CHAPTER 3: THERMAL EVALUATION

3.0 INTRODUCTION

In this chapter, compliance of the HI-STAR System thermal performance to 10CFR71 requirements is established for normal transport and hypothetical accident conditions of transport. The analysis considers passive rejection of decay heat from the spent nuclear fuel (SNF) to an environment under the most severe 10CFR71 mandated design basis ambient conditions.

10CFR71 defines the requirements and acceptance criteria that must be fulfilled by the cask thermal design. The requirements and acceptance criteria applicable to the thermal analysis presented in this chapter are summarized here as follows:

1. The applicant must include a description of the proposed package in sufficient detail to identify the package accurately and provide a sufficient basis for the evaluation of the package. [71.33].

   The description must include, with respect to the packaging, specific materials of construction, weights, dimensions, and fabrication methods of materials specifically used as nonfissile neutron absorbers or moderators [71.33(a)(5)(ii)]; and structural and mechanical means for the transfer and dissipation of heat [71.33(a)(5)(v)].

   The description must include, with respect to the contents of the package, chemical and physical form [71.33(b)(3)]; maximum normal operating pressure [71.33(b)(5)]; maximum amount of decay heat [71.33(b)(7)]; and identification and volumes of any coolants [71.33(b)(8)].

2. A package must be designed, constructed, and prepared for shipment so that under normal conditions of transport there would be no substantial reduction in the effectiveness of the packaging [71.43(f) and 71.51(a)(1)].

3. A package must be designed, constructed, and prepared for shipment so that in still air at 100°F and in the shade, no accessible surface of the package would have a temperature exceeding 185°F in an exclusive use shipment [71.43(g)].

4. Compliance with the permitted activity release limits for a Type B package may not depend on filters or on a mechanical cooling system [71.51(c)].

5. With respect to the initial conditions for the events of normal conditions of transport and hypothetical accident conditions, the demonstration of compliance with the requirements of 10CFR71 must be based on the ambient temperature preceding and following the event remaining constant at that value between -20°F and 100°F which is most unfavorable for the feature under consideration. The initial internal pressure within the containment

system must be considered to be the maximum normal operating pressure, unless a lower internal pressure consistent with the ambient temperature considered to precede and follow the event is more unfavorable [71.71(b) and 71.73(b)].

6. For normal conditions of transport, a heat event consisting of an ambient temperature of 100°F in still air and prescribed insolation must be evaluated [71.71(c)(1)].

7. For normal conditions of transport, a cold event consisting of an ambient temperature of -40°F in still air and shade must be evaluated [71.71(c)(2)].

8. Evaluation for hypothetical accident conditions is to be based on sequential application of the specified events, in the prescribed order, to determine their cumulative effect on a package [71.73(a)].

9. For hypothetical accident conditions, a thermal event consisting of a fully engulfing hydrocarbon fuel/air fire with an average emissivity coefficient of at least 0.9, with an average flame temperature of at least 1475°F for a period of 30 minutes [71.73(c)(4)].

As demonstrated in this chapter, the HI-STAR System design and thermal analyses comply with all nine requirements and acceptance criteria listed above. Subsection 3.2 lists the material properties data required to perform the thermal analyses and Subsection 3.3 provides the applicable temperature limits criteria required to demonstrate the adequacy of the HI-STAR System design under all conditions. All thermal analyses to evaluate the normal conditions of transport performance of a HI-STAR System are described in Subsection 3.4. All thermal analyses for hypothetical accident conditions are described in Subsection 3.5. A summary discussion of regulatory compliance is included in Subsection 3.6.

3.1 DISCUSSION

Sectional views of the HI-STAR System have been presented earlier (see Figures 1.1.3 and 1.1.4). The system essentially consists of a loaded MPC situated inside an overpack equipped with a bolted closure. The fuel assemblies reside inside the MPC that has two redundant welded closures. The MPC contains a stainless steel honeycomb fuel basket that provides square-shaped fuel compartments of appropriate dimensions to facilitate insertion of fuel assemblies prior to welding of the MPC lid. Each fuel cell wall (except outer periphery MPC-32 and MPC-68 cell walls) is provided with thermal neutron absorber panels sandwiched between a stainless steel sheathing plate and the cell wall along the entire length of the active fuel region. Prior to sealing the MPC lid, the MPC is backfilled with helium to the levels specified in Table 1.2.3. This provides a stable and inert environment for the transport of the SNF. Additionally, the annular gap between the MPC and the overpack is backfilled with helium before the overpack vent and drain port plug plugs are installed. Heat is transferred from the SNF in the HI-STAR to the environment by passive heat transport mechanisms only.

The helium backfill gas is an integral part of the MPC and overpack thermal designs. The helium fills all the spaces between solid components and provides an improved conduction medium (compared to air) for dissipating decay heat in the MPC. Additionally, helium in the spaces between the fuel basket and the MPC shell is heated differentially and, therefore, subject to the "Rayleigh" effect which is discussed in detail later (Subsection 3.4.1.1.5). To ensure that the helium gas is retained and is not diluted by lower conductivity air, the MPC helium retention boundary is designed to comply with the provisions of the ASME B&PV Code Section III, Subsection NB, as an all-seal-welded pressure vessel with redundant closures. Similarly, the overpack containment boundary is designed as an ASME B&PV Code Section III, Subsection NB pressure vessel. The overpack containment boundary is required to meet maximum leakage rate requirements included in Section 8.1.4 of this SAR. The leakage rate criterion ensures the presence of helium during transport. The helium gas is therefore retained and undiluted, and may be credited in the thermal analyses.

An important thermal design criterion imposed on the HI-STAR System is to limit the maximum fuel cladding temperature during normal transport to below design basis limits (Table 1.2.3). An equally important design criterion is to reduce temperature gradients within the MPC to minimize thermal stresses. In order to meet these design objectives, the HI-STAR MPC basket is designed to possess certain distinctive characteristics, which are summarized in the following.

The MPC design minimizes resistance to heat transfer within the basket and basket periphery regions. This is ensured by a high structural integrity all-welded honeycomb structure. The MPC design incorporates top and bottom plenums with interconnected downcomer paths. The top plenum is formed between the MPC lid and the top of the honeycomb fuel basket with additional semicircular holes in the top of each fuel cell wall. The bottom plenum is formed by large elongated semicircular holes at the base of all cell walls. The MPC basket is designed to eliminate structural discontinuities (i.e., gaps) which introduce large thermal resistances to heat flow. Consequently, temperature gradients are minimized in this design, which results in lower thermal stresses within the basket. Low thermal stresses are also ensured by an MPC design that

permits unrestrained axial and radial growth of the basket to eliminate the possibility of thermally induced stresses due to restraint of free-end expansion.

The HI-STAR System is designed for transport of PWR and BWR spent fuel assemblies and features two distinct MPC fuel basket geometries. For intact PWR fuel a 24-assembly design (depicted in Figure 1.2.5) and a higher capacity canister (MPC-32) are available. A 68-assembly design for the transport of intact or specified damaged BWR fuel is shown in Figure 1.2.3. Damaged BWR fuel must be placed in a damaged fuel container for transport in the MPC-68. Extensively damaged BWR fuel assemblies (e.g. severed rods) classified as fuel debris shall be transported in the MPC-68F. The MPC-68F is identical to the MPC-68, except for the ^{10}B loading of the neutron absorber panels for criticality control. Each basket design must comply with the required temperature limits under the imposed heat generation loads from the fuel assembly contents. For normal transport conditions, the maximum decay heat loads for the PWR and BWR MPCs are summarized in Table 1.2.3. The complete HI-STAR System consisting of the overpack and MPC under transport conditions is conservatively analyzed for the imposed design heat loads.

Thermal analysis of the HI-STAR System is based on including all three fundamental modes of heat transfer: conduction, natural convection and thermal radiation. Different combinations of these modes are active in different parts of the system. These modes are properly identified and conservatively analyzed within each region of the MPC and overpack, to enable bounding calculations of the temperature distribution within the HI-STAR System for both PWR and BWR MPC basket designs.

On the outside surface of the overpack, heat is dissipated to the environment by buoyancy induced convective air flow (natural convection) and thermal radiation. In the overpack internal metal structure, only conductive heat transport is possible. Between metal surfaces (e.g., between neighboring fuel rod surfaces) heat transport is due to a combination of conduction through a gaseous medium (helium) and thermal radiation. Finally, buoyancy-induced convective heat transport occurs within the open spaces of the MPC, aided by the MPC design which provides low pressure drop helium flow recirculation loops formed by the fuel cells, top plenum, downcomers, and bottom plenum. However, in the interest of conservatism, no credit for buoyancy-induced heat transport in the HI-STAR MPC basket is taken to satisfy either temperature or stress intensity limits. Heat transfer between the fuel basket external surface and MPC enclosure shell inside wall is further influenced by the so-called "Rayleigh" effect in differentially heated vertical cavities and "Rayleigh-Benard" effect in horizontal channels heated from below. A discussion on these effects is provided in Subsection 3.4.1.1.5.

The total heat generation in each assembly is non-uniformly distributed over the active fuel to account for design basis-fuel burnup distribution listed in Chapter 1 (Table 1.2.15 and Figures 1.2.13 and 1.2.14). As discussed later in this chapter (Subsection 3.4.6), an array of conservative assumptions bias the results of the thermal analysis towards much reduced computed margins than would be obtained by a rigorous analysis of the problem.

The complete thermal analysis is performed using the industry standard ANSYS finite element modeling package [3.1.1] and the finite volume Computational Fluid Dynamics (CFD) code FLUENT [3.1.2]. ANSYS has been previously used and accepted by the NRC on numerous dockets. The FLUENT CFD program is independently benchmarked and validated with a wide class of theoretical and experimental studies reported in the technical journals. Additionally, Holtec has confirmed the code's capability to reliably predict temperature fields in dry storage applications using independent full-scale test data from a loaded cask [3.1.3]. This study concluded that FLUENT can be used to model all modes of heat transfer, namely, conduction, convection, and radiation in dry cask systems.

3.2 SUMMARY OF THERMAL PROPERTIES OF MATERIALS

Materials present in the HI-STAR System include stainless steels, carbon steels, aluminum, neutron shield (Holtite-A), neutron absorber and helium. In Table 3.2.1, a summary of references used to obtain cask material properties for performing all thermal analyses is presented.

Tables 3.2.2, 3.2.3 and 3.2.9 provide numerical thermal conductivity data for all materials at several representative temperatures. The neutron absorber materials are made of aluminum powder and boron carbide powder. Although their manufacturing processes differ, from a thermal standpoint, their ability to conduct heat is virtually identical. Therefore, the value of conductivity of one neutron absorber (Boral) is used in the thermal calculations and is applicable to both neutron absorbers used in the HI-STAR 100 cask. Thermal properties of Boral are provided in Table 3.2.8.

Surface emissivity data for key materials of construction are provided in Table 3.2.4. The emissivity properties of painted surfaces are generally excellent. Kern [3.2.5] reports an emissivity range of 0.8 to 0.98 for a wide variety of paints. In the HI-STAR thermal analysis, an emissivity of 0.85[†] is applied to exterior painted surfaces. A conservative solar absorbtivity coefficient of 1.0 is applied to all exposed cask surfaces.

In Table 3.2.5, the heat capacity and density data of different cask materials is presented. These properties are used in performing transient (hypothetical fire accident condition, for example) analyses. MPC Rayleigh effect calculations use helium density, heat capacity, and gas viscosity properties data, which are listed in Tables 3.2.5 and 3.2.6.

The HI-STAR System's outside surface heat transfer coefficient is calculated by accounting for both natural convection heat transfer and radiation. The natural convection coefficient of a heated horizontal cylinder depends upon the product of the Grashof (Gr) and Prandtl (Pr) numbers. Following the approach developed by Jakob and Hawkins [3.2.9], GrPr is expressed as $L^3 \Delta T\ Z$, where L is the diameter of the cask, ΔT is the HI-STAR System overpack surface-to-ambient temperature differential and Z is a parameter which depends upon air properties, which are known functions of temperature, evaluated at the average film temperature. The temperature dependence of Z for air is provided in Table 3.2.7.

The long-term thermal stability and radiation resistance of Holtite-A has been confirmed through qualification testing. The qualification test conditions exceed the Holtite-A thermal and radiation environment (gamma and neutron fluence) in the HI-STAR 100 cask. The Holtite-A thermal stability test temperature, 325°F, is well above the maximum operating temperature of Holtite-A (See Tables 3.4.10 and 3.4.11). The Holtite-A radiation test exposures exceed 50-year HI-STAR service neutron

---

† This is conservative with respect to prior cask industry practice, which has historically accepted higher emissivities. For example, the emissivity for painted surfaces (ε=0.95) is used in the TN-32 cask TSAR (Docket 72-1021).

dose by a factor of 3.75 and gamma dose by a factor of 5.54 (See Table 3.2.10). The Holtite-A qualification test data is archived in the following reports:

i) "Holtite A: Development history and thermal performance data", Holtec Report HI-2002396, Rev. 3.
ii) "Holtite-A: Results of Pre-and-Post-Irradiation Tests and Measurements", Holtec Report HI-2002420, Rev. 1.

The testing referenced above confirms that Holtite-A does not degrade at elevated temperatures and Holtite-A is unaffected by high neutron fluence and megarad gamma doses. Even under very conservative assumptions (20-years of storage under the maximum temperature reached at the beginning of dry storage) only a 2% weight loss is computed (licensing basis commitment is 4%). Nevertheless, periodic thermal testing of HI-STAR 100 is required as specified in Chapter 8.

Table 3.2.1

SUMMARY OF HI-STAR SYSTEM MATERIALS
THERMAL PROPERTY REFERENCES

Material	Emissivity	Conductivity	Density	Heat Capacity
Helium	NA	Handbook [3.2.2]	Ideal Gas Law	Handbook [3.2.2]
Air	NA	Handbook [3.2.2]	Ideal Gas Law	Handbook [3.2.2]
Zircaloy Cladding	EPRI [3.2.3]	NUREG [3.2.6], [3.2.7]	Rust [3.2.4]	Rust [3.2.4]
UO_2	Not Used	NUREG [3.2.6], [3.2.7]	Rust [3.2.4]	Rust [3.2.4]
Stainless Steel (machined forgings)*	Kern [3.2.5]	ASME [3.2.8]	Marks [3.2.1]	Marks [3.2.1]
Stainless Steel Plates†	ORNL [3.2.12], [3.2.13]	ASME [3.2.8]	Marks [3.2.1]	Marks [3.2.1]
Carbon Steel	Kern [3.2.5]	ASME [3.2.8]	Marks [3.2.1]	Marks [3.2.1]
Aluminum Impact Limiters	Not Used	Note 1	Note 1	Note 1
Aluminum Alloy 1100 (Heat Conduction Elements)‡	Handbook [3.2.2]	ASME [3.2.8]	ASME [3.2.8]	ASME [3.2.8]
Boral†	Not Used	Test Data	Test Data	Test Data
Holtite-A	Not Used	Test Data [3.2.14]	Test Data [3.2.14]	Test Data [3.2.13]
METAMIC§	Not Used	Test Data [3.2.10], [3.2.11]	Test Data [3.2.10], [3.2.11]	Test Data [3.2.10], [3.2.11]
Note 1: Properties of solid aluminum *are* used during fire to maximize heat input and properties of air used during normal transport and post-fire cooldown to minimize heat dissipation. *The solid aluminum properties are taken from the ASME Code [3.2.8] for alloy 5052, and thermal conductivity values are extrapolated linearly to 450°F and 700°F.*				

* Used in the MPC lid.
† Used in the basket panels & sheathing, MPC shell& baseplate.
‡ Heat conduction elements used in certain early vintage MPCs
† AAR Structures' Boral thermophysical test data.
§ Table lists all sources consulted for material properties.

Table 3.2.2

SUMMARY OF HI-STAR SYSTEM MATERIALS
THERMAL CONDUCTIVITY DATA

Material	@ 200°F (Btu/ft-hr-°F)	@ 450°F (Btu/ft-hr-°F)	@ 700°F (Btu/ft-hr-°F)
Helium	0.0976	0.1289	0.1575
Air	0.0173	0.0225	0.0272
Alloy X	8.4	9.8	11.0
Carbon Steel Radial Connectors	29.2	27.1	24.6
Carbon Steel Gamma Shield Layers	24.4	23.9	22.4
Aluminum Honeycomb Impact Limiter*	84.4	90.9	97.4
Holtite-A†	See Footnote		
Cryogenic Steel	23.8	23.7	22.3

* Properties of solid Aluminum used during fire to maximize heat input and properties of air used during normal transport and post-fire cooldown to minimize heat dissipation.

† No credit taken for conduction through radial Holtite for the steady-state analysis, and before and after fire conditions for fire accident analysis. A conservative upper bound conductivity (1.0 Btu/ft-hr-°F) is applied during the fire condition to the radial neutron shield (between intermediate shells and overpack enclosure shell).

Table 3.2.3

SUMMARY OF FUEL ELEMENT COMPONENTS
THERMAL CONDUCTIVITY DATA

Fuel Cladding		**Fuel (UO_2)**	
Temperature (°F)	**Conductivity (Btu/ft-hr-°F)**	**Temperature (°F)**	**Conductivity (Btu/ft-hr-°F)**
392	8.28†	100	3.48
572	8.76	448	3.48
752	9.60	570	3.24
932	10.44	793	2.28†

† Lowest value of conductivity is used in the thermal analysis for conservatism.

Table 3.2.4

SUMMARY OF MATERIALS SURFACE EMISSIVITY DATA

Material	Emissivity
Fuel cladding	0.80
Painted exterior surface	0.85
Rolled carbon steel	0.66
Stainless steel (machined forgings)	0.36
Stainless Steel Plates	0.587*
Sandblasted aluminum†	0.40

Note: The emissivities of package interior surfaces are understated to maximize normal operating temperatures of the package payload. As justified next, the lowerbound emissivities are used under hypothetical fire accident evaluations. The temperature elevation from the initial conditions, T_{fire}, of the HI-STAR package SNF under a hypothetical fire accident is principally a function of heat absorbed by the package during fire (Q_{fire}) and the thermal inertia (C) of the package. As Q_{fire} is unaffected by the emissivity of package internals (stainless steel basket panels and MPC pressure boundaries) and C is independent of emissivity, T_{fire} is unaffected by emissivity.

* Lowerbound value of stainless steel plates from cited references in Table 3.2.1. For conservatism, an even lower emissivity ($\varepsilon = 0.36$) was used in the thermal calculations.

† Reported data covers the use of aluminum heat conduction elements in certain early vintage MPCs

Table 3.2.5

MATERIALS DENSITY AND HEAT CAPACITY PROPERTIES SUMMARY

Materials	**Density (lbm/ft^3)**	**Heat Capacity (Btu/lbm-°F)**
Helium	(Ideal Gas Law)	1.24
Zircaloy Cladding	409	0.0728
Fuel (UO_2)	684	0.056
Carbon Steel	489	0.1
Stainless Steel	501	0.12
Boral	154.7	0.13
Aluminum Honeycomb Impact Limiter*	167.6	0.23
Aluminum Alloy 1100	169.3	0.23
Holtite-A†	105.0	0.39

* Properties of solid Aluminum used during fire to maximize heat input and properties of air used during normal transport and post-fire cooldown to minimize heat dissipation.

† Conservatively postulated to underestimate thermal inertia for fire accident analysis.

Table 3.2.6

HELIUM GAS VISCOSITY† VARIATION WITH TEMPERATURE

Temperature (°F)	Viscosity (Micropoise)
167.4	220.5
200.3	228.2
297.4	250.6
346.9	261.8
463.0	288.7
537.8	299.8
737.6	338.8

† Obtained from Rohsenow and Hartnett [3.2.2].

Table 3.2.7

VARIATION OF NATURAL CONVECTION PROPERTIES
PARAMETER "Z" FOR AIR WITH TEMPERATURE

Temperature (°F)	**Z (ft^{-3} °F^{-1})**†
40	2.1×10^{6}
140	9.0×10^{5}
240	4.6×10^{5}
340	2.6×10^{5}
440	1.5×10^{5}

† Obtained from Jakob and Hawkins [3.2.9].

Table 3.2.8

BORAL COMPONENT MATERIALS*
THERMAL CONDUCTIVITY DATA

Temperature (°F)	B_4C Core Conductivity (Btu/ft-hr-°F)	Aluminum Cladding Conductivity (Btu/ft-hr-°F)
212	48.09	100.00
392	48.03	104.51
572	47.28	108.04
752	46.35	109.43

* Thermal properties of Boral used in the calculations are tabulated herein. As heat conduction properties of METAMIC are essentially same as Boral (See Section 3.2) tabulation of METAMIC properties is not necessary.

Table 3.2.9

HEAT CONDUCTION ELEMENTS (ALUMINUM ALLOY 1100)
THERMAL CONDUCTIVITY DATA

Temperature (°F)	**Conductivity (Btu/ft×hr×°F)**
100	131.8
200	128.5
300	126.2
400	124.5

Table 3.2.10

Holtite-A Radiation Exposure*

	Under 50-Year Service Life	Test Exposure
Neutron Fluence (n/cm^2)	$4x10^{14}$	$1.28x10^{15}$
Gamma Dose (rad)	$3.55x10^5$	$1.7x10^6$
Note: As tabulated above the Holtite-A qualification test exposures exceed 50-year service exposures by significant margins.		

* "Holtite-A: Results of Pre-and-Post-Irradiation Tests and Measurements", Holtec Report HI-2002420, Rev. 1.

3.3 TECHNICAL SPECIFICATIONS FOR COMPONENTS

HI-STAR System materials and components which are required to be maintained within their safe operating temperature ranges to ensure their intended function are summarized in Table 3.3.1. Long-term stability and continued neutron shielding ability of the Holtite-A neutron shield material under normal transport conditions are ensured when material exposure temperatures are maintained below the maximum allowable limit. The overpack metallic seals will continue to ensure sealing of the closure plate, and drain and vent ports if the manufacturer's recommended design temperature limits are not exceeded. Integrity of SNF during transport requires demonstration of HI-STAR fuel cladding temperatures to remain below regulatory limits. Neutron absorber materials used in MPC baskets for criticality control are stable in excess of 1000°F. For conservatism temperature limits below the threshold of material integrity† are adopted (See Table 3.3.1).

Compliance to 10CFR71 requires evaluation of hypothetical accident conditions. The inherent mechanical stability characteristics of the HI-STAR System materials and components ensure that no significant functional degradation is possible due to exposure to short-term temperature excursions outside the normal long-term temperature limits. For evaluation of the HI-STAR System's thermal performance under hypothetical accident conditions, material temperature limits for short-duration events are also provided in Table 3.3.1. In this Table, the cladding temperature limits of ISG-11, Rev. 3 [3.1.5] are adopted for Commercial Spent Fuel (CSF). These limits are applicable to all fuel types, burnup levels and cladding materials approved by the NRC for power generation.

3.3.1 Evaluation of Moderate Burnup Fuel

It is recognized that hydrides present in irradiated fuel rods (predominantly circumferentially oriented) dissolve at cladding temperatures above 400°C [3.3.8]. Upon cooling below a threshold temperature (T_p), the hydrides precipitate and reorient to an undesirable (radial) direction if cladding stresses at the hydride precipitation temperature T_p are excessive. For moderate burnup fuel, T_p is conservatively estimated as 350°C [3.3.8].

Moderate Burnup Fuel (MBF) temperature limits for short term operations have been addressed in the PNNL report "Estimated Maximum Cladding Stresses for Bounding PWR Fuel Rods During Short Term Operations for Dry Cask Storage" published in Jan. 2004 [3.3.8]. In this report the potential for hydride re-orientation was evaluated in a simulated drying event in which fuel was heated to the cladding temperature limit (570°C (1058°F)) and then cooled below the hydride precipitation temperature T_p. The study concluded that hydride re-orientation is not a concern in moderate burnup fuel because the coincident cladding stress at the hydride precipitation temperature is below the critical cladding stress. Accordingly, the 570°C (1058°F) temperature limit is justified

† Neutron absorber materials are manufactured using B_4C and aluminum. B_4C is a refractory material that is unaffected by high temperatures and aluminum is solid at temperatures in excess of 1000°F.

for moderate burnup fuel and is adopted in the HI-STAR SAR for short-term operations with MBF fueled MPCs.

Table 3.3.1

HI-STAR SYSTEM MATERIAL TEMPERATURE LIMITS

Material	Normal Condition Temperature Limits	Short Term and Accident Temperature Limits
CSF Cladding	752°F	1058°F
Neutron Absorber	800°F	1000°F
Overpack Closure Plate Mechanical Seals	See Table 4.1.1	See Table 4.1.1
Overpack Vent and Drain Port Plug Seals	See Table 4.1.1	See Table 4.1.1
Aluminum Alloy 5052	176°F[††]	1105°F[†††]
Holtite-A	300°F[††††]	N/A[†††††]
Aluminum Heat Conduction Elements (Alloy 1100)[1]	725°F	950°F

†† AL-STAR impact limiter aluminum honeycomb test data.

††† Melting range of alloy is 1105°F-1200°F [3.3.1].

†††† Neutron shield manufacturer's test data (Appendix 1.B).

††††† For shielding analysis (Chapter 5), Holtite-A is conservatively assumed to be lost during the fire accident.

1 Temperature limits provided to cover the use of aluminum heat conduction elements in certain early vintage MPCs.

Tables 3.3.2 through 3.3.8

[INTENTIONALLY DELETED]

3.4 THERMAL EVALUATION FOR NORMAL CONDITIONS OF TRANSPORT

3.4.1 Thermal Model

The HI-STAR MPC basket designs consist of four distinct geometries engineered to hold 24 and 32 PWR (MPC-24, MPC-24E and MPC-32) or 68 BWR (MPC-68) fuel assemblies. The fuel basket forms a honeycomb matrix of square-shaped fuel compartments to retain the fuel assemblies during transport (refer to Figures 1.2.3 and 1.2.5 for an illustration of PWR and BWR baskets). The basket is formed by an interlocking honeycomb structure of steel plates and full-length edge welding of the cell corners to form an integral basket configuration. Individual cell walls (except outer periphery MPC-68 and MPC-32 cell walls) are provided with neutron absorber panels sandwiched between the cell wall and a stainless steel sheathing plate, for the full length of the active fuel region.

The design basis decay heat generation per PWR or BWR assembly for normal transport for each MPC type is specified in Table 1.2.13. The decay heat is considered to be non-uniformly distributed over the active fuel length based on the design basis axial burnup distribution specified in Chapter 1 (see Table 1.2.15 and Figures 1.2.13 and 1.2.14).

Transport of heat from the MPC basket interior to the basket periphery is accomplished by conduction through the MPC basket metal grid structure and the narrow helium gaps between the fuel assemblies and fuel cell walls. Heat dissipation in the MPC basket periphery-to-MPC shell gap is by a combination of helium conduction, natural convection (by means of the "Rayleigh" effect) and radiation across the gap. Between the MPC shell and the overpack inner shell is a small clearance, which is evacuated and backfilled with helium. Helium, besides being inert, is a better conductor of heat than air. Thus, heat conduction through the helium gap between the MPC and the overpack will minimize temperature differentials across this region.

The overpack, under normal transport conditions, passively rejects heat to the environment. Cooling of the exterior system surfaces is by natural convection and radiation. During transport, the HI-STAR System is placed in a horizontal position with stainless steel encased aluminum honeycomb impact limiters installed at both ends of the overpack. To conservatively maximize the calculated internal temperatures, the thermal conductivity of the impact limiters is set essentially equal to zero. Under normal transport conditions, the MPC shell rests on the overpack internal cavity surface forming an eccentric gap. Direct contact between the MPC and overpack surfaces is expected to minimize heat transfer resistance in this region of intimate contact. Significantly improved conductive heat transport due to reduction in the helium gap near the contact region is accounted for in the thermal analysis of the HI-STAR System. The HI-STAR System is conservatively analyzed assuming a minimum 0.02-inch gap at the line of metal-to-metal contact. Analytical modeling details of the various thermal transport mechanisms are provided in the following.

3.4.1.1 Analytical Model - General Remarks

Transport of heat from the heat generation region (fuel assemblies) to the outside environment is analyzed broadly in terms of three interdependent thermal models.

i. The first model considers transport of heat from the fuel assembly to the basket cell walls.

This model recognizes the combined effects of conduction (through helium) and radiation, and is essentially a finite element technology-based update of the classical Wooton & Epstein [3.4.1] formulation (which considers radiative heat exchange between fuel rod surfaces).

ii. The second model considers heat transport within an MPC cross section by conduction and radiation. The effective cross sectional thermal conductivity of the basket region obtained from the combined fuel assembly/basket heat conduction radiation model is applied to an axisymmetric thermal model of the HI-STAR System on the FLUENT [3.1.2] code.

iii. The third model deals with the transmission of heat from the MPC exterior surface to the external environment (heat sink). From the MPC shell to the cask exterior surface, heat is conducted through an array of concentric shells representing the MPC-to-overpack helium gap, the overpack inner shell, the intermediate shells, the Holtite-A neutron shielding and finally the overpack outer shell. Heat rejection from the outside cask surfaces to ambient air is considered by accounting for natural convection and thermal radiation heat transfer mechanisms from the exposed cask surfaces. Insolation on exposed cask surfaces is based on 12-hour levels prescribed in 10CFR71, averaged over a 24-hour period.

The following subsections contain a systematic description of the mathematical models devised to articulate the temperature field in the HI-STAR System. Table 3.4.2 shows the relationship between the mathematical models and the corresponding regions (i.e., fuel, MPC, overpack, etc.) of the HI-STAR System. The description begins with the method to characterize the heat transfer behavior of the prismatic (square) opening referred to as the "fuel space" containing a heat emitting fuel assembly. The methodology utilizes a finite-volume procedure to replace the heterogeneous SNF/fuel space region with an equivalent solid body having a well-defined temperature-dependent conductivity. In the following subsection, the method to replace the composite walls of the fuel basket cells with equivalent "solid" walls is presented. Having created the mathematical equivalents for the SNF/fuel spaces and the fuel basket walls, the method to represent the MPC cylinder containing the fuel basket by an equivalent cylinder whose thermal conductivity is a function of the spatial location and coincident temperature is presented.

Following the approach of presenting descriptions starting from the inside and moving to the outer region of a cask, the next subsections present the mathematical model to simulate the overpack. Subsection 3.4.1.1.12 concludes the presentation with a description of how the different models for the specific regions within the HI-STAR System are assembled into the final finite element model.

3.4.1.1.1 Overview of the Thermal Model

Thermal analysis of the HI-STAR System is performed by assuming that the system is subject to its maximum heat duty with each storage location occupied and with the heat generation rate in each stored fuel assembly equal to the design basis maximum value. While the assumption of equal heat generation imputes a certain symmetry to the cask thermal problem, the thermal model must incorporate three attributes of the physical problem to perform a rigorous analysis:

i. While the rate of heat conduction through metals is a relatively weak function of

temperature, radiation heat exchange is a nonlinear function of surface temperatures.

ii. Heat generation in the MPC is axially non-uniform due to a non-uniform axial burnup profile in the fuel assemblies.

iii. Inasmuch as the transfer of heat occurs from the inside of the basket region to the outside, the temperature field in the MPC is spatially distributed with the maximum values reached in the central region.

It is clearly impractical to explicitly model every fuel rod in every stored fuel assembly explicitly. Instead, the cross section bounded by the inside of the storage cell, which surrounds the assemblage of fuel rods and the interstitial helium gas, is replaced with an "equivalent" square (solid) section characterized by an effective thermal conductivity. Figure 3.4.1 pictorially illustrates the homogenization concept. Further details on this process for determining the effective conductivity is presented in Subsection 3.4.1.1.2. It suffices to state here that the effective conductivity of the cell space will be a function of temperature, because radiation heat transfer (a major component of the heat transport mechanism between the fuel rods to the basket metal square) is a strong function of the absolute temperatures of the participating bodies. Therefore, in effect, every storage cell location will have a different value of effective conductivity in the homogenized model. The process of determining the temperature-dependent effective conductivity is carried out using a finite volume procedure.

In the next step of homogenization, a planar section of MPC is considered. With each storage cell inside space replaced with an equivalent solid square, the MPC cross section consists of a metallic gridwork (basket cell walls with each cell space containing a solid fuel square with an effective thermal conductivity) circumscribed by a circular ring (MPC shell). There are four principal materials in this section that are included in all MPCs, namely the homogenized fuel cell squares, the Alloy X MPC structural materials in the MPC (including sheathing material), neutron absorber and helium gas. Aluminum heat conduction elements (AHCEs), included optionally in the MPC design, are appropriately ignored in the heat dissipation calculations. Each of the four constituent materials in this section has a different conductivity. As discussed earlier, the conductivity of the homogenized fuel cell is a strong function of temperature.

In order to replace this thermally heterogeneous MPC section with an equivalent conduction-only lamina, resort to the finite-element procedure is necessary. Because the rate of transport of heat within the MPC is influenced by radiation, which is a temperature-dependent effect, the equivalent conductivity of the MPC lamina must be computed as a function of temperature. Finally, it is recognized that the MPC section consists of two discrete regions, namely, the basket region and the periphery region. The periphery region is the space between the peripheral storage cells and the MPC enclosure shell. This space is essentially full of helium gas surrounded by Alloy X plates and optionally aluminum heat conduction elements. Accordingly, as illustrated in Figure 3.4.2 for MPC-68, the MPC cross section is replaced with two homogenized regions with temperature-dependent conductivities. In particular, the effective conductivity of the fuel cells is subsumed into the equivalent conductivity of the basket cross section using a finite element procedure. The ANSYS finite-element code is the vehicle for all modeling efforts described in the foregoing.

In summary, appropriate finite element models are used to replace the MPC cross section with an equivalent two-region homogeneous conduction lamina whose local conductivity is a known function of coincident absolute temperature. Thus, the MPC cylinder containing discrete fuel assemblies, helium, neutron absorber, Alloy X and optionally AHCEs* is replaced with a right circular cylinder whose material conductivity will vary with radial and axial position as a function of the coincident temperature.

The MPC-to-overpack gap is simply an annular space that is readily modeled with an equivalent conductivity that reflects the conduction and radiation modes of heat transfer. The overpack is a radially symmetric structure except for the neutron absorber region which is built from radial connectors and Holtite. Using the classical equivalence procedure as described in Section 3.4.1.1.9, this region is replaced with an equivalent radially symmetric annular cylinder.

The thermal analysis procedure described above makes frequent use of equivalent thermal properties to ease the geometric modeling of the cask components. These equivalent properties are rigorously calculated values based on detailed evaluations of actual cask system geometries. All these calculations are performed conservatively to ensure a bounding representation of the cask system. This process commonly referred to as submodeling, yields accurate (not approximate) results. Given the detailed nature of the submodeling process, experimental validation of the individual submodels is not necessary.

In this manner, a HI-STAR System overpack containing a loaded MPC is replaced with a right circular cylinder with spatially varying temperature-dependent conductivity. Heat is generated within the basket space in this cylinder in the manner of the prescribed axial distribution. In addition, heat is deposited from insolation on its external surface. Natural convection and thermal radiation to ambient air dissipate heat. Details of the elements of mathematical modeling are provided in the following sections.

3.4.1.1.2 Fuel Region Effective Thermal Conductivity Calculation

Thermal properties of a large number of PWR and BWR fuel assembly configurations manufactured by the major fuel suppliers (i.e., Westinghouse, CE, B&W, and GE) have been evaluated for inclusion in the HI-STAR System thermal analysis. Bounding PWR and BWR fuel assembly configurations are determined using the simplified procedure described below. This is followed by the determination of temperature-dependent properties of the bounding PWR and BWR fuel assembly configurations to be used for cask thermal analysis using a finite-volume (FLUENT) approach.

To determine which of the numerous PWR assembly types listed in Table 3.4.4 should be used in the thermal model for the PWR fuel baskets, we must establish which assembly has the maximum thermal resistance. The same determination must be made for the MPC-68, out of the menu of SNF types listed in Table 3.4.5. For this purpose, we utilize a simplified procedure that we describe below.

* In the thermal model, AHCEs are appropriately ignored.

Each fuel assembly consists of a large array of fuel rods typically arranged on a square layout. Every fuel rod in this array is generating heat due to radioactive decay in the enclosed fuel pellets. There is a finite temperature difference required to transport heat from the innermost fuel rods to the storage cell walls. Heat transport within the fuel assembly is based on principles of conduction heat transfer combined with the highly conservative analytical model proposed by Wooton and Epstein [3.4.1]. The Wooton-Epstein model considers radiative heat exchange between individual fuel rod surfaces as a means to bound the hottest fuel rod cladding temperature.

Transport of heat energy within any cross section of a fuel assembly is due to a combination of radiative energy exchange and conduction through the helium gas that fills the interstices between the fuel rods in the array. With the assumption of uniform heat generation within any given horizontal cross section of a fuel assembly, the combined radiation and conduction heat transport effects result in the following heat flow equation:

$$Q = \sigma C_o F_\varepsilon A [T_C^4 - T_B^4] + 13.5740 L K_{cs} [T_C - T_B]$$

where,

$$F_\varepsilon = Emissivity\ Factor = \frac{1}{\left(\frac{1}{\varepsilon_C} + \frac{1}{\varepsilon_B} - 1\right)}$$

ε_C, ε_B = emissivities of fuel cladding, fuel basket (see Table 3.2.4)

$$C_o = Assembly\ Geometry\ Factor$$
$$= \frac{4N}{(N+1)^2}\ (when\ N\ is\ odd)$$
$$= \frac{4}{N+2}\ (when\ N\ is\ even)$$

N	=	Number of rows or columns of rods arranged in a square array
A	=	fuel assembly "box" heat transfer area
	=	4 × width × length (ft^2)
L	=	fuel assembly length (ft)
K_{cs}	=	fuel assembly constituent materials volume fraction weighted mixture conductivity (Btu/ft-hr-°F)
T_C	=	hottest fuel cladding temperature (°R)
T_B	=	box temperature (°R)

Q = net radial heat transport from the assembly interior (Btu/hr)

σ = Stefan-Boltzman Constant (0.1714×10^{-8} Btu/ft^2-hr-°R^4)

In the above heat flow equation, the first term is the Wooten-Epstein radiative heat flow contribution while the second term is the conduction heat transport contribution based on the classical solution to the temperature distribution problem inside a square shaped block with uniform heat generation [3.4.3]. The 13.574 factor in the conduction term of the equation is the shape factor for two-dimensional heat transfer in a square section. Planar fuel assembly heat transport by conduction occurs through a series of resistances formed by the interstitial helium fill gas, fuel cladding and enclosed fuel. An effective planar mixture conductivity is determined by a volume fraction weighted sum of the individual constituent materials resistances. For BWR assemblies, this formulation is applied to the region inside the fuel channel. A second conduction and radiation model is applied between the channel and the fuel basket gap. These two models are combined, in series, to yield a total effective conductivity.

The effective thermal conductivities of several representative intact PWR and BWR assemblies are presented in Tables 3.4.4 and 3.4.5. At higher temperatures (greater than 450°F), the zircaloy clad fuel assemblies with the lowest effective thermal conductivities are the Westinghouse 17×17 OFA (PWR) and the General Electric GE-11 9×9 (BWR). A discussion of fuel assembly conductivities for some of the newer 10×10 array and plant specific BWR fuel designs is presented near the end of this subsection. Based on this simplified analysis, the Westinghouse 17×17 OFA PWR and GE-11 9×9 BWR fuel assemblies are determined to be the bounding configurations for analysis at design basis maximum heat loads.

Several of the assemblies listed in Tables 3.4.5 were excluded from consideration when determining the bounding assembly because of their extremely low decay heat loads. The excluded assemblies, which were each used at a single reactor only, are physically small and have extremely low burnups and long cooling times. These factors combine to result in decay heat loads that are much lower than the design basis maximum. The excluded assemblies are:

Dresden Unit 1 8×8
Dresden Unit 1 6×6
Allis-Chalmers 10×10 Stainless
Exxon Nuclear 10×10 Stainless
Humboldt Bay 7x7
Quad$^+$ 8x8

The Allis-Chalmers and Exxon assemblies are used only in the LaCrosse reactor of the Dairyland Power Cooperative. The design basis assembly decay heat loads for Dresden Unit 1 and LaCrosse SNF (Tables 1.2.14 and 1.2.19) are approximately 58% lower and 69% lower, respectively, than the MPC-68 design basis assembly maximum heat load (Table 1.2.13). Examining Table 3.4.5, the effective thermal conductivity of damaged Dresden Unit 1 fuel assemblies inside DFCs (the lowest of any Dresden Unit 1 assembly) and LaCrosse fuel assemblies are approximately 40% lower and

30% lower, respectively, than that of the bounding (GE-11 9×9) fuel assembly. Consequently, the fuel cladding temperatures in the HI-STAR System with Dresden Unit 1 and LaCrosse fuel assemblies (intact or damaged) will be bounded by design basis fuel cladding temperatures.

To accommodate Trojan Nuclear Plant (TNP) SNF in a HI-STAR System's MPC-24E canister*, the discharged fuel characteristics at this permanently shutdown site are evaluated herein. To permit TNP fuel in the HI-STAR System, it is necessary to confirm that certain key fuel parameters, viz. burnup (B) and cask decay heat (D) are bounded by the thermal design limits (42,500 MWD/MTU and 20 kW for PWR MPCs). The TNP SNF is a member of the 17x17 class of fuel types. The bulk of the fuel inventory is from Westinghouse and balance from B&W. The B&W SNF configuration and cladding dimensions are same as that of the Westinghouse 17x17 SNF. The fuel is more than nine years old and the burnups are in the range of 5073 MWD/MTU to 41889 MWD/MTU. The TNP SNF burnups are bounded by the design maximum for PWR class of fuel (i.e. B < 42500 MWD/MTU). Because the fuel decay heat is exponentially attenuating with time, it is conservative to evaluate decay heat on a date that precedes fuel loading. For this purpose, a reference date (RD) of 11/9/2001 is employed herein. The decay heat from the most emissive Trojan fuel is bounded by 725 W on RD. Postulating every cell location in an MPC-24E is occupied by this most heat emissive fuel assembly, a conservatively bounding D = 17.4 kW† is computed. The Trojan MPC-24E heat loads are below the HI-STAR System design heat load (i.e. D < 20 kW) by a significant margin.

A limited number of Trojan assemblies have poison inserts (RCCAs and BPRAs) and other non-fuel hardware (Thimble Plugs). The inclusion of PWR non-fuel hardware influences the MPC thermal response in two ways: (i) The presence of non-fuel hardware increases the effective basket conductivity, thus enhancing heat dissipation and lowering fuel temperatures and (ii) Volume displaced by the mass of non-fuel hardware lowers the available cavity free volume for accommodating gas released in hypothetical rod rupture scenarios. For a conservatively bounding evaluation, the thermal modeling ignores the presence of non-fuel hardware and the MPC cavity volume is computed based on volume displacement by the heaviest fuel (bounding weight) with non-fuel hardware included.

Having established the governing (most resistive) PWR and BWR SNF types, a finite-volume code is used to determine the effective conductivities in a conservative manner. Detailed conduction-radiation finite-volume models of the bounding PWR and BWR fuel assemblies are developed in the FLUENT code as shown in Figures 3.4.7 and 3.4.8, respectively. The PWR model was originally developed on the ANSYS code which enables individual rod-to-rod and rod-to-basket wall view factor calculations to be performed using that code's AUX12 processor. Limitations of radiation modeling techniques implemented in ANSYS make it difficult to take advantage of the symmetry of the fuel assembly geometry. Unacceptably long CPU time and large workspace requirements necessary for performing gray body radiation calculations for a complete fuel assembly geometry on ANSYS prompted the development of an alternate simplified model on the FLUENT code. The FLUENT model was benchmarked with the ANSYS model results for a Westinghouse 17×17 OFA fuel assembly geometry for the case of black body radiation (emissivities = 1). The FLUENT model was found to yield conservative results in comparison to the ANSYS model for the "black" surface

* The height of MPC-24E for Trojan SNF is shorter than the height of generic HI-STAR MPCs.
† Projected MPC heat loads are much lower (in the range of 6 kW to 14.5 kW in circa 2003).

case. The FLUENT model benchmarked in this manner is used to solve the gray body radiation problem to provide the necessary results for determining the effective thermal conductivity of the governing PWR fuel assembly. The same modeling approach using FLUENT is then applied to the governing BWR fuel assembly and the effective conductivity of GE-11 9×9 fuel is determined.

An equivalent homogeneous material that fills the basket opening replaces the combined fuel rods-helium matrix by the following two-step procedure. In the first step, the FLUENT-based fuel assembly model is solved by applying equal heat generation per unit length to the individual fuel rods and a uniform boundary temperature along the basket cell opening inside periphery. The temperature difference between the peak cladding and boundary temperatures is used to determine an effective conductivity as described in the next step. For this purpose, we consider a two-dimensional cross section of a square shaped block of size equal to 2L and a uniform volumetric heat source (q_g) cooled at the periphery with a uniform boundary temperature. Under the assumption of constant material thermal conductivity (K), the temperature difference (ΔT) from the center of the cross section to the periphery is analytically given by [3.4.3]:

$$\Delta T = 0.29468 \frac{q_g L^2}{K}$$

This analytical formula is applied to determine the effective material conductivity from a known quantity of heat generation applied in the FLUENT model (smeared as a uniform heat source, q_g), basket opening size and ΔT calculated in the first step.

As discussed earlier, the effective fuel space conductivity is a function of the temperature coordinate. The above two step analysis is carried out for a number of reference temperatures. In this manner, the effective conductivity as a function of temperature is established.

In Table 3.4.25, 10×10 array type BWR fuel assembly effective thermal conductivity results from a simplified analysis are presented to determine the most resistive fuel assembly in this class. Using the simplified analysis procedure discussed earlier, the Atrium-10 fuel type is determined to be the most resistive in this class of fuel assemblies. A detailed finite-element model of this assembly type was developed to rigorously quantify the heat dissipation characteristics. The results of this study are presented in Table 3.4.26 and compared to the bounding BWR fuel assembly effective thermal conductivity depicted in Figure 3.4.13. The results of this study demonstrate that the bounding BWR fuel assembly effective thermal conductivity is conservative with respect to the 10×10 class of BWR assemblies. Table 3.4.34 summarizes plant specific fuel types' effective conductivities. From these analytical results, the SPC-5 is determined to be the most resistive fuel assembly in this group of fuel types. A rigorous finite element model of SPC-5 fuel assembly was developed to confirm that its in-plane heat dissipation characteristics are bounded from below by the design basis BWR fuel conductivities used in the HI-STAR thermal analysis.

Temperature-dependent effective conductivities of PWR and BWR design basis fuel assemblies (most resistive SNF types) are shown in Figure 3.4.13. The finite-volume results are also compared to results reported from independent technical sources. From this comparison, it is readily apparent that FLUENT-based fuel assembly conductivities are conservative. The FLUENT computed values

(not the published literature data) are used in the MPC thermal analysis presented in this document.

3.4.1.1.3 Effective Thermal Conductivity of Sheathing/Neutron Absorber/Cell Wall Sandwich

Each MPC basket cell wall (except outer periphery MPC-68 & MPC-32 cell walls) is manufactured with a neutron absorbing plate for criticality control. Each neutron absorbing plate is sandwiched in a sheathing-to-basket wall pocket. A schematic of the "Box Wall-Neutron Absorber-Sheathing" sandwich geometry of an MPC basket is illustrated in Figure 3.4.5. During fabrication, a uniformly applied normal pressure on each sheathing-Neutron Absorber-cell wall sandwich prior to stitch welding of the sheathing periphery to the box wall ensures adequate surface-to-surface contact for elimination of any macroscopic gaps. The mean coefficient of linear expansion of neutron absorber is higher than the basket materials thermal expansion coefficients. Consequently, basket heat-up from the contained SNF will further ensure a tight fit of the neutron absorber plate in the sheathing-to-cell wall pocket. The presence of small microscopic gaps due to less than perfect surface finish characteristics requires consideration of an interfacial contact resistance between the neutron absorber and the box and sheathing surfaces. A conservative contact resistance resulting from a 2 mils neutron absorber-to-pocket gap is applied to the analysis. Note that this gap would actually be filled with helium. In other words, no credit is taken for the interfacial pressure between neutron absorber and stainless plate/sheet stock produced by the fixturing and welding process.

Heat conduction properties of a composite "Box Wall-Neutron Absorber-Sheathing" sandwich in the two principal basket cross sectional directions as illustrated in Figure 3.4.5 (i.e., lateral "out-of-plane" and longitudinal "in-plane") are unequal. In the lateral direction, heat is transported across layers of sheathing, helium-gap, neutron absorber, helium-gap, and cell wall resistances that are in series (except for the small helium filled end regions shown in Figure 3.4.6). Heat conduction in the longitudinal direction, in contrast, is through an array of essentially parallel resistances comprised of these same layers. For the ANSYS based MPC basket thermal model, corresponding non-isotropic effective thermal conductivities in the two orthogonal directions are determined and applied in the analysis.

The non-isotropic conductivities are determined by constructing ANSYS models of the composite "Box Wall-Neutron Absorber-Sheathing" sandwich for the "in-plane" and "out-of-plane" directions. For determining the effective conductivity (K_{eff}), a heat flux is applied to one end of the sandwich and an ANSYS numerical solution to the sandwich temperature differential obtained. From Fourier equation for one-dimensional conduction heat transfer, the following equation for K_{eff} is obtained:

$$K_{eff} = \frac{qL}{\Delta T}$$

where:

q = Sandwich heat flux
L = Sandwich length in the direction of heat transfer
ΔT = Sandwich temperature differential (obtained from ANSYS solution)

In the equation above, L is the width or thickness of the sandwich, respectively, for in-plane or out-

of-plane heat transfer directions.

3.4.1.1.4 Modeling of Basket Conductive Heat Transport

Conduction of heat in a fuel basket is a combination of planar and axial contributions. These component contributions are individually calculated for each MPC basket design and combined (as described later in this subsection) to obtain an equivalent isotropic thermal conductivity. The heat rejection capability of each MPC design (i.e., MPC-24, MPC-24E, MPC-32 and MPC-68) is evaluated by developing a thermal model of the combined fuel assemblies and composite basket walls geometry on the ANSYS finite element code. The ANSYS model includes a geometric layout of the basket structure in which the "Box Wall-Neutron Absorber-Sheathing" sandwich is replaced by a "homogeneous wall" with an equivalent thermal conductivity. Since the thermal conductivity of the Alloy X material is a weakly varying function of temperature, the equivalent "homogeneous wall" must have a temperature-dependent effective conductivity. Similarly, as illustrated in Figure 3.4.6, the conductivities in the in-plane and through-thickness direction of the equivalent "homogeneous wall" are different. Finally, as discussed earlier, the fuel assemblies occupying the basket cell openings are modeled as homogeneous heat generating regions with effective temperature dependent in-plane conductivities. The methodology used to reduce the heterogeneous MPC basket - fuel assemblage to an equivalent homogeneous region with effective thermal properties is discussed in the following.

Consider a cylinder of height L and radius r_o with a uniform volumetric heat source term q_g, with insulated top and bottom faces and its cylindrical boundary maintained at a uniform temperature T_c. The maximum centerline temperature (T_h) to boundary temperature difference is readily obtained from classical one-dimensional conduction relationships (for the case of a conducting region with constant thermal conductivity K_s):

$$(T_h - T_c) = q_g r_o^2/(4 K_s)$$

Noting that the total heat generated in the cylinder (Q_t) is $\pi r_o^2 L q_g$, the above temperature rise formula can be reduced to the following simplified form in terms of the total heat generation per unit length (Q_t/L):

$$(T_h - T_c) = (Q_t / L)/ (4 \pi K_s)$$

This simple analytical approach is employed to determine an effective basket cross-sectional conductivity by applying an equivalence between the ANSYS finite element model of the basket and the analytical case. The equivalence principle employed in the HI-STAR System thermal analysis is depicted in Figure 3.4.2. The 2-dimensional ANSYS finite element model of the MPC basket is solved by applying a uniform heat generation per unit length in each basket cell region and a constant basket periphery boundary temperature, T_c'. Noting that the basket region with uniformly distributed heat sources and a constant boundary temperature is equivalent to the analytical case of a cylinder with uniform volumetric heat source discussed earlier, an effective MPC basket conductivity (K_{eff}) is readily derived from the analytical formula and the ANSYS solution leading to the following relationship:

$$K_{eff} = N\,(Q_f'/L) / (4\,\pi\,[T_h' - T_c'])$$

where:

N = number of fuel assemblies

(Q_f'/L) = each fuel assembly heat generation per unit length applied in ANSYS model

T_h' = peak basket cross-section temperature from ANSYS model

Cross sectional views of MPC basket ANSYS models are illustrated in Figures 3.4.10 and 3.4.11 for a PWR and BWR MPC. Notice that many of the basket supports and all shims have been conservatively neglected in the models. This conservative geometry simplification, coupled with the conservative neglect of thermal expansion which would minimize the gaps, yields conservative gap thermal resistances. Temperature dependent equivalent thermal conductivities of the fuel region and composite basket walls, as determined from analysis procedures described earlier, are applied to the ANSYS model. The planar ANSYS conduction model is solved by applying a constant basket periphery temperature with uniform heat generation in the fuel region. Table 3.4.6 summarizes effective thermal conductivity results of each basket design obtained from the ANSYS models. It is recalled that the equivalent thermal conductivity values presented in Table 3.4.6 are lower bound values because, among other elements of conservatism, the effective conductivity of the most resistive SNF type (Tables 3.4.4 and 3.4.5) is used in the MPC finite-element simulations.

The axial conductivity of a fuel basket is determined by calculating a cross-sectional area-weighted sum of the component conductivities (Helium, Alloy-X, neutron absorber and fuel cladding). In accordance with NUREG-1536 guidelines, credit for fuel rod axial heat conduction is conservatively limited to cladding.

Having obtained planar and axial thermal conductivities as described above, an equivalent isotropic conductivity (defined as the Square Root of the Mean Sum of Squares (SRMSS[†])) is obtained as shown below:

$$k_{iso} = \sqrt{\frac{k_{rad}^{\ 2} + k_{ax}^{\ 2}}{2}}$$

where:

k_{iso} = equivalent isotropic thermal conductivity
k_{rad} = equivalent planar thermal conductivity
k_{ax} = equivalent axial thermal conductivity

The equivalent isotropic conductivities are employed in the HI-STAR thermal modeling as discussed in Subsection 3.4.2.

3.4.1.1.5 Heat Transfer in MPC Basket Peripheral Regions

† This formulation has been benchmarked for specific application to the MPC basket designs and confirmed to yield conservative results.

Each of the MPC designs for storing PWR or BWR fuel are provided with relatively large helium filled regions formed between the relatively cooler MPC shell and hot basket peripheral panels. For a horizontally oriented cask under normal transport conditions, heat transfer in these helium-filled regions is similar to heat transfer in closed cavities under three cases listed below:

i. differentially heated short vertical cavity

ii. horizontal channel heated from below

iii. horizontal channel heated from above

In a closed cavity (case i scenario), an exchange of hot and cold fluids occurs near the top and bottom ends of the cavity, resulting in a net transport of heat across the gap.

The case (ii) scenario is similar to the classical Rayleigh-Benard instability of a layer of fluid heated from below [3.4.6]. If the condition for onset of fluid motion is satisfied, then a multi-cellular natural convection pattern is formed. The flow pattern results in upward motion of heated fluid and downward motion of relatively cooler fluid from the top plate, resulting in a net transport of heat across the heated fluid channel.

The case (iii) is a special form of case (ii) with an inverted (stably stratified) temperature profile. No fluid motion is possible in this circumstance and heat transfer is thus limited to fluid (helium) conduction only.

The three possible cases of closed cavity natural convection are illustrated in Figure 3.4.3 for an MPC-68 basket geometry. Peripheral spaces labeled B and B' illustrate the case (i) scenario, the space labeled D illustrates the case (ii) scenario, and the space labeled D' illustrates the case (iii) scenario. The basket is oriented to conservatively maximize the number of peripheral spaces having *no* fluid motion. A small alteration in the basket orientation will result in a non-zero gravity component in the x-direction which will induce case (i) type fluid motion in the D' space. The rate of natural convection heat transfer is characterized by a Rayleigh number for the cavity defined as follows:

$$R_{a_L} = \frac{C_p \rho^2 g \beta \Delta T L^3}{\mu K}$$

where:

C_p = fluid heat capacity

ρ = average fluid density

g = acceleration due to gravity

β = coefficient of thermal expansion (equal to reciprocal of absolute temperature

for gases)

ΔT = temperature difference between hot and cold surfaces

L = spacing between hot and cold surfaces

μ = fluid viscosity

K = fluid conductivity

Hewitt et al. [3.4.5] report Nusselt number correlations for the closed cavity natural convection cases discussed earlier. A Nusselt number equal to unity implies heat transfer by fluid conduction only. A higher than unity Nusselt number is due to the so-called "Rayleigh" effect, which monotonically rises with increasing Rayleigh number. Nusselt numbers applicable to helium filled PWR and BWR MPCs in the peripheral voids are provided in Table 3.4.1. For conservatively maximizing HI-STAR normal transport temperatures, the heat dissipation enhancement due to Rayleigh effect is ignored.

3.4.1.1.6 Effective Conductivity of Multi-Layered Intermediate Shell Region

Fabrication of the layered overpack intermediate shells is discussed in Section 1.2 of this SAR. In the thermal analysis, each intermediate shell metal-to-metal interface presents an additional resistance to heat transport. The contact resistance arises from microscopic pockets of air trapped between surface irregularities of the contacting surfaces. Since air is a relatively poor conductor of heat, this results in a reduction in the ability to transport heat across the interface compared to that of the base metal. Interfacial contact conductance depends upon three principal factors, namely: (i) base material conductivity, (ii) interfacial contact pressure, and (iii) surface finish.

Rohsenow and Hartnett [3.2.2] have reported results from experimental studies of contact conductance across air entrapped stainless steel surfaces with a typical 100 μ-inch surface finish. A minimum contact conductance of 350 Btu/ft-hr-°F is determined from extrapolation of results to zero contact pressure.

The thermal conductivity of carbon steel is about three times that of stainless steel. Thus the choice of carbon steel as the base material in a multi-layered construction significantly improves heat transport across interfaces. The fabrication process guarantees interfacial contact. Contact conductance values extrapolated to zero contact pressures are therefore conservative. The surface finish of hot-rolled carbon steel plate stock is generally in the range of 250-1000 μ-inch [3.2.1]. The process of forming hot-rolled flat plate stock to cylindrical shapes to form the intermediate shells by rolling will result in a smoother surface finish. This results from the large surface pressures exerted by the hardened roller faces that flatten out any surface irregularities.

In the HI-STAR thermal analysis, a conservatively bounding interfacial contact conductance value is determined based on the following assumptions:

1. No credit is taken for high base metal conductivity.

2. No credit is taken for interfacial contact pressure.
3. No credit is taken for a smooth surface finish resulting from rolling of hot-rolled plate stock to cylindrical shapes.
4. Contact conductance is based on a uniform 2000 μ-inch (1000 μ-inch for each surface condition) interfacial air gap at all interfaces.
5. No credit for radiation heat exchange across this hypothetical inter-surface air gap.
6. Bounding low thermal conductivity at 200°F.

These assumptions guarantee a conservative assessment of heat dissipation characteristics of the multi-layered intermediate shell region. The resistances of the five carbon steel layers along with the associated interfacial resistances are combined as resistances in series to determine an effective conductivity of this region leading to the following relationship:

$$K_{gs} = r_o \ell n\left[\frac{r_5}{r_o}\right]\left[\sum_{i=1}^{5}\frac{\delta}{K_{air}}\frac{r_o}{r_i} + \frac{r_o \ell n\left[\frac{r_5}{r_o}\right]}{K_{cst}}\right]^{-1}$$

where (in conventional U.S. units):

K_{gs}	=	effective intermediate shell region thermal conductivity
r_o	=	inside radius of inner gamma shield layer
r_i	=	outer radius of ith intermediate shell layer
δ	=	interfacial air gap (2000 μ-inch)
K_{air}	=	air thermal conductivity
K_{cst}	=	carbon steel thermal conductivity

3.4.1.1.7 <u>Heat Rejection from Overpack and Impact Limiter Outside Surfaces</u>

Jakob and Hawkins [3.2.9] recommend the following correlations for natural convection heat transfer to air from heated vertical surfaces (flat impact limiter ends) and from single horizontal cylinders (overpack and impact limiter curved surfaces):

Turbulent range:

$$h = 0.19\,(\Delta T)^{1/3}\ (\text{Vertical}, GrPr > 10^9)$$

$$h = 0.18\,(\Delta T)^{1/3}\ (\text{Horizontal Cylinder}, GrPr > 10^9)$$

(in conventional U.S. units)

Laminar range:

$$h = 0.29\,(\frac{\Delta T}{L})^{1/4}\ (\text{Vertical}, GrPr < 10^9)$$

$$h = 0.27\,(\frac{\Delta T}{D})^{1/4}\ (\text{Horizontal Cylinder}, GrPr < 10^9)$$

(in conventional U.S. units)

where ΔT is the temperature differential between the system exterior surface and ambient air. During normal transport conditions, the surfaces to be cooled are the impact limiter and overpack cylindrical surfaces, and the flat vertical faces of the impact limiters. The corresponding length scales for these surfaces are the impact limiter diameter, overpack diameter, and impact limiter diameter, respectively. Noting that Gr×Pr is expressed as $L^3\Delta TZ$, where Z (from Table 3.2.7) is at least 2.6×10^5 at a conservatively high upper bound system exterior surface temperature of 340°F, it is apparent that the turbulent condition is always satisfied for ΔT in excess of a few degrees Fahrenheit. Under turbulent conditions, the more conservative heat transfer correlation for horizontal cylinders (i.e., $h = 0.18\ \Delta T^{1/3}$) is utilized for thermal analyses on all exposed system surfaces.

Including both convective and radiative heat loss from the system exterior surfaces, the following relationship for surface heat flux is developed:

$$q_s = 0.18\,(T_s - T_A)^{4/3} + \sigma \times \varepsilon \times [(T_s + 460)^4 - (T_A + 460)^4]$$

where:

T_s, T_A = surface, ambient temperatures (°F)
q_s = surface heat flux (Btu/ft^2-hr)
ε = surface emissivity (see Table 3.2.4)
σ = Stefan-Boltzman Constant (0.1714×10^{-8} Btu/ft^2-hr-°R^4)

3.4.1.1.8 Determination of Solar Heat Input

The intensity of solar radiation incident on an exposed surface depends on a number of time varying parameters. The solar heat flux strongly depends upon the time of the day as well as on latitude and day of the year. Also, the presence of clouds and other atmospheric conditions (dust, haze, etc.) can significantly attenuate solar intensity levels. Rapp [3.4.2] has discussed the influence of such factors in considerable detail.

The HI-STAR System thermal analysis is based upon insolation levels specified in 10CFR71, Subpart F, which are for a 12-hour daytime period. During normal transport conditions, the HI-STAR System is cyclically subjected to solar heating during the 12-hour daytime period followed by cooling during the 12-hour nighttime. However, due to the large mass of metal and the size of the system, the inherent dynamic time lag in the temperature response is substantially larger than the 24-hour heating-cooling time period. Accordingly, the HI-STAR System cask model includes insolation at exposed surfaces averaged over a 24-hour time period. A bounding solar absorption coefficient of 1.0 is applied to cask exterior surfaces. The 10CFR71 mandated 12-hour average incident solar radiation levels are summarized in Table 3.4.7. The combined incident insolation heat flux absorbed by exposed cask surfaces and decay heat load from the MPC is rejected by natural convection and radiation to ambient air.

3.4.1.1.9 Effective Thermal Conductivity of Radial Channels - Holtite Region

In order to minimize heat transfer resistance limitations due to the poor thermal conductivity of the

Holtite-A neutron shield material, a large number of thick radial channels formed from high strength and conductivity carbon steel material are embedded in the neutron shield region. These radial channels form highly conductive heat transfer paths for efficient heat removal. Each channel is welded to the outside surface of the outermost intermediate shell and at the overpack enclosure shell, thereby providing a continuous path for heat removal to the ambient environment.

The effective thermal conductivity of the composite neutron shielding and radial channels region is determined by combining the heat transfer resistance of individual components in a parallel network. In determining the heat transfer capability of this region to the outside ambient environment for normal transport conditions, no credit is taken for conduction through the neutron shielding material. Thus, heat transport from the outer intermediate shell surface to the overpack outer shell is conservatively based on heat transfer through the carbon steel radial channel legs alone. Thermal conductivity of the parallel neutron shield and radial channel leg region is given by the following formula:

$$K_{ne} = \frac{K_R\, N_R\, t_R \ln\left[\frac{r_B}{r_A}\right]}{2\pi L_R} + \frac{K_{ns}\, N_R\, t_{ns} \ln\left[\frac{r_B}{r_A}\right]}{2\pi L_R}$$

where (in consistent U.S. units):

K_{ne}	=	effective thermal conductivity of neutron shield region
r_A	=	inner radius of neutron shielding
r_B	=	outer radius of neutron shielding
K_R	=	effective thermal conductivity of carbon steel radial channel leg
N_R	=	total number of radial channel legs (also equal number of neutron shield sections)
t_R	=	minimum (nominal) thickness of each radial channel leg
L_R	=	effective radial heat transport length through radial channel leg
K_{ns}	=	neutron shield thermal conductivity
t_{ns}	=	neutron shield circumferential thickness (between two radial channel legs)

The radial channel leg to outer intermediate shell surface weld thickness is equal to half the plate thickness. The additional weld resistance is accounted for by reducing the plate thickness in the weld region for a short radial span equal to the weld size. Conductivity of the radial carbon steel channel legs based on the full thickness for the entire radial span is correspondingly reduced. Figure 3.4.4 depicts a resistance network developed to combine the neutron shield and radial channel legs resistances to determine an effective conductivity of the neutron shield region. Note that in the resistance network analogy only the annulus region between overpack outer enclosure inner surface and intermediate shells outer surface is considered in this analysis. The effective thermal conductivity of neutron shield region is provided in Table 3.4.8.

3.4.1.1.10 Effective Thermal Conductivity of the Eccentric MPC to Overpack Gap

During horizontal shipment of the HI-STAR System under normal transport conditions, the MPC will rest on the inside surface of the overpack. In the region of line contact, the resistance to heat

transfer across the gap will be negligibly small due to a vanishingly small gap thickness. The resistance to heat transfer at other regions along the periphery of the MPC will, however, increase in direct proportion to the thickness of the local gap. This variation in gap thickness can be accounted for in the thermal model by developing a relation for the total heat transferred across the gap as given below:

$$Q_E = 2\int_0^{\pi} \frac{K_{He}}{g(\theta)} L\, R_o\, \Delta T\, d\theta$$

where:

Q_E	=	total heat transfer across the gap (Btu/hr)
K_{He}	=	helium conductivity Btu/ft-hr-°F
L	=	length of MPC (ft.)
R_o	=	MPC radius (ft.)
θ	=	angle from point of line contact
g(θ)	=	variation of gap thickness with angle (ft.)
ΔT	=	temperature difference across the gap (°F)

A corresponding relationship for heat transferred across a uniform gap is given by:

$$Q_c = \frac{K_{eff}}{(R_1 - R_0)} 2\pi\, R_0\, L\, \Delta T$$

where R_1 is the inside radius of the overpack and K_{eff} is the effective thermal conductivity of an equivalent concentric MPC/overpack gap configuration. From these two relationships, the ratio of effective gap conductivity to helium thermal conductivity in the MPC/overpack region is shown below:

$$\frac{K_{eff}}{K_{He}} = \frac{R_1 - R_0}{\pi} \int_0^{\pi} \frac{1}{g(\theta)} d\theta$$

Based on an analysis of the geometry of a thin gap between two eccentrically positioned cylinders, the following relationship is developed for variation of the gap thickness with position:

$$g(\theta) = (R_1 - R_0)(1 - \cos\theta) + \varepsilon \cos\theta$$

The above equation conservatively accounts for imperfect contact by postulating a minimum gap ε at the point where the two surfaces would ideally form a line of perfect contact. The relatively thin MPC shell is far more flexible than the much thicker overpack inner shell, and will ovalize to yield greater than line contact. The substantial weight of the fuel basket and contained fuel assemblies will also cause the MPC shell to conform to the overpack inner shell. An evaluation based on contact along a line would therefore be reasonable and conservative. However, a minimum gap is assumed to further increase conservatism in this calculation.

Based on an applied gap of 0.02-inch, which is conservative compared to contact along a line, the effective gap thermal conductivity determined from analytical integration [3.4.7] is in excess of

200% of the conductivity of helium gas. In the HI-STAR analysis, a conservative effective gap conductivity equal to twice the helium gas conductivity is applied to the performance evaluation.

3.4.1.1.11 Effective Thermal Conductivity of MPC Basket-to-Shell Aluminum Heat Conduction Elements

The HI-STAR MPCs feature an option to install full-length heat conduction elements fabricated from aluminum alloy 1100 in the large MPC basket-to-shell gaps. Due to the high aluminum alloy 1100 thermal conductivity (about 15 times that of Alloy X), a significant rate of net heat transfer is possible along the thin plates. For conservatism, heat dissipation by the Aluminum Heat Conduction Elements (AHCEs) is ignored in normal transport analyses. This overstates the initial fuel temperature for hypothetical fire accident evaluation. To conservatively compute heating of MPC contents in a hypothetical fire condition, the presence of heat conduction elements in AHCE equipped MPCs is duly recognized.

Figure 3.4.12 shows a mathematical idealization of a heat conduction element inserted between basket periphery panels and the MPC shell. The aluminum insert is shown to cover the MPC basket Alloy X peripheral panel and MPC shell surfaces (Regions I and III depicted in Figure 3.4.12) along the full-length of the basket. Heat transport to and from the aluminum insert is conservatively postulated to occur across a thin helium gap as shown in the figure (i.e., no credit is considered for aluminum insert to Alloy X metal-to-metal contact). Aluminum surfaces inside the hollow region are sandblasted prior to fabrication to result in a rough surface finish which has a significantly higher emissivity compared to smooth surfaces of rolled aluminum. The untreated aluminum surfaces directly facing Alloy X panels have a smooth finish to minimize contact resistance.

Net heat transfer resistance from the hot basket periphery panel to the relatively cooler MPC shell along the aluminum heat conduction element pathway is a sum of three individual resistances in regions labeled I, II, and III. In Region I, heat is transported from the basket to the aluminum insert surface directly facing the basket panel across a thin helium resistance gap. Longitudinal transport of heat (in the z direction) in the aluminum plate (in Region I) will result in an axially non-uniform temperature distribution. Longitudinal one-dimensional heat transfer in the Region I aluminum plate is analytically formulated to result in the following ordinary differential equation for the non-uniform temperature distribution:

$$t\,K_{Al}\frac{\partial^2 T}{\partial z^2} = -\frac{K_{He}}{h}(T_h - T) \qquad \text{(Equation a)}$$

Boundary Conditions

$$\frac{\partial T}{\partial z} = 0 \text{ at } z = 0$$
$$T = T_h' \text{ at } z = P \qquad \text{(Equation b)}$$

where (see Figure 3.4.12):

$T(z)$	=	non-uniform aluminum metal temperature distribution
t	=	conduction element thickness
K_{Al}	=	conduction element conductivity
K_{He}	=	helium conductivity
h	=	helium gap thickness
T_h	=	hot basket temperature
T_h'	=	conduction element Region I boundary temperature at z = P
P	=	conduction element Region I length

Solution of this ordinary differential equation subject to the imposed boundary condition is:

$$(T_h - T) = (T_h - T_h')\left[\frac{e^{\frac{z}{\sqrt{\alpha}}} + e^{-\frac{z}{\sqrt{\alpha}}}}{e^{\frac{P}{\sqrt{\alpha}}} + e^{-\frac{P}{\sqrt{\alpha}}}}\right] \qquad \text{(Equation c)}$$

where α is a dimensional parameter equal to htK_{Al}/K_{He}. The net heat transfer (Q_I) across the Region I helium gap can be determined by the following integrated heat flux to a conduction element of length L as:

$$Q_I = \int_0^P \frac{K_{He}}{h}(T_h - T)(L)\,dz \qquad \text{(Equation d)}$$

Substituting the analytical temperature distribution result obtained in Equation c into Equation d and then integrating, the following expression for net heat transfer is obtained:

$$Q_I = \frac{K_{He} L \sqrt{\alpha}}{h}\left(1 - \frac{1}{e^{\frac{P}{\sqrt{\alpha}}} + e^{-\frac{P}{\sqrt{\alpha}}}}\right)(T_h - T_h') \qquad \text{(Equation e)}$$

Based on this result, an expression for Region I resistance is obtained as shown below:

$$R_I = \frac{T_h - T_{h'}}{Q_I} = \frac{h}{K_{He} L \sqrt{\alpha}}\left(1 - \frac{1}{e^{\frac{P}{\sqrt{\alpha}}} + e^{-\frac{P}{\sqrt{\alpha}}}}\right)^{-1} \qquad \text{(Equation f)}$$

Similarly, a Region III resistance expression can be analytically determined as shown below:

$$R_{III} = \frac{(T_c' - T_c)}{Q_{III}} = \frac{h}{K_{He} L \sqrt{\alpha}} \left(1 - \frac{1}{e^{\frac{P}{\sqrt{\alpha}}} + e^{-\frac{P}{\sqrt{\alpha}}}} \right)^{-1} \qquad \text{(Equation g)}$$

A Region II resistance expression can be developed from the following net heat transfer equation in the vertical leg of the conduction element as shown below:

$$Q_{II} = \frac{K_{Al} L t}{W} (T_h' - T_c') \qquad \text{(Equation h)}$$

Hence,

$$R_{II} = \frac{T_h' - T_c'}{Q_{II}} = \frac{W}{K_{Al} L t} \qquad \text{(Equation i)}$$

This completes the analysis for the total thermal resistance attributable to the heat conduction elements equal to sum of the three individual resistances. The total resistance is smeared across the basket-to-MPC shell region as an effective uniform annular gap conductivity (see Figure 3.4.2). Note that heat transport along the conduction elements is an independent conduction path in parallel with conduction and radiation mechanisms in the large helium gaps. Helium conduction and radiation between the MPC basket and the MPC shell is accounted for separately in the ANSYS MPC models described earlier in this section. Therefore, the total MPC basket-to-MPC shell peripheral gaps conductivity will be the sum of the conduction elements effective conductivity and the helium conduction-radiation gap effective conductivity.

3.4.1.1.12 FLUENT Model for HI-STAR Temperature Field Computation

In the preceding subsections, the series of analytical and numerical models to define the thermal characteristics of the various elements of the HI-STAR System are presented. The thermal modeling begins with the replacement of the SNF cross section and surrounding fuel cell space by a solid lamina with an equivalent conductivity. Since radiation is an important constituent of the heat transfer process in the SNF/storage cell space and the rate of radiation heat transfer is a strong function of the surface temperatures, it is necessary to treat the equivalent lamina conductivity as a function of temperature. In fact, because of the relatively large range of temperatures which will exist in a loaded HI-STAR System under the design basis heat loads, it is necessary to include the effect of variation in the thermal conductivity of materials with temperature throughout the system finite volume model. The presence of significant radiation effect in the storage cell spaces adds to the imperative to treat the equivalent lamina conductivity as temperature-dependent.

FLUENT finite volume simulations have been performed to establish the equivalent thermal conductivity as a function of temperature for the limiting (thermally most resistive) BWR and PWR spent fuel types. By utilizing the most limiting SNF (established through a simplified analytical process for comparing conductivities) the numerical idealization for the fuel space conductivity is ensured to be conservative for all non-limiting fuel types.

Having replaced the interior of the cell spaces by solid prismatic (square) columns possessing a temperature-dependent conductivity essentially renders the basket into a non-homogeneous three-dimensional solid where the non-homogeneity is introduced by the honeycomb basket structure. The basket panels themselves are a composite of Alloy X cell wall, neutron absorber, and Alloy X sheathing metal. A conservative approach to replace this composite section with an equivalent "solid wall" is described in a preceding subsection.

In the next step, a planar section of the MPC is considered. The MPC, externally radially symmetric, contains a non-symmetric basket lamina wherein the equivalent fuel space solid squares are separated by the "equivalent" solid metal walls. The space between the basket and the MPC, called the peripheral gap, is filled with helium gas and optionally aluminum heat conduction elements. The equivalent thermal conductivity of this MPC section is computed using a finite element procedure on ANSYS, as described previously. For hypothetical fire conditions the "helium-conduction-radiation" based peripheral gap conductivity and the effective conductivity of aluminum conduction elements are added to obtain a combined effective conductivity. At this stage in the thermal analysis, the SNF/basket/MPC assemblage has been replaced with a two-zone (Figure 3.4.2) cylindrical solid whose thermal conductivity is a strong function of temperature.

The idealization for the overpack is considerably more straightforward. The overpack is radially symmetric except for the Holtite region (discussed in Subsection 3.4.1.1.9). The procedure to replace the multiple shell layers, Holtite-A and radial connectors with an equivalent solid utilizes classical heat conduction analogies, as described in the preceding subsections.

In the final step of the analysis, the equivalent two-zone MPC cylinder, the equivalent overpack shell, the top and bottom plates, and the impact limiters are assembled into a comprehensive finite volume model. A cross section of this axisymmetric model implemented on FLUENT is shown in Figure 3.4.14. A summary of the essential features of this model is presented in the following:

- The overpack shell is represented by 840×9 elements. The effective thermal conductivity of the overpack shell elements is set down as a function of temperature based on the analyses described earlier.

- The overpack bottom plate and bolted closure plate are modeled by 312×9 axisymmetric elements.

- The two-zone MPC "solid" is represented by 1,144×9 axisymmetric elements.

- The space between the MPC "solid" and the overpack interior space is assumed to contain helium.

- Heat input due to insolation is applied to the impact limiter surfaces and the cylindrical surface of the overpack.

- The heat generation in the MPC solid basket region is assumed to be uniform in each horizontal plane, but to vary in the axial direction to correspond to the axial burnup distribution in the active fuel region postulated in Chapter 1.

The finite volume model constructed in this manner will produce an axisymmetric temperature distribution. The peak temperature will occur near the centerline and is expected to correspond to the axial location of peak heat generation. As is shown later, the results from the finite element solution bear out these observations.

3.4.1.1.13 Effect of Fuel Cladding Crud Resistance

In this subsection, a conservatively bounding estimate of the temperature drop across a crud film adhering to a fuel rod during dry storage conditions is determined. The evaluation is performed for a BWR fuel assembly based on an upper bound crud thickness obtained from PNL-4835 report ([3.3.5], Table 3). The crud present on fuel assemblies is predominantly iron oxide mixed, with small quantities of other metals such as cobalt, nickel, chromium, etc. Consequently, the effective conductivity of the crud mixture is expected to be in the range of typical metal alloys. Metals have thermal conductivities several orders of magnitude larger than that of helium. In the interest of extreme conservatism, however, a film of helium with the same thickness replaces the crud layer. The calculation is performed in two steps. In the first step, a crud film resistance is determined based on bounding maximum crud layer thickness replaced as a helium film on the fuel rod surfaces. This is followed by a peak local cladding heat flux calculation for the smaller GE 7×7 fuel assembly postulated to emit a conservatively bounding decay heat equal to 0.5kW. The temperature drop across the crud film obtained as a product of the heat flux and crud resistance terms is determined to be less than 0.1°F. The calculations are presented below:

Bounding Crud Thickness (δ)= (PNL-4835)		130μm (4.26×10^{-4} ft)
Crud Conductivity (K)	=	0.1 Btu/ft-hr-°F (conservatively assumed as helium)

GE 7×7 Fuel Assembly:

Rod O.D.	=	0.563"
Active Fuel Length	=	150"
Heat Transfer Area	=	$(7\times7)\ (\pi \times 0.563) \times 150/144$
	=	90.3 ft^2
Axial Peaking Factor	=	1.195 (Burnup distribution Table 1.2.15)
Decay Heat	=	500W (conservative assumption)

$$\text{Crud Resistance} = \frac{\delta}{K} = \frac{4.26\times10^{-4}}{0.1} = 4.26\times10^{-3}\,\frac{\text{ft}^2\text{-hr-}^\circ\text{F}}{\text{Btu}}$$

$$\text{Peak Heat Flux} = \frac{(500\times3.417)\ \text{Btu/hr}}{90.3\ \text{ft}^2}\times1.195$$

$$= 18.92\times1.195 = 22.6\,\frac{\text{Btu}}{\text{ft}^2\text{-hr}}$$

Temperature drop (ΔT_c) across crud film:

$$= 4.26\times10^{-3}\,\frac{\text{ft}^2\text{-hr-}^\circ\text{F}}{\text{Btu}}\times22.6\,\frac{\text{Btu}}{\text{ft}^2\text{-hr}}$$

$$= 0.096^\circ\text{F}$$

$$(\text{i.e., less than } 0.1^\circ\text{F})$$

Therefore, it is concluded that deposition of crud does not materially change the SNF cladding temperature.

3.4.1.1.14 Maximum Time Limit During Wet Transfer

While loading an empty HI-STAR System for transport directly from a spent fuel pool, water inside the MPC cavity is not permitted to boil. Consequently, uncontrolled pressures in the de-watering, purging, and recharging system that may result from two-phase condition are completely avoided. This requirement is accomplished by imposing a limit on the maximum allowable time duration for fuel to be submerged in water after a loaded HI-STAR cask is removed from the pool and prior to the start of vacuum drying operations.

When the HI-STAR overpack and the loaded MPC under water-flooded conditions are removed from the pool, the combined mass of the water, the fuel, the MPC, and the overpack will absorb the decay heat emitted by the fuel assemblies. This results in a slow temperature rise of the entire system with time, starting from an initial temperature of the contents. The rate of temperature rise is limited by the thermal inertia of the HI-STAR system. To enable a bounding heat-up rate determination for the HI-STAR system, the following conservative assumptions are imposed:

i. Heat loss by natural convection and radiation from the exposed HI-STAR surfaces to the pool building ambient air is neglected (i.e., an adiabatic temperature rise calculation is performed).

ii. Design Basis maximum decay heat input from the loaded fuel assemblies is imposed on the HI-STAR system.

iii. The smallest of the *minimum* MPC cavity-free volumes between the two MPC types is considered for flooded water mass determination.

iv. Fifty percent of the water mass in the MPC cavity is credited towards water thermal inertia evaluation.

Table 3.4.19 summarizes the weights and thermal inertias of several components in the loaded HI-STAR system. The rate of temperature rise of the HI-STAR and its contents during an adiabatic heat-up is governed by the following equation:

$$\frac{dT}{d\tau} = \frac{Q}{C_h}$$

where:

Q = decay heat load (Btu/hr) [equal to Design Basis maximum (between the two MPC types) 20.0 kW (i.e., 68,260 Btu/hr)]

C_h = combined thermal inertia of the loaded HI-STAR system (Btu/°F)

T = temperature of the contents (°F)

τ = time after HI-STAR system is removed from the pool (hr)

A bounding heat-up rate for the HI-STAR system contents is determined to be equal to 2.19°F/hr. From this adiabatic rate of temperature rise estimate, the maximum allowable time duration (t_{max}) for fuel to be submerged in water is determined as follows:

$$t_{\max} = \frac{T_{boil} - T_{initial}}{dT/d\tau}$$

where:

T_{boil} = boiling temperature of water (equal to 212°F at the water surface in the MPC cavity)

$T_{initial}$ =initial temperature of the HI-STAR contents when removed from the pool

Table 3.4.20 provides a summary of t_{max} at several initial HI-STAR contents temperatures.

As set forth in Section 7.4, in the unlikely event where the maximum allowable time provided in Table 3.4.20 is found to be insufficient to complete all wet transfer operations, a forced water circulation shall be initiated and maintained to remove the decay heat from the MPC cavity. In this case, relatively cooler water will enter via the MPC lid drain port connection and heated water will exit from the vent port. The minimum water flow rate required to maintain the MPC cavity water temperature below boiling with an adequate subcooling margin is determined as follows:

$$M_W = \frac{Q}{C_{pw}(T_{\max} - T_{in})}$$

where:

M_W = minimum water flow rate (lb/hr)

C_{pw} = water heat capacity (Btu/lb-°F)

T_{max} = maximum MPC cavity water mass temperature

T_{in} = temperature of water supply to MPC

With the MPC cavity water temperature limited to 150°F, MPC inlet water maximum temperature equal to 125°F and at the design basis maximum heat load, the water flow rate is determined to be 2,731 lb/hr (5.5 gpm).

3.4.1.1.15 Cask Cooldown and Reflood Analysis During Fuel Unloading Operation

Before a loaded HI-STAR System can be unloaded (i.e., fuel removed from the MPC) the cask must be cooled from the operating temperatures and reflooded with water[†]. Past industry experience generally supports cooldown of cask internals and fuel from hot storage conditions by direct water quenching. However, the extremely rapid cooldown rates that are typical during water injection, to which the hot cask internals and fuel cladding are subjected to, may result in uncontrolled thermal stresses and failure in the structural members. Moreover, water injection results in large amounts of steam generation and unpredictable transient two-phase flow conditions inside the MPC cavity, which may result in over-pressurization of the MPC helium retention boundary and a potentially unacceptable reduction in the safety margins to prevent criticality. To avoid potential safety concerns related to rapid cask cooldown by direct water quenching, the HI-STAR MPCs are designed to be cooled in a gradual manner, thereby eliminating thermal shock loads on the cask internals and fuel cladding.

In the unlikely event that a HI-STAR system is required to be unloaded, it will be transported back to the fuel handling building. Prior to reflooding the MPC cavity with water, a forced flow helium recirculation system with adequate flow capacity shall be operated to remove the decay heat and initiate a slow cask cooldown lasting for several days. The operating procedures in Section 7.2 provide a detailed description of the steps involved in the cask unloading. In this section, an analytical evaluation is presented to provide the basis for helium flow rates and time of forced cooling to meet the objective of eliminating thermal shock when the MPC cavity is eventually flooded with water.

Under a closed loop forced helium circulation condition, the helium gas is cooled via an external chiller, down to 100°F, and then introduced inside the MPC cavity from the drain line near the bottom baseplate. The helium gas enters the MPC basket from the bottom oversized flow holes and moves upward through the hot fuel assemblies, removing heat and cooling the MPC internals. The heated helium gas exits from the basket top and collects in the top plenum, from where it is expelled through the MPC lid vent connection to the helium recirculation and cooling system. The bulk

† Certain fuel configurations in PWR MPCs require Borated water for criticality control (Chapter 6). Such MPCs are reflooded with Borated water.

average temperature reduction of the MPC contents as a function of time is principally dependent upon the rate of helium circulation. The temperature transient is governed by the following heat balance equation:

$$C_h \frac{dT}{d\tau} = Q_D - m C_p (T - T_i) - Q_c$$

Initial Condition: $T = T_o$ at $\tau = 0$

where:

T = MPC bulk average temperature (°F)

T_o = initial MPC bulk average temperature in the HI-STAR system (483°F†)

τ = time after start of forced circulation (hr)

Q_D = decay heat load (Btu/hr) (equal to Design Basis maximum 20.0 kW (i.e., 68,260 Btu/hr))

m = helium circulation rate (lb/hr)

C_p = helium heat capacity (Btu/lb-°F) (equal to 1.24 Btu/lb-°F)

Q_c = heat rejection from cask exposed surfaces to ambient (Btu/hr) (conservatively neglected)

C_h = thermal capacity of the loaded MPC (Btu/°F) (For a bounding upper bound 100,000 lb loaded MPC weight, and heat capacity of Alloy X equal to 0.12 Btu/lb-°F, the heat capacity is equal to 12,000 Btu/°F)

T_i = MPC helium inlet temperature (°F)

The differential equation is analytically solved, yielding the following expression for time-dependent MPC bulk temperature:

$$T(t) = (T_i + \frac{Q_D}{m C_p})(1 - e^{-\frac{m C_p}{C_h} t}) + T_o e^{-\frac{m C_p}{C_h} t}$$

This equation is used to determine the minimum helium mass flow rate that would cool the MPC cavity down from initially hot conditions to less than 200°F. For example, to cool the MPC to less

† Bounding for HI-STAR normal transport.

than 200°F in 72 hours would required a helium mass flow rate of 574 lb/hr (i.e., 859 SCFM).

Once the helium gas circulation has cooled the MPC internals to less than 200°F, water can be injected to the MPC without risk of boiling and the associated thermal stress concerns. Because of the relatively long cooldown period, the thermal stress contribution to the total cladding stress would be negligible, and the total stress would therefore be bounded by the normal (dry) condition. The elimination of boiling eliminates any concern of over-pressurization due to steam production.

3.4.1.1.16 MPC Evaluation Under Drying Conditions

The initial loading of SNF in the MPC requires that the water within the MPC be drained, residual moisture removed and MPC filled with helium. This operation on the HI-STAR MPCs will be carried out using a Forced Helium Dehydrator (FHD) for a "load-and-go" operation. A "load-and-go" operation is defined as an activity wherein an MPC is loaded for direct off-site shipment in a HI-STAR transport cask. MPCs prepared via other competent methods for MPC drying as approved by the NRC on other dockets (1008 and 1014) are duly recognized for transport under this docket.

To reduce moisture to trace levels in the MPC using a Forced Helium Dehydration (FHD) system, a closed loop system consisting of a condenser, a demoisturizer, a compressor, and a pre-heater is utilized to extract moisture from the MPC cavity through repeated displacement of its contained helium, accompanied by vigorous flow turbulation. Appendix 3.B contains detailed discussion of the design and operation criteria for the FHD system.

The FHD system provides concurrent fuel cooling during the moisture removal process through forced convective heat transfer. The attendant forced convection-aided heat transfer occurring during operation of the FHD system ensures that the fuel cladding temperature will remain below the applicable peak cladding temperature limit for normal conditions of transport (752°F) for all combinations of SNF type, burnup, decay heat, and cooling time. Because the FHD operation induces a state of forced convection heat transfer in the MPC, (in contrast to the quiescent mode of natural convection in transport), it is readily concluded that the peak fuel cladding temperature under the latter condition will be greater than that during the FHD operation phase. In the event that the FHD system malfunctions, the forced convection state will degenerate to natural convection, which corresponds to the conditions of normal transport. As a result, the peak fuel cladding temperatures will approximate the values reached during normal transport as described elsewhere in this chapter.

3.4.1.1.17 Effects of Helium Dilution from Fuel Rod Gases

In this subsection, the generic cask transportation accident issue raised in a USNRC Spent Fuel Project Office (SFPO) staff guidance letter† is addressed. This issue directs cask designers to evaluate the impact of fission gas release into the canister, from a 100% fuel rods rupture accident, on the cask component temperatures and pressures when the MNOP†† is within 10% of the design

† SFPO Director's Interim Staff Guidance Letter(s), W.F. Kane, (Interim Staff-Guidance-7), October 8, 1998.

†† MNOP is a regulatory term defined in NUREG-1617 as the maximum gauge pressure that would

pressure. To determine whether the HI-STAR System falls within the stipulated criteria, the MNOP results from Table 3.4.15 are provided below:

Canister	MNOP (psig)	Threshold Criteria††† for Accident Evaluation (psig)
MPC-24	88.8	90
MPC-68	86.9	90
MPC-24E	88.9	90
MPC-32	89.3	90

As shown above the MNOPs are below the threshold and an accident evaluation is not required. Nevertheless, for illustrative purposes, a 100% rods rupture accident for a HI-STAR package with an MPC-24 canister is evaluated.

Under a severe hypothetical accident scenario 100% of the fuel rods may rupture, releasing the rod fill gas (helium) and a portion of the gaseous fission products (^{3}H, ^{85}Kr, ^{129}I and ^{131}Xe). The gaseous fission products release fractions are stipulated in NUREG-1536. The released gases will mix with the MPC backfill gas and reduce its thermal conductivity. This reduction in conductivity will result in a small increase in MPC temperatures and pressures.

Appendix C of NUREG/CR-0497 [3.4.13] describes a method for calculating the effective thermal conductivity of a mixture of gases. The same method is also described by Rohsenow and Hartnett [3.2.2]. The following expression is provided by both references:

$$k_{mix} = \sum_{i=1}^{n} \left(\frac{k_i x_i}{x_i + \sum_{\substack{j=1 \\ j \neq i}}^{n} \varphi_{ij} x_j} \right)$$

where:

k_{mix} = thermal conductivity of the gas mixture (Btu/hr-ft-°F)
n = number of gases
k_i = thermal conductivity of gas component i (Btu/hr-ft-°F)
x_i = mole fraction of gas component i

In the preceding equation, the term φ_{ij} is given by the following:

develop in the containment in a period of 1 year under the heat condition specified in 10 CFR 71.71(c)(1) in the absence of venting, external ancillary cooling or operational controls.

††† Accident evaluation required when MNOP is within 10% of the design pressure. This translates to a pressure that is between 100 psig (HI-STAR design pressure (Table 2.1.1)) and 90 psig.

$$\varphi_{ij} = \phi_{ij}\left[1 + 2.41\frac{(M_i - M_j)(M_i - 0.142 \cdot M_j)}{(M_i + M_j)^2}\right]$$

where M_i and M_j are the molecular weights of gas components i and j, and ϕ_{ij} is:

$$\phi_{ij} = \frac{\left[1 + \left(\frac{k_i}{k_j}\right)^{\frac{1}{2}}\left(\frac{M_i}{M_j}\right)^{\frac{1}{4}}\right]^2}{2^{\frac{3}{2}}\left(1 + \frac{M_i}{M_j}\right)^{\frac{1}{2}}}$$

Table 3.4.30 presents a summary of the gas mixture thermal conductivity calculations for MPC-24 containing design basis PWR fuel assemblies.

Having calculated the gas mixture thermal conductivity, the effective thermal conductivity of the design basis PWR fuel assembly is calculated using the finite-volume model described in Subsection 3.4.1.1.2. Only the helium gas conductivity is changed, all other modeling assumptions are the same. The fuel assembly effective thermal conductivity with diluted helium is compared to that with undiluted helium in Table 3.4.31.

Next, the effective thermal conductivities of the MPC fuel basket and basket periphery regions are determined as described in Subsections 3.4.1.1.3 and 3.4.1.1.4. This calculation incorporates both the diluted helium thermal conductivity and the effective thermal conductivity of the fuel assembly with diluted helium. In the evaluation of helium dilution by high molecular weight gases (fission gas releases from hypothetical rupture of fuel rods) the increase in convection heat transfer in the basket peripheral spaces due to a substantial rise in gas density is recognized. The effective thermal conductivities with diluted helium are compared to those with undiluted helium in Table 3.4.31.

The MPC fuel basket effective thermal conductivities are input to a finite-volume model of the HI-STAR System arranged for transport. The cask system temperature distribution with diluted MPC helium is determined using the finite-volume model, as described in Subsection 3.4.1.1.12. Design basis normal environmental conditions are applied to the model and a temperature field solution obtained. Cask system temperatures with diluted MPC helium are summarized in Table 3.4.32.

The slightly higher MPC cavity temperature with MPC helium dilution will result in a small perturbation in MPC internal pressure. Based on the temperature field obtained with helium dilution, the MPC internal pressure is determined using the Ideal Gas Law. The calculated MPC internal pressure with helium dilution is presented in Table 3.4.33.

The results of analyses presented in this subsection are performed to illustrate the effect of a hypothetical 100% rods rupture on a HI-STAR package with an MPC-24. Even under the extreme postulated conditions, the MPC component temperatures and pressures remain substantially below

the design limits.

3.4.1.1.18 HI-STAR Temperature Field With Low Heat Emitting Fuel

The HI-STAR 100 thermal evaluations for BWR fuel are divided in two groups of fuel assemblies proposed for storage in MPC-68. These groups are classified as Low Heat Emitting (LHE) fuel assemblies and Design Basis (DB) fuel assemblies. The LHE group of fuel assemblies are characterized by low burnup, long cooling time, and short active fuel lengths. Consequently, their heat loads are dwarfed by the DB group of fuel assemblies. The Dresden-1 (6x6 and 8x8), QUAD+, and Humboldt Bay (7x7 and 6x6) fuel characteristics warrant their classification as LHE fuel. These characteristics, including burnup and cooling time limits imposed on this class of fuel, are presented in Table 1.2.23. This fuel (except Quad+) is permitted to be loaded when encased in Damaged Fuel Containers (DFCs). As a result of interruption of radiation heat exchange between the fuel assembly and the fuel basket by the DFC boundary, this loading configuration is bounding for thermal evaluation. In Subsection 3.4.1.1.2, two canister designs for encasing LHE fuel are evaluated – a previously approved Holtec Design (Figure 1.2.10) and an existing canister in which some of the Dresden-1 fuel is currently stored (Transnuclear D-1 Canister). The most resistive fuel assembly determined by analytical evaluation is considered for thermal evaluation (see Table 3.4.5). The MPC-68 basket effective conductivity, loaded with the most resistive fuel assembly from the LHE group of fuel (encased in a canister) is provided in Table 3.4.6. To this basket, LHE fuel decay heat load, is applied and a HI-STAR 100 System temperature field obtained. The low heat load burden limits the initial peak cladding temperature to less than 579°F which is substantially below the cladding temperature limit (Table 3.3.1).

A thoria rod canister designed to hold a maximum of 20 fuel rods arrayed in a 5x4 configuration is currently stored at the Dresden-1 spent fuel pool. The fuel rods contain a mixture of enriched UO_2 and Thorium Oxide in the fuel pellets. The fuel rods were originally constituted as part of an 8x8 fuel assembly and used in the second and third cycle of Dresden-1 operation. The maximum fuel burnup of these rods is quite low (~13,100 MWD/MTU). The thoria rod canister internal design is a honeycomb structure formed from 12 gage stainless steel plates. The rods are loaded in individual square cells and are isolated from each other by the cell walls. The few number of rods (18 per assembly) and very low burnup of fuel stored in these Dresden-1 canisters render them as miniscule sources of decay heat. The canister all-metal internal honeycomb construction serves as an additional means of heat dissipation in the fuel cell space. In accordance with preferential fuel loading requirements, low burnup fuel shall be loaded toward the basket periphery (i.e., away from the hot central core of the fuel basket). All these considerations provide ample assurance that these fuel rods will be stored in a benign thermal environment and therefore remain protected during transport.

3.4.1.2 Test Model

A detailed analytical model for evaluating the thermal design of the HI-STAR System was developed using the FLUENT CFD code and the industry standard ANSYS modeling system as discussed in Subsection 3.4.1.1. Furthermore, the analysis incorporates many conservative assumptions in order to demonstrate compliance with specified temperature limits for operation with adequate margins. In view of these considerations, the HI-STAR thermal design complies with the

thermal criteria set forth in the design basis for normal transport conditions. Additional experimental verification of the thermal design is therefore not required. Acceptance and periodic thermal testing for the HI-STAR System is discussed in Sections 8.1 and 8.2.

3.4.2 Maximum Temperatures Under Normal Transport Conditions

Both MPC-basket designs developed for the HI-STAR System have been analyzed to determine temperature distributions under normal transport conditions. In the HI-STAR System thermal analysis models developed on FLUENT, the overpack impact limiters are included in the finite volume geometry. However, no credit is considered for the presence of heat conducting aluminum honeycomb material. In other words, heat transmission through the ends is conservatively neglected in the analysis. The thermal results are therefore bounding with respect to impact limiter design. The MPC baskets are considered to be loaded at design-basis maximum heat load with PWR or BWR fuel assemblies, as appropriate.

As discussed in Subsection 3.4.1.1.1, the thermal analysis is performed using a submodeling process where the results of an analysis on an individual component are incorporated into the analysis of a larger set of components. Specifically, the submodeling process yields directly computed fuel temperatures from which fuel basket temperatures are indirectly calculated. This modeling process differs from previous analytical approaches wherein the basket temperatures were evaluated first and then a basket-to-cladding temperature difference calculation by Wooten-Epstein or other means provided a basis for cladding temperatures. Subsection 3.4.1.1.2 describes the calculation of an effective fuel assembly thermal conductivity for an equivalent homogenous region. It is important to note that the result of this analysis is a function for thermal conductivity versus temperature. This function for fuel thermal conductivity is then input to the fuel basket effective thermal conductivity calculation described in Subsection 3.4.1.1.4. This calculation uses a finite-element methodology, wherein each fuel cell region containing multiple finite-elements has temperature varying thermal conductivity properties. The resultant temperature varying fuel basket thermal conductivity computed by this basket-fuel composite model is then input to the fuel basket region of the FLUENT cask model.

Because the FLUENT cask model incorporates the results of the fuel basket submodel, which in turn incorporates the fuel assembly submodel, the peak temperature reported from the FLUENT model is the peak temperature in any component. In a dry storage cask, the hottest components are the fuel assemblies. It should be noted that, because the fuel assembly models described in Subsection 3.4.1.1.2 include the fuel pellets, the FLUENT calculated peak temperatures reported in Tables 3.4.10 and 3.4.11 are actually peak pellet centerline temperatures which bound the peak cladding temperatures. We conservatively assume that the peak clad temperature is equal to the peak pellet centerline temperature.

From a thermal/hydraulic standpoint, the HI-STAR transport cask must cover two scenarios:

i. MPCs equipped with AHCEs
ii. MPCs without AHCEs

In the thermal analysis submitted in support of HI-STAR's original transport certification, which we

now refer to as the Baseline Thermal Model (BTM), the AHCEs are included in the thermal models and the basket thermal model is constructed in an exceedingly conservative manner. In particular, the axial conductance of the basket fuel assemblage is assumed to be equal to the in-plane conductance (in reality, the in-plane conductance is much smaller than the axial conductance due to the presence of physical gaps between the fuel and the cell and within the fuel assemblies). For the Scenario (ii) analysis, such an overarching conservatism is removed while certain other less sweeping conservatisms are retained. The revised model, which we refer to as the Refined Thermal Model (RTM), forms the licensing basis for thermal evaluation. The conservatisms germane to the RTM are summarized in Appendix 3.A. To summarize, the principal difference between the BTM and RTM are as follows:

Item	*Description*	*BTM Assumption*	*RTM Assumption*
1	AHCE heat dissipation	Included	Excluded
2	Rayleigh effect	Included	Excluded
3	Basket Axial Conductivity	Grossly Understated	Realistic modeling of axial conductivity (See discussion in Subsection 3.4.1.1.4)

For representative PWR (MPC-24) and BWR (MPC-68) MPC-basket configurations with AHCEs installed, the temperature contours obtained with the Baseline Thermal Model (BTM) corresponding to steady-state hot conditions (100°F ambient, maximum design basis maximum decay heat and full insolation) are shown in Figures 3.4.16 and 3.4.17. Figures 3.4.19 and 3.4.20 show the axial temperature variation of the hottest fuel rod in the MPC-24 and MPC-68 basket designs, respectively. Figures 3.4.22 and 3.4.23 show the radial temperature profile in the MPC-24 and MPC-68 basket designs, respectively, in the horizontal plane where maximum fuel cladding temperature is indicated. Tables 3.4.10 and 3.4.11 summarize maximum calculated temperatures in different parts of the HI-STAR System at design-basis maximum decay heat loads. Tables 3.4.28 and 3.4.29 summarize the peak fuel cladding temperatures with heat loads lower than the design basis maximum. In Tables 3.4.22 and 3.4.23, maximum calculated temperatures in different parts of the HI-STAR System under steady-state cold conditions (-40°F ambient, maximum design basis maximum decay heat and no insolation) are summarized. To confirm the BTM fuel temperatures provided herein are bounding for all MPCs without the AHCEs option (MPC-24, MPC-24E, MPC-32 and MPC-68) a Refined Thermal Model (RTM) is articulated as discussed in the preceding paragraph. As shown next, the results of the refined calculations confirm the BTM results are bounding.

Maximum Cladding Temperatures		
MPC Type	BTM [°F]	RTM [°F]
PWR	701	671 (MPC-24) 668 (MPC-24E) 699 (MPC-32)
BWR	713	642 (MPC-68)

The following additional observations can be derived by inspecting the temperature field obtained

from the finite element analysis:

- The maximum fuel cladding temperature is well within the PNL recommended temperature limit.
- The maximum temperature of basket structural material is well within the stipulated design temperatures.
- The maximum temperature of the neutron absorber is below the material temperature limit.
- The maximum temperatures of the MPC helium retention boundary materials are well below their respective ASME Code limits.
- The maximum temperatures of the aluminum heat conduction elements are well below the stipulated design temperature limits.
- The maximum temperature of the HI-STAR containment boundary materials is well below their respective ASME Code limits.
- The neutron shielding material (Holtite-A) will not experience temperatures in excess of its qualified limit.

The above observations lead us to conclude that the temperature field in the HI-STAR System with a fully loaded MPC containing design-basis heat emitting SNF complies with all regulatory and industry thermal requirements for normal conditions of transport. In other words, the thermal environment in the HI-STAR System will be conducive to safe transport of spent nuclear fuel.

3.4.2.1 Maximum Accessible Surface Temperatures

Access to the HI-STAR overpack cylindrical surface is restricted by the use of a personnel barrier (See Holtec Drawing 3930, Sheet 3 in Chapter 1, Section 1.4). Therefore, the HI-STAR System surfaces accessible during normal transport are the exposed impact limiter surfaces outside the personnel barrier. In this subsection, the exposed impact limiter surface temperatures are computed by including heat transmission from the hot overpack ends through the impact limiters. A conservatively bounding analysis is performed by applying the thermal conductivity of aluminum to the encased aluminum-honeycomb material in the impact limiter shells to the normal condition thermal model discussed earlier in this chapter. In this manner heat transport to the exposed surfaces from the hot overpack is maximized and accessible surface temperatures over estimated. The maximum exposed cask surface temperatures for a PWR MPC (MPC-24) and a BWR MPC (MPC-68) at design maximum heat loads are 142°F and 139°F respectively. In Figure 3.4.28, a color contour map of the regions of HI-STAR System less than 185°F (358°K) is depicted for the hotter MPC-24 basket design. From this map, it is apparent that the accessible (impact limiter) surface temperatures are below the 10CFR71.43(g) mandated limit by a significant margin.

3.4.3 Minimum Temperatures

As specified in 10CFR71, the minimum ambient temperature conditions for the HI-STAR System are -20°F and a cold environment at -40°F. The HI-STAR System design does not have any minimum decay heat load restrictions for transport. Therefore, under zero decay heat load in combination with no solar input conditions, the temperature distribution will be uniformly equal to the imposed minimum ambient conditions. All HI-STAR System materials of construction would satisfactorily perform their intended function in the transport mode at this minimum postulated temperature condition. Evaluations in Chapter 2 demonstrate the acceptable structural performance of the overpack and MPC steel materials at low temperature. Shielding and criticality functions of the HI-STAR System materials (Chapters 5 and 6) are unaffected by exposure to this minimum temperature.

3.4.3.1 Post Rapid Ambient Temperature Drop Overpack Cooldown Event

In this section, the thermal response of the HI-STAR overpack to a rapid ambient temperature drop is analyzed and evaluated. The ambient temperature is postulated to drop from the maximum to minimum temperature under normal condition of transport in a very short time (100°F to –40°F during a 1 hour period) and is assumed to hold steady at –40°F thereafter. The initial overpack condition prior to this rapid temperature drop corresponds to normal steady state transport with maximum design basis heat load. During this postulated cooldown event, the outer surface of the overpack will initially cool more rapidly than the bulk of metal away from the exposed surfaces. Consequently, it is expected that the through-thickness temperature gradients will increase for a period of time, reach a maximum and follow an asymptotic return to the initial steady condition through thickness temperature gradients as the overpack temperature field approaches the –40°F ambient steady condition. The results of the transient analysis reported in this sub-section verify these observations.

Noting that the state of thermal stress is influenced by changes in the overpack temperature field during the cooldown transient, a number of critical locations in the containment boundary depicted in Figure 3.4.24 are identified as pertinent to a structural integrity evaluation discussed in Subsection 2.6.2.3 of this SAR. Locations (1) and (2) are chosen to track the through-thickness temperature gradients in the overpack top forging which is directly exposed to the ambient. Locations (3) and (4) are chosen to track the overpack inner containment shell through-thickness temperature gradient in a plane of maximum heat generation (i.e. active fuel mid-height) where the heat fluxes and corresponding temperature gradients are highest. Locations (A) and (B) are similarly chosen to track the temperature differential in the multi-layered shells (outer-to-inner shells).

The normal transport condition thermal model discussed previously in this chapter is employed in the overpack cooldown transient analysis. This analysis is carried out by applying time-dependent thermal boundary conditions to the model and starting the transient solution in the FLUENT program. In the cooldown event, the ambient temperature is decreased from 100°F to –40°F in 10°F steps every 4 minutes (i.e. a total of 14 steps lasting 56 minutes). The ambient temperature is held constant thereafter. The maximum design basis heat load cask (i.e. the MPC-24 design) was selected to maximize the thermal gradients (by Fourier's Law, thermal gradient is proportional to heat flow). The overpack cooldown event is tracked by the thermal model for a period of 24 hours and results are reported in Figures 3.4.25 through 3.4.27 as discussed below.

In Figure 3.2.25, the overpack containment through-thickness temperature gradient responses are plotted. From this figure, it is evident that the exposed surface of the overpack forging (location (2)) initially cools at a faster rate than the recessed location (1). A similar but less pronounced result is observed in the multi-layered shells temperature changes depicted in Figure 3.4.26. This out-of-phase rate of cooling results in an increasing temperature gradient through the overpack metal layers. The thermal response of deeply recessed locations (3) and (4) show gradual temperature changes that follow each other closely. In other words, while through-thickness temperature gradients in the forging are somewhat altered the overpack inner shell gradients are essentially unchanged during the cooldown period. A closer examination of the forging temperature gradient is therefore warranted.

In Figure 3.4.27, the time dependent forging through thickness temperature differential is depicted. The gradient increases to a maximum in a short time period followed by a slow return towards the starting state. In absolute terms, both the steady state and transient temperature gradients in the forging are quite modest. In the steady state the forging through thickness temperature gradient is approximately 3°F. This value reaches a maximum plateau of 7°F during the transient event (Figure 3.4.27). The incremental thermal stress arising from this short-term gradient elevation is computed and discussed in Subsection 2.6.2.3 of this SAR.

3.4.4 Maximum Internal Pressures

The MPC is initially filled with dry helium after fuel loading and prior to sealing the MPC lid port cover plates and closure ring. During normal transport conditions, the gas temperature within the MPC rises to its maximum operating temperature as determined by the thermal analysis methodology described earlier (see Subsection 3.4.1). The gas pressure inside the MPC will increase with rising temperature. The pressure rise is determined using the Ideal Gas Law which states that the absolute pressure of a fixed volume of entombed gas is proportional to its absolute temperature.

The HI-STAR Maximum Normal Operating Pressure (MNOP) is calculated for10 CFR71.71(c)(1) heat condition (100°F ambient & insolation) and the HI-STAR Overpack passively cooled at design maximum heat load. For other lower than design maximum heat load scenarios, (e.g. transport with Trojan fuel) the MNOP results are confirmed to be bounding. . In Tables 3.4.13 and 3.4.14, summary calculations for determining net free volume in the PWR and BWR canisters are presented. Based on a 30% release of the significant radioactive gases, a 100% release of the rod fill gas from postulated cladding breaches, the net free volume and the initial fill gas pressure, the MNOP results are given in Table 3.4.15. The overpack containment boundary MNOP for a hypothetical MPC breach condition is bounded by the MPC pressure results reported in this table.

3.4.5 Maximum Thermal Stresses

Thermal expansion induced mechanical stresses due to imposed non-uniform temperature distributions have been determined and reported in Chapter 2. Tables 3.4.17 and 3.4.18 summarize the HI-STAR System components temperatures, under steady-state hot conditions, for structural evaluation.

Additionally, Table 3.4.24 provides a summary of MPC helium retention boundary temperatures during normal transport conditions (steady state hot). Structural evaluations in Section 2.6 reference these temperature results to demonstrate the MPC helium retention boundary integrity.

3.4.6 Evaluation of System Performance for Normal Conditions of Transport

The HI-STAR System thermal analysis is based on detailed and complete heat transfer models that properly account for radiation, conduction and natural convection modes of heat transfer. The thermal models incorporate many conservative assumptions that are listed below. A quantitative evaluation of HI-STAR conservatisms is provided in Appendix 3.A.

1. No credit for gap reduction between the MPC and overpack due to differential thermal expansion under hot condition is considered.

2. No credit is considered for MPC basket internal thermosiphon heat transfer. Under a perfectly horizontal transport condition, axial temperature gradients with peaking at active fuel mid-height induces buoyancy flows from both ends of the basket in each MPC cell. Buoyancy flow in shallow horizontal channels has been widely researched and reported in the technical literature [3.4.10 to 3.4.12]. An additional mode of heat transport due to thermosiphon flow within the basket cells is initiated for any cask orientation other than a perfectly horizontal condition. In practice this is a highly likely scenario. However, in the interest of conservatism, no credit is considered for this mode of heat transfer.

3. An upper bound solar absorbtivity of unity is applied to all exposed surfaces.

4. No credit considered for radiative heat transfer between the neutron absorber panels and the neutron absorber pocket walls.

5. No credit is considered for conduction through the neutron shielding materials.

6. No credit is considered for contact between fuel assemblies and the MPC basket wall or between the MPC basket and the MPC basket supports. The fuel assemblies and MPC basket are conservatively considered to be in concentric alignment.

7. No credit considered for presence of highly conducting aluminum honeycomb material inside impact limiters.

8. The fuel assembly contribution to MPC basket axial conductivity is conservatively limited to the fuel cladding only (i.e. axial heat transfer through fuel pellets is neglected).

9. The MPC is assumed to be loaded with the SNF type which has the maximum equivalent thermal resistance of all fuel types in its category (BWR or PWR), as applicable.

10. The design basis maximum decay heat loads are used for all thermal-hydraulic analyses. For casks loaded with fuel assemblies having decay heat generation rates less than design basis, additional thermal margins of safety will exist.

11. Interfacial contact conductance of multi-layered intermediate shell contacting layers was conservatively determined to bound surface finish, contact pressure, and base metal conductivity conditions.

12. Flow turbulation in the MPC space neglected.

Temperature distribution results obtained from a conservatively developed thermal model show that maximum fuel cladding temperature limits are met with adequate margins. Margins during actual normal transport conditions are expected to be greater due to the many conservative assumptions incorporated in the analysis. The maximum local temperatures in the neutron shield and overpack seals are lower than design limits. The maximum local MPC basket temperature level is below the recommended limits for structural materials in terms of susceptibility to stress, corrosion and creep induced degradation. Furthermore, structural evaluation (Chapter 2) has demonstrated that stresses (including those induced due to imposed temperature gradients) are within ASME B&PV Code limits. Section 3.6 provides a discussion of compliance with the regulatory requirements and acceptance criteria listed in Section 3.0. As a result of the above-mentioned considerations, it is concluded that the HI-STAR thermal design is in compliance with 10CFR71 requirements for normal conditions of transport.

Table 3.4.1

CLOSED CAVITY NUSSELT NUMBER†
RESULTS FOR HELIUM FILLED MPC PERIPHERAL VOIDS

	Case (i) Nusselt Number		Case (ii) Nusselt Number	
Temperature (°F)	MPC-24, MPC-24E, MPC-32	MPC-68	MPC-24, MPC-24E, MPC-32	MPC-68
200	6.93	4.72	5.45	3.46
450	5.44	3.71	4.09	2.58
700	4.60	3.13	3.36	2.12

† For conservatism, the heat dissipation enhancement due to Rayleigh effect discussed in Sub-section 3.4.1.1.5 is ignored

Table 3.4.2

RELATIONSHIP BETWEEN HI-STAR SYSTEM REGIONS AND MATHEMATICAL MODEL DESCRIPTIONS

HI-STAR System Region	Mathematical Model	Subsections
Fuel Assembly	Fuel Region Effective Thermal Conductivity	3.4.1.1.2
MPC	Effective Thermal Conductivity of Neutron Absorber/Sheathing/Box Wall Sandwich	3.4.1.1.3
	Basket In-Plane Conductive Heat Transport	3.4.1.1.4
	Heat Transfer in MPC Basket Peripheral Region	3.4.1.1.5
	Effective Thermal Conductivity of MPC Basket-to-Shell Aluminum Heat Conduction Elements	3.4.1.1.11
Overpack	Effective Conductivity of Multi-Layered Intermediate Shell Region	3.4.1.1.6
	Effective Thermal Conductivity of Holtite Neutron Shielding Region	3.4.1.1.9
Ambient Environment	Heat Rejection from Overpack Exterior Surfaces	3.4.1.1.7
	Solar Heat Input	3.4.1.1.8
Assembled Cask Model	Overview of the Thermal Model	3.4.1.1.1
	Effective Conductivity of MPC to Overpack Gap	3.4.1.1.10
	FLUENT Model for HI-STAR	3.4.1.1.12

Table 3.4.3

THIS TABLE IS INTENTIONALLY DELETED.

Table 3.4.4

SUMMARY OF PWR FUEL ASSEMBLIES
EFFECTIVE THERMAL CONDUCTIVITIES

No.	Fuel	@ 200°F (Btu/ft-hr-°F)	@ 450°F (Btu/ft-hr-°F)	@ 700°F (Btu/ft-hr-°F)
1	W 17×17 OFA	0.182	0.277	**0.402**
2	W 17×17 Std	0.189	0.286	0.413
3	W 17×17 Vantage-5H	0.182	0.277	0.402
4	W 15×15 Std	0.191	0.294	0.430
5	W 14×14 Std	0.182	0.284	0.424
6	W 14×14 OFA	**0.175**	**0.275**	0.413
7	B&W 17×17	0.191	0.289	0.416
8	B&W 15×15	0.195	0.298	0.436
9	CE 16×16	0.183	0.281	0.411
10	CE 14×14	0.189	0.293	0.435
11	HN† 15×15 SS	0.180	0.265	0.370
12	W 14×14 SS	0.170	0.254	0.361
13	B&W 15x15 Mark B-11	0.187	0.289	0.424
14	CE 14x14 (MP2)	0.188	0.293	0.434

Note: Boldface values denote the lowest thermal conductivity in each column (excluding stainless steel clad fuel assemblies).

† Haddam Neck B&W or Westinghouse stainless steel clad fuel assemblies.

Table 3.4.5

SUMMARY OF BWR FUEL ASSEMBLIES EFFECTIVE THERMAL CONDUCTIVITIES

No.	Fuel	@ 200°F (Btu/ft-hr-°F)	@ 450°F (Btu/ft-hr-°F)	@ 700°F (Btu/ft-hr-°F)
1	Dresden 1 8×8†	0.119	0.201	0.319
2	Dresden 1 6×6	0.126	0.215	0.345
3	GE 7×7	0.171	0.286	0.449
4	GE 7×7R	0.171	0.286	0.449
5	GE 8×8	0.168	0.278	0.433
6	GE 8×8R	**0.166**	0.275	0.430
7	GE-10 8×8	0.168	0.280	0.437
8	GE-11 9×9	0.167	**0.273**	**0.422**
9	AC†† 10×10 SS	0.152	0.222	0.309
10	Exxon 10×10 SS	0.151	0.221	0.308
11	Damaged Dresden 1 8×8 in a DFC†	0.107	0.169	0.254
12	Dresden-1 Thin Clad 6x6†	0.124	0.212	0.343
13	Humboldt Bay-7x7†	0.127	0.215	0.343
14	Damaged Dresden-1 8x8 (in TND-1 canister)†	0.107	0.168	0.252
15	8x8 QUAD+ Westinghouse†	0.164	0.278	0.435

Note: Boldface values denote the lowest thermal conductivity in each column (excluding Dresden and LaCrosse clad fuel assemblies).

† Low heat emitting fuel assemblies excluded from list of fuel assemblies (zircaloy clad) evaluated to determine the most resistive SNF type

†† Allis-Chalmers stainless steel clad fuel assemblies

Table 3.4.6

MPC BASKET EFFECTIVE THERMAL CONDUCTIVITY RESULTS
FROM ANSYS MODELS

Basket	@200°F (Btu/ft-hr-°F)	@450°F (Btu/ft-hr-°F)	@700°F (Btu/ft-hr-°F)
MPC-24 (Zircaloy Clad Fuel)	1.127	1.535	2.026
MPC-68 (Zircaloy Clad Fuel)	1.025	1.257	1.500
MPC-24 (Stainless Steel Clad Fuel) (Note 1)	0.901	1.230	1.615
MPC-68 (Stainless Steel Clad Fuel) (Note 1)	0.987	1.180	1.360
MPC-68 (Dresden-1 8x8 in canisters)	0.921	1.118	1.306
MPC-32 (Zircaloy Clad Fuel)	0.964	1.214	1.486
MPC-32 (Stainless Steel Clad Fuel) (Note 1)	0.762	0.936	1.104
MPC-24E (Zircaloy Clad Fuel)	1.211	1.635	2.137
MPC-24E (Stainless Steel Clad Fuel) (Note 1)	0.988	1.348	1.766

Note-1: Evaluated for a conservatively bounding configuration (fuel in a damaged fuel canister)

Table 3.4.7

INSOLATION DATA SPECIFIED BY 10CFR71, SUBPART F

Surface Type	**12-Hour Total Insolation Basis**	
	(g-cal/cm^2)	**(Watts/m^2)**
Horizontally Transported Flat Surfaces		
- Base	None	None
- Other Surfaces	800	774.0
Non-Horizontal Flat Surfaces	200	193.5
Curved Surfaces	400	387.0

Table 3.4.8

EFFECTIVE THERMAL CONDUCTIVITY OF THE NEUTRON SHIELD/RADIAL CHANNELS REGION

Condition/Temperature (°F)	**Thermal Conductivity (Btu/ft-hr-°F)**
Normal Condition:	
200	1.953
450	1.812
700	1.645
Fire Condition:	
200	3.012
450	2.865
700	2.689

Table 3.4.9

THIS TABLE IS INTENTIONALLY DELETED.

Table 3.4.10

HI-STAR SYSTEM NORMAL TRANSPORT† MAXIMUM TEMPERATURES
(PWR MPCs)

	Bounding Temperature [°F]	**Normal Condition Temperature Limit [°F]**
Fuel Cladding	701	752
MPC Basket Centerline	667	725
MPC Basket Periphery	430	725
MPC Outer Shell Surface	315	450
MPC/Overpack Helium Gap Outer Surface	291	400
Radial Neutron Shield Inner Surface	271	300
Overpack Enclosure Shell Surface	222	350
Axial Neutron Shield	292	300
Impact Limiter Exposed Surface	121	176
Overpack Closure Plate††	163	400
Overpack Bottom Plate††	295	350

† Steady-state hot (100°F ambient) with maximum decay heat and insolation.

†† Overpack closure plate and vent/drain port plug seals normal condition design temperature is 400°F. The maximum seals temperatures are bounded by the reported closure plate and bottom plate maximum temperatures. Consequently, a large margin of safety exists to permit safe operation of seals in the overpack helium retention boundary.

Table 3.4.11

HI-STAR SYSTEM NORMAL TRANSPORT† MAXIMUM TEMPERATURES
(MPC-68)

	Bounding Temperature [°F]	**Normal Condition Temperature Limit [°F]**
Fuel Cladding	713	752
MPC Basket Centerline	697	725
MPC Basket Periphery	365	725
MPC Outer Shell Surface	306	450
MPC/Overpack Gap Outer Surface	282	400
Radial Neutron Shield Inner Surface	264	300
Overpack Enclosure Shell Surface	217	350
Axial Neutron Shield	255	300
Impact Limiter Exposed Surface	121	176
Overpack Closure Plate††	162	400
Overpack Bottom Plate††	256	350

† Steady-state hot (100°F ambient) with maximum decay heat and insolation.

†† Overpack closure plate and vent/drain port plug seals normal condition design temperature is 400°F. The maximum seals temperatures are bounded by the reported closure plate and bottom plate maximum temperatures. Consequently, a large margin of safety exists to permit safe operation of seals in the overpack helium retention boundary.

Table 3.4.12

THIS TABLE IS INTENTIONALLY DELETED.

Table 3.4.13

SUMMARY OF BOUNDING MINIMUM
FREE VOLUME CALCULATIONS (PWR MPCs)

Item	**MPC-24 Volume (ft^3)**	**MPC-24E Volume (ft^3)**	**MPC-32 Volume (ft^3)**
Cavity Volume	367	367	367
Basket Metal Volume	45	52	25
Bounding Fuel Assemblies Volume	79	79	106
Basket Supports and Fuel Spacers Volume	7	7	9
Aluminum Conduction Elements†	6	6	6
Net Free Volume	230 (6512 liters)	223 (6314 liters)	221 (6258 liters)

† Bounding 1,000 lbs aluminum weight.

Table 3.4.14

SUMMARY OF BOUNDING MINIMUM
MPC-68 FREE VOLUME CALCULATIONS

Item	**Volume (ft^3)**
Cavity Volume	367
Basket Metal Volume	35
Bounding Fuel Assemblies Volume	93
Basket Supports and Fuel Spacers Volume	12
Aluminum Conduction Elements†	6
Net Free Volume	221 (6258 liters)

† Bounding 1,000 lbs aluminum weight.

Table 3.4.15

SUMMARY OF MAXIMUM NORMAL OPERATING PRESSURE (MNOP)†
FOR HORIZONTAL TRANSPORT CONDITIONS

Condition	**Pressure (psig)**	**Bounding MPC Cavity Bulk Temperature (°F)**
MPC-24:		
Initial Backfill (at 70°F)	42.8	483
Normal Condition	87.7	
With 3% Rods Rupture(Note 1)	88.8	
MPC-68:		
Initial Backfill (at 70°F)	42.8	468
Normal Condition	86.0	
With 3% Rods Rupture(Note 1)	86.9	
MPC-24E:		
Initial Backfill (at 70°F)	42.8	483
Normal Condition	87.7	
With 3% Rods Rupture(Note 1)	88.9	
MPC-32:		
Initial Backfill (at 70°F)	42.8	483
Normal Condition	87.7	
With 3% Rods Rupture(Note 1)	89.3	

Note 1: NUREG-1617 requires an assumption for normal transport that 3% of the rods are breached with release of 100% fill gas and 30% fission gas to containment.

† Pressure analysis in accordance with heat condition specified in 10 CFR 71.71(c)(1) in the absence of venting, external ancillary cooling or operational controls.

Table 3.4.16

THIS TABLE IS INTENTIONALLY DELETED.

Table 3.4.17

PWR MPCs NORMAL HORIZONTAL TRANSPORT CONDITION
HI-STAR SYSTEM COMPONENTS BOUNDING TEMPERATURE SUMMARY

	MPC Basket Axial Mid-Length [°F]	**MPC Basket Axial Ends** [°F]
Overpack enclosure shell	222	147
Overpack inner shell	291	163
MPC shell	315	164
Basket periphery	430	166
Basket center	667	177

Table 3.4.18

MPC-68 NORMAL HORIZONTAL TRANSPORT CONDITION
HI-STAR SYSTEM COMPONENTS TEMPERATURE [°F] SUMMARY

	MPC Basket Axial Mid-Length	**MPC Basket Axial Ends**
Overpack enclosure shell	217	146
Overpack inner shell	282	161
MPC shell	306	163
Basket periphery	365	164
Basket center	697	175

Table 3.4.19

SUMMARY OF LOADED HI-STAR SYSTEM
BOUNDING COMPONENT WEIGHTS AND THERMAL INERTIAS

Component	Weight (lbs)	Heat Capacity (Btu/lb-°F)	Thermal Inertia (Btu/°F)
Holtite-A	11,000	0.39	4,290
Carbon Steel	140,000	0.1	14,000
Alloy-X MPC (empty)	35,000	0.12	4,200
Fuel	40,000	0.056	2,240
MPC Cavity Water†	6,500	1.0	6,500
			31,230 (Total)

† Based on smallest MPC-68 cavity net free volume with 50% credit for flooded water mass.

Table 3.4.20

MAXIMUM ALLOWABLE TIME DURATION
FOR WET TRANSFER OPERATIONS

Initial Temperature (°F)	Time Duration (hr)
115	44.3
120	42.0
125	39.7
130	37.4
135	35.2
140	32.9
145	30.6
150	28.3

Table 3.4.21

THIS TABLE IS INTENTIONALLY DELETED.

Table 3.4.22

HI-STAR SYSTEM BOUNDING TEMPERATURES [°F]
UNDER STEADY-STATE COLD† CONDITIONS (PWR MPCs)

Fuel Cladding	620
MPC Basket Centerline	586
MPC Basket Periphery	329
MPC Outer Shell Surface	190
MPC/Overpack Gap Outer Surface	165
Radial Neutron Shield Inner Surface	141
Overpack Enclosure Shell Surface	96
Axial Neutron Shield	165
Impact Limiter Exposed Surface	-40

† -40°F ambient temperature with maximum decay heat and no insolation.

Table 3.4.23

HI-STAR SYSTEM MAXIMUM TEMPERATURES [°F]
UNDER STEADY-STATE COLD† CONDITIONS (MPC-68)

Fuel Cladding	621
MPC Basket Centerline	605
MPC Basket Periphery	254
MPC Outer Shell Surface	178
MPC/Overpack Gap Outer Surface	153
Radial Neutron Shield Inner Surface	130
Overpack Enclosure Shell Surface	88
Axial Neutron Shield	123
Impact Limiter Exposed Surface	-40

† -40°F ambient temperature with maximum decay heat and no insolation.

Table 3.4.24

SUMMARY OF MPC HELIUM RETENTION BOUNDARY BOUNDING TEMPERATUREDISTRIBUTION DURING NORMAL STORAGE CONDITIONS

Location	**Figure 2.6.20 Designation**	**PWR MPCs [°F]**	**MPC-68 [°F]**
MPC Lid Inside Surface at Centerline	A	176	173
MPC Lid Outside Surface at Centerline	B	171	169
MPC Lid Inside Surface at Periphery	C	164	163
MPC Lid Outside Surface at Periphery	D	162	161
MPC Baseplate Inside Surface at Centerline	E	301	260
MPC Baseplate Outside Surface at Centerline	F	295	256
MPC Baseplate Inside Surface at Periphery	G	267	239
MPC Baseplate Outside Surface at Periphery	H	267	239
MPC Shell Maximum	I	315	306

Table 3.4.25

SUMMARY OF 10×10 ARRAY BWR FUEL ASSEMBLY TYPES
EFFECTIVE THERMAL CONDUCTIVITIES†

Fuel	**k_{eff} at 200°F [Btu/(ft-hr-°F)]**	**k_{eff} at 450°F [Btu/(ft-hr-°F)]**	**k_{eff} at 700°F [Btu/(ft-hr-°F)]**
GE-12/14	0.166	0.269	0.412
Atrium-10	0.164	0.266	0.409
SVEA-96	0.164	0.269	0.416

† The conductivities reported in this table are obtained by the simplified method described in the beginning of Subsection 3.4.1.1.2.

Table 3.4.26

COMPARISON OF ATRIUM-10† AND BOUNDING†† BWR FUEL ASSEMBLY EFFECTIVE THERMAL CONDUCTIVITIES

Temperature	**Atrium-10 Assembly**		**Bounding BWR Assembly**	
°F	**Btu/(ft-hr-°F)**	**W/m-K**	**Btu/(ft-hr-°F)**	**W/m-K**
200	0.225	0.389	0.171	0.296
450	0.345	0.597	0.271	0.469
700	0.504	0.872	0.410	0.710

† The reported effective thermal conductivity has been obtained from a rigorous finite-element modeling of the Atrium-10 assembly.

†† The bounding BWR fuel assembly effective thermal conductivity applied in the MPC-68 basket thermal analysis.

Table 3.4.27

THIS TABLE IS INTENTIONALLY DELETED.

Table 3.4.28

PWR MPCs BOUNDING PEAK FUEL CLADDING TEMPERATURE
AS A FUNCTION OF TOTAL HEAT LOAD

Total MPC Decay Heat Load (kW)	Peak Fuel Cladding Temperature (°F)
20.0†	700.6
19.0	678.9
17.0	633.9
15.5	598.8

† Design Basis Maximum.

Table 3.4.29

MPC-68 PEAK FUEL CLADDING TEMPERATURE
AS A FUNCTION OF TOTAL HEAT LOAD

Total MPC Decay Heat Load (kW)	Peak Fuel Cladding Temperature (°F)
18.5†	712.7
17.0	674.0
15.5	634.1

† Design Basis Maximum.

Table 3.4.30

SUMMARY OF THERMAL CONDUCTIVITY CALCULATIONS
FOR MPC HELIUM DILUTED BY RELEASED ROD GASES

Component Gas	**Molecular Weight (g/mole)**	**Mole Fraction**	**Thermal Conductivity* (Btu/hr-ft-°F)**
MPC and Fuel Rod Backfill Helium	4	0.817	0.098 @ 200°F 0.129 @ 450 °F 0.158 @ 700°F
Rod Tritium	3	8.007×10^{-5}	0.119 @ 200 0.148 @ 450°F 0.177 @ 700°F
Rod Krypton	85	0.016	6.76×10^{-3} @ 200°F 8.782×10^{-3} @ 450°F 0.011 @ 700°F
Rod Xenon	131	0.160	3.987×10^{-3} @ 200°F 5.258×10^{-3} @ 450°F 6.471×10^{-3} @ 700°F
Rod Iodine	129	6.846×10^{-3}	2.496×10^{-3} @ 200°F 3.351×10^{-3} @ 450°F 4.201×10^{-3} @ 700°F
Mixture of Gases (diluted helium)	N/A	1.000	0.053 @ 200°F 0.069 @ 450°F 0.085 @ 700°F

* References [3.2.2], [3.4.18] & [3.4.19] consulted for fission gases (Tritium, Krypton, Xenon and Iodine) conductivities.

Table 3.4.31

COMPARISON OF COMPONENT EFFECTIVE THERMAL CONDUCTIVITIES WITH AND WITHOUT MPC HELIUM DILUTION

	Effective Thermal Conductivity (Btu/hr-ft-°F)		
	Value at 200°F	**Value at 450°F**	**Value at 700°F**
Fuel Assembly with Undiluted Helium	0.257	0.406	0.604
Fuel Assembly with Diluted Helium	0.160	0.278	0.458
MPC Fuel Basket with Undiluted Helium	1.127	1.535	2.026
MPC Fuel Basket with Diluted Helium	0.948	1.338	1.829

Table 3.4.32

MPC-24 HYPOTHETICAL 100% RODS RUPTURE ACCIDENT
MAXIMUM TEMPERATURES*

	Calculated Maximum Temperature (°F)	**Accident Condition Temperature Limit (°F)**
Fuel Cladding	743	1058
MPC Basket Centerline	709	950
MPC Basket Periphery	444	950
MPC Outer Shell Surface	314	775
MPC/Overpack Helium Gap Outer Surface	291	500
Radial Neutron Shield Inner Surface	271	N/A
Overpack Enclosure Shell Surface	222	1350
Overpack Closure Plate	176	700
Overpack Bottom Plate	296	700

* The results reported herein are obtained from thermal models employing grossly understated fuel basket conductivities.

Table 3.4.33

MPC-24 HYPOTHETICAL 100% RODS RUPTURE ACCIDENT PRESSURES

Calculated Accident Pressure (psig)	Accident Condition Design Pressure (psig)
134	200

Table 3.4.34

PLANT SPECIFIC BWR FUEL TYPES EFFECTIVE THERMAL CONDUCTIVITY*

Fuel	@200°F [Btu/ft-hr-°F]	@450°F [Btu/ft-hr-°F]	@700F° [Btu/ft-hr-°F]
Oyster Creek (7x7)	0.165	0.273	0.427
Oyster Creek (8x8)	0.162	0.266	0.413
TVA Browns Ferry (8x8)	0.160	0.264	0.411
SPC-5 (9x9)	0.149	0.245	0.380

* The conductivities reported in this table are obtained by a simplified analytical method described in Subsection 3.4.1.1.2.

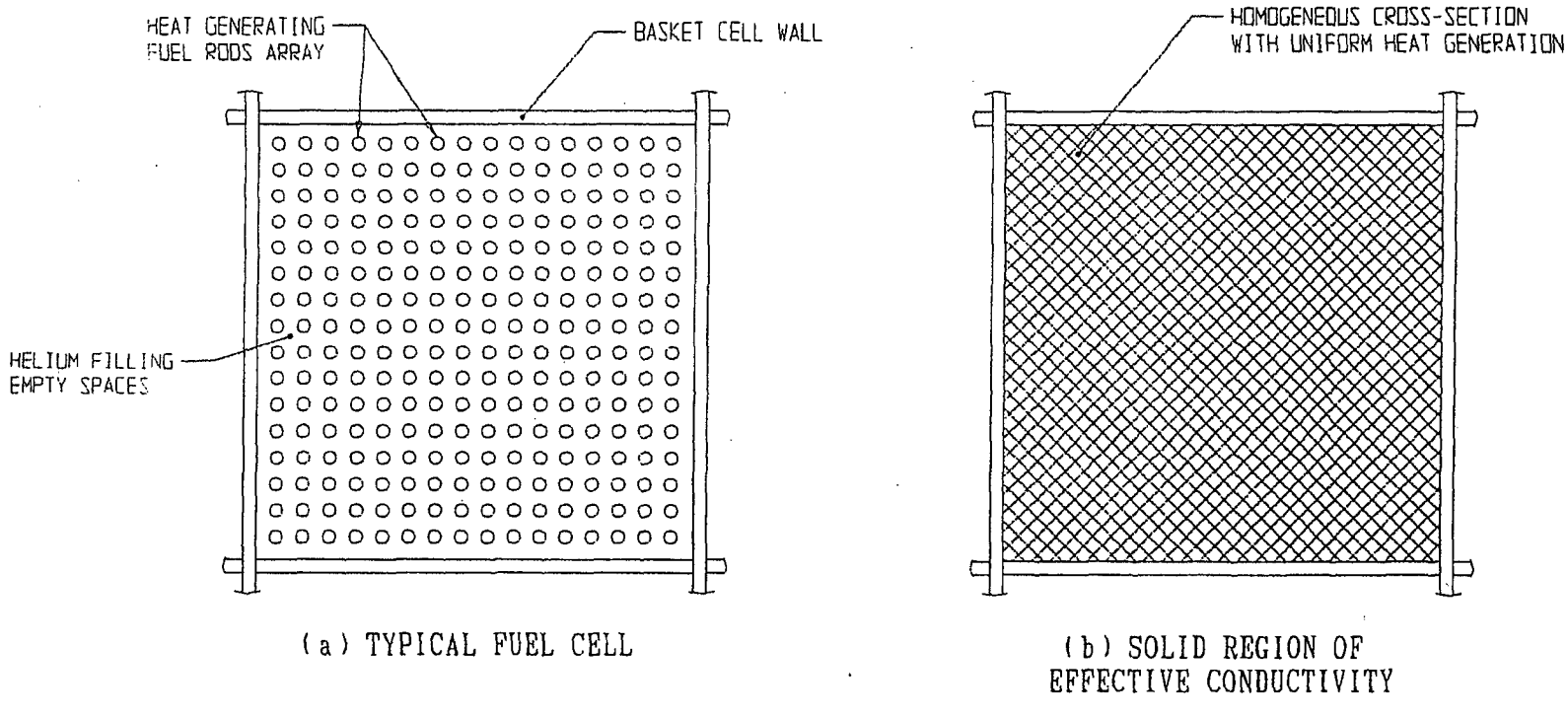

(a) TYPICAL FUEL CELL

(b) SOLID REGION OF
EFFECTIVE CONDUCTIVITY

FIGURE 3.4.1; HOMOGENIZATION OF THE STORAGE CELL CROSS-SECTION

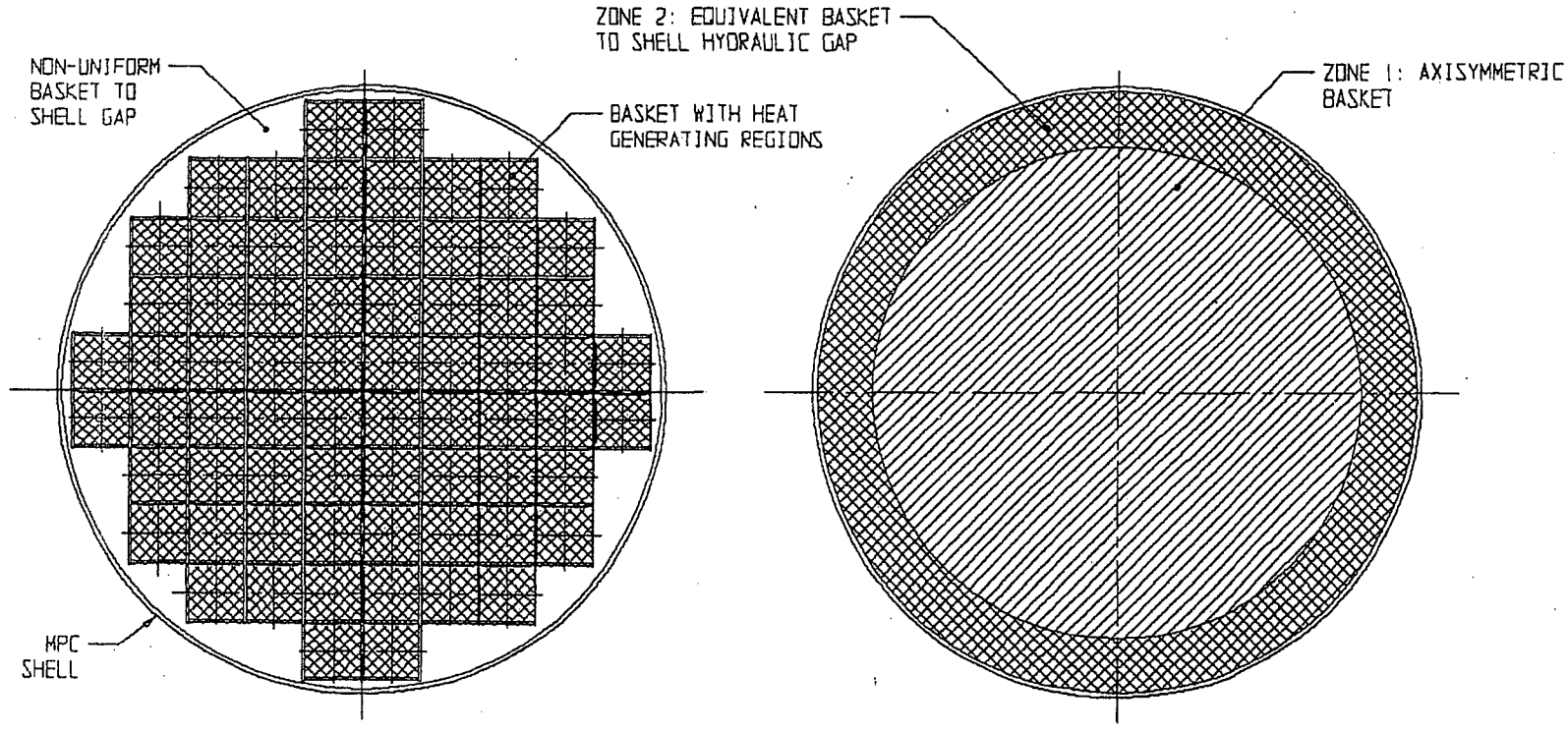

(a) TYPICAL MPC CROSS-SECTION

(b) EQUIVALENT TWO ZONE MODEL

FIGURE 3.4.2; MPC CROSS-SECTION REPLACED WITH AN EQUIVALENT TWO ZONE AXISYMMETRIC BODY

\PROJECTS\5014\HI951251\CH_3\3_4_2

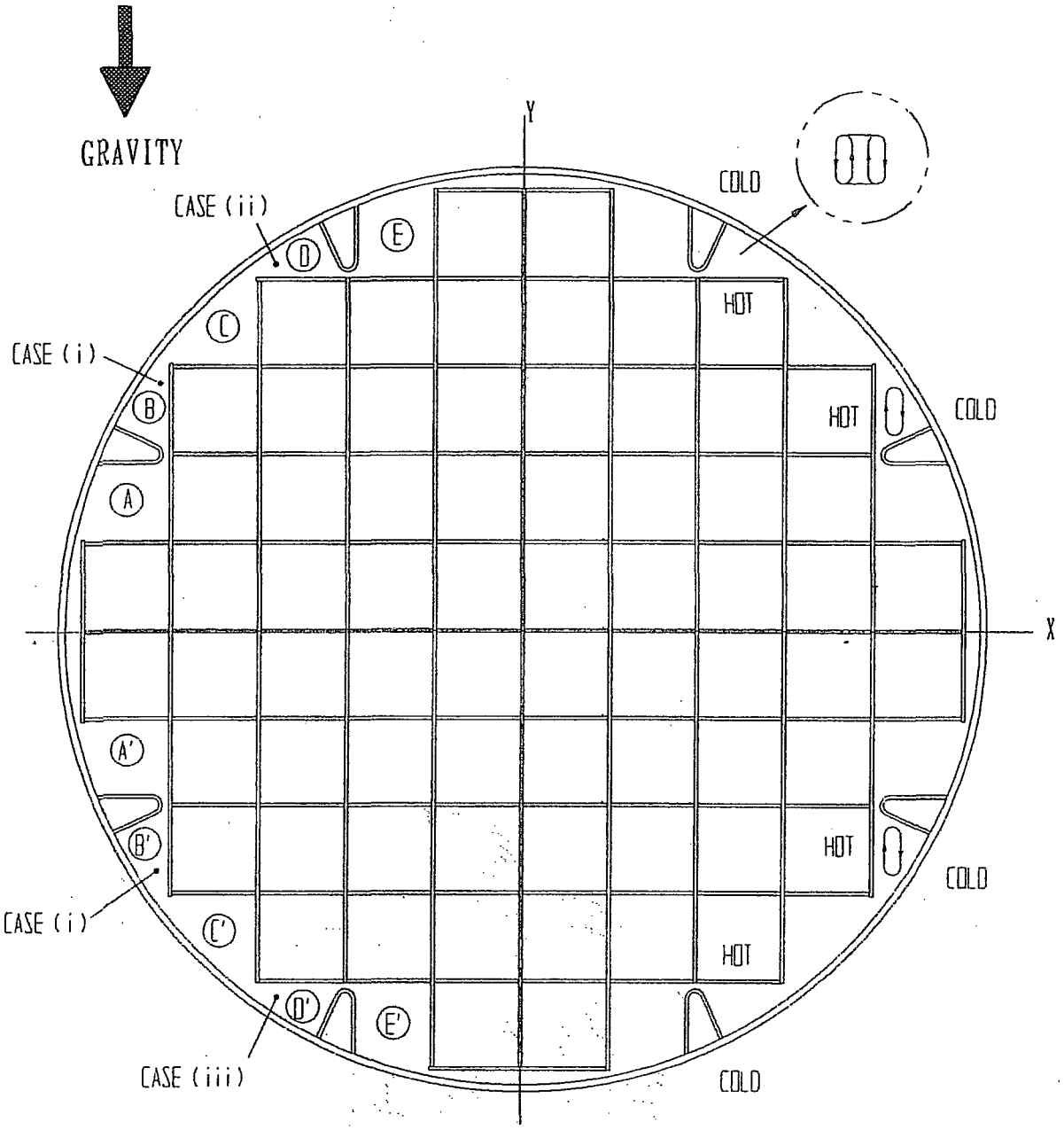

FIGURE 3.4.3; NATURAL CONVECTION IN MPC BASKET PERIPHERY REGION

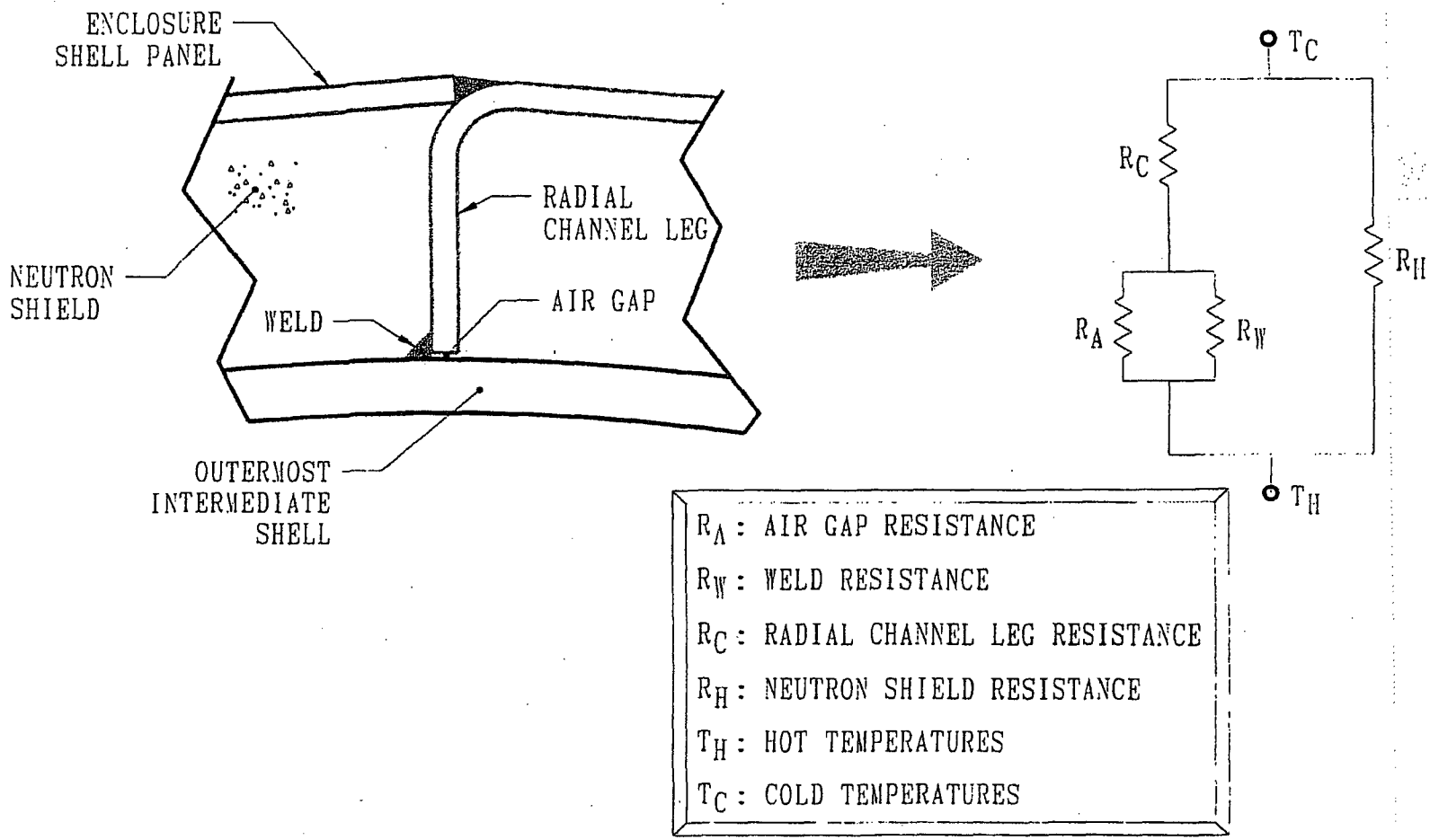

FIGURE 3.4.4; NEUTRON SHIELD REGION RESISTANCE NETWORK ANALOGY FOR EFFECTIVE CONDUCTIVITY CALCULATION

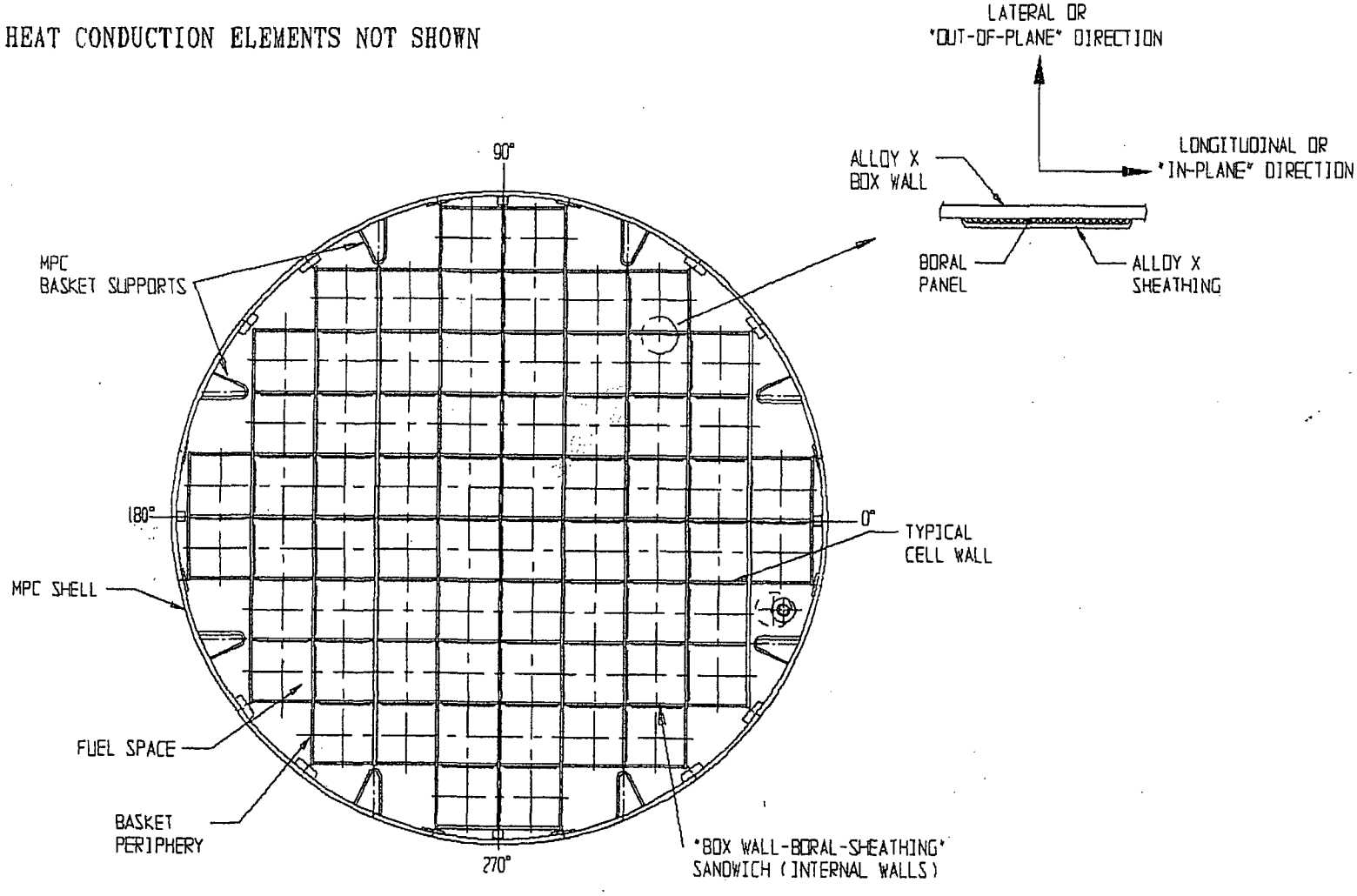

FIGURE 3.4.5; TYPICAL MPC BASKET PARTS IN A CROSS-SECTIONAL VIEW

\PROJECTS\5014\HI951251\CH_3\3_4_5

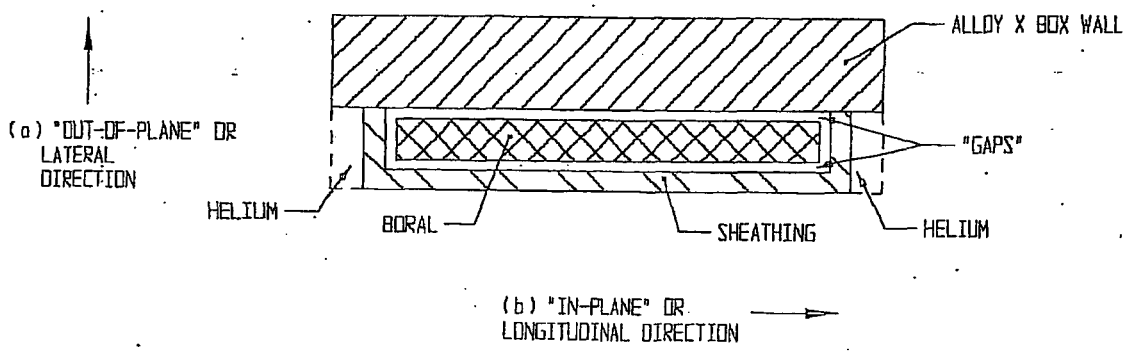

FIGURE 3.4.6: "BOX WALL-BORAL-SHEATHING" SANDWICH

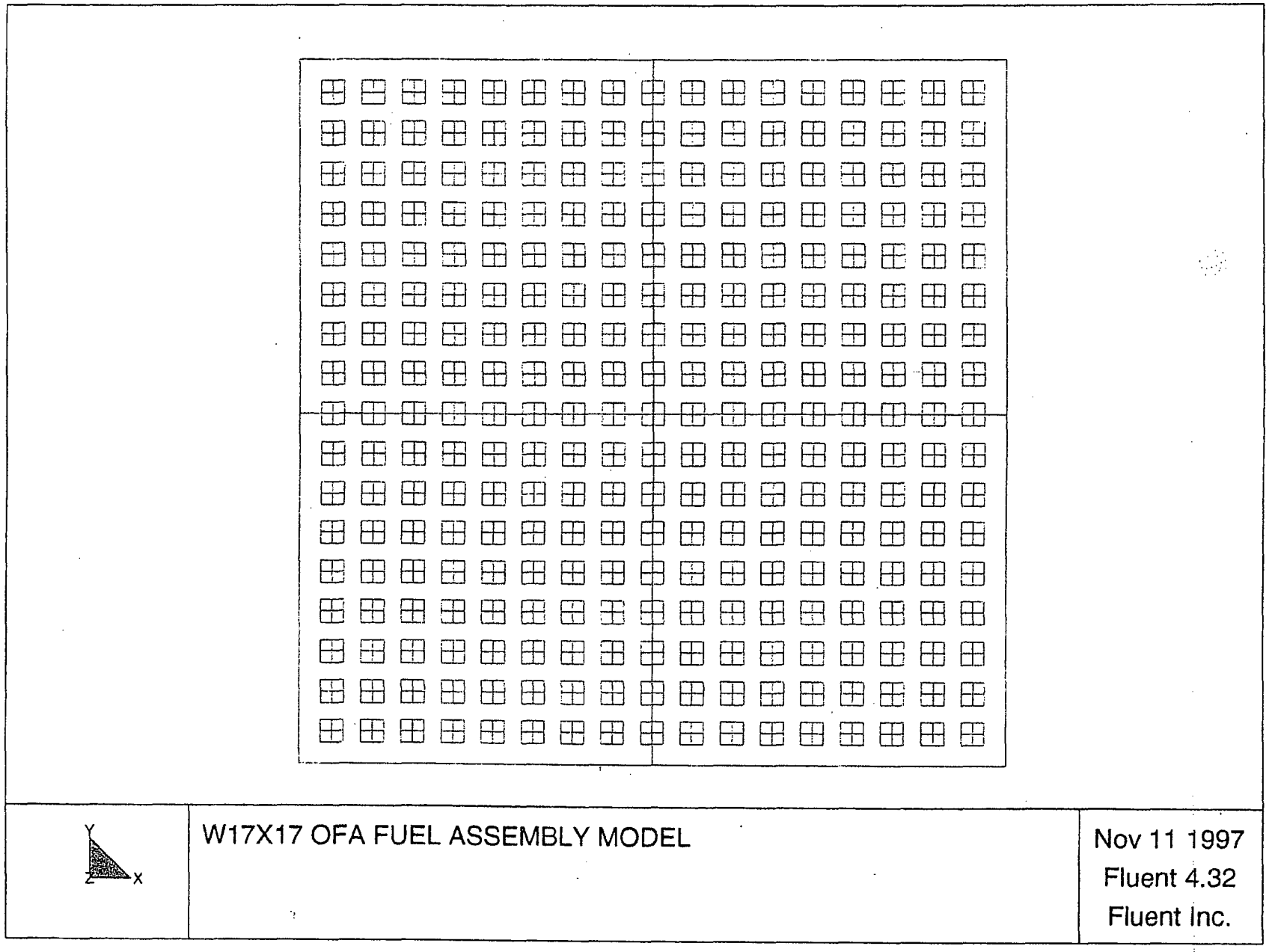

FIGURE 3.4.7: WESTINGHOUSE 17x17 OFA PWR FUEL ASSEMBLY MODEL

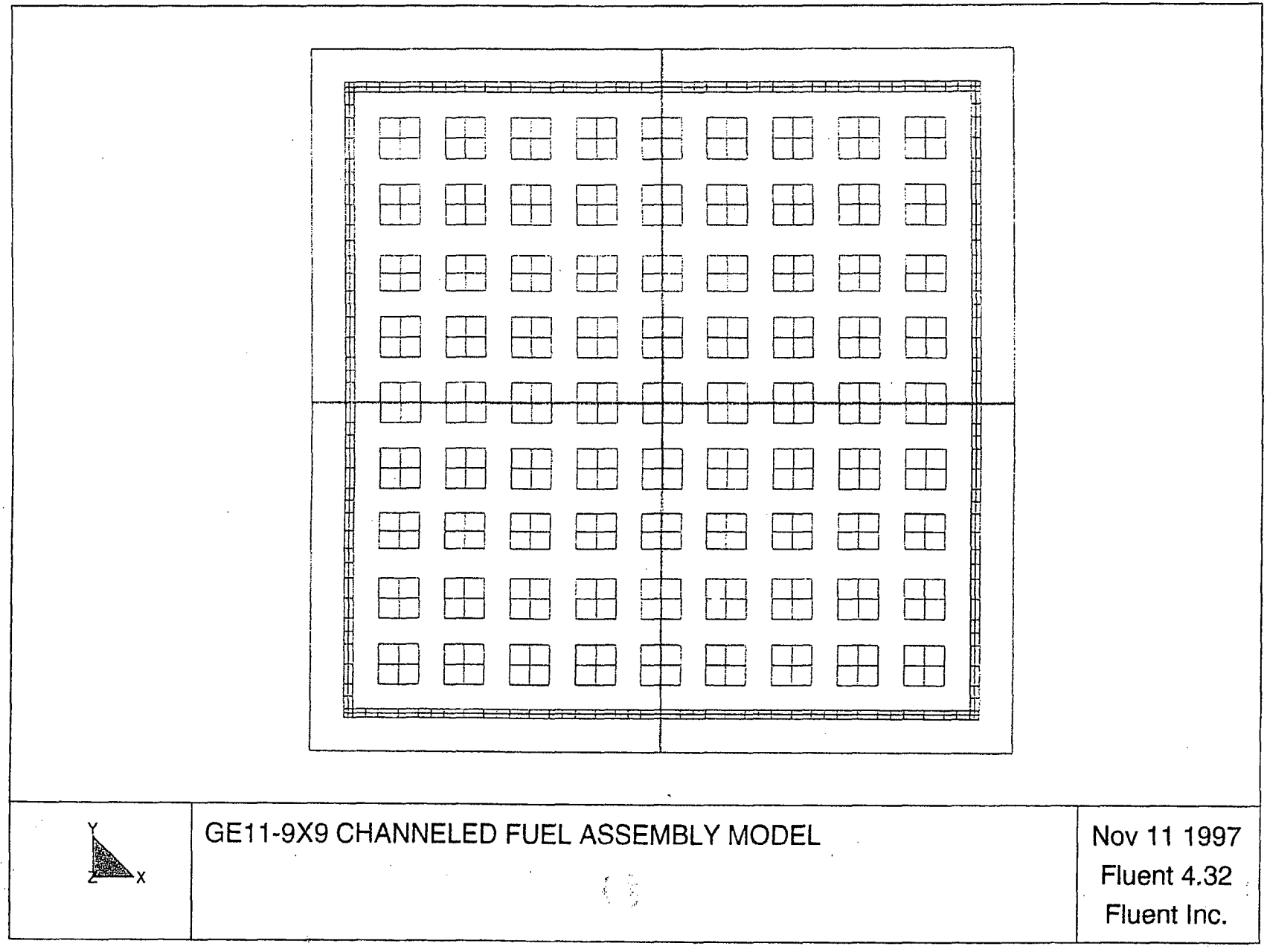

FIGURE 3.4.8: GENERAL ELECTRIC 9x9 BWR FUEL ASSEMBLY MODEL

FIGURE 3.4.9

THIS FIGURE IS INTENTIONALLY DELETED.

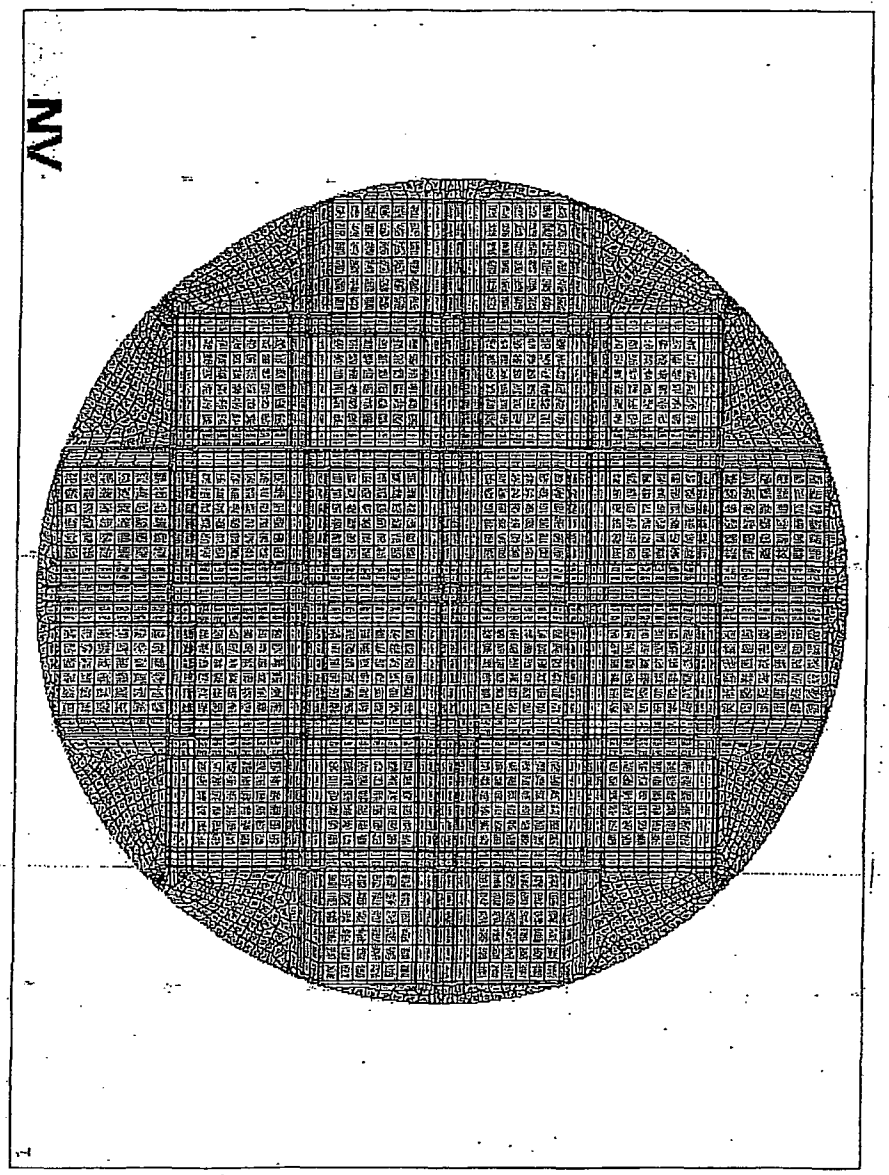

FIGURE 3.4.10: MPC-24 BASKET CROSS-SECTION ANSYS FINITE ELEMENT MODEL

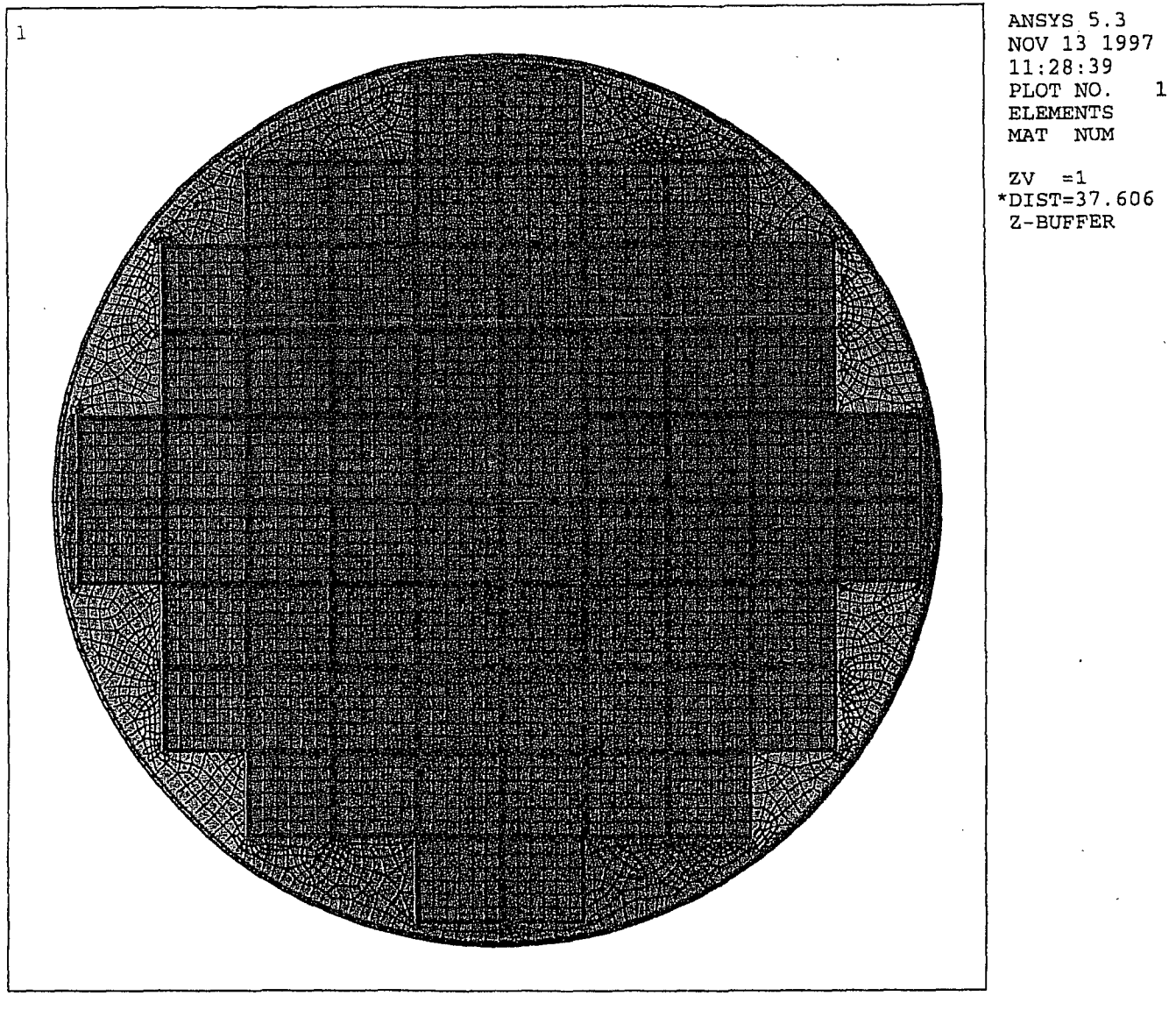

FIGURE 3.4.11; MPC-68 BASKET CROSS-SECTION ANSYS FINITE ELEMENT MODEL

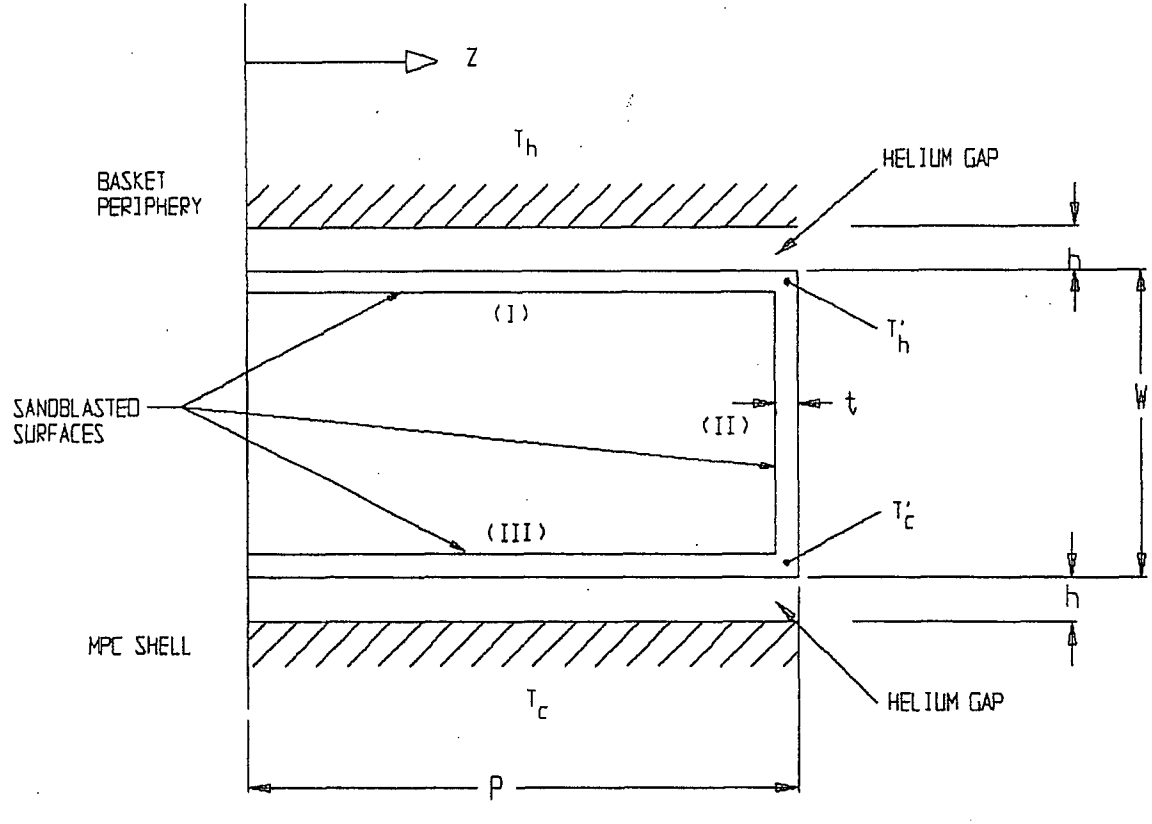

FIGURE 3.4.12; ILLUSTRATION OF AN MPC BASKET TO SHELL ALUMINUM HEAT CONDUCTION ELEMENT

\5014\HI951251\CH_3\3_4_12

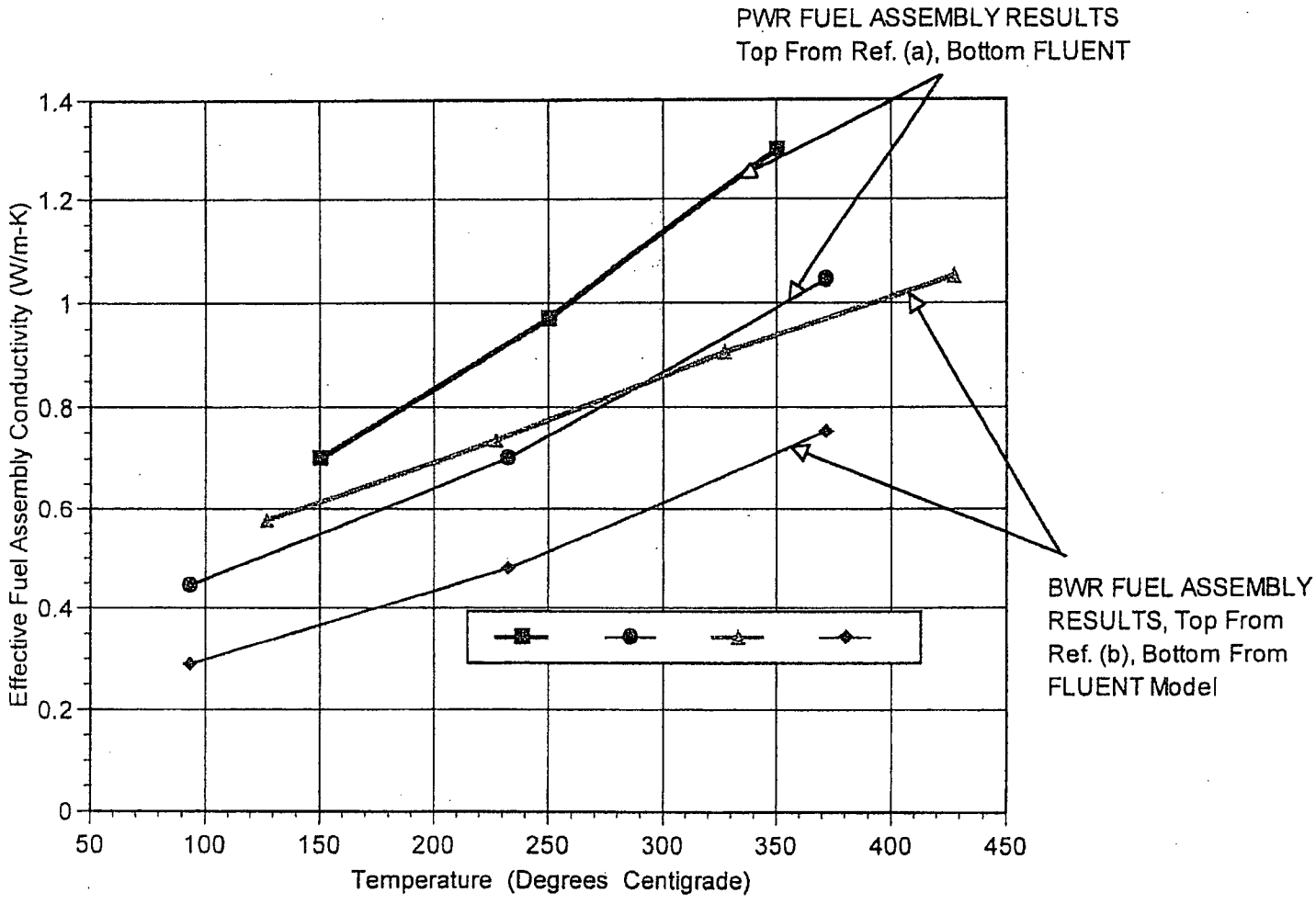

(a) "Determination of SNF Peak Temperatures in the Waste Package", Bahney & Doering, *HLRWM Sixth Annual Conf.*, Pages 671-673, (April 30 - May 5, 1995)
(b) "A Method for Determining the Spent-Fuel Contribution to Transport Cask Containment Requirements", *Sandia Report SAND90-2406*, page II-132, (1992)

FIGURE 3.4.13: COMPARISON OF FLUENT BASED FUEL ASSEMBLY EFFECTIVE CONDUCTIVITY RESULTS WITH PUBLISHED TECHNICAL DATA

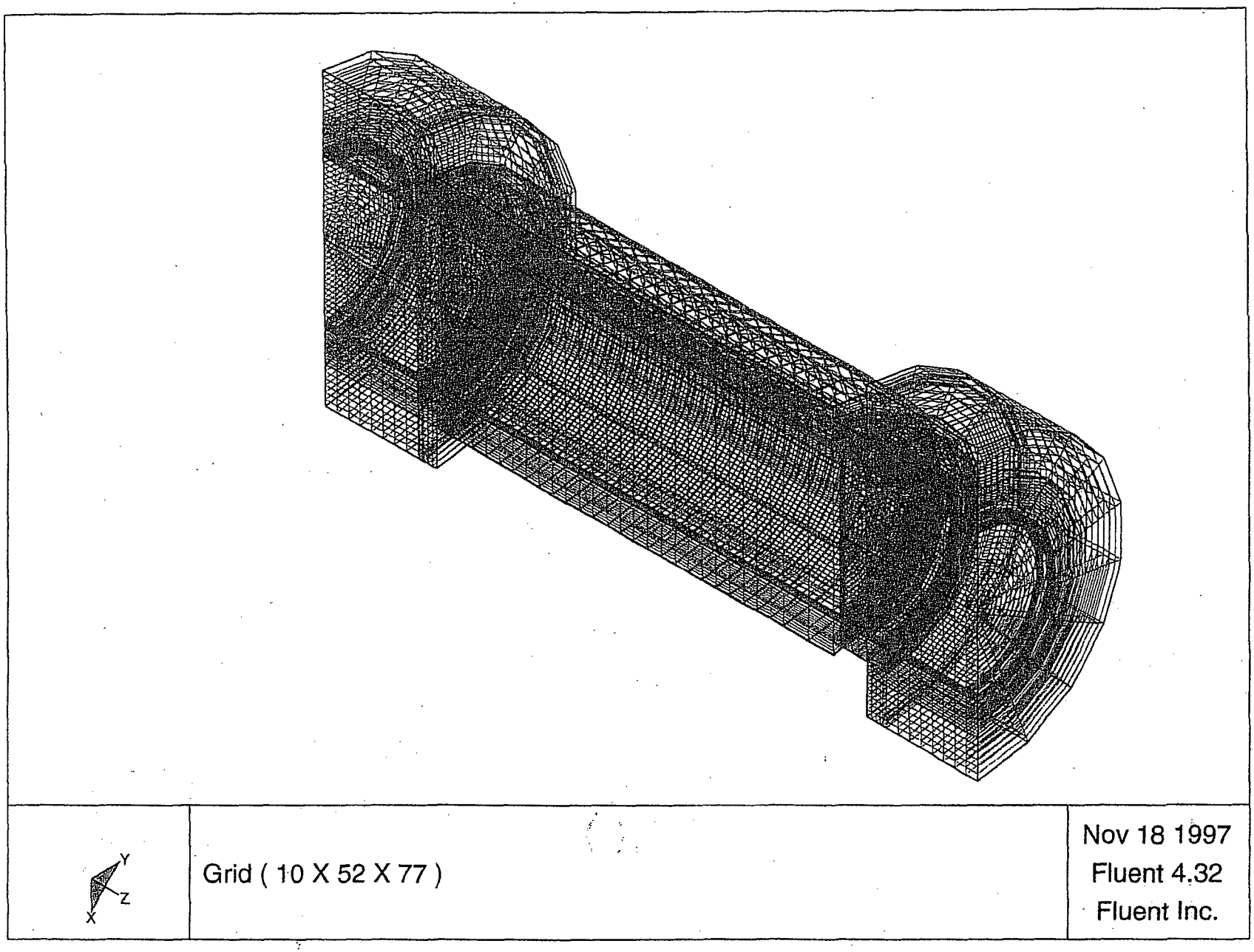

FIGURE 3.4.14: HI-STAR 100 SYSTEM FINITE ELEMENT MESH FOR THERMAL ANALYSIS

FIGURE 3.4.15

THIS FIGURE IS INTENTIONALLY DELETED.

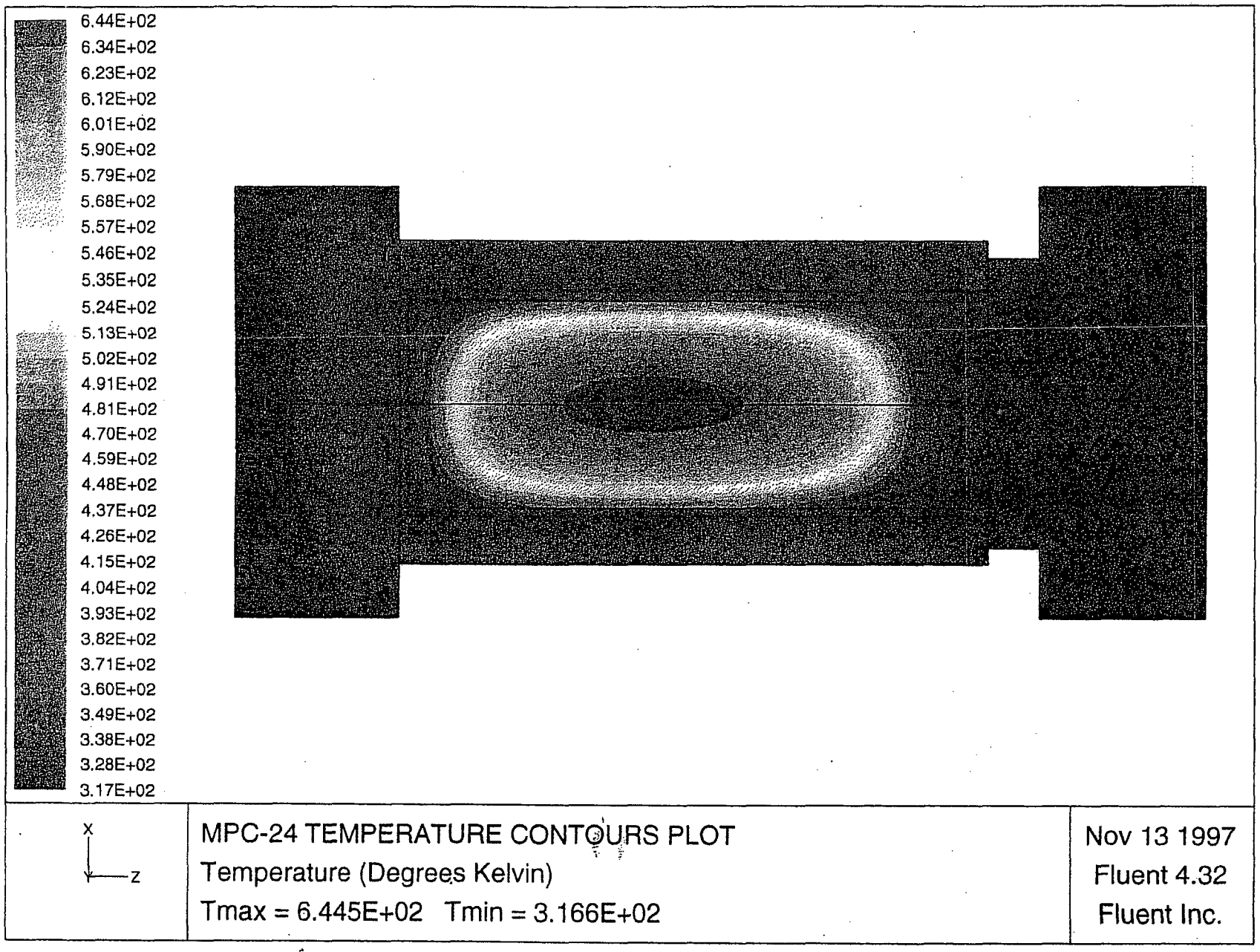

FIGURE 3.4.16: HI-STAR 100 SYSTEM NORMAL TRANSPORT CONDITION TEMPERATURE CONTOURS PLOT (MPC-24 BASKET)

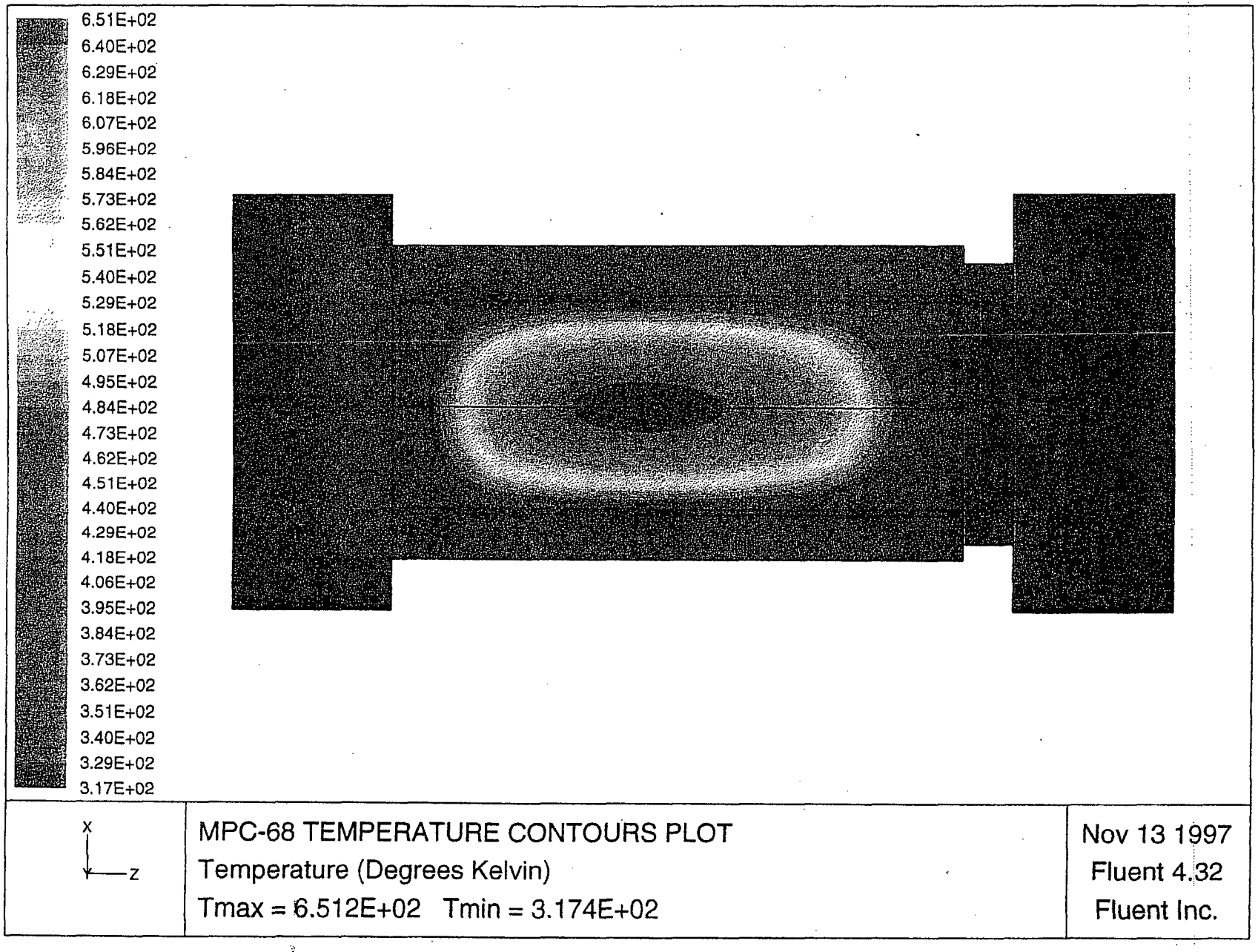

FIGURE 3.4.17: HI-STAR 100 SYSTEM NORMAL TRANSPORT CONDITION TEMPERATURE CONTOURS PLOT (MPC-68 BASKET)

FIGURE 3.4.18

THIS FIGURE IS INTENTIONALLY DELETED.

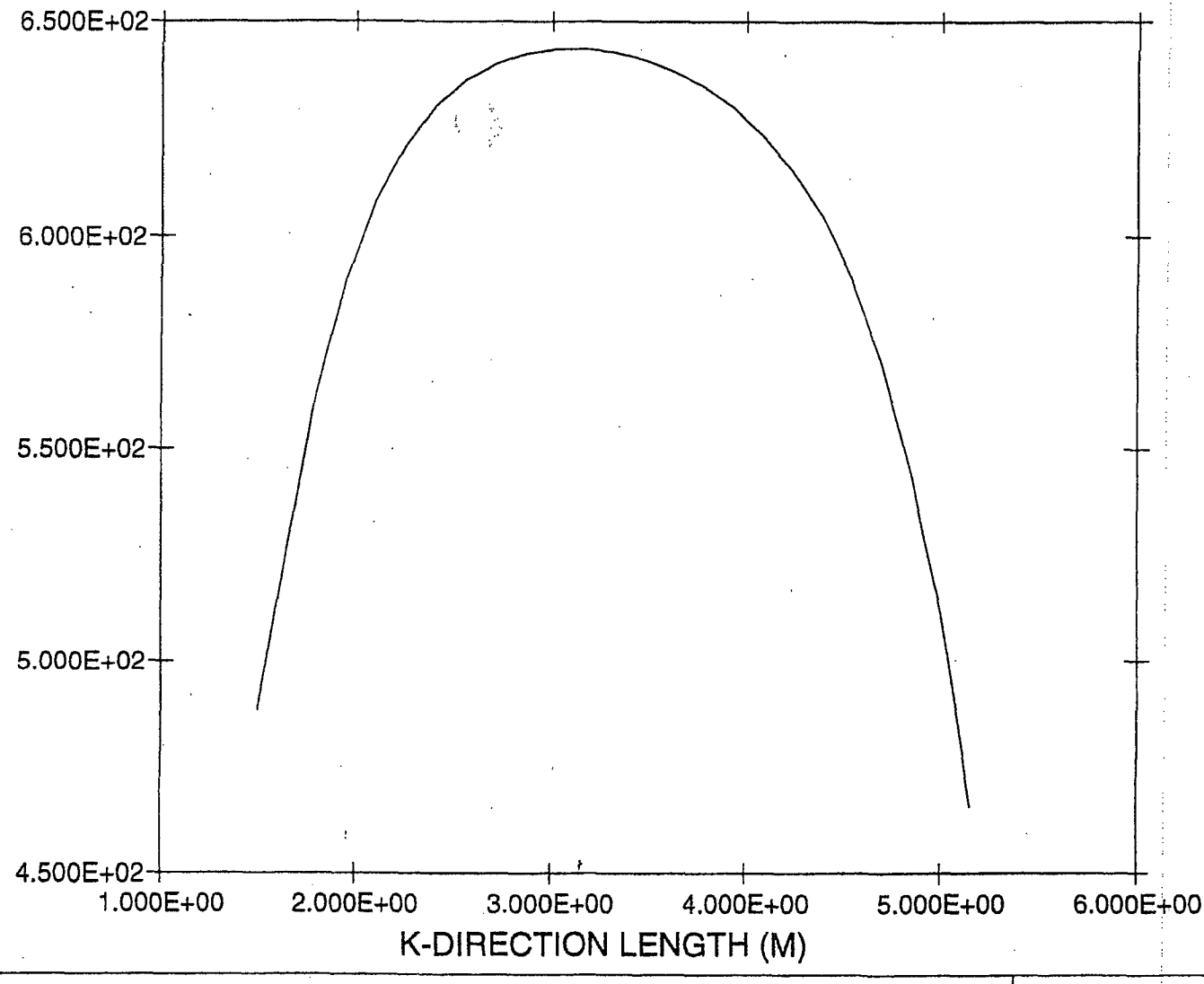

Y, Z, X	FIGURE 3.4.19: MPC-24 HOTTEST ROD TEMPERATURE PROFILE Temperature (Kelvin) Vs. Axial Length (Meters)	May 24 1998 Fluent 4.32 Fluent Inc.

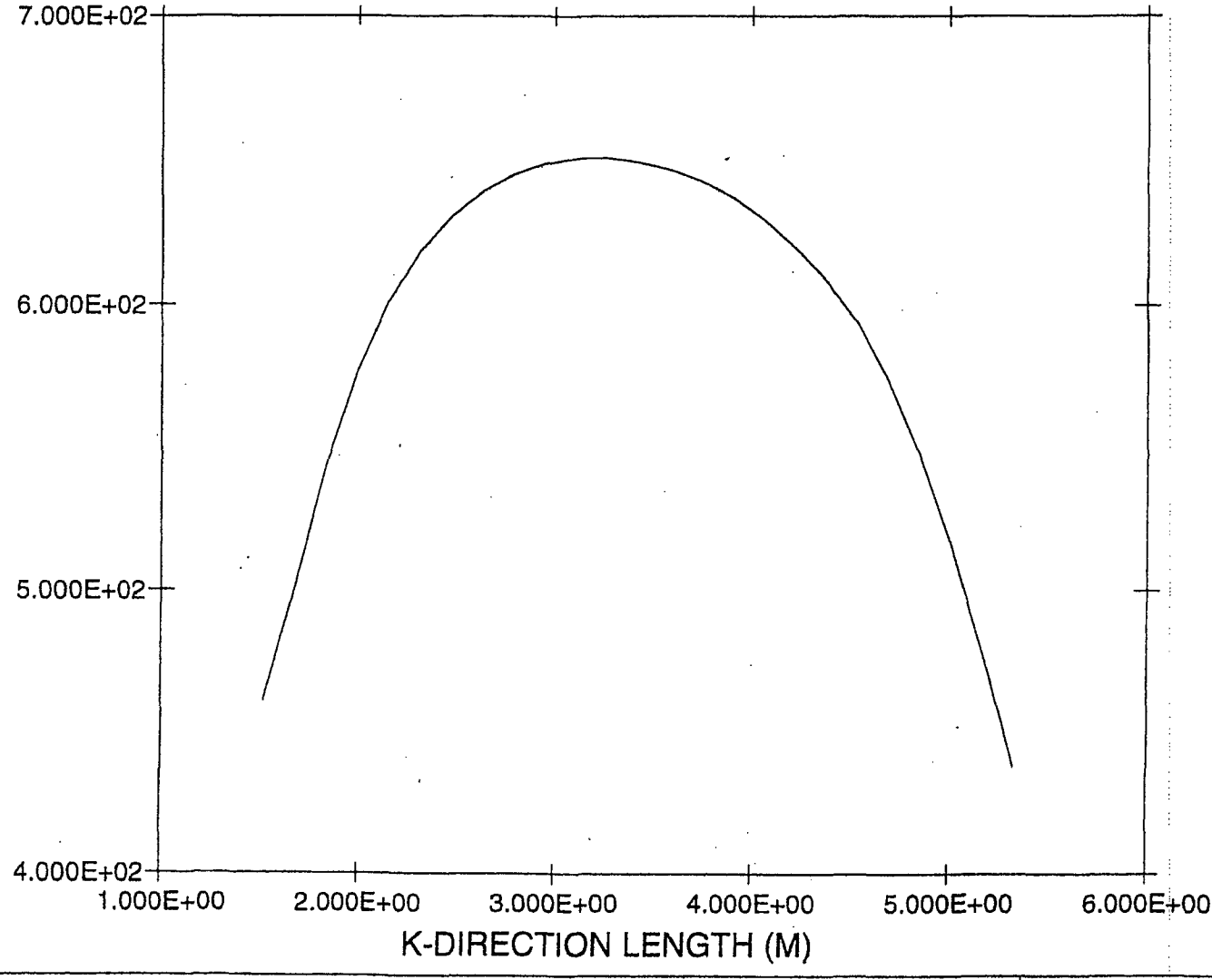

Y, Z, X	FIGURE 3.4.20: MPC-68 HOTTEST ROD TEMPERATURE PROFILE Temperature (Kelvin) Vs. Axial Length (Meters)	May 24 1998 Fluent 4.32 Fluent Inc.

FIGURE 3.4.21

THIS FIGURE IS INTENTIONALLY DELETED.

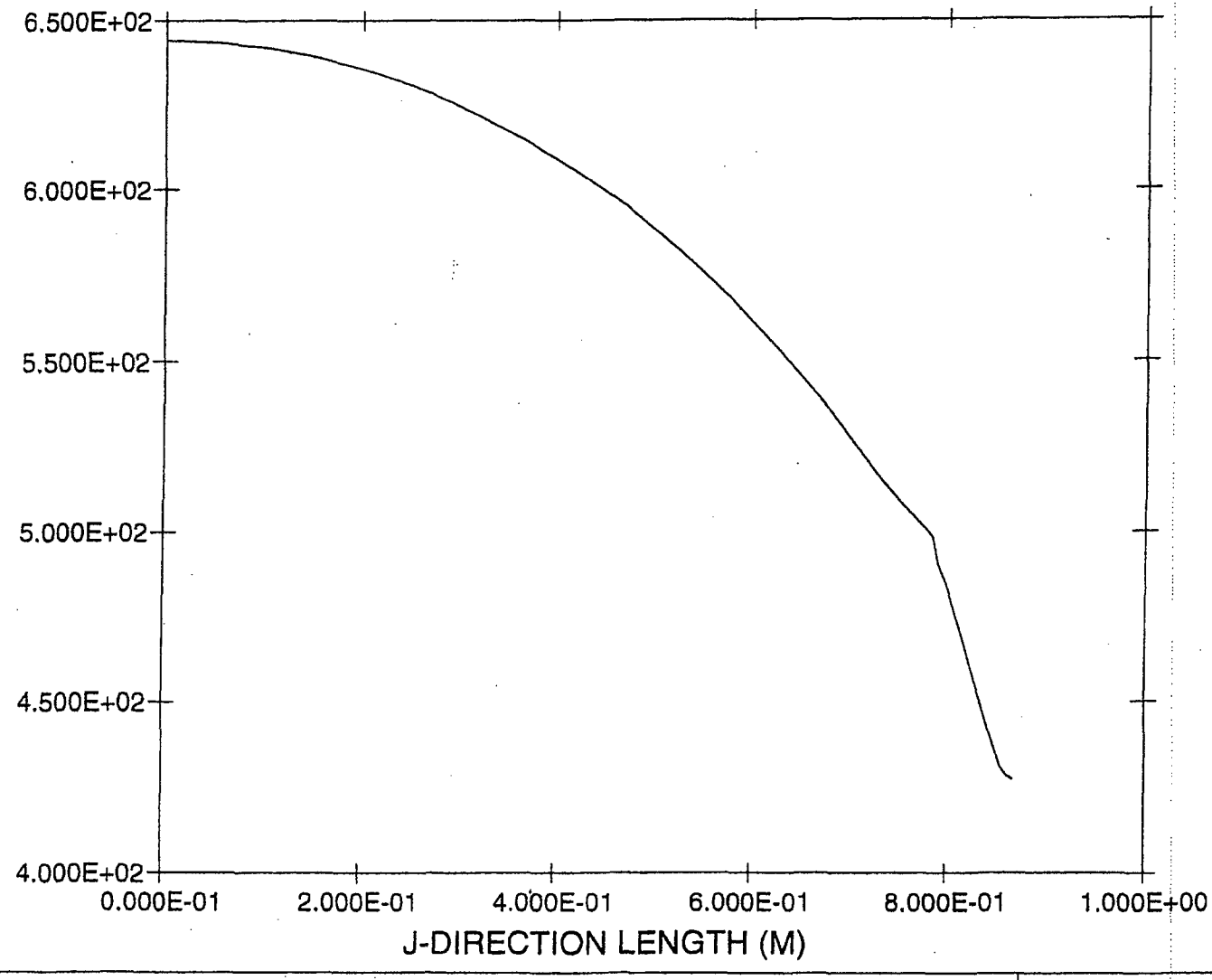

Y, Z, X	FIGURE 3.4.22: MPC-24 RADIAL TEMPERATURE PROFILE Temperature (Kelvin) Vs. Radial Distance (Meters)	May 24 1998 Fluent 4.32 Fluent Inc.

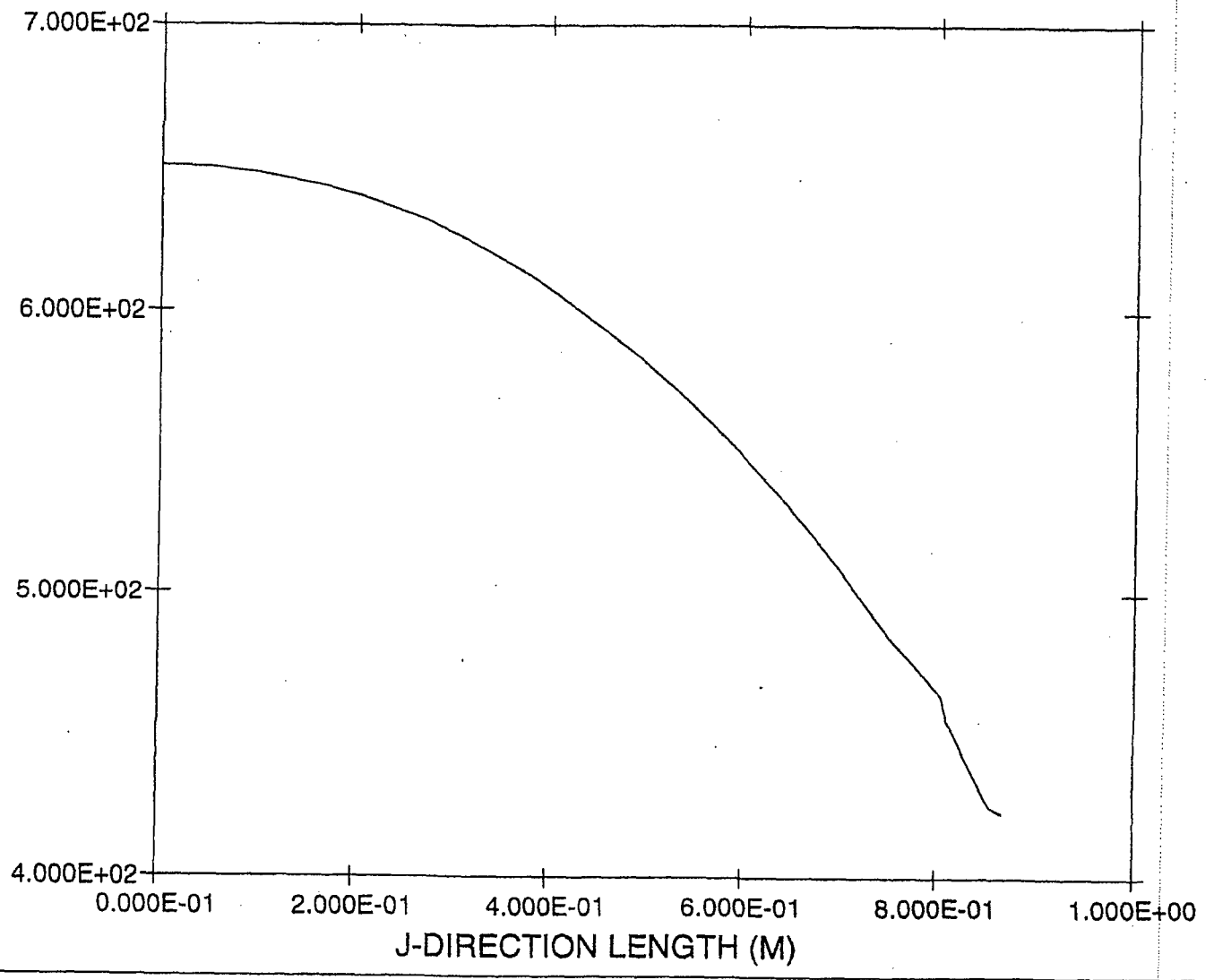

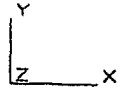

FIGURE 3.4.23: MPC-68 RADIAL TEMPERATURE PROFILE

Temperature (Kelvin) Vs. Radial Position (Meters)

May 24 1998
Fluent 4.32
Fluent Inc.

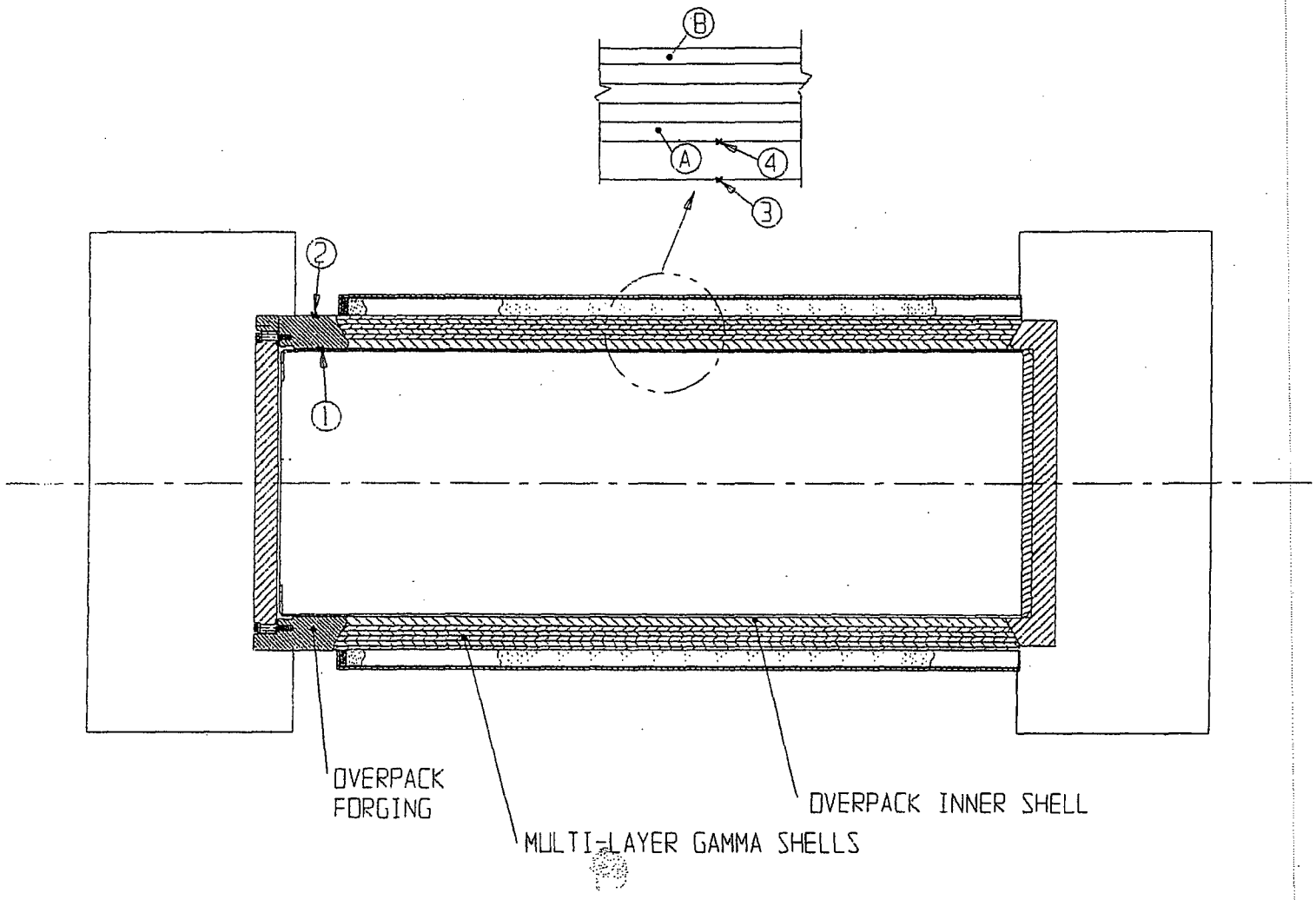

FIGURE 3.4.24; HI-STAR 100 PACKAGE CONTROL LOCATIONS TRACKED IN THE COOLDOWN EVENT

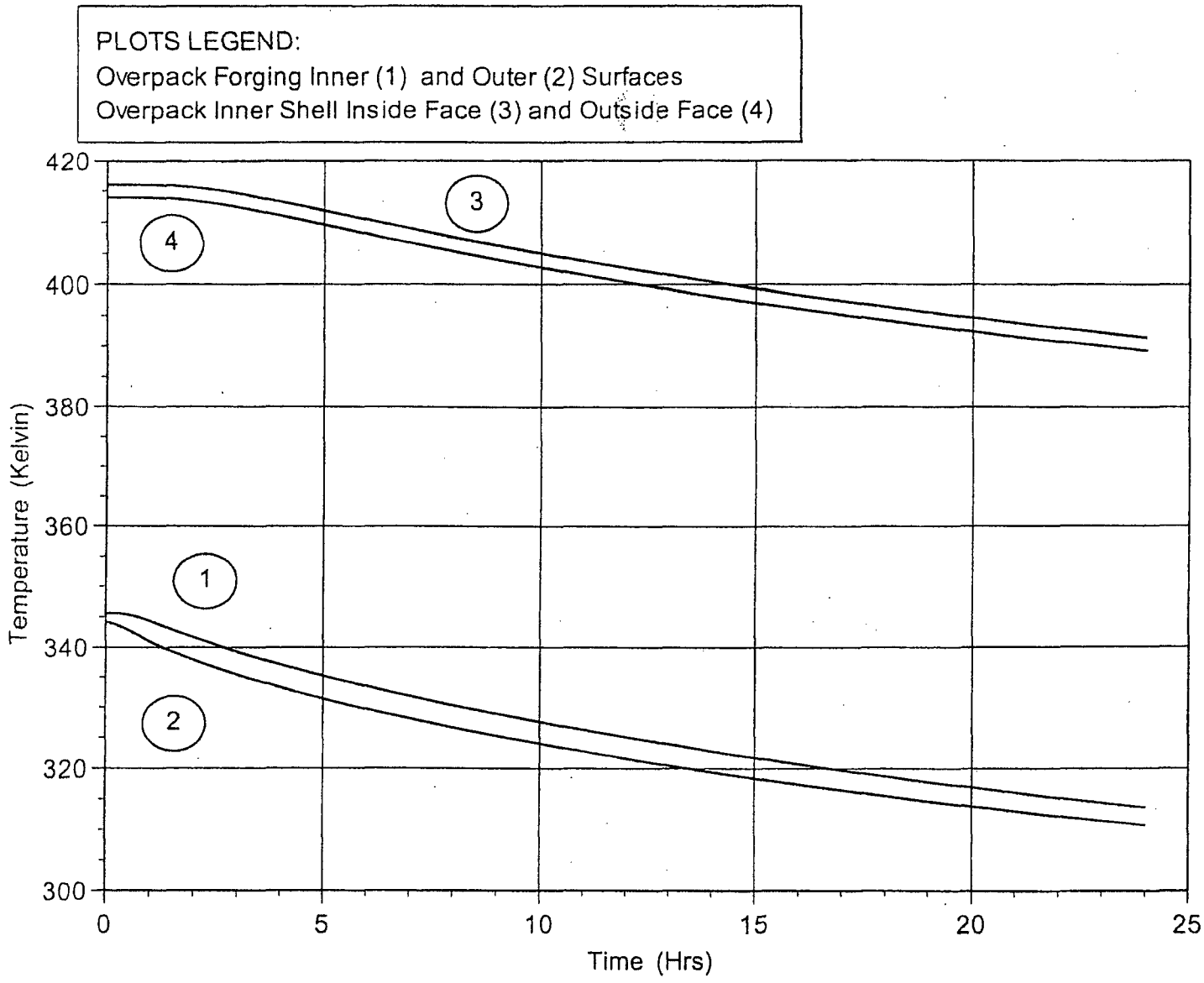

FIGURE 3.4.25: CONTAINMENT BOUNDARY COOLDOWN TEMPERATURE PROFILES

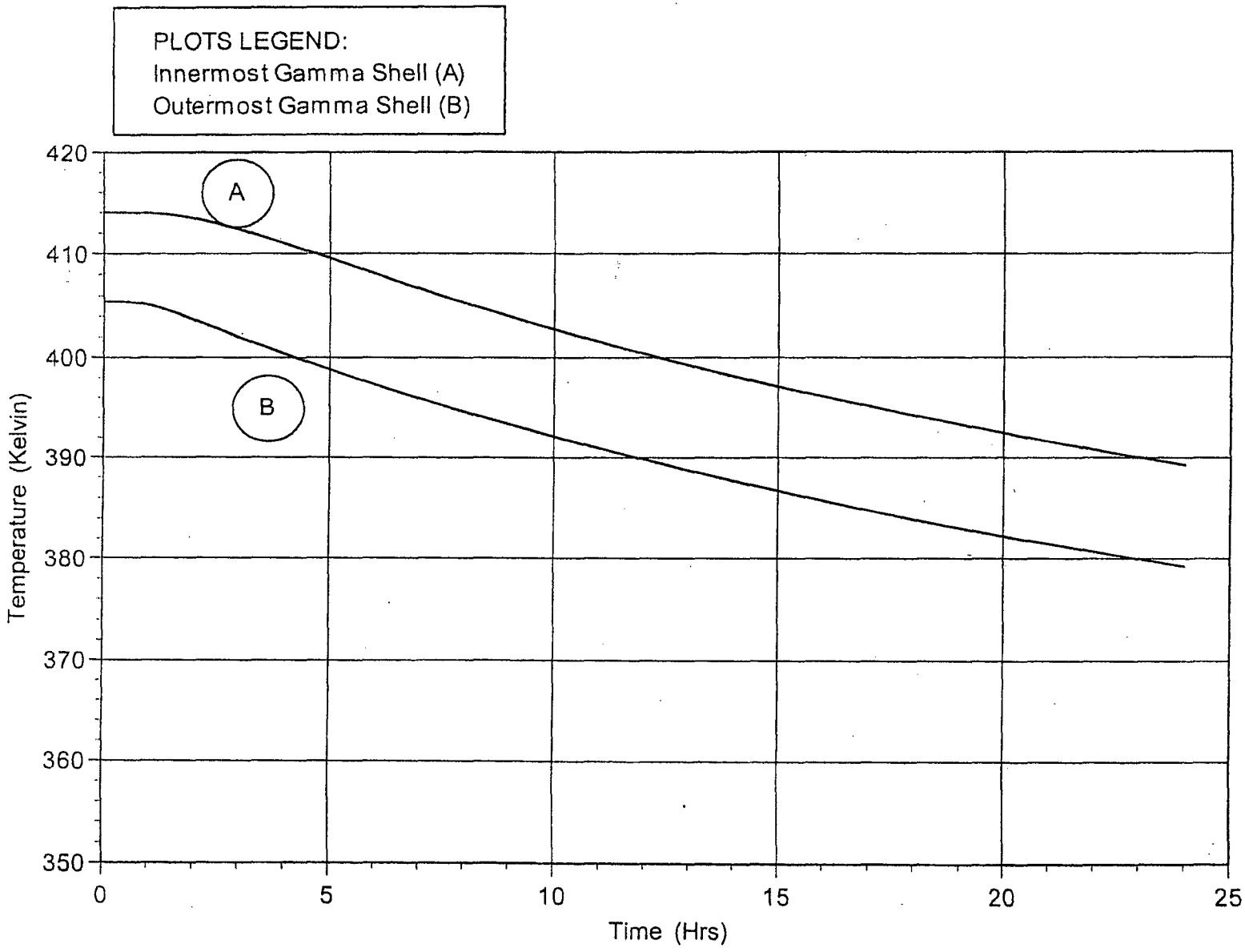

FIGURE 3.4.26: MULTI-LAYERED SHELLS COOLDOWN TEMPERATURE PROFILES

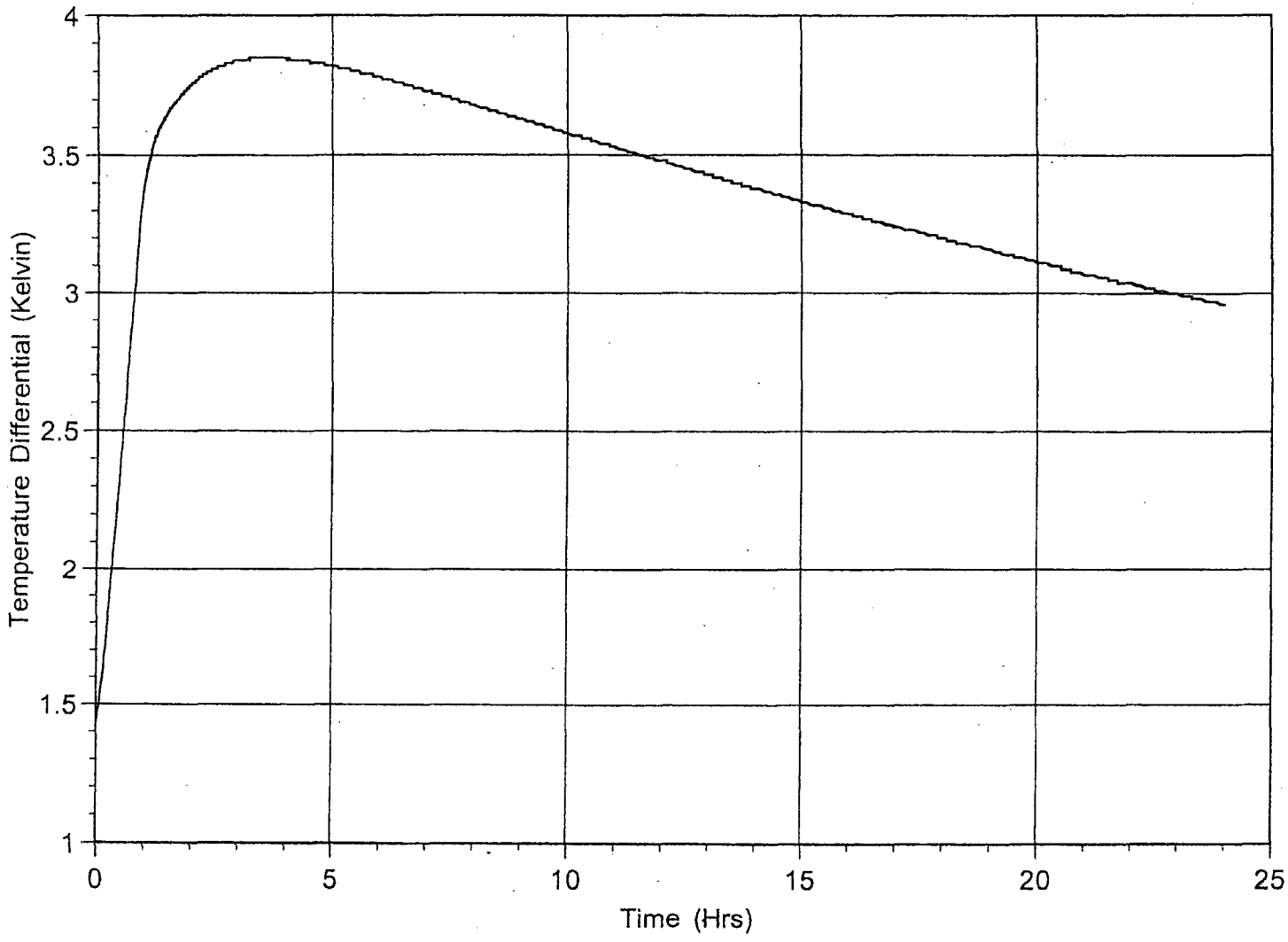

FIGURE 3.4.27: OVERPACK FORGING THROUGH THICKNESS TEMPERATURE GRADIENT DURING COOLDOWN TRANSIENT

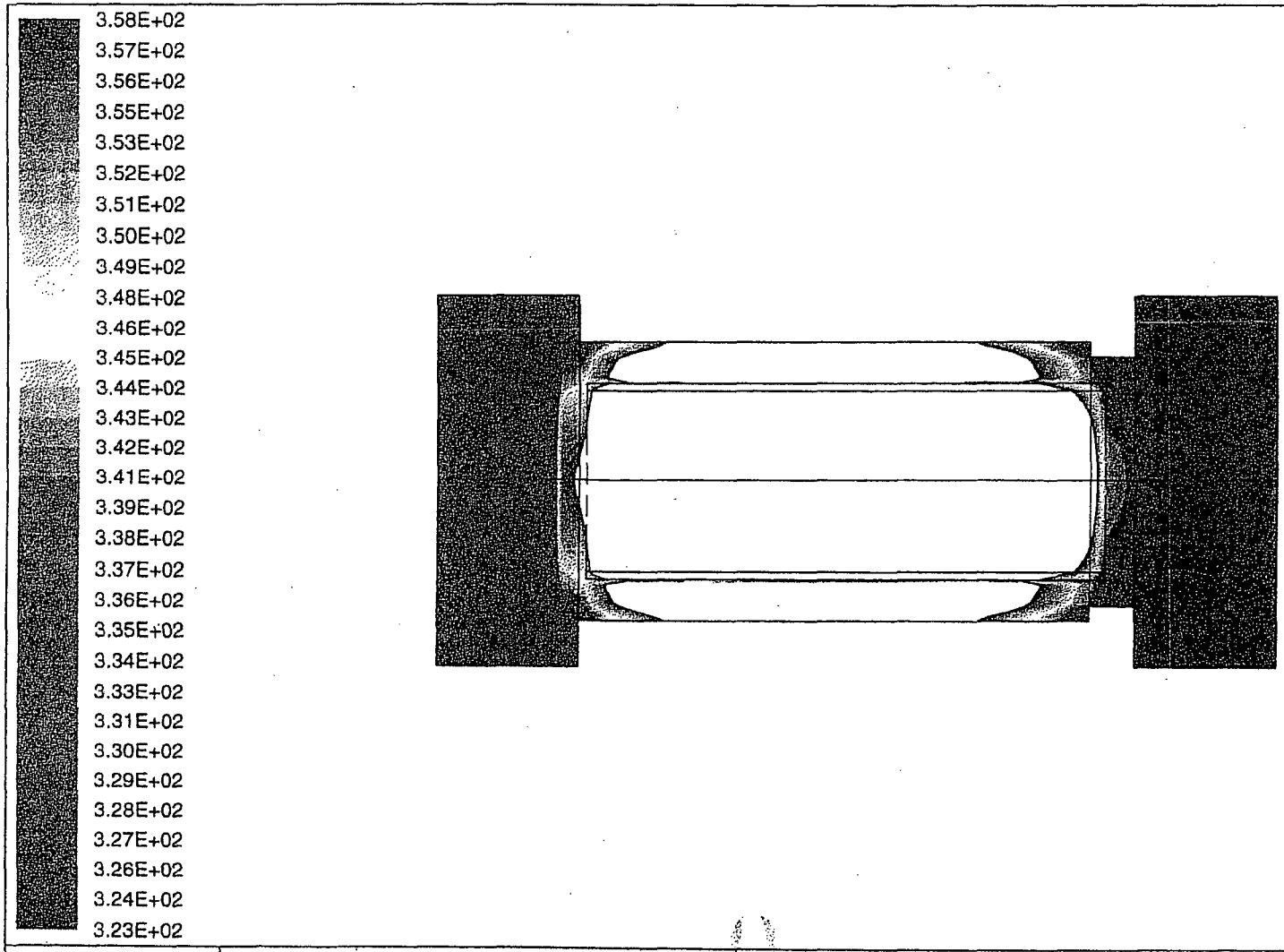

FIGURE 3.4.28: IMPACT LIMITERS SURFACE TEMPERATURE MAP
Temperature (Degrees Kelvin)
Tmax = 3.580E+02 Tmin = 3.232E+02

Feb 04 1999
Fluent 4.32
Fluent Inc.

3.5 HYPOTHETICAL ACCIDENT THERMAL EVALUATION

As mandated by 10CFR71 requirements, the HI-STAR System is subjected to a sequence of hypothetical accident conditions. The objective is to determine and assess the cumulative damage sustained by the system. The accident scenarios specified in order are: (1) a 30 foot free drop onto an unyielding surface; (2) a 40-inch drop onto a mild steel bar; and (3) exposure to a 30-minute fire at 1475°F. The initial conditions for the fire accident specify steady state at an ambient temperature between -20°F and 100°F [3.5.1]. In the HI-STAR System hypothetical fire accident evaluation, full effects of insolation before, during, and after the fire are considered. The effects of the first two drop accidents are evaluated in Chapter 2. In this section, the transient thermal response of the HI-STAR System to a 30-minute fire followed by a post-fire cooldown is determined. The fire accident evaluation is performed by consideration of a worst case combination of factors which conservatively overestimate heat input to the HI-STAR System during the fire followed by an underestimation of the ability of the cask to reject heat to the environment after the fire.

The impact limiters are designed to crush and absorb energy during the hypothetical drops. In the hypothetical fire accident evaluation, the impact limiter is assumed to be crushed to the bounding maximum condition of a solid block of highly conducting aluminum, resulting in increased heat input to the overpack ends through the reduced impact limiter thickness during the fire. The fire condition thermal analysis results are therefore bounding with respect to impact limiter design and amount of crush experienced during a hypothetical drop accident.

A puncture event may locally buckle some of the radial connector plates through the neutron shielding, thereby reducing the ability of the system to reject heat after the fire. As described in Section 2.7, the puncture bar is 6 inches in diameter and correspondingly has a face area of approximately 28.3 in^2. The enclosure shell area is greater than 52,200 in^2. Therefore, while the puncture bar would directly impact less than 0.06% of the exposed area, a conservative 10% reduction in the neutron shield region effective thermal conductivity is considered during the post-fire cooldown phase.

During the initial 30-minute fire event, some of the neutron shield will be exposed to high temperatures. Therefore, in determining heat input to the system, a conservative value maximizing the heat input is utilized for the neutron shield thermal conductivity. During the post-fire cooldown phase, no credit is considered for conduction through the neutron shield material. During the fire, a 10CFR71 mandated cask surface emissivity is considered to maximize radiant heat input to the cask. Destruction of the painted surfaces due to exposure to intense heat during the fire event is a credible possibility. Therefore, the lower emissivity of exposed carbon steel is conservatively considered for post-fire cooldown analysis.

The initial condition prior to the start of the fire accident is based on the bounding normal transport condition MPC basket temperature distribution. The smallest of the four baskets (MPC-24, MPC-24E, MPC-32 and MPC-68) average density and heat capacity are applied to the fire transient analysis. Thus, maximum basket heat load coincident with minimum thermal inertia provides a conservatively bounding response of the HI-STAR System to a fire accident condition.

In the fire event, analyzed in this Section of the SAR, the aim of the analysis is to bound two HI-STAR cask scenarios namely (a) MPCs installed with AHCEs and (b) MPCs without AHCEs. To achieve this objective, the analysis to characterize the response of the HI-STAR package in enveloping a Part 71 fire event assumes that the AHCE heat transfer bridge is present while the fire is raging so that the computed heat flow to the fuel is maximized. Further, the absorptivity of the overpack is increased from its normal operating condition value of 0.85 to the Part 71 value of 0.9. To account for the "no-AHCE" scenario, the emissivity of the overpack is reduced below its normal operating condition value (Table 3.5.2), as soon as the fire event ends, thus retarding the rejection of heat to the environment.

The temperature history of a number of critical control points in the HI-STAR System are monitored during the 30-minute fire and the subsequent relaxation of temperature profiles during the post-fire cooldown phase. The impact of transient temperature excursions on HI-STAR System materials is assessed in this section.

3.5.1 Thermal Model

3.5.1.1 Analytical Model

A thermal transient simulation model to determine the fire condition temperature response is developed on the FLUENT CFD code [3.1.2]. The basic underlying finite volume model is based on the steady-state FLUENT model developed and described in Section 3.4. This basic model is modified by incorporating time dependent thermal loads on the exposed surfaces of the HI-STAR System for determining transient responses at every computational cell defined in the FLUENT model.

The HI-STAR System configuration during a hypothetical fire accident is schematically depicted in Figure 3.5.1. The initial thermal condition of the HI-STAR System prior to the accident condition is the normal transport steady-state temperature distribution. The HI-STAR System is then subjected to a 1475°F fire environment for 30 minutes. During this fire event, the impact limiters installed on both ends are assumed to be in a fully crushed state. This is a conservative assumption which results in an increased heat input to the overpack due to the higher thermal conductivity and reduced thickness of the crushed impact limiter. After 30 minutes, the ambient temperature is restored to 100°F and the HI-STAR System is allowed to proceed through a post-fire cooldown phase. During this entire transient event (fire and post-fire cooldown), the temperature history of several control points in the HI-STAR System is monitored. These points are schematically depicted in Figure 3.5.1.

Heat input to the HI-STAR System while it is engulfed in a fire is from a combination of radiation and forced convection heat transfer to all overpack/impact limiter exposed surfaces. This can be expressed by the following equation:

$$q_F = h_{fc}(T_F - T_s) + \sigma \varepsilon [(T_F + 460)^4 - (T_s + 460)^4]$$

where:

q_F = surface heat input flux (Btu/ft^2-hr)
T_F = fire condition temperature (1475°F)

T_S = transient surface temperature (°F)
h_{fc} = forced convection heat transfer coefficient [Btu/ft-hr-°F]
ε = surface emissivity = 0.9 (per 10CFR71)
σ = Stefan-Boltzmann Constant (0.1714×10^{-8} Btu/ft^2-hr-°R^4)

The forced convection heat transfer coefficient is calculated to bound the convective heat flux contribution to the exposed cask surfaces due to a fire induced air flow velocity of 15 m/s. For the case of air flow past a heated cylinder, Jakob [3.5.2] recommends the following correlation for convective heat transfer, obtained from experimental data:

$$Nu_{fc} = 0.028\, Re^{0.8} \left[1 + 0.4 \left(\frac{L_{st}}{L_{tot}}\right)^{2.75} \right]$$

where:

L_{tot} = length traversed by flow
L_{st} = length of unheated section
K_f = thermal conductivity of air evaluated at the average film temperature
Re = flow Reynolds Number based on L_{tot}
Nu_{fc} = Nusselt Number ($h_{fc}\, L_{tot}/K_f$)

Consideration of the wide range of temperatures to which the exposed surfaces are subjected to during the fire and the temperature dependent trend of air properties requires a careful selection of parameters to determine a conservatively large bounding value of the convective heat transfer coefficient. In Table 3.5.1, a summary of the parameter selections with justifications provides an appropriate basis for application of this correlation to determine forced convection heating of the HI-STAR System during the short-term fire event.

After the 30-minute fire event, the ambient temperature is restored to 100°F. The HI-STAR System cools down during this post-fire cooldown phase. Heat loss from outside exposed surfaces of the overpack is determined by the following equations:

$$q_S = 0.18\,(T_S - T_A)^{4/3} + \sigma\,\varepsilon\,[(T_S + 460)^4 - (T_A + 460)^4]$$

where:

q_s= surface heat loss flux (Btu/ft^2-hr)
T_S = transient surface temperature (°F)
T_A = ambient temperature (100°F)
ε = surface emissivity
σ = Stefan-Boltzmann Constant (0.1714×10^{-8} Btu/ft^2-hr-°R^4)

During the fire event, some region of Holtite will be overheated and thus lose its ability to conduct heat. In the fire transient analysis, full credit is given to conduction through Holtite to conservatively increase heat input to the overpack. In the post-fire cooldown phase, all of the Holtite is conservatively assumed to be lost (no conduction through Holtite material).

During the 30-foot drop and puncture accident events, the mechanical integrity of the HI-STAR System is maintained. From a thermal analysis standpoint, the impact limiters are crushed and there

is at most localized damage to radial channels. While the resulting localized damage would not significantly degrade the heat transfer ability of the Holtite region, a 10% effective conductivity reduction is conservatively (as described earlier in Section 3.5) applied during the post-fire cooldown phase. In Table 3.5.2, a summary of inputs used in the determination of the effect of a hypothetical fire accident is provided.

3.5.1.2 Test Model

For determining the transient response of the HI-STAR System under a hypothetical fire accident condition, a detailed finite volume model has been developed on the validated and benchmarked FLUENT code. The dynamic model features several conservative assumptions to bound temperature excursions during the heat up and cooldown phases of the accident. Accordingly, development of a separate test model to verify the results is not considered necessary. Evaluation of the HI-STAR System thermal design in the event of a hypothetical fire event is shown to be in compliance with 10CFR71 requirements.

3.5.2 System Conditions and Environment

The HI-STAR System is shown to maintain its mechanical integrity following a 30 foot drop and puncture accident with stresses within applicable ASME Code requirements. The impact limiters absorb the impact forces and are crushed in the drop event. Completely crushed impact limiters provide a conservatively limiting situation for increased heat absorption during the 30-minute fire. The effect of a puncture accident results in localized damage to the radial connectors embedded in Holtite neutron shielding. This will *not* reduce the heat transfer capability of the region containing Holtite by a significant factor. The fire is specified to be at a temperature of 1475°F and last for 30 minutes. Emissivity of all exposed surfaces is set to 0.9. Some of the Holtite will decompose and lose its ability to conduct heat during the fire event due to exposure to severe temperature conditions. Thermal analysis of the HI-STAR System is performed by postulating worst case conditions whereby increased heat absorption takes place during the 30-minute fire and a reduced ability of the HI-STAR System to reject heat takes place during the post-fire cooldown phase.

3.5.3 System Temperatures

The hypothetical fire accident condition is evaluated by imposing a 1475°F fire temperature for 30 minutes followed by a post-fire equilibrium phase that is followed for more than 30 hours. The temperature-time history of several control points is monitored. These points are selected because of their importance relating to safety evaluation. In Figures 3.5.2 to 3.5.4, the transient temperature profiles of the monitored points shown in Figure 3.5.1 are plotted. From these plots, the temperature of exposed surfaces is seen to increase rapidly and peak at about 1348°F at the end of the fire (i.e., 30 minutes). Figure 3.5.5 shows the peak axial fuel cladding temperature profile during post-fire cooldown. In the post-fire equilibrium phase, there is an initial rapid cooldown of the peak surface temperature followed by an asymptotic approach to the final steady-state condition. The closure bolts and mechanical seals peak temperatures are below short-term limits. The MPC basket center temperature rises sluggishly to a broad peak and then slowly decays to a final steady-state condition. Portions of Holtite neutron shielding material near the overpack enclosure shell experience a short duration high temperature excursion. The crushed aluminum alloy inside the impact limiter begins to

melt at 1105°F. The latent heat of melting of aluminum alloy during the melting phase would absorb the incident heat flux from the fire. This ablation mechanism will protect the cask by limiting the surface temperature excursion and restricting the amount of heat input to the overpack lid. In the HI-STAR System fire transient evaluation, credit for this protective feature is not considered.

The HI-STAR fire event model is depicted in Figure 3.5.6. Fire condition containment boundary through thickness temperature profiles are presented in Figures 3.5.7, 3.5.8, and 3.5.9 across Sections A-A, B-B, and C-C, as shown in Figure 3.5.6. The figures present through-thickness temperature profiles at the end of the 30-minute fire and 60 minutes after the start of the fire (30 minutes into the post-fire cooldown period).

In the fire event, the dominant heat input source is located on the outside of the cask. The temperature gradient, as seen in Figures 3.5.7, 3.5.8, and 3.5.9, is reversed from the normal condition, with the maximum temperature occurring at the outermost layer. From Figure 3.5.7, it is apparent that the overpack inner shell remains below the 500°F short-term design basis temperature limit. At the end of the 30-minute fire, the outermost layer of the multi-layered shells is heated to approximately 540°F. During the post-fire cooldown phase the temperature of this outer layer rapidly drops below 500°F, as shown on the 60-minute profile.

An examination of the overpack forging temperature profile (Section B-B, Figure 3.5.8) shows that the outer layers of the forging, directly adjacent to the surface exposed to the fire, are heated to in excess of 700°F during the fire. The bulk of the forging metal mass (in excess of 6 inches out of the total 8.5 inches) remains below the 700°F short-term design basis temperature limit. The portion of the overpack forging which is covered by the impact limiters remains below 700°F both during and after the fire. This is illustrated by the temperature profiles presented in Figure 3.5.9.

The following observations can be drawn from an examination of Figures 3.5.6 through 3.5.9:

- The containment boundary regions that are within the confines of the multi-layered shells remain below 500°F.
- The containment boundary regions that are within the confines of the impact limiters remain below 700°F.
- The bulk of the containment boundary in the regions that are directly exposed to the fire remain below 700°F.

The outer region of the HI-STAR 100 overpack consists of forty sector shaped annular spaces enclosed in half inch thick carbon steel plates. These annular spaces contain Holtite-A neutron absorber material. Holtite-A is a stable material under the environmental and thermal conditions corresponding to normal operation. Under a fire condition, the temperature in the enclosure shell cavity rises resulting in loosening of the water intermolecular bonds to the neutron shield material leading to liberation of water vapor. For conservatism, a 6% weight loss factor for the neutron shield when exposed to a direct fire is assumed. Under a conservatively postulated scenario wherein all of the radial neutron shield material (approximately 12,850 lbs required to completely fill the forty

spaces) is exposed to a direct fire, 771 lbs of water vapor (i.e 6% of neutron shield) generation in 30 minutes is required to be expelled from the neutron shield cavities. To protect the enclosure shell from overpressure, two rupture discs (each having the required vapor expulsion capacity) are incorporated in the HI-STAR overpack design. The rupture discs have a relatively low set pressure (30 psig) to relieve water vapor if the generation is rapid during a fire condition.

3.5.4 Maximum Internal Pressure

Based on bounding transient temperature excursions calculated for the HI-STAR System during a hypothetical fire accident condition, maximum calculated cask internal pressures are reported in Table 3.5.3. Maximum pressure calculations assume 100% of the fuel rods rupture, releasing conservatively determined rod fill gas and fission gases volumes into the MPC cavity.

3.5.5 Maximum Thermal Stresses

Maximum thermal stresses generated during transient temperature excursions within the HI-STAR System are reported in Chapter 2.

3.5.6 Evaluation of System Performance for the Hypothetical Accident Thermal Conditions

The HI-STAR System was subjected to a hypothetical fire accident condition with the impact limiters crushed and enclosure shell punctured as a result of previously imposed drop and puncture accidents. However, mechanical integrity of the overpack intermediate and inner shells, mechanical seals, and MPC shell is retained. During the fire accident event, portions of neutron shielding material in the overpack enclosure shell experience high transient temperature excursions and thus partially lose the ability to conduct heat and shield neutrons. Portions of aluminum alloy inside the crushed impact limiters near the exposed surfaces melt, but do not ignite.

For assessing the impact of transient temperature excursions on the integrity of the HI-STAR System, the significant components and quantities of interest are the closure plate bolts temperatures, the mechanical seals temperatures, the neutron shield temperature, the peak pressure and the peak fuel cladding temperature. The closure plate bolts maintain their ability to hold the seals. The neutron shield material in the post-accident shielding analysis is conservatively assumed to be completely lost. The peak system pressure remains below the design basis accident pressure. The fuel cladding temperature peak does not exceed short-term accident limits. Consequently, the HI-STAR System integrity during the most severe fire event followed by a post-fire cooldown phase is not compromised. In Table 3.5.4, a summary of peak HI-STAR System component temperatures during fire and post-fire accident conditions is provided. The calculated results demonstrate that the HI-STAR System is in compliance with 10CFR71 thermal requirements for hypothetical accident conditions of transport.

Table 3.5.1

SUMMARY OF TEMPERATURE-DEPENDENT FORCED CONVECTION HEAT TRANSFER CORRELATION PARAMETERS FOR AIR

Parameter	**Trend with Increasing Temperatures**	**Criteria to Maximize h_{fc}**	**Conservative Parameter Value**	**Evaluated At**
Temperature Range	100°F-1475°F	NA	NA	NA
Density	Decreases	Reynolds Number	High	100°F
Viscosity	Increases	Reynolds Number	Low	100°F
Conductivity (K_f)	Increases	h_{fc} Proportional to K_f	High	1475°F

Table 3.5.2

SUMMARY OF HYPOTHETICAL FIRE ACCIDENT INPUTS

		Steady-State Initial† Condition	**30-minute Fire**	**Post-Fire Equilibrium**
1.	Conduction through Holtite	No	Yes	No
2.	Holtite Region Conductivity Reduction (Loss of Radial Connectors)	No	No	Yes
3.	Insolation	Yes	Yes	Yes
4.	Radiation Heat Transfer	Yes	Yes	Yes
5.	Surface Convection	Natural	Forced	Natural
6.	Impact Limiters Installed††	Yes	Yes (crushed)	Yes (crushed)
7.	Surface Emissivity	0.85	0.9	0.66

† A bounding initial temperature condition is imposed for fire transient analysis.

†† Based on minimum 15,000 lbs impact limiter weight modeled as a solid aluminum cap to maximize heat input to cask.

Table 3.5.3

MAXIMUM HI-STAR SYSTEM HYPOTHETICAL FIRE CONDITION EVENT PRESSURES†

Condition	**Pressure (psig)**			
	MPC-24	**MPC-68**	**MPC-24E**	**MPC-32**
Without fuel rods rupture	99.6	98.0	99.6	99.6
With 100% fuel rods rupture	143.8	128.5	145.2	160.9

† Pressure analysis is based on release of 100% of the rods fill gas and 30% of the significant radioactive gases from a ruptured rod.

Table 3.5.4

MAXIMUM HI-STAR SYSTEM COMPONENTS AND MATERIALS TEMPERATURES DURING AND AFTER HYPOTHETICAL FIRE CONDITION

Material/Component	Initial Condition (°F)	During Fire (°F)	Post Fire Cooldown (°F)	Accident Limit (°F)
Fuel cladding	708	708	751	1058
Overpack closure bolts	159	415	514	600
Overpack closure plate seals	160	392	490	1200
Drain port plug seal	259	645	662	932
Vent port plug seal	160	283	443	932
Holtite outer surface	223	1232	1232	N/A†
Holtite inner surface	259	604	604	N/A
MPC shell	309	313	419	775
Impact limiter surface	127	983	983	1105
Overpack outer enclosure	226	1348	1348	1350

† Holtite is conservatively assumed to be completely lost during the fire accident.

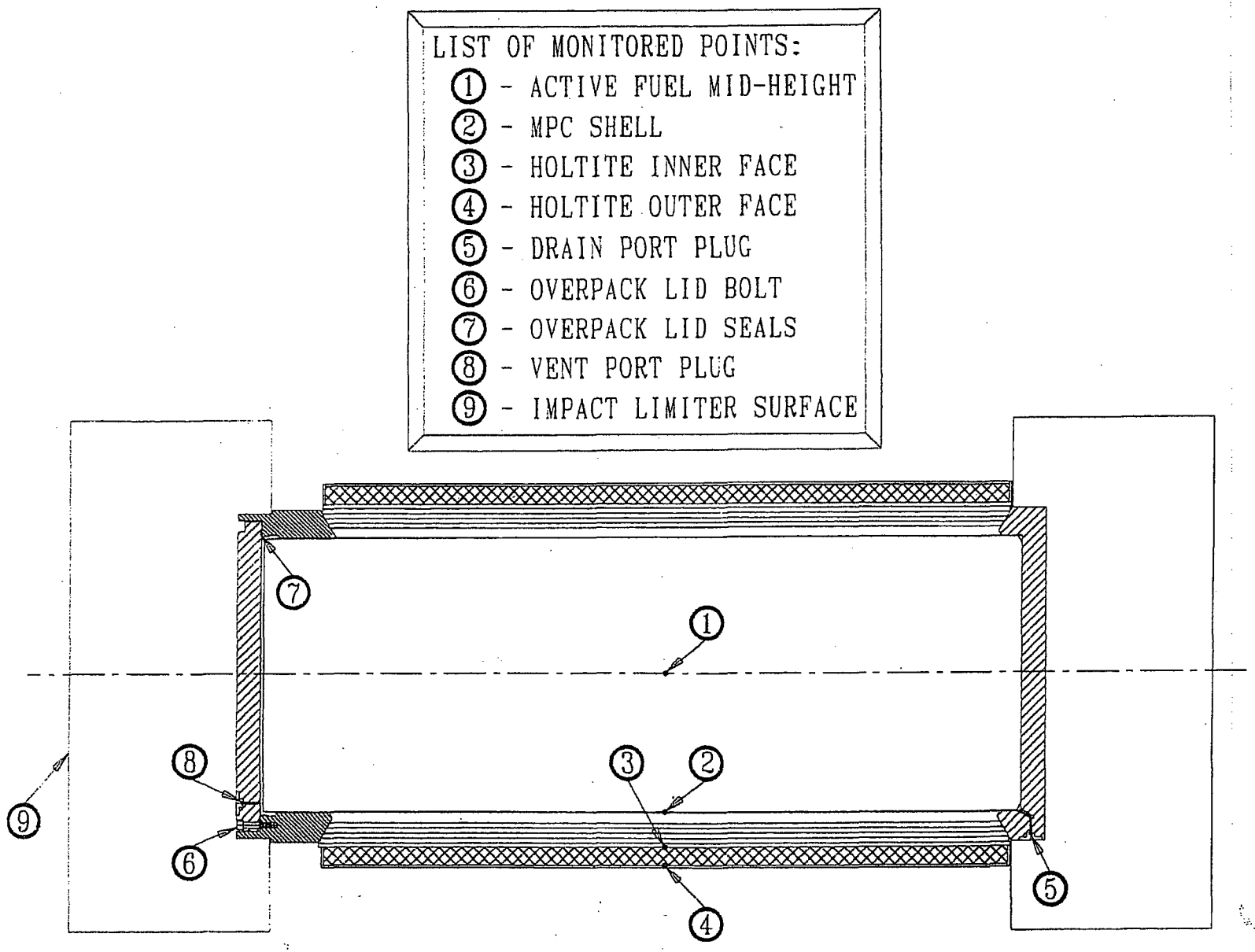

FIGURE 3.5.1; LOCATION OF HI-STAR 100 PACKAGE CONTROL POINTS MONITORED DURING HYPOTHETICAL FIRE ACCIDENT CONDITION

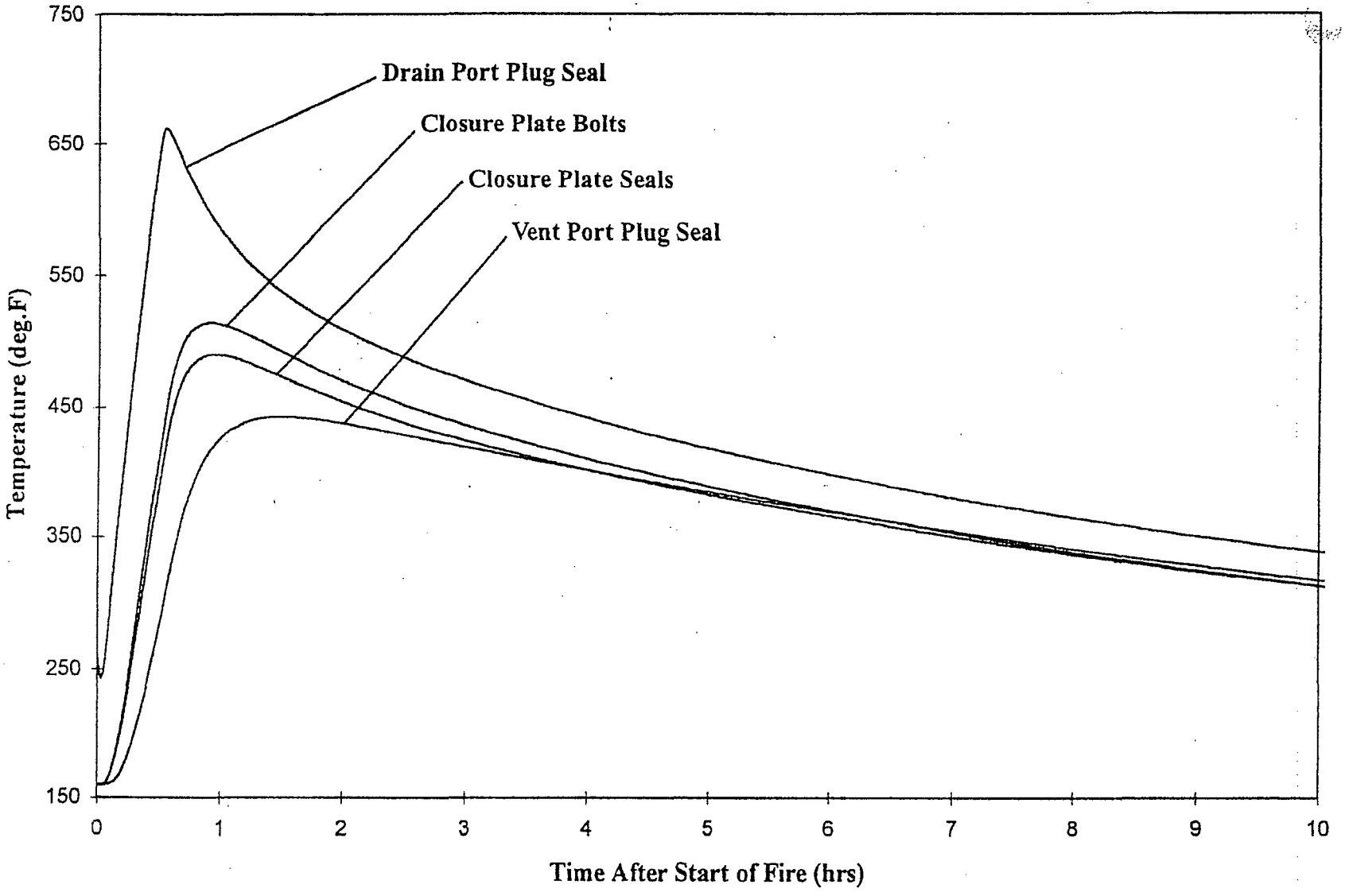

FIGURE 3.5.2; HI-STAR 100 PACKAGE CONTAINMENT BOUNDARY COMPONENTS FIRE ACCIDENT TRANSIENT TEMPERATURE RESPONSE

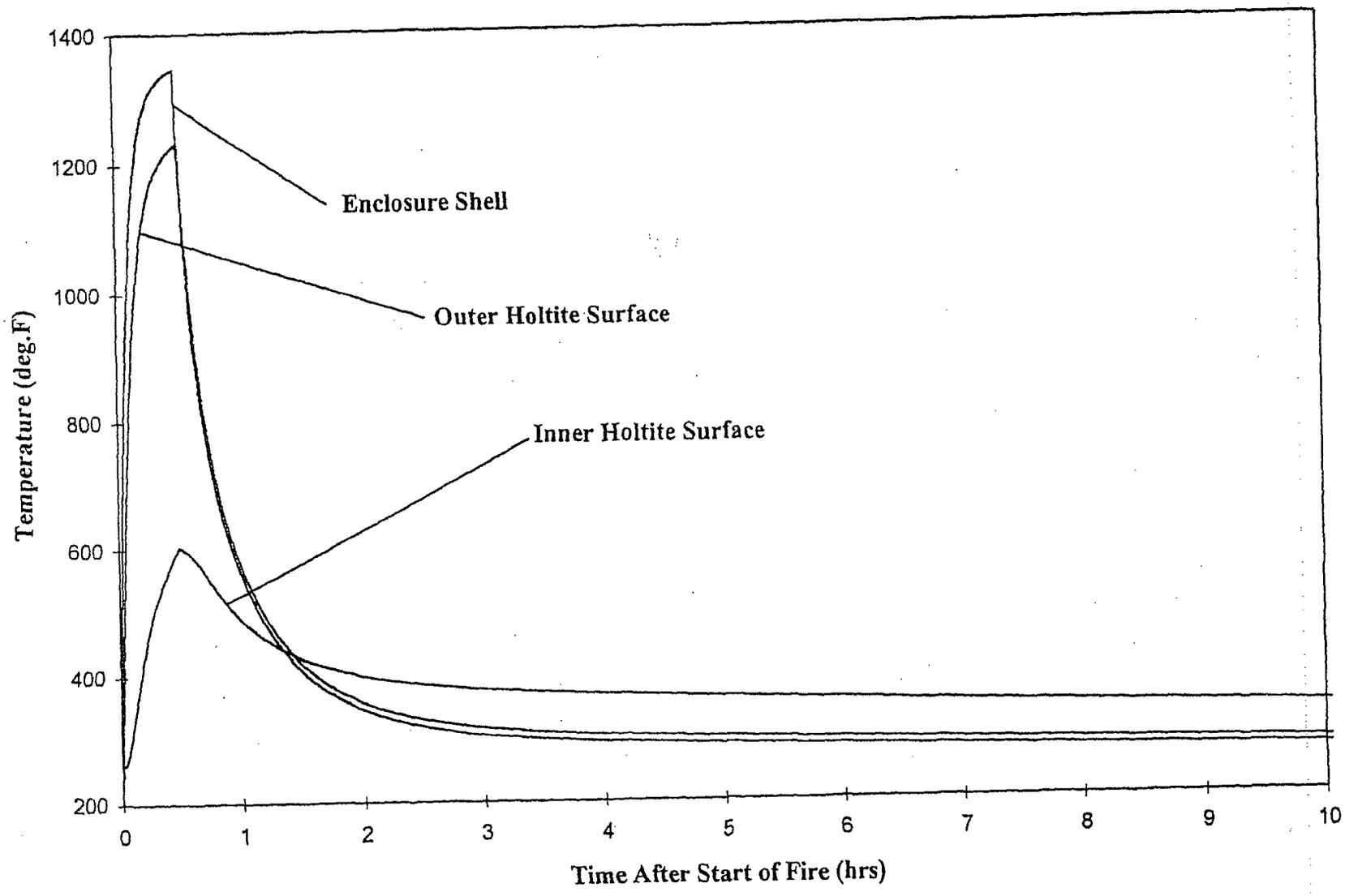

FIGURE 3.5.3; HI-STAR 100 PACKAGE NEUTRON SHIELDING REGION FIRE ACCIDENT TRANSIENT TEMPERATURE RESPONSE

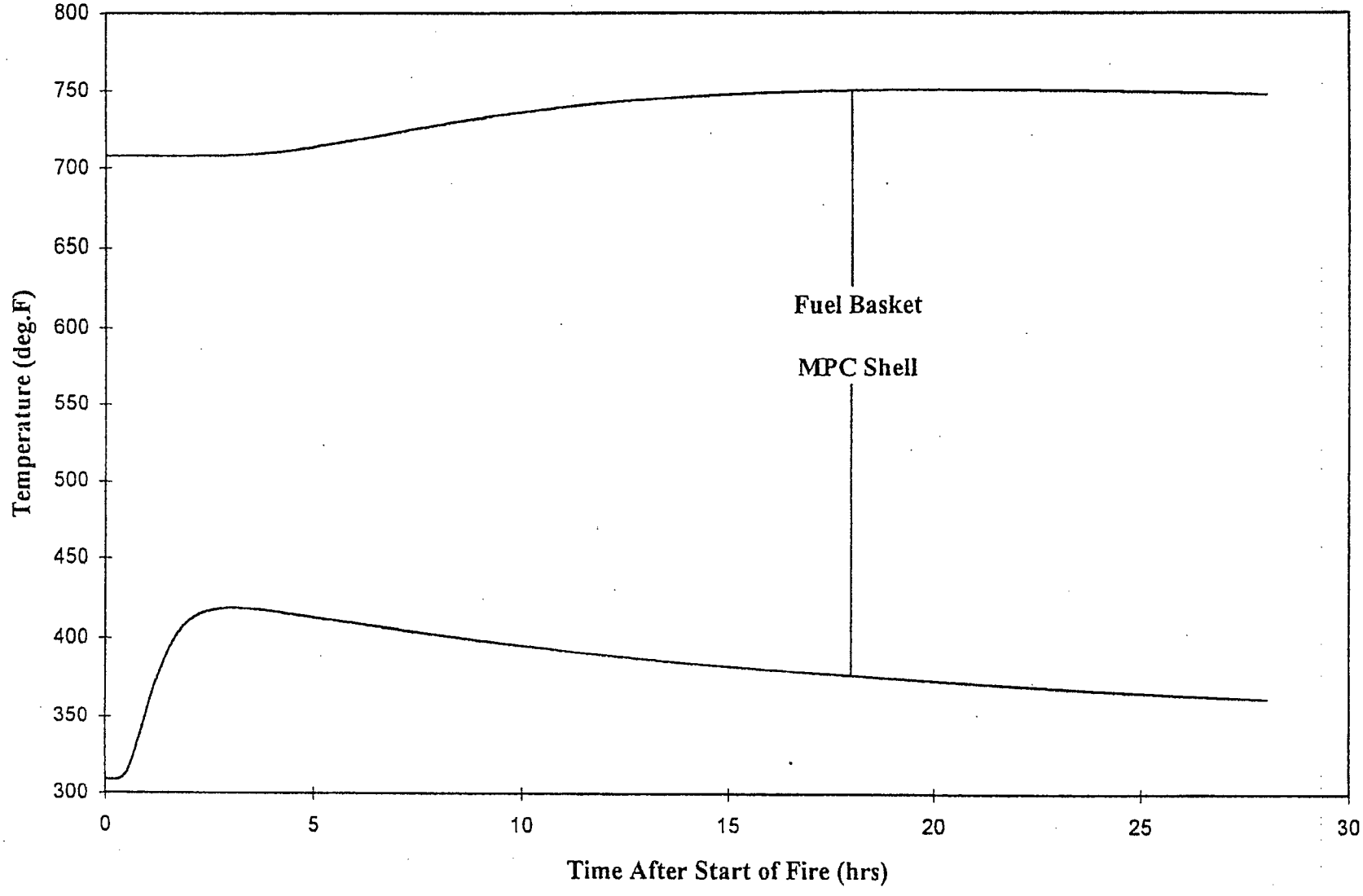

FIGURE 3.5.4; HI-STAR 100 PACKAGE MPC SHELL AND FUEL BASKET FIRE ACCIDENT TRANSIENT TEMPERATURE RESPONSE

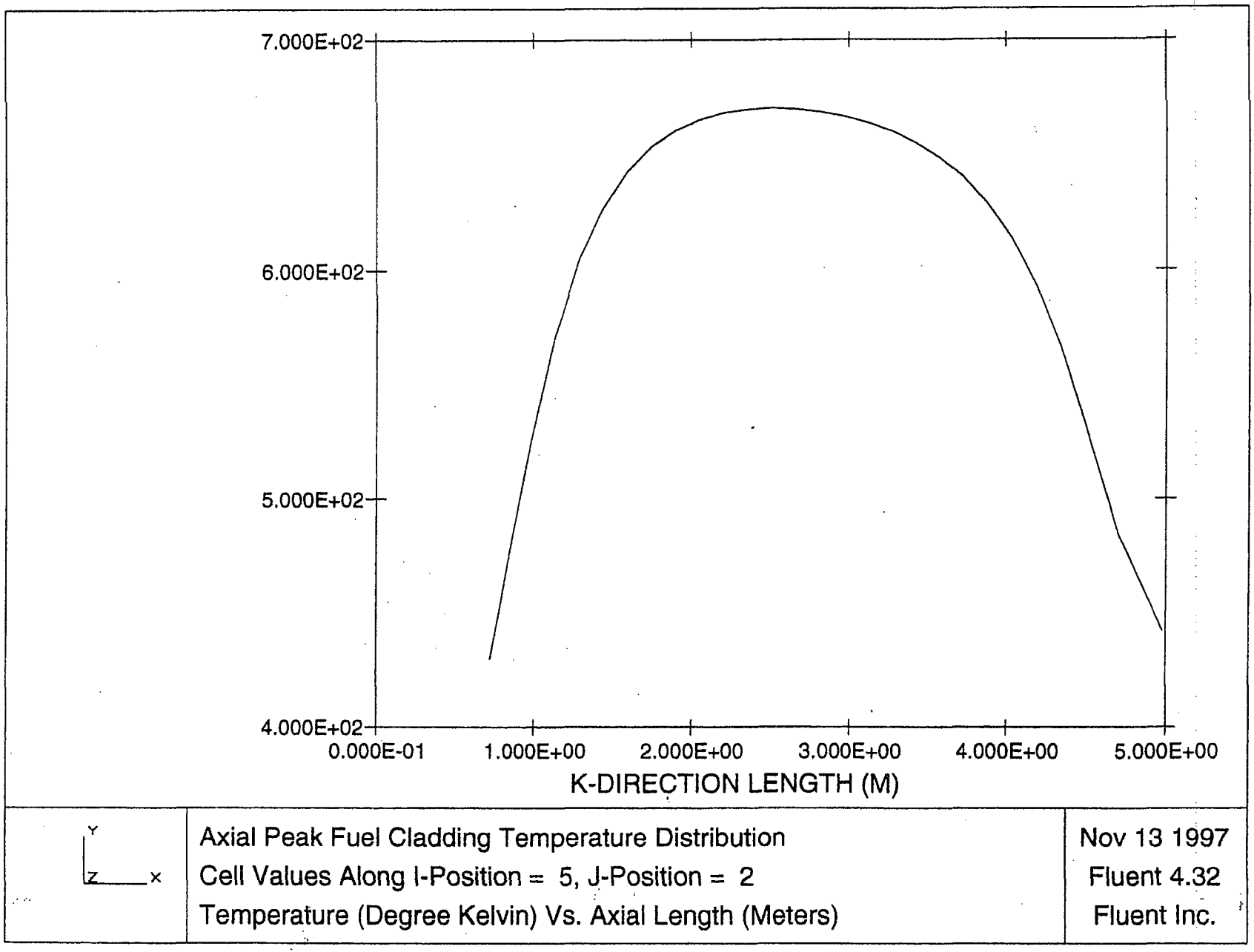

FIGURE 3.5.5: FUEL CLADDING PEAK AXIAL TEMPERATURE DISTRIBUTION DURING POST FIRE COOLDOWN

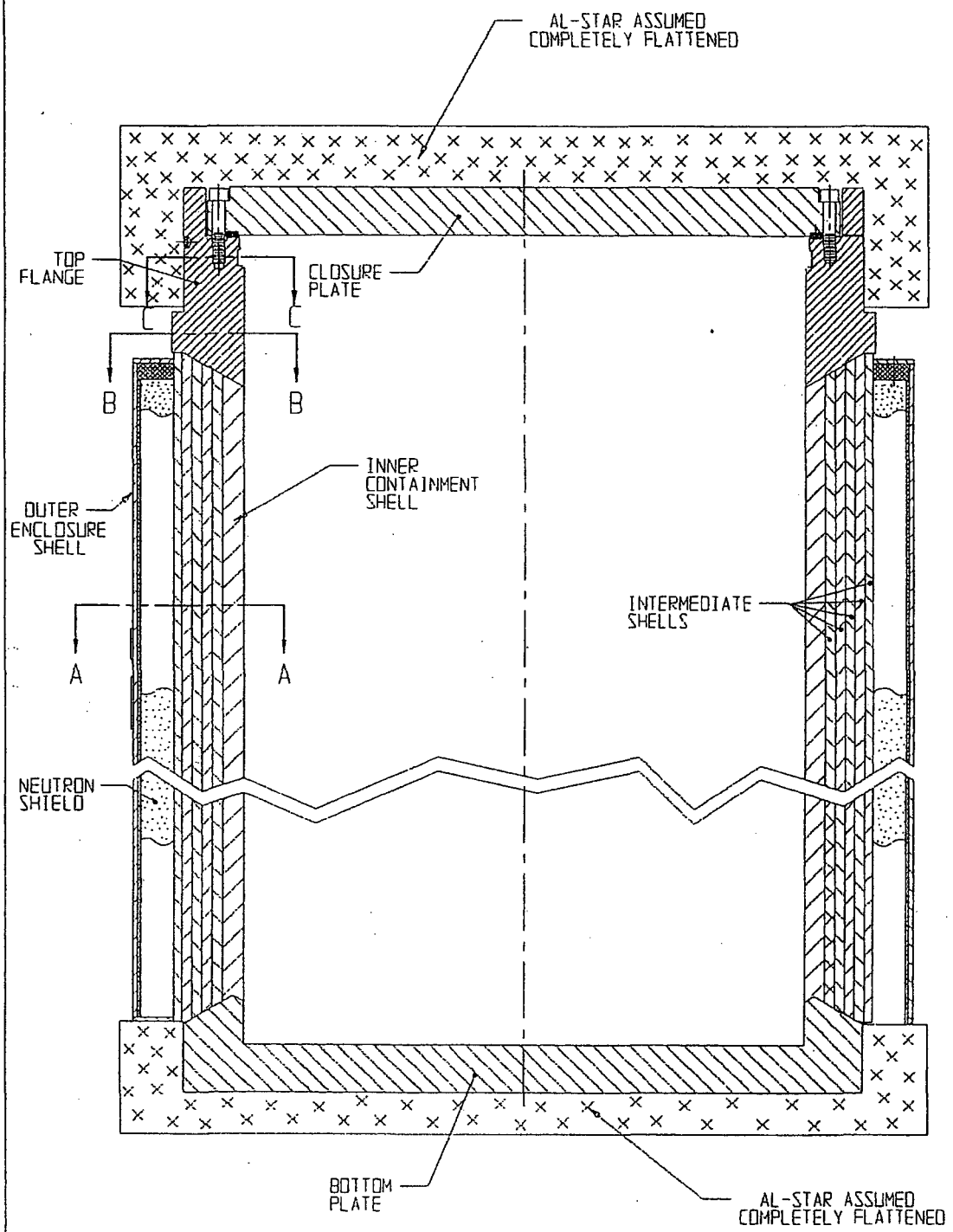

FIGURE 3.5.6; HI-STAR MODEL FOR TRANSPORT FIRE

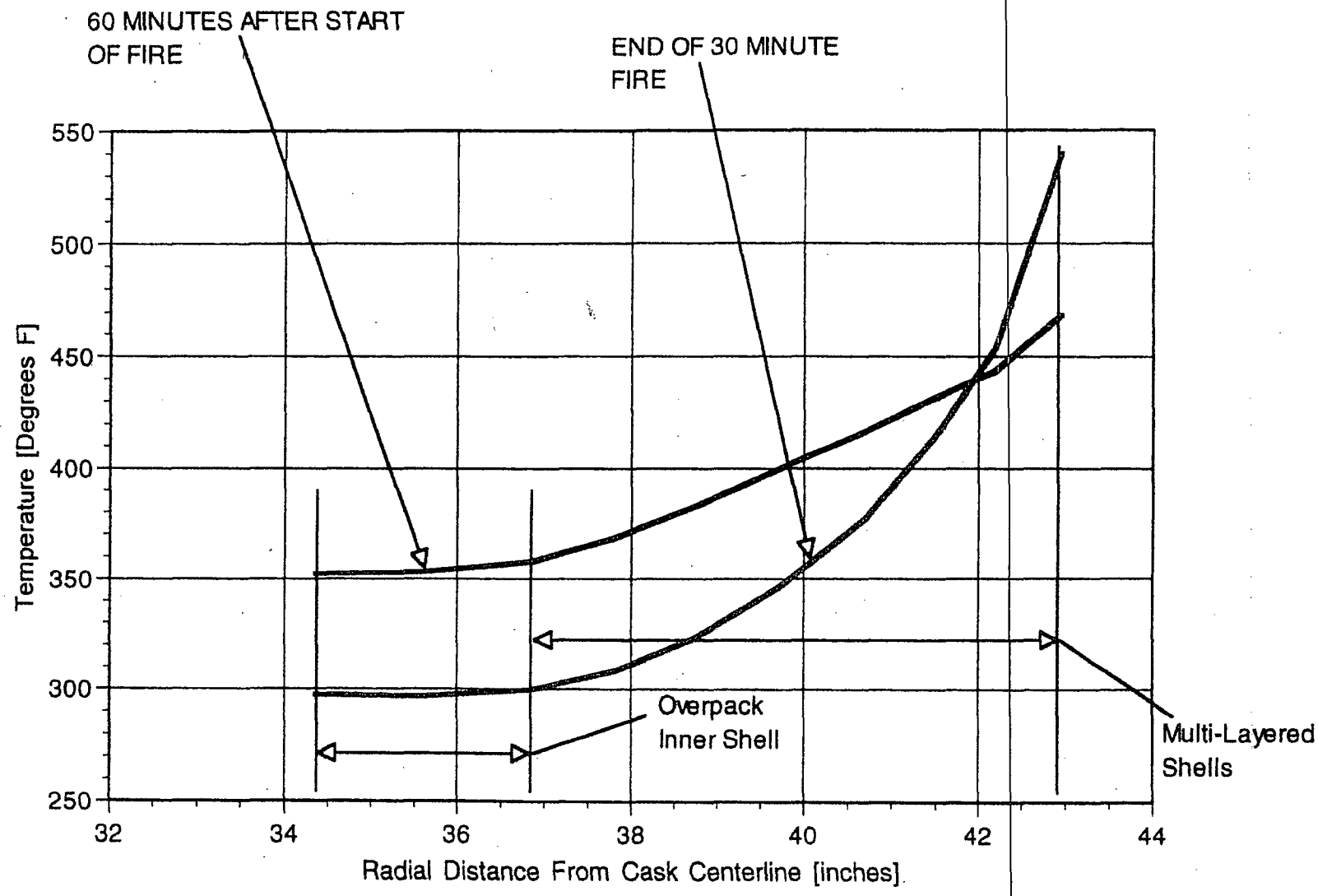

FIGURE 3.5.7: TRANSPORT FIRE CONDITION CONTAINMENT BOUNDARY AND LAYERED SHELLS TEMPERATURE DISTRIBUTIONS (SECTION A-A)

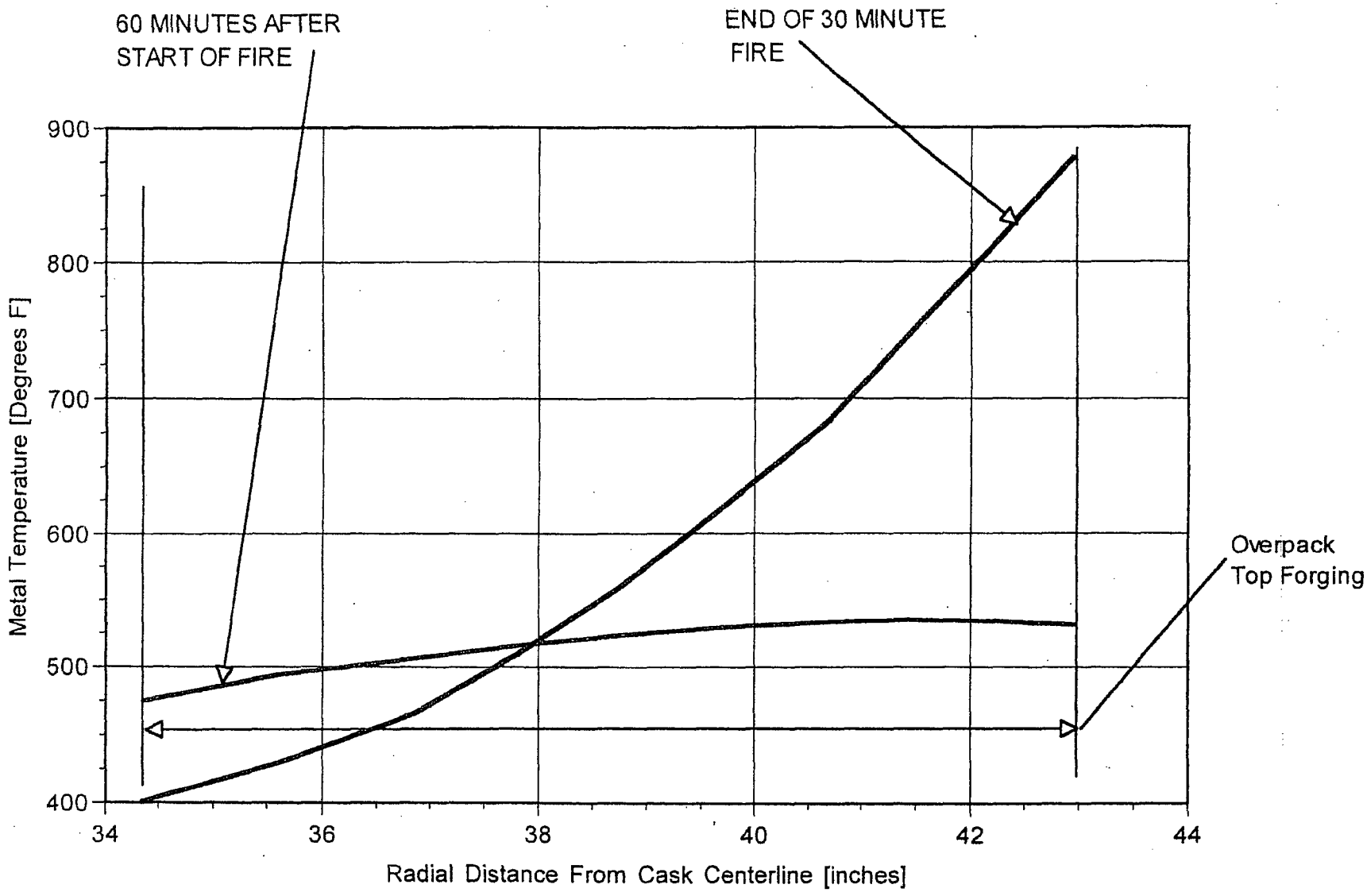

FIGURE 3.5.8: TRANSPORT FIRE CONDITION OVERPACK TOP FORGING TEMPERATURE DISTRIBUTIONS (SECTION B-B)

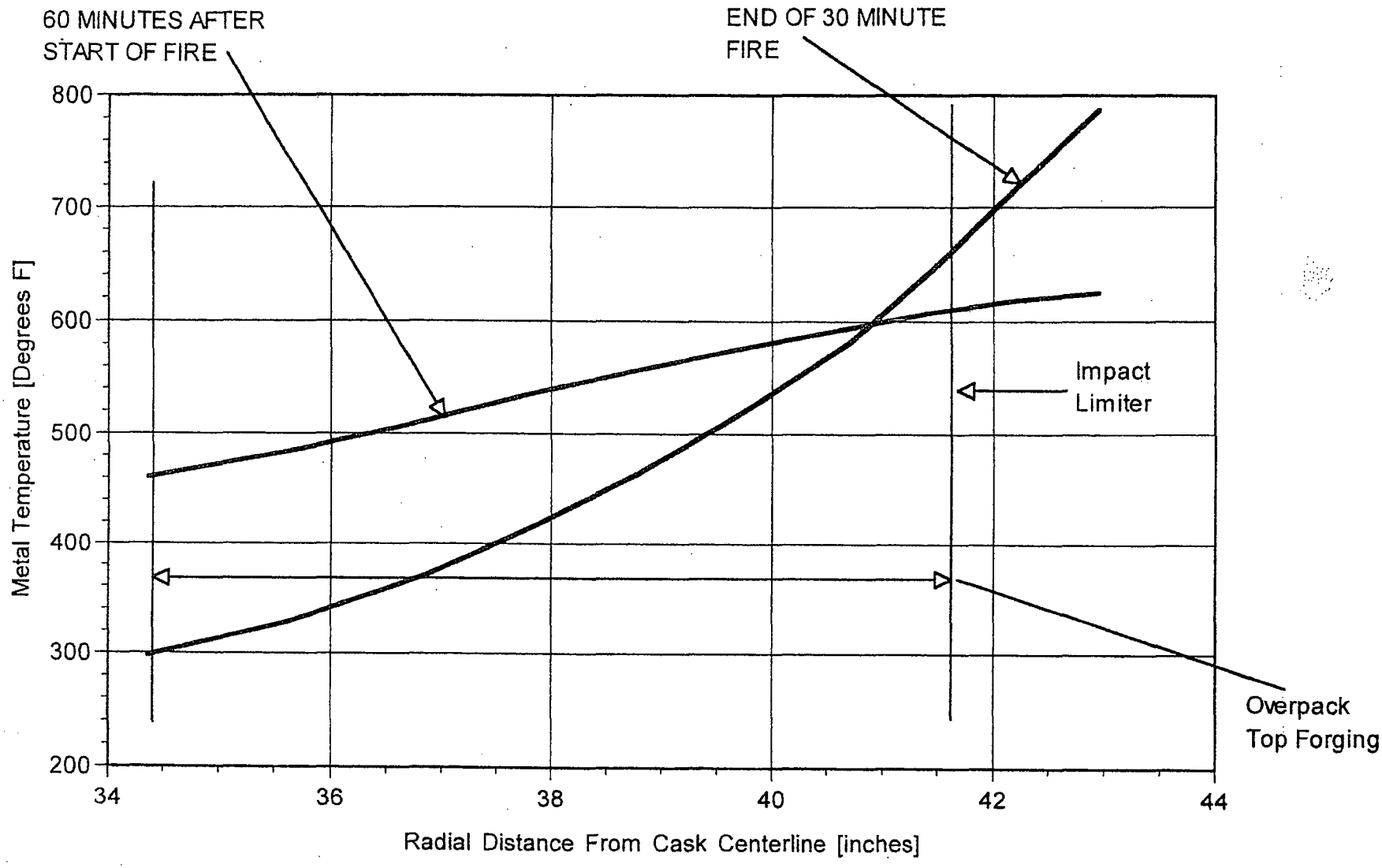

FIGURE 3.5.9: TRANSPORT FIRE CONDITION OVERPACK TOP FORGING TEMPERATURE DISTRIBUTIONS (SECTION C-C)

3.6 REGULATORY COMPLIANCE

Section 3.1 defines the requirements of 10CFR71 and ISG-11, Rev. 3 [3.1.5]) that must be met by the HI-STAR cask thermal design. The cask thermal evaluations in support of these requirements are provided in Sections 3.1 through 3.5. In this Section, a summary of the requirements and results of the evaluations are provided.

1. The applicant must include a description of the proposed package in sufficient detail to identify the package accurately and provide a sufficient basis for the evaluation of the package. The description must include, with respect to the packaging: specific materials of construction, weights, dimensions, and fabrication methods of materials specifically used as non-fissile neutron absorbers or moderators; and structural and mechanical means for the transfer and dissipation of heat. The description must include, with respect to the contents of the package: chemical and physical form; maximum normal operating pressure; maximum amount of decay heat; and identification and volumes of any coolants.

   A general description of the HI-STAR System is included in Chapter 1. Descriptions of cask materials are presented in Subsection 1.2.1, Section 1.4 and Appendices 1.A, 1.B and 1.C. Shielding materials are specifically addressed in Subsection 1.2.1.4. Cask component weights are presented in Subsections 1.2.1.1 and 2.2. Cask component dimensions are presented in Subsection 1.2.1.2 and in engineering drawings included in Section 1.4. The transfer and dissipation of heat are discussed generally in Subsection 1.2.1.6, and in detail in this chapter.

   General descriptions of and requirements for fuel assemblies for transport are presented in Subsection 1.2.3, including design basis maximum decay heat load specifications in Subsection 1.2.3.5. Maximum normal operating pressures are reported in Subsection 3.4.4. As stated in Subsection 1.2.1.7, there are no coolant volumes (reservoirs) in the HI-STAR System.

2. A package must be designed, constructed, and prepared for shipment so that under normal conditions of transport there would be no substantial reduction in the effectiveness of the packaging.

   The results of thermal evaluations presented in Section 3.4 demonstrate that the HI-STAR System performs as designed under all normal conditions of transport.

3. A package must be designed, constructed, and prepared for shipment so that in still air at 100°F and in the shade, no accessible surface of the package would have a temperature exceeding 185°F in an exclusive use shipment.

   Maximum exposed surface temperatures for the HI-STAR System are reported in Subsection 3.4.2. All impact limiter surface temperatures are shown to be below 185°F. The personnel

barrier, described in Chapter 7, renders the hot overpack enclosure shell surfaces inaccessible.

4. Compliance with the permitted activity release limits for a Type B package may not depend on filters or on a mechanical cooling system.

   As stated in Section 3.1, all cooling mechanisms in the HI-STAR System are completely passive.

5. With respect to the initial conditions for the events of normal conditions of transport and hypothetical accident conditions, the demonstration of compliance with the requirements of 10CFR71 must be based on the ambient temperature preceding and following the event remaining constant at that value between -20°F and 100°F, which is most unfavorable for the feature under consideration. The initial internal pressure within the containment system must be considered to be the maximum normal operating pressure (MNOP), unless a lower internal pressure consistent with the ambient temperature considered to precede and follow the event is more unfavorable.

   Hypothetical fire accident transient calculations for the HI-STAR System are described in Section 3.5. The initial condition for this event corresponds to the most severe steady-state solution for normal conditions of transport, which correspond to a 100°F ambient temperature with full insolation. These same environmental conditions are applied during the post-accident phase of the evaluation as well. All calculated temperatures for this event are below the specified design temperature limits.

   Maximum calculated normal condition internal pressures (MNOPs) are reported in Subsection 3.4.4. Maximum calculated hypothetical accident condition internal pressures are reported in Subsection 3.5.4. All calculated MNOPs are below the design pressure limits for the MPC helium retention boundary and the overpack containment boundary.

6. For normal conditions of transport, a heat event consisting of an ambient temperature of 100°F in still air and prescribed insolation must be evaluated.

   The maximum temperatures in the HI-STAR System reported in Subsection 3.4.2 correspond to the heat event. All calculated temperatures for this event are below the appropriate design temperature limits. As stated in Subsection 3.4.5, thermal stresses are determined and reported in Chapter 2.

7. For normal conditions of transport, a cold event consisting of an ambient temperature of –40°F in still air and shade must be evaluated.

   The minimum temperatures in the HI-STAR System reported in Subsection 3.4.3 correspond to the cold event. All calculated temperatures for this event are below the appropriate design

temperature limits. As stated in Subsection 3.4.5, thermal stresses are determined and reported in Chapter 2.

8. Evaluation for hypothetical accident conditions is to be based on sequential application of the specified events, in the prescribed order, to determine their cumulative effect on a package.

   As described in Section 3.5, the HI-STAR System hypothetical accident thermal condition (hydrocarbon fuel/air fire) evaluation incorporates bounding representations of the results of the preceding accident conditions. Specifically, the impact limiters are assumed to be completely crushed (drop event) and the heat transfer effectiveness of the radial channels region is reduced (puncture event). All calculated temperatures for this event are below the appropriate design temperature limits.

9. For hypothetical accident conditions, a thermal event consisting of a fully engulfing hydrocarbon fuel/air fire with an average emissivity coefficient of at least 0.9, with an average flame temperature of at least 1475°F for a period of 30 minutes.

   The description of the HI-STAR System hypothetical accident thermal event model (Subsection 3.5.1.1) specifies the fire condition input parameters. All input parameters are in accordance with the requirements of 10CFR71.73(c)(4). All calculated temperatures for this event are below the appropriate design temperature limits.

The thermal evaluations in Sections 3.4, 3.5, 3.I.4 and 3.I.5 demonstrate compliance with ISG-11, Rev. 3 [3.1.5] temperature limits. Specifically, the maximum cladding temperatures for normal transport and accident conditions are below the prescribed limits (normal (752°F) and accident (1058°F)). The thermal evaluations provided in this SAR demonstrate that the HI-STAR and HI-STAR HB System description and evaluation satisfy the thermal requirements of 10 CFR Part 71. Specifically:

- The material properties and component specifications used in the thermal evaluation are sufficient to provide a basis for evaluation of the HI-STAR System against the thermal requirements of 10 CFR Part 71.

- The methods used in the thermal evaluation are described in sufficient detail to permit an independent review, with confirmatory calculations, of the HI-STAR System thermal design.

- The accessible surface temperatures of the HI-STAR System as it will be prepared for shipment satisfy 10 CFR 71.43(g) for exclusive use shipments.

- The HI-STAR System design, construction, and preparations for shipment ensure that the material and component temperatures will not extend beyond the specified allowable limits during normal conditions of transport consistent with 10 CFR 71.71.

- The HI-STAR System design, construction, and preparations for shipment ensure that the material and component temperatures will not exceed the specified allowable temperature limits during hypothetical accident conditions consistent with 10 CFR 71.73.

It is therefore concluded that the thermal design of the HI-STAR System is in compliance with 10 CFR Part 71, and that the applicable design and acceptance criteria have been satisfied. The evaluation of the thermal design provides reasonable assurance that the HI-STAR System will allow safe transport of spent fuel. This conclusion is based on the technical data and analyses presented in this chapter in conjunction with provisions of 10 CFR Part 71, appropriate regulatory guides, applicable codes and standards, and accepted engineering practices.

3.7 REFERENCES

[3.1.1] ANSYS Finite Element Modeling Package, Swanson Analysis Systems, Inc., Houston, PA, 1993.

[3.1.2] FLUENT Computational Fluid Dynamics Software (Fluent, Inc., Centerra Resource Park, 10 Cavendish Court, Lebanon, NH 03766).

[3.1.3] Greer et al., "The TN-24P PWR Spent Fuel Storage Cask: Testing and Analyses," EPRI NP-5128, PNL-6054, UC-85, (April 1987).

[3.1.4] Deleted.

[3.1.5] "Cladding Considerations for the Transportation and Storage of Spent Fuel", Interim Staff Guidance – 11, Revision 3, (11/17/2003).

[3.2.1] Baumeister, T., Avallone, E.A. and Baumeister III, T., "Marks' Standard Handbook for Mechanical Engineers", 8th Edition, McGraw Hill Book Company, 1978.

[3.2.2] Rohsenow, W.M. and Hartnett, J.P., "Handbook of Heat Transfer," McGraw Hill Book Company, New York, 1973.

[3.2.3] Greer et al., "The TN-24P Spent Fuel Storage Cask: Testing and Analyses," EPRI NP-5128, PNL-6054, UC-85, (April 1987).

[3.2.4] Rust, J.H., "Nuclear Power Plant Engineering," Haralson Publishing Company, (1979).

[3.2.5] Kern, D.Q., "Process Heat Transfer," McGraw Hill Kogakusha, (1950).

[3.2.6] "A Handbook of Materials Properties for Use in the Analysis of Light Water Reactor Fuel Rod Behavior", NUREG/CR-0497, (August 1981).

[3.2.7] "Safety Analysis Report for the NAC Storable Transport Cask," Docket No. 71-9235.

[3.2.8] ASME Boiler and Pressure Vessel Code, Section II, Part D, (1995).

[3.2.9] Jakob, M. and Hawkins, G.A., "Elements of Heat Transfer," John Wiley & Sons, New York, 1957.

[3.2.10] "Qualification of METAMIC for Spent-Fuel Storage Application", EPRI Report 1003137, (October 2001), EPRI, Palo Alto, CA.

[3.2.11] "Sourcebook for METAMIC Performance Assessment", Holtec Report HI-2043215, Holtec International, Marlton, NJ, 08053.

[3.2.12] "Nuclear Systems Materials Handbook, Vol. 1, Design Data", ORNL TID 26666.

[3.2.13] "Scoping Design Analyses for Optimized Shipping Casks Containing 1-, 2-, 3-, 5-, 7-, or 10-Year-Old PWR Spent Fuel", ORNL/CSD/TM-149 TTC-0316, (1983).

[3.2.14] "Holtite A: Development History and Thermal Performance Data", Holtec Report HI-2002396, Rev. 3., Holtec International, Marlton, NJ, 08053.

[3.3.1] "Handbook of Aluminum," Alcan Aluminum Corporation, 3rd Edition, page 170, (1970).

[3.3.2] Deleted.

[3.3.3] Deleted.

[3.3.4] Deleted.

[3.3.5] Johnson, Jr., A.B. and Gilbert, E.R., "Technical Basis for Storage of Zircaloy-Clad Spent Fuel in Inert Gases," PNL-4835, (September 1983).

[3.3.6] Deleted.

[3.3.7] Deleted.

[3.3.8] Lanning and Beyer, "Estimated Maximum Cladding Stresses for Bounding PWR Fuel Rod During Short Term Operations for Dry Cask Storage," PNNL White Paper, (January 2004).

[3.4.1] Wooton, R.O. and Epstein, H.M., "Heat Transfer from a Parallel Rod Fuel Element in a Shipping Container," Battelle Memorial Institute, 1963.

[3.4.2] Rapp, D., "Solar Energy," Prentice-Hall, Inc., Englewood Cliffs, NJ, 1981.

[3.4.3] Sanders et al., "A Method for Determining the Spent-Fuel Contribution to Transport Cask Containment Requirements," Sandia Report SAND90-2406-TTC-1019UC-820, page II-127, (November 1992).

[3.4.4] Holman, J.P., "Heat Transfer," 6th ed., McGraw Hill Book Company, 1986.

[3.4.5] Hewitt, G.F., Shires, G.L., and Bott, T.R., "Process Heat Transfer," CRC Press,

(1994).

[3.4.6] Chandrasekhar, S., "Hydrodynamic and Hydromagnetic Stability," Dover, (1961).

[3.4.7] Gradshteyn, I.S. and Ryzhik, I.M., "Table of Integrals Series and Products," Academic Press, Fourth Edition, page 366, (1965).

[3.4.8] Deleted.

[3.4.9] Deleted.

[3.4.10] Cormack, D.E., L.G. Leal and J. Imberger, "Natural Convection in a Shallow Cavity With Differentially Heated End Walls. Part 1 Asymptotic Theory," J. Fluid Mechanics, 65, 209-229, (1974).

[3.4.11] Cormack, D.E., L.G. Leal and J.H. Seinfeld, "Natural Convection in a Shallow Cavity With Differentially Heated End Walls. Part 2 Numerical Solutions," J. Fluid Mechanics, 65, 231-246, (1974).

[3.4.12] Imberger, J., "Natural Convection in a Shallow Cavity with Differentially Heated End Walls. Part 3 Experimental Results," J. Fluid Mechanics, 65, 247-260, (1974).

[3.4.13] Hagrman, Reymann and Mason, "MATPRO-Version 11 (Revision 2) A Handbook of Materials Properties for Use in the Analysis of Light Water Reactor Fuel Rod Behavior," NUREG/CR-0497, Tree 1280, Rev. 2, EG&G Idaho, August 1981.

[3.4.14] Deleted.

[3.4.15] Deleted.

[3.4.16] Deleted.

[3.4.17] Deleted.

[3.4.18] Perry and Green, "Perry's Chemical Engineers' Handbook", 6th Edition, McGraw-Hill, 1984.

[3.4.19] Reid, Prauznitz and Poling, "The Properties of Gases and Liquids", Fourth Edition, McGraw-Hill, 1987.

[3.5.1] 10CFR Part 71, Paragraph 71.73, (January 1, 1998).

[3.5.2] Jakob, M., "Heat Transfer," John Wiley & Sons, Inc., page 555, (1967).

APPENDIX 3.A: CONSERVATISMS IN THE THERMAL ANALYSIS OF THE HI-STAR SYSTEM

3.A.1 INTRODUCTION

The HI-STAR 100 overpack is a thick walled, multi-layered cylindrical vessel with an internal cavity suited for emplacement of a cylindrical canister containing spent nuclear fuel (SNF). The canister rests on the inside surface of a horizontally oriented overpack during transport. One principal safety function of the cask is to ensure that the Spent Nuclear Fuel (SNF) cladding temperatures remain below prescribed regulatory limits. For this purpose a thermal model is articulated with modeling assumptions that overstate the temperature of cask contents and provide a conservative upperbound to cladding temperature field that would be obtained inside the canister. In this appendix, the underlying modeling assumptions are evaluated and an assessment of thermal margins reported.

Storage of SNF in casks is characterized by relatively large temperature elevations above the ambient. The cladding temperature rise is the cumulative sum of temperature increments arising from individual elements of thermal resistance. To assure that cladding temperatures are below regulatory limits with robust margins, analytical assumptions adversely impacting heat transfer are chosen with particular attention given to those temperature increments which form the bulk of the temperature rise. In this appendix, a quantitative estimate of some of the principal conservatisms in the thermal model of the HI-STAR 100 System are presented to provide an insight into the extent of overall conservatism in the predicted peak cladding temperatures.

3.A.2 CONSERVATISM IN REPRESENTING HEAT DISSIPATION TO AMBIENT

Heat dissipation from a HI-STAR cask occurs principally by convection and radiation heat transfer to ambient air. The rate of decay heat dissipation from the external surfaces is, of course, influenced by several factors, some of which aid the process (e.g. wind), and others (radiation heating by sun) that oppose it. In the HI-STAR modeling, factors aiding heat transfer are neglected (still air) and those opposing it (insolation) are included. A concomitant effect of assuming no wind is that heat transfer is limited to natural convection cooling. To represent heat transfer from the HI-STAR cask, natural convection correlations for heat transfer (h) from heated surfaces are reported in Chapter 3 (Sub-section 3.4.1.1.7). The numerical values obtained for the HI-STAR cask modeling are in the neighborhood of 1 Btu/ft^2-hr-^{o}F. As we show in the following, these h values are extremely conservative when the effects of wind are considered.

For considering the effects of wind, we present a heat transfer correlation from Jakob [3.A.1] for air flow past a heated cylinder [3.A.1].

$$Nu = 0.028\, Re^{0.8}\, [1 + 0.4\, (L_h/L)^{2.75}] \qquad \text{[Eq. 1]}$$

where:

L = Length of cylinder
L_h = Length of heated section
Re = Reynolds number ($LV\rho/\mu$)

V = Air velocity
ρ = Air density
μ = Air viscosity
Nu = Nusselt number (hL/k)
k = Air conductivity

For illustrative purposes, let us consider a slight wind (10 MPH) and representative air properties (ρ = 0.075 lbm/ft^3, k = 0.015 Btu/ft-hr-^{o}F and μ = 180 μP). The length (L) of the HI-STAR overpack cylinder is 203.125 inch (Section 1.4 HI-STAR Drawings). The length of overpack heating (L_h) is assumed to be equal to a representative height of active fuel zone (12 ft). Employing consistent units, Re is computed as:

$$Re = 16.92 \text{ ft} * 14.66 \text{ ft/s} * 0.075 \text{ lbm/ft}^3 / 1.2\text{x}10^{-5} \text{ lbm/ft-s}$$
$$= 1.5\text{x}10^6$$

The Nusselt number is computed by substituting numerical values for Re, L and L_h in Eq. 1. The numerical value is 2822. From the definition of Nu (=hL/k), h is computed as 2.5 Btu/ft^2-hr-^{o}F. In other words, the principal mode of heat transfer – convection cooling of the HI-STAR cask – is approximately 150% greater than the values used in the thermal analysis.

3.A.3 CONSERVATISM IN REPRESENTING BASKET AXIAL RESISTANCE

Much of the elevation in fuel cladding temperatures in a HI-STAR cask occurs within the MPC[1]. Therefore, it stands to reason that conservatism in the basket thermal simulation would have a pronounced effect on the conservatism in the final solution. The thermal model of the fuel basket in the HI-STAR was accordingly constructed with a number of conservative assumptions to ensure robust margins. Most notable assumptions in this regard are:

a) Axial heat dissipation in the fuel pellets ignored
b) Convection heat transfer in the MPC space ignored

We illustrate these conservatisms by examining one of them (item a) in some detail in the following. It is recognized that the heat emission from a fuel assembly is axially non-uniform. The maximum heat generation occurs at about the mid-height region of the enriched uranium column, and tapers off toward its extremities. The axial heat conduction in the fuel basket would act to diffuse and levelize the temperature field in the basket. The axial conductivity of the basket, quite clearly, is the key determinant in how well the thermal field in the basket would be homogenized. In the interest of conservatism, axial heat dissipation in the fuel pellets is ignored. This assumption has the direct effect of throttling the axial flow of heat and thus of elevating the computed value of mid-height cladding temperature (where the peak temperature occurs) above its actual value. In actuality, the axial conductivity of the fuel basket is greater than used in the analysis. Had the axial conductivity of the basket been modeled less conservatively in the thermal analysis, the temperature peaking would be depressed and the temperature field would be more uniform.

1 See for example temperature results Table 3.4.10 for PWR MPCs wherein the cladding is elevated 386°F above the MPC shell temperature. This elevation is 64% of the cladding temperature rise above ambient (601°F).

To estimate the conservatism in restricting the basket axial resistance, we perform a numerical exercise using mathematical perturbation techniques. The axial conductivity (K_z) of the MPC is, as explained previously, is higher than used in the analysis (K). The thermal solution to the higher axial conductivity problem (i.e. $K_z > K$) is mathematically expressed as a sum of a baseline solution T_o at K and a perturbation T^* which accounts for the higher axial conductivity. From Fourier's Law of heat conduction in solids, a perturbation equation for T* is articulated below:

$$K_z \frac{d^2T^*}{dz^2} = -\Delta K \frac{d^2T_o}{dz^2}$$

Where, ΔK is a perturbation parameter (axial conductivity offset $\Delta K = K_z - K$). The boundary conditions for the perturbation solution are zero slope at peak cladding temperature location ($dT^*/dz = 0$) (which occurs at about the active fuel mid- height) and $T^* = 0$ at the ends of the active fuel length. The object of this calculation is to compute T* where the peak fuel cladding temperature is reached. To this end, the baseline thermal solution T_o is employed to characterize d^2T_o/dz^2 for the hottest fuel cell. This is computed as $(-\Delta T_{ax}/L^2)$ where ΔT_{ax} is the cladding temperature rise from the ends of the active fuel length to mid-height and L is half the active fuel length (~6 ft). Conservatively postulating a lower bound ΔT_{ax} of 300°F d^2T_o/dz^2 is computed as $-8.33°F/ft^2$. Integrating the perturbation equation shown above, the following formula for T* is obtained:

$$T^* = \left(\frac{\Delta K}{K_z}\right)\frac{d^2T_o}{dz^2}\frac{L^2}{2}$$

Employing a conservative low value for the $(\Delta K/K_z)$ parameter of 0.05, T* is computed as – 7.5°F. In other words, the baseline HI-STORM solution over predicts the peak cladding temperature by over 7°F, because of the conservatism in the value of axial conductivity.

3.A.4 CONSERVATISM IN REPRESENTING FUEL BASKET CONFIGURATION

The HI-STAR System is designed for normal transport in a horizontal orientation. This orientation ensures physical contact between: (i) Fuel assemblies and the fuel basket, (ii) Fuel basket and MPC (iii) MPC and HI-STAR overpack. From a heat transfer perspective, this is an optimal orientation because (a) Gap resistances are minimized and (b) Heat dissipation is maximized through physical contact. In the MPC modeling, we assume a physical configuration that is opposite of (a) and (b) for the MPC space. This configuration assumes:

I. Each fuel assembly is levitating coaxially in it's storage cell
II. Fuel basket is levitating coaxially in the MPC shell

The assumptions described in I and II maximize gap resistance and completely ignore physical contact. In the thermal analysis of the HI-STAR system the fuel storage cell space is modeled with a uniform gap between the fuel assembly envelope and the cell walls (See Figure 3.4.7). The fuel basket-to-MPC space is modeled as a helium filled concentric annular gap (See Figure 3.4.2). Because gaps depress heat transfer, it follows that deliberately postulating gaps between physically

contacting parts considerably elevates the MPC planar resistance and the computed fuel and basket temperatures. In the MPC-to-overpack space, the thermal modeling includes partial recognition of gap reduction (See Sub-section 3.4.1.1.10 for eccentric gap evaluation) and completely ignores physical contact between the MPC and overpack.

3.A.5 OTHER CONSERVATISMS

Section 3.4.6 of the SAR lists an array of conservatisms, of which certain unobvious and individually significant items are discussed in detail in this appendix. These conservatisms are primarily intrinsic to the solution methodology or are product of assumptions in the input data. Examples in the latter category are values assumed in the thermal analysis for key inputs such as insolation heat and ambient temperature. Apart from the input data and methodology related conservatisms, the modeling includes assumptions to under represent heat transfer. A listing of such conservatisms is summarized below:

i) Insolation heating assumed with a bounding absorbtivity of 1.0
ii) Heat dissipation from the HI-STAR overpack ends ignored
iii) Conduction heat transfer in Holtite is neglected.
iv) MPCs are assumed to be loaded with the most thermally resistive fuel type in its category (BWR or PWR) as applicable

The assumptions inherent in the FLUENT methodology, in the thermal modeling and in the input data, are estimated to have an aggregate effect of overestimating cladding temperatures by a considerable amount, as estimated in Table 3.A.1.

3.A.6 CONCLUSIONS

The foregoing narrative provides a physical description of the many elements of conservatism in the HI-STORM 100 thermal model. The conservatisms may be broadly divided into two categories:

1. Those intrinsic to the FLUENT methodology.

2. Those arising from the input data and thermal modeling.

The conservatism in Category (1) may be identified by reviewing the Holtec International Benchmark Report [3.A.2], which shows that the FLUENT solution methodology, when applied to the prototype cask (TN 24P) over-predicts the peak cladding temperature by as much as 79 °F. and as much as 37°F relative to the PNNL results (see Attachment 1 to Reference [3.A.2]) from their COBRA SFS solution as compared against Holtec's FLUENT solution.

Category (2) conservatisms are those that we have deliberately embedded in the HI-STAR thermal models to ensure that the computed value of the peak fuel cladding temperature is further exaggerated. Table 3.A.1 contains a listing of the major conservatisms in the HI-STAR thermal model, along with an estimate of the effect (increase) of each on the computed peak cladding temperature. Finally, we note that the computed peak cladding temperatures for all MPCs are also

lower than the 400°C limit by varying amounts, which can be viewed as an additional thermal margin in the system.

The cumulative effect of conservatisms listed in Table 3.A.1 would be additive if the thermal resistances were all arrayed in series. In reality some resistances are in series and others in parallel. For obtaining a reasonable estimate of the cumulative effect, a square root of sum of squares of the individual conservatisms is computed and reported in the last row of the Table 3.A.1.

Table 3.A.1

Estimated Conservatisms in the Computed Peak Cladding Temperature for the HI-STAR 100 System

MODELING ASSUMPTION	CONSERVATISM [°F]
1. Wind effects neglected	45
2. Axial heat dissipation understated	7
3. MPC convection heat transfer neglected	40
4. Holtite conduction neglected	10
5. Miscellaneous	20
Cumulative Effect[2] of 1 thru 5:	64.6

3.A.6 REFERENCES

[3.A.1] Jakob, M., "Heat Transfer", John Wiley & Sons, Inc., (1967).

[3.A.2] "Topical Report on the HI-STAR/HI-STORM Thermal Model and its Benchmarking with Full-Size Cask Test Data", Holtec Report HI-992252, Rev. 1.

2 See cumulative effect discussion in the last paragraph of 3.A.6.

APPENDIX 3.B: THE FORCED HELIUM DEHYDRATION (FHD) SYSTEM

3.B.1 System Overview

The Forced Helium Dehydration (FHD) system is used to remove the remaining moisture in the MPC cavity after all of the water that can practically be removed through the drain line using a hydraulic pump or an inert gas has been expelled in the water blowdown operation. Expelling the water from the MPC using a conventional pump or a water displacement method using inert gas would remove practically all of the contained water except for the small quantity remaining on the MPC baseplate below the bottom of the drain line and an even smaller adherent amount wetting the internal surfaces. A skid-mounted, closed loop dehydration system will be used to remove the residual water from the MPC such that the partial pressure of the trace quantity of water vapor in the MPC cavity gas is brought down to ≤ 3 torr. The FHD system, engineered for this purpose, shall utilize helium gas as the working substance.

The FHD system, schematically illustrated in Figure 3.B.1, can be viewed as an assemblage of four thermal modules, namely, (i) the condensing module, (ii) the demoisturizer module, (iii) the helium circulator module and (iv) the pre-heater module. The condensing module serves to cool the helium/vapor mixture exiting the MPC to a temperature well below its dew point such that water may be extracted from the helium stream. The condensing module is equipped with suitable instrumentation to provide a direct assessment of the extent of condensation that takes place in the module during the operation of the FHD system. The demoisturizer module, engineered to receive partially cooled helium exiting the condensing module, progressively chills the recirculating helium gas to a temperature that is well below the temperature corresponding to the partial pressure of water vapor at 3 torr.

The motive energy to circulate helium is provided by the helium circulator module, which is sized to provide the pressure rise necessary to circulate helium at the requisite rate. The last item, labeled the pre-heater module, serves to pre-heat the flowing helium to the desired temperature such that it is sufficiently warm to boil off any water present in the MPC cavity.

The pre-heater module, in essence, serves to add supplemental heat energy to the helium gas (in addition to the heat generated by the stored SNF in the MPC) so as to facilitate rapid conversion of water into vapor form. The heat input from the pre-heater module can be adjusted in the manner of a conventional electric heater so that the recirculating helium entering the MPC is sufficiently dry and hot to evaporate water, but not unduly hot to place unnecessary thermal burden on the condensing module.

The FHD system described in the foregoing performs its intended function by continuously removing water entrained in the MPC through successive cooling, moisture removal and reheating of the working substance in a closed loop. In a classical system of the FHD genre, the moisture removal operation occurs in two discrete phases. In the beginning of the FHD system's operation (Phase 1), the helium exiting the MPC is laden with water vapor produced by boiling of the entrained bulk water. The condensing module serves as the principal device to condense out the water vapor from the helium stream in Phase 1. Phase 1 ends when all of the bulk water in the MPC cavity is vaporized. At this point, the operation of the FHD system moves on to steadily lowering the

relative humidity and bulk temperature of the circulating helium gas (Phase 2). The demoisturizer module, equipped with the facility to chill flowing helium, plays the principal role in the dehydration process in Phase 2.

3.B.2 Design Criteria

The design criteria set forth below are intended to ensure that design and operation of the FHD system will drive the partial pressure of the residual vapor in the MPC cavity to ≤ 3 torr if the temperature of helium exiting the demoisturizer has met the value and duration criteria provided in the HI-STORM technical specifications. The FHD system shall be designed to ensure that during normal operation (i.e., excluding startup and shutdown ramps) the following criteria are met:

i. The temperature of helium gas in the MPC shall be at least 15°F higher than the saturation temperature at coincident pressure.

ii. The pressure in the MPC cavity space shall be less than or equal to 60.3 psig (75 psia).

iii. The recirculation rate of helium shall be sufficiently high (minimum hourly throughput equal to ten times the nominal helium mass backfilled into the MPC for fuel storage operations) so as to produce a turbulated flow regime in the MPC cavity.

iv. The partial pressure of the water vapor in the MPC cavity will not exceed 3 torr if the helium temperature at the demoisturer outlet is ≤ 21°F for a period of 30 minutes.

In addition to the above system design criteria, the individual modules shall be designed in accordance with the following criteria:

i. The condensing module shall be designed to de-vaporize the recirculating helium gas to a dew point of 120°F or less.

ii. The demoisturizer module shall be configured to be introduced into its helium conditioning function <u>after</u> the condensing module has been operated for the required length of time to assure that the bulk moisture vaporization in the MPC (defined as Phase 1 in Section 2.B.1) has been completed.

iii. The helium circulator shall be sized to effect the minimum flow rate of circulation required by the system design criteria described above.

iv. The pre-heater module shall be engineered to ensure that the temperature of the helium gas in the MPC meets the system design criteria described above.

3.B.3 Analysis Requirements

The design of the FHD system shall be subject to the confirmatory analyses listed below to ensure that the system will accomplish the performance objectives set forth in this FSAR.

i. System thermal analysis in Phase 1: Characterize the rate of condensation in the condensing module and helium temperature variation under Phase 1 operation (i.e., the scenario where there is some unevaporated water in the MPC) using a classical thermal-hydraulic model wherein the incoming helium is assumed to fully mix with the moist helium inside the MPC.

ii. System thermal analysis in Phase 2: Characterize the thermal performance of the closed loop system in Phase 2 (no unvaporized moisture in the MPC) to predict the rate of condensation and temperature of the helium gas exiting the condensing and the demoisturizer modules. Establish that the system design is capable to ensure that partial pressure of water vapor in the MPC will reach ≤ 3 torr if the temperature of the helium gas exiting the demoisturizer is predicted to be at a maximum of 21°F for 30 minutes.

iii. Fuel Cladding Temperature Analysis: A steady-state thermal analysis of the MPC under the forced helium flow scenario shall be performed using the methodology described in SAR Subsections 3.4.1.1.1 through 3.4.1.1.4 with due recognition of the forced convection process during FHD system operation. This analysis shall demonstrate that the peak temperature of the fuel cladding under the most adverse condition of FHD system operation (design maximum heat load, no moisture, and maximum helium inlet temperature), is below the peak cladding temperature limit for normal conditions of storage for the applicable fuel type (PWR or BWR) and cooling time at the start of dry storage.

3.B.4 Acceptance Testing

The first FHD system designed and built for the MPC drying function required by HI-STORM's technical specifications shall be subject to confirmatory testing as follows:

a. A representative quantity of water shall be placed in a manufactured MPC (or equivalent mock-up) and the closure lid and RVOAs installed and secured to create a hermetically sealed container.

b. The MPC cavity drying test shall be conducted for the worst case scenario (no heat generation within the MPC available to vaporize water).

c. The drain and vent line RVOAs on the MPC lid shall be connected to the terminals located in the pre-heater and condensing modules of the FHD system, respectively.

d. The FHD system shall be operated through the moisture vaporization (Phase 1) and subsequent dehydration (Phase 2). The FHD system operation will be stopped after the temperature of helium exiting the demoisturizer module has been at or below 21°F for thirty minutes (nominal). Thereafter, a sample of the helium gas from the MPC will be extracted and tested to determine the partial pressure of the residual water vapor in it.

The FHD system will be deemed to have passed the acceptance testing if the partial pressure in the extracted helium sample is less than or equal to 3 torr.

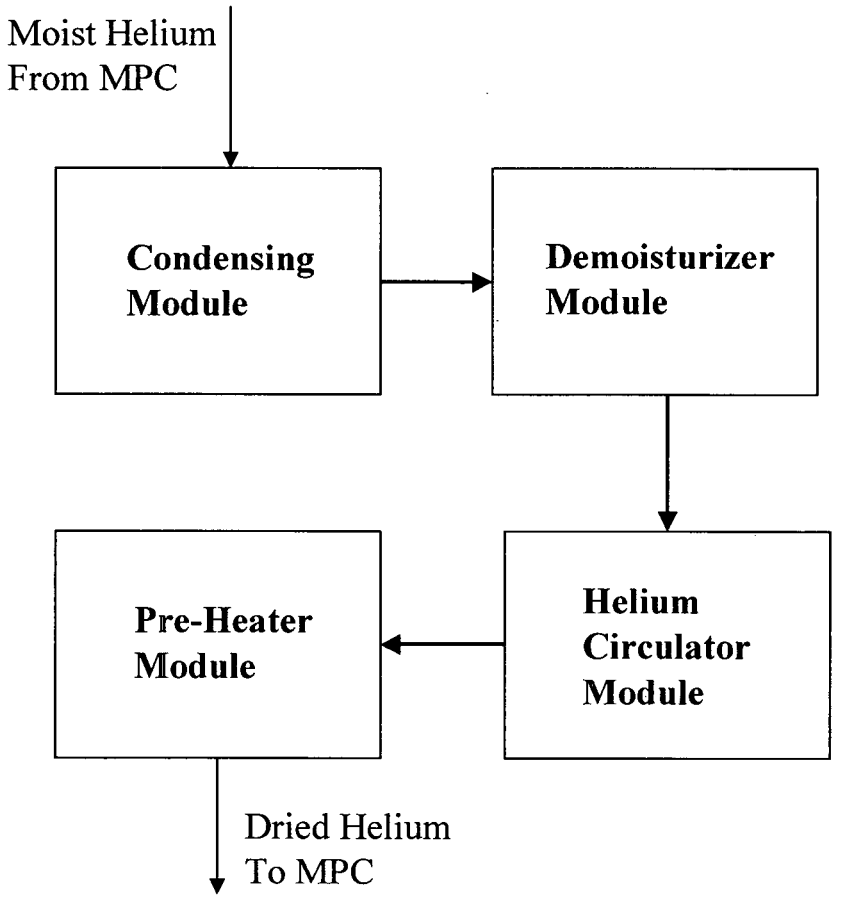

FIGURE 3.B.1: SCHEMATIC OF THE FORCED HELIUM DEHYDRATION SYSTEM

SUPPLEMENT 3.I

THERMAL EVALUATION OF HI-STAR HB

3.I.0 INTRODUCTION

The Humboldt Bay HI-STAR HB cask is licensed to store permanently shutdown Unit 3 BWR spent nuclear fuel (SNF) at the Humboldt Bay ISFSI. In this supplement compliance of the HI-STAR HB cask to 10CFR71 and ISG-11, Rev. 3 thermal requirements are evaluated for transport. The analysis considers passive rejection of decay heat from the spent nuclear fuel to an environment under the 10CFR71 mandated ambient conditions for normal and accident scenarios. The regulatory requirements and acceptance criteria for transport evaluation are listed in Section 3.0.

3.I.1 DISCUSSION

The HI-STAR HB, with the exception noted below, is an essentially shortened version of the HI-STAR 100 cask. The HI-STAR 100 cask thermal design features discussed in Section 3.1 are applicable to the HI-STAR HB design. Prior to sealing the HI-STAR HB MPC lid, the MPC-HB is backfilled with helium to Table 1.I.2 specifications.

The HI-STAR HB overpack design features a neutron shield placed in the annulus region between the multi-layered shells and enclosure shell without connecting ribs. (See HI-STAR HB overpack dwg. 4082, Sht. 6 included in the Chapter 1 Supplement, Section 1.I.4). This feature is unique to the "HB" version of the generic HI-STAR 100 overpack design. As the annular shield is a thick layer of a low conductivity material, Holtite A, it retards the lateral transmission of fire heat during hypothetical accidents, thus minimizing the heating of HI-STAR HB package internals and the stored fuel during fires.

3.I.2 THERMAL PROPERTIES OF MATERIALS

The thermophysical data compiled in Section 3.2 of the SAR provides the required materials information except for Holtite thermal conductivity. Holtite conductivity data [3.I.1] is provided in Table 3.I.1.

Holtite-A is qualified to withstand the effects of much elevated temperatures and high radiation exposures reached in the generic HI-STAR 100 Cask (heat loads upto 20 kW). As the HI-STAR HB package heat loads (2 kW) are dwarfed by the generic design, much larger margins against thermal and radiation degradation are realized. The Holtite-A thermal characterization and qualification testing for use in dry storage casks are archived in references [3.I.1] and [3.I.2].

3.I.3 TECHNICAL SPECIFICATIONS OF COMPONENTS

The HI-STAR materials and components required to be maintained within safe operating limits are listed in Section 3.3. The temperature limits specified in this section are adopted for transport evaluation.

3.I.4 NORMAL TRANSPORT THERMAL EVALUATION

The HI-STAR HB cask features an all-welded multi-purpose canister (MPC) containing spent nuclear fuel emplaced in a bolted steel overpack. From a thermal standpoint the HI-STAR HB cask is identical to the generic HI-STAR cask except for the following differences:

a) The height of the cask is reduced to be compatible with the short-length Humboldt Bay fuel.
b) To accommodate the narrow width Humboldt Bay fuel the fuel storage cells count is increased to 80.
c) Radial connectors in the neutron shield region are replaced with a continuous neutron shield ring to minimize streaming.

The thermal payload of the HI-STAR HB transport package is given in Table 3.I.2.

3.I.4.1 Thermal Model

Thermal modeling of the HI-STAR HB adopts the same methodology used for HI-STAR thermal evaluation. An overview of the thermal methodology is given in the following.

Transport of heat from the HI-STAR HB to the ambient is analyzed broadly using three connected thermal models.

i. The first model considers transport of heat from the fuel assembly to the basket cell walls. This model recognizes the combined effects of conduction (through helium) and radiation using finite element methods.

ii. The second model considers heat transport within an MPC cross section by conduction and radiation. This model computes an effective cross sectional conductivity of the fuel basket.

iii. The third model deals with the transmission of heat from the MPC exterior surface to the external environment (heat sink). From the MPC shell to the cask exterior surface, heat is conducted through an array of concentric shells representing the MPC-to-overpack helium gap, the overpack inner shell, the intermediate shells, the Holtite-A neutron shielding and finally the overpack outer shell. Heat rejection from the outside cask surfaces to ambient air is considered by accounting for natural convection and thermal radiation heat transfer from the cask external surfaces. Insolation on exposed cask surfaces is based on 12-hour

levels prescribed in 10CFR71, averaged over a 24-hour period.

Detailed descriptions of the above models are provided in Section 3.4. Using these steps, effective properties of the fuel, MPC and HI-STAR HB overpack are obtained and used in an axi-symmetric rendering of the cask geometry. For a conservative portrayal of cask temperatures the thermal evaluation incorporates the following assumptions:

a) Fuel basket conductivity is understated.
b) Neutron shield conductivity is understated.
c) A theoretical bounding absorbtivity of 1.0 assumed for ins*u*lation.
d) Heat dissipation by internal helium motion is ignored.
e) The ends of the overpack are assumed to be insulated.
f) To conservatively bound the hottest fuel the cask decay heat is non-uniformly distributed with a robust peaking in the interior.

Thermal analysis results are provided in the next section.

3.I.4.1.1 Evaluation of Damaged and Undamaged Fuel Assemblies

The HI-STAR HB cask is designed to store damaged and undamaged fuel assemblies ("Damaged" and "Undamaged Fuel Assemblies" are defined in Table 1.0.1). From a thermal perspective, damaged fuel assemblies storage is limiting because damaged fuel must be placed in a Damaged Fuel Container (DFC) which blocks radiation heat dissipation from the fuel assemblies. To bound the HI-STAR HB thermal condition in a conservative manner all fuel assemblies placed in the HI-STAR HB cask are assumed to be "Damaged" and in DFCs.

3.I.4.2 Maximum Temperatures

As discussed in the previous section, an axi-symmetric model of the HI-STAR HB is constructed for thermal evaluation. This model adopts the same methodology used in the generic HI-STAR cask thermal analysis. To this model design basis heat loads (Table 3.I.2) and 10CFR71 inputs (100°F ambient temperature and Table 3.4.7 insolation) are imposed and steady state cask temperatures obtained. The results are provided in Table 3.I.3.

3.I.4.3 Minimum Temperatures

As specified in 10CFR71, the minimum ambient temperature conditions for the HI-STAR System are -20°F and a cold environment at -40°F. The HI-STAR System design does not have any minimum decay heat load restrictions for transport. Therefore, under bounding cold conditions (zero decay heat and no insolation), the cask temperatures will approach ambient conditions. All HI-STAR System materials of construction satisfactorily perform their intended function at these cold temperatures. Evaluations in Chapter 2 demonstrate the acceptable structural performance of the overpack and MPC steel materials at low temperature. Shielding and criticality functions of the cask materials are unaffected by cold.

3.I.4.4 Maximum Internal Pressures

The Humboldt Bay multi-purpose canisters (MPC HB) are pressurized with helium prior to sealing the lid ports. In Table 3.I.4 the initial backfill pressures are listed. In response to higher than ambient transport temperatures the helium pressure rises above the initial backfill pressures. In accordance with NUREG-1617 the maximum normal operating pressure (MNOP) is computed assuming normal operating temperatures and 3% fuel rods are ruptured. For conservatism, the MPC HB is assumed to be backfilled at the maximum backfill pressure (See Table 3.I.4). The normal transport pressures are provided in Table 3.I.5.

3.I.4.5 Maximum Thermal Stresses

Thermal expansion induced mechanical stresses are evaluated, using bounding temperature distributions, in Chapter 2.

3.I.4.6 Evaluation of Normal Transport

Based on a comparison of HI-STAR HB normal transport conditions (Tables 3.I.3 and 3.I.5) with generic HI-STAR temperatures and pressures (Tables 3.4.10, 3.4.11 and 3.4.15) we conclude the following:

a) Fuel temperatures are bounded by generic HI-STAR.
b) Containment boundary temperatures are bounded by generic HI-STAR.
c) Surface temperatures are bounded by generic HI-STAR.
d) MNOP is bounded by generic HI-STAR.

As the HI-STAR HB temperatures and pressures are bounded by the generic HI-STAR package transport evaluation and the HI-STAR complies with 10CFR Part 71 and ISG 11, Rev. 3 requirements (See Section 3.6) we conclude that the HI-STAR HB package is in compliance with the 10CFR Part 71 and ISG 11, Rev. 3 requirements for normal transport.

3.I.5 HYPOTHETICAL ACCIDENT THERMAL EVALUATION

In compliance with 10CFR71 requirements, the HI-STAR System is evaluated for hypothetical accident conditions. The accident scenarios are: (1) a 30 foot free drop onto an unyielding surface; (2) a 40-inch drop onto a mild steel bar; and (3) exposure to a 30-minute fire at 1475°F. The effects of the drop accidents (items (1) and (2)) are evaluated in Chapter 2. In this section the effect of a 30-minute fire are evaluated.

The HI-STAR HB is a short height version of the generic HI-STAR overpack. This version includes a solid shell of a low conductivity material (Holtite-A) in the neutron shield region. The HI-STAR HB initial conditions (normal transport) are bounded by HI-STAR generic temperatures and pressures. Based on the above information the following observations apply to HI-STAR HB fire evaluation:

Observation	Basis
Fire heat input to HI-STAR HB overpack is bounded by the generic HI-STAR	Exposed area of overpack is bounded by generic design
Rate of through-overpack fire heat transmission is bounded by generic HI-STAR	HI-STAR HB overpack design features a neutron shield ring without ribs (See discussion in Section 3.I.1)
Start of fire conditions are bounded by generic HI-STAR	See 3.I.4.6

Based on the observations above we conclude that the generic HI-STAR fire evaluation is bounding and the HI-STAR HB package complies with the 10CFR Part 71 requirements for hypothetical accidents.

3.I.6 REGULATORY COMPLIANCE

The Humboldt Bay cask evaluations for normal transport and hypothetical accident conditions show that the HI-STAR HB is bounded by the generic HI-STAR (See Sections 3.I.4.6 and 3.I.5). Accordingly, the regulatory compliance evaluated in Section 3.6 for HI-STAR cask applies to HI-STAR HB.

3.I.7 REFERENCES

[3.I.1] "Holtite A: Development History and Thermal Performance Data", Holtec Report HI-2002396, Rev. 3, Holtec International, Marlton, NJ, 08053.
[3.I.2] "Holtite-A: Results of Pre-and-Post-Irradiation Tests and Measurements", Holtec Report HI-2002420, Rev. 1.

Table 3.I.1: Holtite A Thermal Conductivity Data [3.I.1]

Temperature	Conductivity (Btu/ft-hr-°F)
106	0.543
154	0.537
208	0.509
252	0.488
306	0.480

Table 3.I.2: HI-STAR HB Thermal Payload

Fuel Decay Heat	2 kW

Table 3.I.3: Maximum Normal Transport Temperatures

Component	Temperature (°F)
Fuel Cladding	419
MPC Shell	162
Overpack Inner Shell	156
Overpack Top Plate	129
Overpack Bottom Plate	154
Overpack Outer Shell	147

Table 3.I.4: Helium Backfill Pressures

Minimum Pressure[1]	45.2 psig @ 70°F
Maximum Pressure	48.8 psig @ 70°F

[1] As MPC internal convection is conservatively neglected in transport evaluations the minimum required helium backfill pressure is 0 psig. This value is adopted in the transport CoC requirements for HI-STAR HB.

Table 3.I.5: HI-STAR HB Normal Operating Pressures

Condition	Pressure (psig)
Initial Backfill	48.8
Normal Transport	68.82
MNOP (with 3% rods rupture)	69.72[2]

[2] According to ISG-7, a 100% rods rupture evaluation is required for casks within 10% of the vessel design pressure (See Section 3.4.1.1.17). As the HI-STAR HB maximum normal operating pressure is below the regulatory threshold (90 psig) a 100% rods rupture evaluation is not required.

CHAPTER 4: CONTAINMENT

4.0 INTRODUCTION

This chapter demonstrates the HI-STAR 100 containment boundary compliance with the permitted activity release limits specified in 10CFR71, 71.51(a)(1) and 71.51(a)(2) for both normal and hypothetical accident conditions of transport [4.0.1]. Satisfaction of the containment criteria, expressed as the leakage rate acceptance criterion (atm-cm^3/sec, Helium), ensures that the HI-STAR 100 package will not exceed the specified allowable radionuclide release rates. Leakage rates are determined in accordance with the recommendations of ANSI N14.5 [4.0.2], and utilizing NUREG/CR-6487, *Containment Analysis for Type B Packages Used to Transport Various Contents* [4.0.3], Regulatory Guide 7.4, *Leakage Tests on Packages for Shipment of Radioactive Materials* [4.0.4] as content guides, and Draft NUREG-1617, *Standard Review Plan for Transportation Packages for Spent Nuclear Fuel* [4.0.5].

The HI-STAR 100 packaging allowable leakage rates established herein ensures that the requirements of 10CFR71.51 are met. The containment system boundary for the HI-STAR 100 packaging consists of the overpack inner shell, the bottom plate, the top flange, the top closure plate, closure bolts, the overpack vent and drain port plugs, and their respective mechanical seals.

Chapter 2 of this SAR shows that all containment boundary components are maintained within their code-allowable stress limits during all normal and hypothetical accident conditions of transport as defined in 10CFR71.71 and 10CFR71.73. Chapter 3 of this SAR shows that the peak containment component temperatures and pressures are within the design basis limits for all normal and hypothetical accident conditions of transport as defined in 10CFR71.71 and 10CFR71.73. Since both the containment boundary is shown to remain intact, and the temperature and pressure design bases are not exceeded, the design basis leakage rates are not exceeded during normal or hypothetical accident conditions of transport.

The HI-STAR overpack is subjected to a containment system fabrication verification test before the first use as described in Chapter 8. The containment system fabrication verification test is performed at the factory as part of the HI-STAR 100 acceptance testing. The welds of the containment boundary, the closure plate inner seal, and the vent and drain port plug seals are helium leakage tested in accordance with ANSI N14.5. A containment system periodic verification test as described in Chapter 8, will be performed prior to each loaded transport. The mechanical seals of the HI-STAR 100 overpack will be replaced and retested each time the HI-STAR 100 is loaded.

As the containment system periodic verification leakage test shall be performed on the containment boundary prior to each loaded transport, this test takes the place of and is performed in lieu of the assembly verification.

4.1 CONTAINMENT BOUNDARIES

The containment system boundary for the HI-STAR 100 packaging consists of the overpack inner shell, the bottom plate, the top flange, the top closure plate, closure bolts, the overpack vent and drain port plugs, and their respective mechanical seals. The containment boundary system components for the HI-STAR 100 system are designed and fabricated in accordance with the requirements of ASME Code, Section III, Subsection NB [4.1.1], to the maximum extent practicable. Chapter 1 provides design criteria for the containment design. Section 1.3 provides applicable Code requirements. Exceptions to specific Code requirements with complete justifications are presented in Table 1.3.2. The containment boundary components are shown on Figure 4.1.1 with additional details provided in Figures 4.1.2 and 4.1.3.

Chapter 2 provides design criteria for the containment design. Section 1.3 provides applicable Code requirements. Alternatives to specific Code requirements with complete justifications are presented in Table 1.3.2.

4.1.1 Containment Vessel

The containment vessel for the HI-STAR 100 packaging consists of the overpack components which form the inner cavity volume used to house any of the MPC designs which contain spent nuclear fuel. The containment vessel is represented by the overpack inner shell, bottom plate, the top flange, and the closure plate. These components create an enclosed cylindrical cavity sufficient for insertion and enclosure of an MPC. The materials of construction for the packaging containment vessel are specified in the drawings in Section 1.4.

Table 4.1.1 provides a summary of the containment boundary design specifications.

4.1.2 Containment Penetrations

The containment system boundary penetrations for the HI-STAR 100 package include the closure plate test port plug, the vent port plug, the drain port plug, and their respective mechanical seals. Each penetration has redundant mechanical seals. The vent port is located in the closure plate and the drain port is located in the bottom plate. The closure configuration of the vent and drain ports is essentially identical (See Figure 4.1.3). The containment penetrations are designed and tested to ensure that the radionuclide release rates specified in 10CFR71.51 will not be exceeded.

4.1.3 Seals and Welds

The HI-STAR 100 containment vessel uses a combination of seals and welds designed and tested during normal transport conditions, and during and after the hypothetical transport accident conditions. Seals and welds are individually discussed below.

The seals and welds discussed below provides a containment system which is securely closed and cannot be opened unintentionally or by an internal pressure within the package as required in 10CFR71.43(c).

4.1.3.1 Containment Seals

The HI-STAR 100 closure plate uses two concentric metallic seals to form the closure between the top flange surface and the closure plate. To protect the sealing surfaces against corrosion, a stainless steel weld inlay is provided during manufacturing on both the closure plate and mating overpack surfaces. The closure plate inner seal is tested for leakage through a small test port in the overpack closure plate (See Figure 4.1.2). The test port provides access to the volume between the two mechanical lid seals for leakage testing of the closure plate inner seal. Following leakage testing, a threaded plug with a metallic seal is installed in the test port hole to provide redundant closure.

Closure of the vent and drain ports is achieved via a threaded plug with a single metallic seal. The metallic seal is compressed between the underside of the threaded plug head and the overpack body to form the seal. The sealing surfaces are not subject to corrosion due to the presence of the cover plates and their seals preventing exposure of the seal surfaces to the elements. Each port plug seal is independently tested for leakage to verify containment performance. A bolted cover plate, with a machined seal groove, is installed over the vent and drain ports. A metallic seal, installed in the cover plate groove, is compressed between the cover plate and the overpack body during cover plate bolt torquing. These cover plates provide redundant closure of the drain and vent port penetrations.

Details on the seals are provided in the drawings in Section 1.4 and in Appendix 4.B. Table 4.1.1 contains reference information for the seals from the selected supplier. Note that the seals selected are designed and fabricated to meet the design requirements of the HI-STAR 100 System. The Chapter 7 procedures require replacement of any used seal after closure opening except for transportation of an empty overpack.

4.1.3.2 Containment Welds

The containment boundary welds of the HI-STAR 100 overpack body include the welds forming the inner closure shell, the weld connecting the inner shell to the top flange, and the weld connecting the bottom plate to the inner shell. All containment boundary welds are fabricated and inspected in accordance with ASME Code Section III, Subsection NB (no stamp required). Full-penetration welds are specified for the plates that form the overpack inner shell. Full-penetration welds are also specified for the inner shell to the top flange and bottom plate welds. The weld details are shown in the drawings in Section 1.4. The containment boundary welds are volumetrically examined by radiography (RT) as described in Chapter 8.

4.1.4 Closure

The HI-STAR 100 packaging closure plate is secured using multiple closure bolts around the perimeter. Torquing of the closure plate bolts compresses the closure plate concentric mechanical seals between the closure plate and the overpack flange forming the closure plate seal.

Closure of the overpack vent and drain ports is provided by a single threaded plug installed in each penetration (see Figure 4.1.3). The mechanical seal is compressed between the underside of the port plug head and the overpack body forming the port closure. A cover plate, containing a single

metallic seal, is installed over each of the ports forming the redundant closure of the vent and drain port penetrations. The cover plate is secured by bolts. The closure plate test port is sealed using a port plug and mechanical seal in the same manner as the vent and drain port penetrations (see Figure 4.1.2).

The installation procedures, bolt torquing patterns, required lubrication, and torque values are provided in Table 7.1.1. The torque values are established to maintain containment during normal and accident conditions of transport. Torque values for the closure plate bolts were determined to preclude separation of the closure plate from the overpack flange. Appendix 4.A contains the calculations for the test, vent and drain port plugs and the vent and drain port cover plates bolt torques.

Table 4.1.2 provides a summary of the containment closure bolting for the HI-STAR 100 overpack penetrations.

4.1.5 Damaged Fuel Container

Fuel assemblies classified as damaged fuel or fuel debris (assembly array/class 6x6A, 6x6B, 6x6C, 7x7A, and 8x8A for BWR fuel as specified in Table 1.2.11 and Trojan damaged fuel and fuel debris for PWR fuel as specified in Table 1.2.10) have been evaluated.

The MPC is designed to transport damaged fuel, fuel debris, or intact fuel. To aid in loading and unloading, damaged fuel assemblies and fuel debris will be loaded into stainless steel DFCs. The damaged fuel container (DFC) is shown in the drawings in Section 1.4. The DFC is designed to provide SNF loose component retention and handling capabilities. The DFC consists of a smooth-walled, welded stainless steel square canister with a removable lid. The canister lid provides the means of DFC closure and handling. The DFC is provided with stainless steel wire mesh screens in the top and bottom for draining, drying and helium backfill operations. The screens are specified as a 250-by-250-mesh with an effective opening of 0.0024 inches. There are no other openings in the DFC. Chapter 1 specifies the fuel assembly characteristics for damaged fuel acceptable for loading in the MPC-68, MPC-68F, or MPC-24EF and for fuel debris acceptable for loading in the MPC-68F or MPC-24EF.

Up to four (4) DFCs containing specified fuel debris may be placed in a custom-designed Trojan MPC-24EF (Trojan PWR fuel debris) or an MPC-68F (BWR fuel debris). Up to 4 PWR damaged fuel assemblies in DFCs may be transported in a custom-designed Trojan MPC-24EF or up to 68 BWR damaged fuel assemblies in DFCs may be transported in an MPC-68 or MPC-68F, respectively. The quantity of fuel debris is limited to meet the off-site transportation requirements of 10CFR71, specifically, 10CFR71.51(a)(1). Analyses provided in this chapter conservatively assume 100% of the rods of the fuel debris are breached under normal conditions of transport. Therefore, 100% of the contents of the DFCs are available for release.

Table 4.1.1

SUMMARY OF CONTAINMENT BOUNDARY DESIGN SPECIFICATIONS

Design Attribute	Design Rating
Closure Plate Mechanical Seals:[††] Design Temperature Pressure Rating Design Leakage Rate	 1200°F 1,000 psig $1x10^{-6}$ cm^3/s, Helium
Overpack Vent and Drain Port Cover Plate Mechanical Seals: [†,††] Design Temperature Pressure Rating Design Leakage Rate	 1200°F 1,000 psig $1x10^{-6}$ cm^3/sec, Helium
Overpack Vent and Drain Port Plug Mechanical Seals: [††] Design Temperature Pressure Rating Design Leakage Rate	 1200°F 1,000 psig $1x10^{-6}$ cm^3/sec, Helium
Leakage Rate Acceptance Criterion	4.3×10^{-6} atm cm^3/s, He
Leakage Rate Test Sensitivity	2.15×10^{-6} atm cm^3/s, He

† No credit is taken for the overpack vent and drain port cover plate seals as part of the containment boundary. Specifications are provided for information.

†† Per manufacturer's recommended operating limits.

Table 4.1.2

CONTAINMENT CLOSURE BOLTING SUMMARY

Item	Qty	Type	Material
Closure Plate Bolt (Long)	52	1-5/8"-8 UNC x 7-3/8" LG Cap Screw	SB-637-N07718
Closure Plate Bolt (Short)	2	1-5/8"-8 UNC x 7-1/8" LG Cap Screw	SB-637-N07718
Vent/Drain Port Cover Plate Bolt	4 ea	3/8 -16 UNC x 5/8" LG Cap Screw	SA-193 GRADE B7
Vent/Drain/Closure Plate Test Port Plugs	1 ea	7/8" diameter Fabricated Plug	SA-193 GRADE B8

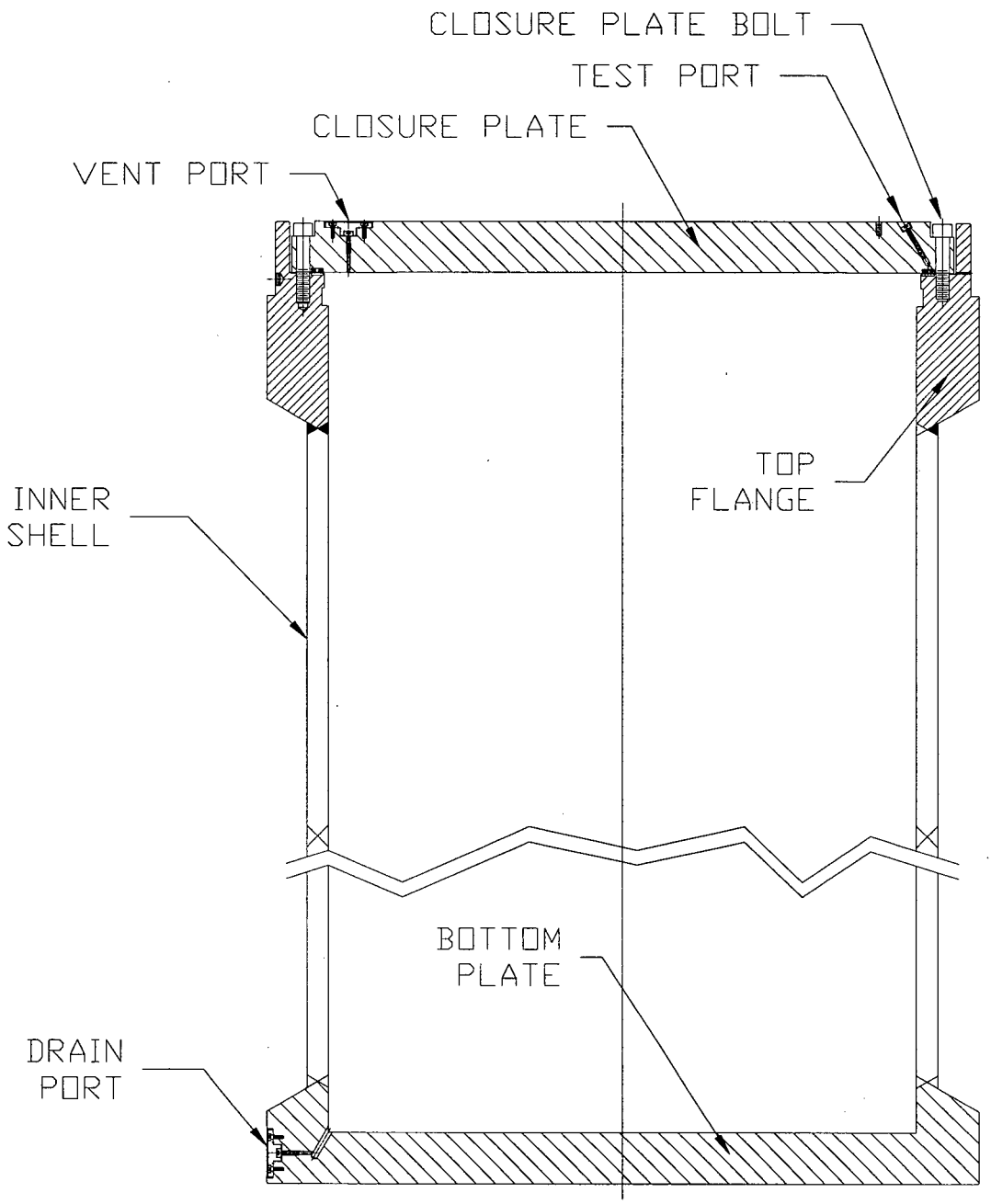

FIGURE 4.1.1; HI-STAR 100 OVERPACK PRIMARY CONTAINMENT BOUNDARY COMPONENTS

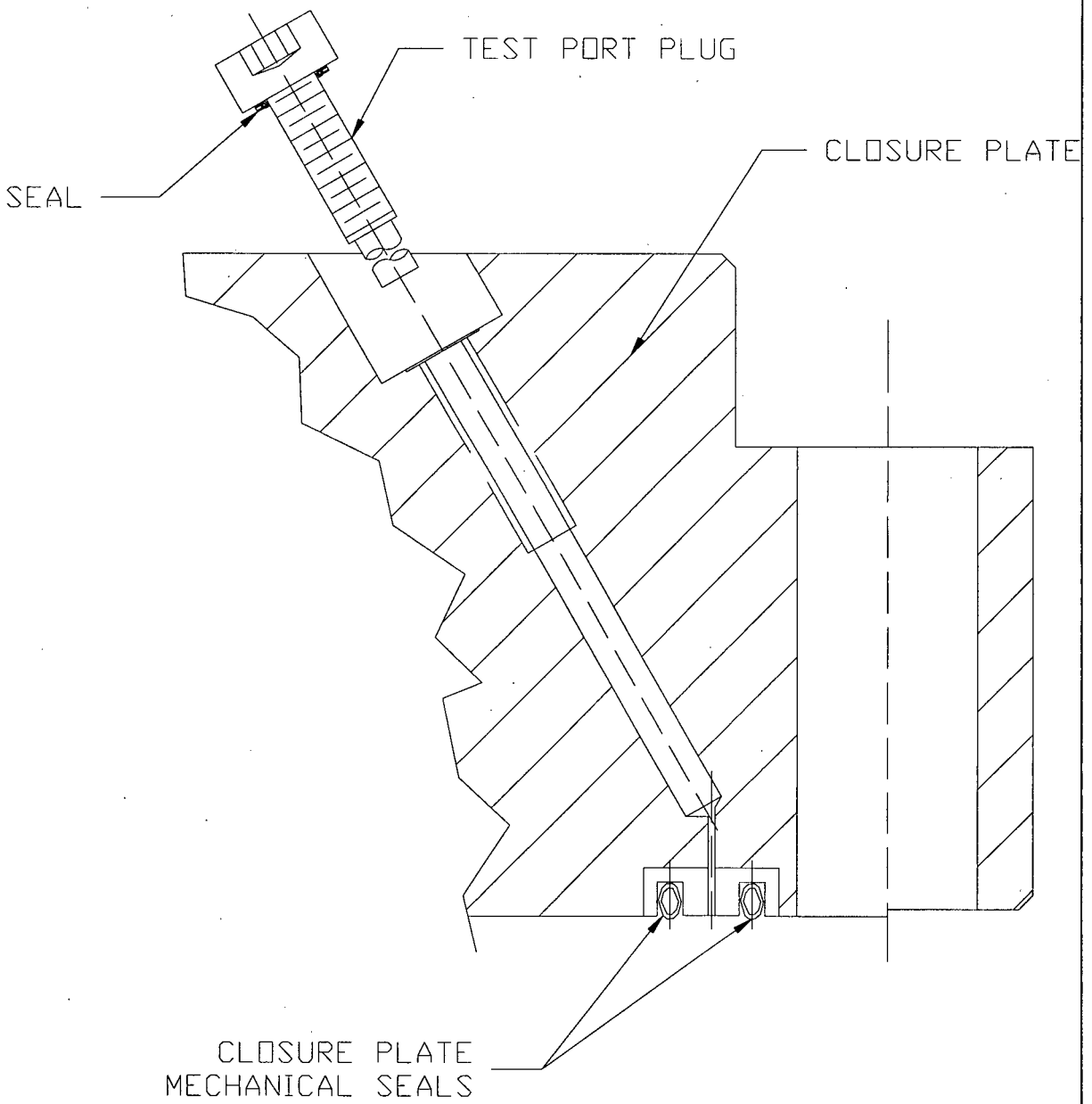

FIGURE 4.1.2; HI-STAR 100 CLOSURE PLATE CONTAINMENT DETAILS

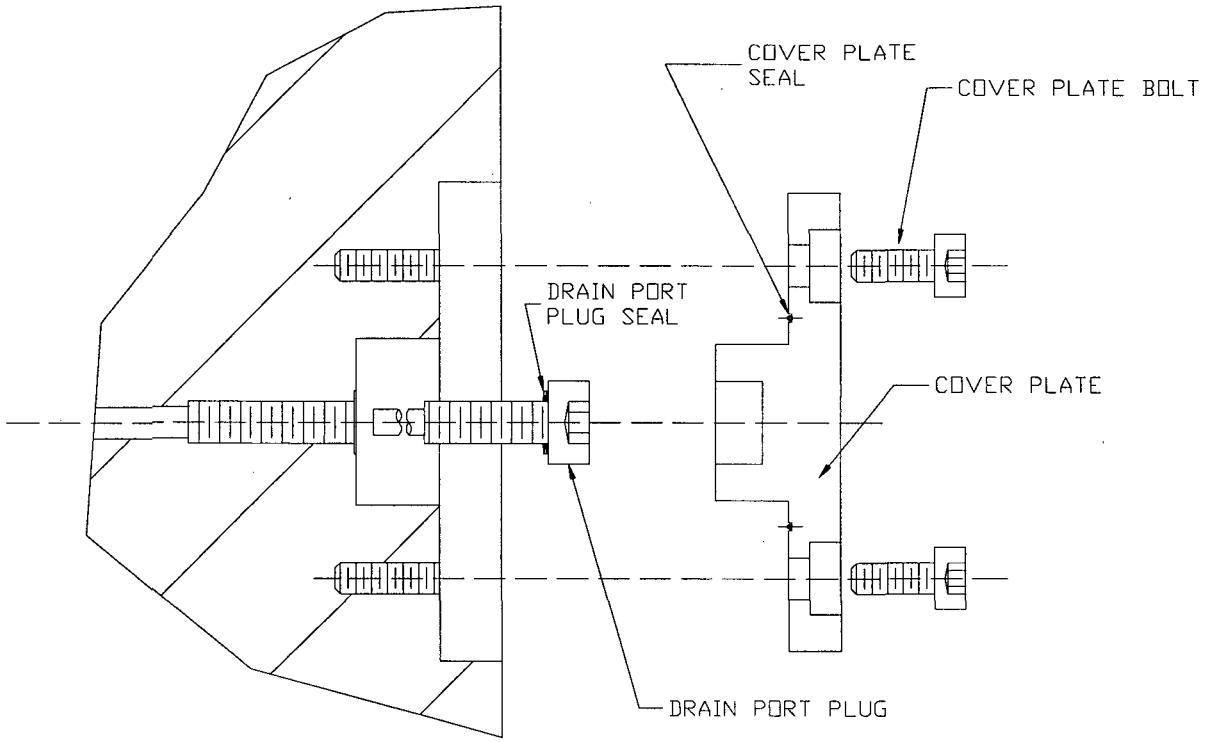

FIGURE 4.1.3; HI-STAR 100 OVERPACK VENT AND DRAIN PORT DETAILS

FIGURE 4.1.4;
THIS FIGURE WAS INTENTIONALLY DELETED

4.2 REQUIREMENTS FOR NORMAL AND HYPOTHETICAL ACCIDENT CONDITIONS OF TRANSPORT

Chapter 2 shows that all containment components are maintained within their code-allowable stress limits during all normal and hypothetical accident conditions of transport as defined in 10CFR71.71 and 10CFR71.73 [4.0.1]. Chapter 3 shows that the peak containment component temperatures and pressure are within the design basis limits for all normal and hypothetical accident conditions of transport as defined in 10CFR71.71 and 10CFR71.73. Since the containment vessel remains intact, and the temperature and pressure design bases are not exceeded, the design basis leakage rate (see Table 4.1.1) will not be exceeded during normal or hypothetical accident conditions of transport.

4.2.1 Containment Criteria

The allowable leakage rates presented in this chapter were determined in accordance with ANSI N14.5-1997 [4.0.2] and shall be used for containment system fabrication verification and containment system periodic verification tests of the HI-STAR 100 containment boundary. Measured leakage rates shall not exceed the values presented in Table 4.1.1. Compliance with these leakage rates ensures that the radionuclide release rates specified in 10CFR71.51 will not be exceeded during normal or hypothetical accident conditions of transport.

4.2.2 Containment of Radioactive Material

The HI-STAR 100 packaging allowable leakage rate (See Table 4.1.1) ensures that the requirements of 10CFR71.51 are met. Section 4.2.5 determines the maximum leakage rate for normal and hypothetical accident conditions of transport and the allowable leakage rate criterion for the HI-STAR 100 packaging containing each of the MPC types. The maximum calculated leakage rates for normal transport conditions assume a full complement of design basis fuel assembly types with bounding radiological source terms. The calculations also assume 3% fuel rod rupture for normal conditions. This bounds all possible MPC fuel loading configurations. For calculating the maximum leakage rates for normal conditions of transport, the internal pressure is conservatively assumed to be greater than the MPC internal pressure for the most limiting MPC type determined in Chapter 3. Following testing, no credit is taken for the MPC as a containment boundary.

The allowable leakage rate is then conservatively chosen to be less than the calculated maximum leakage rates from all MPC types for normal conditions of transport. This ensures that the 10CFR71.51(a)(1) limit for radionuclide release are not exceeded.

4.2.3 Pressurization of Containment Vessel

The HI-STAR 100 overpack contains a sealed MPC during normal conditions of transport. Except for the small space between the MPC and overpack, the overpack internal cavity is essentially filled. This space (annulus) is drained, dried, evacuated and backfilled with helium gas prior to final closure of the overpack; therefore, no vapors or gases are present which could cause a reaction or explosion inside the overpack. Procedural steps (Chapter 7) prevent overpack over-pressurization during closure operations. The enclosed MPC is also drained, dried, and backfilled with helium gas

prior to final closure; therefore, any MPC leak would not introduce any explosive gases into the overpack cavity. Since the exterior of the MPC is entirely composed of stainless steel, there is no possibility of chemical reaction that would produce gas or vapor. The overpack accident condition design basis internal pressure analysis assumes a non-mechanistic event resulting in the loss of MPC closure welds, a full-complement of design basis fuel with 100% fill gas and 30% of significant fission gas release, and the hypothetical 10CFR71.73(c)(4) fire condition. Even in this event, structural integrity and containment of the HI-STAR 100 packaging are maintained.

As the MPC is drained, dried, evacuated and backfilled with helium gas, no vapors or gases are present which could cause a reaction or explosion inside the MPC. Procedural steps (Chapter 7) prevent MPC over-pressurization during closure operations. The interior of the MPC contains stainless steel, neutron absorber, and optional aluminum heat conductive inserts. There is no possibility of chemical reaction that would produce gas or vapor.

4.2.4 Assumptions

The HI-STAR 100 System is designed to meet the radioactive release limit requirements of 10CFR71.51. Allowable leakage rates are determined in accordance with the requirements of ANSI N14.5, and utilizing NUREG/CR-6487, *Containment Analysis for Type B Packages Used to Transport Various Contents* [4.0.3] and Regulatory Guide 7.4, *Leakage Tests on Packages for Shipment of Radioactive Materials* [4.0.4] as guides.

The following assumptions have been used in determining the allowable leakage rates:

1. For MPCs other than the MPC-24EF with Trojan fuel debris and MPC-68F, three percent of the fuel rods are assumed to have failed during normal conditions of transportation. One-hundred percent of the fuel rods are assumed to have failed during hypothetical accident conditions.

2. Thirty percent of the radioactive gases are assumed to escape each failed fuel rod.

3. Fifteen percent of the ^{60}Co from the crud on the surface of the fuel rods is released as an aerosol in normal conditions of transport. One-hundred percent of the ^{60}Co is released as an aerosol from the surfaces of the fuel assemblies during accident conditions.

4. Since the overpack internals are never exposed to contaminants, the residual activity on the overpack interior surface and the MPC exterior surface is negligible compared to crud deposits on the fuel and is neglected as a source term.

5. Up to four (4) DFCs containing specified fuel debris may be placed in an MPC-24EF (only the custom-designed Trojan MPC-24EF) or an MPC-68F.

6. Crud spallation and cladding breaches occur instantaneously after fuel loading and container closure operations.

7. The calculation for normal transport conditions of an MPC containing fuel debris assumes 100% of the rods of the fuel debris are breached.

8. For containment analysis purposes, the MPC-24, MPC-24E or MPC-24EF contain up to 24 PWR assemblies, of which 4 of these in the custom-designed Trojan MPC-24EF may be DFCs with Trojan fuel debris, the MPC-32 contains up to 32 PWR assemblies, the MPC-68 contains up to 68 BWR assemblies, and the MPC-68F contains up to 68 intact BWR fuel assemblies, of which 4 of those may be specified BWR fuel debris in damaged fuel containers.

9. 0.003% of the total fuel mass contained in a rod is assumed to be released as fines if the cladding on the rod ruptures (i.e., $f_f=3x10^{-5}$).

10. Bounding values for the crud surface activity for PWR rods is $140x10^{-6}$ Ci/cm^2 and for BWR rods is $1254x10^{-6}$ Ci/cm^2.

11. The rod surface area per assembly is $3x10^5$ cm^2 for PWR and $1x10^5$ cm^2 for BWR fuel assemblies. These surface areas are also conservatively used for the surface area of damaged fuel or fuel debris..

12. The release fractions for volatiles (^{89}Sr, ^{90}Sr, ^{103}Ru, ^{106}Ru, ^{134}Cs, ^{135}Cs, and ^{137}Cs) are all assumed to be $2x10^{-4}$ ($f_V=2x10^{-4}$).

13. In the analysis of the containment boundary, no credit is taken for the presence of the seal welded MPC.

14. In calculating the leakage rates of the containment system for normal conditions of transport, the internal pressure of the overpack is conservatively assumed to be equal to or larger than the maximum internal pressure of all MPC types determined in Chapter 3.

15. The average cavity temperature for accident conditions is conservatively assumed to be the design basis peak cladding temperature of 1058°F (843K).

16. All of the activity associated with crud is assumed to be Cobalt-60.

17. It is assumed that the flow is unchoked for all leakage analyses.

18. Deleted

19. Deleted

4.2.5 Analysis and Results

The allowable leakage rates for the containment boundary under normal and hypothetical accident

conditions of transport at operating conditions for the HI-STAR 100 packaging containing each of the MPC types were determined and are presented in this chapter. To calculate the leakage rates for a particular contents type and transportation condition, the following were determined: the source term concentration for the releasable material; the effective A_2 of the individual contributors; the releasable activity; the effective A_2 for the total source term; the allowable radionuclide release rates; and the allowable leakage rates at transport (operating) conditions. Using the equations for continuum and molecular flow, the corresponding leakage hole diameters were calculated. Then, using these leak hole diameters, the corresponding allowable leakage rates at test conditions were calculated. Parameters were utilized in a way that ensured conservatism in the final leakage rates for the conditions, contents, and package arrangements considered.

The methodology and analysis results are summarized below.

4.2.5.1 Volume in the Containment Vessel

As discussed above, the containment system boundary for the HI-STAR 100 packaging consists of the overpack inner shell and associated components.

Except for a small volume between the MPC and the overpack (the annulus), the overpack internal cavity is essentially filled. Therefore, the free gas volume for the containment boundary includes the free gas volume for the MPC plus the overpack annulus volume. The free gas volume in each of the MPC types is presented in Chapter 3. The free gas volumes of the containment system are repeated in Table 4.2.1 for completeness. The MPC-24E and MPC-24EF basket designed for Trojan are shorter to allow for storage in their overpacks. These shorter baskets are designated as the Trojan MPC-24E and Trojan MPC-24EF, respectively, where necessary. For calculating the free volume in the containment system (overpack) with either of the Trojan MPCs, the annulus space is assumed to be the same as that for the larger generic MPCs (i.e. the larger annulus space between the Trojan MPC and HI-STAR overpack is neglected). This will conservatively underestimate the free volume inside the containment boundary.

4.2.5.2 Source Terms For Spent Nuclear Fuel Assemblies

In accordance with NUREG/CR-6487 [4.0.3], the following contributions are considered in determining the releasable source term for packages designed to transport irradiated fuel rods: (1) the radionuclides comprising the fuel rods, (2) the radionuclides on the surface of the fuel rods, and (3) the residual contamination on the inside surfaces of the vessel. NUREG/CR-6487 goes on to state that a radioactive aerosol can be generated inside a vessel when radioactive material from the fuel rods or from the inside surfaces of the container become airborne. The sources for the airborne material are (1) residual activity on the cask interior, (2) fission and activation-product activity associated with corrosion-deposited material (crud) on the fuel assembly surface, and (3) the radionuclides within the individual fuel rods. In accordance with NUREG/CR-6487, contamination due to residual activity on the cask interior surfaces is negligible as compared to crud deposits on the fuel rods themselves and therefore may be neglected. The source term considered for this calculation results from the spallation of crud from the fuel rods and from the fines, gases and volatiles which result from cladding breaches.

The inventory for isotopes other than ^{60}Co is calculated with the SAS2H and ORIGEN-S modules of the SCALE 4.3 system as described in Chapter 5. The inventory for the MPC-24, MPC-24E, MPC-24EF, and MPC-32 was conservatively based on the B&W 15x15 fuel assembly with a burnup of 45,000 MWD/MTU, 5 years of cooling time, and an enrichment of 3.6%. The inventory for the Trojan MPCs (Trojan MPC-24E, Trojan MPC-24EF) was based on the Westinghouse 17x17 fuel assembly with a burnup of 42,000 MWD/MTU, 9 years cooling time, and an enrichment of 3.09%. The inventory for the MPC-68 was based the GE 7x7 fuel assembly with a burnup of 45,000 MWD/MTU, 5 years of cooling time, and 3.2% enrichment. The inventory for the MPC-68F was based on the GE 6x6 fuel assembly with a burnup of 30,000 MWD/MTU, 18 years of cooling time, and 1.8% enrichment. Additionally, an MPC-68F was analyzed containing 67 GE 6x6 assemblies and a DFC containing 18 thorium rods. Finally, an Sb-Be source stored in one fuel rod in one assembly with 67 GE 6x6 assemblies was analyzed. The isotopes which contribute greater than 0.01% to the total curie inventory for the fuel assembly are considered in the evaluation as fines. Additionally, isotopes with A_2 values less than 1.0 in Table A-1, Appendix A, 10CFR71 are included as fines. Isotopes which contribute greater than 0.01% but which do not have an assigned A_2 value in Table A-1 are assigned an A_2 value based on the guidance in Table A-3, Appendix A, 10CFR71. Finally, those radionuclides that have no A_2 value in Table A-1 from Appendix A of 10CFR71, have a half-life shorter than 10 days, and have a half-life less than their parent radionuclide (i.e, are in secular equilibrium with their parent nuclide),, are in accordance with 10CFR71, Appendix A, III treated as a single radionuclide along with the parent nuclide. Table 4.2.2 presents the isotope inventory used in the calculation.

A. Source Activity Due to Crud Spallation from Fuel Rods

The majority of the activity associated with crud is due to ^{60}Co [4.0.3]. The inventory for ^{60}Co was determined by using the crud surface activity for PWR rods (140×10^{-6} Ci/cm^2) and for BWR rods (1254×10^{-6} Ci/cm^2) provided in NUREG/CR-6487 [4.0.3] multiplied by the surface area per assembly (3×10^5 cm^2 and 1×10^5 cm^2 for PWR and BWR, respectively, also provided in NUREG/CR-6487).

The source terms were then decay corrected (5 years for the MPC-24, MPC-24E, MPC-24EF, MPC-32 and the MPC-68; 18 years for the MPC-68F; 9 years for the Trojan MPCs) using the basic radioactive decay equation:

$$A(t) = A_0 e^{-\lambda t} \qquad \textbf{(4-1)}$$

where:

$A(t)$ is activity at time t [Ci]
A_o is the initial activity [Ci]
λ is the $\ln 2/t_{1/2}$ (where $t_{1/2} = 5.272$ years for ^{60}Co)
t is the time in years (5 years for the MPC-24, MPC-24E, MPC-24EF, MPC-32 and the MPC-68; 18 years for the MPC-68F; 9 years for the Trojan MPCs)

The inventory for ^{60}Co was determined using the methodology described above with the following results:

PWR
Surface area per Assy = 3.0E+05 cm^2
140 $\mu Ci/cm^2$ x 3.0E+05 cm^2 = 42.0 Ci/assy

BWR
Surface area per Assy = 1.0E+05 cm^2
1254 $\mu Ci/cm^2$ x 1.0E+05 cm^2 = 125.4 Ci/assy

$^{60}Co(t) = {}^{60}Co_0\, e^{-(\lambda t)}$, where $\lambda = \ln 2/t_{1/2}$, t = 5 years (for the MPC-24, MPC-24E, MPC-24EF, MPC-32 and MPC-68), t = 18 years (MPC-68F), t = 9 years (Trojan MPCs), $t_{1/2}$ = 5.272 years for ^{60}Co [4.2.4]

MPC-24, MPC-24E, MPC-24EF, MPC-32
$^{60}Co(5) = 42.0\ Ci\ e^{-(\ln 2/5.272)(5)}$
$^{60}Co(5) = 21.77$ Ci/assy

MPC-68
$^{60}Co(5) = 125.4\ Ci\ e^{-(\ln 2/5.272)(5)}$
$^{60}Co(5) = 64.98$ Ci/assy

Trojan MPC-24E, Trojan MPC-24EF
$^{60}Co(5) = 42.0\ Ci\ e^{-(\ln 2/5.272)(9)}$
$^{60}Co(5) = 12.86$ Ci/assy

MPC-68F
$^{60}Co(18) = 125.4\ Ci\ e^{-(\ln 2/5.272)(18)}$
$^{60}Co(18) = 11.76$ Ci/assy

A summary of the ^{60}Co inventory available for release is provided in Table 4.2.2.

The activity density that results inside the containment vessel as a result of crud spallation from spent fuel rods can be formulated as:

$$C_{crud} = \frac{f_C\, M_A\, N_A}{V} \qquad \textbf{(4-2)}$$

where:

C_{crud} is the activity density inside the containment vessel as a result of crud spallation [Ci/cm^3],
M_A is the total crud activity inventory per assembly [Ci/assy],
f_C is the crud spallation fraction,
N_A is the number of assemblies, and
V is the free volume inside the containment vessel [cm^3].

NUREG/CR-6487 states that measurements have shown 15% to be a reasonable value for the percent of crud spallation for both PWR and BWR fuel rods under normal transportation conditions. For hypothetical accident conditions, it is assumed that there is 100% crud spallation [4.0.3].

B. Source Activity Due to Releases of Fines from Cladding Breaches

A breach in the cladding of a fuel rod may allow radionuclides to be released from the resulting cladding defect into the interior of the MPC. If there is a leak in the containment vessel, then the radioisotopes emitted from a cladding breach that were aerosolized may be entrained in the gases escaping from the package and result in a radioactive release to the environment.

NUREG/CR-6487 suggests that a bounding value of 3% of the rods develop cladding breaches during normal transportation (i.e., f_B=0.03). For hypothetical accident conditions, it is assumed that all of the rods develop a cladding breach (i.e., f_B=1.0). These values were used for both PWR and BWR fuel rods. As described in NUREG/CR-6487, roughly 0.003% of the fuel mass contained in a rod is released as fines if the cladding on the rod ruptures (i.e., $f_f=3x10^{-5}$).

The calculation for normal transport conditions of either a Trojan MPC-24EF or an MPC-68F containing four (4) DFCs containing fuel debris assumes that for the four DFCs, 100% of the rods of the fuel debris are breached. The remaining 20 or 64 assemblies in either the Trojan MPC-24EF or the MPC-68F, respectively, were assumed to have a 3% cladding rupture. Therefore, f_B for a Trojan MPC-24EF or an MPC-68F containing fuel debris is:

$$f_B = (0.03)\frac{20}{24} + (1.0)\frac{4}{20}$$
$$f_B = 0.192 \qquad \textbf{(4-3a)}$$

$$f_B = (0.03)\frac{64}{68} + (1.0)\frac{4}{68}$$
$$f_B = 0.087 \qquad \textbf{(4-3b)}$$

The activity concentration inside the containment vessel due to fines being released from cladding breaches is given by:

$$C_{fines} = \frac{f_f\, I_{fines}\, N_A\, f_B}{V} \qquad \textbf{(4-4)}$$

where:

C_{fines} is the activity concentration inside the containment vessel as a result of fines released from cladding breaches [Ci/cm^3],
f_f is the fraction of a fuel rod's mass released as fines as a result of a cladding breach ($f_f=3x10^{-5}$),
I_{fines} is the total activity inventory [Ci/assy],
N_A is the number of assemblies,
f_B is the fraction of rods that develop cladding breaches, and
V is the free volume inside the containment vessel [cm^3].

C. Source Activity from Gases due to Cladding Breaches

If a cladding failure occurs in a fuel rod, a large fraction of the gap fission gases will be introduced into the free volume of the system. Tritium and Krypton-85 are typically the major sources of radioactivity among the gases present [4.0.3]. NUREG/CR-6487 suggests that a bounding value of

30% of the fission product gases escape from a fuel rod as a result of a cladding breach (i.e., f_g=0.3).

The activity concentration due to the release of gases form a cladding breach is given by:

$$C_{gases} = \frac{f_g I_{gases} N_A f_B}{V} \quad \textbf{(4-5)}$$

where:

C_{gases} is the releasable activity concentration inside the containment vessel due to gases released from cladding breaches [Ci/cm^3],
f_g is the fraction of gas that would escape from a fuel rod that developed a cladding breach,
I_{gases} is the gas activity inventory [^{3}H, ^{129}I, ^{85}Kr, ^{81}Kr, ^{127}Xe] [Ci/assy],
N_A is the number of assemblies,
f_B is the fraction of rods that develop cladding breaches, and
V is the free volume inside the containment vessel [cm^3].

D. Source Activity from Volatiles due to Cladding Breaches

Volatiles such as cesium, strontium, and ruthenium, can also be released from a fuel rod as a result of a cladding breach. NUREG/CR-6487 estimates that $2x10^{-4}$ is a conservative bounding value for the fraction of the volatiles released from a fuel rod (i.e., f_V=$2x10^{-4}$).

The activity concentration due to the release of volatiles is given by:

$$C_{vol} = \frac{f_v I_{vol} N_A f_B}{V} \quad \textbf{(4-6)}$$

where:

C_{vol} is the releasable activity concentration inside the containment vessel due to volatiles released from cladding breaches [Ci/cm^3],
f_V is the fraction of volatiles that would escape from a fuel rod that developed a cladding breach,
I_{vol} is the volatile activity inventory [^{89}Sr, ^{90}Sr, ^{134}Cs, ^{135}Cs, ^{137}Cs, ^{134}Cs, ^{103}Ru, ^{106}Ru] [Ci/assy],
N_A is the number of assemblies,
f_B is the fraction of rods that develop cladding breaches, and
V is the free volume inside the containment vessel [cm^3].

E. Total Source Term for the HI-STAR 100 System

The total source term was determined by combining Equations 4-2, 4-4, 4-5, and 4-6:

$$C_{total} = C_{crud} + C_{fines} + C_{gases} + C_{vol} \quad \textbf{(4-7)}$$

where C_{total} has units of Ci/cm^3.

Table 4.2.3 presents the total source term determined using the above methodology. Table 4.2.4 summarizes the parameters from NUREG/CR-6487 used in this analysis.

4.2.5.3 Effective A_2 of Individual Contributors (Crud, Fines, Gases, and Volatiles)

The A_2 of the individual contributions (i.e., crud, fines, gases, and volatiles) were determined in accordance with NUREG/CR-6487. As previously described, the majority of the activity due to crud is from Cobalt-60. Therefore, the A_2 value of 10.8 Ci used for crud for both PWR and BWR fuel is the same as that for Cobalt-60 found in 10CFR71, Appendix A.

In accordance with 10CFR71.51(b) the methodology presented in 10CFR71, Appendix A for mixtures of different radionuclides was used to determine the A_2 values for the gases, fines and volatiles.

$$A_2 \text{ for a mixture} = \frac{1}{\sum_{i=1}^{I} \frac{f_i}{(A_2)_i}} \qquad \textbf{(4-8)}$$

Where f(i) is the fraction of activity of nuclide I in the mixture and $A_2(i)$ is the appropriate A_2 value for the nuclide I.

10CFR71.51(b) also states that for Krypton-85, an effective A_2 value equal to 10 A_2 may be used. Table 4.2.5 summarizes the effective A_2 for all individual contributors.

4.2.5.4 Releasable Activity

The releasable activity is the product of the respective activity concentrations (C_{fines}, C_{gas}, C_{crud}, and C_{vol}) and the respective MPC volume. The releasable activity of fines, volatiles, gases, and crud were determined using this methodology.

$$\text{Releasable Activity [Ci]} = \text{Activity Concentration } [\frac{Ci}{cm^3}] \text{ x Volume } [cm^3] \qquad \textbf{(4-9)}$$

4.2.5.5 Effective A_2 for the Total Source Term

Using the releasable activity and the effective A_2 values from the individual contributors (i.e., crud, fines, gases, and volatiles), the effective A_2 for the total source term was calculated for each MPC type, for normal transportation and hypothetical accident conditions. The methodology used to determine the effective A_2 is the same as that used for a mixture, which is provided in Equation 4-8.

The results are summarized in Table 4.2.6. As stated in 4.2.5.3, the effective A_2 used for Krypton-85 is 10 A_2 (2700 Ci).

4.2.5.6 Allowable Radionuclide Release Rates

The containment criterion for the HI-STAR 100 System under normal conditions of transport is given in 10CFR71.51(a)(1). This criterion requires that a package have a radioactive release rate less than $A_2 \times 10^{-6}$ in one hour, where A_2 is the effective A_2 for the total source term in the packaging determined in 4.2.5.5. Additionally, 10CFR71.51(b)(2) specifies that for hypothetical accident conditions, the quantity that may be released in one week is A_2 (effective A_2 for the total source term determined in 4.2.5.5).

NUREG/CR-6487 and ANSI N14.5 provides the following equations for the allowable release rates.

Release rate for normal conditions of transport:

$$R_N = L_N C_N \leq A_2 \times 2.78\text{x}10^{-10}/\text{second} \qquad \textbf{(4-10)}$$

where:

R_N is the release rate for normal transport [Ci/s]
L_N is the volumetric gas leakage rate [cm^3/s]
C_N is the total source term activity concentration [Ci/cm^3]
A_2 is the appropriate effective A_2 value [Ci].

Release rate for hypothetical accident conditions:

$$R_A = L_A C_A \leq A_2 \times 1.65\text{x}10^{-6}/\text{second} \qquad \textbf{(4-11)}$$

where:

R_A is the release rate for hypothetical accident conditions [Ci/s]
L_A is the volumetric gas leakage rate [cm^3/s]
C_A is the total source term activity concentration [Ci/cm^3]
A_2 is the appropriate effective A_2 value [Ci].

Equations 4-10 and 4-11 were used to determine the allowable radionuclide release rates for each MPC type and transport condition. The release rates are summarized in Table 4.2.7.

4.2.5.7 Allowable Leakage Rates at Operating Conditions

The allowable leakage rates at operating conditions were determined by dividing the allowable release rates by the appropriate source term activity concentration (modifying Equations 4-10 and 4-11).

$$L_N = \frac{R_N}{C_N} \text{ or } L_A = \frac{R_A}{C_A} \quad \textbf{(4-12)}$$

where,

L_N or L_A is the allowable leakage rate at the upstream pressure for normal (N) or accident (A) conditions [cm^3/s],
R_N or R_A is the allowable release rate for normal (N) or accident (A) conditions [Ci/s], and
C_N or C_A is the allowable release rate for normal (N) or accident (A) conditions [Ci/cm^3].

The allowable leakage rates determined using Equation 4-12 are the allowable leakage rates at the upstream pressure. Table 4.2.9 summarizes the allowable leakage rates at the upstream pressures. The most limiting allowable leakage rate presented in Table 4.2.9 was conservatively selected and used to determine the leakage rate acceptance criterion.

Equation deleted **(4-13)**

4.2.5.8 Leakage Rate Acceptance Criteria for Test Conditions

The leakage rates discussed thus far were determined at operating conditions (see normal and accident conditions in Table 4.2.12). The following provides details of the methodology used to convert the allowable leakage rate at operating conditions to a leakage rate acceptance criterion at reference test conditions.

For conservatism, unchoked flow correlations were used as the unchoked flow correlations better approximate the true measured flow rate for the leakage rates associated with transportation packages. Using the equations for molecular and continuum flow provided in NUREG/CR-6487, the corresponding leak hole diameter was calculated by solving Equation 4-14a for D, the leak hole diameter. The capillary length required for Equation 4-14a for the containment was conservatively chosen as the closure plate inner seal seating width which is 0.25 cm.

$$L_{@P_u} = \left[\frac{2.49x10^6\, D^4}{a\, u} + \frac{3.81x10^3\, D^3 \sqrt{\frac{T}{M}}}{a\, P_a} \right] [P_u - P_d] \frac{P_a}{P_u} \quad \textbf{(4-14a)}$$

where:

$L_{@Pu}$ is the allowable leakage rate at the upstream pressure for normal and accident conditions [cm^3/s],
a is the capillary length [cm],
T is the temperature for normal and accident conditions [K],
M is the gas molecular weight [g/mole] = 4.0 from ANSI N14.5, Table B1 [4.0.2],
u is the fluid viscosity for helium [cP] from Rosenhow and Hartnett [4.2.3]

P_u is the upstream pressure [ATM],
D leak hole diameter [cm],
P_d is the downstream pressure for normal and accident conditions [ATM], and
P_a is the average pressure; $P_a = (P_u + P_d)/2$ for normal and accident conditions [ATM].

The actual leakage tests performed on the containment boundary are typically not performed under exactly the same conditions every time. Therefore, reference test conditions are specified to provide a consistent comparison of the measured leakage rate to the leakage rate acceptance criterion. The reference test conditions, and approximate actual test conditions are specified in Table 4.2.12.

The corresponding leak hole diameter at operating conditions was determined by solving Equation 4-14a for 'D' where $L_{@Pu}$ is the most restrictive allowable leakage rate at the upstream pressure from Table 4.2.9 and using the parameters for normal conditions of transport presented in Table 4.2.12.

Using this leak hole diameter and the temperature and pressure specified for reference test conditions provided in Table 4.2.12, Equation 4-14a was solved for the volumetric leakage rate at reference test conditions.

Equation B-1 of ANSI N14.5-1997 [4.0.2] is used to express this volumetric leakage rate into a mass-like helium flow rate (Q_u) as follows:

$$Q_u = L_u * P_u \text{ (atm-cm}^3\text{/sec)} \qquad \textbf{(4-14b)}$$

where:

L_u is the upstream volumetric leakage rate [cm^3/sec],
Q_u is the mass-like helium leak rate [atm-cm^3/sec], and
P_u is the upstream pressure [atm].

Using Equation 4-14b to convert the volumetric flow rate into a mass-like flow, the leakage rate acceptance criteria is calculated and conservatively reduced to the value presented in Table 4.1.1.

Table 4.2.12 provides additional parameters used in the analysis.

4.2.5.9 Leak Test Sensitivity

The sensitivity for the overpack leakage test procedures is equal to one-half of the allowable leakage rate. The HI-STAR 100 containment packaging tests in Chapter 8 incorporate the appropriate leakage test procedure sensitivity. The leakage rates for the HI-STAR 100 containment packaging with its corresponding sensitivity are presented in Table 4.1.1.

Table 4.2.1

FREE GAS VOLUME OF THE CONTAINMENT SYSTEM

MPC Type	Containment Volume (cm^3)
MPC-24	6.70×10^6
MPC-24E MPC-24EF	6.55×10^6
Trojan MPC-24E Trojan MPC-24EF	6.12×10^6
MPC-32	6.35×10^6
MPC-68	6.15×10^6
MPC-68F	6.15×10^6

Table 4.2.2

ISOTOPE INVENTORY
Ci/Assembly

Nuclide	PWR MPCs Ci/Assembly	MPC-68 Ci/Assembly	MPC-68F Ci/Assembly	Trojan MPCs Ci/Assembly
Gases				
^{3}H	2.76E+02	1.09E+02	1.78E+01	1.75E+02
^{129}I	2.17E-02	8.66E-03	3.49E-03	1.93E-02
^{85}Kr	4.69E+03	1.79E+03	2.37E+02	2.76E+03
^{81}Kr	7.97E-08	3.50E-08	1.19E-08	6.80E-08
^{127}Xe	5.95E-11	2.05E-11	0.00E+00	3.39E-29
Crud				
^{60}Co	2.18E+01	6.50E+01	1.18E+01	1.29E+01
Volatiles				
^{90}Sr	4.53E+04	1.76E+04	4.29E+03	3.36E+04
^{106}Ru	4.97E+04	1.74E+04	2.30E-01	7.99E+02
^{134}Cs	4.43E+04	1.66E+04	3.16E+01	5.14E+03
^{137}Cs	6.76E+04	2.68E+04	7.21E+03	5.20E+04
^{89}Sr	1.25E-01	3.47E-02	2.41E-35	1.01E-14
^{103}Ru	3.65E-03	1.13E-03	0.00E+00	5.47E-20
^{135}Cs	2.79E-01	1.11E-01	4.54E-02	2.16E-01
Fines				
^{225}Ac*	3.05E-08	2.14E-08	9.69E-09	4.02E-08
^{227}Ac*	2.36E-06	1.18E-06	1.45E-06	2.08E-06
^{110m}Ag	1.73E+02	6.58E+01	4.97E-06	3.32E-01
^{241}Am*	4.76E+02	1.61E+02	2.52E+02	9.50E+02

Table 4.2.2 (continued)
ISOTOPE INVENTORY

	PWR MPCs Ci/Assembly	MPC-68 Ci/Assembly	MPC-68F Ci/Assembly	Trojan MPCs Ci/Assembly
^{242M}Am*	5.60E+00	1.94E+00	9.35E-01	4.12E+00
^{243}Am*	2.23E+01	9.42E+00	3.30E+00	2.06E+01
^{210M}Bi*	0.00E+00	0.00E+00	0.00E+00	8.62E-19
^{247}Bk*	0.00E+00	0.00E+00	0.00E+00	0.00E+00
^{144}Ce	4.77E+04	1.45E+04	7.33E-03	2.13E+02
^{248}Cf*	0.00E+00	0.00E+00	0.00E+00	0.00E+00
^{249}Cf*	8.01E-05	4.47E-05	3.62E-06	5.86E-05
^{250}Cf*	2.92E-04	1.86E-04	6.69E-06	1.57E-04
^{251}Cf*	3.40E-06	2.06E-06	1.36E-07	2.31E-06
^{252}Cf*	4.11E-04	3.14E-04	3.64E-07	6.17E-05
^{254}Cf*	1.19E-13	1.05E-13	0.00E+00	1.28E-24
^{240}Cm*	0.00E+00	0.00E+00	0.00E+00	0.00E+00
^{242}Cm*	3.21E+02	1.26E+02	7.71E-01	3.42E+00
^{243}Cm*	1.61E+01	6.51E+00	1.54E+00	1.16E+01
^{244}Cm*	3.26E+03	1.45E+03	2.17E+02	2.30E+03
^{245}Cm*	3.25E-01	1.23E-01	2.48E-02	2.61E-01
^{246}Cm*	1.06E-01	5.40E-02	1.01E-02	9.26E-02
^{247}Cm*	7.07E-07	3.72E-07	5.26E-08	5.71E-07
^{248}Cm*	4.20E-06	2.43E-06	2.53E-07	3.17E-06

Table 4.2.2 (continued)

ISOTOPE INVENTORY

Ci/Assembly

	PWR MPCs Ci/Assembly	MPC-68 Ci/Assembly	MPC-68F Ci/Assembly	Trojan MPCs Ci/Assembly
^{154}Eu	4.03E+03	1.47E+03	1.44E+02	2.06E+03
^{155}Eu	1.34E+03	5.46E+02	2.23E+01	4.93E+02
^{55}Fe	6.98E+01	3.23E+01	2.94E-01	1.80E+01
^{148}Gd*	0.00E+00	0.00E+00	0.00E+00	0.00E+00
^{236}Np*	9.77E-06	3.29E-06	7.30E-07	7.23E-06
^{237}Np*	2.33E-01	8.07E-02	2.55E-02	1.90E-01
^{239}Np	2.23E+01	9.42E+00	3.30E+00	2.06E+01
^{231}Pa*	1.82E-05	8.17E-06	3.16E-06	7.94E-06
^{147}Pm	4.28E+04	1.52E+04	1.18E+02	7.93E+03
^{210}Po*	3.92E-09	1.98E-09	1.08E-08	1.21E-08
^{236}Pu*	2.04E-01	6.32E-02	3.66E-04	3.59E-02

Table 4.2.2 (continued)

ISOTOPE INVENTORY

Ci/Assembly

	PWR MPCs Ci/Assembly	MPC-68 Ci/Assembly	MPC-68F Ci/Assembly	Trojan MPCs Ci/Assembly
^{238}Pu*	2.56E+03	9.55E+02	2.50E+02	1.93E+03
^{239}Pu*	1.91E+02	6.24E+01	2.95E+01	1.63E+02
^{240}Pu*	3.27E+02	1.34E+02	6.81E+01	3.01E+02
^{241}Pu	7.55E+04	2.47E+04	5.16E+03	4.92E+04
^{242}Pu*	1.65E+00	7.05E-01	3.06E-01	1.60E+00
^{244}Pu*	1.11E-13	6.58E-14	3.73E-14	2.34E-13
^{223}Ra*	2.37E-06	1.18E-06	1.45E-06	2.08E-06
^{224}Ra*	8.57E-03	3.40E-03	1.72E-03	1.31E-02
^{225}Ra*	3.05E-08	2.14E-08	9.69E-09	4.02E-08
^{226}Ra*	2.82E-08	1.32E-08	5.94E-08	1.12E-07
^{228}Ra*	9.87E-12	4.63E-12	1.24E-11	3.07E-11
^{222}Rn*	2.82E-08	1.32E-08	5.94E-08	1.12E-07
^{125}Sb	2.87E+03	1.15E+03	9.46E+00	5.82E+02
^{151}Sm	2.60E+02	7.92E+01	2.53E+01	2.01E+02
^{119m}Sn	5.46E+02	3.08E+02	1.98E-04	3.18E+00
^{125m}Te	6.99E+02	2.82E+02	2.31E+00	1.42E+02
^{227}Th*	2.33E-06	1.16E-06	1.43E-06	2.05E-06
^{228}Th*	8.56E-03	3.40E-03	1.71E-03	1.31E-02
^{229}Th*	3.05E-08	2.14E-08	9.69E-09	4.02E-08
^{230}Th*	2.16E-05	8.26E-06	1.29E-05	4.40E-05

Table 4.2.2 (continued)
ISOTOPE INVENTORY
Ci/Assembly

	PWR MPCs Ci/Assembly	MPC-68 Ci/Assembly	MPC-68F Ci/Assembly	Trojan MPCs Ci/Assembly
^{231}Th*	7.11E-03	1.67E-03	5.43E-04	5.07E-03
^{230}U*	1.33E-23	4.74E-24	0.00E+00	0.00E+00
^{232}U*	1.51E-02	5.58E-03	1.69E-03	1.48E-02
^{233}U*	1.41E-05	4.20E-06	3.03E-06	1.60E-05
^{234}U*	4.97E-01	1.70E-01	7.26E-02	4.37E-01
^{236}U*	1.60E-01	5.85E-02	1.84E-02	1.29E-01
^{90}Y	4.53E+04	1.76E+04	4.29E+03	3.36E+04

Note: The isotopes which contribute greater than 0.01% to the total curie inventory for the fuel assembly are considered in the evaluation as fines. Additionally, isotopes with A_2 values less than 1.0 in Table A-1, Appendix A, 10CFR71 are included as fines and are designated in the table by an "*".

Table 4.2.3

TOTAL SOURCE TERM FOR THE HI-STAR 100 SYSTEM (Ci/cm^3)

	C_{crud} (Ci/cm^3)	C_{fines} (Ci/cm^3)	C_{vol} (Ci/cm^3)	C_{gas} (Ci/cm^3)	Total (Ci/cm^3)
Normal Transport Conditions					
MPC-24	1.17E-05	7.37E-07	4.45E-06	1.60E-04	1.77E-04
MPC-24E, MPC-24EF	1.20E-05	7.53E-07	4.55E-06	1.64E-04	1.81E-04
Trojan MPC-24E	7.56E-06	3.53E-07	2.15E-06	1.04E-04	1.14E-04
Trojan MPC-24EF	7.56E-06	2.26E-06	1.38E-05	6.63E-04	6.87E-04
MPC-32	1.64E-05	1.04E-06	6.26E-06	2.25E-04	2.49E-04
MPC-68	1.08E-04	7.85E-07	5.20E-06	1.89E-04	3.03E-04
MPC-68F	1.95E-05	3.06E-07	2.22E-06	7.35E-05	9.56E-05
Accident Conditions					
MPC-24	7.79E-05	2.46E-05	1.48E-04	5.34E-03	5.59E-03
MPC-24E, MPC-24EF	7.97E-05	2.51E-05	1.52E-04	5.46E-03	5.72E-03
Trojan MPC-24E	5.04E-05	1.18E-05	7.18E-05	3.45E-03	3.59E-03
Trojan MPC-24EF	5.04E-05	1.18E-05	7.18E-05	3.45E-03	3.59E-03
MPC-32	1.10E-04	3.45E-05	2.09E-04	7.51E-03	7.86E-03
MPC-68	7.18E-04	2.62E-05	1.73E-04	6.30E-03	7.22E-03
MPC-68F	1.30E-04	3.52E-06	2.55E-05	8.45E-04	1.00E-03

Table 4.2.4

VARIABLES FOUND IN NUREG/CR-6487 USED IN THE LEAKAGE RATE ANALYSIS

Variable	PWR		BWR	
	Normal	Accident	Normal	Accident
Fraction of crud that spalls, f_C	0.15	1.0	0.15	1.0
Crud surface activity (Ci/cm^2)	140×10^{-06}	140×10^{-06}	1254×10^{-06}	1254×10^{-06}
Surface area per assembly, cm^2	3×10^5	3×10^5	1×10^5	1×10^5
Fraction of rods that develop cladding breach, f_B†	0.03	1.0	0.03	1.0
Fraction of fines that are released, f_f	3×10^{-5}	3×10^{-5}	3×10^{-5}	3×10^{-5}
Fraction of gases that are released, f_G	0.3	0.3	0.3	0.3
Fraction of volatiles that are released, f_V	2×10^{-04}	2×10^{-04}	2×10^{-04}	2×10^{-04}

† The calculation for normal transport conditions of the Trojan MPC-24EF and MPC-68F each containing four (4) DFCs with fuel debris assumes that for the four DFCs, 100% of the rods of the fuel debris are breached. The remaining 20 or 64 assemblies in the Trojan MPC-24EF and MPC-68F, respectively, were assumed to have a 3% cladding rupture. Therefore, f_B for the Trojan MPC-24EF and the MPC-68F containing fuel debris is 0.192 and 0.087, respectively.

Table 4.2.5

INDIVIDUAL CONTRIBUTOR EFFECTIVE A_2
FOR GASES, CRUD, FINES, AND VOLATILES

MPC Type	A_2 (Ci)
Gases	
PWR MPCs	282
MPC-68	282
MPC-68F	285
Trojan MPCs	479
Crud	
All MPCs	10.8
Fines	
PWR MPCs	0.889
MPC-68	0.812
MPC-68F	0.351
Trojan MPCs	0.494
Volatiles	
PWR MPCs	9.72
MPC-68	9.90
MPC-68F	11.8
Trojan MPCs	11.8

Table 4.2.6

TOTAL SOURCE TERM EFFECTIVE A_2 FOR NORMAL AND HYPOTHETICAL ACCIDENT CONDITIONS

Normal Transport Conditions	
	Effective A_2 (Ci)
MPC-24	60.3
MPC-24E MPC-24EF	60.3
Trojan MPC-24E	62.6
Trojan MPC-24EF	87.7
MPC-32	60.3
MPC-68	24.9
MPC-68F	30.6
Accident Conditions	
MPC-24	81.0
MPC-24E MPC-24EF	81.0
Trojan MPC-24E	85.8
Trojan MPC-24EF	85.8
MPC-32	81.0
MPC-68	52.1
MPC-68F	37.0

Table 4.2.7

RADIONUCLIDE RELEASE RATES

	Allowable Release Rate (R_N or R_A) (Ci/s)
Normal Conditions	
MPC-24	1.68E-08
MPC-24E, MPC-24EF	1.68E-08
Trojan MPC-24E	1.74E-08
Trojan MPC-24EF	2.44E-08
MPC-32	1.68E-08
MPC-68	6.93E-09
MPC-68F	8.51E-09
Accident Conditions	
MPC-24	1.34E-04
MPC-24E, MPC-24EF	1.34E-04
Trojan MPC-24E	1.42E-04
Trojan MPC-24EF	1.42E-04
MPC-32	1.34E-04
MPC-68	8.59E-05
MPC-68F	6.10E-05

Table 4.2.8

Table Deleted

Table 4.2.9

ALLOWABLE LEAKAGE RATES AT UPSTREAM PRESSURE

	C_{total} (Ci/cm^3)	Allowable Leakage Rate at P_u L_N or L_A (cm^3/s)
Normal Transport Conditions		
MPC-24	1.77E-04	9.47E-05
MPC-24E, MPC-24EF	1.81E-04	9.26E-05
Trojan MPC-24E	1.14E-04	1.53E-04
Trojan MPC-24EF	6.87E-04	3.55E-05
MPC-32	2.49E-04	6.73E-05
MPC-68	3.03E-04	2.29E-05
MPC-68F	9.56E-05	8.91E-05
Accident Conditions		
MPC-24	5.59E-03	2.39E-02
MPC-24E, MPC-24EF	5.72E-03	2.34E-02
Trojan MPC-24E	3.59E-03	3.95E-02
Trojan MPC-24EF	3.59E-03	3.95E-02
MPC-32	7.86E-03	1.70E-02
MPC-68	7.22E-03	1.19E-02
MPC-68F	1.00E-03	6.07E-02

Table 4.2.10

Table Deleted

Table 4.2.11

DELETED

Table 4.2.12

PARAMETERS FOR NORMAL, HYPOTHETICAL ACCIDENT AND TEST CONDITIONS

Parameter	Normal Conditions	Hypothetical Accident Conditions	Reference Test Conditions	Actual Test Conditions
P_u	104 psia[1] (7.07 ATM)	214.7 psia (14.61 ATM)	1.68 ATM	1.68 ATM (min)
P_d	14.7 psia (1 ATM)	14.7 psia (1 ATM)	14.7 psia (1 ATM)	14.7 psia (1 ATM)
T	495°F (530 K)	1058°F (843 K)	373 K	373 K (max)
M	4 g/mol	4 g/mol	4 g/mol	4 g/mol
u	0.0293 cP	0.0397 cP	0.0231 cP	0.0231 cP
a	0.25 cm	0.25 cm	0.25 cm	0.25 cm

[1] The maximum upstream pressure for normal operating conditions in the Trojan MPCs is 83.2 psia (5.66 ATM). This value has been used to determine the maximum allowable leakage rate from the Trojan MPCs.

Table 4.2.13
DELETED

Table 4.2.14
DELETED

4.3 REGULATORY COMPLIANCE

Chapter 4 of this SAR has been prepared to summarize the containment features and capabilities of the HI-STAR 100 packaging. The containment boundary of the HI-STAR 100 packaging are designed and tested to ensure that the radionuclide release rates specified in 10CFR71.51 [4.0.1] will not be exceeded.

Leakage rates presented in Chapter 4 are determined in accordance with the requirements of ANSI N14.5 [4.0.2], and utilizing NUREG/CR-6487, *Containment Analysis for Type B Packages Used to Transport Various Contents* [4.0.3], Regulatory Guide 7.4, *Leakage Tests on Packages for Shipment of Radioactive Materials* [4.0.4] as content guides, and NUREG-1617, Standard Review Plan for Transportation Packages for Spent Nuclear Fuel [4.0.5].

The containment features and capabilities of the HI-STAR 100 packaging can be summarized in the following evaluation statements:

1. The HI-STAR 100 packaging, as presented in Chapter 4, complies with all applicable codes and standards for the containment system as identified in the chapter.

2. The containment boundary is securely closed by using multiple bolts and plugs. The closure of the containment boundary is sufficient to prevent unintentional opening or opening by pressure that may arise in the package as required by 10CFR71.43(c).

3. The materials of construction for the packaging containment are specified in the Bills-of-Material in Section 1.4. All materials and construction assure that there will be no significant chemical, galvanic, or other reaction as required by 10CFR71.43(d).

4. The overpack and MPC penetrations are designed to prevent leakage and protect against unauthorized operation by using cover plates to provide redundant closure as required by 10CFR71.43(e).

5. The containment system boundary for the HI-STAR 100 packaging consists of the overpack inner shell, the bottom plate, the top flange, the top closure plate, closure bolts, the overpack vent and drain port plugs, and their respective mechanical seals.

6. The HI-STAR 100 packaging is design, constructed, and prepared for shipment so that under the tests specified in 10CFR71.71 (normal conditions of transport), the package satisfies the containment requirement of 10CFR71.43(f) and 10CFR71.51(a)(1) for normal conditions of transport and 10CFR71.51(a)(2) for hypothetical accident conditions with no dependence on filters or a mechanical cooling system as required by 10CFR71.51(c).

7. The HI-STAR 100 packaging satisfies the containment requirements of 10CFR71, and the packaging meets the containment criteria of ANSI N14.5.

4.4 REFERENCES

[4.0.1] 10CFR71. "Packaging and Transportation of Radioactive Material." 2006

[4.0.2] ANSI N14.5-1997. "American National Standard for Radioactive Materials-Leakage Tests on Packages for Shipment."

[4.0.3] B.L. Anderson et al. *Containment Analysis for Type B Packages Used to Transport Various Contents.* NUREG/CR-6487, UCRL-ID-124822. Lawrence Livermore National Laboratory, November 1996.

[4.0.4] U.S. Nuclear Regulatory Commission, Regulatory Guide 7.4, *Leakage Tests on Packages for Shipment of Radioactive Materials*, June 1975.

[4.0.5] NUREG-1617, "Standard Review Plan for Transportation Packages for Spent Nuclear Fuel", Draft Report for Comment, March 1998.

[4.1.1] American Society of Mechanical Engineers (ASME), Boiler and Pressure Vessel Code, Section III, Division 1, Subsection NB, Class 1 Components, 1995 Edition.

[4.2.1] Deleted.

[4.2.2] Deleted.

[4.2.3] Rosenhow, W.M. and Hartnett, J.P., *Handbook of Heat Transfer*, Hemisphere Publishing Corporation, New York, 1973.

[4.2.4] Shleien, B., *The Health Physics and Radiological Health Handbook*, Scinta, Inc. Silver Spring, MD, 1992.

APPENDIX 4.A: BOLT AND PLUG TORQUES

This appendix provides the calculations used to determine the torque values for the vent and drain port plugs and cover plate bolts.

4.A.1 HI-STAR 100 Vent and Drain Port Plug Torques†

The HI-STAR 100 vent and drain port are sealed with plugs under which a mechanical seal is compressed. The objective of this calculation is to determine the torque required on the plug and to provide the required compressive load.

Given:

O-Ring (Mechanical Seal) Diameter: D_{OR} =0.683 in

O-Ring Compression: q_{OR} =800 lbf/in (pound force per linear inch)

Internal Pressure: p_i =100 psi

Plug Diameter: D_B =0.5 inch

Load due to internal overpack pressure: $q_i = p_i \ \pi D_B^2/4 =$ 19.6 lbf

Determine the required seating load:

The circumference of the O-Ring is: $C_{OR}=\pi D_{OR}$ C_{OR}= 2.14 in

The required seating load is: $F_i = q_i + P_{OR}$

$p_{OR}=C_{OR}q_{OR}$ p_{OR}= 1712 lbf

F_i=1732 lbf

The procedure presented here is taken from Shingley, Joseph Edward and Mischke, Charles R., Mechanical Engineering Design, Fifth Edition, McGraw Hill, p. 344-346.

Given a torque factor K= 0.30 (for non-plated, non-lubricated plug).

† Since the closure plate test port plug is the same material, diameter and uses the same seal, this calculation also applies to the closure plate test port plug.

Determine the required torque:

$T= KFiD_B$

T=0.30 (1732 lbf)0.5 in T=259 in-lbf T=22 ft-lbf

4.A.2 HI-STAR 100 Vent and Drain Port Cover Plate Bolt Torques

The HI-STAR 100 vent and drain port cover plates are sealed with a mechanical seal that is compressed under a bolted cover plate. The objective of this calculation is to determine the torque required on the bolts and to provide the required compressive load.

Given:

O-Ring (Mechanical Seal) Diameter: D_{OR} =2.5 in

Required O-Ring Compression: q_{OR} =1150 lbf/in (pound force per linear inch)

Internal Pressure: p_i =100 psi (assumed)

Bolt Diameter:D_B =0.375 inch

Number of Bolts: n= 4 bolts

Determine the required seating load:

The circumference of the O-Ring is: $C_{OR}=\pi D_{OR}$ C_{OR}= 7.85 in

The required seating load per bolt is: $F_i = q_i + P_{OR}/n$

$qi= p_i \pi D_{OR}^2/4$ qi= 491 lbf
$P_{OR}=C_{OR}q_{OR}$ P_{OR}= 9028 lbf

F_i=9516 lbf/4 F_i=2380 ft-lbf

The procedure presented here is taken from Shingley, Joseph Edward and Mischke, Charles R., Mechanical Engineering Design, Fifth Edition, McGraw Hill, p. 344-346.

Given a torque factor K= 0.15 (See technical Bulletin for FELPRO N-5000 in Appendix

1.C).

For conservatism, the torque factor is increased by an additional 5 percent in the following calculation.

Determine the required torque:

$T = KFiD_B$

T=0.1575 (2380 lbf)0.375 in T=141 in-lbf T=11.8 ft-lbf

APPENDIX 4.B: Manufacturer Seal Information
(Total of 5 Pages Including This Page)

The information provided in this appendix provides additional details on the mechanical seals specified to ensure containment. The following is a listing of the drawings provided in this appendix.

- ASE Drawing No. 050038-TAB, Rev B, ".375 C-Ring, Spring Ener., Internal Pressure" (Detail of Closure Plate Mechanical Seals, Holtec Dwg. 1397 and Bill-of-Material 1476, Items 26 and 27)

- ASE Drawing No. 050033, Rev. B, "C-Ring, .062 Spring Energized, Internal Pressure" (Detail of Port Plug Mechanical Seal, Holtec Dwg. 1397 and Bill-of-Material 1476, Item 19)

- ASE Drawing No. 050118, Rev. A, ".062 C-Ring, Spring Ener., Internal Pressure" (Detail of Port Cover Mechanical Seal, Holtec Dwg. 1398 and Bill-of-Material 1476, Item 30)

The detailed dimensions, materials, and groove requirements are provided below for each mechanical seal.

<u>Closure Plate Outer Seal:</u>

Holtec Item No.	27
ASE Part No.	ASE050038-TAB-1
Seal Type	Spring energized C-ring, internal pressure
Seal Size	72.50 OD x 3/8 free height
Material	Jacket Alloy X750
	Spring Alloy X750
Plating	Silver
Groove OD	72.545 inches nominal
Groove ID	71.685 inches nominal
Groove Depth	0.300 inches nominal

Closure Plate Inner Seal:

Holtec Item No.	26
ASE Part No.	ASE050038-TAB-2
Seal Type	Spring energized C-ring, internal pressure
Seal Size	71.00 OD x 3/8 free height
Material	Jacket Alloy X750
	Spring Alloy X750
Plating	Silver
Groove OD	71.045 inches nominal
Groove ID	70.175 inches nominal
Groove Depth	0.300 inches nominal

Port Plug Seal:

Holtec Item No.	19
ASE Part No.	ASE050033
Seal Type	Spring energized C-ring, internal pressure
Seal Size	0.75 OD x 0.062 free height
Material	Jacket Alloy X750
	Spring Alloy X750
Plating	Silver
Groove OD	0.760 inches nominal
Groove Depth	0.052 inches nominal

Port Cover Seal:

Holtec Item No.	30
ASE Part No.	ASE050118
Seal Type	Spring energized C-ring, internal pressure
Seal Size	2.50 OD x 0.062 free height
Material	Jacket Alloy X750
	Spring Alloy X750
Plating	Silver
Groove OD	2.52 inches nominal
Groove ID	2.31 inches nominal
Groove Depth	0.052 inches nominal

DRAWING NO. 050038-TAB | REV B

DASH NO.	DIAMETER A (IN)
001	72.500/72.460
002	71.000/70.960

REVISIONS

LTR.	DESCRIPTION	ECO	DATE	APPROVED
-	INITIAL RELEASE	96021	11-12-97	CAP
A	ADDED TESTING NOTE 8.	96021	06-10-98	CAP
B	LOAD INCREASED TO 1700-2200 LB	96021	12-01-99	CAP

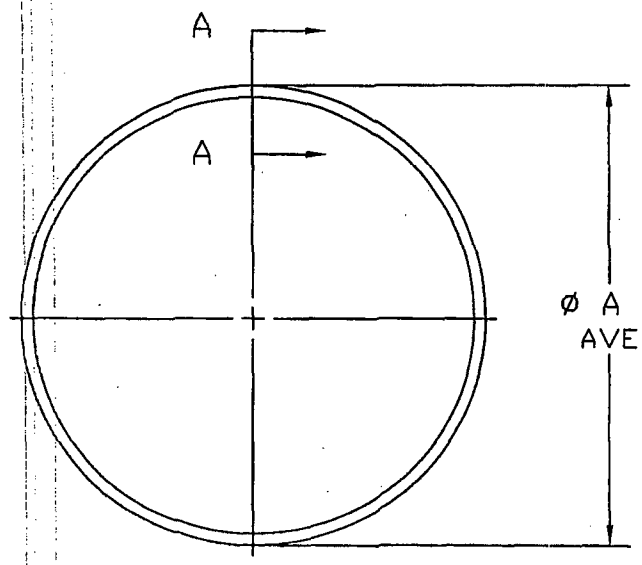

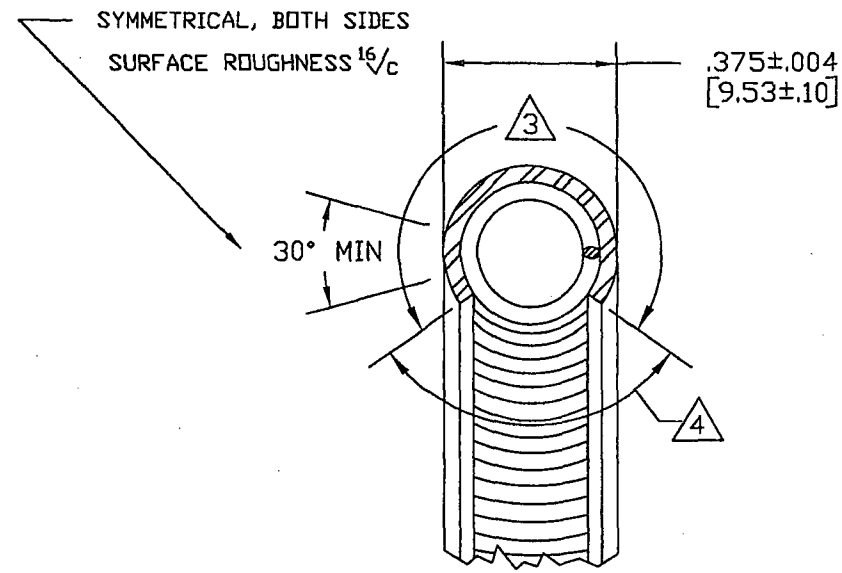

SECTION A-A

SCALE: 4/1

NOTES:

1. DIMENSIONS SHOWN ARE PRIOR TO PLATING.
2. WELDED CONSTRUCTION PERMITTED.
3. PLATING: SILVER .004-.006 THICK PER AMS 2410.
4. PLATING IS OPTIONAL AND MAY BE INCOMPLETE IN THIS AREA.
5. MATERIAL: JACKET: ALLOY X750 PER AMS 5598.
   SPRING: ALLOY X750 PER AMS 5699.
6. TEMPER: WORK HARDENED
7. DIMENSIONS IN [ ] ARE IN MILLIMETERS.
8. TESTING: LOAD & SPRINGBACK TESTING PER ASE010063.
   TEST TWO 2" LONG SAMPLES PER ORDER/LOT.
   LOAD TO COMPRESS SEAL TO A HEIGHT OF .300" SHALL BE 1700-2200 LB/INCH
   MINIMUM SPRINGBACK SHALL BE .018".
9. REF. HOLTEC INTERNATIONAL

UNLESS OTHERWISE SPECIFIED			
1. DECIMALS: .XX ±.010 .XXX ±.005	DRAWN	CAP	11-12-97
2. ANGLES: ±2°	CHECKED	JRP	11-12-97
3. FRACTIONS: ±1/64	Q.A.	CAP	11-12-97
4. All DIMENSIONS ARE IN INCHES	ENGR.	CAP	11-12-97
5. INTERPRET PER MIL-STD-100	MATERIAL: AS NOTED		
6. SURFACE ROUGHNESS 125/			
THIRD ANGLE PROJECTION	TEMPER: AS NOTED		
	FINNISH: AS NOTED		

American Seal & Engineering Co., Inc.
156 Gando Drive
New Haven, CT 06513, USA

TITLE: .375 C-RING, SPRING ENER., INTERNAL PRESSURE

SIZE	CAGE NUMBER	DRAWING NO.	REV.
B	9G389	050038-TAB	B

SCALE: NOTED | NEXT ASSY: - | SHEET: 1 OF 1

DRAWING NO.	REV
050033	B

REVISIONS

LTR.	DESCRIPTION	ECO	DATE	APPROVED
-	INITIAL RELEASE	96012	09-06-96	CAP
A	REDRAWN TO LATEST STD.	96012	01-13-98	CAP
B	Ag PER AMS 2410 WAS Ni PER AMS 2424	96012	07-21-00	CAP

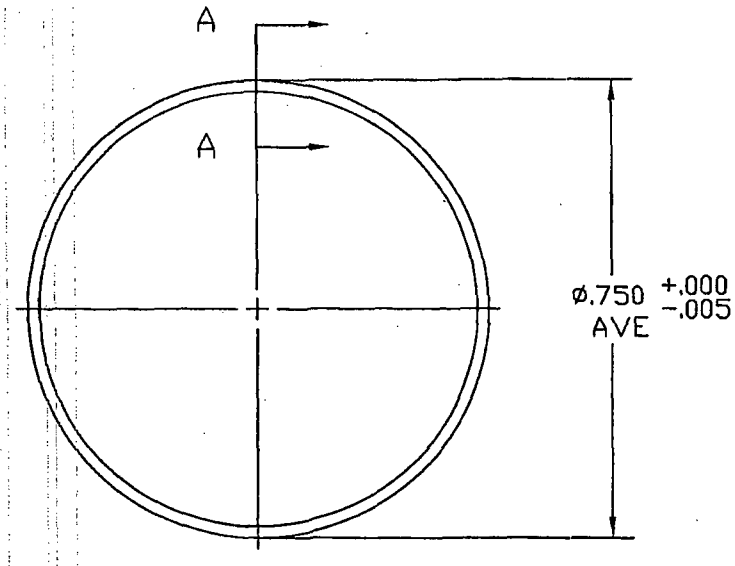

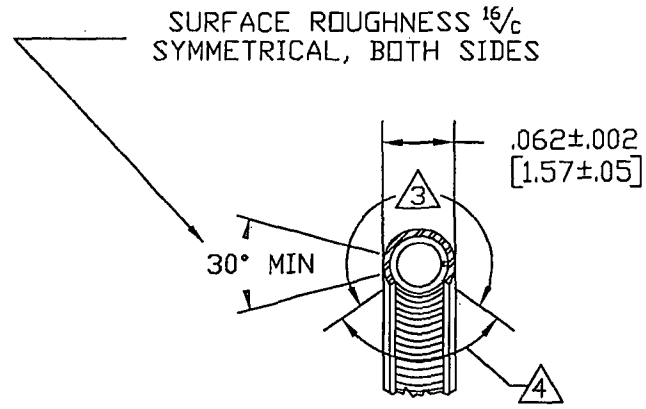

SECTION A-A

SCALE: 10/1

NOTES:

1. DIMENSIONS SHOWN ARE PRIOR TO PLATING.
2. WELDED CONSTRUCTION PERMITTED.
3. PLATING: SILVER .0015-.0025 THICK PER AMS 2410.
4. PLATING IS OPTIONAL AND MAY BE INCOMPLETE IN THIS AREA.
5. MATERIAL: JACKET: ALLOY X750 PER AMS 5598.
   SPRING: ALLOY X750 PER AMS 5699.
6. TEMPER: WORK HARDENED
7. DIMENSIONS IN [ ] ARE IN MILLIMETERS.
8. REF: HOLTEC INTERNATIONAL

UNLESS OTHERWISE SPECIFIED			
1. DECIMALS: .XX ±.010 .XXX ±.005	DRAWN	CAP	09-06-96
2. ANGLES: ±2°	CHECKED	JRP	09-06-98
3. FRACTIONS: ±1/64	Q.A.	CAP	09-06-96
4. All DIMENSIONS ARE IN INCHES	ENGR.	CAP	09-06-96
5. INTERPRET PER MIL-STD-100	MATERIAL: AS NOTED		
6. SURFACE ROUGHNESS 125/			
THIRD ANGLE PROJECTION	TEMPER: AS NOTED		
	FINISH: AS NOTED		

American Seal & Engineering Co., Inc.
156 Gando Drive
New Haven, CT 06513, USA

TITLE: .062 C-RING, SPRING ENER., INTERNAL PRESSURE

SIZE	CAGE NUMBER	DRAWING NO.	REV.
B	9G389	050033	B

SCALE: NOTED | NEXT ASSY: - | SHEET: 1 OF 1

DRAWING NO.	REV
050118	A

REVISIONS

LTR.	DESCRIPTION	ECO	DATE	APPROVED
-	INITIAL RELEASE	97141	12-17-97	CAP
A	Ag PER AMS 2410 WAS NI PER AMS 2424	97141	07-21-00	CAP

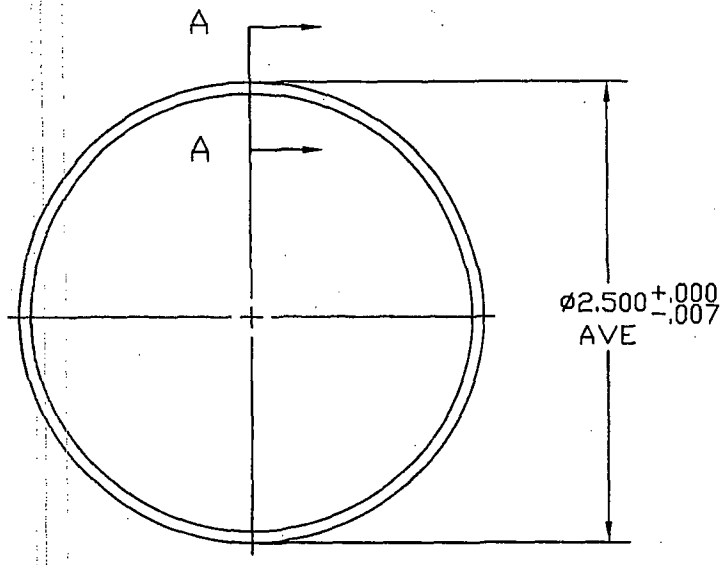

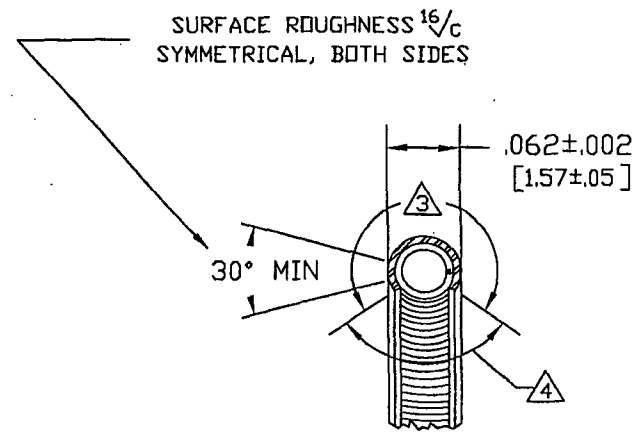

SECTION A-A

SCALE: 10/1

NOTES:
1. DIMENSIONS SHOWN ARE PRIOR TO PLATING.
2. WELDED CONSTRUCTION PERMITTED.
3. PLATING: SILVER .0015-.0025 THICK PER AMS 2410.
4. PLATING IS OPTIONAL AND MAY BE INCOMPLETE IN THIS AREA.
5. MATERIAL: JACKET: ALLOY X750 PER AMS 5598.
   SPRING: ALLOY X750 PER AMS 5699.
6. TEMPER: WORK HARDENED
7. DIMENSIONS IN [ ] ARE IN MILLIMETERS.
8. REF: HOLTEC INTERNATIONAL

UNLESS OTHERWISE SPECIFIED	DRAWN	CAP	12-17-97
1. DECIMALS: .XX ±.010, .XXX ±.005	CHECKED	JRP	12-17-97
2. ANGLES: ±2°	Q.A.	CAP	12-17-97
3. FRACTIONS: ±1/64	ENGR.	CAP	12-17-97
4. ALL DIMENSIONS ARE IN INCHES	MATERIAL: AS NOTED		
5. INTERPRET PER MIL-STD-100			
6. SURFACE ROUGHNESS 125/			
THIRD ANGLE PROJECTION	TEMPER: AS NOTED		
	FINNISH: AS NOTED		

American Seal & Engineering Co., Inc.
156 Gando Drive
New Haven, CT 06513, USA

TITLE: .062 C-RING, SPRING ENER., INTERNAL PRESSURE

SIZE	CAGE NUMBER	DRAWING NO.	REV.
B	9G389	050118	A

SCALE: NOTED | NEXT ASSY: - | SHEET: 1 OF 1

SUPPLEMENT 4.I

CONTAINMENT EVALUATION OF HUMBOLDT BAY FUEL IN THE HI-STAR HB

4.I.0 INTRODUCTION

This supplement is focused on providing containment evaluations for fuel from the Humboldt Bay Power Plant (HBPP) in the HI-STAR HB. The evaluation presented herein supplements those evaluations contained in the main body of Chapter 4 of this FSAR, and information in the main body of Chapter 4 is not repeated in this supplement. To aid the reader, the sections in this supplement are numbered in the same fashion as the corresponding sections in the main body of this chapter, i.e., Sections 4.I.1 through 4.I.3 correspond to Sections 4.1 through 4.3. Tables and figures in this supplement are labeled sequentially. The results of the evaluations in this supplement demonstrates the HI-STAR HB containment boundary compliance with the permitted activity release limits specified in 10 CFR 71, 71.51(a)(1) and 71.51(a)(2) for both normal and hypothetical accident conditions of transport.

4.I.1 CONTAINMENT BOUNDARIES

The containment system boundary for the HI-STAR HB is identical to that of the HI-STAR 100 System described in Section 4.1. Therefore, the discussion provided in the main part of the chapter on the containment vessel, penetrations, seals, welds, closure and damaged fuel containers for the HI-STAR 100 System are directly applicable to the HI-STAR HB.

4.I.2 REQUIREMENTS FOR NORMAL AND HYPOTHETICAL ACCIDENT CONDITIONS OF TRANSPORT

Supplement 2.I shows that all containment components for the HI-STAR HB are maintained within their code-allowable stress limits during all normal and hypothetical accident conditions of transport as defined in 10CFR71.71 and 10CFR71.73 [4.0.1]. Supplement 3.I shows that the peak containment component temperatures and pressure are within the design basis limits for all normal and hypothetical accident conditions of transport as defined in 10CFR71.71 and 10CFR71.73. Since the containment vessels remain intact, and the temperature and pressure design bases are not exceeded, the design basis leakage rate will not be exceeded during normal or hypothetical accident conditions of transport.

4.I.2.1 Containment Criteria

The containment criteria are identical to those identified in Section 4.2.1 of the main part of the chapter.

4.I.2.2 Containment of Radioactive Material

The HI-STAR HB packaging allowable leakage rate ensures that the requirements of 10CFR71.51 are met. Section 4.I.2.5 determines the maximum leakage rate for normal and hypothetical accident conditions of transport and the allowable leakage rate criterion for the HI-STAR HB packaging containing the MPC-HB. Following testing, no credit is taken for the MPC as a containment boundary for the transport of spent fuel.

4.I.2.3 Pressurization of Containment Vessel

The HI-STAR HB is drained, dried, evacuated and backfilled with helium gas prior to final closure of the overpack in an identical way as the HI-STAR 100 System described in the main part of the chapter.

4.I.2.4 Assumptions

The following assumptions have been used in determining the allowable leakage rates in addition to those already listed in Section 4.2.4:

1. The MPC-HB contains 80 Humboldt Bay fuel assemblies of which up to forty (40) may be DFCs containing specified fuel debris or damaged fuel.

2. In calculating the leakage rates of the containment system for normal conditions of transport, the internal pressure of the overpack is assumed to be equal to the maximum internal pressure determined in Supplement 3.I with 3% rod rupture.

3. The average cavity temperature for normal conditions is conservatively assumed to be the maximum cladding temperature from Supplement 3.I.

4. The average cavity temperature for hypothetical accident conditions is conservatively assumed to be the design basis peak cladding temperature.

4.I.2.5 Analysis and Results

The methodology to determine the allowable leakage rates from the HI-STAR HB for normal and hypothetical accident conditions is identical to the methodology employed in the main part of the chapter for the HI-STAR 100 System. The only differences are in the input information, which is detailed in the following sections.

4.I.2.5.1 Volume in the Containment Vessel

The free gas volume in the MPC-HB is presented in Table 4.I.2.1. For calculating the free volume in the containment system (overpack) the volume of the annulus space is added to the free volume of the MPC-HB. This will conservatively underestimate the free volume inside the containment boundary.

4.I.2.5.2 Source Terms for Spent Nuclear Fuel Assemblies

The inventory for isotopes other than ^{60}Co is calculated with the SAS2H and ORIGEN-S modules of the SCALE 4.3 system as described in Chapter 5. The inventory for the MPC-HB was based the Humboldt Bay 6x6 fuel assembly with a burnup of 23,000 MWD/MTU, 29 years of cooling time, and 2.09 wt% enrichment. The isotopes which contribute greater than 0.01% to the total curie inventory for the fuel assembly are considered in the evaluation as fines. Additionally, isotopes with A_2 values less than 1.0 in Table A-1, Appendix A, 10CFR71 are included as fines. Isotopes which contribute greater than 0.01% but which do not have an assigned A_2 value in Table A-1 are assigned an A_2 value based on the guidance in Table A-3, Appendix A, 10CFR71. Isotopes which contribute greater than 0.01% but have a radiological half life less than 10 days are neglected. Table 4.I.2.2 presents the isotope inventory used in the calculation.

A. Source Activity Due to Crud Spallation from Fuel Rods

The source term activity associated with crud for the Humboldt Bay fuel was calculated in the same way as in the main part of the chapter. The inventory for ^{60}Co was determined by using the crud surface activity for BWR rods (1254×10^{-6} Ci/cm^2) provided in NUREG/CR-6487 [4.0.3] multiplied by the surface area per assembly (1×10^5 cm^2 for BWR fuel, also provided in NUREG/CR-6487). The source terms were then decay corrected 29 years using equation 4-1.

BWR

Surface area per Assy = 1.0E+05 cm^2

1254 μCi/cm^2 x 1.0E+05 cm^2 = 125.4 Ci/assy

MPC-HB

$$^{60}Co(29) = 125.4 \text{ Ci } e^{-(\ln 2/5.272)(29)}$$

$$^{60}Co(29) = 2.769 \text{ Ci/assy}$$

A summary of the ^{60}Co inventory available for release is provided in Table 4.I.2.2.

The activity density that results inside the HI-STAR HB containment vessel as a result of crud spallation from spent fuel rods is calculated using Equation 4-2.

B. Source Activity Due to Releases of Fines from Cladding Breaches

The source term activity associated with fines for the Humboldt Bay fuel was calculated in the same way as in the main part of the chapter.

The calculation for normal transport conditions of a MPC-HB containing forty (40) DFCs containing fuel debris assumes that for the forty DFCs, 100% of the rods of the fuel debris are

breached. The remaining 40 in the MPC-HB were assumed to have a 3% cladding rupture. Therefore, f_B for an MPC-HB containing fuel debris is:

$$f_B = (0.03)\frac{40}{80} + (1.0)\frac{40}{80}$$
$$f_B = 0.515 \qquad \textbf{(4.I-1)}$$

The activity concentration inside the containment vessel due to fines being released from cladding breaches is given by Equation 4-4.

C. Source Activity from Gases due to Cladding Breaches

The source term activity associated with gases for the Humboldt Bay fuel was calculated in the same way as in the main part of the chapter.

The activity concentration due to the release of gases from a cladding breach is given by Equation 4-5.

D. Source Activity from Volatiles due to Cladding Breaches

The source term activity associated with volitiles for the Humboldt Bay fuel was calculated in the same way as in the main part of the chapter.

The activity concentration due to the release of volatiles from a cladding breach is given by Equation 4-6.

E. Total Source Term for the HI-STAR HB System

The total source term was determined using Equation 4-7. Table 4.I.2.3 presents the total source term determined using the above methodology.

4.I.2.5.3 Effective A_2 of Individual Contributors (Crud, Fines, Gases, and Volatiles)

Table 4.I.2.3 presents the total source term determined using the above methodology. Table 4.2.4 in the main part of the chapter summarizes the parameters from NUREG/CR-6487 used in this analysis, with the exception of the fraction of rods that develop cladding breaches, which is explained in the previous section. Table 4.I.2.4 summarizes the effective A_2 for all individual contributors.

4.I.2.5.4 Releasable Activity

The release activity of fines, volatiles, gases, and crud were determined using Equation 4-9.

4.I.2.5.5 Effective A_2 for the Total Source Term

The total source term effective A_2 was calculated in the same way as in the main chapter. The results are summarized in Table 4.I.2.5

4.I.2.5.6 Allowable Radionuclide Release Rates

The HI-STAR HB containment system is designed to the same containment criteria as the HI-STAR 100 System. These criterion are given in 10CFR71.51(a)(1) for normal conditions and 10CFR71.51(b)(2) for hypothetical accident conditions.

Equations 4-10 and 4-11 were used to determine the allowable radionuclide release rate for the MPC-HB under normal and hypothetical accident conditions. The release rates for the MPC-HB are summarized in Table 4.I.2.6.

4.I.2.5.7 Allowable Leakage Rates at Operating Conditions

The allowable leakage rates at operating conditions were determined using Equation 4-12. Table 4.I.2.7 summarizes the allowable leakage rates at the upstream pressures. The most limiting allowable leakage rate presented in Table 4.I.2.7 was conservatively selected and used to determine the leakage rate acceptance criterion for the MPC-HB.

4.I.2.5.8 Leakage Rate Acceptance Criteria for Test Conditions

The leakage rate acceptance criteria for test conditions was determined using the same methodology presented in Section 4.2.5.8 of the main part of the chapter. The reference test conditions, and approximate actual test conditions for the MPC-HB are specified in Table 4.I.2.8.

4.I.2.5.9 Leak Test Sensitivity

The sensitivity for the overpack leakage test procedures is equal to one-half of the allowable leakage rate. The HI-STAR HB containment packaging tests in Chapter 8 incorporate the appropriate leakage test procedure sensitivity. The leakage rates for the HI-STAR 100 containment packaging with its corresponding sensitivity are presented in Table 4.1.1.

4.I.3 REGULATORY COMPLIANCE

The HI-STAR HB is identical to the HI-STAR 100 System in that it is designed and tested to ensure compliance with the radionuclide release rates specified in 10CFR71.51 [4.0.1] for normal and hypothetical accident transport conditions.

Table 4.I.2.1

FREE GAS VOLUME OF THE HI-STAR HB CONTAINMENT SYSTEM

Containment Volume [cm^3]	3.40×10^6

Table 4.I.2.2

Isotopic Inventory for the HI-STAR HB

Nuclide	Ci/Assembly
Gases	
^{3}H	5.09E+00
^{129}I	1.77E-03
^{85}Kr	7.26E+01
^{81}Kr	3.76E-09
^{127}Xe	0.00E+00
Crud	
^{60}Co	2.77E+00
Volatiles	
^{90}Sr	2.02E+03
^{106}Ru	6.97E-05
^{134}Cs	3.39E-01
^{137}Cs	3.00E+03
^{89}Sr	0.00E+00
^{103}Ru	0.00E+00
^{135}Cs	2.39E-02
Fines	
^{225}Ac*	6.21E-09
^{227}Ac*	6.72E-07
^{110m}Ag	2.36E-11
^{241}Am	1.61E+02

Table 4.I.2.2 (continued)
ISOTOPE INVENTORY

^{242M}Am*	3.55E-01
^{243}Am*	8.13E-01
^{210M}Bi*	4.04E-20
^{247}Bk*	1.27E-07
^{144}Ce	3.26E-07
^{248}Cf*	0.00E+00
^{249}Cf*	7.07E-08
^{250}Cf*	6.71E-08
^{251}Cf*	1.98E-09
^{252}Cf*	1.99E-10
^{254}Cf*	0.00E+00
^{240}Cm*	0.00E+00
^{242}Cm*	2.93E-01
^{243}Cm*	2.95E-01
^{244}Cm	2.20E+01
^{245}Cm*	2.95E-03
^{246}Cm*	7.58E-04
^{247}Cm*	2.54E-09
^{248}Cm*	7.32E-09

Table 4.I.2.2 (continued)
ISOTOPE INVENTORY

^{154}Eu	2.41E+01
^{155}Eu	1.92E+00
^{148}Gd*	0.00E+00
^{236}Np*	2.29E-07
^{237}Np*	1.36E-02
^{239}Np	8.13E-01
^{231}Pa*	1.31E-06
^{147}Pm	4.68E+00
^{210}Po*	3.17E-08
^{236}Pu*	9.26E-06
^{238}Pu	7.91E+01
^{239}Pu	1.87E+01
^{240}Pu	3.53E+01
^{241}Pu	1.55E+03

Table 4.I.2.2 (continued)
ISOTOPE INVENTORY

^{242}Pu*	1.06E-01
^{244}Pu*	1.71E-15
^{223}Ra*	6.73E-07
^{224}Ra*	5.29E-04
^{225}Ra*	6.21E-09
^{226}Ra*	1.27E-07
^{222}Rn*	1.27E-07
^{151}Sm	1.42E+01
^{227}Th*	6.64E-07
^{228}Th*	5.27E-04
^{229}Th*	6.21E-09
^{230}Th*	1.84E-05
^{231}Th*	8.36E-04
^{230}U*	0.00E+00
^{232}U*	5.13E-04
^{233}U*	2.47E-06
^{234}U*	6.53E-02
^{236}U*	1.35E-02
^{90}Y	2.02E+03

Table 4.I.2.3

TOTAL SOURCE TERM FOR THE HI-STAR HB (Ci/cm^3)

	C_{crud} (Ci/cm^3)	C_{fines} (Ci/cm^3)	C_{gas} (Ci/cm^3)	C_{vol} (Ci/cm^3)	Total (Ci/cm^3)
Normal Transport Conditions					
HI-STAR HB	9.77E-06	1.43E-06	2.82E-04	1.22E-05	3.06E-04
Accident Conditions					
HI-STAR HB	6.52E-05	2.78E-06	5.48E-04	2.36E-05	6.40E-04

Table 4.I.2.4

INDIVIDUAL CONTRIBUTOR EFFECTIVE A_2 FOR GASES, CRUD, FINES, AND VOLATILES FOR THE HI-STAR HB

HI-STAR HB	A_2 (Ci)
Gases	2.46E+03
Crud	10.8
Fines	3.13E-01
Volatiles	1.16E+01

Table 4.I.2.5

TOTAL SOURCE TERM EFFECTIVE A_2 FOR NORMAL AND HYPOTHETICAL ACCIDENT CONDITIONS FOR THE HI-STAR HB

	Effective A_2 (Ci)
Normal Transport Conditions	
HI-STAR HB	46.1
Accident Conditions	
HI-STAR HB	37.3

Table 4.I.2.6

RADIONUCLIDE RELEASE RATES FOR THE HI-STAR HB

	Allowable Release Rate (R_N or R_A) (Ci/s)
Normal Conditions	
HI-STAR HB	1.28E-08
Accident Conditions	
HI-STAR HB	6.15E-05

Table 4.I.2.7

ALLOWABLE LEAKAGE RATES AT UPSTREAM PRESSURE FOR THE HI-STAR HB

	Allowable Leakage Rate at P_u L_N or L_A (cm^3/s)
Normal Transport Conditions	
HI-STAR HB	4.19E-05
Accident Conditions	
HI-STAR HB	9.61E-02

Table 4.I.2.8

PARAMETERS FOR NORMAL, HYPOTHETICAL ACCIDENT AND TEST CONDITIONS FOR THE HI-STAR HB

Parameter	Normal Conditions	Hypothetical Accident Conditions	Reference Test Conditions	Actual Test Conditions
P_u	84.4 psia (5.74 ATM)	214.7 psia (14.61 ATM)	1.68 ATM	1.68 ATM (min)
P_d	14.7 psia (1 ATM)	14.7 psia (1 ATM)	14.7 psia (1 ATM)	14.7 psia (1 ATM)
T	419°F (488 K)	1058°F (843 K)	373 K	373 K (max)
M	4 g/mol	4 g/mol	4 g/mol	4 g/mol
u	0.0276 cP	0.0397 cP	0.0231 cP	0.0231 cP
a	0.25 cm	0.25 cm	0.25 cm	0.25 cm

CHAPTER 5: SHIELDING EVALUATION

5.0 INTRODUCTION

The shielding analysis of the HI-STAR 100 System is presented in this chapter. The HI-STAR 100 System is designed to accommodate different MPCs within one standard HI-STAR 100 overpack. The MPCs are designated as MPC-24, MPC-24E, and MPC-24EF (24 PWR fuel assemblies), MPC-32 (32 PWR fuel assemblies), and MPC-68 and MPC-68F (68 BWR fuel assemblies). The MPC-24E and MPC-24EF are essentially identical to the MPC-24 from a shielding perspective. Therefore, only the MPC-24 is analyzed in this chapter. Throughout this chapter, unless stated otherwise, MPC-24 refers to either the MPC-24, MPC-24E, or MPC-24EF and MPC-68 refers to the MPC-68 or MPC-68F.

In addition to housing intact PWR and BWR fuel assemblies, the HI-STAR 100 System is designed to transport damaged BWR fuel assemblies and BWR fuel debris. Damaged fuel assemblies and fuel debris are defined in Subsection 1.2.3. Both damaged BWR fuel assemblies and BWR fuel debris are required to be loaded into Damaged Fuel Containers (DFCs). DFCs containing BWR fuel debris must be stored in the MPC-68F. DFCs containing BWR damaged fuel assemblies may be stored in either the MPC-68 or the MPC-68F. Only the fuel assemblies in the Dresden 1 and Humboldt Bay fuel assembly classes identified in Table 1.2.9 are authorized as contents for transport in the HI-STAR 100 system as either BWR damaged fuel or fuel debris.

The MPC-68 and MPC-68F are also capable of transporting Dresden Unit 1 antimony-beryllium neutron sources and the single Thoria rod canister which contains 18 thoria rods that were irradiated in two separate fuel assemblies.

Slightly modified versions of the MPC-24E and MPC-24EF are being used for the transportation of Trojan nuclear power plant spent nuclear fuel, non-fuel hardware, neutron sources, and damaged fuel and fuel debris as described in Subsection 1.2.3. These MPCs are referred to as the Trojan MPC-24E and Trojan MPC-24EF. The Trojan MPC-24E/EF is explicitly analyzed in this chapter for the inclusion of the Trojan non-fuel hardware, damaged fuel, and Antimony-Beryllium and Californium neutron sources.

This chapter contains the following information:

- A description of the shielding features of the HI-STAR 100 System.
- A description of the bounding source terms.
- A general description of the shielding analysis methodology.
- A description of the analysis assumptions and results for the HI-STAR 100 System.

- Analyses for the HI-STAR 100 System's content conditions to show that the 10CFR71.47 radiation limits are met during normal conditions of transport and that the 10CFR71.51 dose rate limit is not exceeded following hypothetical accident conditions.
- Analyses which demonstrate that the storage of BWR damaged fuel in the HI-STAR 100 System is bounded by the BWR intact fuel analysis during normal and hypothetical accident conditions.
- Analyses for the Trojan Nuclear Power Plant spent fuel contents, including damaged fuel and fuel debris, and non-fuel hardware.

5.1 DISCUSSION AND RESULTS

The principal sources of radiation in the HI-STAR 100 System are:

- Gamma radiation originating from the following sources

    1. Decay of radioactive fission products
    2. Hardware activation products generated during core operations
    3. Secondary photons from neutron capture in fissile and non-fissile nuclides

- Neutron radiation originating from the following sources

    1. Spontaneous fission
    2. α,n reactions in fuel materials
    3. Secondary neutrons produced by fission from subcritical multiplication
    4. γ,n reactions (this source is negligible)
    5. Dresden Unit 1 and Trojan neutron sources

Shielding from gamma radiation is provided by the steel structure of the MPC and overpack. In order for the neutron shielding to be effective, the neutrons must be thermalized and then absorbed in a material of high neutron cross section. In the HI-STAR 100 System design, a neutron shielding material, Holtite-A, is used to thermalize the neutrons. Boron carbide, dispersed in the neutron shield, utilizes the high neutron absorption cross section of ^{10}B to absorb the thermalized neutrons.

The shielding analyses were performed with MCNP-4A [5.1.1] from Los Alamos National Laboratory. The source terms for the design basis fuels were calculated with the SAS2H and ORIGEN-S sequences from the SCALE 4.3 system [5.1.2, 5.1.3] from Oak Ridge National Laboratory. The source terms for the Trojan specific inventory were calculated with the SAS2H and ORIGEN-S sequences from the SCALE 4.4 system [5.1.4, 5.1.5] as described in the Trojan FSAR [5.1.6]. A detailed description of the MCNP models and the source term calculations are presented in Sections 5.3 and 5.2, respectively.

The design basis intact zircaloy clad fuels used in calculating the dose rates presented in this chapter are the B&W 15x15 (with zircaloy and non-zircaloy incore spacers) and the GE 7x7, for PWR and BWR fuel types, respectively. The design basis intact 6x6, damaged, and mixed oxide (MOX) fuel assemblies are the GE 6x6. Tables 1.2.22 through 1.2.27 specify the acceptable intact zircaloy clad fuel characteristics for transport. Tables 1.2.23 and 1.2.24 specify the acceptable damaged and MOX zircaloy clad fuel characteristics for transport.

The design bases intact stainless steel clad fuels are the WE 15x15 and the AC 10x10, for PWR and BWR fuel types, respectively. Tables 1.2.22, 1.2.23, 1.2.25, and 1.2.26 specify the acceptable fuel characteristics of stainless steel clad fuel for transport.

The Trojan spent fuel contents were analyzed separately, as discussed in later sections, and therefore are not covered by the design basis fuel assemblies mentioned above.

Tables 1.2.28 through 1.2.33 specify, in tabular form, the minimum enrichment, burnup and cooling time combinations for spent nuclear fuel that were analyzed for transport in the MPC-24, MPC-32, and MPC-68. Each combination provides a dose rate equal to or below the maximum values reported in this section. These tables represent the fuel assembly acceptance criteria.

The burnup, cooling time, and minimum enrichment combinations specified in Tables 1.2.28 through 1.2.33 were determined strictly based on the shielding analysis in this chapter. Each combination was specifically analyzed and it was verified that the calculated dose rates were less than the regulatory limits. Detailed results (e.g. dose from gammas, neutrons, co-60, etc...) are not presented in this chapter for each burnup, cooling time, and minimum enrichment combination analyzed. Rather, the detailed results for the combination that produced the highest dose rate for each of the three regulatory acceptance criteria and locations (i.e. surface normal condition, 2 meter normal condition, 1 meter accident condition) in a specific MPC are presented in this section. However, the total dose rates for all approved burnup and cooling time combinations are presented in Section 5.4. The choice of burnup and cooling time combinations for which detailed (i.e. individual dose components in addition to total) results are provided is discussed further in the following subsections.

Unless otherwise stated, all dose rates reported in this chapter are average surface dose rates. The effect of radiation peaking due to azimuthal variations in the fuel loading pattern and the steel radial channels is specifically addressed in Subsection 5.4.1.

5.1.1 Normal Operations

The 10CFR71.47 external radiation requirements during normal transport operations for an exclusive use shipment are:

1. 200 mrem/hr (2 mSv/hr) on the external surface of the package, unless the following conditions are met, in which case the limit is 1000 mrem/hr (10 mSv/hr).
   i. The shipment is made in a closed transport vehicle;
   ii. The package is secured within the vehicle so that its position remains fixed during transportation; and
   iii. There are no loading and unloading operations between the beginning and end of the transportation.

2. 200 mrem/hr (2 mSv/hr) at any point on the outer surface of the vehicle, including the top and underside of the vehicle; or in the case of a flat-bed style vehicle, at any point on the vertical planes projected from the outer edges of the vehicle, on the upper surface of the load or enclosure, if used, and on the lower external surface of the vehicle.

3. 10 mrem/hr (0.1 mSv/hr) at any point 2 meters (80 in) from the outer lateral surfaces of the vehicle (excluding the top and underside of the vehicle); or in the case of a flat-bed style vehicle, at any point 2 meters (6.6 feet) from the vertical planes projected by the outer edges of the vehicle (excluding the top and underside of the vehicle).

4. 2 mrem/h (0.02 mSv/hr) in any normally occupied space, except that this provision does not apply to private carriers, if exposed personnel under their control wear radiation dosimetry devices in conformance with 10CFR20.1502.

The Standard Review Plan for Transportation Packages of Spent Nuclear Fuel, NUREG-1617 [5.2.1] states that "Personnel barriers and similar devices that are attached to the conveyance, rather than the package, can, however, qualify the vehicle as a closed vehicle (NUREG/CR-5569A and NUREG/CR-5569B) as defined in 49 CFR 173.403."

When the HI-STAR is transported, a personnel barrier will be placed over the HI-STAR as depicted in Figure 1.2.8. This personnel barrier spans the distance between the impact limiters. The outer radial location of the personnel barrier is equal to the outer radial surface of the impact limiters and the personnel barrier is attached to the saddle on the rail car rather than the HI-STAR overpack. Therefore, the personnel barrier acts as an enclosure for the main body of the HI-STAR overpack. Consequently, the 1000 mrem/hr limit for the enclosed package is applicable for the outer radial surface of the overpack in the region between the impact limiters. Since the impact limiters are not enclosed, the surface of the impact limiters is required to meet the lower 200 mrem/hr limit for the package.

The HI-STAR 100 System will be transported on either a flat-bed rail car, heavy haul vehicle, or a barge. The smallest width of a transport vehicle is equivalent to the width of the impact limiters. Therefore, the vertical planes projected by the outer side edges of the transport vehicle are equivalent to the outer edge of the impact limiters. The minimum length of any transport vehicle will be 12 feet longer than the length of the overpack, with impact limiters attached. The bottom impact limiter of the HI-STAR 100 System will be conservatively positioned a minimum of 9 feet from the end of the transport vehicle. Therefore, the vertical planes projected from the outer edge of the ends of the vehicle will be taken as the end of the top impact limiter and 9 feet from the end of the bottom impact limiter.

Figure 5.1.1 shows the HI-STAR 100 System during normal transport conditions. The impact limiters and personnel barrier are outlined on the figure and various dose point locations are shown on the surface of the enclosure (personnel barrier) and the HI-STAR 100 System. The

dose values reported at the locations shown on Figure 5.1.1 are averaged over a region that is approximately 1 foot in width. Each of the dose locations in Figure 5.1.1 (with the exception of 2a and 3a) has a corresponding location at 2 meters from the surface of the transport vehicle as defined above.

Dose locations 2a, 3a, and 2 shown in Figure 5.1.1 and Figure 5.1.2 (discussed below) do not correspond to single dose locations. Rather the dose rate for multiple axial segments of approximately 1 foot or less were calculated and the highest value was chosen for the corresponding dose location. Dose locations 2a and 2 encompass 14 axial segments that range from the pocket trunnion to the top of the Holtite. The highest dose rate of these 14 axial segments was chosen as the value for dose locations 2a and 2. Dose location 3a corresponds to two axial segments while dose locations 1, 3, and 4 correspond to a single axial segment. Dose locations 5 and 6 correspond to either the center radial segment of the overpack along the axis or the adjacent location radial segment.

Tables 5.1.1 through 5.1.3, 5.1.10, and 5.1.11 provide the maximum dose rates on the surface of the system during normal transport conditions for the MPC-24, MPC-32, and MPC-68 with design basis intact zircaloy clad fuel. Tables 5.1.4 through 5.1.6, 5.1.12, and 5.1.13 list the maximum dose rates two meters from the edge of the transport vehicle during normal conditions. Section 5.4 provides a detailed list of the total dose rates at several cask locations for all burnup and cooling times analyzed. The burnup and cooling time combinations chosen for the tables mentioned above was the combination that resulted in the absolute highest dose rate for the normal condition regulatory locations (i.e. surface and 2 meter). For example, Table 5.1.1 presents the burnup and cooling time combination that results in the highest dose rate from a review of the dose rates, in Table 5.4.8, for locations 2a, 3a, and 1-6 for all allowable burnup and cooling time combinations. This combination may not result in the highest dose rate at each individual dose location (e.q. 2a, 3a, 1-6) but it is the combination that results in the absolute highest dose rate for the surface or 2 meter locations.

Subsections 5.2.1 and 5.2.2 list the gamma and neutron sources for the design basis zircaloy clad intact, zircaloy clad damaged and MOX fuel assemblies. Since the source strengths of the damaged and MOX fuel are significantly smaller in all energy groups than the intact design basis fuel source strengths, the damaged and MOX fuel dose rates for normal conditions are bounded by the MPC-68 analysis with design basis intact fuel. Therefore, no explicit analysis of the MPC-68 with either damaged or MOX fuel for normal conditions is required to demonstrate that the MPC-68 with damaged fuel or MOX fuel will meet the normal condition regulatory requirements.

Subsection 5.2.6 lists the gamma and neutron sources from the Dresden Unit 1 Thoria rod canister and demonstrates that the Thoria rod canister is bounded by the design basis 6x6 intact fuel.

Subsection 5.4.5 demonstrates that the Dresden Unit 1 fuel assemblies containing antimony-beryllium neutron sources are bounded by the shielding analysis presented in this section.

Subsections 5.4.7 and 5.4.8 present the results for the Trojan contents in the MPC-24E/EF and demonstrate that these contents are acceptable for transportation.

Subsection 5.2.3 lists the gamma and neutron sources for the design basis intact stainless steel clad fuels. The dose rates from these fuels are provided in Subsection 5.4.4.

Tables 5.1.4 through 5.1.6, 5.1.12, and 5.1.13 show that the dose rate at Dose Location #5 (the top of the HI-STAR 100 System, see Figure 5.1.1) at 2 meters from the edge of the transport vehicle is less than 2 mrem/hr. It is, therefore, recommended that the HI-STAR 100 System be positioned such that the top impact limiter is facing the normally occupied space. If this is the orientation, radiation dosimetry will not be required as long as the normally occupied space is a minimum of 2 meters from the impact limiter on the top of the HI-STAR 100 System. If a different orientation is chosen for the HI-STAR 100 System, the dose rate in the normally occupied space will have to be evaluated against the dose requirement for the normally occupied space to determine if radiation dosimetry is required.

The analyses summarized in this section demonstrate the HI-STAR 100 System's compliance with the 10CFR71.47 limits.

5.1.2 Hypothetical Accident Conditions

The 10CFR71.51 external radiation dose limit for design basis accidents is:

- The external radiation dose rate shall not exceed 1 rem/hr (10 mSv/hr) at 1 m (40 in.) from the external surface of the package.

The hypothetical accident conditions of transport have two bounding consequences which affect the shielding materials. They are the damage to the neutron shield as a result of the design basis fire and damage of the impact limiters as a result of the 30 foot drop. In a conservative fashion, the dose analysis assumes that as a result of the fire, the neutron shield is completely destroyed and replaced by a void. Additionally, the impact limiters are assumed to have been lost. These are highly conservative assumptions since some portion of the neutron shield would be expected to remain after the fire as the neutron shield material is fire retardant, and the impact limiters have been shown by 1/4-scale testing to remain attached following impact.

Throughout the hypothetical accident condition the axial location of the fuel will remain fixed within the MPC because of the fuel spacers or by the MPC lid and baseplate if spacers are not used. Chapter 2 provides an analysis to show that the fuel spacers do not fail under all normal and hypothetical accident conditions. Chapter 2 also shows that the inner shell, intermediate

shell, radial channels, and outer enclosure shell of the overpack remain unaltered throughout the hypothetical accident conditions. Localized damage of the overpack outer enclosure shell could be experienced during the pin puncture. However, the localized deformations will have only a negligible impact on the dose rate at 1 meter from the surface.

Figure 5.1.2 shows the HI-STAR 100 System after the postulated accident. The various dose point locations at 1 meter from the HI-STAR 100 System are shown on the figure. Tables 5.1.7 through 5.1.9, 5.1.14 and 5.1.15 provide the maximum dose rates at 1 meter for the accident conditions. The burnup and cooling time combinations chosen for the aforementioned tables were the combinations that resulted in the absolute highest dose rate for the accident condition regulatory location (i.e. 1 meter).

The consequences of the hypothetical accident conditions for the MPC-68F storing either damaged or MOX (which can also be considered damaged) fuel differ slightly from those with intact fuel. For this accident condition, it is conservatively assumed that during a drop accident the damaged fuel collapses and the pellets rest in the bottom of the damaged fuel container. The analysis presented in Subsections 5.4.2 and 5.4.3 demonstrate that the damaged fuel in the post-accident condition has lower source terms (both gamma and neutron) per inch than the intact BWR design basis fuel. Therefore, the damaged fuel post-accident dose rates are bounded by the BWR intact fuel post-accident dose rates.

Subsections 5.4.7 and 5.4.8 present the results for the Trojan contents in the MPC-24E/EF and demonstrate that these contents are acceptable for transportation.

Analyses summarized in this section demonstrate the HI-STAR 100 System's compliance with the 10CFR71.51 radiation dose limit.

Table 5.1.1

DOSE RATES ON THE SURFACE OF THE HI-STAR 100 SYSTEM FOR NORMAL CONDITIONS
MPC-24 WITH DESIGN BASIS ZIRCALOY CLAD FUEL WITH ZIRCALOY INCORE SPACERS
AT WORST CASE BURNUP AND COOLING TIME
44,500 MWD/MTU AND 14-YEAR COOLING

Dose Point† Location	Fuel Gammas†† (mrem/hr)	Gammas from Incore Spacers (mrem/hr)	^{60}Co Gammas (mrem/hr)	Neutrons (mrem/hr)	Totals (mrem/hr)	10 CFR 71.47 Limit
2a	23.91	0.00	0.01	22.27	46.19	1000
3a	0.96	0.00	28.52	108.98	138.47	1000
1	1.92	0.00	13.98	18.95	34.85	200
2	15.33	0.00	0.09	12.82	28.24	200
3	1.11	0.00	10.45	18.63	30.19	200
4	0.62	0.00	9.21	18.22	28.05	200
5	0.50	0.00	0.02	3.63	4.15	200
6	4.74	0.00	55.85	29.42	90.02	200

† Refer to Figure 5.1.1.

†† Gammas generated by neutron capture are included with fuel gammas.

Table 5.1.2

DOSE RATES ON THE SURFACE OF THE HI-STAR 100 SYSTEM FOR NORMAL CONDITIONS
MPC-24 WITH DESIGN BASIS ZIRCALOY CLAD FUEL WITH NON-ZIRCALOY INCORE SPACERS
AT WORST CASE BURNUP AND COOLING TIME
44,500 MWD/MTU AND 18-YEAR COOLING

Dose Point† Location	Fuel Gammas†† (mrem/hr)	Gammas from Incore Spacers (mrem/hr)	^{60}Co Gammas (mrem/hr)	Neutrons (mrem/hr)	Totals (mrem/hr)	10 CFR 71.47 Limit
2a	18.10	8.92	0.01	19.22	46.24	1000
3a	0.78	0.14	16.91	94.04	111.87	1000
1	1.48	0.63	8.29	16.35	26.75	200
2	11.56	5.93	0.05	11.07	28.62	200
3	0.85	0.35	6.19	16.08	23.47	200
4	0.49	0.19	5.46	15.72	21.85	200
5	0.44†††	-	0.01	3.13	3.58	200
6	4.85†††	-	33.10	25.39	63.35	200

† Refer to Figure 5.1.1.

†† Gammas generated by neutron capture are included with fuel gammas.

††† Gammas from incore spacers are included with fuel gammas.

Table 5.1.3

DOSE RATES ON THE SURFACE OF THE HI-STAR 100 SYSTEM FOR NORMAL CONDITIONS
MPC-68 WITH DESIGN BASIS ZIRCALOY CLAD FUEL AT
WORST CASE BURNUP AND COOLING TIME
20,000 MWD/MTU AND 7-YEAR COOLING

Dose Point† Location	Fuel Gammas†† (mrem/hr)	Gammas from Incore Spacers (mrem/hr)	^{60}Co Gammas (mrem/hr)	Neutrons (mrem/hr)	Totals (mrem/hr)	10 CFR 71.47 Limit
2a	0.50	0.10	49.98	2.10	52.69	1000
3a	0.33	0.12	140.66	13.30	154.42	1000
1	2.03	0.54	31.63	5.09	39.29	200
2	1.21	0.31	24.28	1.73	27.53	200
3	0.59	0.14	34.17	2.85	37.75	200
4	0.31	0.08	32.67	2.69	35.76	200
5	0.07†††	-	0.04	0.49	0.60	200
6	2.52†††	-	111.69	7.00	121.21	200

† Refer to Figure 5.1.1.

†† Gammas generated by neutron capture are included with fuel gammas.

††† Gammas from incore spacers are included with fuel gammas.

Table 5.1.4

DOSE RATES AT TWO METERS FOR NORMAL CONDITIONS
MPC-24 WITH DESIGN BASIS ZIRCALOY CLAD FUEL WITH ZIRCALOY INCORE SPACERS
AT WORST CASE BURNUP AND COOLING TIME
24,500 MWD/MTU AND 6-YEAR COOLING

Dose Point† Location	Fuel Gammas†† (mrem/hr)	Gammas from Incore Spacers (mrem/hr)	^{60}Co Gammas (mrem/hr)	Neutrons (mrem/hr)	Totals (mrem/hr)
1	3.06	0.00	3.56	0.78	7.41
2	7.52	0.00	1.16	0.88	9.57
3	2.57	0.00	3.41	0.74	6.72
4	2.03	0.00	3.43	0.70	6.16
5	0.01	0.00	0.01	0.07	0.09
6	0.28	0.00	7.85	0.26	8.39
10CFR71.47 Limit					10.00

† Refer to Figure 5.1.1.

†† Gammas generated by neutron capture are included with fuel gammas.

Table 5.1.5

DOSE RATES AT TWO METERS FOR NORMAL CONDITIONS
MPC-24 WITH DESIGN BASIS ZIRCALOY CLAD FUEL WITH NON-ZIRCALOY INCORE SPACERS
AT WORST CASE BURNUP AND COOLING TIME
24,500 MWD/MTU AND 9-YEAR COOLING

Dose Point† Location	Fuel Gammas†† (mrem/hr)	Gammas from Incore Spacers (mrem/hr)	^{60}Co Gammas (mrem/hr)	Neutrons (mrem/hr)	Totals (mrem/hr)
1	1.42	1.90	2.40	0.70	6.42
2	3.38	4.56	0.80	0.77	9.51
3	1.18	1.54	2.30	0.66	5.68
4	0.94	1.21	2.31	0.63	5.08
5	0.01†††	-	0.01	0.07	0.08
6	0.32†††	-	5.29	0.23	5.84
10CFR71.47 Limit					10.00

† Refer to Figure 5.1.1.

†† Gammas generated by neutron capture are included with fuel gammas.

††† Gammas from incore spacers are included with fuel gammas.

Table 5.1.6

DOSE RATES AT TWO METERS FOR NORMAL CONDITIONS
MPC-68 WITH DESIGN BASIS ZIRCALOY CLAD FUEL
AT WORST CASE BURNUP AND COOLING TIME
34,500 MWD/MTU AND 11-YEAR COOLING

Dose Point† Location	Fuel Gammas†† (mrem/hr)	Gammas from Incore Spacers (mrem/hr)	^{60}Co Gammas (mrem/hr)	Neutrons (mrem/hr)	Totals (mrem/hr)
1	2.38	0.43	2.33	2.45	7.59
2	5.19	0.95	0.65	2.83	9.62
3	1.56	0.28	3.14	1.64	6.62
4	1.21	0.21	3.33	1.57	6.32
5	0.02†††	-	0.01	0.13	0.15
6	0.17†††	-	4.39	0.45	5.01
10CFR71.47 Limit					10.00

† Refer to Figure 5.1.1.

†† Gammas generated by neutron capture are included with fuel gammas.

††† Gammas from incore spacers are included with fuel gammas.

Table 5.1.7

DOSE RATES AT ONE METER FOR ACCIDENT CONDITIONS
MPC-24 WITH DESIGN BASIS ZIRCALOY CLAD FUEL WITH ZIRCALOY INCORE SPACERS
AT WORST CASE BURNUP AND COOLING TIME
29,500 MWD/MTU AND 7-YEAR COOLING

Dose Point† Location	Fuel Gammas†† (mrem/hr)	^{60}Co Gammas (mrem/hr)	Neutrons (mrem/hr)	Totals (mrem/hr)
1	7.11	34.28	56.17	97.55
2	37.07	1.19	185.96	224.23
3	4.67	19.87	39.87	64.41
4	2.70	15.08	29.35	47.12
5	0.03	0.24	6.32	6.59
6	20.66	618.44	47.99	687.08
10CFR71.51 Limit				1000.00

† Refer to Figure 5.1.2.

†† Gammas generated by neutron capture and gammas from incore spacers are included with fuel gammas.

Table 5.1.8

DOSE RATES AT ONE METER FOR ACCIDENT CONDITIONS
MPC-24 WITH DESIGN BASIS ZIRCALOY CLAD FUEL WITH NON-ZIRCALOY INCORE SPACERS
AT WORST CASE BURNUP AND COOLING TIME
24,500 MWD/MTU AND 9-YEAR COOLING

Dose Point† Location	Fuel Gammas†† (mrem/hr)	^{60}Co Gammas (mrem/hr)	Neutrons (mrem/hr)	Totals (mrem/hr)
1	8.40	23.69	30.24	62.33
2	44.07	0.82	100.11	145.00
3	5.51	13.73	21.46	40.70
4	3.17	10.42	15.80	29.39
5	0.02	0.17	3.40	3.59
6	25.07	427.37	25.84	478.28
10CFR71.51 Limit				1000.00

† Refer to Figure 5.1.2.

†† Gammas generated by neutron capture and gammas from incore spacers are included with fuel gammas.

Table 5.1.9

DOSE RATES AT ONE METER FOR ACCIDENT CONDITIONS
MPC-68 WITH DESIGN BASIS ZIRCALOY CLAD FUEL
AT WORST CASE BURNUP AND COOLING TIME
20,000 MWD/MTU AND 7-YEAR COOLING

Dose Point† Location	Fuel Gammas†† (mrem/hr)	^{60}Co Gammas (mrem/hr)	Neutrons (mrem/hr)	Totals (mrem/hr)
1	7.90	37.54	40.74	86.18
2	38.84	0.80	133.11	172.74
3	3.07	25.51	20.81	49.39
4	1.71	22.73	14.88	39.33
5	0.02	0.26	2.42	2.70
6	9.72	631.00	27.37	668.09
10CFR71.51 Limit				1000.00

† Refer to Figure 5.1.2.

†† Gammas generated by neutron capture and gammas from incore spacers are included with fuel gammas.

Table 5.1.10

DOSE RATES ON THE SURFACE OF THE HI-STAR 100 SYSTEM FOR NORMAL CONDITIONS
MPC-32 WITH DESIGN BASIS ZIRCALOY CLAD FUEL WITH ZIRCALOY INCORE SPACERS
AT WORST CASE BURNUP AND COOLING TIME
44,500 MWD/MTU AND 19-YEAR COOLING

Dose Point† Location	Fuel Gammas†† (mrem/hr)	Gammas from Incore Spacers (mrem/hr)	^{60}Co Gammas (mrem/hr)	Neutrons (mrem/hr)	Totals (mrem/hr)	10 CFR 71.47 Limit
2a	2.77	0.00	17.29	30.84	50.90	1000
3a	2.01	0.00	27.39	234.56	263.95	1000
1	1.90	0.00	11.60	29.02	42.51	200
2	2.80	0.00	8.42	24.26	35.48	200
3	1.45	0.00	9.60	38.62	49.68	200
4	0.74	0.00	8.99	37.58	47.31	200
5	0.93	0.00	0.02	7.52	8.46	200
6	5.69	0.00	44.21	45.55	95.45	200

† Refer to Figure 5.1.1.

†† Gammas generated by neutron capture are included with fuel gammas.

Table 5.1.11

DOSE RATES ON THE SURFACE OF THE HI-STAR 100 SYSTEM FOR NORMAL CONDITIONS
MPC-32 WITH DESIGN BASIS ZIRCALOY CLAD FUEL WITH NON-ZIRCALOY INCORE SPACERS
AT WORST CASE BURNUP AND COOLING TIME
42,500 MWD/MTU AND 20-YEAR COOLING

Dose Point† Location	Fuel Gammas†† (mrem/hr)	Gammas from Incore Spacers (mrem/hr)	^{60}Co Gammas (mrem/hr)	Neutrons (mrem/hr)	Totals (mrem/hr)	10 CFR 71.47 Limit
2a	18.92	9.15	0.01	16.46	44.54	1000
3a	1.65	0.29	22.98	188.28	213.21	1000
1	1.61	0.70	9.73	23.29	35.33	200
2	2.38	1.01	7.06	19.48	29.93	200
3	1.22	0.46	8.06	31.01	40.74	200
4	0.63	0.24	7.54	30.17	38.57	200
5	0.75†††	-	0.01	6.04	6.79	200
6	5.97†††	-	37.10	36.56	79.64	200

† Refer to Figure 5.1.1.

†† Gammas generated by neutron capture are included with fuel gammas.

††† Gammas from incore spacers are included with fuel gammas.

Table 5.1.12

DOSE RATES AT TWO METERS FOR NORMAL CONDITIONS
MPC-32 WITH DESIGN BASIS ZIRCALOY CLAD FUEL WITH ZIRCALOY INCORE SPACERS
AT WORST CASE BURNUP AND COOLING TIME
39,500 MWD/MTU AND 14-YEAR COOLING

Dose Point† Location	Fuel Gammas†† (mrem/hr)	Gammas from Incore Spacers (mrem/hr)	^{60}Co Gammas (mrem/hr)	Neutrons (mrem/hr)	Totals (mrem/hr)
1	2.29	0.00	2.59	3.56	8.43
2	5.25	0.00	0.82	3.58	9.65
3	1.92	0.00	2.66	4.52	9.10
4	1.57	0.00	2.67	4.56	8.79
5	0.06	0.00	0.01	0.49	0.55
6	0.19	0.00	4.55	0.92	5.66
10CFR71.47 Limit					10.00

† Refer to Figure 5.1.1.

†† Gammas generated by neutron capture are included with fuel gammas.

Table 5.1.13

DOSE RATES AT TWO METERS FOR NORMAL CONDITIONS
MPC-32 WITH DESIGN BASIS ZIRCALOY CLAD FUEL WITH NON-ZIRCALOY INCORE SPACERS
AT WORST CASE BURNUP AND COOLING TIME
42,500 MWD/MTU AND 20-YEAR COOLING

Dose Point† Location	Fuel Gammas†† (mrem/hr)	Gammas from Incore Spacers (mrem/hr)	^{60}Co Gammas (mrem/hr)	Neutrons (mrem/hr)	Totals (mrem/hr)
1	1.68	0.80	1.22	3.43	7.13
2	3.81	1.96	0.38	3.46	9.61
3	1.43	0.67	1.25	4.36	7.71
4	1.16	0.54	1.26	4.40	7.36
5	0.06†††	-	0.00	0.47	0.53
6	0.21†††	-	2.14	0.89	3.24
10CFR71.47 Limit					10.00

† Refer to Figure 5.1.1.

†† Gammas generated by neutron capture are included with fuel gammas.

††† Gammas from incore spacers are included with fuel gammas.

Table 5.1.14

DOSE RATES AT ONE METER FOR ACCIDENT CONDITIONS
MPC-32 WITH DESIGN BASIS ZIRCALOY CLAD FUEL WITH ZIRCALOY INCORE SPACERS
AT WORST CASE BURNUP AND COOLING TIME
29,500 MWD/MTU AND 9-YEAR COOLING

Dose Point† Location	Fuel Gammas†† (mrem/hr)	^{60}Co Gammas (mrem/hr)	Neutrons (mrem/hr)	Totals (mrem/hr)
1	6.51	43.30	68.18	117.99
2	32.65	1.42	196.89	230.95
3	4.37	25.54	60.00	89.91
4	2.64	20.54	43.37	66.55
5	0.06	0.27	14.76	15.09
6	18.89	720.63	77.64	817.16
10CFR71.51 Limit				1000.00

† Refer to Figure 5.1.2.

†† Gammas generated by neutron capture and gammas from incore spacers are included with fuel gammas.

Table 5.1.15

DOSE RATES AT ONE METER FOR ACCIDENT CONDITIONS
MPC-32 WITH DESIGN BASIS ZIRCALOY CLAD FUEL WITH NON-ZIRCALOY INCORE SPACERS
AT WORST CASE BURNUP AND COOLING TIME
24,500 MWD/MTU AND 12-YEAR COOLING

Dose Point† Location	**Fuel Gammas†† (mrem/hr)**	**^{60}Co Gammas (mrem/hr)**	**Neutrons (mrem/hr)**	**Totals (mrem/hr)**
1	8.07	26.23	35.50	69.80
2	40.10	0.86	102.53	143.48
3	5.43	15.47	31.25	52.15
4	3.29	12.44	22.58	38.31
5	0.04	0.16	7.69	7.89
6	23.63	436.48	40.43	500.54
10CFR71.51 Limit				1000.00

† Refer to Figure 5.1.2.

†† Gammas generated by neutron capture and gammas from incore spacers are included with fuel gammas.

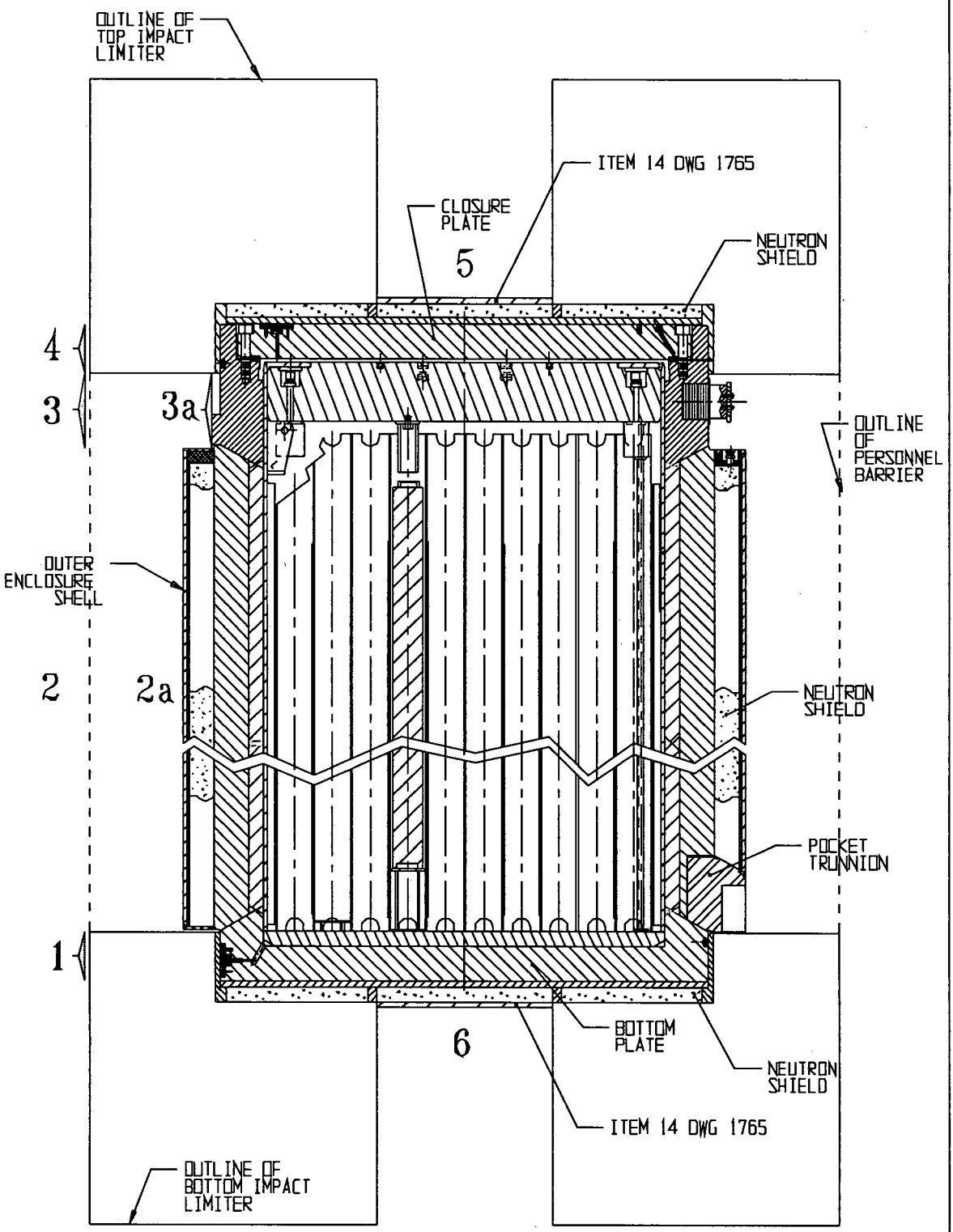

FIGURE 5.1.1; CROSS SECTION ELEVATION VIEW OF THE HI-STAR 100 SYSTEM WITH DOSE POINT LOCATIONS DURING NORMAL CONDITIONS

REPORT HI-951251 | REVISION 10

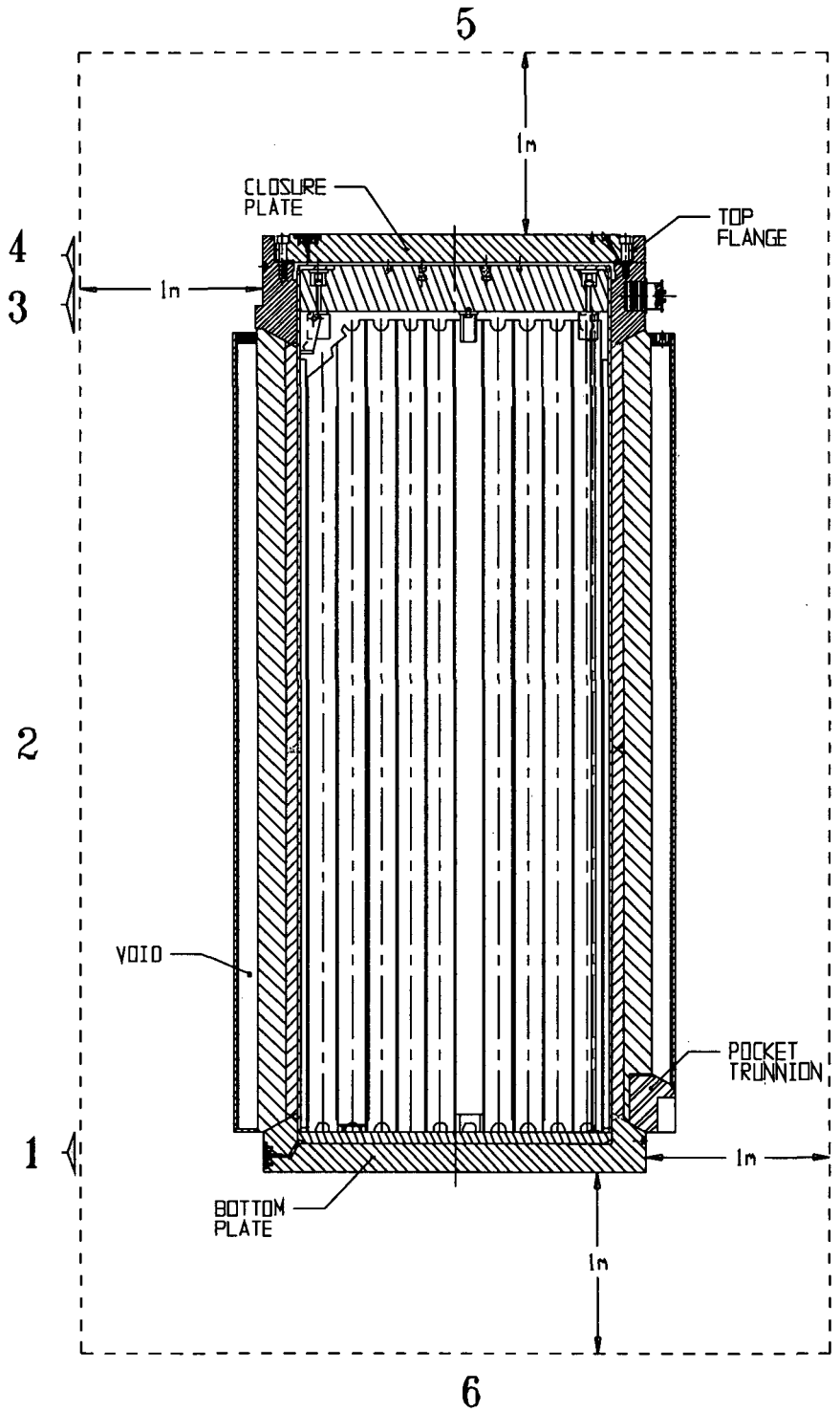

FIGURE 5.1.2; CROSS SECTION ELEVATION VIEW OF THE HI-STAR 100 SYSTEM WITH DOSE POINT LOCATIONS DURING ACCIDENT CONDITIONS

5.2 SOURCE SPECIFICATION

The neutron and gamma source terms, decay heat values, and quantities of radionuclides available for release were calculated with the SAS2H and ORIGEN-S modules of the SCALE 4.3 system [5.1.2, 5.1.3]. The source terms for the Trojan specific inventory were calculated with the SAS2H and ORIGEN-S sequences from the SCALE 4.4 system [5.1.4, 5.1.5] as described in the Trojan FSAR [5.1.6]. Sample input files for SAS2H and ORIGEN-S are provided in Appendices 5.A and 5.B, respectively. The gamma source term is actually comprised of three distinct sources. The first is a gamma source term from the active fuel region due to decay of fission products. The second source term is from ^{60}Co activity of the steel structural material in the fuel assembly above and below the active fuel region. The third source is from (n,γ) reactions described below.

A description of the design basis intact zircaloy clad fuel for the source term calculations is provided in Table 5.2.1. The PWR fuel assembly described is the assembly that produces the highest neutron and gamma sources and the highest decay heat load from the following fuel assembly classes listed in Table 1.2.8: B&W 15x15, B&W 17x17, CE 14x14, CE 16x16, WE 14x14, WE 15x15, WE 17x17, St. Lucie, and Ft. Calhoun. The BWR fuel assembly described is the assembly that produces the highest neutron and gamma sources and the highest decay heat load from the following fuel assembly classes listed in Table 1.2.9: GE BWR/2-3, GE BWR/4-6, Humboldt Bay 7x7, and Dresden 1 8x8. Multiple SAS2H and ORIGEN-S calculations were performed to confirm that the B&W 15x15 and the GE 7x7, which have the highest UO_2 mass, bound all other PWR and BWR fuel assemblies, respectively. Subsection 5.2.5 discusses, in detail, the determination of the design basis fuel assemblies.

The design basis Humboldt Bay and Dresden 1 6x6 fuel assembly, which is also the design basis damaged fuel assembly for the Humboldt Bay and Dresden 1 damaged fuel or fuel debris, is described in Table 5.2.2. The design basis damaged fuel assembly is also the design basis fuel assembly for fuel debris. The fuel assembly type listed produces the highest total neutron and gamma sources from the fuel assemblies at Dresden 1 and Humboldt Bay. Table 5.2.15 provides a description of the design basis Dresden 1 MOX fuel assembly used in this analysis. The design basis 6x6, damaged, and MOX fuel assemblies which are smaller than the GE 7x7, are assumed to have the same hardware characteristics as the GE 7x7. This is conservative because the larger hardware mass of the GE 7x7 results in a larger ^{60}Co activity.

The design basis stainless steel clad fuel assembly for the Indian Point 1, Haddam Neck and San Onofre 1 assembly classes is described in Table 5.2.18. This table also describes the design basis stainless steel clad LaCrosse fuel assembly.

Since the MPC-24E being used for Trojan fuel is slightly different than the standard MPC-24E, the Trojan contents were specifically analyzed and are not covered by the design basis PWR fuel assembly described above. The design basis Trojan WE 17x17 fuel assembly is described in Table 5.2.32 and was taken from the site specific Trojan FSAR analysis [5.1.6].

In performing the SAS2H and ORIGEN-S calculations, a single full power cycle was used to achieve the desired burnup. This assumption, in conjunction with the above-average specific powers listed in Tables 5.2.1, 5.2.2, 5.2.15, 5.2.18, and 5.2.32 resulted in conservative source term calculations.

Subsections 5.2.1 and 5.2.2 describe the calculation of the gamma and neutron source terms for zircaloy clad fuel while Subsection 5.2.3 discusses the calculation of the gamma and neutron source terms for the stainless steel clad fuel.

5.2.1 Gamma Source

Tables 5.2.3 through 5.2.6, 5.2.33, 5.2.40, and 5.2.41 provide the gamma source in MeV/s and photons/s as calculated with SAS2H and ORIGEN-S for the design bases intact fuels for the MPC-24, MPC-32, MPC-68, the design basis damaged fuel, and the Trojan fuel. Table 5.2.16 provides the gamma source in MeV/s and photons/s for the design basis MOX fuel. NUREG-1617 [5.2.1] states that "In general, only gammas from approximately 0.8 MeV-2.5 MeV will contribute significantly to the external radiation levels." However, specific analysis for the HI-STAR 100 system has revealed that, due to the magnitude of the gamma source in the energy range just below 0.8 MeV, gammas with energies as low as 0.45 MeV must be included in the shielding analysis. The effect of gammas with energies above 3.0 MeV, on the other hand, was found to be insignificant (less than 1% of the total gamma dose). This is due to the fact that the source of gammas in this range (i.e., above 3.0 MeV) is extremely low (less than 1% of the total source). Therefore, all gammas with energies in the range of 0.45 to 3.0 MeV are included in the shielding calculations. Photons with energies below 0.45 MeV are too weak to penetrate the steel of the overpack, and photons with energies above 3.0 MeV are too few to contribute significantly to the external dose. As discussed earlier, the MPC-24, MPC-32, and the MPC-68 are analyzed for transportation of spent nuclear fuel with varying minimum enrichments, burnup levels and cooling times. This section provides the radiation source for each of the burnup levels and cooling times evaluated.

The primary source of activity in the non-fuel regions of an assembly arise from the activation of ^{59}Co to ^{60}Co. The primary source of ^{59}Co in a fuel element is the steel and inconel structural material. The zircaloy in these regions is neglected since it does not have a significant ^{59}Co impurity level. Reference [5.2.3] indicates that the ^{59}Co impurity level in steel is 800 ppm or 0.8 gm/kg and in inconel is approximately 4700 ppm or 4.7 gm/kg. In the early to mid 1980s, the fuel vendors reduced the ^{59}Co impurity level in both inconel and steel to less than 500 ppm or 0.5 gm/kg. Prior to that, the impurity level in inconel in fuel assemblies was typically less than 1200 ppm or 1.2 gm/kg. Nevertheless, a conservative ^{59}Co impurity level of 1.0 gm/kg was used for the stainless steel end fittings and a highly conservative impurity level of 4.7 gm/kg was used for the inconel.

PWR fuel assemblies are currently manufactured with zircaloy incore grid spacers (the plenum spacer and the lower spacer are still inconel in some cases). However, earlier assemblies were manufactured with inconel incore grid spacers. Since the mass of the spacers is significant and since the cobalt impurity level assumed for inconel is very conservative, the Cobalt-60 activity from the incore spacers contributes significantly to the external dose rate. As a result, separate burnup and cooling times were developed for PWR assemblies that utilize zircaloy and non-zircaloy incore spacers. Since steel has a lower cobalt impurity level than inconel, any zircaloy clad PWR assemblies with stainless steel grid spacers are bounded by the analysis performed in this chapter utilizing inconel grid spacers. The BWR assembly grid spacers are zircaloy, however, some assembly designs have inconel springs in conjunction with the grid spacers. The gamma source for the BWR fuel assembly includes the activation of these springs associated with the grid spacers.

The non-fuel data listed in Table 5.2.1 was taken from References [5.2.3], [5.2.4], and [5.2.5]while the non-fuel data listed in Table 5.2.32 was taken from References [5.2.5] and [5.2.8]. The BWR masses are for an 8x8 fuel assembly. These masses are also appropriate for the 7x7 assembly since the masses of the non-fuel hardware from a 7x7 and an 8x8 are approximately the same. The masses listed are those of the steel components. The zircaloy in these regions was not included because zircaloy does not produce significant activation. These masses are larger than most other fuel assemblies from other manufacturers. This, in combination with the conservative ^{59}Co impurity level, results in a conservative estimate of the ^{60}Co activity.

The masses in Table 5.2.1 and 5.2.32 were used to calculate a ^{59}Co impurity level in the fuel material. The grams of impurity were then used in ORIGEN-S to calculate a ^{60}Co activity level for the desired burnup and decay time. The methodology used to determine the activation level was developed from Reference [5.2.2] and is described here.

1. The activity of the ^{60}Co is calculated using ORIGEN-S. The flux used in the calculation was the in-core fuel region flux at full power.

2. The activity calculated in Step 1 for the region of interest was modified by the appropriate scaling factors listed in Table 5.2.7. These scaling factors were taken from Reference [5.2.2]. In the case of the Trojan fuel, the higher value of 0.2 was used for both the gas plenum springs and spacer consistent with the Trojan FSAR [5.1.6].

Tables 5.2.8 through 5.2.10, 5.2.34, 5.2.42, and 5.2.43 provide the ^{60}Co activity utilized in the shielding calculations in the non-fuel regions of the assemblies for the MPC-24, MPC-32, MPC-68, and Trojan fuel. The design basis damaged and MOX fuel assemblies are conservatively assumed to have the same ^{60}Co source strength as the BWR intact design basis fuel. This is a conservative assumption as the design basis damaged fuel and MOX fuel are limited to a significantly lower burnup and longer cooling time than the intact design basis zircaloy clad fuel.

In addition to the two sources already mentioned, a third source arises from (n,γ) reactions in the material of the MPC and the overpack. This source of photons is properly accounted for in MCNP when a neutron calculation is performed in a coupled neutron-gamma mode.

5.2.2 Neutron Source

It is well known that the neutron source strength increases as enrichment decreases, for a constant burnup and decay time. This is due to the increase in Pu content in the fuel which increases the inventory of other transuranium nuclides such as Cm. The gamma source also varies with enrichment, although only slightly. Because of this effect and in order to obtain conservative source terms, low initial fuel enrichments were chosen for the BWR and PWR design basis fuel assemblies as a function of burnup and cooling time. Conservatively, the minimum enrichments used to develop the source terms and dose rates presented in this chapter are specified in Tables 1.2.28 through 1.2.33 as fuel assembly acceptance criteria. The minimum enrichments for the design basis PWR and BWR assemblies are also listed in Table 5.2.23 for convenience.

The neutron source calculated for the design basis intact fuel assemblies for the MPC-24, MPC-32, MPC-68, Trojan fuel, and the design basis damaged fuel are listed in Tables 5.2.11 through 5.2.14, 5.2.35, 5.2.44, and 5.2.45 in neutrons/s. Table 5.2.17 provides the neutron source in neutrons/sec for the design basis MOX fuel assembly. ^{244}Cm accounts for approximately 96% of the total number of neutrons produced, with slightly over 2% originating from (α,n) reactions within the UO_2 fuel. The remaining 2% derive from spontaneous fission in various Pu and Cm radionuclides. In addition, any neutrons generated from subcritical multiplication, (n,2n) or similar reactions are properly accounted for in the MCNP calculation.

5.2.3 Stainless Steel Clad Fuel Source

Table 5.2.18 lists the characteristics of the design basis stainless steel clad fuel. The fuel characteristics listed in this table are the input parameters that were used in the shielding calculations described in this chapter. The active fuel length listed in the table is actually longer than the true active fuel length of 122 inches for the W15x15 and 83 inches for the A/C 10x10. Since the true active fuel length is shorter than the design basis zircaloy clad active fuel length, it would be incorrect to calculate source terms for the stainless steel fuel using the actual fuel length and compare them directly to the source terms from the zircaloy clad fuel with a longer active fuel length.

In order to eliminate the potential confusion when comparing source terms, the stainless steel clad fuel source terms were calculated with the same active fuel length as the design basis zircaloy clad fuel. Reference [5.2.3] indicates that the Cobalt-59 impurity level in steel is 800 ppm or 0.8 gm/kg and in inconel is approximately 4700 ppm or 4.7 gm/kg. In the early to mid 1980s, the fuel vendors reduced the Cobalt-59 impurity level in both inconel and steel to less than 500 ppm or 0.5 gm/kg. Prior to that, the impurity level in inconel in fuel assemblies was

typically less than 1200 ppm or 1.2 gm/kg. Nevertheless, a conservative Cobalt-59 impurity level of 0.8 gm/kg was used for the stainless steel cladding and a highly conservative impurity level of 4.7 gm/kg was used for the inconel incore spacers. It is assumed that the end fitting masses of the stainless steel clad fuel are the same as the end fittings masses of the zircaloy clad fuel. Therefore, separate source terms are not provided for the end fittings of the stainless steel fuel.

Tables 5.2.19 through 5.2.22 list the neutron and gamma source strengths for the design basis stainless steel clad fuel. The gamma source strengths include the contribution from the cobalt activation in the incore spacers. Subsection 5.4.4 presents the dose rates around the HI-STAR 100 for the normal and hypothetical accident conditions for the stainless steel fuel. In the calculation of these dose rates the length of the active fuel was conservatively assumed to be 144 inches. In addition, the fuel assembly configuration used in the MCNP calculations was identical to the configuration used for the design basis fuel assemblies as described in Table 5.3.1.

5.2.4 Non-fuel Hardware

Generic PWR non-fuel hardware is not permitted for transport in the HI-STAR 100 system. However, certain non-fuel hardware from the Trojan Nuclear plant has been analyzed and is approved for transportation. These components include rod cluster control assemblies (RCCAs), burnable poison rod assemblies (BPRAs) and thimble plug devices (TPDs). The methodology for analyzing the non-fuel hardware authorized for transportation is described below and has been previously approved in the HI-STORM 100 FSAR [5.2.9].

5.2.4.1 BPRAs and TPDs

Burnable poison rod assemblies (BPRA) and thimble plug devices (TPD) are an integral, yet removable, part of a large portion of PWR fuel. The TPDs are not used in all assemblies in a reactor core but are reused from cycle to cycle. Therefore, these devices can achieve very high burnups. In contrast, BPRAs are burned with a fuel assembly in core and are not reused. In fact, many BPRAs are removed after one or two cycles before the fuel assembly is discharged. Therefore, the achieved burnup for BPRAs is not significantly different than fuel assemblies.

TPDs are made of stainless steel and may contain a small amount of inconel. These devices extend down into the plenum region of the fuel assembly but do not extend into the active fuel region. Since these devices are made of stainless steel, there is a significant amount of cobalt-60 produced during irradiation. This is the only significant radiation source from the activation of steel and inconel.

BPRAs are made of stainless steel in the region above the active fuel zone and may contain a small amount of inconel in this region. Within the active fuel zone the BPRAs may contain 2-24 rodlets which are burnable absorbers clad in either zircaloy or stainless steel. The stainless steel clad BPRAs create a significant radiation source (Co-60) while the zircaloy clad BPRAs create a negligible radiation source. Therefore the stainless steel clad BPRAs are bounding.

SAS2H and ORIGEN-S were used to calculate a radiation source term for the Trojan TPDs and BPRAs. In the ORIGEN-S calculations the cobalt-59 impurity level was conservatively assumed to be 0.8 gm/kg for stainless steel and 4.7 gm/kg for inconel. These calculations were performed by irradiating the appropriate mass of steel and inconel using the flux calculated for the design basis Trojan 17x17 fuel assembly. The mass of material in the regions above the active fuel zone was scaled by the appropriate scaling factors listed in Table 5.2.7 in order to account for the reduced flux levels above the fuel assembly. The total curies of cobalt were calculated for the Trojan TPDs and BPRAs for the actual burnups and cooling times (the BPRAs were only used in the first cycle whereas the TPDs were used in all but the last cycle). The accumulated burnup and cooling time for the BPRAs and TPDs are 15,998 MWD/MTU and 24 years cooling and 118,674 MWD/MTU and 11 years cooling, respectively. Since the operating history of the shutdown Trojan reactor is well known the actual cycle lengths and conservatively short downtimes between cycles were used in the calculation of the source terms. In the ORIGEN-S calculations it was assumed that the burned fuel assembly was replaced with a fresh fuel assembly after every cycle. This was achieved in ORIGEN-S by resetting the flux levels and cross sections to the 0 MWD/MTU condition after every cycle.

Currently only the Trojan non-fuel hardware is permitted for transportation in the HI-STAR 100 System. The masses of the Trojan TPD and BPRA are listed in Table 5.2.36. This information was taken from references [5.2.5] and [5.2.7] and is the same information used in the Trojan FSAR [5.1.6].

Table 5.2.37 shows the curies of Co-60 that were calculated for BPRAs and TPDs in each region of the fuel assembly (e.g. incore, plenum, top). An allowable cooling time, separate from the fuel assemblies, of 24 years and 11 years is used for the Trojan BPRAs and TPDs, respectively.

Subsection 5.4.7 discusses the analysis of cask dose rates from Trojan fuel including the effect of the insertion of BPRAs or TPDs into Trojan fuel assemblies.

5.2.4.2 RCCAs

Rod cluster control assemblies (RCCAs) are an integral, yet reusable, portion of a PWR fuel assembly. These devices are utilized for many years (upwards of 20 years) prior to discharge into the spent fuel pool. The manner in which the RCCAs are utilized varies from plant to plant. Some utilities maintain the RCCAs fully withdrawn during normal operation while others may operate with a bank of rods partially inserted (approximately 10%) during normal operation. Even when fully withdrawn, the ends of the RCCAs are present in the upper portion of the fuel assembly since they are never fully removed from the fuel assembly during operation. The result of the different operating styles is a variation in the source term for the RCCAs. In all cases, however, only the lower portion of the RCCAs will be significantly activated. Therefore, when the RCCAs are stored with the PWR fuel assembly, the activated portion of the RCCAs will be in the lower portion of the cask. RCCAs are fabricated of various materials. The cladding is

typically stainless steel, although inconel has been used. The absorber can be a single material or a combination of materials. AgInCd is possibly the most common absorber although B_4C in aluminum is used, and hafnium has also been used. AgInCd produces a noticeable source term in the 0.3-1.0 MeV range due to the activation of Ag. The Trojan RCCAs, the only RCCAs currently authorized for transport, were made of AgInCd clad in stainless steel.

In order to determine the impact on the dose rates around the HI-STAR 100 System, source terms for the Trojan RCCAs were calculated using SAS2H and ORIGEN-S. In the ORIGEN-S calculations the cobalt-59 impurity level was conservatively assumed to be 0.8 gm/kg for stainless steel and 4.7 gm/kg for inconel. These calculations were performed by irradiating 1 kg of steel, inconel, and AgInCd using the flux calculated for the Trojan W 17x17 fuel assembly. The total curies of cobalt for the steel and inconel and the 0.3-1.0 MeV source for the AgInCd were calculated for a single burnup, 125,515 MWD/MTU, and cooling time, 9 years, corresponding to the lifetime operation of the Trojan reactor. Since the operating history of the shutdown Trojan reactor is well known the actual cycle lengths and conservatively short downtimes between cycles were used in the calculation of the source terms. In the ORIGEN-S calculations it was assumed that the burned fuel assembly was replaced with a fresh fuel assembly after every cycle. This was achieved in ORIGEN-S by resetting the flux levels and cross sections to the 0 MWD/MTU condition after every cycle. The sources were then scaled by the appropriate mass using the flux weighting factors for the different regions of the assembly to determine the final source term. Since the Trojan reactor normally operated with all RCCA rods fully withdrawn only one configuration was analyzed for the RCCAs. The configuration, which is summarized below, is described in Table 5.2.38 for the RCCAs. The masses of the materials listed in these tables were determined from reference [5.2.5]. The masses listed in Table 5.2.38 do not match exact values from [5.2.5] because the values in the reference were adjusted to the lengths shown in the tables.

RCCA Configuration

This configuration represents a fully removed RCCA during normal core operations. The activated portion corresponds to the upper portion of a fuel assembly above the active fuel length with the appropriate flux weighting factors used.

Table 5.2.38 presents the source terms that were calculated for the Trojan RCCAs. The only significant source from the activation of inconel or steel is Co-60 and the only significant source from the activation of AgInCd is from 0.3-1.0 MeV.

Subsection 5.4.7 discusses the analysis of cask dose rates from Trojan fuel including the effect of the insertion of RCCAs into Trojan fuel assemblies.

5.2.5 Choice of Design Basis Assembly

The analysis presented in this chapter was performed to bound the fuel assembly classes listed in Tables 1.2.8 and 1.2.9. In order to perform a bounding analysis, a design basis fuel assembly

must be chosen. Therefore, a fuel assembly from each fuel class was analyzed and a comparison of the neutrons/sec, photons/sec, and thermal power (watts) was performed. The fuel assembly which produced the highest source for a specified burnup, cooling time, and enrichment was chosen as the design basis fuel assembly. A separate design basis assembly was chosen for the PWR baskets (MPC-24 and MPC-32) and the BWR basket (MPC-68).

5.2.5.1 PWR Design Basis Assembly

Table 1.2.8 lists the PWR fuel assembly classes that were evaluated to determine the design basis PWR fuel assembly. Within each class, the fuel assembly with the highest UO_2 mass was analyzed. Since the variations of fuel assemblies within a class are very minor (pellet diameter, clad thickness, etc.), it is conservative to choose the assembly with the highest UO_2 mass. For a given class of assemblies, the one with the highest UO_2 mass will produce the highest radiation source because, for a given burnup (MWD/MTU) and enrichment, the highest UO_2 mass will have produced the most energy and therefore the most fission products.

Table 5.2.24 presents the characteristics of the fuel assemblies analyzed to determine the design basis zircaloy clad PWR fuel assembly. The fuel assembly listed for each class is the assembly with the highest UO_2 mass. The St. Lucie and Ft. Calhoun classes are not present in Table 5.2.24. These assemblies are shorter versions of the CE 16x16 and CE 14x14 assembly classes, respectively. Therefore, these assemblies are bounded by the CE 16x16 and CE 14x14 classes and were not explicitly analyzed. Since the Haddam Neck and San Onofre 1 classes are stainless steel clad fuel, these classes were analyzed separately and are discussed below. All fuel assemblies in Table 5.2.24 were analyzed at the same burnup and cooling time. The results of the comparison are provided in Table 5.2.26. These results indicate that the B&W 15x15 fuel assembly has the highest radiation source term of the zircaloy clad fuel assembly classes considered in Table 1.2.8. This fuel assembly also has the highest UO_2 mass (see Table 5.2.24) which confirms that, for a given initial enrichment, burnup, and cooling time, the assembly with the highest UO_2 mass produces the highest radiation source term.

The Haddam Neck and San Onofre 1 classes are shorter stainless steel clad versions of the WE 15x15 and WE 14x14 classes, respectively. Since these assemblies have stainless steel clad, they were analyzed separately as discussed in Subsection 5.2.3. Based on the results in Table 5.2.26, which show that the WE 15x15 assembly class has a higher source term than the WE 14x14 assembly class, the Haddam Neck, WE 15x15, fuel assembly was analyzed as the bounding PWR stainless steel clad fuel assembly.

5.2.5.2 BWR Design Basis Assembly

Table 1.2.9 lists the BWR fuel assembly classes that were evaluated to determine the design basis BWR fuel assembly. Since there are minor differences between the array types in the GE BWR/2-3 and GE BWR/4-6 assembly classes, these assembly classes were not considered individually but rather as a single class. Within that class, the array types, 7x7, 8x8, 9x9, and

10x10 were analyzed to determine the bounding BWR fuel assembly. Since the Humboldt Bay 7x7 and Dresden 1 8x8 are smaller versions of the 7x7 and 8x8 assemblies they are bounded by the 7x7 and 8x8 assemblies in the GE BWR/2-3 and GE BWR/4-6 classes. Within each array type, the fuel assembly with the highest UO_2 mass was analyzed. Since the variations of fuel assemblies within an array type are very minor, it is conservative to choose the assembly with the highest UO_2 mass. For a given array type of assemblies, the one with the highest UO_2 mass will produce the highest radiation source because, for a given burnup (MWD/MTU) and enrichment, it will have produced the most energy and therefore the most fission products. The Humboldt Bay 6x6, Dresden 1 6x6, and LaCrosse assembly classes were not considered in the determination of the bounding fuel assembly. However, these assemblies were analyzed explicitly as discussed below.

Table 5.2.25 presents the characteristics of the fuel assemblies analyzed to determine the design basis zircaloy clad BWR fuel assembly. The fuel assembly listed for each array type is the assembly that has the highest UO_2 mass. All fuel assemblies in Table 5.2.25 were analyzed at the same burnup and cooling time. The results of the comparison are provided in Table 5.2.27. These results indicate that the 7x7 fuel assembly has the highest radiation source term of the zircaloy clad fuel assembly classes considered in Table 1.2.9. This fuel assembly also has the highest UO_2 mass which confirms that, for a given initial enrichment, burnup, and cooling time, the assembly with the highest UO_2 mass produces the highest radiation source term. According to Reference [5.2.6], the last discharge of a 7x7 assembly was in 1985 and the maximum average burnup for a 7x7 during their operation was 29,000 MWD/MTU. This clearly indicates that the existing 7x7 assemblies have an average burnup and minimum cooling time that is well within the burnup and cooling time limits in Table 1.2.20. Therefore, the 7x7 assembly has never reached the burnup level analyzed in this chapter. However, in the interest of conservatism the 7x7 was chosen as the bounding fuel assembly array type.

Since the LaCrosse fuel assembly type is a stainless steel clad 10x10 assembly, it was analyzed separately. The maximum burnup and minimum cooling times for this assembly are limited to 22,500 MWD/MTU and 15-year cooling as specified in Table 1.2.19. This assembly type is discussed further in Subsection 5.2.3.

The Humboldt Bay 6x6 and Dresden 1 6x6 fuel are older and shorter than the other array types analyzed and therefore are considered separately. The Dresden 1 6x6 was chosen as the design basis fuel assembly for the Humboldt Bay 6x6 and Dresden 1 6x6 fuel assembly classes because it has the higher UO_2 mass. Dresden 1 also contains a few 6x6 MOX fuel assemblies which were explicitly analyzed as well.

Reference [5.2.6] indicates that the Dresden 1 6x6 fuel assembly has a higher UO_2 mass than the Dresden 1 8x8 or the Humboldt Bay fuel (6x6 and 7x7). Therefore, the Dresden 1 6x6 fuel assembly was also chosen as the bounding assembly for damaged fuel and fuel debris for the Humboldt Bay and Dresden 1 fuel assembly classes.

Since the design basis damaged fuel assembly and the design basis intact 6x6 fuel assembly are identical, the analysis presented in Subsection 5.4.2 for the damaged fuel assembly also demonstrates the acceptability of transporting intact 6x6 fuel assemblies from the Dresden 1 and Humboldt Bay fuel assembly classes.

5.2.5.3 Decay Heat Loads

The decay heat values per assembly were calculated using the methodology described in Section 5.2. As demonstrated in Tables 5.2.26 and 5.2.27, the design basis fuel assembly produces a higher decay heat value than the other assembly types considered. This is due to the higher heavy metal mass in the design basis fuel assemblies. Conservatively, Tables 1.2.10 and 1.2.11 limit the heavy metal mass of the design basis fuel assembly classes to a value less than the design basis value utilized in this chapter. This provides additional assurance that the radiation source terms are bounding values.

As further demonstration that the decay heat values (calculated using the design basis fuel assemblies) are conservative, a comparison between these calculated decay heats and the decay heats reported in Reference [5.2.7] are presented in Table 5.2.28. This comparison is made for a burnup of 30,000 MWD/MTU and a cooling time of 5 years. The burnup was chosen based on the limited burnup data available in Reference [5.2.7].

The heavy metal mass of the non-design basis fuel assembly classes in Tables 1.2.10 and 1.2.11 are limited to the masses used in Tables 5.2.24 and 5.2.25. No margin is applied between the allowable mass and the analyzed mass of heavy metal for the non-design basis fuel assemblies. This is acceptable because additional assurance that the radiation source terms for the non-design basis fuel assemblies are bounding values is obtained by using the radiation source terms for the design basis fuel assemblies in determining the acceptable loading criteria for all fuel assemblies.

5.2.6 Thoria Rod Canister

Dresden Unit 1 has a single DFC containing 18 thoria rods which have obtained a relatively low burnup, 16,000 MWD/MTU. These rods were removed from two 8x8 fuel assemblies which contained 9 rods each. The irradiation of thorium produces an isotope which is not commonly found in depleted uranium fuel. Th-232 when irradiated produces U-233. The U-233 can undergo an (n,2n) reaction which produces U-232. The U-232 decays to produce Tl-208 which produces a 2.6 MeV gamma during Beta decay. This results in a significant source in the 2.5-3.0 MeV range which is not commonly present in depleted uranium fuel. Therefore, this single DFC container was analyzed to determine if it was bounded by the current shielding analysis.

A radiation source term was calculated for the 18 thoria rods using SAS2H and ORIGEN-S for a burnup of 16,000 MWD/MTU and a cooling time of 18 years. Table 5.2.29 describes the 8x8 fuel assembly that contains the thoria rods. Table 5.2.30 and 5.2.31 show the gamma and neutron source terms, respectively, that were calculated for the 18 thoria rods in the thoria rod canister.

Comparing these source terms to the design basis 6x6 source terms for Dresden Unit 1 fuel in Tables 5.2.6 and 5.2.14 clearly indicates that the design basis source terms bound the thoria rods source terms in all neutron groups and in all gamma groups except the 2.5-3.0 MeV group. As mentioned above, the thoria rods have a significant source in this energy range due to the decay of Tl-208.

Subsection 5.4.6 provides a further discussion of the thoria rod canister and its acceptability for transport in the HI-STAR 100 System.

5.2.7 Fuel Assembly Neutron Sources

Neutron sources are used in reactors during initial startup of reactor cores. There are different types of neutron sources (e.g. californium, americium-beryllium, plutonium-beryllium, antimony-beryllium). These neutron sources are typically inserted into the water rod of a fuel assembly and are usually removable.

Currently the only neutron source permitted for transport in the HI-STAR 100 System are from Dresden Unit 1 and Trojan Nuclear Plant as discussed below.

5.2.7.1 Dresden Unit 1 Neutron Source Assemblies

Dresden Unit 1 has a few antimony-beryllium neutron sources. These sources have been analyzed in Subsection 5.4.5 to demonstrate that they are acceptable for transport in the HI-STAR 100 System.

5.2.7.2 Trojan Nuclear Plant Neutron Source Assemblies

Trojan Nuclear Power has two primary (californium) neutron source assemblies and four secondary (antimony-beryllium) neutron source assemblies. The neutron source assemblies are basically BPRAs with the source material placed in a few of the rods instead of burnable absorber. In the case of the californium source, a single rod contained a nominally 1.5 inch long californium capsule while the remaining locations consisted of 19 burnable poison rods and 4 thimble plug rods. The initial source strength of the primary sources were approximately 6.0E+8 neutrons/sec. Since these devices were delivered prior to startup, they have realized more than 24 years of decay time. Based on the half-life of Cf-252 (2.65 years), the neutron source strength of these devices would be less than 1.2E+6 neutrons/sec after 24 years of decay time. Therefore, the neutron contribution from these devices is negligible and is not considered in the analysis in this chapter. Since these devices are clad in stainless steel, there is the potential for significant Co-60 activation from in-core activation of the cladding material. The primary sources were only operated during the first cycle of the Trojan nuclear plant and as a result achieved a burnup of 15,998 MWD/MTU and have a cooling time of more than 24 years. This burnup and cooling time is identical to the burnup and cooling time for the Trojan BPRAs as discussed in Subsection

5.2.4.1. Therefore, the primary sources are not explicitly considered in this analysis but are bounded by the analysis of the BPRAs.

The Trojan Nuclear Plant secondary neutron source assemblies used 4 rods for the antimony-beryllium source and the remaining rods were either burnable poison rods or thimble plug rods. The 4 source rods in a secondary neutron source assembly each contained 88 inches of antimony-beryllium. Since the antimony-beryllium neutron sources are regenerative sources they will be producing a steady state level of neutrons while in the MPC. This production of neutrons has been explicitly analyzed in Subsection 5.4.8. In addition to the neutron source from the secondary sources, there will be a substantial Co-60 source from the activation of the stainless steel cladding. There are two different levels of activation since the first two source assemblies were used in-core for cycles 1-4 and the latter two source assemblies were used in-core for cycles 4-14. The operating history for these devices results in a burnup of 45,361 MWD/MTU and a cooling time of 19 years for the source assemblies that operated in the first four cycles. The burnup and cooling time for the other two source assemblies is 88,547 MWD/MTU and 9 years. In addition to the difference in the burnup and cooling times between the two sets of secondary source assemblies, the number of burnable poison rods and thimble plug rods is different. The two source assemblies used in Cycles 1-4 each contained 4 source rods, 16 burnable poison rods and 4 thimble plug rods. The two source assemblies used in Cycles 4-14 each contained 4 source rods and 20 thimble plug rods. Table 5.2.39 shows the physical description of these devices that was used in the source term calculation and the resultant Co-60 source term in each region. Subsection 5.4.8 discusses the effect of the secondary source assemblies on the calculated dose rates and demonstrates that these devices are acceptable for transport.

5.2.8 Trojan Non-Fuel Bearing Components, Damaged Fuel and Fuel Debris

Trojan Nuclear Power has failed fuel cans containing fuel process can capsules and fuel debris. The fuel process can capsules contain only a limited amount of fuel in the form of fuel debris (metal fragments). The source term from the fuel process can capsules is therefore bounded by the source from a fuel assembly.

The fuel assemblies classified as fuel debris consist of a few assemblies with each containing a maximum of 17 rods. There is also a single damaged fuel container that has 23 individual rods not bound in a fuel assembly configuration. If it is assumed that the 23 individual rods are from a design basis Trojan fuel assembly and have not collapsed, then the source strength per inch of active fuel is a small fraction (23 rods/264 rods in an intact assembly) of the source in an intact assembly. If it is assumed that the source strength per rod is "A" then the source per inch in an intact assembly is 264A/144=1.833A. The damaged fuel assembly with 23 rods would have to collapse from 144 inches in height to 12.5 inches (height = 23A/1.833A) in order for the source strength per unit inch in the collapsed assembly to be equivalent to the source strength per unit

inch in an intact assembly. Further collapse would increase the source strength per inch beyond that of a design basis assembly but it is not considered likely that this would occur. Therefore, even in a collapsed state which might exist after a transport accident, this fuel debris is bounded by an intact fuel assembly and therefore is not explicitly considered in the analysis in this chapter.

There are also a couple of fuel assemblies classified as damaged fuel because of missing rods. These assemblies are also bounded by an intact assembly and during the transport accident it is expected that these damaged assemblies would react the same as intact assemblies. Therefore, the Trojan damaged fuel assemblies were not explicitly considered in the analysis in this chapter.

Trojan fuel assembly hardware, non-fuel bearing components and one fuel skeleton will also be transported. These components are made of stainless steel, zircaloy and inconel. The source term from these additional components were not explicitly considered but are bounded by intact fuel assemblies. Therefore, the source term from these components were not explicitly considered.

Table 5.2.1

DESCRIPTION OF DESIGN BASIS INTACT ZIRCALOY CLAD FUEL

	PWR	BWR
Assembly type/class	B&W 15×15	GE 7×7
Active fuel length (in.)	144	144
No. of fuel rods	208	49
Rod pitch (in.)	0.568	0.738
Cladding material	zircaloy-4	zircaloy-2
Rod diameter (in.)	0.428	0.570
Cladding thickness (in.)	0.0230	0.0355
Pellet diameter (in.)	0.3742	0.488
Pellet material	UO_2	UO_2
Pellet density (gm/cc)	10.412 (95% of theoretical)	10.412 (95% of theoretical)
Enrichment (w/o ^{235}U)	See Tables 1.2.28, 1.2.29, 1.2.32, 1.2.33	See Table 1.2.31
Burnup (MWD/MTU)	See Table 1.2.28, 1.2.29, 1.2.32, 1.2.33	See Table 1.2.31
Cooling Time (years)	See Table 1.2.28, 1.2.29, 1.2.32, 1.2.33	See Table 1.2.31
Specific power (MW/MTU)	40	30
Weight of UO_2 (kg)†	562.029	225.177
Weight of U (kg)†	495.485	198.516

Notes:
1. The B&W 15x15 is the design basis assembly for the following fuel assembly classes listed in Table 1.2.8: B&W 15x15, B&W 17x17, CE 14x14, CE 16x16, WE 14x14, WE 15x15, WE 17x17, St. Lucie, and Ft. Calhoun.
2. The GE 7x7 is the design basis assembly for the following fuel assembly classes listed in Table 1.2.9: GE BWR/2-3, GE BWR/4-6, Humboldt Bay 7x7, and Dresden 1 8x8.

† Derived from parameters in this table.

Table 5.2.1 (continued)

DESCRIPTION OF DESIGN BASIS INTACT ZIRCALOY CLAD FUEL

	PWR	BWR
No. of Water Rods/Guide Tubes	17	0
Water Rod O.D. (in.)	0.53	N/A
Water Rod Thickness (in.)	0.0160	N/A
Lower End Fitting (kg)	8.16 (steel) 1.3 (inconel)	4.8 (steel)
Gas Plenum Springs (kg)	0.48428 (inconel) 0.23748 (steel)	1.1 (steel)
Gas Plenum Spacer (kg)	0.55572 (inconel) 0.27252 (steel)	N/A
Expansion Springs (kg)	N/A	0.4 (steel)
Upper End Fitting (kg)	9.28 (steel)	2.0 (steel)
Handle (kg)	N/A	0.5 (steel)
Incore Grid Spacers (kg)	4.9 (inconel)†	0.33 (inconel springs)

† This mass of inconel was used for fuel assemblies with non-zircaloy grid spacers. For fuel assemblies with zircaloy grid spacers the mass was 0.0. However, the mass of the inconel and steel in the other assembly components are identical for assemblies with zircaloy and non-zircaloy incore grid spacers.

Table 5.2.2

DESCRIPTION OF DESIGN BASIS DAMAGED ZIRCALOY CLAD FUEL

	BWR
Fuel type	GE 6x6
Active fuel length (in.)	110
No. of fuel rods	36
Rod pitch (in.)	0.694
Cladding material	zircaloy-2
Rod diameter (in.)	0.5645
Cladding thickness (in.)	0.035
Pellet diameter (in.)	0.494
Pellet material	UO_2
Pellet density (gm/cc)	10.412 (95% of theoretical)
Enrichment (w/o ^{235}U)	1.45
Burnup (MWD/MTU)	30,000
Cooling Time (years)	18
Specific power (MW/MTU)	16.5
Weight of UO_2 (kg)†	129.5
Weight of U (kg)†	114.2
Incore spacers (kg inconel)	1.07

Notes:
1. The 6x6 is the design basis damaged fuel assembly for the Humboldt Bay (all array types) and the Dresden 1 (all array types) damaged fuel assembly classes. It is also the design basis fuel assembly for the intact Humboldt Bay 6x6 and Dresden 1 6x6 fuel assembly classes.
2. This design basis damaged fuel assembly is also the design basis fuel assembly for fuel debris.

† Derived from parameters in this table.

Table 5.2.3
CALCULATED MPC-24 PWR FUEL GAMMA SOURCE PER ASSEMBLY FOR DESIGN BASIS ZIRCALOY CLAD FUEL WITH NON-ZIRCALOY INCORE SPACERS FOR VARYING BURNUPS AND COOLING TIMES

Lower Energy	**Upper Energy**	**24,500 MWD/MTU 9 Year Cooling**		**29,500 MWD/MTU 11 Year Cooling**		**34,500 MWD/MTU 13 Year Cooling**	
(MeV)	(MeV)	(MeV/s)	(Photons/s)	(MeV/s)	(Photons/s)	(MeV/s)	(Photons/s)
0.45	0.7	7.61E+14	1.32E+15	8.35E+14	1.45E+15	9.05E+14	1.57E+15
0.7	1.0	8.94E+13	1.05E+14	6.95E+13	8.18E+13	5.54E+13	6.52E+13
1.0	1.5	3.29E+13	2.63E+13	3.33E+13	2.67E+13	3.41E+13	2.73E+13
1.5	2.0	1.70E+12	9.74E+11	1.73E+12	9.91E+11	1.84E+12	1.05E+12
2.0	2.5	2.19E+11	9.71E+10	5.49E+10	2.44E+10	1.89E+10	8.40E+09
2.5	3.0	1.32E+10	4.81E+09	4.06E+09	1.47E+09	1.49E+09	5.42E+08
Totals		8.85E+14	1.46E+15	9.39E+14	1.56E+15	9.96E+14	1.67E+15
Lower Energy	**Upper Energy**	**39,500 MWD/MTU 15 Year Cooling**		**44,500 MWD/MTU 18 Year Cooling**			
(MeV)	(MeV)	(MeV/s)	(Photons/s)	(MeV/s)	(Photons/s)		
0.45	0.7	9.70E+14	1.69E+15	1.00E+15	1.74E+15		
0.7	1.0	4.49E+13	5.28E+13	3.32E+13	3.90E+13		
1.0	1.5	3.39E+13	2.71E+13	3.07E+13	2.46E+13		
1.5	2.0	1.89E+12	1.08E+12	1.78E+12	1.02E+12		
2.0	2.5	1.11E+10	4.92E+09	9.00E+09	4.00E+09		
2.5	3.0	8.82E+08	3.21E+08	8.14E+08	2.96E+08		
Totals		1.05E+15	1.77E+15	1.07E+15	1.81E+15		

Table 5.2.4
CALCULATED MPC-24 PWR FUEL GAMMA SOURCE PER ASSEMBLY FOR DESIGN BASIS ZIRCALOY CLAD FUEL WITH ZIRCALOY INCORE SPACERS FOR VARYING BURNUPS AND COOLING TIMES

Lower Energy	**Upper Energy**	**24,500 MWD/MTU 6 Year Cooling**		**29,500 MWD/MTU 7 Year Cooling**		**34,500 MWD/MTU 9 Year Cooling**	
(MeV)	(MeV)	(MeV/s)	(Photons/s)	(MeV/s)	(Photons/s)	(MeV/s)	(Photons/s)
0.45	0.7	9.60E+14	1.67E+15	1.06E+15	1.85E+15	1.08E+15	1.88E+15
0.7	1.0	2.17E+14	2.55E+14	2.09E+14	2.46E+14	1.48E+14	1.74E+14
1.0	1.5	5.67E+13	4.54E+13	5.96E+13	4.77E+13	5.44E+13	4.35E+13
1.5	2.0	3.71E+12	2.12E+12	3.24E+12	1.85E+12	2.70E+12	1.54E+12
2.0	2.5	2.48E+12	1.10E+12	1.19E+12	5.27E+11	2.57E+11	1.14E+11
2.5	3.0	1.02E+11	3.70E+10	5.83E+10	2.12E+10	1.67E+10	6.08E+09
Totals		1.24E+15	1.97E+15	1.33E+15	2.14E+15	1.29E+15	2.10E+15
Lower Energy	**Upper Energy**	**39,500 MWD/MTU11 Year Cooling**		**44,500 MWD/MTU14 Year Cooling**			
(MeV)	(MeV)	(MeV/s)	(Photons/s)	(MeV/s)	(Photons/s)		
0.45	0.7	1.12E+15	1.94E+15	1.12E+15	1.95E+15		
0.7	1.0	1.05E+14	1.24E+14	6.36E+13	7.48E+13		
1.0	1.5	5.06E+13	4.05E+13	4.35E+13	3.48E+13		
1.5	2.0	2.58E+12	1.47E+12	2.37E+12	1.35E+12		
2.0	2.5	6.36E+10	2.83E+10	1.55E+10	6.89E+09		
2.5	3.0	5.07E+09	1.84E+09	1.41E+09	5.12E+08		
Totals		1.28E+15	2.11E+15	1.23E+15	2.06E+15		

Table 5.2.5
CALCULATED MPC-68 BWR FUEL GAMMA SOURCE PER ASSEMBLY FOR DESIGN BASIS ZIRCALOY CLAD FUEL FOR VARYING BURNUPS AND COOLING TIMES

Lower Energy	**Upper Energy**	**10,000 MWD/MTU 5 Year Cooling**		**20,000 MWD/MTU 7 Year Cooling**		**24,500 MWD/MTU 8 Year Cooling**		**29,500 MWD/MTU 9 Year Cooling**	
(MeV)	(MeV)	(MeV/s)	(Photons/s)	(MeV/s)	(Photons/s)	(MeV/s)	(Photons/s)	(MeV/s)	(Photons/s)
0.45	0.7	1.68E+14	2.93E+14	2.83E+14	4.92E+14	3.21E+14	5.57E+14	3.64E+14	6.34E+14
0.7	1.0	3.28E+13	3.86E+13	4.89E+13	5.75E+13	4.54E+13	5.34E+13	4.46E+13	5.25E+13
1.0	1.5	9.61E+12	7.69E+12	1.42E+13	1.13E+13	1.46E+13	1.17E+13	1.63E+13	1.30E+13
1.5	2.0	1.11E+12	6.34E+11	8.42E+11	4.81E+11	7.68E+11	4.39E+11	8.20E+11	4.69E+11
2.0	2.5	1.22E+12	5.40E+11	3.47E+11	1.54E+11	1.65E+11	7.34E+10	8.09E+10	3.60E+10
2.5	3.0	4.73E+10	1.72E+10	1.87E+10	6.82E+09	9.32E+09	3.39E+09	5.31E+09	1.93E+09
Total		2.13E+14	3.40E+14	3.47E+14	5.62E+14	3.82E+14	6.23E+14	4.26E+14	7.00E+14
Lower Energy	**Upper Energy**	**34,500 MWD/MTU 11 Year Cooling**		**39,500 MWD/MTU 14 Year Cooling**		**44,500 MWD/MTU 19 Year Cooling**			
(MeV)	(MeV)	(MeV/s)	(Photons/s)	(MeV/s)	(Photons/s)	(MeV/s)	(Photons/s)		
0.45	0.7	3.87E+14	6.73E+14	3.96E+14	6.89E+14	3.87E+14	6.73E+14		
0.7	1.0	3.31E+13	3.89E+13	2.03E+13	2.39E+13	1.09E+13	1.28E+13		
1.0	1.5	1.57E+13	1.26E+13	1.38E+13	1.10E+13	1.05E+13	8.38E+12		
1.5	2.0	8.10E+11	4.63E+11	7.59E+11	4.34E+11	6.17E+11	3.53E+11		
2.0	2.5	2.05E+10	9.10E+09	5.27E+09	2.34E+09	3.33E+09	1.48E+09		
2.5	3.0	1.62E+09	5.91E+08	4.16E+08	1.51E+08	2.84E+08	1.03E+08		
Total		4.36E+14	7.25E+14	4.31E+14	7.24E+14	4.09E+14	6.95E+14		

Table 5.2.6

CALCULATED MPC-68 and MPC-68F BWR FUEL GAMMA SOURCE PER ASSEMBLY FOR DESIGN BASIS ZIRCALOY CLAD DAMAGED FUEL

Lower Energy	**Upper Energy**	**30,000 MWD/MTU 18 Year Cooling**	
(MeV)	(MeV)	(MeV/s)	(Photons/s)
0.45	0.7	1.52E+14	2.65E+14
0.7	1.0	4.14E+12	4.87E+12
1.0	1.5	3.91E+12	3.13E+12
1.5	2.0	2.28E+11	1.30E+11
2.0	2.5	1.17E+09	5.21E+08
2.5	3.0	7.48E+07	2.72E+07
Totals		1.60E+14	2.73E+14

Table 5.2.7

SCALING FACTORS USED IN CALCULATING THE ^{60}Co SOURCE

Region	**PWR**	**BWR**
Handle	N/A	0.05
Top end fitting	0.1	0.1
Gas plenum spacer	0.1	N/A
Expansion springs	N/A	0.1
Gas plenum springs	0.2	0.2
Grid spacer spring	N/A	1.0
Bottom end fitting	0.2	0.15

Table 5.2.8

CALCULATED MPC-24 ^{60}Co SOURCE PER ASSEMBLY FOR DESIGN BASIS ZIRCALOY CLAD FUEL WITH NON-ZIRCALOY INCORE SPACERS AT VARYING BURNUPS AND COOLING TIMES

Location	**24,500 MWD/MTU 9 Year Cooling (curies)**	**29,500 MWD/MTU 11 Year Cooling (curies)**	**34,500 MWD/MTU 13 Year Cooling (curies)**	**39,500 MWD/MTU 15 Year Cooling (curies)**	**44,500 MWD/MTU 18 Year Cooling (curies)**
Lower end fitting	95.83	81.89	68.71	56.79	41.33
Gas plenum springs	18.64	15.93	13.37	11.05	8.04
Gas plenum spacer	10.70	9.14	7.67	6.34	4.61
Expansion springs	N/A	N/A	N/A	N/A	N/A
Grid spacers	870.53	743.87	624.11	515.87	375.39
Upper end fitting	35.08	29.97	25.15	20.79	15.13
Handle	N/A	N/A	N/A	N/A	N/A

Table 5.2.9

CALCULATED MPC-24 ^{60}Co SOURCE PER ASSEMBLY FOR DESIGN BASIS ZIRCALOY CLAD FUEL WITH ZIRCALOY INCORE SPACERS AT VARYING BURNUPS AND COOLING TIMES

Location	**24,500 MWD/MTU 6 Year Cooling (curies)**	**29,500 MWD/MTU 7 Year Cooling (curies)**	**34,500 MWD/MTU 9 Year Cooling (curies)**	**39,500 MWD/MTU 11 Year Cooling (curies)**	**44,500 MWD/MTU 14 Year Cooling (curies)**
Lower end fitting	142.23	138.68	116.12	96.09	69.72
Gas plenum springs	27.67	26.98	22.59	18.69	13.56
Gas plenum spacer	15.88	15.48	12.96	10.73	7.78
Expansion springs	N/A	N/A	N/A	N/A	N/A
Grid spacers†	N/A	N/A	N/A	N/A	N/A
Upper end fitting	52.06	50.76	42.50	35.17	25.52
Handle	N/A	N/A	N/A	N/A	N/A

† These burnup and cooling times represent fuel with zircaloy grid spacers. Therefore, the cobalt activation is negligible.

Table 5.2.10

CALCULATED MPC-68 ^{60}CO SOURCE PER ASSEMBLY FOR DESIGN BASIS ZIRCALOY CLAD FUEL AT VARYING BURNUPS AND COOLING TIMES

Location	**10,000 MWD/MTU 5 Year Cooling (curies)**	**20,000 MWD/MTU 7 Year Cooling (curies)**	**24,500 MWD/MTU 8 Year Cooling (curies)**	**29,500 MWD/MTU 9 Year Cooling (curies)**	**34,500 MWD/MTU 11 Year Cooling (curies)**	**39,500 MWD/MTU 14 Year Cooling (curies)**	**44,500 MWD/MTU 19 Year Cooling (curies)**
Lower end fitting	39.71	40.80	34.04	30.55	27.49	19.64	11.08
Gas plenum springs	12.13	12.47	10.40	9.33	8.40	6.00	3.39
Gas plenum spacer	N/A	N/A	N/A	N/A	N/A	N/A	N/A
Expansion springs	2.21	2.27	1.89	1.70	1.53	1.09	0.62
Grid spacers	85.54	87.89	73.32	65.80	59.22	42.30	23.88
Upper end fitting	11.03	11.33	9.45	8.48	7.64	5.45	3.08
Handle	1.38	1.42	1.18	1.06	0.95	0.68	0.38

Table 5.2.11

CALCULATED MPC-24 PWR NEUTRON SOURCE PER ASSEMBLY
FOR DESIGN BASIS ZIRCALOY CLAD FUEL WITH NON-ZIRCALOY
INCORE SPACERS FOR VARYING BURNUPS AND COOLING TIMES

Lower Energy (MeV)	**Upper Energy (MeV)**	**24,500 MWD/MTU 9 Year Cooling (Neutrons/s)**	**29,500 MWD/MTU 11 Year Cooling (Neutrons/s)**	**34,500 MWD/MTU 13 Year Cooling (Neutrons/s)**	**39,500 MWD/MTU 15 Year Cooling (Neutrons/s)**	**44,500 MWD/MTU 18 Year Cooling (Neutrons/s)**
1.0E-01	4.0E-01	2.50E+06	4.04E+06	6.01E+06	8.09E+06	1.05E+07
4.0E-01	9.0E-01	1.28E+07	2.06E+07	3.07E+07	4.13E+07	5.35E+07
9.0E-01	1.4	1.18E+07	1.90E+07	2.82E+07	3.79E+07	4.91E+07
1.4	1.85	8.77E+06	1.41E+07	2.09E+07	2.81E+07	3.63E+07
1.85	3.0	1.58E+07	2.52E+07	3.73E+07	5.00E+07	6.47E+07
3.0	6.43	1.40E+07	2.25E+07	3.35E+07	4.50E+07	5.82E+07
6.43	20.0	1.23E+06	1.98E+06	2.94E+06	3.96E+06	5.13E+06
TOTALS		6.69E+07	1.07E+08	1.60E+08	2.14E+08	2.77E+08

Table 5.2.12

CALCULATED MPC-24 PWR NEUTRON SOURCE PER ASSEMBLY
FOR DESIGN BASIS ZIRCALOY CLAD FUEL WITH ZIRCALOY
INCORE SPACERS FOR VARYING BURNUPS AND COOLING TIMES

Lower Energy (MeV)	Upper Energy (MeV)	24,500 MWD/MTU 6 Year Cooling (Neutrons/s)	29,500 MWD/MTU 7 Year Cooling (Neutrons/s)	34,500 MWD/MTU 9 Year Cooling (Neutrons/s)	39,500 MWD/MTU 11 Year Cooling (Neutrons/s)	44,500 MWD/MTU 14 Year Cooling (Neutrons/s)
1.0E-01	4.0E-01	2.80E+06	4.69E+06	6.98E+06	9.40E+06	1.22E+07
4.0E-01	9.0E-01	1.43E+07	2.40E+07	3.57E+07	4.80E+07	6.22E+07
9.0E-01	1.4	1.32E+07	2.20E+07	3.27E+07	4.40E+07	5.70E+07
1.4	1.85	9.76E+06	1.63E+07	2.42E+07	3.26E+07	4.21E+07
1.85	3.0	1.75E+07	2.90E+07	4.30E+07	5.78E+07	7.47E+07
3.0	6.43	1.56E+07	2.61E+07	3.88E+07	5.22E+07	6.75E+07
6.43	20.0	1.37E+06	2.29E+06	3.42E+06	4.60E+06	5.96E+06
TOTALS		7.45E+07	1.24E+08	1.85E+08	2.49E+08	3.22E+08

Table 5.2.13

CALCULATED MPC-68 BWR NEUTRON SOURCE PER ASSEMBLY
FOR DESIGN BASIS ZIRCALOY CLAD FUEL
FOR VARYING BURNUPS AND COOLING TIMES

Lower Energy (MeV)	Upper Energy (MeV)	10,000 MWD/MTU 5 Year Cooling (Neutrons/s)	20,000 MWD/MTU 7 Year Cooling (Neutrons/s)	24,500 MWD/MTU 8 Year Cooling (Neutrons/s)	29,500 MWD/MTU 9 Year Cooling (Neutrons/s)	34,500 MWD/MTU 11 Year Cooling (Neutrons/s)	39,500 MWD/MTU 14 Year Cooling (Neutrons/s)	44,500 MWD/MTU 19 Year Cooling (Neutrons/s)
1.0E-01	4.0E-01	1.62E+05	1.01E+06	1.08E+06	1.81E+06	2.80E+06	3.61E+06	4.57E+06
4.0E-01	9.0E-01	8.29E+05	5.15E+06	5.52E+06	9.23E+06	1.43E+07	1.84E+07	2.33E+07
9.0E-01	1.4	7.68E+05	4.72E+06	5.08E+06	8.47E+06	1.31E+07	1.69E+07	2.14E+07
1.4	1.85	5.79E+05	3.50E+06	3.77E+06	6.27E+06	9.71E+06	1.25E+07	1.58E+07
1.85	3.0	1.07E+06	6.25E+06	6.75E+06	1.12E+07	1.73E+07	2.22E+07	2.80E+07
3.0	6.43	9.26E+05	5.61E+06	6.04E+06	1.01E+07	1.56E+07	2.00E+07	2.53E+07
6.43	20.0	7.91E+04	4.93E+05	5.29E+05	8.84E+05	1.37E+06	1.77E+06	2.24E+06
TOTALS		4.41E+06	2.67E+07	2.88E+07	4.79E+07	7.42E+07	9.54E+07	1.21E+08

Table 5.2.14

CALCULATED MPC-68 and MPC-68F BWR NEUTRON SOURCE PER ASSEMBLY FOR DESIGN BASIS DAMAGED ZIRCALOY CLAD FUEL

Lower Energy (MeV)	**Upper Energy (MeV)**	**30,000 MWD/MTU 18 Year Cooling (Neutrons/s)**
1.0E-01	4.0E-01	1.59E+6
4.0E-01	9.0E-01	8.10E+6
9.0E-01	1.4	7.43E+6
1.4	1.85	5.49E+6
1.85	3.0	9.76E+6
3.0	6.43	8.80E+6
6.43	20.0	7.76E+5
Totals		4.19E+7

Table 5.2.15

DESCRIPTION OF DESIGN BASIS ZIRCALOY CLAD MIXED OXIDE FUEL

	BWR
Fuel type	GE 6x6
Active fuel length (in.)	110
No. of fuel rods	36
Rod pitch (in.)	0.696
Cladding material	zircaloy-2
Rod diameter (in.)	0.5645
Cladding thickness (in.)	0.036
Pellet diameter (in.)	0.482
Pellet material	UO_2 and $PuUO_2$
No. of UO_2 Rods	27
No. of $PuUO_2$ Rods	9
Pellet density (gm/cc)	10.412 (95% of theoretical)
Enrichment (w/o ^{235}U)†	1.8 (UO_2 rods) 0.711 ($PuUO_2$ rods)
Burnup (MWD/MTU)	30,000
Cooling Time (years)	18
Specific power (MW/MTU)	16.5
Weight of UO_2, $PuUO_2$ (kg)††	123.3
Weight of U,Pu (kg)††	108.7
Incore spacers (kg inconel)	1.07

† See Table 5.3.3 for detailed composition of $PuUO_2$ rods.

†† Derived from parameters in this table.

Table 5.2.16

CALCULATED MPC-68 BWR FUEL GAMMA SOURCE PER ASSEMBLY FOR DESIGN BASIS ZIRCALOY CLAD MIXED OXIDE FUEL

Lower Energy	**Upper Energy**	**30,000 MWD/MTU 18-Year Cooling**	
(MeV)	(MeV)	(MeV/s)	(Photons/s)
0.45	0.7	1.45E+14	2.52E+14
0.7	1.0	3.95E+12	4.65E+12
1.0	1.5	3.82E+12	3.06E+12
1.5	2.0	2.22E+11	1.27E+11
2.0	2.5	1.11E+9	4.93E+8
2.5	3.0	9.31E+7	3.39E+7
Totals		1.53E+14	2.60E+14

Table 5.2.17

CALCULATED MPC-68 BWR NEUTRON SOURCE PER ASSEMBLY
FOR DESIGN BASIS ZIRCALOY CLAD MIXED OXIDE FUEL

Lower Energy (MeV)	**Upper Energy (MeV)**	**30,000 MWD/MTU 18-Year Cooling (Neutrons/s)**
1.0E-01	4.0E-01	1.50E+6
4.0E-01	9.0E-01	7.67E+6
9.0E-01	1.4	7.09E+6
1.4	1.85	5.31E+6
1.85	3.0	9.67E+6
3.0	6.43	8.47E+6
6.43	20.0	7.33E+5
Totals		4.04E+7

Table 5.2.18
DESCRIPTION OF DESIGN BASIS INTACT STAINLESS STEEL CLAD FUEL

	PWR	BWR
Fuel type	WE 15x15	A/C 10x10
Active fuel length (in.)	144	144
No. of fuel rods	204	100
Rod pitch (in.)	0.563	0.565
Cladding material	304 SS	348H SS
Rod diameter (in.)	0.422	0.396
Cladding thickness (in.)	0.0165	0.02
Pellet diameter (in.)	0.3825	0.35
Pellet material	UO_2	UO_2
Pellet density (gm/cc)	10.412 (95% of theoretical)	10.412 (95% of theoretical)
Enrichment (w/o ^{235}U)	3.1	3.5
Burnup (MWD/MTU)	30,000 @ 19 yr (MPC-24) 40,000 @ 24 yr (MPC-24)	22,500 (MPC-68)
Cooling Time (years)	19 (MPC-24) 24 (MPC-24)	16 (MPC-68)
Specific power (MW/MTU)	37.96	29.17
No. of Water Rods	21	0
Water Rod O.D. (in.)	0.546	N/A
Water Rod Thickness (in.)	0.017	N/A
Incore spacers (kg inconel)	5.1	0.83

Notes:
1. The WE 15x15 is the design basis assembly for the following fuel assembly classes listed in Table 1.2.8: Indian Point, Haddam Neck and San Onofre 1.
2. The A/C 10x10 is the design basis assembly for the following fuel assembly class listed in Table 1.2.9: LaCrosse.

Table 5.2.19

CALCULATED BWR FUEL GAMMA SOURCE PER ASSEMBLY
FOR STAINLESS STEEL CLAD FUEL

Lower Energy	**Upper Energy**	**22,500 MWD/MTU 16-Year Cooling**	
(MeV)	(MeV)	(MeV/s)	(Photons/s)
0.45	0.7	2.26E+14	3.94E+14
0.7	1.0	6.02E+12	7.08E+12
1.0	1.5	4.04E+13	3.23E+13
1.5	2.0	2.90E+11	1.66E+11
2.0	2.5	2.94E+9	1.31E+9
2.5	3.0	7.77E+7	2.83E+7
Totals		2.73E+14	4.33E+14

Note:
1. These source terms were calculated for a 144 inch active fuel length. The actual active fuel length is 83 inches.
2. The ^{60}Co activation from incore spacers is included in the 1.0-1.5 MeV energy group.

Table 5.2.20

CALCULATED PWR FUEL GAMMA SOURCE PER ASSEMBLY
FOR STAINLESS STEEL CLAD FUEL

Lower Energy	**Upper Energy**	**30,000 MWD/MTU 19-Year Cooling**		**40,000 MWD/MTU 24-Year Cooling**	
(MeV)	(MeV)	(MeV/s)	(Photons/s)	(MeV/s)	(Photons/s)
0.45	0.7	6.81E+14	1.18E+15	7.97E+14	1.39E+15
0.7	1.0	1.83E+13	2.16E+13	1.70E+13	2.01E+13
1.0	1.5	1.13E+14	9.06E+13	8.24E+13	6.60E+13
1.5	2.0	1.06E+12	6.04E+11	1.12E+12	6.42E+11
2.0	2.5	7.25E+9	3.22E+9	7.42E+9	3.30E+9
2.5	3.0	3.52E+8	1.28E+8	6.43E+8	2.34E+8
Totals		8.14E+14	1.30E+15	8.98E+14	1.47E+15

Note:
1. These source terms were calculated for a 144 inch active fuel length. The actual active fuel length is 122 inches.
2. The ^{60}Co activation from incore spacers is included in the 1.0-1.5 MeV energy group.

Table 5.2.21

CALCULATED BWR NEUTRON SOURCE PER ASSEMBLY
FOR STAINLESS STEEL CLAD FUEL

Lower Energy (MeV)	**Upper Energy (MeV)**	**22,500 MWD/MTU 16-Year Cooling (Neutrons/s)**
1.0E-01	4.0E-01	1.81E+5
4.0E-01	9.0E-01	9.26E+5
9.0E-01	1.4	8.75E+5
1.4	1.85	6.85E+5
1.85	3.0	1.34E+6
3.0	6.43	1.08E+6
6.43	20.0	8.77E+4
Total		5.18E+6

Note:
These source terms were calculated for a 144 inch active fuel length. The actual active fuel length is 83 inches.

Table 5.2.22

CALCULATED PWR NEUTRON SOURCE PER ASSEMBLY
FOR STAINLESS STEEL CLAD FUEL

Lower Energy (MeV)	**Upper Energy (MeV)**	**30,000 MWD/MTU 19-Year Cooling (Neutrons/s)**	**40,000 MWD/MTU 24-Year Cooling (Neutrons/s)**
1.0E-01	4.0E-01	2.68E+6	7.07E+6
4.0E-01	9.0E-01	1.37E+7	3.61E+7
9.0E-01	1.4	1.27E+7	3.32E+7
1.4	1.85	9.50E+6	2.47E+7
1.85	3.0	1.74E+7	4.43E+7
3.0	6.43	1.52E+7	3.95E+7
6.43	20.0	1.31E+6	3.46E+6
Totals		7.24E+7	1.88E+8

Note:
These source terms were calculated for a 144 inch active fuel length. The actual active fuel length is 122 inches.

Table 5.2.23

MINIMUM ENRICHMENTS AS A FUNCTION OF BURNUP
FOR THE SHIELDING ANALYSIS

Minimum Enrichment (wt.% ^{235}U)	Maximum Burnup Analyzed (MWD/MTU)	
PWR assemblies with non-zircaloy incore spacers	MPC-24	MPC-32
2.3	24,500	24,500
2.6	29,500	29,500
2.9	34,500	34,500
3.2	39,500	39,500
3.4	44,500	42,500
PWR assemblies with zircaloy incore spacers	MPC-24	MPC-32
2.3	24,500	24,500
2.6	29,500	29,500
2.9	34,500	34,500
3.2	39,500	39,500
3.4	44,500	44,500
MPC-68		
0.7	10,000	
1.35	20,000	
2.1	24,500	
2.4	29,500	
2.6	34,500	
2.9	39,500	
3.0	44,500	

Table 5.2.24

DESCRIPTION OF EVALUATED INTACT ZIRCALOY CLAD PWR FUEL

Assembly class	WE 14×14	WE 15×15	WE 17×17	CE 14×14	CE 16×16	B&W 15×15	B&W 17×17
Active fuel length (in.)	144	144	144	144	150	144	144
No. of fuel rods	179	204	264	176	236	208	264
Rod pitch (in.)	0.556	0.563	0.496	0.580	0.5063	0.568	0.502
Cladding material	Zr-4	Zr-4	Zr-4	Zr-4	Zr-4	Zr-4	Zr-4
Rod diameter (in.)	0.422	0.422	0.374	0.440	0.382	0.428	0.377
Cladding thickness (in.)	0.0243	0.0245	0.0225	0.0280	0.0250	0.0230	0.0220
Pellet diameter (in.)	0.3659	0.366	0.3225	0.377	0.3255	0.3742	0.3252
Pellet material	UO_2	UO_2	UO_2	UO_2	UO_2	UO_2	UO_2
Pellet density (gm/cc) (95% of theoretical)	10.412	10.412	10.412	10.412	10.412	10.412	10.412
Enrichment (wt.% ^{235}U)	3.4	3.4	3.4	3.4	3.4	3.4	3.4
Burnup (MWD/MTU)	40,000	40,000	40,000	40,000	40,000	40,000	40,000
Cooling time (years)	5	5	5	5	5	5	5
Specific power (MW/MTU)	40	40	40	40	40	40	40
Weight of UO_2 (kg)†	462.451	527.327	529.848	482.706	502.609	562.029	538.757
Weight of U (kg)†	407.697	464.891	467.114	425.554	443.100	495.485	474.968
No. of Guide Tubes	17	21	25	5	5	17	25
Guide Tube O.D. (in.)	0.539	0.546	0.474	1.115	0.98	0.53	0.564
Guide Tube Thickness (in.)	0.0170	0.0170	0.0160	0.0400	0.0400	0.0160	0.0175

† Derived from parameters in this table.

Table 5.2.25

DESCRIPTION OF EVALUATED INTACT ZIRCALOY CLAD BWR FUEL

Array Type	7×7	8×8	9×9	10×10
Active fuel length (in.)	144	144	144	144
No. of fuel rods	49	63	74	92
Rod pitch (in.)	0.738	0.640	0.566	0.510
Cladding material	Zr-2	Zr-2	Zr-2	Zr-2
Rod diameter (in.)	0.570	0.493	0.440	0.404
Cladding thickness (in.)	0.0355	0.0340	0.0280	0.0260
Pellet diameter (in.)	0.488	0.416	0.376	0.345
Pellet material	UO_2	UO_2	UO_2	UO_2
Pellet density (gm/cc) (95% of theoretical)	10.412	10.412	10.412	10.412
Enrichment (wt.% ^{235}U)	3.0	3.0	3.0	3.0
Burnup (MWD/MTU)	40,000	40,000	40,000	40,000
Cooling time (years)	5	5	5	5
Specific power (MW/MTU)	30	30	30	30
Weight of UO_2 (kg)†	225.177	210.385	201.881	211.307
Weight of U (kg)†	198.516	185.475	177.978	186.288
No. of Water Rods	0	1	2	2
Water Rod O.D. (in.)	n/a	0.493	0.980	0.980
Water Rod Thickness (in.)	n/a	0.0340	0.0300	0.0300

† Derived from parameters in this table.

Table 5.2.26

COMPARISON OF SOURCE TERMS FOR INTACT ZIRCALOY CLAD PWR FUEL
3.4 wt.% ^{235}U - 40,000 MWD/MTU - 5 years cooling

Assembly class	WE 14×14	WE 15×15	WE 17×17	CE 14×14	CE 16×16	B&W 15×15	B&W 17×17
Neutrons/sec	2.29E+8 / 2.31E+8	2.63E+8 / 2.65E+8	2.62E+8	2.31E+8	2.34E+8	2.94E+8	2.64E+8
Photons/sec (0.45-3.0 MeV)	3.28E+15/ 3.33E+15	3.74E+15/ 3.79E+15	3.76E+15	3.39E+15	3.54E+15	4.01E+15	3.82E+15
Thermal power (watts)	926.6 / 936.8	1056 / 1068	1062	956.6	995.7	1137	1077

Note:
The WE 14x14 and WE 15x15 have both zircaloy and stainless steel guide tubes. The first value presented is for the assembly with zircaloy guide tubes and the second value is for the assembly with stainless steel guide tubes.

Table 5.2.27

COMPARISON OF SOURCE TERMS FOR INTACT ZIRCALOY CLAD BWR FUEL
3.0 wt.% ^{235}U - 40,000 MWD/MTU - 5 years cooling

Assembly class	7×7	8×8	9×9	10×10
Neutrons/sec	1.33E+8	1.17E+8	1.11E+8	1.22E+8
Photons/sec (0.45-3.0 MeV)	1.55E+15	1.44E+15	1.38E+15	1.46E+15
Thermal power (watts)	435.5	402.3	385.3	407.4

Table 5.2.28

COMPARISON OF CALCULATED DECAY HEATS FOR DESIGN BASIS FUEL AND VALUES REPORTED IN THE DOE CHARACTERISTICS DATABASE † FOR 30,000 MWD/MTU AND 5-YEAR COOLING

Fuel Assembly Class	Decay Heat from the DOE Database (watts/assembly)	Decay Heat from Design Basis Fuel (watts/assembly)
PWR Fuel		
B&W 15x15	752.0	827.5
B&W 17x17	732.9	827.5
CE 16x16	653.7	827.5
CE 14x14	601.3	827.5
WE 17x17	742.5	827.5
WE 15x15	762.2	827.5
WE 14x14	649.6	827.5
BWR Fuel		
7x7	310.9	315.7
8x8	296.6	315.7
9x9	275.0	315.7

Notes:
1. The PWR and BWR design basis fuels are the B&W 15x15 and the GE 7x7, respectively.
2. The decay heat values from the database include contributions from in-core material (e.g. spacer grids).
3. Information on the 10x10 was not available in the DOE database. However, based on the results in Table 5.2.27, the actual decay heat values from the 10x10 would be very similar to the values shown above for the 8x8.

† Reference [5.2.7].

Table 5.2.29
DESCRIPTION OF FUEL ASSEMBLY USED TO ANNALYZE THORIA RODS IN THE THORIA ROD CANISTER

	BWR
Fuel type	8x8
Active fuel length (in.)	110.5
No. of UO_2 fuel rods	55
No. of UO_2/ThO_2 fuel rods	9
Rod pitch (in.)	0.523
Cladding material	zircaloy
Rod diameter (in.)	0.412
Cladding thickness (in.)	0.025
Pellet diameter (in.)	0.358
Pellet material	98.2% ThO_2 and 1.8% UO_2 for UO_2/ThO_2 rods
Pellet density (gm/cc)	10.412
Enrichment (w/o ^{235}U)	93.5 in UO_2 for UO_2/ThO_2 rods and 1.8 for UO_2 rods
Burnup (MWD/MTIHM)	16,000
Cooling Time (years)	18
Specific power (MW/MTIHM)	16.5
Weight of THO_2 and UO_2 (kg)†	121.46
Weight of U (kg)†	92.29
Weight of Th (kg)†	14.74

† Derived from parameters in this table.

Table 5.2.30

CALCULATED FUEL GAMMA SOURCE FOR THORIA ROD CANISTER CONTAINING EIGHTEEN THORIA RODS

Lower Energy	**Upper Energy**	**16,000 MWD/MTIHM 18-Year Cooling**	
(MeV)	(MeV)	(MeV/s)	(Photons/s)
7.0E-01	1.0	5.79E+11	6.81E+11
1.0	1.5	3.79E+11	3.03E+11
1.5	2.0	4.25E+10	2.43E+10
2.0	2.5	4.16E+8	1.85E+8
2.5	3.0	2.31E+11	8.39E+10
Totals		1.23E+12	1.09E+12

Table 5.2.31

CALCULATED FUEL NEUTRON SOURCE FOR THORIA ROD CANISTER CONTAINING EIGHTEEN THORIA RODS

Lower Energy (MeV)	**Upper Energy (MeV)**	**16,000 MWD/MTIHM 18-Year Cooling (Neutrons/s)**
1.0E-01	4.0E-01	5.65E+2
4.0E-01	9.0E-01	3.19E+3
9.0E-01	1.4	6.79E+3
1.4	1.85	1.05E+4
1.85	3.0	3.68E+4
3.0	6.43	1.41E+4
6.43	20.0	1.60E+2
Totals		7.21E+4

Table 5.2.32

DESCRIPTION OF DESIGN BASIS TROJAN FUEL

	PWR
Assembly type/class	WE 17×17
Active fuel length (in.)	144
No. of fuel rods	264
Rod pitch (in.)	0.496
Cladding material	zircaloy-4
Rod diameter (in.)	0.374
Cladding thickness (in.)	0.0225
Pellet diameter (in.)	0.3225
Pellet material	UO_2
Pellet density (gm/cc)	10.412 (95% of theoretical)
Enrichment (w/o ^{235}U)[††]	2.1, 2.6, 3.09
Burnup (MWD/MTU)	30,000, 37,500, 42,000
Cooling Time (years)	16
Specific power (MW/MTU)	40
Weight of UO_2 (kg)[†]	529.85
Weight of U (kg)[†]	467.11
No. of Water Rods/Guide Tubes	25
Water Rod O.D. (in.)	0.482
Water Rod Thickness (in.)	0.016
Lower End Fitting (kg)	5.9 (steel)
Gas Plenum Springs (kg)	1.15 (steel)
Gas Plenum Spacer (kg)	0.84 (steel) 0.79 (inconel)
Upper End Fitting (kg)	6.89 (steel) 0.96 (inconel)
Incore Grid Spacers (kg)	4.9 (inconel)

[††] The enrichments correspond directly to the burnups (e.g. 2.1 for 30,000 MWD/MTU)

[†] Derived from parameters in this table.

Table 5.2.33
CALCULATED TROJAN PWR FUEL GAMMA SOURCE PER ASSEMBLY

Lower Energy	**Upper Energy**	**30,000 MWD/MTU 16 Year Cooling**		**37,500 MWD/MTU 16 Year Cooling**		**42,000 MWD/MTU 16 Year Cooling**	
(MeV)	(MeV)	(MeV/s)	(Photons/s)	(MeV/s)	(Photons/s)	(MeV/s)	(Photons/s)
0.45	0.7	6.80E+14	1.18E+15	8.46E+14	1.47E+15	9.44E+14	1.64E+15
0.7	1.0	2.52E+13	2.96E+13	3.35E+13	3.94E+13	3.82E+13	4.50E+13
1.0	1.5	2.04E+13	1.64E+13	2.71E+13	2.17E+13	3.09E+13	2.47E+13
1.5	2.0	1.16E+12	6.65E+11	1.53E+12	8.77E+11	1.75E+12	9.99E+11
2.0	2.5	6.72E+09	2.99E+09	8.28E+09	3.68E+09	9.33E+09	4.15E+09
2.5	3.0	4.10E+08	1.49E+08	6.13E+08	2.23E+08	7.47E+08	2.72E+08
Totals		7.26E+14	1.23E+15	9.08E+14	1.53E+15	1.01E+15	1.71E+15

Table 5.2.34
CALCULATED TROJAN FUEL ^{60}Co SOURCE PER ASSEMBLY

Location	**30,000 MWD/MTU 16 Year Cooling (curies)**	**37,500 MWD/MTU 16 Year Cooling (curies)**	**42,000 MWD/MTU 16 Year Cooling (curies)**
Lower End Fitting	21.48	23.72	24.19
Gas Plenum Springs	4.19	4.62	4.72
Gas Plenum Spacer	15.99	17.66	18.02
Grid Spacers	419.15	462.90	472.12
Upper End Fitting	18.29	20.20	20.60

Table 5.2.35
CALCULATED TROJAN FUEL NEUTRON SOURCE PER ASSEMBLY

Lower Energy (MeV)	Upper Energy (MeV)	30,000 MWD/MTU 16 Year Cooling (Neutrons/s)	37,500 MWD/MTU 16 Year Cooling (Neutrons/s)	42,000 MWD/MTU 16 Year Cooling (Neutrons/s)
1.0E-01	4.0E-01	4.71E+06	8.11E+06	9.55E+06
4.0E-01	9.0E-01	2.41E+07	4.15E+07	4.88E+07
9.0E-01	1.4	2.21E+07	3.80E+07	4.47E+07
1.4	1.85	1.64E+07	2.81E+07	3.31E+07
1.85	3.0	2.93E+07	5.00E+07	5.88E+07
3.0	6.43	2.63E+07	4.51E+07	5.30E+07
6.43	20.0	2.30E+06	3.97E+06	4.67E+06
Total		1.25E+08	2.15E+08	2.53E+08

Table 5.2.36

DESCRIPTION OF TROJAN BURNABLE POISON ROD ASSEMBLY
AND THIMBLE PLUG DEVICE

Region	**BPRA**	**TPD**
Upper End Fitting (kg of steel)	2.62	2.31
Upper End Fitting (kg of inconel)	0.42	0.42
Gas Plenum Spacer (kg of steel)	0.72	1.6
Gas Plenum Springs (kg of steel)	0.73	1.6
In-core (kg of steel)	12.10	N/A

Table 5.2.37

COBALT-60 ACTIVITIES FOR TROJAN BURNABLE POISON ROD ASSEMBLIES AND THIMBLE PLUG DEVICES

Region	**BPRA**	**TPD**
Burnup (MWD/MTU)	15,998	118,674
Cooling Time (years)	24	11
Upper End Fitting (curies Co-60)	1.20	18.86
Gas Plenum Spacer (curies Co-60)	0.34	12.80
Gas Plenum Springs (curies Co-60)	0.34	12.80
In-core (curies Co-60)	28.68	N/A

Table 5.2.38

DESCRIPTION OF TROJAN ROD CLUSTER CONTROL ASSEMBLY
FOR SOURCE TERM CALCULATIONS

Physical Description

Axial Dimensions Relative to Bottom of Active Fuel			Flux Weighting Factor	Mass of cladding (kg Steel)	Mass of absorber (kg AgInCd)
Start (in)	Finish (in)	Length (in)			
Configuration - Fully Removed					
0.0	8.358	8.358	0.2	0.76	3.18
8.358	12.028	3.67	0.1	0.34	1.40

Radiological Description
125,515 MWD/MTU
9 Year Cooling

Axial Dimensions Relative to Bottom of Active Fuel			Photons/sec from AgInCd			Curies Co-60 from Steel
Start (in)	Finish (in)	Length (in)	0.3-0.45 MeV	0.45-0.7 MeV	0.7-1.0 MeV	
Configuration - Fully Removed						
0.0	8.358	8.358	7.66E+12	7.12E+12	5.66E+12	7.34
8.358	12.028	3.67	1.68E+12	1.56E+13	1.24E+12	1.61

Table 5.2.39

DESCRIPTION OF TROJAN SECONDARY SOURCE ASSEMBLIES

Physical Description

Region	Source in Cycles 1-4	Sources in Cycles 4-14
Upper End Fitting (kg of steel)	2.62	2.62
Upper End Fitting (kg of inconel)	0.42	0.42
Gas Plenum Spacer (kg of steel)	1.6	1.6
Gas Plenum Springs (kg of steel)	1.6	1.6
In-core (kg of steel)	10.08	2.02

Radiological Description

Region	Source in Cycles 1-4	Sources in Cycles 4-14
Burnup (MWD/MTU)	45,361	88,547
Cooling Time (years)	19	9
Upper End Fitting (curies Co-60)	10.08	45.09
Gas Plenum Spacer (curies Co-60)	3.18	14.30
Gas Plenum Springs (curies Co-60)	3.18	14.30
In-core (curies Co-60)	100.20	90.29

Table 5.2.40
CALCULATED MPC-32 PWR FUEL GAMMA SOURCE PER ASSEMBLY FOR DESIGN BASIS ZIRCALOY CLAD FUEL WITH NON-ZIRCALOY INCORE SPACERS FOR VARYING BURNUPS AND COOLING TIMES

Lower Energy	**Upper Energy**	**24,500 MWD/MTU 12 Year Cooling**		**29,500 MWD/MTU 14 Year Cooling**		**34,500 MWD/MTU 16 Year Cooling**	
(MeV)	(MeV)	(MeV/s)	(Photons/s)	(MeV/s)	(Photons/s)	(MeV/s)	(Photons/s)
0.45	0.7	6.67E+14	1.16E+15	7.51E+14	1.31E+15	8.26E+14	1.44E+15
0.7	1.0	4.19E+13	4.94E+13	3.59E+13	4.23E+13	3.18E+13	3.74E+13
1.0	1.5	2.29E+13	1.83E+13	2.45E+13	1.96E+13	2.59E+13	2.07E+13
1.5	2.0	1.23E+12	7.05E+11	1.36E+12	7.80E+11	1.48E+12	8.47E+11
2.0	2.5	2.57E+10	1.14E+10	1.14E+10	5.06E+09	8.42E+09	3.74E+09
2.5	3.0	1.87E+09	6.78E+08	7.75E+08	2.82E+08	5.66E+08	2.06E+08
Totals		7.33E+14	1.23E+15	8.13E+14	1.37E+15	8.85E+14	1.50E+15
Lower Energy	**Upper Energy**	**39,500 MWD/MTU 19 Year Cooling**		**42,500 MWD/MTU 20 Year Cooling**			
(MeV)	(MeV)	(MeV/s)	(Photons/s)	(MeV/s)	(Photons/s)		
0.45	0.7	8.72E+14	1.52E+15	9.13E+14	1.59E+15		
0.7	1.0	2.51E+13	2.95E+13	2.46E+13	2.89E+13		
1.0	1.5	2.42E+13	1.94E+13	2.46E+13	1.97E+13		
1.5	2.0	1.43E+12	8.17E+11	1.46E+12	8.35E+11		
2.0	2.5	7.78E+09	3.46E+09	8.08E+09	3.59E+09		
2.5	3.0	5.98E+08	2.17E+08	6.89E+08	2.51E+08		
Totals		9.22E+14	1.57E+15	9.63E+14	1.64E+15		

Table 5.2.41
CALCULATED MPC-32 PWR FUEL GAMMA SOURCE PER ASSEMBLY FOR DESIGN BASIS ZIRCALOY CLAD FUEL WITH ZIRCALOY INCORE SPACERS FOR VARYING BURNUPS AND COOLING TIMES

Lower Energy	**Upper Energy**	**24,500 MWD/MTU 8 Year Cooling**		**29,500 MWD/MTU 9 Year Cooling**		**34,500 MWD/MTU 12 Year Cooling**	
(MeV)	(MeV)	(MeV/s)	(Photons/s)	(MeV/s)	(Photons/s)	(MeV/s)	(Photons/s)
0.45	0.7	8.09E+14	1.41E+15	9.20E+14	1.60E+15	9.38E+14	1.63E+15
0.7	1.0	1.19E+14	1.40E+14	1.17E+14	1.38E+14	6.91E+13	8.13E+13
1.0	1.5	3.84E+13	3.07E+13	4.30E+13	3.44E+13	3.78E+13	3.02E+13
1.5	2.0	2.04E+12	1.17E+12	2.17E+12	1.24E+12	1.99E+12	1.14E+12
2.0	2.5	4.83E+11	2.15E+11	2.40E+11	1.07E+11	3.18E+10	1.41E+10
2.5	3.0	2.60E+10	9.46E+09	1.51E+10	5.48E+09	2.53E+09	9.20E+08
Totals		9.69E+14	1.58E+15	1.08E+15	1.77E+15	1.05E+15	1.74E+15
Lower Energy	**Upper Energy**	**39,500 MWD/MTU 14 Year Cooling**		**44,500 MWD/MTU 19 Year Cooling**			
(MeV)	(MeV)	(MeV/s)	(Photons/s)	(MeV/s)	(Photons/s)		
0.45	0.7	1.00E+15	1.74E+15	9.78E+14	1.70E+15		
0.7	1.0	5.41E+13	6.37E+13	2.92E+13	3.44E+13		
1.0	1.5	3.71E+13	2.97E+13	2.84E+13	2.27E+13		
1.5	2.0	2.03E+12	1.16E+12	1.66E+12	9.50E+11		
2.0	2.5	1.42E+10	6.32E+09	8.63E+09	3.84E+09		
2.5	3.0	1.17E+09	4.25E+08	7.88E+08	2.87E+08		
Totals		1.09E+15	1.83E+15	1.04E+15	1.76E+15		

Table 5.2.42

CALCULATED MPC-32 ^{60}Co SOURCE PER ASSEMBLY FOR DESIGN BASIS ZIRCALOY CLAD FUEL WITH NON-ZIRCALOY INCORE SPACERS AT VARYING BURNUPS AND COOLING TIMES

Location	**24,500 MWD/MTU 12 Year Cooling (curies)**	**29,500 MWD/MTU 14 Year Cooling (curies)**	**34,500 MWD/MTU 16 Year Cooling (curies)**	**39,500 MWD/MTU 19 Year Cooling (curies)**	**42,500 MWD/MTU 20 Year Cooling (curies)**
Lower end fitting	64.65	55.27	46.40	33.47	30.42
Gas plenum springs	12.58	10.75	9.03	6.51	5.92
Gas plenum spacer	7.22	6.17	5.18	3.74	3.40
Expansion springs	N/A	N/A	N/A	N/A	N/A
Grid spacers	587.27	502.05	421.45	304.00	276.36
Upper end fitting	23.66	20.23	16.98	12.25	11.14
Handle	N/A	N/A	N/A	N/A	N/A

Table 5.2.43

CALCULATED MPC-32 ^{60}Co SOURCE PER ASSEMBLY FOR DESIGN BASIS ZIRCALOY CLAD FUEL WITH ZIRCALOY INCORE SPACERS AT VARYING BURNUPS AND COOLING TIMES

Location	**24,500 MWD/MTU 8 Year Cooling (curies)**	**29,500 MWD/MTU 9 Year Cooling (curies)**	**34,500 MWD/MTU 12 Year Cooling (curies)**	**39,500 MWD/MTU 14 Year Cooling (curies)**	**44,500 MWD/MTU 19 Year Cooling (curies)**
Lower end fitting	109.27	106.74	78.34	64.65	36.25
Gas plenum springs	21.26	20.77	15.24	12.58	7.05
Gas plenum spacer	12.20	11.91	8.74	7.22	4.05
Expansion springs	N/A	N/A	N/A	N/A	N/A
Grid spacers†	N/A	N/A	N/A	N/A	N/A
Upper end fitting	40.00	39.07	28.68	23.66	13.27
Handle	N/A	N/A	N/A	N/A	N/A

† These burnup and cooling times represent fuel with zircaloy grid spacers. Therefore, the cobalt activation is negligible.

Table 5.2.44

CALCULATED MPC-32 PWR NEUTRON SOURCE PER ASSEMBLY
FOR DESIGN BASIS ZIRCALOY CLAD FUEL WITH NON-ZIRCALOY
INCORE SPACERS FOR VARYING BURNUPS AND COOLING TIMES

Lower Energy (MeV)	Upper Energy (MeV)	24,500 MWD/MTU 12 Year Cooling (Neutrons/s)	29,500 MWD/MTU 14 Year Cooling (Neutrons/s)	34,500 MWD/MTU 16 Year Cooling (Neutrons/s)	39,500 MWD/MTU 19 Year Cooling (Neutrons/s)	42,500 MWD/MTU 20 Year Cooling (Neutrons/s)
1.0E-01	4.0E-01	2.24E+06	3.61E+06	5.37E+06	6.97E+06	8.08E+06
4.0E-01	9.0E-01	1.15E+07	1.84E+07	2.74E+07	3.56E+07	4.13E+07
9.0E-01	1.4	1.06E+07	1.70E+07	2.52E+07	3.27E+07	3.79E+07
1.4	1.85	7.88E+06	1.26E+07	1.87E+07	2.43E+07	2.81E+07
1.85	3.0	1.43E+07	2.27E+07	3.35E+07	4.34E+07	5.02E+07
3.0	6.43	1.26E+07	2.02E+07	3.00E+07	3.89E+07	4.50E+07
6.43	20.0	1.10E+06	1.76E+06	2.63E+06	3.41E+06	3.95E+06
TOTALS		6.01E+07	9.63E+07	1.43E+08	1.85E+08	2.15E+08

Table 5.2.45

CALCULATED MPC-32 PWR NEUTRON SOURCE PER ASSEMBLY
FOR DESIGN BASIS ZIRCALOY CLAD FUEL WITH ZIRCALOY
INCORE SPACERS FOR VARYING BURNUPS AND COOLING TIMES

Lower Energy (MeV)	Upper Energy (MeV)	24,500 MWD/MTU 8 Year Cooling (Neutrons/s)	29,500 MWD/MTU 9 Year Cooling (Neutrons/s)	34,500 MWD/MTU 12 Year Cooling (Neutrons/s)	39,500 MWD/MTU 14 Year Cooling (Neutrons/s)	44,500 MWD/MTU 19 Year Cooling (Neutrons/s)
1.0E-01	4.0E-01	2.60E+06	4.35E+06	6.24E+06	8.40E+06	1.01E+07
4.0E-01	9.0E-01	1.33E+07	2.22E+07	3.19E+07	4.29E+07	5.16E+07
9.0E-01	1.4	1.22E+07	2.04E+07	2.92E+07	3.94E+07	4.73E+07
1.4	1.85	9.08E+06	1.51E+07	2.17E+07	2.91E+07	3.50E+07
1.85	3.0	1.63E+07	2.70E+07	3.86E+07	5.19E+07	6.24E+07
3.0	6.43	1.45E+07	2.42E+07	3.47E+07	4.67E+07	5.61E+07
6.43	20.0	1.27E+06	2.13E+06	3.05E+06	4.11E+06	4.94E+06
TOTALS		6.93E+07	1.16E+08	1.65E+08	2.23E+08	2.67E+08

5.3 MODEL SPECIFICATIONS

The shielding analysis of the HI-STAR 100 System was performed with MCNP-4A [5.1.1]. MCNP is a Monte Carlo transport code that offers a full three-dimensional combinatorial geometry modeling capability including such complex surfaces as cones and tori. This means that no gross approximations were required to represent the HI-STAR 100 System in the shielding analysis. A sample input file for MCNP is provided in Appendix 5.C.

Subsection 5.1.2 discussed the accident conditions and stated that the only accident that would impact the shielding analysis would be a loss of the neutron shield and impact limiters. Therefore, the MCNP models of the HI-STAR 100 System normal condition have the neutron shield and impact limiters in place while the hypothetical accident condition replaces the neutron shield with void and removes the impact limiters. The aluminum honeycomb in the impact limiters was conservatively neglected in the MCNP modeling. However, credit was taken for the outer dimensions of the impact limiters.

5.3.1 Description of the Radial and Axial Shielding Configuration

Section 1.4 provides the drawings that describe the HI-STAR 100 System. These drawings were used to create the MCNP models used in the radiation transport calculations. Figures 5.3.1 through 5.3.3 show cross sectional views of the HI-STAR 100 overpack and MPC as it was modeled in MCNP for each of the MPCs. These figures were created with the MCNP two-dimensional plotter and are drawn to scale. The figures clearly illustrate the radial steel fins and pocket trunnions in the neutron shield region. Since the fins and pocket trunnions were modeled explicitly, neutron streaming through these components is accounted for in the calculations of the dose adjacent to the overpack and 1 meter dose. In Subsection 5.4.1, the dose effect of localized streaming through these compartments is analyzed. Figures 5.3.4 through 5.3.6 show the MCNP models of the MPC-32, MPC-24, and MPC-68 fuel baskets including the as-modeled dimensions. Figure 5.3.9 shows a cross sectional view of the HI-STAR 100 overpack with the as-modeled thickness of the various materials. Figure 5.3.10 is an axial representation of the HI-STAR 100 overpack with the various as-modeled dimensions indicated. As Figure 5.3.10 indicates, the thickness of the MPC lid is 9.5 inches. Earlier versions of the MPC-68 used a 10 inch thick lid with a correspondingly smaller MPC-internal cavity height. The analysis in this chapter conservatively represents the 9.5 inch thick lid. Figures 5.3.11 and 5.3.12 provide the as-modeled dimensions of the impact limiters during normal conditions. The aluminum honeycomb material in the impact limiter is not shown in Figure 5.3.11 because it was conservatively not modeled in the MCNP calculations.

Calculations were performed to determine the acceptability of homogenizing the fuel assembly versus explicit modeling. Based on these calculations it was concluded that it was acceptable to homogenize the fuel assembly without loss of accuracy. The width of the PWR and BWR homogenized fuel assembly is equal to 15 times the pitch and 7 times the pitch, respectively.

Several conservative approximations were made in modeling the MPC and overpack. The conservative approximations are listed below.

1. The basket material in the top and bottom 0.9 inches where the MPC basket flow holes are located is not modeled. The length of the basket not modeled (0.9 inches) was determined by calculating the equivalent area removed by the flow holes. This method of approximation is conservative because no material for the basket shielding is provided in the 0.9 inch area at the top and bottom of the MPC basket.

2. The upper and lower fuel spacers are not modeled. The fuel spacers are not needed on all fuel assembly types. However, most PWR fuel assemblies will have upper and lower fuel spacers. The positioning of the fuel assembly for the shielding analysis is determined by the fuel spacer length for the design basis fuel assembly type, but the fuel spacer materials are not modeled. This is conservative since it removes steel which would provide a small amount of additional shielding.

3. For the MPC-24, MPC-32, and the MPC-68, the MPC basket supports are not modeled. This is conservative since it removes steel which would provide a small increase in shielding. The optional aluminum heat conduction elements were also conservatively not modeled.

4. Deleted.

5. In the modeling of the BWR fuel assemblies, the zircaloy flow channels were not represented. This was done because it cannot be guaranteed that all BWR fuel assemblies will have an associated flow channel when placed in the MPC. The flow channel does not contribute to the source, but does provide some small amount of shielding. However, no credit is taken for this additional shielding.

6. In the modeling of the impact limiters, only the neutron shield (Holtite-A) and the steel, shown in Figure 5.1.1, were represented. Conservatively, the aluminum honeycomb of the impact limiters was not modeled. However, credit was taken for the outer boundary of the impact limiter as the external surface of the HI-STAR 100 System.

7. Deleted

8. The Trojan MPC-24E was modeled explicitly with its shorter cavity length and larger cell sizes with shorter height on the four corner locations. The Trojan MPC was properly positioned in the bottom portion of the HI-STAR and the spacer device between the top of the MPC and the underside of the HI-STAR lid was conservatively not modeled.

During this project several design changes occurred that affected the drawings, but did not significantly affect the MCNP models of the HI-STAR 100 overpack or MPC. Therefore, in

some cases, these models do not exactly represent the drawings. The discrepancies between models and drawings are listed and discussed here.

MPC Modeling Discrepancies

1. In the newer MPCs, there is a sump in the baseplate to enhance draining of the MPC. This localized reduction in the thickness of the baseplate was not modeled. Since there is significant shielding and distance in the HI-STAR outside the MPC baseplate, this localized reduction in shielding will not affect the calculated dose rates outside the HI-STAR.
2. The MPC-24 has narrower boral (6.25 inches compared to 7.5 inches) on 16 of the 24 exterior panels. Conservatively, all 24 panels were modeled as 6.5 inches wide. This dimension is slightly larger than the actual 6.25 inch dimension but is considerably smaller than the 7.5 inch dimension and results in a net reduction in boral around the periphery of the basket.
3. An enhanced version of the MPC-24 design, the MPC-24E, has been created. The MPC-24E is superior to the MPC-24 from a criticality perspective. From a shielding perspective, the two designs are almost identical. The cell openings in the MPC-24E are slightly smaller than in the MPC-24 and the boral and sheathing are slightly thicker in the MPC-24E than in the MPC-24. As a result, the MPC-24E has slightly better shielding characteristics than the MPC-24 and the MPC-24 analysis bounds the MPC-24E.
4. In the newer MPC's, the MPC lid may be fabricated as a two-piece lid with the bottom piece made of an alternative construction of carbon steel covered or coated within stainless steel. In MCNP, the MPC lid is modeled entirely of stainless steel; however the shielding analyses conservatively uses a density of 0.286 lbs/cubic inch for stainless steel, whereas the density of carbon steel is typically 0.284 lbs/cubic inch. Therefore, even an MPC lid constructed entirely of carbon still represents a decrease in density of less than 0.7%, which has a negligible effect on the calculated dose rates.

5.3.1.1 Fuel Configuration

As described above, the active fuel region is modeled as a homogenous zone. The end fittings and the plenum regions are also modeled as homogenous regions of steel. The masses of steel used in these regions are shown in Tables 5.2.1 and 5.2.32. The axial description of the design basis fuel assemblies is provided in Table 5.3.1. The axial description of the Trojan fuel assembly is provided in Table 5.3.4. Figures 5.3.7 and 5.3.8 graphically depict the location of the PWR and BWR fuel assemblies within the HI-STAR 100 System. The impact limiters are not depicted in the figures for clarity. The axial locations of the Boral, basket, pocket trunnion, and transition areas are shown in these figures.

The axial position of the fuel assembly within the basket is maintained with the use of the upper and lower fuel spacers. These fuel spacers are used to position the active fuel region next to the Boral. Chapter 2 demonstrates that these fuel spacers do not fail under all normal and hypothetical accident conditions. Therefore, movement of the fuel assembly during transport is not considered.

5.3.1.2 Streaming Considerations

The streaming from the radial channels and pocket trunnions in the neutron shield is evaluated in Subsection 5.4.1. The MCNP model of the HI-STAR 100 completely describes the radial channels and pocket trunnions, thereby properly accounting for the streaming effect. In newer designs of the HI-STAR 100 overpack, the pocket trunnion has been removed. However, the analysis presented in this chapter using the pocket trunnion bounds the new configuration due to the reduction in streaming when the pocket trunnion is not present.

The design of the HI-STAR 100 System, as described in the drawings in Section 1.4, has eliminated all other possible streaming paths. Therefore, the MCNP model does not represent any additional streaming paths. A brief justification of this assumption is provided for each penetration.

- The lifting trunnions will remain installed in the overpack top flange. No credit is taken for any part of the trunnion that extends outside of the overpack.

- The pocket trunnions are modeled as solid blocks of steel. The pocket trunnion will be filled with a solid steel rotation trunnion attached to the transport frame during handling and shipping or a plug will be installed if rotation trunnions are not inserted into the pocket trunnion.

- The threaded holes in the MPC lid are plugged with solid plugs during shipping and, therefore, do not create a void in the MPC lid.

- The drain and vent ports in the MPC lid are designed to eliminate streaming paths. The steel lost in the MPC lid at the port location is replaced with a block of steel approximately 6 inches thick below the port opening and attached to the underside of the lid. This design feature is shown on the drawings in Section 1.4. The MCNP model did not explicitly represent this arrangement but, rather, modeled the MPC lid as a solid piece.

- The penetrations in the overpack are filled with bolts that extend into the penetration, thereby eliminating any potential direct streaming paths. Cover plates are also designed in such a way as to maintain the thickness of the overpack to the maximum extent practical. Therefore, the MCNP model does not represent any streaming paths due to penetrations in the overpack.

5.3.2 Regional Densities

Composition and densities of the various materials used in the HI-STAR 100 System shielding analyses are given in Tables 5.3.2 and 5.3.3. All of the materials and their actual geometries are represented in the MCNP model. All steel in the MPC was modeled as stainless steel and all steel in the overpack was modeled as carbon steel.

The MPCs in the HI-STAR 100 System can be manufactured with one of two possible neutron absorbing materials: Boral or Metamic. Both materials are made of aluminum and B_4C powder. The Boral contains an aluminum and B_4C powder mixture sandwiched between two aluminum plates while the Metamic is a single plate. The thickness and minimum ^{10}B areal density are the same for Boral and Metamic while the thicknesses are essentially the same. Therefore, the mass of Aluminum and B_4C are essentially equivalent and there is no distinction between the two materials from a shielding perspective. As a result, Table 5.3.2 identifies the composition for Boral and no explicit calculations were performed with Metamic.

Section 3.4 demonstrates that all materials used in the HI-STAR 100 System remain below their design temperatures as specified in Table 2.1.2 during all normal conditions. Therefore, the shielding analysis does not address changes in the material density or composition as a result of temperature changes.

During normal operations, the depletion of B-10 in the Boral and the Holtite-A neutron shield is negligible. The fraction of B-10 atoms that are depleted in 50 years is approximately 3.0E-9 and 4.0E-8 in the Boral and Holtite-A, respectively. Therefore, the shielding analysis does not address changes in the composition of the Boral or Holtite-A as a result of neutron absorption.

As discussed in Section 1.2.1.4.2, the density of the Holtite-A during normal condition was reduced by approximately 4% to account for any potential water loss. In addition, the Hydrogen weight percent was conservatively reduced from 6% to 5.92%.

Section 3.5 discusses the effect of the hypothetical accident condition (fire) on the temperatures of the shielding materials and the resultant impact on their shielding effectiveness. As stated in Subsection 5.1.2, the only consequence that has any significant impact on the shielding configuration is the loss of the neutron shield in the HI-STAR 100 System as a result of fire. The change in the neutron shield was conservatively analyzed by assuming that the entire volume of the neutron shield was replaced by void.

Table 5.3.1

DESCRIPTION OF THE AXIAL MCNP MODEL OF THE DESIGN BASIS FUEL ASSEMBLIES†

Region	Start (in.)	Finish (in.)	Length (in.)	Actual Material	Modeled Material
PWR					
Lower End Fitting	0.0	7.375	7.375	SS304	SS304
Space	7.375	8.375	1.0	zircaloy	void
Fuel	8.375	152.375	144	fuel & zircaloy	fuel
Gas Plenum Springs	152.375	156.1875	3.8125	SS304 & zircaloy	SS304
Gas Plenum Spacer	156.1875	160.5625	4.375	SS304 & zircaloy	SS304
Upper End Fitting	160.5625	165.625	5.0625	SS304	SS304
BWR					
Lower End Fitting	0.0	7.385	7.385	SS304	SS304
Fuel	7.385	151.385	144	fuel & zircaloy	fuel
Space	151.385	157.385	6	zircaloy	void
Gas Plenum Springs	157.385	166.865	9.48	SS304 & zircaloy	SS304
Expansion Springs	166.865	168.215	1.35	SS304	SS304
Upper End Fitting	168.215	171.555	3.34	SS304	SS304
Handle	171.555	176	4.445	SS304	SS304

† All dimensions start at the bottom of the fuel assembly. The length of the lower fuel spacer must be added to the distances to determine the distance from the top of the MPC baseplate.

Table 5.3.2

COMPOSITION OF THE MATERIALS IN THE HI-STAR 100 SYSTEM

Component	Density (g/cm^3)	Elements	Mass Fraction (%)
Uranium Oxide	10.412	^{235}U	2.9971(BWR) 3.2615(PWR)
		^{238}U	85.1529(BWR) 84.8885(PWR)
		O	11.85
Boral	2.644	^{10}B	4.4226 (MPC-68 & MPC-32) 4.367 (MPC-24)
		^{11}B	20.1474 (MPC-68 & MPC-32) 19.893 (MPC-24)
		Al	68.61 (MPC-68 & MPC-32) 69.01 (MPC-24)
		C	6.82 (MPC-68 & MPC-32) 6.73 (MPC-24)
SS304	7.92	Cr	19
		Mn	2
		Fe	69.5
		Ni	9.5
Carbon Steel	7.82	C	0.5
		Fe	99.5
Zircaloy	6.55	Zr	100

Table 5.3.2 (continued)

COMPOSITION OF THE MATERIALS IN THE HI-STAR 100 SYSTEM

Component	Density (g/cm^3)	Elements	Mass Fraction (%)
Neutron Shield Holtite-A	1.61	C	27.66039
		H	5.92
		Al	21.285
		N	1.98
		O	42.372
		^{10}B	0.14087
		^{11}B	0.64174
BWR Fuel Region Mixture	4.29251	^{235}U	2.4966
		^{238}U	70.9315
		O	9.8709
		Zr	16.701
PWR Fuel Region Mixture	3.853705	^{235}U	2.6944
		^{238}U	70.1276
		O	9.7895
		Zr	17.3885

Table 5.3.2 (continued)

COMPOSITION OF THE MATERIALS IN THE HI-STAR 100 SYSTEM

Component	Density (g/cm^3)	Elements	Mass Fraction (%)
Lower End Fitting (PWR)	1.0783	SS304	100
Gas Plenum Springs (PWR)	0.1591	SS304	100
Gas Plenum Spacer (PWR)	0.1591	SS304	100
Upper End Fitting (PWR)	1.5410	SS304	100
Lower End Fitting (BWR)	1.4862	SS304	100
Gas Plenum Springs (BWR)	0.2653	SS304	100
Expansion Springs (BWR)	0.6775	SS304	100
Upper End Fitting (BWR)	1.3692	SS304	100
Handle (BWR)	0.2572	SS304	100

Table 5.3.3

COMPOSITION OF THE FUEL IN THE MIXED OXIDE FUEL ASSEMBLIES IN THE MPC-68 OF THE HI-STAR 100 SYSTEM

Component	Density (g/cm^3)	Elements	Mass Fraction (%)
Mixed Oxide Pellets	10.412	^{238}U	85.498
		^{235}U	0.612
		^{238}Pu	0.421
		^{239}Pu	1.455
		^{240}Pu	0.034
		^{241}Pu	0.123
		^{242}Pu	0.007
		O	11.85
Uranium Oxide Pellets	10.412	^{238}U	86.175
		^{235}U	1.975
		O	11.85

Table 5.3.4

DESCRIPTION OF THE AXIAL MCNP MODEL OF THE TROJAN FUEL ASSEMBLY†

Region	Start (in.)	Finish (in.)	Length (in.)	Actual Material	Modeled Material
PWR					
Lower End Fitting	0.0	2.738	2.738	SS304	SS304
Space	2.738	3.738	1.0	zircaloy	Void
Fuel	3.738	147.738	144	fuel & zircaloy	Fuel
Gas Plenum Springs	147.738	151.916	4.178	SS304 & zircaloy	SS304
Gas Plenum Spacer	151.916	156.095	4.179	SS304 & zircaloy	SS304
Upper End Fitting	156.095	159.765	3.67	SS304	SS304

† All dimensions start at the bottom of the fuel assembly. The length of the lower fuel spacer must be added to the distances to determine the distance from the top of the MPC baseplate.

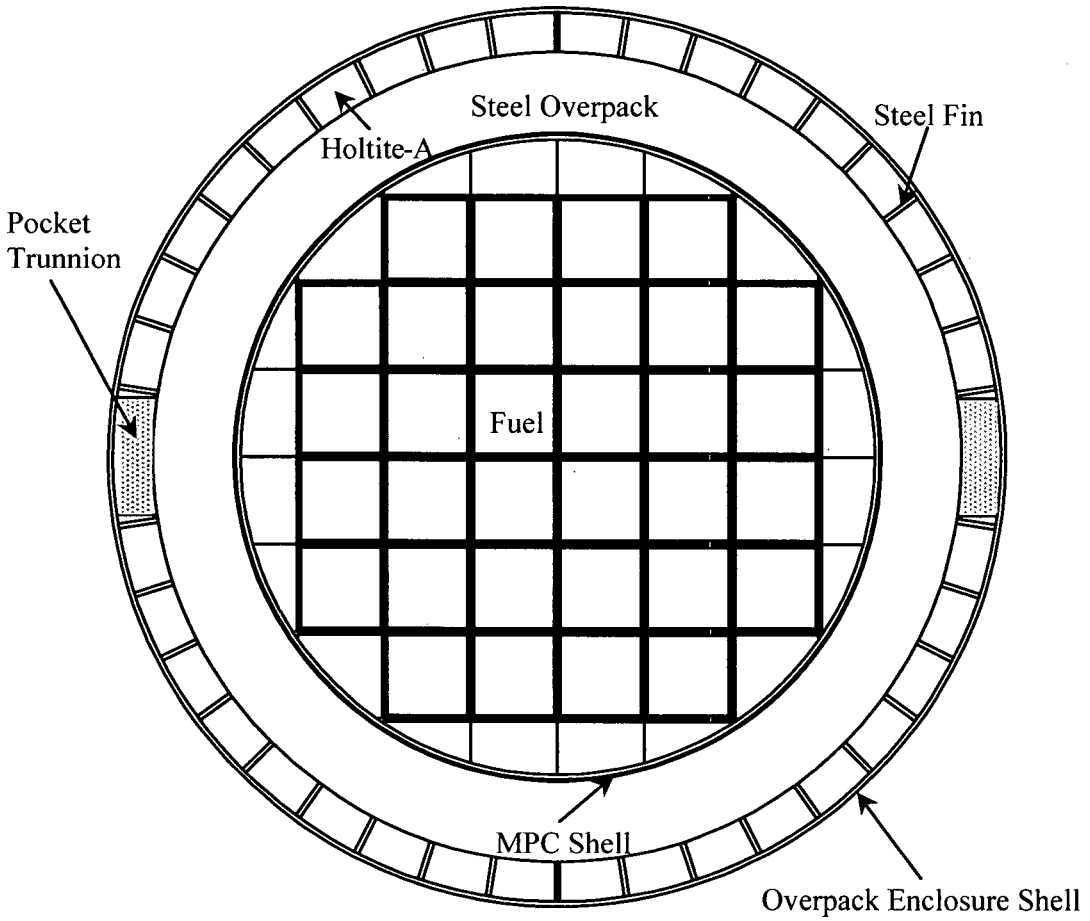

FIGURE 5.3.1; HI-STAR 100 OVERPACK WITH MPC-32 CROSS SECTIONAL VIEW AS MODELLED IN MCNP†

† This figure is drawn to scale using the MCNP plotter.

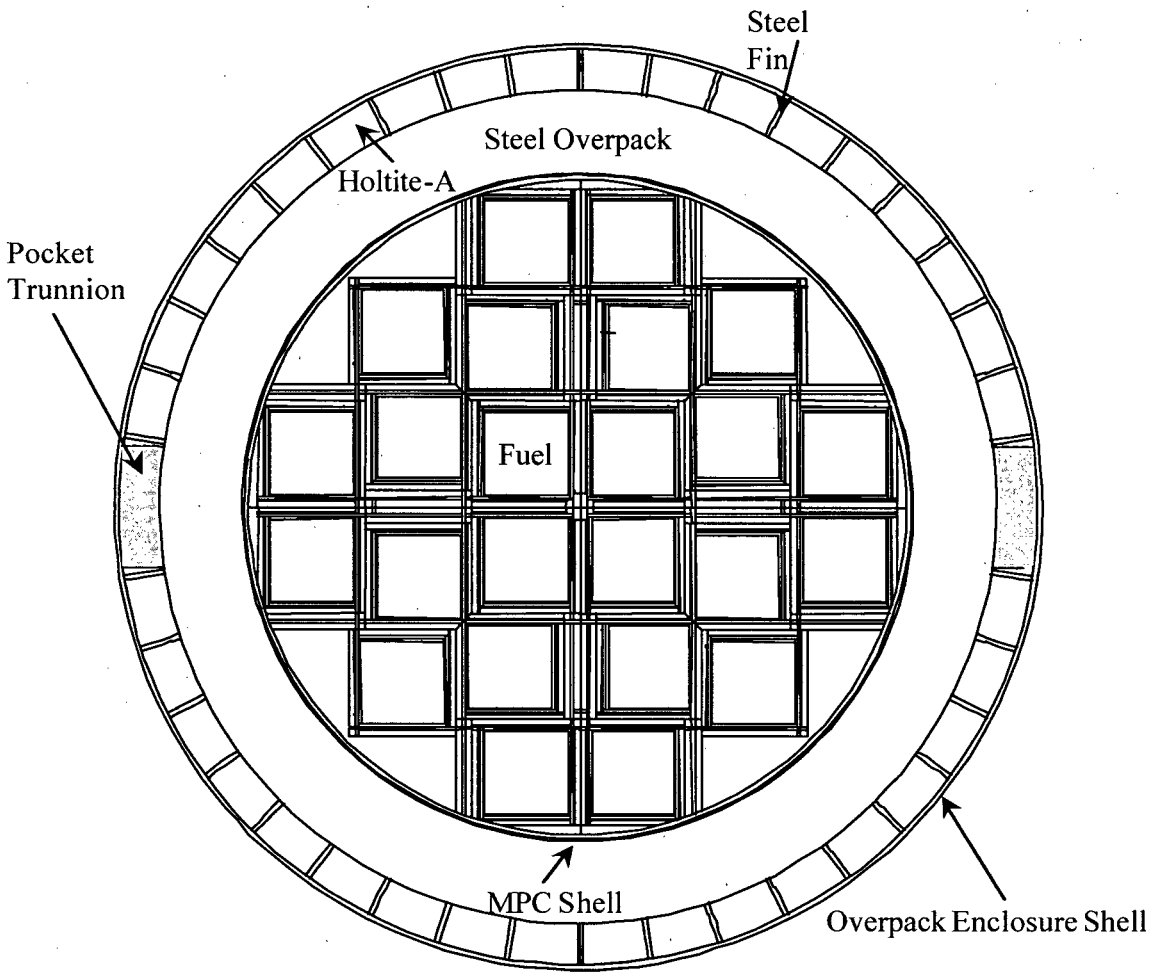

FIGURE 5.3.2; HI-STAR 100 OVERPACK WITH MPC-24 CROSS SECTIONAL VIEW AS MODELLED IN MCNP†

† This figure is drawn to scale using the MCNP plotter.

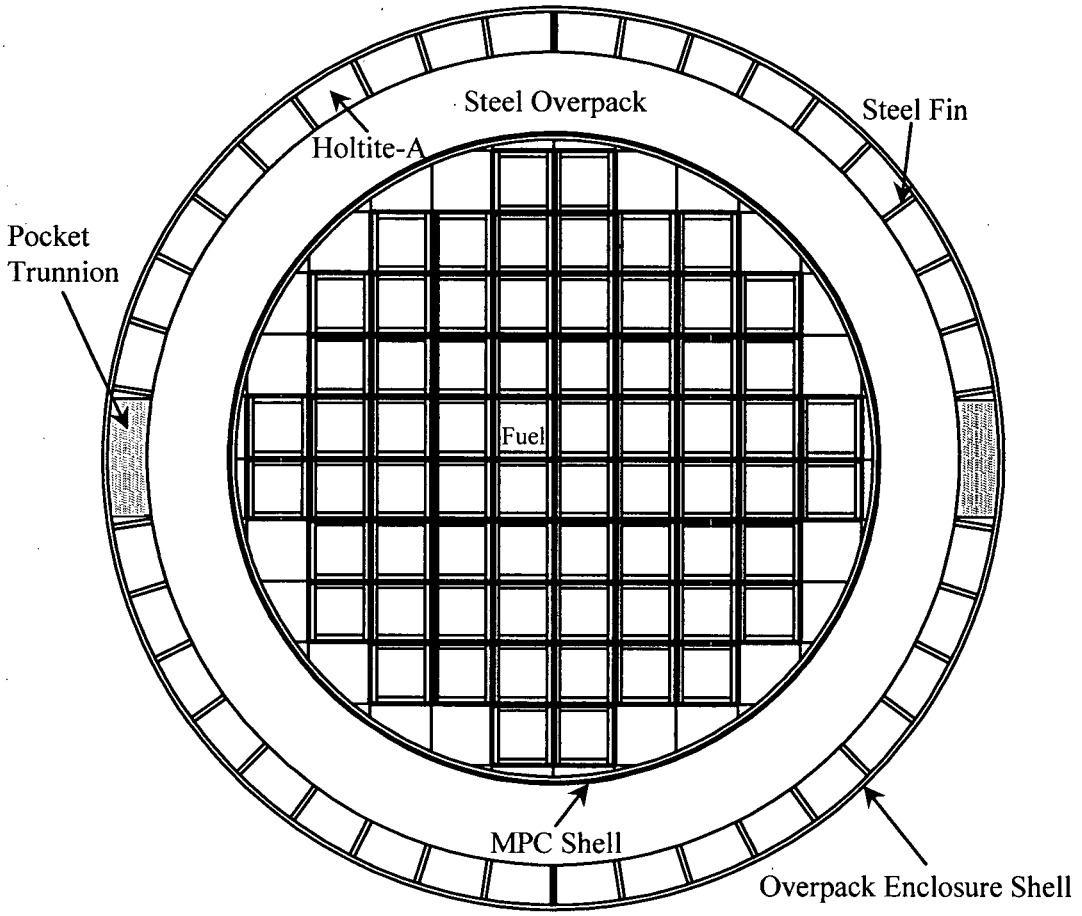

FIGURE 5.3.3; HI-STAR 100 OVERPACK WITH MPC-68 CROSS SECTIONAL VIEW AS MODELLED IN MCNP†

† This figure is drawn to scale using the MCNP plotter.

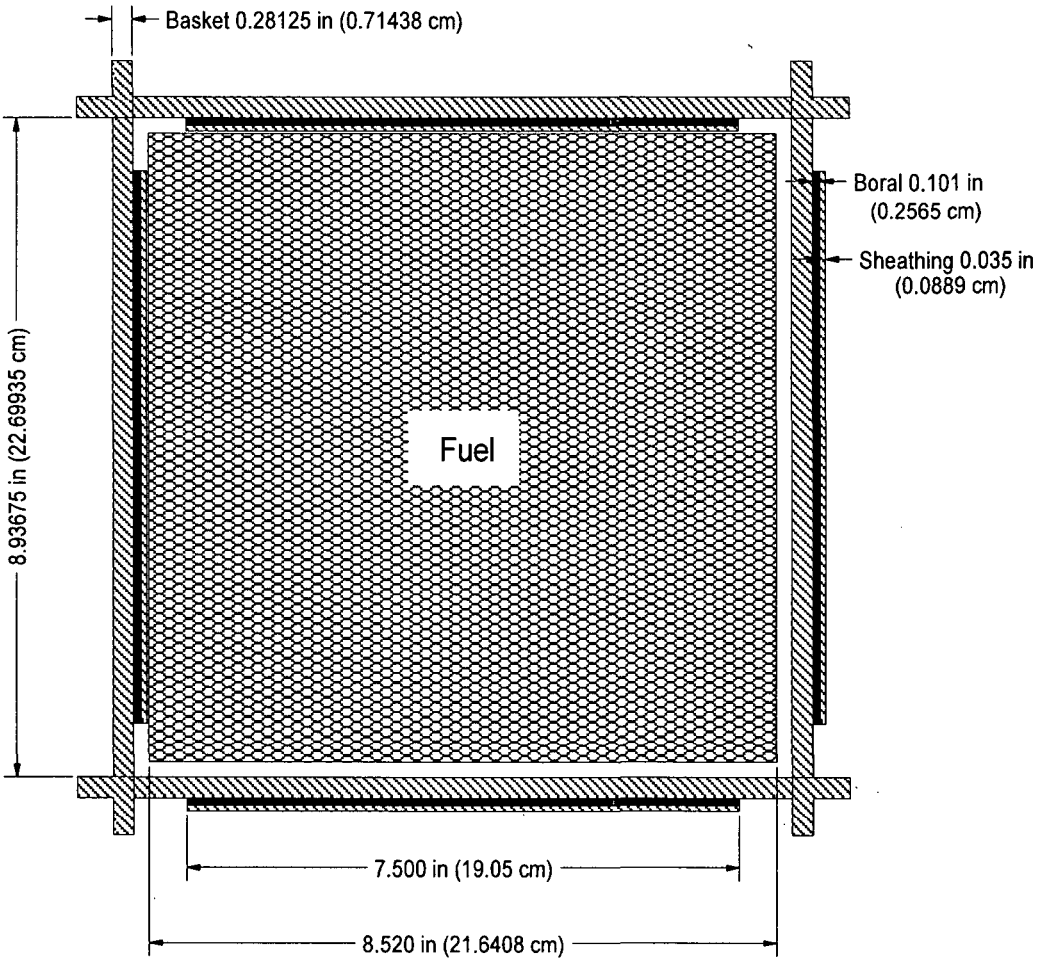

FIGURE 5.3.4; CROSS SECTIONAL VIEW OF AN MPC-32 BASKET CELL AS MODELED IN MCNP

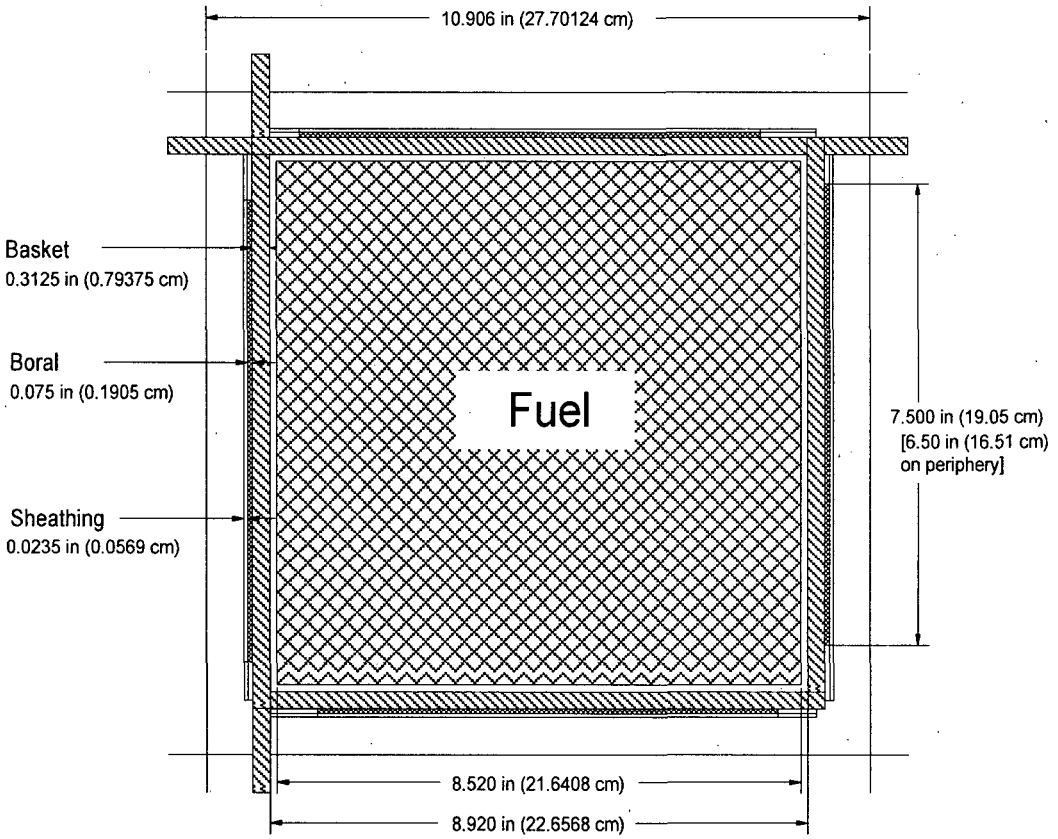

FIGURE 5.3.5; CROSS SECTIONAL VIEW OF AN MPC-24 BASKET CELL AS MODELED IN MCNP

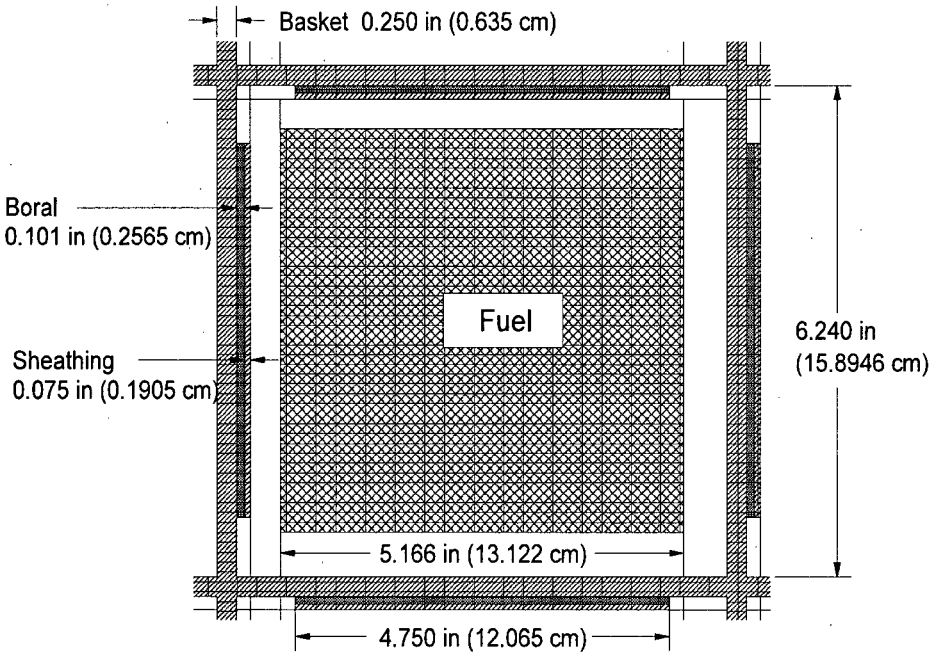

FIGURE 5.3.6; CROSS SECTIONAL VIEW OF AN MPC-68 BASKET CELL AS MODELED IN MCNP

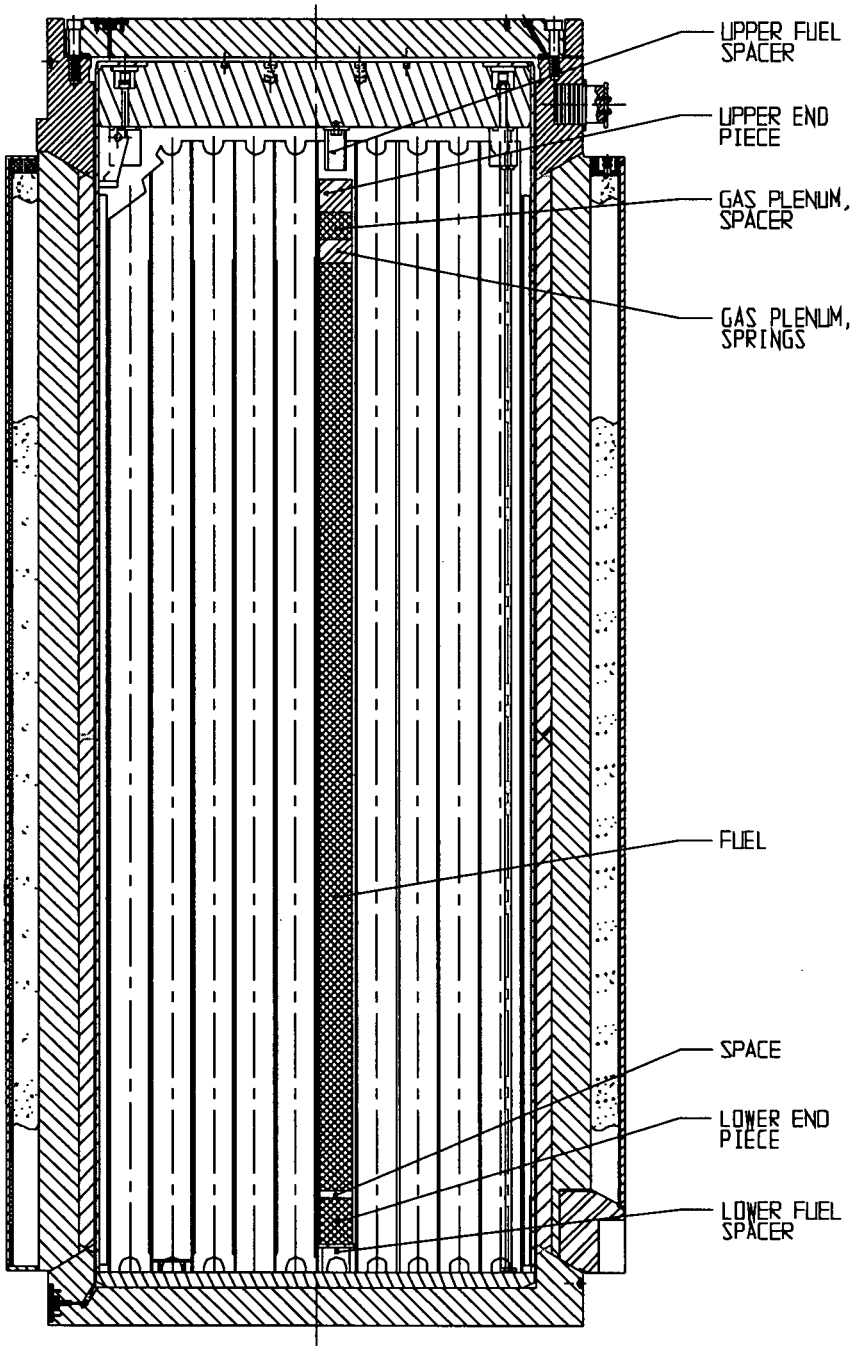

FIGURE 5.3.7; AXIAL LOCATION OF PWR DESIGN BASIS FUEL IN THE HI-STAR 100 SYSTEM

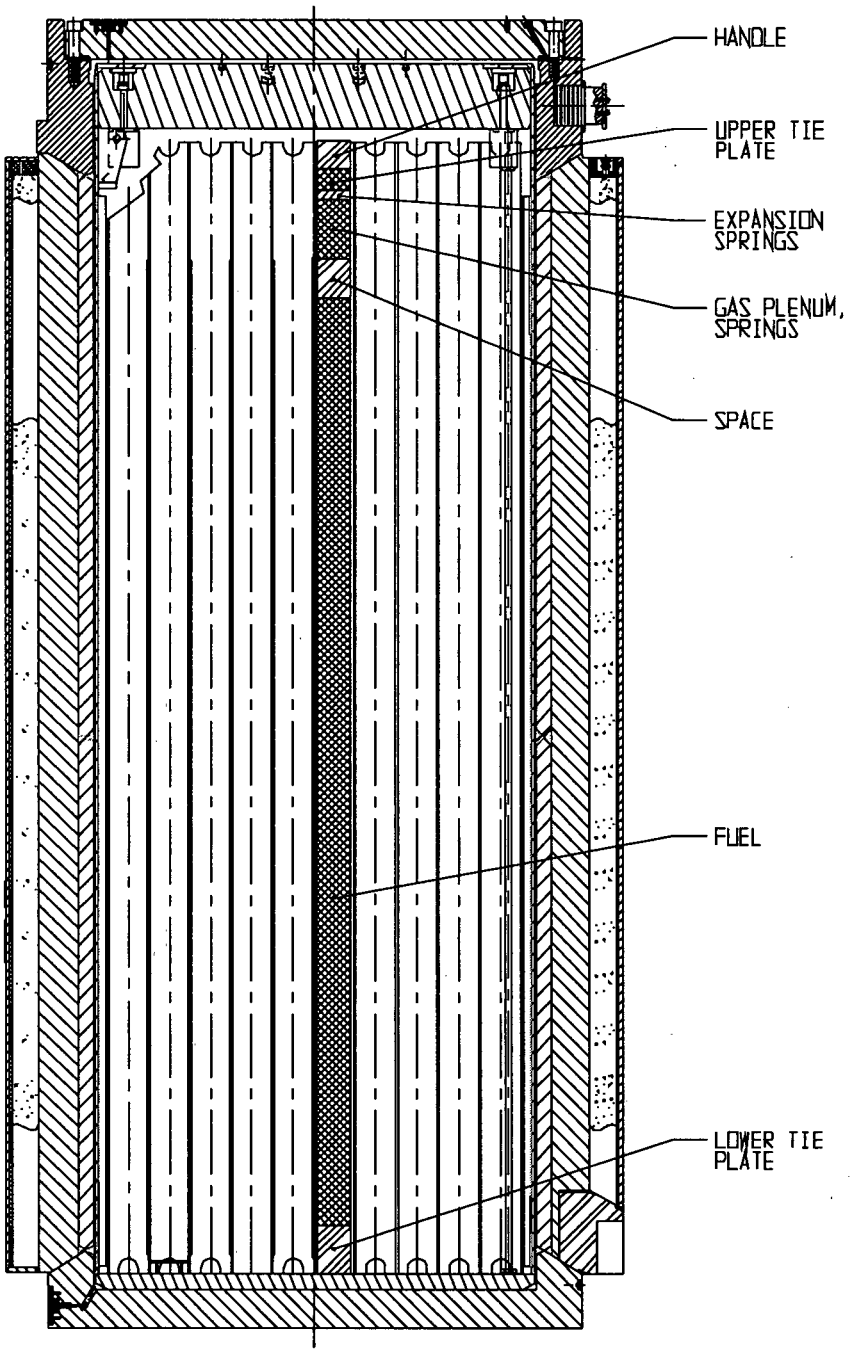

FIGURE 5.3.8; AXIAL LOCATION OF BWR DESIGN BASIS FUEL IN THE HI-STAR 100 SYSTEM

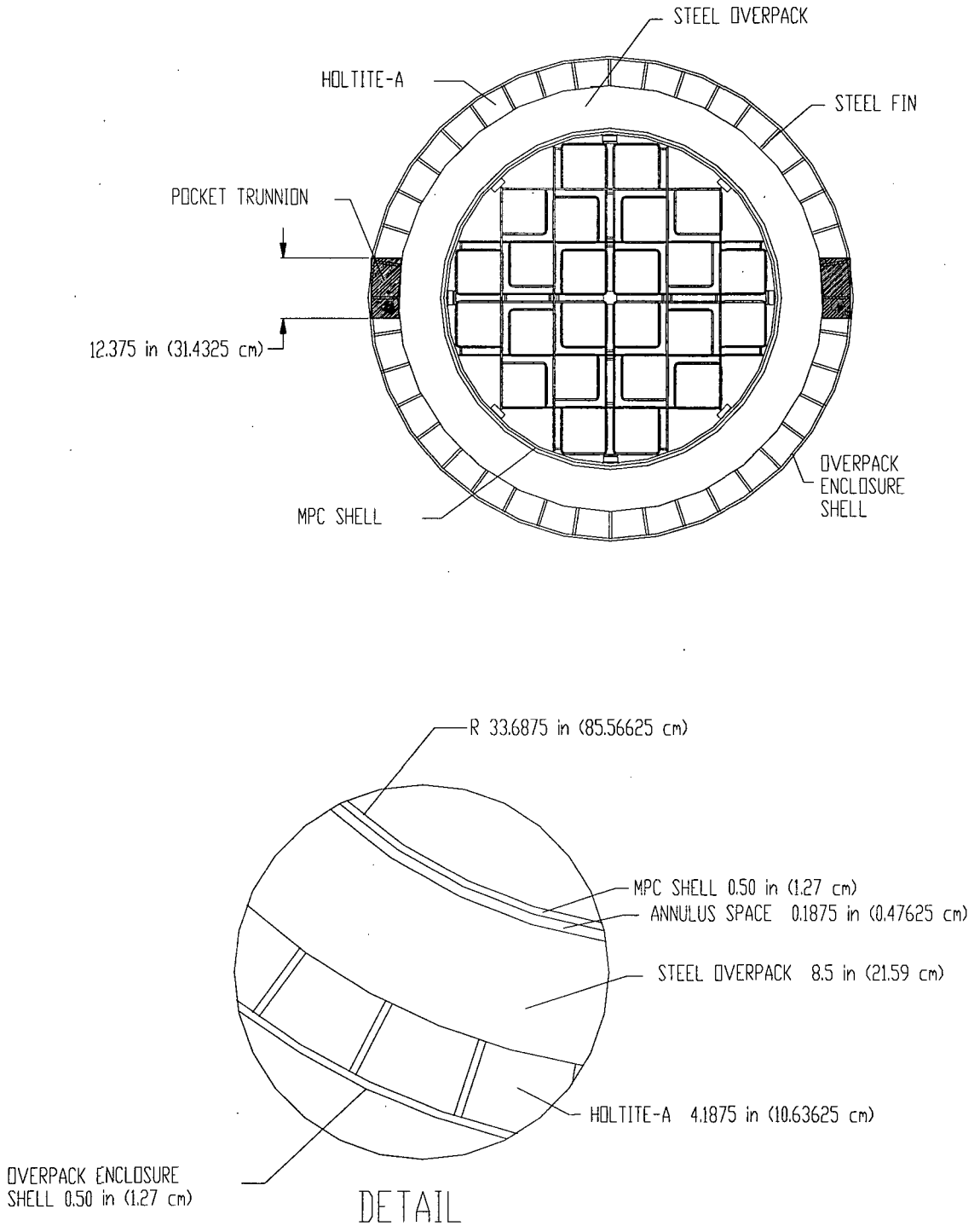

FIGURE 5.3.9; HI-STAR 100 OVERPACK CROSS SECTIONAL VIEW SHOWING THE THICKNESS OF THE MPC SHELL AND OVERPACK AS MODELED IN MCNP. THE MPC-24 IS SHOWN FOR ILLUSTRATIVE PURPOSES ONLY.

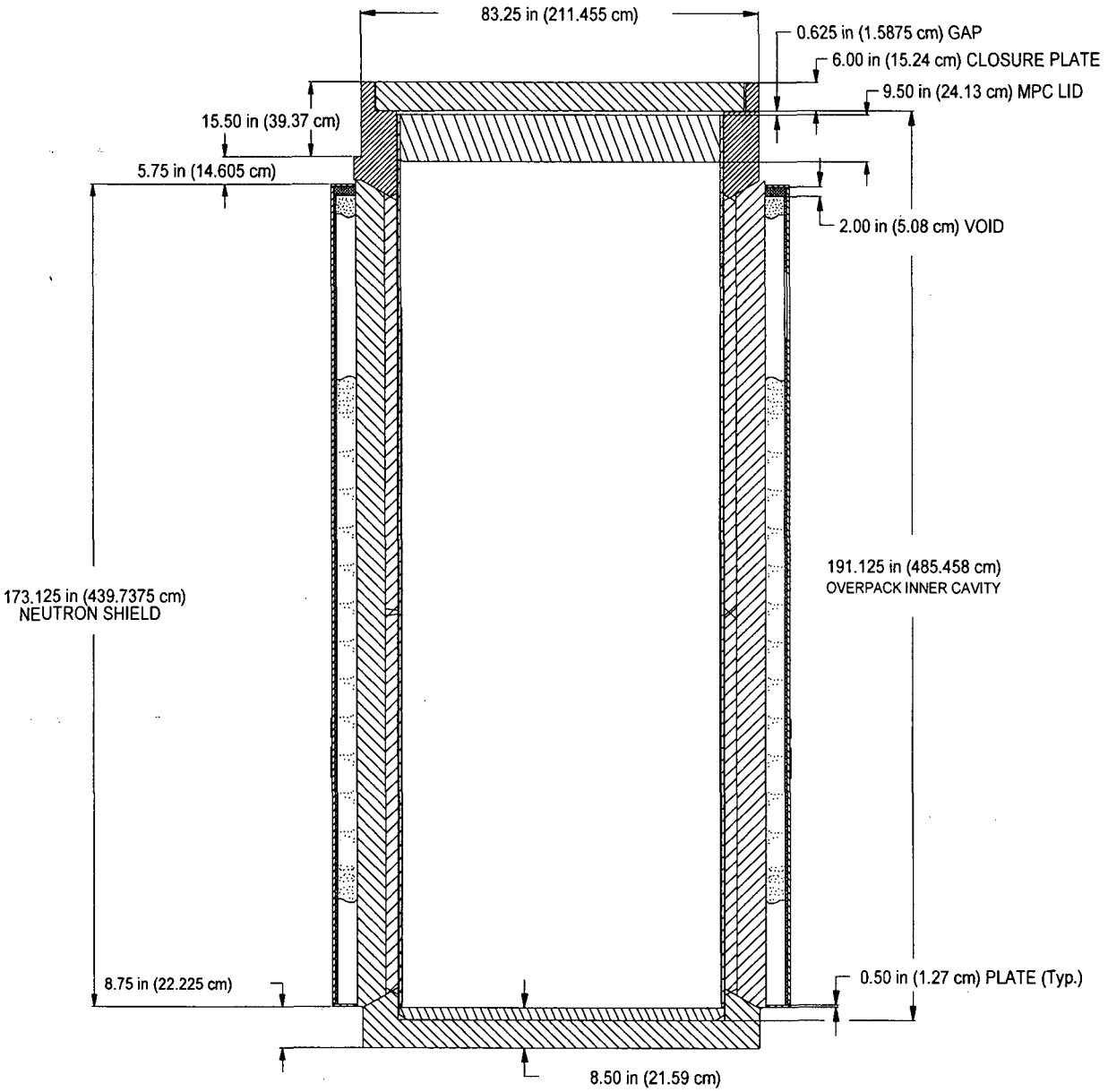

FIGURE 5.3.10; AXIAL VIEW OF HI-STAR 100 OVERPACK AND MPC WITH AXIAL DIMENSIONS SHOWN AS MODELED IN MCNP

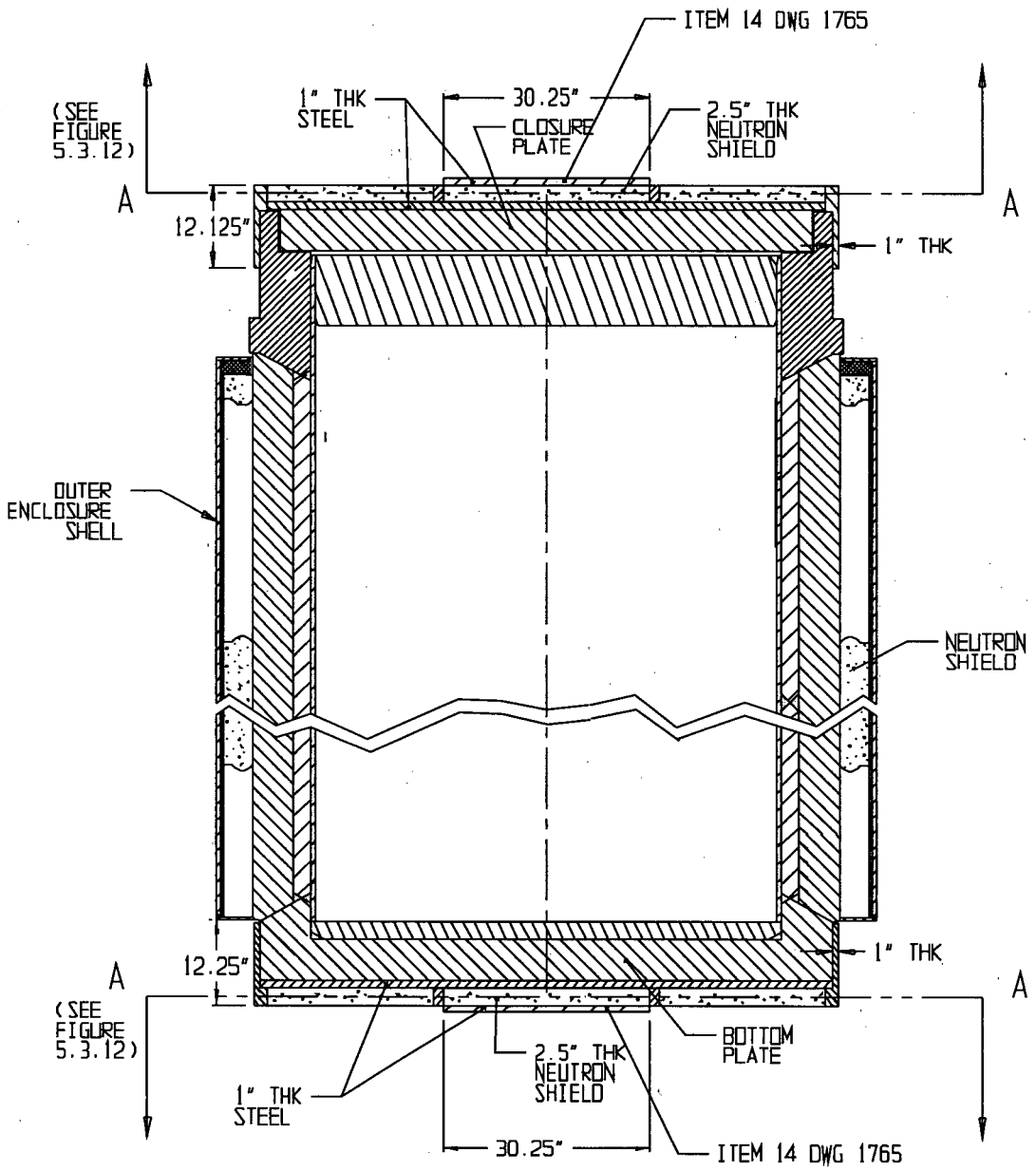

FIGURE 5.3.11; CROSS SECTION ELEVATION VIEW OF THE HI-STAR 100 SYSTEM WITH AS MODELED DIMENSIONS FOR THE IMPACT LIMITER

REPORT HI-951251 | REVISION 8

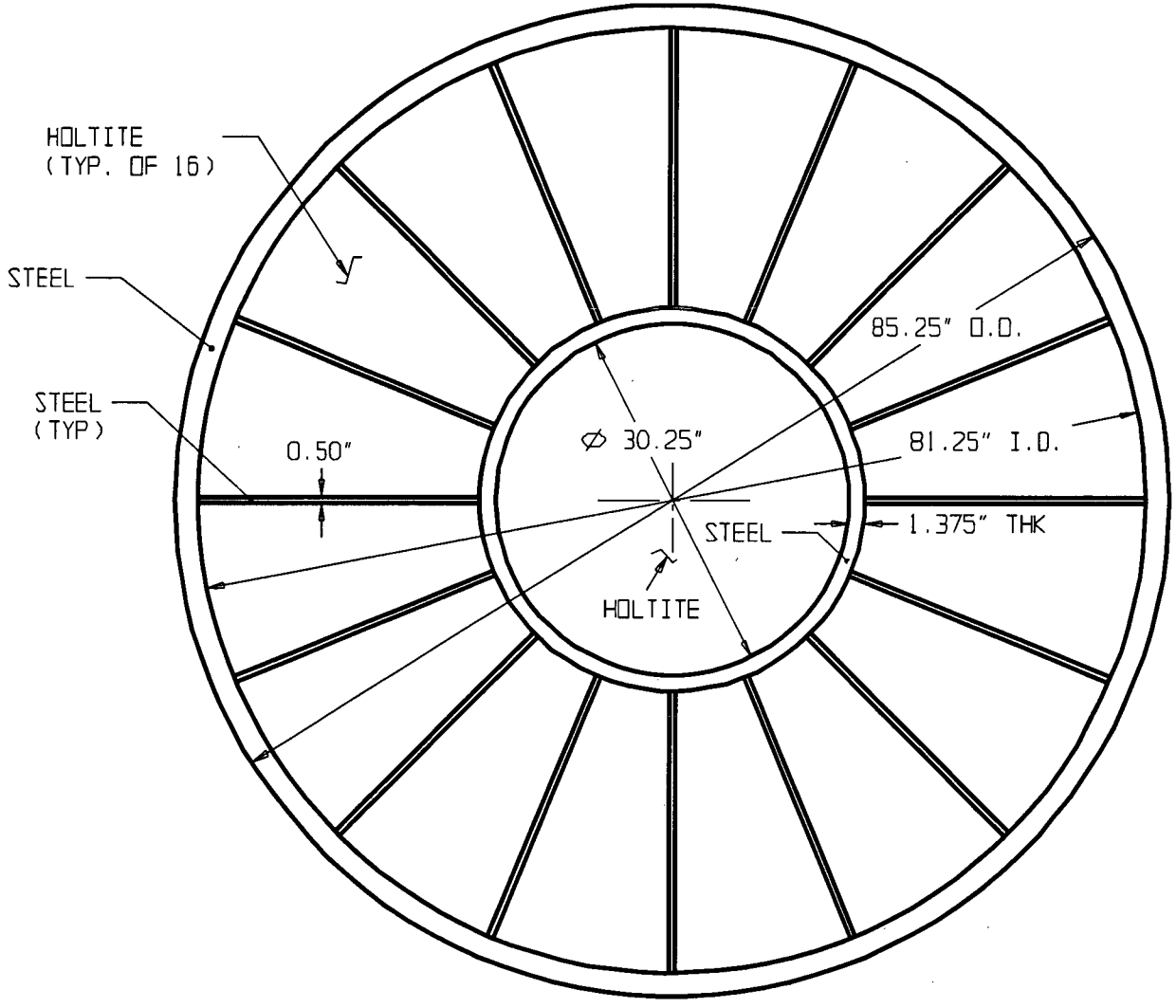

SECTION A - A

FIGURE 5.3.12; CROSS SECTIONAL VIEW OF IMPACT LIMITER WITH AS MODELED DIMENSIONS

5.4 SHIELDING EVALUATION

The MCNP-4A code[5.1.1] was used for all of the shielding analyses. MCNP is a continuous energy, three-dimensional, coupled neutron-photon-electron Monte Carlo transport code. Continuous energy cross section data is represented with sufficient energy points to permit linear-linear interpolation between these points. The individual cross section libraries used for each nuclide are those recommended by the MCNP manual. All of these data are based on ENDF/B-V data. MCNP has been extensively benchmarked against experimental data by the large user community. References [5.4.2], [5.4.3], and [5.4.4] are three examples of the benchmarking that has been performed.

The energy distribution of the source term, as described earlier, is used explicitly in the MCNP model. A different MCNP calculation is performed for each of the three source terms (neutron, decay gamma, and ^{60}Co). The axial distribution of the fuel source term is described in Table 1.2.15 and Figures 1.2.13 and 1.2.14. The PWR and BWR axial burnup distributions were obtained from References [5.4.5] and [5.4.6] respectively. These axial distributions were obtained from operating plants and are representative of PWR and BWR fuel with burnups greater than 30,000 MWD/MTU. The ^{60}Co source in the hardware was assumed to be uniformly distributed over the appropriate regions. The axial distribution used for the Trojan Plant fuel was similar but not identical to the generic PWR distribution. Table 1.2.15 and Figure 1.2.13a present the axial burnup distribution used for the Trojan Plant fuel taken from the Trojan FSAR [5.1.6].

It has been shown that the neutron source strength varies as the burnup level raised by the power of 4.2. Since this relationship is non-linear and since the burnup in the axial center of a fuel assembly is greater than the average burnup, the neutron source strength in the axial center of the assembly is greater than the relative burnup times the average neutron source strength. In order to account for this effect, the neutron source strength in each of the 10 axial nodes listed in Table 1.2.15 was determined by multiplying the average source strength by the relative burnup level raised to the power of 4.2. The peak relative burnups listed in Table 1.2.15 for the generic PWR and BWR fuels are 1.105 and 1.195 respectively. Using the power of 4.2 relationship results in a 37.6% ($1.105^{4.2}/1.105$) and 76.8% ($1.195^{4.2}/1.195$) increase in the neutron source strength in the peak nodes for the PWR and BWR fuel respectively. The total neutron source strength increases by 15.6% for the PWR fuel assemblies and 36.9% for the BWR fuel assemblies.

MCNP was used to calculate dose at the various desired locations. MCNP calculates neutron or photon flux and these values can be converted into dose by the use of dose response functions. This is done internally in MCNP and the dose response functions are listed in the input file. The response functions used in these calculations are listed in Table 5.4.1 and were taken from ANSI/ANS 6.1.1, 1977 [5.4.1].

The dose rate at the various locations were calculated with MCNP using a two step process. The first step was to calculate the dose rate for each dose location per starting particle for each neutron and gamma group and each axial location in the end fittings. The second and last step was to multiply the dose rate per starting particle for each group by the source strength (i.e. particles/sec) in that group and sum the resulting dose rates for all groups in each dose location. The standard deviations of the various results were statistically combined to determine the standard deviation of the total dose in each dose location.

Figures 5.1.1 and 5.1.2 depict the dose point locations during normal and hypothetical accident conditions of transport. Dose point location 3a in Figure 5.1.1 covers two regions of different radii. The outermost region is 5.75 inches in height and the innermost region is 6.875 inches in height. The dose rate was calculated over both segments and the highest value was reported for dose location 3a. Dose point locations 1 through 4 in Figure 5.1.2 are conservatively located at a radial position that is approximately 1 meter from the outer radial surface of the bottom plate.

Tables 5.4.8, 5.4.9, 5.4.19, 5.4.29, and 5.4.32 provide the total dose rate on the surface of the HI-STAR 100 System for each burnup level and cooling time. Tables 5.4.10 through 5.4.13, 5.4.20, 5.4.21, 5.4.30, 5.4.31, 5.4.33, and 5.4.34 provide the total dose rate at 2 meters for normal conditions and at 1 meter for accident conditions for each burnup level and cooling time for the MPC-24, MPC-68 and the MPC-32. This information was used to determine the worst case burnup level and cooling time and corresponding maximum dose rates reported in Section 5.1.

Since MCNP is a statistical code, there is an uncertainty associated with the calculated values. In MCNP the uncertainty is expressed as the relative error which is defined as the standard deviation of the mean divided by the mean. Therefore, the standard deviation is represented as a percentage of the mean. The relative error for the total dose rates presented in this chapter were typically less than 2% and the relative error for the individual dose components was typically less than 5%.

5.4.1 Streaming Through Radial Steel Fins and Pocket Trunnions

The HI-STAR 100 overpack utilizes 0.5 inch thick radial channels for structural support and cooling. The attenuation of neutrons through steel is substantially less than the attenuation of neutrons through the neutron shield. Therefore, it is possible to have neutron streaming through the channels which could result in a localized dose peak. The reverse is true for photons which would result in a localized reduction in the photon dose. Analyses were performed to determine the magnitude of the dose peaks and depressions and the impact on localized dose as compared to average total dose. This effect was evaluated at the radial surface of the HI-STAR 100 System and a distance of two meters.

In addition to the radial channels, the pocket trunnions are essentially blocks of steel that are approximately 12 inches wide and 12 inches high. The effect of the pocket trunnion on neutron

streaming and photon transmission will be more substantial than the effect of a single fin. Therefore, analyses were performed to quantity this effect. Figures 5.3.7 and 5.3.8 illustrate the location of the pocket trunnion and its axial position relative to the active fuel.

The fuel loading pattern in the MPC-32, MPC-24 and the MPC-68, as depicted in Figures 5.3.1 through 5.3.3, is not cylindrical. Therefore, there is a potential to experience peaking as a result of azimuthal variations in the fuel loading. Since the MCNP models represent the fuel in the correct positions (i.e., cylindrical homogenization is not performed) the effect of azimuthal variations in the loading pattern is automatically accounted for in the calculations that are discussed below.

The effect of streaming through the pocket trunnion and the radial channels was analyzed using the full three-dimensional MCNP models of the MPC-24 and the MPC-68. The effect of peaking was calculated on the surface of the overpack adjacent to the pocket trunnion and dose locations 2a and 3a in Figures 5.1.1. The effect of peaking was also analyzed at 2 meters from the overpack at dose location 2 and at the axial height of the impact limiter. Dose location 3 was not analyzed at two meters because the dose at that point is less than the dose at location 2 as demonstrated in the tables at the end of this section. Figure 5.4.1 shows a quarter of the HI-STAR 100 overpack with 41 azimuthal bins drawn. There is one bin per steel fin and 3 bins in each neutron shield region. This azimuthal binning structure was used over the axial height of the overpack. The dose was calculated in each of these bins and then compared to the average dose calculated over the surface to determine a peak-to-average ratio for the dose in that bin. The azimuthal location of the pocket trunnion is shown in Figure 5.4.1. The pocket trunnion was modeled as solid steel. During shipping, a steel rotation trunnion or plug shall be placed in the pocket trunnion recess. To conservatively evaluate the peak to average ratio, the pocket trunnion is assumed to be solid steel.

Table 5.4.14 provides representative peak-to-average ratios that were calculated for the various dose components and locations. Table 5.4.15 presents the dose rates at the dose locations analyzed including the effect of peaking. These results can be compared with the surface average results in Tables 5.1.1, 5.1.3, 5.1.4, and 5.1.6. The peak dose on the surface of the overpack at dose location 2a occurs at a steel channel (fin). This is evident by the high neutron peaking at dose location 2a on the surface of the overpack. The dose rate at the pocket trunnion, in those overpacks containing pocket trunnions, is higher than the dose rate at dose location 2 on the surface of the overpack. However, these results clearly indicate that, at two meters, the peaking associated with the pocket trunnion is not present and that the peak dose location is #2.

The MPC-32 was not explicitly analyzed to determine peak-to-average ratios. This is acceptable because the peaking outside the HI-STAR for the MPC-32 will be similar if not smaller than in the MPC-24 due to the fact that the fuel assemblies in the MPC-24 are not as closely positioned to each other as in the MPC-32. Section 5.5, Regulatory Compliance, presents results which take

into account peaking due to radiation streaming or azimuthal variation. For the MPC-32, the peak-to-average values calculated for the MPC-24 were used.

5.4.2 Damaged Fuel Post-Accident Shielding Evaluation

As discussed in Subsection 5.2.5.2, the analysis presented below, even though it is for damaged fuel, demonstrates the acceptability of transporting intact Humboldt Bay 6x6 and intact Dresden 1 6x6 fuel assemblies. As discussed in Subsection 5.2.8, the Trojan damaged fuel and fuel debris were not explicitly analyzed because they are bounded by the intact fuel assemblies.

For the damaged fuel and fuel debris accident condition, it is conservatively assumed the damaged fuel cladding ruptures and all the fuel pellets fall and collect at the bottom of the damaged fuel container. The inner dimension of the damaged fuel container, specified in the Design Drawings of Section 1.4, and the design basis damaged fuel and fuel debris assembly dimensions in Table 5.2.2 are used to calculate the axial height of the rubble in the damaged fuel container assuming 50% compaction. Neglecting the fuel pellet to cladding inner diameter gap, the volume of cladding and fuel pellets available for deposit is calculated assuming the fuel rods are solid. Using the volume in conjunction with the damaged fuel container, the axial height of rubble is calculated to be 80 inches.

Some of the 6x6 assemblies described in Table 5.2.2 were manufactured with Inconel grid spacers (the mass of inconel is listed in Table 5.2.2). The calculated ^{60}Co activity from these spacers was 66.7 curies for a burnup of 30,000 MWD/MTU and a cooling time of 18 years. Including this source with the total fuel gamma source for damaged fuel in Table 5.2.6 and dividing by the 80 inch rubble height provides a gamma source per inch of 3.47E+12 photon/s. Dividing the total neutron source for damaged fuel in Table 5.2.14 by 80 inches provides a neutron source per inch of 5.24E+5 neutron/s. These values are both bounded by the BWR design basis fuel gamma source per inch and neutron source per inch values of 5.03E+12 photon/s and 6.63E+5 neutron/s. These BWR design basis values were calculated by dividing the total source strengths as calculated from Tables 5.2.5 and 5.2.13 (39,500 MWD/MTU and 14 year cooling values) by the active fuel length of 144 inches. Additionally, a separate analysis added the calculated ^{60}Co activity from the Inconel grid spacers to the 1.0 to 1.5 MeV energy range of the gamma source rather than to the total of the fuel gamma source. While the gamma source in the 1.0 to 1.5 MeV range is not bounded, the resulting dose rate is still below the limit, since the contribution from the other energy ranges are lower. The resulting side dose rates from the damaged fuel assemblies are approximately 20 to 25% lower than the side dose rates from the design basis BWR intact fuel assemblies. Therefore, the design basis damaged fuel assembly is bounded by the design basis intact BWR fuel assembly for accident conditions. No explicit analysis of the damaged fuel dose rates are provided as they are bounded by the intact fuel analysis.

5.4.3 Mixed Oxide Fuel Evaluation

The source terms calculated for the Dresden Unit 1 GE 6x6 MOX fuel assemblies can be compared to the design basis source terms for the BWR assemblies which demonstrates that the MOX fuel source terms are bounded by the design basis source terms and no additional shielding analysis is needed.

Since the active fuel length of the MOX fuel assemblies is shorter than the active fuel length of the design basis fuel, the source terms must be compared on a per inch basis. Including the ^{60}Co source from grid spacers as calculated in the previous subsection (66.7 curies) with the total fuel gamma source for the MOX fuel in Table 5.2.16 and dividing by the 110 inch active fuel height provides a gamma source per inch of 2.41E+12 photons/s. Dividing the total neutron source for the MOX fuel assemblies in Table 5.2.17 by 110 inches provides a neutron source strength per inch of 3.67E+5 neutrons/s. These values are both bounded by the BWR design basis fuel gamma source per inch and neutron source per inch values of 5.03E+12 photons/s and 6.63E+5 neutrons/s. These BWR design basis values were calculated by dividing the total source strengths as calculated from Tables 5.2.5 and 5.2.13 (39,500 MWD/MTU and 14 year cooling values) by the active fuel length of 144 inches. This comparison shows that the MOX fuel source terms are bound by the design basis source terms. Therefore, no explicit analysis of dose rates is provided for MOX fuel.

Since the MOX fuel assemblies are Dresden Unit 1 6x6 assemblies, they can also be considered as damaged fuel. Using the same methodology as described in Subsection 5.4.2, the source term for the MOX fuel is calculated on a per inch basis assuming a post-accident rubble height of 80 inches. The resulting gamma and neutron source strengths are 3.31E+12 photons/s and 5.05E+5 neutrons/s. These values are also bounded by the design basis fuel gamma source per inch and neutron source per inch. Therefore, no explicit analysis of dose rates is provided for MOX fuel in a post-accident configuration.

5.4.4 Stainless Steel Clad Fuel Evaluation

Tables 5.4.22 through 5.4.24 present the dose rates from the stainless steel clad fuel at various dose locations around the HI-STAR 100 overpack for the MPC-24 and the MPC-68 for normal and hypothetical accident conditions. These dose rates are below the regulatory limits indicating that these fuel assemblies are acceptable for transport.

As described in Subsection 5.2.3, the source term for the stainless steel fuel was calculated conservatively with an artificial active fuel length of 144 inches. The end fitting masses of the stainless steel clad fuel are also assumed to be identical to the end fitting masses of the zircaloy clad fuel. In addition, the fuel assembly configuration used in the MCNP calculations was identical to the configuration used for the design basis fuel assemblies as described in Table 5.3.1.

5.4.5 Dresden Unit 1 Antimony-Beryllium Neutron Sources

Dresden Unit 1 has antimony-beryllium neutron sources which are placed in the water rod location of their fuel assemblies. These sources are steel rods which contain a cylindrical antimony-beryllium source which is 77.25 inches in length. The steel rod is approximately 95 inches in length. Information obtained from Dresden Unit 1 characterizes these sources in the following manner: "About one-quarter pound of beryllium will be employed as a special neutron source material. The beryllium produces neutrons upon gamma irradiation. The gamma rays for the source at initial start-up will be provided by neutron-activated antimony (about 865 curies). The source strength is approximately 1E+8 neutrons/second."

As stated above, beryllium produces neutrons through gamma irradiation and in this particular case antimony is used as the gamma source. The threshold gamma energy for producing neutrons from beryllium is 1.666 MeV. The outgoing neutron energy increases as the incident gamma energy increases. Sb-124, which decays by Beta decay with a half life of 60.2 days, produces a gamma of energy 1.69 MeV which is just energetic enough to produce a neutron from beryllium. Approximately 54% of the Beta decays for Sb-124 produce gammas with energies greater than or equal to 1.69 MeV. Therefore, the neutron production rate in the neutron source can be specified as 5.8E-6 neutrons per gamma (1E+8/865/3.7E+10/0.54) with energy greater than 1.666 MeV or 1.16E+5 neutrons/curie (1E+8/865) of Sb-124.

With the short half life of 60.2 days all of the initial Sb-124 is decayed and any Sb-124 that was produced while the neutron source was in the reactor is also decayed since these neutron sources are assumed to have the same minimum cooling time as the Dresden 1 fuel assemblies (array classes 6x6A, 6x6B, 6x6C, and 8x8A) of 18 years. Therefore, there are only two possible gamma sources which can produce neutrons from this antimony-beryllium source. The first is the gammas from the decay of fission products in the fuel assemblies in the MPC. The second gamma source is from Sb-124 which is being produced in the MPC from neutron activation from neutrons from the decay of fission products.

MCNP calculations were performed to determine the gamma source as a result of decay gammas from fuel assemblies and Sb-124 activation. The calculations explicitly modeled the 6x6 fuel assembly described in Table 5.2.2. A single fuel rod was removed and replaced by a guide tube. In order to determine the amount of Sb-124 that is being activated from neutrons in the MPC it was necessary to estimate the amount of antimony in the neutron source. The O.D. of the source was assumed to be the I.D. of the steel rod encasing the source (0.345 in.). The length of the source is 77.25 inches. The beryllium is assumed to be annular in shape encompassing the antimony. Using the assumed O.D. of the beryllium and the mass and length, the I.D. of the beryllium was calculated to be 0.24 inches. The antimony is assumed to be a solid cylinder with an O.D. equal to the I.D. of the beryllium. These assumptions are conservative since the antimony and beryllium are probably encased in another material which would reduce the mass

of antimony. A larger mass of antimony is conservative since the calculated activity of Sb-124 is directly proportional to the initial mass of antimony.

The number of gammas from fuel assemblies with energies greater than 1.666 MeV entering the 77.25 inch long neutron source was calculated to be 1.04E+8 gammas/sec which would produce a neutron source of 603.2 neutrons/sec (1.04E+8 * 5.8E-6). The steady state amount of Sb-124 activated in the antimony was calculated to be 39.9 curies. This activity level would produce a neutron source of 4.63E+6 neutrons/sec (39.9 * 1.16E+5) or 6.0E+4 neutrons/sec/inch (4.63E+6/77.25). These calculations conservatively neglect the reduction in antimony and beryllium which would have occurred while the neutron sources were in the core and being irradiated at full reactor power.

Since this is a localized source (77.25 inches in length) it is appropriate to compare the neutron source per inch from the design basis Dresden Unit 1 fuel assembly, 6x6, containing an Sb-Be neutron source to the design basis fuel neutron source per inch. This comparison, presented in Table 5.4.25, demonstrates that a Dresden Unit 1 fuel assembly containing an Sb-Be neutron source is bounded by the design basis fuel.

As stated above, the Sb-Be source is encased in a steel rod. Therefore, the gamma source from the activation of the steel was considered assuming a burnup of 120,000 MWD/MTU which is the maximum burnup assuming the Sb-Be source was in the reactor for the entire 18 year life of Dresden Unit 1. The cooling time assumed was 18 years which is the minimum cooling time for Dresden Unit 1 fuel. The source from the steel was bounded by the design basis fuel assembly. In conclusion, transport of a Dresden Unit 1 Sb-Be neutron source in a Dresden Unit 1 fuel assembly is acceptable and bounded by the current analysis.

5.4.6 Thoria Rod Canister

Based on a comparison of the gamma spectra from Tables 5.2.30 and 5.2.6 for the thoria rod canister and design basis 6x6 fuel assembly, respectively, it is difficult to determine if the thoria rods will be bounded by the 6x6 fuel assemblies. However, it is obvious that the neutron spectra from the 6x6, Table 5.2.14, bounds the thoria rod neutron spectra, Table 5.2.31, with a significant margin. In order to demonstrate that the gamma spectrum from the single thoria rod canister is bounded by the gamma spectrum from the design basis 6x6 fuel assembly, the gamma dose rate on the outer radial surface of the overpack was estimated conservatively assuming an MPC full of thoria rod canisters. This gamma dose rate was compared to an estimate of the dose rate from an MPC full of design basis 6x6 fuel assemblies. The gamma dose rate from the 6x6 fuel was higher than the dose rate from an MPC full of thoria rod canisters. This in conjunction with the significant margin in neutron spectrum and the fact that there is only one thoria rod canister clearly demonstrates that the thoria rod canister is acceptable for transport in the MPC-68 or the MPC-68F.

5.4.7 Trojan Fuel Contents

Tables 5.4.26 through 5.4.28 present the results for the Trojan MPC-24E for normal surface and 2 meter as well as accident results. These results are presented for a single burnup and cooling time of 42,000 MWD/MTU and 16 year cooling. This burnup and cooling time combination is shown in Tables 5.2.33 through 5.2.35 to bound the other allowable burnup and cooling time combinations for Trojan fuel. Since the Trojan MPCs will contain BPRAs, RCCAs, and TPDs, the source from these devices was considered in the analysis. The source from BPRAs and TPDs were added to the fuel source in the appropriate location. The mass from these devices was conservatively neglected. Separate calculations were performed for the BPRAs and the TPDs since both devices can not be present in the same fuel assembly. The results presented in Tables 5.4.26 through 5.4.28 represent the configuration (fuel plus non-fuel hardware: BPRA or TPD) that produces the highest dose rate at that location. Separate results for the different non-fuel hardware are not provided. Separate MCNP calculations were performed for the consideration of the RCCAs since this source is localized at the bottom of the MPC. The results for the RCCAs indicate that the presence of RCCAs will increase the dose rate on the surface of the overpack by a maximum of 1.3 mrem/hr and the dose rate at 2 meters will increase by a maximum of 0.09 mrem/hr for normal conditions. During accident conditions the dose rate will increase by a maximum of 6 mrem/hr with the presence of RCCAs.

These dose rates are less than the regulatory limits and therefore the Trojan contents are approved for transportation.

5.4.8 Trojan Antimony-Beryllium Neutron Sources

The analysis of the Trojan secondary antimony-beryllium neutron sources was performed in a manner very similar to that described above in Subsection 5.4.5. The secondary sources are basically BPRAs with four rods containing the antimony-beryllium with a length of 88 inches in each rod. As mentioned in Subsection 5.4.5, the antimony-beryllium source is a regenerative source in which the antimony is activated and the gammas released from the antimony induce a gamma,n reaction in the beryllium.

The steady state production of neutrons from this antimony-beryllium source was conservatively calculated in the MPC using an approach very similar to that described in Subsection 5.4.5. The depletion of antimony from the operation in the reactor core was conservatively neglected in the analysis. MCNP calculations were performed with explicitly modeled fuel assemblies in a Trojan MPC model to calculate the steady state activity of Sb-124 in the antimony-beryllium source due to the neutrons from the spent fuel. This activity level was used in a subsequent MCNP calculation to determine the gamma,n reaction rate in the beryllium. The gamma,n cross section for beryllium, which exhibits peaks at 1.5E-3 with lows at approximately 0.3E-3 barns, was used in MCNP as a reaction rate multiplier for the flux tallies. Additionally, the gamma,n reaction rate due to gammas from the spent fuel was determined. In the latter case, gammas from the spent

fuel with energies up to 11 MeV were considered in the analysis compared to an upper limit of 3 MeV for the cask dose rate analysis. Finally, the gamma,n reaction rate was converted to neutrons/sec to yield the neutron source per secondary source assembly. In this conversion process the spectrum of neutrons emitted from the Sb-Be source was determined based on the energy spectrum of the gammas reacting in the beryllium [5.4.7]. The neutron source strength per secondary source assembly was calculated to be 9.9E+5 neutrons/sec with more than 99% of these having an upper energy of 0.03 MeV. The remaining 1% of the secondary source neutrons had energies up to 0.74 MeV. This is a conservative estimate of the neutrons/sec from the secondary source because it neglects depletion of the antimony that has occurred during core operation and it assumes that all assemblies in the MPC are design basis Trojan fuel assemblies.

In order to determine the impact of the secondary neutron sources on the dose rates, MCNP calculations were performed. Since the dose rate that is closest to the regulatory limit is at 2 meters from the overpack, this was the only location considered in the analysis. Rather than calculate the average dose rate around the overpack at the 2 meter location, the dose rate was calculated for a specific location. Figure 5.4.2 shows the location where the dose rate was calculated. This location (an 8.2 inch diameter cylinder) is at 2 meters from the transport vehicle on a line drawn from the center of the MPC through the center of a corner assembly. The dose rate in this cylinder was calculated using the same axial segmentation as in the design basis calculations. In this analysis, the corner assembly was the only assembly considered to have the secondary source assembly. This choice of assembly position and dose location bounds all other possible locations for the single Trojan secondary source assembly permitted in any MPC.

The dose rates were calculated for the following combinations of fuel assemblies and non-fuel hardware inserts. In all dose rate calculations, both the neutron and gamma source from the secondary sources was considered.

1. One fuel assembly with secondary source assembly from cycles 1-4 and the remaining 23 fuel assemblies with BPRAs.
2. One fuel assembly with secondary source assembly from cycles 1-4 and the remaining 23 fuel assemblies with TPDs.
3. One fuel assembly with secondary source assembly from cycles 4-14 and the remaining 23 fuel assemblies with BPRAs.
4. One fuel assembly with secondary source assembly from cycles 4-14 and the remaining 23 fuel assemblies with TPDs.

The worst case dose rate from the configurations listed above was less than 9.8 mrem/hr from configuration 4. This value was conservatively calculated assuming all fuel assemblies were identical design basis Trojan fuel assemblies with design basis Trojan non-fuel hardware. This dose rate is slightly higher than the design basis dose rates for the Trojan fuel. However, this value is still below the regulatory limit of 10.0 mrem/hr. Therefore, the insertion of a single secondary source assembly into a Trojan MPC is acceptable for transport.

Table 5.4.1

FLUX-TO-DOSE CONVERSION FACTORS
(FROM [5.4.1])

Gamma Energy (MeV)	(rem/hr)/(photon/cm^2-s)
0.01	3.96E-06
0.03	5.82E-07
0.05	2.90E-07
0.07	2.58E-07
0.1	2.83E-07
0.15	3.79E-07
0.2	5.01E-07
0.25	6.31E-07
0.3	7.59E-07
0.35	8.78E-07
0.4	9.85E-07
0.45	1.08E-06
0.5	1.17E-06
0.55	1.27E-06
0.6	1.36E-06
0.65	1.44E-06
0.7	1.52E-06
0.8	1.68E-06
1.0	1.98E-06
1.4	2.51E-06
1.8	2.99E-06
2.2	3.42E-06

Table 5.4.1 (continued)

FLUX-TO-DOSE CONVERSION FACTORS
(FROM [5.4.1])

Gamma Energy (MeV)	**(rem/hr)/(photon/cm^2-s)**
2.6	3.82E-06
2.8	4.01E-06
3.25	4.41E-06
3.75	4.83E-06
4.25	5.23E-06
4.75	5.60E-06
5.0	5.80E-06
5.25	6.01E-06
5.75	6.37E-06
6.25	6.74E-06
6.75	7.11E-06
7.5	7.66E-06
9.0	8.77E-06
11.0	1.03E-05
13.0	1.18E-05
15.0	1.33E-05

Table 5.4.1 (continued)

FLUX-TO-DOSE CONVERSION FACTORS
(FROM [5.4.1])

Neutron Energy (MeV)	Quality Factor	(rem/hr)/(n/cm^2-s)†
2.5E-8	2.0	3.67E-6
1.0E-7	2.0	3.67E-6
1.0E-6	2.0	4.46E-6
1.0E-5	2.0	4.54E-6
1.0E-4	2.0	4.18E-6
1.0E-3	2.0	3.76E-6
1.0E-2	2.5	3.56E-6
0.1	7.5	2.17E-5
0.5	11.0	9.26E-5
1.0	11.0	1.32E-4
2.5	9.0	1.25E-4
5.0	8.0	1.56E-4
7.0	7.0	1.47E-4
10.0	6.5	1.47E-4
14.0	7.5	2.08E-4
20.0	8.0	2.27E-4

† Includes the Quality Factor.

Table 5.4.2

DELETED

Table 5.4.3

DELETED

Table 5.4.4

DELETED

Table 5.4.5

DELETED

Table 5.4.6

DELETED

Table 5.4.7

DELETED

Table 5.4.8

TOTAL DOSE RATES
DOSE LOCATION ON THE SURFACE OF THE HI-STAR 100 SYSTEM FOR NORMAL CONDITIONS
MPC-24 DESIGN BASIS ZIRCALOY CLAD FUEL WITH ZIRCALOY INCORE SPACERS
AT VARYING BURNUPS AND COOLING TIMES

Dose Point† Location	**24,500 MWD/MTU 6 Year Cooling (mrem/hr)**	**29,500 MWD/MTU 7 Year Cooling (mrem/hr)**	**34,500 MWD/MTU 9 Year Cooling (mrem/hr)**	**39,500 MWD/MTU 11 Year Cooling (mrem/hr)**	**44,500 MWD/MTU 14 Year Cooling (mrem/hr)**
2a	49.81	50.88	46.38	43.02	46.19
3a	95.80	108.16	113.72	124.43	138.47
1	35.33	37.42	36.18	35.89	34.85
2	29.01	28.87	26.11	26.57	28.24
3	27.02	29.30	29.26	29.94	30.19
4	23.73	26.05	26.43	27.40	28.05
5	1.00	1.64	2.41	3.22	4.15
6	125.44	127.01	114.18	104.20	90.02
10CFR71.47 Limit	1000.00 (2a,3a) 200.00 (1-6)	1000.00 (2a,3a) 200.00 (1-6)	1000.00 (2a,3a) 200.00 (1-6)	1000.00 (2a,3a) 200.00 (1-6)	1000.00 (2a,3a) 200.00 (1-6)

† Refer to Figure 5.1.1.

Table 5.4.9

TOTAL DOSE RATES
DOSE LOCATION ON THE SURFACE OF THE HI-STAR 100 SYSTEM FOR NORMAL CONDITIONS
MPC-68 DESIGN BASIS ZIRCALOY CLAD FUEL AT VARYING BURNUPS AND COOLING TIMES

Dose Point† Location	**10,000 MWD/MTU 5 Year Cooling (mrem/hr)**	**20,000 MWD/MTU 7 Year Cooling (mrem/hr)**	**24,500 MWD/MTU 8 Year Cooling (mrem/hr)**	**29,500 MWD/MTU 9 Year Cooling (mrem/hr)**	**34,500 MWD/MTU 11 Year Cooling (mrem/hr)**	**39,500 MWD/MTU 14 Year Cooling (mrem/hr)**	**44,500 MWD/MTU 19 Year Cooling (mrem/hr)**
2a	49.51	52.69	44.53	44.60	50.12	52.65	55.25
3a	139.50	154.42	132.09	129.62	132.20	115.66	103.70
1	34.25	39.29	34.23	35.33	37.96	35.72	33.64
2	25.50	27.53	24.21	27.97	31.12	32.05	33.07
3	34.44	37.75	32.25	31.43	31.69	27.33	22.81
4	32.63	35.76	30.52	29.69	29.91	25.74	21.42
5	0.14	0.60	0.64	1.03	1.58	2.01	2.53
6	112.26	121.21	103.06	98.97	97.96	82.26	65.73
10CFR71.47 Limit	1000.00 (2a,3a) 200.00 (1-6)	1000.00 (2a,3a) 200.00 (1-6)	1000.00 (2a,3a) 200.00 (1-6)	1000.00 (2a,3a) 200.00 (1-6)	1000.00 (2a,3a) 200.00 (1-6)	1000.00 (2a,3a) 200.00 (1-6)	1000.00 (2a,3a) 200.00 (1-6)

† Refer to Figure 5.1.1.

Table 5.4.10

TOTAL DOSE RATES
DOSE LOCATION AT TWO METERS FOR NORMAL CONDITIONS
MPC-24 DESIGN BASIS ZIRCALOY CLAD FUEL WITH ZIRCALOY INCORE SPACERS
AT VARYING BURNUPS AND COOLING TIMES

Dose Point† Location	**24,500 MWD/MTU 6 Year Cooling (mrem/hr)**	**29,500 MWD/MTU 7 Year Cooling (mrem/hr)**	**34,500 MWD/MTU 9 Year Cooling (mrem/hr)**	**39,500 MWD/MTU 11 Year Cooling (mrem/hr)**	**44,500 MWD/MTU 14 Year Cooling (mrem/hr)**
1	7.41	7.61	7.26	7.31	7.27
2	9.57	9.45	8.77	8.95	9.10
3	6.72	6.93	6.61	6.64	6.59
4	6.16	6.39	6.13	6.16	6.11
5	0.09	0.15	0.21	0.28	0.35
6	8.39	8.34	7.26	6.36	5.15
10CFR71.47 Limit	10.00	10.00	10.00	10.00	10.00

† Refer to Figure 5.1.1.

Table 5.4.11

TOTAL DOSE RATES
DOSE LOCATION AT TWO METERS FOR NORMAL CONDITIONS
MPC-68 DESIGN BASIS ZIRCALOY CLAD FUEL AT VARYING BURNUPS AND COOLING TIMES

Dose Point† Location	**10,000 MWD/MTU 5 Year Cooling (mrem/hr)**	**20,000 MWD/MTU 7 Year Cooling (mrem/hr)**	**24,500 MWD/MTU 8 Year Cooling (mrem/hr)**	**29,500 MWD/MTU 9 Year Cooling (mrem/hr)**	**34,500 MWD/MTU 11 Year Cooling (mrem/hr)**	**39,500 MWD/MTU 14 Year Cooling (mrem/hr)**	**44,500 MWD/MTU 19 Year Cooling (mrem/hr)**
1	6.67	7.33	6.58	7.05	7.59	7.34	7.07
2	8.32	8.71	8.03	8.94	9.62	9.55	9.39
3	6.66	7.20	6.31	6.44	6.62	6.02	5.36
4	6.43	6.98	6.09	6.15	6.32	5.70	5.03
5	0.02	0.06	0.07	0.10	0.15	0.19	0.24
6	6.55	6.85	5.77	5.34	5.01	3.87	2.65
10CFR71.47 Limit	10.00	10.00	10.00	10.00	10.00	10.00	10.00

† Refer to Figure 5.1.1.

Table 5.4.12

TOTAL DOSE RATES
DOSE LOCATION AT ONE METER FOR ACCIDENT CONDITIONS
MPC-24 DESIGN BASIS ZIRCALOY CLAD FUEL WITH ZIRCALOY INCORE SPACERS
AT VARYING BURNUPS AND COOLING TIMES

Dose Point† Location	**24,500 MWD/MTU 6 Year Cooling (mrem/hr)**	**29,500 MWD/MTU 7 Year Cooling (mrem/hr)**	**34,500 MWD/MTU 9 Year Cooling (mrem/hr)**	**39,500 MWD/MTU 11 Year Cooling (mrem/hr)**	**44,500 MWD/MTU 14 Year Cooling (mrem/hr)**
1	76.55	97.55	117.95	141.21	166.93
2	153.26	224.23	307.31	399.33	504.35
3	49.37	64.41	79.67	96.85	116.00
4	35.97	47.12	58.44	71.10	85.20
5	4.06	6.59	9.62	12.83	16.51
6	685.36	687.08	605.96	539.45	447.78
10CFR71.51 Limit	1000.00	1000.00	1000.00	1000.00	1000.00

† Refer to Figure 5.1.2.

Table 5.4.13

TOTAL DOSE RATES
DOSE LOCATION AT ONE METER FOR ACCIDENT CONDITIONS
MPC-68 DESIGN BASIS ZIRCALOY CLAD FUEL AT VARYING BURNUPS AND COOLING TIMES

Dose Point† Location	**10,000 MWD/MTU 5 Year Cooling (mrem/hr)**	**20,000 MWD/MTU 7 Year Cooling (mrem/hr)**	**24,500 MWD/MTU 8 Year Cooling (mrem/hr)**	**29,500 MWD/MTU 9 Year Cooling (mrem/hr)**	**34,500 MWD/MTU 11 Year Cooling (mrem/hr)**	**39,500 MWD/MTU 14 Year Cooling (mrem/hr)**	**44,500 MWD/MTU 19 Year Cooling (mrem/hr)**
1	51.38	86.18	82.43	108.56	145.23	169.25	198.52
2	62.71	172.74	179.75	275.87	403.87	504.00	622.86
3	31.39	49.39	46.51	59.30	77.64	88.84	102.65
4	26.31	39.33	36.57	45.32	58.13	65.34	74.36
5	0.66	2.70	2.84	4.55	6.92	8.80	11.04
6	629.12	668.09	564.75	530.59	509.65	408.69	300.71
10CFR71.51 Limit	1000.00	1000.00	1000.00	1000.00	1000.00	1000.00	1000.00

† Refer to Figure 5.1.2.

Table 5.4.14

PEAK-TO-AVERAGE RATIOS FOR THE DOSE COMPONENTS
AT VARIOUS LOCATIONS

Location	Fuel Gammas	Gammas from Neutrons	^{60}Co Gammas	Neutron
MPC-24				
Surface				
Pocket Trunnion	0.081	0.262	0.075	6.695
2a	0.713	0.955	0.407	2.362
3a	1.317	1.011	1.005	1.177
2 meter				
Pocket Trunnion	1.109	1.232	1.059	0.809
2	1.034	0.974	1.086	0.990
MPC-68				
Surface				
Pocket Trunnion	0.070	0.432	0.074	7.340
2a	0.737	0.977	1.123	2.284
3a	0.908	0.816	1.217	0.940
2 meter				
Pocket Trunnion	1.121	0.982	1.144	1.171
2	1.070	0.939	1.146	0.950

Table 5.4.15

DOSE RATES FOR NORMAL CONDITIONS SHOWING THE EFFECT OF PEAKING

Dose Point† Location	Fuel Gammas (mrem/hr)	Gammas from Neutrons (mrem/hr)	^{60}Co Gammas (mrem/hr)	Neutrons (mrem/hr)	Total (mrem/hr)
MPC-24					
Surface 44,500 MWD/MTU 14-Year Cooling					
Pocket Trunnion	0.15	0.37	1.98	97.92	100.42
2a	12.30	6.35	0.00	52.60	71.26
3a	0.40	0.67	28.67	128.27	158.01
2 meter 24,500 MWD/MTU 6-Year Cooling					
Pocket Trunnion	4.03	0.17	3.50	0.64	8.34
2	7.55	0.21	1.26	0.87	9.90
MPC-68					
Surface 34,500 MWD/MTU 11-Year Cooling					
Pocket Trunnion	0.25	0.45	1.97	77.42	80.09
2a	19.24	5.35	0.02	42.33	66.93
3a	0.33	0.12	115.34	34.69	150.49
2 meter 34,500 MWD/MTU 11-Year Cooling					
Pocket Trunnion	3.23	0.46	2.06	3.03	8.77
2	5.80	0.68	0.74	2.69	9.91

† Refer to Figure 5.1.1.

Table 5.4.16

DELETED

Table 5.4.17

DELETED

Table 5.4.18

DELETED

Table 5.4.19

TOTAL DOSE RATES
DOSE LOCATION ON THE SURFACE OF THE HI-STAR 100 SYSTEM FOR NORMAL CONDITIONS
MPC-24 DESIGN BASIS ZIRCALOY CLAD FUEL WITH NON-ZIRCALOY INCORE SPACERS
AT VARYING BURNUPS AND COOLING TIMES

Dose Point† Location	**24,500 MWD/MTU 9 Year Cooling (mrem/hr)**	**29,500 MWD/MTU 11 Year Cooling (mrem/hr)**	**34,500 MWD/MTU 13 Year Cooling (mrem/hr)**	**39,500 MWD/MTU 15 Year Cooling (mrem/hr)**	**44,500 MWD/MTU 18 Year Cooling (mrem/hr)**
2a	42.91	42.11	43.11	45.08	46.24
3a	69.70	74.06	83.00	96.79	111.87
1	25.77	25.19	25.54	26.31	26.75
2	26.97	26.54	27.34	28.35	28.62
3	19.70	19.86	20.87	22.23	23.47
4	17.23	17.64	18.84	20.37	21.85
5	0.89	1.40	2.07	2.77	3.58
6	87.60	80.03	74.35	69.97	63.35
10CFR71.47 Limit	1000.00 (2a,3a) 200.00 (1-6)	1000.00 (2a,3a) 200.00 (1-6)	1000.00 (2a,3a) 200.00 (1-6)	1000.00 (2a,3a) 200.00 (1-6)	1000.00 (2a,3a) 200.00 (1-6)

† Refer to Figure 5.1.1.

Table 5.4.20

TOTAL DOSE RATES
DOSE LOCATION AT TWO METERS FOR NORMAL CONDITIONS
MPC-24 DESIGN BASIS ZIRCALOY CLAD FUEL WITH NON-ZIRCALOY INCORE SPACERS
AT VARYING BURNUPS AND COOLING TIMES

Dose Point† Location	**24,500 MWD/MTU 9 Year Cooling (mrem/hr)**	**29,500 MWD/MTU 11 Year Cooling (mrem/hr)**	**34,500 MWD/MTU 13 Year Cooling (mrem/hr)**	**39,500 MWD/MTU 15 Year Cooling (mrem/hr)**	**44,500 MWD/MTU 18 Year Cooling (mrem/hr)**
1	6.42	6.24	6.29	6.42	6.40
2	9.51	9.16	9.18	9.27	9.09
3	5.68	5.52	5.58	5.70	5.71
4	5.08	4.96	5.03	5.16	5.19
5	0.08	0.12	0.18	0.24	0.30
6	5.84	5.19	4.62	4.13	3.47
10CFR71.47 Limit	10.00	10.00	10.00	10.00	10.00

† Refer to Figure 5.1.1.

Table 5.4.21

TOTAL DOSE RATES
DOSE LOCATION AT ONE METER FOR ACCIDENT CONDITIONS
MPC-24 DESIGN BASIS ZIRCALOY CLAD FUEL WITH NON-ZIRCALOY INCORE SPACERS
AT VARYING BURNUPS AND COOLING TIMES

Dose Point† Location	**24,500 MWD/MTU 9 Year Cooling (mrem/hr)**	**29,500 MWD/MTU 11 Year Cooling (mrem/hr)**	**34,500 MWD/MTU 13 Year Cooling (mrem/hr)**	**39,500 MWD/MTU 15 Year Cooling (mrem/hr)**	**44,500 MWD/MTU 18 Year Cooling (mrem/hr)**
1	62.33	76.36	95.99	117.23	140.85
2	145.00	201.06	275.44	354.15	442.83
3	40.70	51.15	65.54	81.04	98.36
4	29.39	37.13	47.76	59.20	72.01
5	3.59	5.63	8.26	11.03	14.21
6	478.28	429.22	388.56	354.69	306.90
10CFR71.51 Limit	1000.00	1000.00	1000.00	1000.00	1000.00

† Refer to Figure 5.1.2.

Table 5.4.22

DOSE RATES FOR
MPC-68 DESIGN BASIS STAINLESS STEEL CLAD FUEL
22,500 MWD/MTU AND 16-YEAR COOLING

Dose Point† Location	Fuel Gammas†† (mrem/hr)	^{60}Co Gammas (mrem/hr)	Neutrons (mrem/hr)	Totals (mrem/hr)
Dose Location at Surface for Normal Condition				
1	2.91	9.19	1.00	13.09
2a	39.68	0.00	1.20	40.88
3a	0.62	40.84	2.60	44.07
4	0.45	9.49	0.53	10.47
5	0.02	0.01	0.10	0.12
6	2.37	32.43	1.37	36.18
10CFR71.47 Limit				200.00
Dose Location at Two Meters for Normal Condition				
1	3.45	1.00	0.17	4.63
2	7.71	0.27	0.19	8.18
3	2.26	1.35	0.12	3.73
4	1.67	1.43	0.11	3.21
5	0.00	0.00	0.01	0.01
6	0.20	1.89	0.03	2.12
10CFR71.47 Limit				10.00
Dose Location at One Meter for Accident Condition				
1	9.43	10.90	7.95	28.29
2	46.22	0.23	25.97	72.42
3	3.58	7.41	4.06	15.05
4	2.00	6.60	2.91	11.51
5	0.01	0.07	0.48	0.57
6	11.14	183.23	5.34	199.71
10CFR71.51 Limit				1000.00

Note: The more conservative limit of 200 mrem/hr was applied for dose locations 2a and 3a while dose locations 2 and 3 were not analyzed.

† Refer to Figures 5.1.1 and 5.1.2.

†† Gammas generated by neutron capture and gammas from incore spacers are included with fuel gammas.

Table 5.4.23

DOSE RATES FOR
MPC-24 DESIGN BASIS STAINLESS STEEL CLAD FUEL
30,000 MWD/MTU AND 19-YEAR COOLING

Dose Point† Location	Fuel Gammas†† (mrem/hr)	^{60}Co Gammas (mrem/hr)	Neutrons (mrem/hr)	Totals (mrem/hr)
Dose Location at Surface for Normal Condition				
1	2.40	5.54	4.27	12.22
2a	35.54	0.01	4.41	39.96
3a	0.66	11.31	24.60	36.57
4	0.73	3.65	4.11	8.49
5	0.12	0.01	0.82	0.94
6	4.36	22.14	6.65	33.15
10CFR71.47 Limit				200.00
Dose Location at Two Meters for Normal Condition				
1	3.05	0.69	0.76	4.50
2	7.23	0.23	0.83	8.29
3	2.47	0.66	0.72	3.85
4	1.95	0.67	0.69	3.30
5	0.01	0.00	0.07	0.08
6	0.30	1.53	0.25	2.08
10CFR71.47 Limit				10.00
Dose Location at One Meter for Accident Condition				
1	7.57	6.83	32.78	47.18
2	39.78	0.24	108.52	148.54
3	4.96	3.96	23.27	32.19
4	2.85	3.00	17.13	22.99
5	0.02	0.05	3.69	3.76
6	22.73	123.24	28.03	174.00
10CFR71.51 Limit				1000.00

Note: The more conservative limit of 200 mrem/hr was applied for dose locations 2a and 3a while dose locations 2 and 3 were not analyzed.

† Refer to Figures 5.1.1 and 5.1.2.

†† Gammas generated by neutron capture and gammas from incore spacers are included with fuel gammas.

Table 5.4.24

DOSE RATES FOR
MPC-24 DESIGN BASIS STAINLESS STEEL CLAD FUEL
40,000 MWD/MTU AND 24-YEAR COOLING

Dose Point† Location	Fuel Gammas†† (mrem/hr)	^{60}Co Gammas (mrem/hr)	Neutrons (mrem/hr)	Totals (mrem/hr)
Dose Location at Surface for Normal Condition				
1	2.12	5.80	11.10	19.02
2a	28.04	0.00	13.06	41.10
3a	0.78	11.82	63.88	76.48
4	0.66	3.82	10.68	15.16
5	0.30	0.01	2.13	2.43
6	4.44	23.15	17.25	44.84
10CFR71.47 Limit				200.00
Dose Location at Two Meters for Normal Condition				
1	2.55	0.72	1.98	5.26
2	5.82	0.24	2.23	8.29
3	2.06	0.69	1.86	4.62
4	1.64	0.70	1.78	4.11
5	0.02	0.00	0.19	0.21
6	0.25	1.60	0.65	2.49
10CFR71.47 Limit				10.00
Dose Location at One Meter for Accident Condition				
1	5.88	7.14	85.12	98.14
2	30.69	0.25	281.83	312.76
3	3.85	4.14	60.42	68.41
4	2.24	3.14	44.48	49.86
5	0.04	0.05	9.57	9.66
6	17.44	128.89	72.74	219.07
10CFR71.51 Limit				1000.00

Note: The more conservative limit of 200 mrem/hr was applied for dose locations 2a and 3a while dose locations 2 and 3 were not analyzed.

† Refer to Figures 5.1.1 and 5.1.2.

†† Gammas generated by neutron capture and gammas from incore spacers are included with fuel gammas.

Table 5.4.25

COMPARISON OF NEUTRON SOURCE PER INCH PER SECOND FOR DESIGN BASIS 7X7 FUEL AND DESIGN BASIS DRESDEN UNIT 1 FUEL

Assembly	**Active fuel length (inch)**	**Neutrons per sec per inch**	**Neutrons per sec per inch with Sb-Be source**	**Reference for neutrons per sec per inch**
7x7 design basis	144	6.63E+5	N/A	Table 5.2.13 39.5 GWD/MTU and 14 year cooling
6x6 design basis	110	3.81E+5	4.41E+5	Table 5.2.14
6x6 design basis MOX	110	3.67E+5	4.27E+5	Table 5.2.17

Table 5.4.26

DOSE RATES AT THE SURFACE OF THE HI-STAR 100 SYSTEM FOR NORMAL CONDITIONS
MPC-24 WITH TROJAN ZIRCALOY CLAD FUEL WITH NON-ZIRCALOY INCORE SPACERS
42,000 MWD/MTU AND 16-YEAR COOLING

Dose Point† Location	Fuel Gammas†† (mrem/hr)	Gammas from Incore Spacers (mrem/hr)	^{60}Co Gammas (mrem/hr)	Neutrons (mrem/hr)	Totals (mrem/hr)	10 CFR 71.47 Limit
2a	3.72	2.48	38.39	2.25	46.84	1000
3a	0.39	0.07	14.34	49.81	64.61	1000
1	1.62	1.09	4.54	14.43	21.68	200
2	10.94	7.72	0.05	9.69	28.40	200
3	0.62	0.32	10.66	8.00	19.60	200
4	0.36	0.16	5.01	7.80	13.34	200
5	0.36†††	-	0.08	2.88	3.32	200
6	7.35†††	-	22.44	21.29	51.08	200

† Refer to Figure 5.1.1.

†† Gammas generated by neutron capture are included with fuel gammas.

††† Gammas from incore spacers are included with fuel gammas.

Table 5.4.27

DOSE RATES AT TWO METERS FROM THE HI-STAR 100 SYSTEM FOR NORMAL CONDITIONS
MPC-24 WITH TROJAN ZIRCALOY CLAD FUEL WITH NON-ZIRCALOY INCORE SPACERS
42,000 MWD/MTU AND 16-YEAR COOLING

Dose Point† Location	Fuel Gammas†† (mrem/hr)	Gammas from Incore Spacers (mrem/hr)	^{60}Co Gammas (mrem/hr)	Neutrons (mrem/hr)	Totals (mrem/hr)
1	1.52	1.11	0.55	2.52	5.69
2	3.41	2.53	0.64	2.67	9.24
3	1.20	0.82	2.31	1.71	6.05
4	0.97	0.62	2.13	1.50	5.21
5	0.02†††	-	0.07	0.22	0.31
6	0.62†††	-	2.25	0.80	3.68
10CFR71.47 Limit					10.00

† Refer to Figure 5.1.1.

†† Gammas generated by neutron capture are included with fuel gammas.

††† Gammas from incore spacers are included with fuel gammas.

Table 5.4.28

DOSE RATES AT ONE METER FOR ACCIDENT CONDITIONS
MPC-24 WITH TROJAN ZIRCALOY CLAD FUEL WITH NON- ZIRCALOY INCORE SPACERS
42,000 MWD/MTU AND 16-YEAR COOLING

Dose Point† Location	Fuel Gammas†† (mrem/hr)	^{60}Co Gammas (mrem/hr)	Neutrons (mrem/hr)	Totals (mrem/hr)
1	7.01	5.69	106.18	118.88
2	31.31	0.30	356.39	387.99
3	3.27	15.94	69.43	88.64
4	1.86	8.65	49.17	59.68
5	0.11	0.25	12.42	12.78
6	34.74	128.20	82.48	245.42
10CFR71.51 Limit				1000.00

† Refer to Figure 5.1.2.

†† Gammas generated by neutron capture and gammas from incore spacers are included with fuel gammas.

Table 5.4.29

TOTAL DOSE RATES
DOSE LOCATION ON THE SURFACE OF THE HI-STAR 100 SYSTEM FOR NORMAL CONDITIONS
MPC-32 DESIGN BASIS ZIRCALOY CLAD FUEL WITH ZIRCALOY INCORE SPACERS
AT VARYING BURNUPS AND COOLING TIMES

Dose Point† Location	**24,500 MWD/MTU 8 Year Cooling (mrem/hr)**	**29,500 MWD/MTU 9 Year Cooling (mrem/hr)**	**34,500 MWD/MTU 12 Year Cooling (mrem/hr)**	**39,500 MWD/MTU 14 Year Cooling (mrem/hr)**	**44,500 MWD/MTU 19 Year Cooling (mrem/hr)**
2a	62.31	66.79	58.99	59.34	50.90
3a	162.02	192.08	205.87	245.88	263.95
1	44.46	48.87	45.01	46.94	42.51
2	34.63	38.55	36.17	38.33	35.48
3	40.30	46.47	46.08	50.81	49.68
4	37.52	43.47	43.40	48.09	47.31
5	2.24	3.70	5.26	7.06	8.46
6	149.23	154.74	128.70	122.42	95.45
10CFR71.47 Limit	1000.00 (2a,3a) 200.00 (1-6)	1000.00 (2a,3a) 200.00 (1-6)	1000.00 (2a,3a) 200.00 (1-6)	1000.00 (2a,3a) 200.00 (1-6)	1000.00 (2a,3a) 200.00 (1-6)

† Refer to Figure 5.1.1.

Table 5.4.30

TOTAL DOSE RATES
DOSE LOCATION AT TWO METERS FOR NORMAL CONDITIONS
MPC-32 DESIGN BASIS ZIRCALOY CLAD FUEL WITH ZIRCALOY INCORE SPACERS
AT VARYING BURNUPS AND COOLING TIMES

Dose Point† Location	**24,500 MWD/MTU 8 Year Cooling (mrem/hr)**	**29,500 MWD/MTU 9 Year Cooling (mrem/hr)**	**34,500 MWD/MTU 12 Year Cooling (mrem/hr)**	**39,500 MWD/MTU 14 Year Cooling (mrem/hr)**	**44,500 MWD/MTU 19 Year Cooling (mrem/hr)**
1	7.85	8.67	8.01	8.43	7.69
2	8.22	9.28	8.86	9.65	9.19
3	7.83	8.83	8.44	9.10	8.59
4	7.50	8.48	8.14	8.79	8.34
5	0.18	0.29	0.41	0.55	0.66
6	8.22	8.21	6.37	5.66	3.83
10CFR71.47 Limit	10.00	10.00	10.00	10.00	10.00

† Refer to Figure 5.1.1.

Table 5.4.31

TOTAL DOSE RATES
DOSE LOCATION AT ONE METER FOR ACCIDENT CONDITIONS
MPC-32 DESIGN BASIS ZIRCALOY CLAD FUEL WITH ZIRCALOY INCORE SPACERS
AT VARYING BURNUPS AND COOLING TIMES

Dose Point† Location	**24,500 MWD/MTU 8 Year Cooling (mrem/hr)**	**29,500 MWD/MTU 9 Year Cooling (mrem/hr)**	**34,500 MWD/MTU 12 Year Cooling (mrem/hr)**	**39,500 MWD/MTU 14 Year Cooling (mrem/hr)**	**44,500 MWD/MTU 19 Year Cooling (mrem/hr)**
1	91.38	117.99	134.85	162.88	176.78
2	150.55	230.95	310.10	406.55	477.18
3	66.27	89.91	108.35	134.66	150.49
4	49.53	66.55	79.40	98.17	109.14
5	9.17	15.09	21.41	28.69	34.38
6	802.16	817.16	656.05	601.72	437.06
10CFR71.51 Limit	1000.00	1000.00	1000.00	1000.00	1000.00

† Refer to Figure 5.1.2.

Table 5.4.32

TOTAL DOSE RATES
DOSE LOCATION ON THE SURFACE OF THE HI-STAR 100 SYSTEM FOR NORMAL CONDITIONS
MPC-32 DESIGN BASIS ZIRCALOY CLAD FUEL WITH NON-ZIRCALOY INCORE SPACERS
AT VARYING BURNUPS AND COOLING TIMES

Dose Point† Location	**24,500 MWD/MTU 12 Year Cooling (mrem/hr)**	**29,500 MWD/MTU 14 Year Cooling (mrem/hr)**	**34,500 MWD/MTU 16 Year Cooling (mrem/hr)**	**39,500 MWD/MTU 19 Year Cooling (mrem/hr)**	**42,500 MWD/MTU 20 Year Cooling (mrem/hr)**
2a	40.66	40.41	42.78	42.27	44.54
3a	110.58	127.81	162.16	189.57	213.21
1	29.82	30.69	32.88	33.09	35.33
2	24.88	25.46	27.44	27.93	29.93
3	27.57	30.30	34.70	37.26	40.74
4	25.39	28.15	32.50	35.17	38.57
5	1.93	3.07	4.54	5.87	6.79
6	94.26	89.20	86.67	78.04	79.64
10CFR71.47 Limit	1000.00 (2a,3a) 200.00 (1-6)	1000.00 (2a,3a) 200.00 (1-6)	1000.00 (2a,3a) 200.00 (1-6)	1000.00 (2a,3a) 200.00 (1-6)	1000.00 (2a,3a) 200.00 (1-6)

† Refer to Figure 5.1.1.

Table 5.4.33

TOTAL DOSE RATES
DOSE LOCATION AT TWO METERS FOR NORMAL CONDITIONS
MPC-32 DESIGN BASIS ZIRCALOY CLAD FUEL WITH NON-ZIRCALOY INCORE SPACERS
AT VARYING BURNUPS AND COOLING TIMES

Dose Point† Location	**24,500 MWD/MTU 12 Year Cooling (mrem/hr)**	**29,500 MWD/MTU 14 Year Cooling (mrem/hr)**	**34,500 MWD/MTU 16 Year Cooling (mrem/hr)**	**39,500 MWD/MTU 19 Year Cooling (mrem/hr)**	**42,500 MWD/MTU 20 Year Cooling (mrem/hr)**
1	6.55	6.64	6.95	6.78	7.13
2	8.99	9.14	9.54	9.21	9.61
3	6.38	6.65	7.17	7.23	7.71
4	5.93	6.21	6.76	6.88	7.36
5	0.15	0.24	0.35	0.46	0.53
6	5.10	4.55	4.08	3.32	3.24
10CFR71.47 Limit	10.00	10.00	10.00	10.00	10.00

† Refer to Figure 5.1.1.

Table 5.4.34

TOTAL DOSE RATES
DOSE LOCATION AT ONE METER FOR ACCIDENT CONDITIONS
MPC-32 DESIGN BASIS ZIRCALOY CLAD FUEL WITH NON-ZIRCALOY INCORE SPACERS
AT VARYING BURNUPS AND COOLING TIMES

Dose Point† Location	**24,500 MWD/MTU 12 Year Cooling (mrem/hr)**	**29,500 MWD/MTU 14 Year Cooling (mrem/hr)**	**34,500 MWD/MTU 16 Year Cooling (mrem/hr)**	**39,500 MWD/MTU 19 Year Cooling (mrem/hr)**	**42,500 MWD/MTU 20 Year Cooling (mrem/hr)**
1	69.80	86.91	110.36	128.98	144.97
2	143.48	202.73	279.80	346.19	395.59
3	52.15	68.42	90.21	108.35	122.82
4	38.31	49.93	65.54	78.49	88.90
5	7.89	12.51	18.46	23.84	27.60
6	500.54	460.23	430.39	368.33	367.17
10CFR71.51 Limit	1000.00	1000.00	1000.00	1000.00	1000.00

† Refer to Figure 5.1.2.

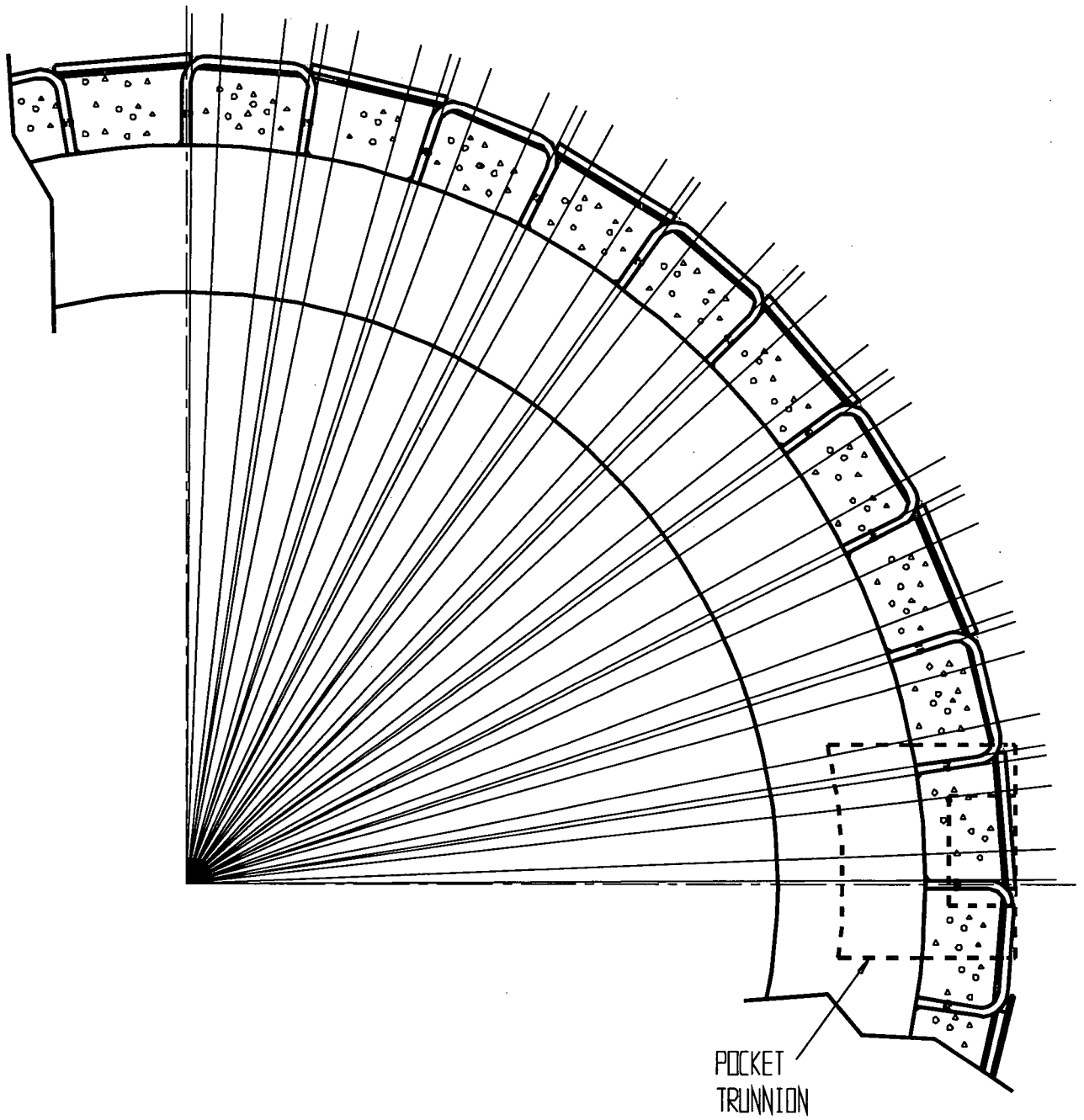

FIGURE 5.4.1; DEPICTION OF THE AZIMUTHAL SEGMENTATION OF THE OVERPACK USED IN ANALYZING NEUTRON AND PHOTON STREAMING

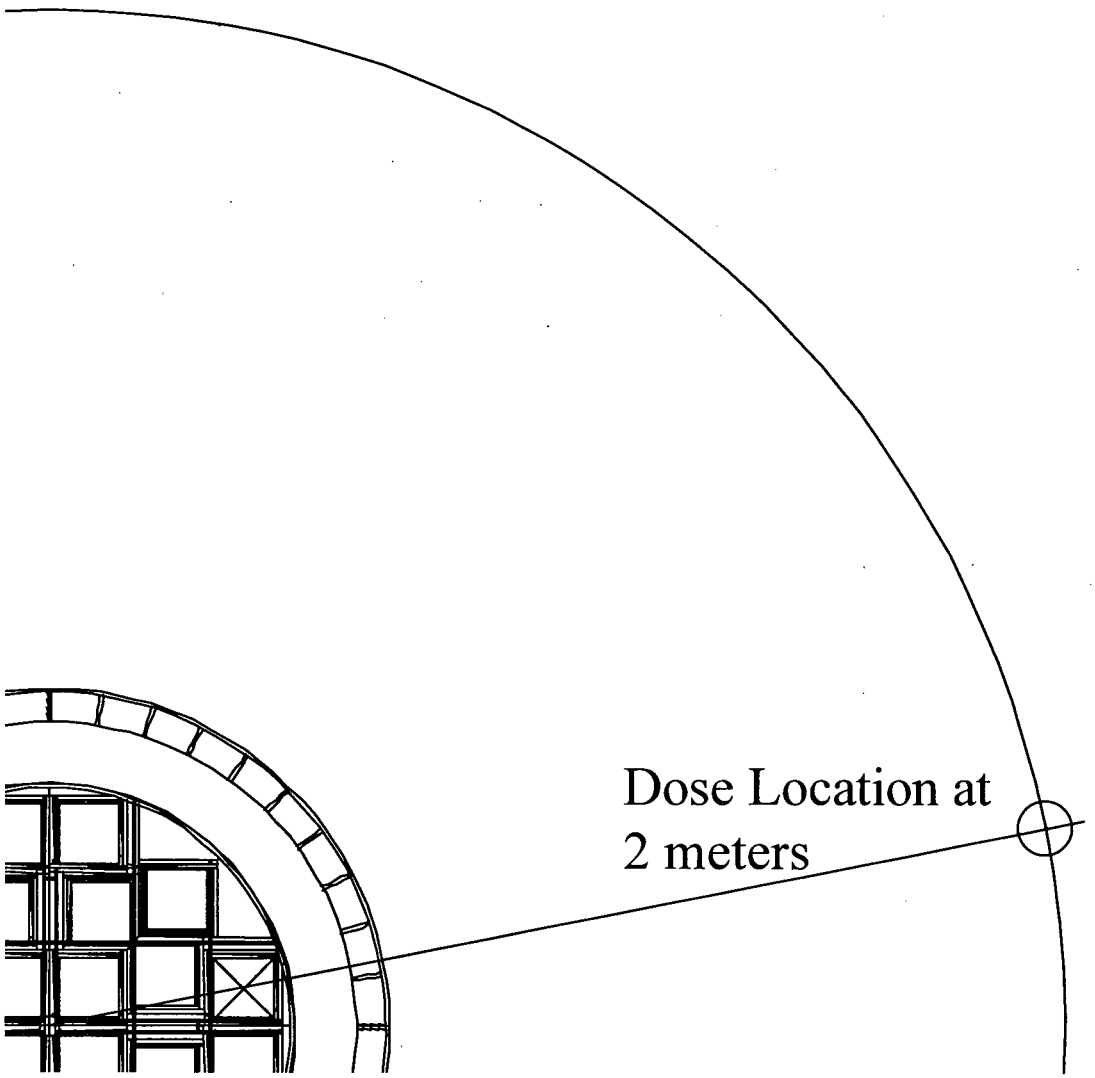

FIGURE 5.4.2: CROSS SECTIONAL VIEW OF THE TROJAN MPC-24E DESIGN SHOWING THE DOSE LOCATION USED FOR THE SECONDARY SOURCE CALCULATIONS.

5.5 REGULATORY COMPLIANCE

The analysis presented in this chapter has shown that the external radiation levels will not increase during normal conditions of transport consistent with the tests specified in 10CFR71.71. This chapter also confirms that the external dose rates from HI-STAR 100 System, when fully loaded with fuel assemblies that meet the acceptance criteria specified in Chapter 1, are less than the regulatory limits specified in 10CFR71.47.

This chapter also demonstrates that the maximum external radiation level at one meter from the external surface of the package does not exceed 1 Rem/hr (10 mSv/hr) during the hypothetical accident conditions consistent with the tests specified in 10CFR71.73.

Tables 5.5.1 through 5.5.3 summarize the maximum dose rates, including the effect of radiation peaking as discussed in Subsection 5.4.1, and demonstrate the HI-STAR 100 System's compliance with the regulatory requirements of 10CFR71.47 and 10CFR71.51. Since these dose rates include the effect of peaking, they may not be equivalent to values reported earlier in this chapter which were surface average dose rates. In these tables "Side" refers to the dose point location that has the maximum dose rate from locations 1-4 (including the pocket trunnion) on Figures 5.1.1 and 5.1.2; "Top" and "Bottom" refer to locations 5 and 6, respectively, on Figures 5.1.1 and 5.1.2. Dose location 2a and 3a from Figure 5.1.1 are not used in Tables 5.5.1 through 5.5.3. Since the maximum dose rate at each location is provided, the corresponding burnup and cooling time may be different between locations and therefore is not listed in the tables. Some of the dose rates in these tables are very close to the regulatory limit. These high dose rates are acceptable because the analysis has been demonstrated to be conservative. In addition, it is extremely unlikely that the casks would be loaded with all fuel assemblies containing the same identical burnup and cooling time analyzed. Finally, the ultimate demonstration of compliance with the 10 CFR 71 regulations will be the measurements that are taken before shipment of the fuel.

Table 5.5.1
MAXIMUM EXTERNAL DOSE RATES FOR THE
HI-STAR 100 SYSTEM CONTAINING THE MPC-24

Normal Conditions of Transport			
	External Surface of Package		
Radiation (mrem/hr)	**Top**	**Side**	**Bottom**
Gamma†	0.52	1.35	115.63
Neutron	3.63	78.65	11.38
Total	4.15	80.00	127.01
10 CFR 71.47(b)(1) Limit	200	200	200
	2 Meters from Vehicle Outer Surface ††		
Radiation (mrem/hr)	**Top**	**Side**	**Bottom**
Gamma†	0.03	9.04	8.13
Neutron	0.32	0.87	0.26
Total	0.35	9.91	8.39
10 CFR 71.47(b)(3) Limit	10	10	10
Hypothetical Accident Conditions			
	1 Meter from Surface of Package †††		
Radiation (mrem/hr)	**Top**	**Side**	**Bottom**
Gamma†	0.18	23.43	639.09
Neutron	16.33	480.92	47.99
Total	16.51	504.35	687.08
10 CFR 71.51(a)(2) Limit	1000	1000	1000

† This includes fuel gammas, gammas from hardware activation including incore spacers, and gammas generated by neutron capture.

†† The vehicle outer surface is the outer radial surface of the impact limiters, the end of the top impact limiter, and 9 feet from the end of the bottom impact limiter.

††† The impact limiters are not present.

Table 5.5.2

MAXIMUM EXTERNAL DOSE RATES FOR THE
HI-STAR 100 SYSTEM CONTAINING THE MPC-32

Normal Conditions of Transport			
	External Surface of Package		
Radiation (mrem/hr)	**Top**	**Side**	**Bottom**
Gamma†	0.95	1.19	135.06
Neutron	7.52	112.38	19.68
Total	8.46	113.57	154.74
10 CFR 71.47(b)(1) Limit	200	200	200
	2 Meters from Vehicle Outer Surface ††		
Radiation (mrem/hr)	**Top**	**Side**	**Bottom**
Gamma†	0.08	5.89	7.98
Neutron	0.58	4.09	0.23
Total	0.66	9.98	8.22
10 CFR 71.47(b)(3) Limit	10	10	10
Hypothetical Accident Conditions			
	1 Meter from Surface of Package †††		
Radiation (mrem/hr)	**Top**	**Side**	**Bottom**
Gamma†	0.22	21.45	739.52
Neutron	34.16	455.73	77.64
Total	34.38	477.18	817.16
10 CFR 71.51(a)(2) Limit	1000	1000	1000

† This includes fuel gammas, gammas from hardware activation including incore spacers, and gammas generated by neutron capture.

†† The vehicle outer surface is the outer radial surface of the impact limiters, the end of the top impact limiter, and 9 feet from the end of the bottom impact limiter.

††† The impact limiters are not present.

Table 5.5.3
MAXIMUM EXTERNAL DOSE RATES FOR THE
HI-STAR 100 SYSTEM CONTAINING THE MPC-68

Normal Conditions of Transport			
	External Surface of Package		
Radiation (mrem/hr)	**Top**	**Side**	**Bottom**
Gamma†	0.34	1.15	114.21
Neutron	2.19	99.04	7.00
Total	2.53	100.19	121.21
10 CFR 71.47(b)(1) Limit	200	200	200
	2 Meters from Vehicle Outer Surface ††		
Radiation (mrem/hr)	**Top**	**Side**	**Bottom**
Gamma†	0.03	5.92	6.69
Neutron	0.21	4.05	0.16
Total	0.24	9.97	6.85
10 CFR 71.47(b)(3) Limit	10	10	10
Hypothetical Accident Conditions			
	1 Meter from Surface of Package †††		
Radiation (mrem/hr)	**Top**	**Side**	**Bottom**
Gamma†	0.11	22.15	640.72
Neutron	10.93	600.71	27.37
Total	11.04	622.86	668.09
10 CFR 71.51(a)(2) Limit	1000	1000	1000

† This includes fuel gammas, gammas from hardware activation including incore spacers, and gammas generated by neutron capture.

†† The vehicle outer surface is the outer radial surface of the impact limiters, the end of the top impact limiter, and 9 feet from the end of the bottom impact limiter.

††† The impact limiters are not present.

5.6 REFERENCES

[5.1.1] J.F. Briesmeister, Ed., "MCNP - A General Monte Carlo N-Particle Transport Code, Version 4A." Los Alamos National Laboratory, LA-12625-M (1993).

[5.1.2] O.W. Hermann, C.V. Parks, "SAS2H: A Coupled One-Dimensional Depletion and Shielding Analysis Module," NUREG/CR-0200, Revision 5, (ORNL/NUREG/CSD-2/V2/R5), Oak Ridge National Laboratory, September 1995.

[5.1.3] O.W. Hermann, R.M. Westfall, "ORIGEN-S: SCALE System Module to Calculate Fuel Depletion, Actinide Transmutation, Fission Product Buildup and Decay, and Associated Radiation Source Terms," NUREG/CR-0200, Revision 5, (ORNL/NUREG/CSD-2/V2/R5), Oak Ridge National Laboratory, September 1995.

[5.1.4] O.W. Hermann, C.V. Parks, "SAS2H: A Coupled One-Dimensional Depletion and Shielding Analysis Module," NUREG/CR-0200, Revision 6, (ORNL/NUREG/CSD-2/V2/R6), Oak Ridge National Laboratory, September 1998.

[5.1.5] O.W. Hermann, R.M. Westfall, "ORIGEN-S: SCALE System Module to Calculate Fuel Depletion, Actinide Transmutation, Fission Product Buildup and Decay, and Associated Radiation Source Terms," NUREG/CR-0200, Revision 6, (ORNL/NUREG/CSD-2/V2/R6), Oak Ridge National Laboratory, September 1998.

[5.1.6] Trojan ISFSI Safety Analysis Report, Revision 3, USNRC Docket 72-0017.

[5.2.1] NUREG-1617, SRP for Transportation Packages for Spent Nuclear Fuel, USNRC, Washington, DC, March 2000.

[5.2.2] A. Luksic, "Spent Fuel Assembly Hardware: Characterization and 10CFR 61 Classification for Waste Disposal," PNL-6906-vol. 1, Pacific Northwest Laboratory, June 1989.

[5.2.3] A.G. Croff, M.A. Bjerke, G.W. Morrison, L.M. Petrie, "Revised Uranium-Plutonium Cycle PWR and BWR Models for the ORIGEN Computer Code," ORNL/TM-6051, Oak Ridge National Laboratory, September 1978.

[5.2.4] J.W. Roddy et al., "Physical and Decay Characteristics of Commercial LWR Spent Fuel," ORNL/TM-9591/V1&R1, Oak Ridge National Laboratory, January 1996.

[5.2.5] "Characteristics of Spent Fuel, High Level Waste, and Other Radioactive Wastes Which May Require Long-Term Isolation," DOE/RW-0184, U.S. Department of Energy, December 1987.

[5.2.6] "Spent Nuclear Fuel Discharges from U.S. Reactors 1994," SR/CNEAF/96-01, Energy Information Administration, U.S. Department of Energy, February 1996.

[5.2.7] "Characteristics Database System LWR Assemblies Database," DOE/RW-0184-R1, U.S. Department of Energy, July 1992.

[5.2.8] S.B. Ludwig and J.P. Renier, "Standard and Extended Burnup PWR and BWR Reactor Models for the ORIGEN2 Computer Code," ORNL/TM-11018, Oak Ridge National Laboratory, December 1989.

[5.2.9] "HI-STORM 100 Final Safety Analysis Report", HI-2002444, Revision 1, September 2002, Holtec International, Docket No. 72-1014.

[5.4.1] "American National Standard Neutron and Gamma-Ray Flux-to-Dose Rate Factors", ANSI/ANS-6.1.1-1977.

[5.4.2] D. J. Whalen, et al., "MCNP: Photon Benchmark Problems," LA-12196, Los Alamos National Laboratory, September 1991.

[5.4.3] D. J. Whalen, et al., "MCNP: Neutron Benchmark Problems," LA-12212, Los Alamos National Laboratory, November 1991.

[5.4.4] J. C. Wagner, et al., "MCNP: Criticality Safety Benchmark Problems," LA-12415, Los Alamos National Laboratory, October 1992.

[5.4.5] S. E. Turner, "Uncertainty Analysis - Axial Burnup Distribution Effects," presented in "Proceedings of a Workshop on the Use of Burnup Credit in Spent Fuel Transport Casks," SAND-89-0018, Sandia National Laboratory, Oct. 1989.

[5.4.6] Commonwealth Edison Company, Letter No. NFS-BND-95-083, Chicago, Illinois.

[5.4.8] S. Cierjacks, "Neutron Sources for Basic Physics and Applications," Pergamon Press, 1983.

APPENDIX 5.A

SAMPLE INPUT FILE FOR SAS2H

(Total number of pages in this appendix : 3)

```
=SAS2H    PARM='halt08,skipshipdata'
bw 15x15 PWR assembly
' fuel temp 923
44groupndf5    LATTICECELL
UO2 1 0.95 923 92234 0.03026 92235 3.4 92236 0.01564
    92238 96.5541 END
'
' Zirc 4 composition
ARBM-ZIRC4 6.55 4 1 0 0 50000 1.7 26000 0.24 24000 0.13 40000 97.93
           2 1.0 595 END
'
' water with 652.5 ppm boron
H2O       3 DEN=0.7135 1  579 END
ARBM-BORMOD  0.7135 1 1 0 0 5000 100 3 652.5E-6  579  END
'
co-59  3 0 1-20 579 end
kr-83  1 0 1-20 923 end
kr-84  1 0 1-20 923 end
kr-85  1 0 1-20 923 end
kr-86  1 0 1-20 923 end
sr-90  1 0 1-20 923 end
y-89   1 0 1-20 923 end
zr-94  1 0 1-20 923 end
zr-95  1 0 1-20 923 end
mo-94  1 0 1-20 923 end
mo-95  1 0 1-20 923 end
nb-94  1 0 1-20 923 end
nb-95  1 0 1-20 923 end
tc-99  1 0 1-20 923 end
ru-106  1 0 1-20 923 end
rh-103  1 0 1-20 923 end
rh-105  1 0 1-20 923 end
sb-124  1 0 1-20 923 end
sn-126  1 0 1-20 923 end
xe-131  1 0 1-20 923 end
xe-132  1 0 1-20 923 end
xe-134  1 0 1-20 923 end
'
xe-135  1 0 1-09 923 end
'
xe-136  1 0 1-20 923 end
cs-133  1 0 1-20 923 end
cs-134  1 0 1-20 923 end
cs-135  1 0 1-20 923 end
cs-137  1 0 1-20 923 end
ba-136  1 0 1-20 923 end
la-139  1 0 1-20 923 end
ce-144  1 0 1-20 923 end
pr-143  1 0 1-20 923 end
nd-143  1 0 1-20 923 end
nd-144  1 0 1-20 923 end
nd-145  1 0 1-20 923 end
nd-146  1 0 1-20 923 end
nd-147  1 0 1-20 923 end
nd-148  1 0 1-20 923 end
nd-150  1 0 1-20 923 end
pm-147  1 0 1-20 923 end
pm-148  1 0 1-20 923 end
pm-149  1 0 1-20 923 end
```

```
sm-147  1 0 1-20 923 end
sm-148  1 0 1-20 923 end
sm-149  1 0 1-20 923 end
sm-150  1 0 1-20 923 end
sm-151  1 0 1-20 923 end
sm-152  1 0 1-20 923 end
eu-151  1 0 1-20 923 end
eu-153  1 0 1-20 923 end
eu-154  1 0 1-20 923 end
eu-155  1 0 1-20 923 end
gd-154  1 0 1-20 923 end
gd-155  1 0 1-20 923 end
gd-157  1 0 1-20 923 end
gd-158  1 0 1-20 923 end
gd-160  1 0 1-20 923 end
'
END COMP
'
' - - - - - - - - - - - - - - - - - - - - - - - - - - - - - - - -
'
'  FUEL-PIN-CELL GEOMETRY:
'
SQUAREPITCH  1.44272 0.950468 1 3 1.08712 2 0.97028 0 END
'
' - - - - - - - - - - - - - - - - - - - - - - - - - - - - - - - -
'
'  MTU in this model is 0.495485 based on fuel dimensions provided
'
'  1 power cycle will be used and a library will be generated every
'  2500 MWD/MTU  power level is 40 MW/MTU
'  therefore 62.5 days per 2500 MWD/MTU
'  Below
'  BURN=62.5*NLIB/CYC
'  POWER=MTU*40
'
'  Number of libraries is 17 which is 42,500 MWD/MTU burnup (17*2500)
'
'  ASSEMBLY AND CYCLE PARAMETERS:
'
NPIN/ASSM=208 FUELNGTH=365.76 NCYCLES=1 NLIB/CYC=17
PRINTLEVEL=1
LIGHTEL=5  INPLEVEL=1   NUMHOLES=17
NUMINStr= 0  ORTUBE= 0.6731  SRTUBE=0.63246   END
POWER=19.81938 BURN=1062.5 END
'
 O  66.54421
 FE  0.24240868
 ZR 98.78151  CR  0.1311304   SN  1.714782
'
END
=SAS2H    PARM='restarts,halt17,skipshipdata'
bw 15x15 PWR assembly
END
```

APPENDIX 5.B

SAMPLE INPUT FILE FOR ORIGEN-S

(Total number of pages in this appendix : 6)

```
#ORIGENS
0$$  A4 33 A8 26 A11 71  E
1$$  1 T
bw 15x15 FUEL -- FT33F001 -
'
' SUBCASE  1 LIBRARY POSITION  1
'
'   lib     pos      grms   photon group
3$$ 33  A3  1  0  A16 2   E T
35$$ 0 T
56$$  5  5  A6 3  A10  0  A13 9  A15 3 A19 1 E
57** 0.0 A3 1.E-5 0.0625 E T
 FUEL 3.4
BW 15x15 0.495485 MTU
58** 19.81938  19.81938 19.81938 19.81938  19.81938
60**  1.0000   3.0000  15.0000  30.0000  62.5
66$$ A1 2 A5 2 A9 2  E
73$$  922350  922340  922360  922380  80000  500000
      260000  240000  400000
74** 16846.48 149.9336 77.49379 478410.7 66544.21 1714.782
     242.0868 131.1304 98781.51
75$$  2  2  2  2  4  4  4  4  4  T
'
' SUBCASE  2 LIBRARY POSITION  2
'
3$$ 33  A3   2  0  A16 2  A33 0  E T
35$$ 0 T
56$$  3  3  A6 3  A10   5  A15 3 A19 1 E
57** 0.0 A3 1.E-5  0.0625 E T
 fuel
BW 15X15
58** 19.81938 19.81938 19.81938
60** 18.5 37.0 62.5
66$$ A1 2 A5 2 A9 2  E T
'
' SUBCASE  3 LIBRARY POSITION  3
'
3$$ 33  A3   3  0  A16 2  A33 0  E T
35$$ 0 T
56$$  3  3  A6 3  A10   3  A15 3 A19 1 E
57** 0.0 A3 1.E-5  0.0625 E T
 fuel
BW 15X15
58** 19.81938 19.81938 19.81938
60** 18.5 37.0 62.5
66$$ A1 2 A5 2 A9 2  E T
'
' SUBCASE  4 LIBRARY POSITION  4
'
3$$ 33  A3   4  0  A16 2  A33 0  E T
35$$ 0 T
56$$  3  3  A6 3  A10   3  A15 3 A19 1 E
57** 0.0 A3 1.E-5  0.0625 E T
 fuel
BW 15X15
58** 19.81938 19.81938 19.81938
60** 18.5 37.0 62.5
66$$ A1 2 A5 2 A9 2  E T
'
```

```
' SUBCASE  5 LIBRARY POSITION  5
'
3$$ 33  A3   5  0  A16 2  A33 0  E T
35$$ 0 T
56$$  3  3  A6 3  A10   3  A15 3 A19 1 E
57** 0.0 A3 1.E-5  0.0625 E T
 fuel
BW 15X15
58** 19.81938 19.81938 19.81938
60** 18.5 37.0 62.5
66$$ A1 2 A5 2 A9 2  E T
'
' SUBCASE  6 LIBRARY POSITION  6
'
3$$ 33  A3   6  0  A16 2  A33 0  E T
35$$ 0 T
56$$  3  3  A6 3  A10   3  A15 3 A19 1 E
57** 0.0 A3 1.E-5  0.0625 E T
 fuel
BW 15X15
58** 19.81938 19.81938 19.81938
60** 18.5 37.0 62.5
66$$ A1 2 A5 2 A9 2  E T
'
' SUBCASE  7 LIBRARY POSITION  7
'
3$$ 33  A3   7  0  A16 2  A33 0  E T
35$$ 0 T
56$$  3  3  A6 3  A10   3  A15 3 A19 1 E
57** 0.0 A3 1.E-5  0.0625 E T
 fuel
BW 15X15
58** 19.81938 19.81938 19.81938
60** 18.5 37.0 62.5
66$$ A1 2 A5 2 A9 2  E T
'
' SUBCASE  8 LIBRARY POSITION  8
'
3$$ 33  A3   8  0  A16 2  A33 0  E T
35$$ 0 T
56$$  3  3  A6 3  A10   3  A15 3 A19 1 E
57** 0.0 A3 1.E-5  0.0625 E T
 fuel
BW 15X15
58** 19.81938 19.81938 19.81938
60** 18.5 37.0 62.5
66$$ A1 2 A5 2 A9 2  E T
'
' SUBCASE  9 LIBRARY POSITION  9
'
3$$ 33  A3   9  0  A16 2  A33 0  E T
35$$ 0 T
56$$  3  3  A6 3  A10   3  A15 3 A19 1 E
57** 0.0 A3 1.E-5  0.0625 E T
 fuel
BW 15X15
58** 19.81938 19.81938 19.81938
60** 18.5 37.0 62.5
66$$ A1 2 A5 2 A9 2  E T
```

```
'
' SUBCASE 10 LIBRARY POSITION 10
'
3$$ 33  A3  10  0  A16 2  A33 0  E T
35$$ 0 T
56$$  3  3  A6 3  A10   3  A15 3 A19 1 E
57** 0.0 A3 1.E-5  0.0625 E T
 fuel
BW 15X15
58** 19.81938 19.81938 19.81938
60** 18.5 37.0 62.5
66$$ A1 2 A5 2 A9 2  E T
'
' SUBCASE 11 LIBRARY POSITION 11
'
3$$ 33  A3  11  0  A16 2  A33 0  E T
35$$ 0 T
56$$  3  3  A6 3  A10   3  A15 3 A19 1 E
57** 0.0 A3 1.E-5  0.0625 E T
 fuel
BW 15X15
58** 19.81938 19.81938 19.81938
60** 18.5 37.0 62.5
66$$ A1 2 A5 2 A9 2  E T
'
' SUBCASE 12 LIBRARY POSITION 12
'
3$$ 33  A3  12  0  A16 2  A33 0  E T
35$$ 0 T
56$$  3  3  A6 3  A10   3  A15 3 A19 1 E
57** 0.0 A3 1.E-5  0.0625 E T
 fuel
BW 15X15
58** 19.81938 19.81938 19.81938
60** 18.5 37.0 62.5
66$$ A1 2 A5 2 A9 2  E T
'
' SUBCASE 13 LIBRARY POSITION 13
'
3$$ 33  A3  13  0  A16 2  A33 0  E T
35$$ 0 T
56$$  3  3  A6 3  A10   3  A15 3 A19 1 E
57** 0.0 A3 1.E-5  0.0625 E T
 fuel
BW 15X15
58** 19.81938 19.81938 19.81938
60** 18.5 37.0 62.5
66$$ A1 2 A5 2 A9 2  E T
'
' SUBCASE 14 LIBRARY POSITION 14
'
3$$ 33  A3  14  0  A16 2  A33 0  E T
35$$ 0 T
56$$  3  3  A6 3  A10   3  A15 3 A19 1 E
57** 0.0 A3 1.E-5  0.0625 E T
 fuel
BW 15X15
58** 19.81938 19.81938 19.81938
60** 18.5 37.0 62.5
```

```
66$$ A1 2 A5 2 A9 2  E T
'
' SUBCASE 15 LIBRARY POSITION 15
'
3$$ 33  A3  15  0  A16 2  A33 0  E T
35$$ 0 T
56$$  3  3  A6 3  A10   3  A15 3 A19 1 E
57** 0.0 A3 1.E-5  0.0625 E T
 fuel
BW 15X15
58** 19.81938 19.81938 19.81938
60** 18.5 37.0 62.5
66$$ A1 2 A5 2 A9 2  E T
'
' SUBCASE 16 LIBRARY POSITION 16
'
3$$ 33  A3  16  A4 7 0  A16 2  A33 18  E T
35$$ 0 T
56$$  3  3  A6 1  A10  3  A15 3 A19 1 E
57** 0.0 A3 1.E-5  0.0625 E T
 fuel
BW 15X15
58** 19.81938 19.81938 19.81938
60** 18.5 37.0 62.5
66$$ A1 2 A5 2 A9 2  E T
'
' SUBCASE - decay
'
54$$ A8 1 E
56$$ 0 9 A6 1 A10 3 A14 3 A15 1 A19 1 E
57** 0.0 0 1.E-5  E T
 fuel enrichment above
60** 0.5 0.75 1.0 4.0 8.0 12.0 24.0 48.0 96.0
61** F0.1
65$$
'GRAM-ATOMS   GRAMS    CURIES     WATTS-ALL  WATTS-GAMMA
     3Z     0  1  0     0 0 0      1 0 0         3Z         6Z
     3Z     0  1  0     0 0 0      1 0 0         3Z         6Z
     3Z     0  1  0     0 0 0      1 0 0         3Z         6Z  T
'
' SUBCASE - decay
'
54$$ A8 1 E
56$$ 0 9 A6 1 A10 9 A14 4 A15 1 A19 1 E
57** 4.0 0 1.E-5  E T
 fuel enrichment above
60** 10.0 20.0 30.0 60.0 90.0 120.0 180.0 240.0 365.0
61** F0.1
65$$
'GRAM-ATOMS   GRAMS    CURIES     WATTS-ALL  WATTS-GAMMA
     3Z     0  1  0     0 0 0      1 0 0         3Z         6Z
     3Z     0  1  0     0 0 0      1 0 0         3Z         6Z
     3Z     0  1  0     0 0 0      1 0 0         3Z         6Z  T
'
' SUBCASE - decay
'
54$$ A8 0 E
56$$ 0 9 A6 1 A10 9 A14 5 A15 1 A19 1 E
57** 1.0 0 1.E-5  E T
```

```
 fuel enrichment above
60** 1.5 3.0 4.0 5.0 6.0 7.0 8.0 9.0 10.0
61** F1.0e-5
65$$
'GRAM-ATOMS   GRAMS    CURIES     WATTS-ALL  WATTS-GAMMA
     3Z     0  1  0     1 0 0      1 0 0         3Z         6Z
     3Z     0  1  0     1 0 0      1 0 0         3Z         6Z
     3Z     0  1  0     1 0 0      1 0 0         3Z         6Z
81$$ 2 0 26 1 E
82$$ 0 2 2 2 2 2 2 2 2
83**  1.1E+7  8.0E+6 6.0E+6 4.0E+6 3.0E+6 2.5E+6 2.0E+6 1.5E+6
      1.0E+6  7.0E+5 4.5E+5 3.0E+5 1.5E+5 1.0E+5 7.0E+4 4.5E+4
      3.0E+4  2.0E+4 1.0E+4
84**  20.0E+6 6.43E+6 3.0E+6 1.85E+6 1.40E+6 9.00E+5 4.00E+5 1.0E+5 T
'
'
'
'
'
'
'
'
' SUBCASE - decay
'
54$$ A8 0 E
56$$ 0 10 A6 1 A10 9 A14 5 A15 1 A19 1 E
57** 10.0 0 1.E-5  E T
 fuel enrichment above
60** 11.0 12.0 13.0 14.0 15.0 16.0 17.0 18.0 19.0 20.0
61** F1.0e-5
65$$
'GRAM-ATOMS   GRAMS    CURIES     WATTS-ALL  WATTS-GAMMA
     3Z     0  1  0     1 0 0      1 0 0         3Z         6Z
     3Z     0  1  0     1 0 0      1 0 0         3Z         6Z
     3Z     0  1  0     1 0 0      1 0 0         3Z         6Z
81$$ 2 0 26 1 E
82$$ 2 2 2 2 2 2 2 2 2 2
83**  1.1E+7  8.0E+6 6.0E+6 4.0E+6 3.0E+6 2.5E+6 2.0E+6 1.5E+6
      1.0E+6  7.0E+5 4.5E+5 3.0E+5 1.5E+5 1.0E+5 7.0E+4 4.5E+4
      3.0E+4  2.0E+4 1.0E+4
84**  20.0E+6 6.43E+6 3.0E+6 1.85E+6 1.40E+6 9.00E+5 4.00E+5 1.0E+5 T
'
'
'
'
'
'
'
'
'
'
' END
'
56$$ F0 T
END
```

APPENDIX 5.C

SAMPLE INPUT FILE FOR MCNP

(Total number of pages in this appendix : 33)

```
message:   outp=m8c7b08o  srctp=m8c7b08s  runtpe=m8c7b08r
           mctal=m8c7b08m  wssa=m8c7b08w  rssa=m8c7b08w

m8c7b08
c       HI STAR 100 MPC68
c
c
c     two pocket trunions modeled
c     holtite present
c     impact limiters present
c     radial model
c
c     origen is at the bottom of the overpack - as an example of the origen
c     item 1 on drawing 1397 is 6 inches thick and extends
c     from 0.0 to 6.0 inches in the axial direction
c
c     universe 1
c
c      egg crate
301    0            -30             -400 u=1
302    0             31             -400 u=1
303    0         30 -31 -32         -400 u=1
304    0         30 -31  33         -400 u=1
305    5 -7.92          28      400 -670 u=1
306    5 -7.92             -23 400 -670 u=1
307    5 -7.92      -15 23 -28 400 -670 u=1
308    5 -7.92  20      23 -28 400 -670 u=1
309    5 -7.92          28      670 -460 u=1
310    5 -7.92             -23 670 -460 u=1
311    5 -7.92      -15 23 -28 670 -460 u=1
312    5 -7.92  20      23 -28 670 -460 u=1
c      boral and inside of egg crate and outside of fuel
314    0         15 -30 23 -28 400 -410 u=-1
315    0         31 -20 23 -28 400 -410 u=-1
316    0         30 -31 33 -28 400 -410 u=-1
317    0         30 -31 23 -32 400 -410 u=-1
318    0         15 -18 26 -28 410 -435 u=-1
319    0         19 -20 26 -28 410 -435 u=-1
320    0         15 -17 23 -24 410 -435 u=-1
321    0         15 -17 25 -26 410 -435 u=-1
322    6 -2.644 18 -19 27 -28 410 -435 u=-1
323    5 -7.92  18 -19 26 -27 410 -435 u=-1
324    6 -2.644 15 -16 24 -25 410 -435 u=-1
325    5 -7.92  16 -17 24 -25 410 -435 u=-1
326    0         17 -30 23 -26 410 -435 u=-1
327    0         31 -20 23 -26 410 -435 u=-1
328    0         30 -31 23 -32 410 -435 u=-1
329    0         30 -31 33 -26 410 -435 u=-1
330    0         15 -30 23 -28 435 -460 u=-1
331    0         31 -20 23 -28 435 -460 u=-1
332    0         30 -31 33 -28 435 -460 u=-1
333    0         30 -31 23 -32 435 -460 u=-1
c      fuel element
338    5 -1.48621  30 -31 32 -33     -420 u=1
339    2 -4.29251 30 -31 32 -33 420 -425 u=-1
340    0            30 -31 32 -33 425 -430 u=-1
341    5 -0.265322 30 -31 32 -33 430 -440 u=-1
342    5 -0.677510 30 -31 32 -33 440 -445 u=-1
343    5 -1.369221 30 -31 32 -33 445 -450 u=-1
344    5 -0.257210 30 -31 32 -33 450 -670 u=-1
345    5 -0.257210 30 -31 32 -33 670 -455 u=-1
346    0            30 -31 32 -33 455  u=1
347    0            -30             460 u=1
348    0             31             460 u=1
349    0         30 -31 -32         460 u=1
350    0         30 -31  33         460 u=1
c
c     universe 2
c
```

```
c       egg crate
401     0            -30             -400 u=2
402     0             31             -400 u=2
403     0         30 -31 -32         -400 u=2
404     0         30 -31  33         -400 u=2
405     5 -7.92          28      400 -670 u=2
406     5 -7.92             -23 400 -670 u=2
407     5 -7.92      -15 23 -28 400 -670 u=2
408     5 -7.92  20      23 -28 400 -670 u=2
409     5 -7.92          28      670 -460 u=2
410     5 -7.92             -23 670 -460 u=2
411     5 -7.92      -15 23 -28 670 -460 u=2
412     5 -7.92  20      23 -28 670 -460 u=2
c       boral and inside of egg crate and outside of fuel
414     0         15 -30 23 -28 400 -460 u=-2
415     0         31 -20 23 -28 400 -460 u=-2
416     0         30 -31 33 -28 400 -460 u=-2
417     0         30 -31 23 -32 400 -460 u=-2
c       fuel element
438     5 -1.48621  30 -31 32 -33     -420 u=2
439     2 -4.29251 30 -31 32 -33 420 -425 u=-2
440     0            30 -31 32 -33 425 -430 u=-2
441     5 -0.265322 30 -31 32 -33 430 -440 u=-2
442     5 -0.677510 30 -31 32 -33 440 -445 u=-2
443     5 -1.369221 30 -31 32 -33 445 -450 u=-2
444     5 -0.257210 30 -31 32 -33 450 -670 u=-2
445     5 -0.257210 30 -31 32 -33 670 -455 u=-2
446     0            30 -31 32 -33 455 u=2
447     0            -30             460 u=2
448     0             31             460 u=2
449     0         30 -31 -32         460 u=2
450     0         30 -31  33         460 u=2
c
c      universe 3
c
c       egg crate
501     0            -30             -400 u=3
502     0             31             -400 u=3
503     0         30 -31 -32         -400 u=3
504     0         30 -31  33         -400 u=3
505     5 -7.92          28      400 -670 u=3
506     5 -7.92             -23 400 -670 u=3
507     5 -7.92      -15 23 -28 400 -670 u=3
508     5 -7.92  20      23 -28 400 -670 u=3
509     5 -7.92          28      670 -460 u=3
510     5 -7.92             -23 670 -460 u=3
511     5 -7.92      -15 23 -28 670 -460 u=3
512     5 -7.92  20      23 -28 670 -460 u=3
c       boral and inside of egg crate and outside of fuel
514     0         15 -30 23 -28 400 -410 u=-3
515     0         31 -20 23 -28 400 -410 u=-3
516     0         30 -31 33 -28 400 -410 u=-3
517     0         30 -31 23 -32 400 -410 u=-3
518     0         15 -18 26 -28 410 -435 u=-3
519     0         19 -20 26 -28 410 -435 u=-3
522     6 -2.644 18 -19 27 -28 410 -435 u=-3
523     5 -7.92  18 -19 26 -27 410 -435 u=-3
526     0         15 -30 23 -26 410 -435 u=-3
527     0         31 -20 23 -26 410 -435 u=-3
528     0         30 -31 23 -32 410 -435 u=-3
529     0         30 -31 33 -26 410 -435 u=-3
530     0         15 -30 23 -28 435 -460 u=-3
531     0         31 -20 23 -28 435 -460 u=-3
532     0         30 -31 33 -28 435 -460 u=-3
533     0         30 -31 23 -32 435 -460 u=-3
c       fuel element
538     5 -1.48621  30 -31 32 -33     -420 u=3
539     2 -4.29251 30 -31 32 -33 420 -425 u=-3
540     0            30 -31 32 -33 425 -430 u=-3
```

```
541     5 -0.265322 30 -31 32 -33 430 -440 u=-3
542     5 -0.677510 30 -31 32 -33 440 -445 u=-3
543     5 -1.369221 30 -31 32 -33 445 -450 u=-3
544     5 -0.257210 30 -31 32 -33 450 -670 u=-3
545     5 -0.257210 30 -31 32 -33 670 -455 u=-3
546     0           30 -31 32 -33 455 u=3
547     0           -30            460 u=3
548     0            31            460 u=3
549     0        30 -31 -32        460 u=3
550     0        30 -31  33        460 u=3
c
c     universe 4
c
c      egg crate
601     0           -30            -400 u=4
602     0            31            -400 u=4
603     0        30 -31 -32        -400 u=4
604     0        30 -31  33        -400 u=4
605     5 -7.92         28     400 -670 u=4
606     5 -7.92            -23 400 -670 u=4
607     5 -7.92     -15 23 -28 400 -670 u=4
608     5 -7.92  20     23 -28 400 -670 u=4
609     5 -7.92         28     670 -460 u=4
610     5 -7.92            -23 670 -460 u=4
611     5 -7.92     -15 23 -28 670 -460 u=4
612     5 -7.92  20     23 -28 670 -460 u=4
c      boral and inside of egg crate and outside of fuel
614     0        15 -30 23 -28 400 -410 u=-4
615     0        31 -20 23 -28 400 -410 u=-4
616     0        30 -31 33 -28 400 -410 u=-4
617     0        30 -31 23 -32 400 -410 u=-4
620     0        15 -17 23 -24 410 -435 u=-4
621     0        15 -17 25 -28 410 -435 u=-4
624     6 -2.644 15 -16 24 -25 410 -435 u=-4
625     5 -7.92  16 -17 24 -25 410 -435 u=-4
626     0        17 -30 23 -28 410 -435 u=-4
627     0        31 -20 23 -28 410 -435 u=-4
628     0        30 -31 23 -32 410 -435 u=-4
629     0        30 -31 33 -28 410 -435 u=-4
630     0        15 -30 23 -28 435 -460 u=-4
631     0        31 -20 23 -28 435 -460 u=-4
632     0        30 -31 33 -28 435 -460 u=-4
633     0        30 -31 23 -32 435 -460 u=-4
c      fuel element
638     5 -1.48621  30 -31 32 -33     -420 u=4
639     2 -4.29251 30 -31 32 -33 420 -425 u=-4
640     0           30 -31 32 -33 425 -430 u=-4
641     5 -0.265322 30 -31 32 -33 430 -440 u=-4
642     5 -0.677510 30 -31 32 -33 440 -445 u=-4
643     5 -1.369221 30 -31 32 -33 445 -450 u=-4
644     5 -0.257210 30 -31 32 -33 450 -670 u=-4
645     5 -0.257210 30 -31 32 -33 670 -455 u=-4
646     0           30 -31 32 -33 455  u=4
647     0           -30            460 u=4
648     0            31            460 u=4
649     0        30 -31 -32        460 u=4
650     0        30 -31  33        460 u=4
c
c     universe 5
c
701     0              -400 u=5
702     5 -7.92 20 400 -670 u=5
704     5 -7.92 20 670 -460 u=5
705     0      -20 400 -460 u=5
706     0          460      u=5
c
c     universe 6
c
710     0                -400 u=6
```

```
711    5 -7.92  -23 400 -670 u=6
713    5 -7.92  -23 670 -460 u=6
714    0         23 400 -460 u=6
715    0            460      u=6
c
c     universe 7
c
720    0                        -400 u=7
721    5 -7.92 20       23 400 -670 u=7
722    5 -7.92    -23      400 -670 u=7
724    5 -7.92 20       23 670 -460 u=7
725    5 -7.92    -23      670 -460 u=7
726    0          -20  23 400 -460 u=7
727    0                   460      u=7
c
c     universe 8
c
730   0                           -400 u=8
731   0        15             400 -460 u=8
739   5 -7.92     -15        400 -670 u=8
740   5 -7.92     -15        670 -460 u=8
741   0                      460      u=8
c
c     universe 9
c
745   0        15     23     400 -460 u=9
753   0                           -400 u=9
754   5 -7.92     -15 23     400 -670 u=9
755   5 -7.92     -23        400 -670 u=9
756   5 -7.92     -15 23     670 -460 u=9
757   5 -7.92     -23        670 -460 u=9
758   0                      460      u=9
c
c     universe 10
c
760   0        15        -28 400 -460 u=10
772   0                           -400 u=10
773   5 -7.92     -15    -28 400 -670 u=10
774   5 -7.92         28     400 -670 u=10
775   5 -7.92     -15    -28 670 -460 u=10
776   5 -7.92         28     670 -460 u=10
777   0                      460      u=10
c
c     universe 11
c
780   0                 -28 400 -460 u=11
788   0                           -400 u=11
789   5 -7.92         28     400 -670 u=11
790   5 -7.92         28     670 -460 u=11
791   0                      460      u=11
c
c     universe 12
c
795   0           -20    -28 400 -460 u=12
803   0                           -400 u=12
804   5 -7.92     -20 28     400 -670 u=12
805   5 -7.92  20            400 -670 u=12
806   5 -7.92     -20 28     670 -460 u=12
807   5 -7.92  20            670 -460 u=12
808   0                      460      u=12
c
c     universe 13
c
c     810   0     -670  u=13
c     811   0      670  u=13
c     storage locations
c
201   0  -301  -106 212 620 -675
202   0  -301  106 -107 212 620 -675
```

```
          fill=6 (-8.2423 90.6653 0.0)
203   0   -301  107 -108 212 620 -675
          fill=6 ( 8.2423 90.6653 0.0)
204   0   -301  108 212 620 -675
c
205   0   -301 -104 211 620 -675
206   0   -301 104 -105 211 620 -675
          fill=6 (-41.2115 74.1807 0.0)
207   0   -301 105 -106 211 -212 620 -675
          fill=7 (-24.7269 74.1807 0.0)
c
101   0   106 -107 211 -212  620 -675
          fill=2 (-8.2423 74.1807 0.0)
102   0   107 -108 211 -212  620 -675
          fill=4 ( 8.2423 74.1807 0.0)
c
208   0   -301 108 -109 211 -212 620 -675
          fill=9 (24.7269 74.1807 0.0)
209   0   -301 109 -110 211 620 -675
          fill=6 (41.2115 74.1807 0.0)
210   0   -301 110 211 620 -675
c
211   0   -301 -103 210 620 -675
212   0   -301 103 -104 210 -211 620 -675
          fill=7 (-57.6961 57.6961 0.0)
c
103   0   104 -105 210 -211  620 -675
          fill=2 (-41.2115 57.6961 0.0)
104   0   105 -106 210 -211  620 -675
          fill=4 (-24.7269 57.6961 0.0)
105   0   106 -107 210 -211  620 -675
          fill=1 (-8.2423 57.6961 0.0)
106   0   107 -108 210 -211  620 -675
          fill=1 ( 8.2423 57.6961 0.0)
107   0   108 -109 210 -211  620 -675
          fill=4 ( 24.7269 57.6961 0.0)
108   0   109 -110 210 -211  620 -675
          fill=4 ( 41.2115 57.6961 0.0)
c
213   0   -301 110 -111 210 -211 620 -675
          fill=9 ( 57.6961 57.6961 0.0)
214   0   -301 111 210 620 -675
c
215   0   -301 -103 209 -210 620 -675
          fill=5 (-74.1807 41.2115 0.0)
c
109   0   103 -104 209 -210  620 -675
          fill=2 (-57.6961 41.2115 0.0)
110   0   104 -105 209 -210  620 -675
          fill=1 (-41.2115 41.2115 0.0)
111   0   105 -106 209 -210  620 -675
          fill=1 (-24.7269 41.2115 0.0)
112   0   106 -107 209 -210  620 -675
          fill=1 (-8.2423 41.2115 0.0)
113   0   107 -108 209 -210  620 -675
          fill=1 ( 8.2423 41.2115 0.0)
114   0   108 -109 209 -210  620 -675
          fill=1 ( 24.7269 41.2115 0.0)
115   0   109 -110 209 -210  620 -675
          fill=1 ( 41.2115 41.2115 0.0)
116   0   110 -111 209 -210  620 -675
          fill=4 ( 57.6961 41.2115 0.0)
c
216   0   -301 111 209 -210 620 -675
          fill=8 (74.1807 41.2115 0.0)
c
217   0   -301 -102 208 620 -675
218   0   -301 102 -103 208 -209 620 -675
          fill=7 (-74.1807 24.7269 0.0)
```

```
c
117   0  103 -104 208 -209  620 -675
         fill=3 (-57.6961 24.7269 0.0)
118   0  104 -105 208 -209  620 -675
         fill=1 (-41.2115 24.7269 0.0)
119   0  105 -106 208 -209  620 -675
         fill=1 (-24.7269 24.7269 0.0)
120   0  106 -107 208 -209  620 -675
         fill=1 (-8.2423 24.7269 0.0)
121   0  107 -108 208 -209  620 -675
         fill=1 ( 8.2423 24.7269 0.0)
122   0  108 -109 208 -209  620 -675
         fill=1 ( 24.7269 24.7269 0.0)
123   0  109 -110 208 -209  620 -675
         fill=1 ( 41.2115 24.7269 0.0)
124   0  110 -111 208 -209  620 -675
         fill=1 ( 57.6961 24.7269 0.0)
c
219   0  -301 111 -112 208 -209 620 -675
         fill=9 (74.1807 24.7269 0.0)
220   0  -301 112 208 620 -675
c
221   0  -301 -102 207 -208 620 -675
         fill=5 (-90.6653 8.2423 0.0)
c
125   0  102 -103 207 -208  620 -675
         fill=2 (-74.1807 8.2423 0.0)
126   0  103 -104 207 -208  620 -675
         fill=1 (-57.6961 8.2423 0.0)
127   0  104 -105 207 -208  620 -675
         fill=1 (-41.2115 8.2423 0.0)
128   0  105 -106 207 -208  620 -675
         fill=1 (-24.7269 8.2423 0.0)
129   0  106 -107 207 -208  620 -675
         fill=1 (-8.2423 8.2423 0.0)
130   0  107 -108 207 -208  620 -675
         fill=1 ( 8.2423 8.2423 0.0)
131   0  108 -109 207 -208  620 -675
         fill=1 ( 24.7269 8.2423 0.0)
132   0  109 -110 207 -208  620 -675
         fill=1 ( 41.2115 8.2423 0.0)
133   0  110 -111 207 -208  620 -675
         fill=1 ( 57.6961 8.2423 0.0)
134   0  111 -112 207 -208  620 -675
         fill=4 ( 74.1807 8.2423 0.0)
c
222   0  -301 112 207 -208 620 -675
         fill=8 (90.6653 8.2423 0.0)
c
223   0  -301 -102 206 -207 620 -675
         fill=5 (-90.6653 -8.2423 0.0)
c
135   0  102 -103 206 -207  620 -675
         fill=3 (-74.1807 -8.2423 0.0)
136   0  103 -104 206 -207  620 -675
         fill=1 (-57.6961 -8.2423 0.0)
137   0  104 -105 206 -207  620 -675
         fill=1 (-41.2115 -8.2423 0.0)
138   0  105 -106 206 -207  620 -675
         fill=1 (-24.7269 -8.2423 0.0)
139   0  106 -107 206 -207  620 -675
         fill=1 (-8.2423 -8.2423 0.0)
140   0  107 -108 206 -207  620 -675
         fill=1 ( 8.2423 -8.2423 0.0)
141   0  108 -109 206 -207  620 -675
         fill=1 ( 24.7269 -8.2423 0.0)
142   0  109 -110 206 -207  620 -675
         fill=1 ( 41.2115 -8.2423 0.0)
143   0  110 -111 206 -207  620 -675
```

```
          fill=1 ( 57.6961 -8.2423 0.0)
144    0  111 -112 206 -207  620 -675
          fill=1 ( 74.1807 -8.2423 0.0)
c
224    0  -301 112 206 -207 620 -675
          fill=8 (90.6653 -8.2423 0.0)
c
225    0  -301 -102 -206 620 -675
226    0  -301 102 -103 205 -206 620 -675
          fill=12 (-74.1807 -24.7269 0.0)
c
145    0  103 -104 205 -206  620 -675
          fill=3 (-57.6961 -24.7269 0.0)
146    0  104 -105 205 -206  620 -675
          fill=1 (-41.2115 -24.7269 0.0)
147    0  105 -106 205 -206  620 -675
          fill=1 (-24.7269 -24.7269 0.0)
148    0  106 -107 205 -206  620 -675
          fill=1 (-8.2423  -24.7269 0.0)
149    0  107 -108 205 -206  620 -675
          fill=1 ( 8.2423  -24.7269 0.0)
150    0  108 -109 205 -206  620 -675
          fill=1 ( 24.7269 -24.7269 0.0)
151    0  109 -110 205 -206  620 -675
          fill=1 ( 41.2115 -24.7269 0.0)
152    0  110 -111 205 -206  620 -675
          fill=1 ( 57.6961 -24.7269 0.0)
c
227    0  -301 111 -112 205 -206 620 -675
          fill=10 (74.1807 -24.7269 0.0)
228    0  -301 112 -206 620 -675
c
229    0  -301 -103 204 -205 620 -675
          fill=5 (-74.1807 -41.2115 0.0)
c
153    0  103 -104 204 -205  620 -675
          fill=3 (-57.6961 -41.2115 0.0)
154    0  104 -105 204 -205  620 -675
          fill=1 (-41.2115 -41.2115 0.0)
155    0  105 -106 204 -205  620 -675
          fill=1 (-24.7269 -41.2115 0.0)
156    0  106 -107 204 -205  620 -675
          fill=1 (-8.2423  -41.2115 0.0)
157    0  107 -108 204 -205  620 -675
          fill=1 ( 8.2423  -41.2115 0.0)
158    0  108 -109 204 -205  620 -675
          fill=1 ( 24.7269 -41.2115 0.0)
159    0  109 -110 204 -205  620 -675
          fill=1 ( 41.2115 -41.2115 0.0)
160    0  110 -111 204 -205  620 -675
          fill=1 ( 57.6961 -41.2115 0.0)
c
230    0  -301 111 204 -205 620 -675
          fill=8 (74.1807 -41.2115 0.0)
c
231    0  -301 -103 -204 620 -675
232    0  -301 103 -104 203 -204 620 -675
          fill=12 (-57.6961 -57.6961 0.0)
c
161    0  104 -105 203 -204  620 -675
          fill=3 (-41.2115 -57.6961 0.0)
162    0  105 -106 203 -204  620 -675
          fill=1 (-24.7269 -57.6961 0.0)
163    0  106 -107 203 -204  620 -675
          fill=1 (-8.2423 -57.6961 0.0)
164    0  107 -108 203 -204  620 -675
          fill=1 ( 8.2423 -57.6961 0.0)
165    0  108 -109 203 -204  620 -675
          fill=1 ( 24.7269 -57.6961 0.0)
```

```
166   0  109 -110 203 -204  620 -675
         fill=1 ( 41.2115 -57.6961 0.0)
c
233   0  -301 110 -111 203 -204 620 -675
         fill=10 ( 57.6961 -57.6961 0.0)
234   0  -301 111 -204 620 -675
c
235   0  -301 -104 -203 620 -675
236   0  -301 104 -105 -203 620 -675
         fill=11 (-41.2115 -74.1807 0.0)
237   0  -301 105 -106 202 -203 620 -675
         fill=12 (-24.7269 -74.1807 0.0)
c
167   0  106 -107 202 -203  620 -675
         fill=3 (-8.2423 -74.1807 0.0)
168   0  107 -108 202 -203  620 -675
         fill=1 ( 8.2423 -74.1807 0.0)
c
238   0  -301 108 -109 202 -203 620 -675
         fill=10 (24.7269 -74.1807 0.0)
239   0  -301 109 -110 -203 620 -675
         fill=11 (41.2115 -74.1807 0.0)
240   0  -301 110 -203 620 -675
c
241   0  -301  -106 -202 620 -675
242   0  -301  106 -107 -202 620 -675
         fill=11 (-8.2423 -90.6653 0.0)
243   0  -301  107 -108 -202 620 -675
         fill=11 ( 8.2423 -90.6653 0.0)
244   0  -301  108 -202 620 -675
c
821   5 -7.92 301 -302 610 -630  $ MPC shell
822   0       302 -501 610 -630  $ Air gap
823   5 -7.92 301 -302 630 -670  $ MPC shell
824   0       302 -501 630 -670  $ Air gap
825   5 -7.92 301 -302 670 -675  $ MPC shell
826   0       302 -501 670 -675  $ Air gap
827   5 -7.92 301 -302 675 -680  $ MPC shell
828   0       301 -302 680 -685  $ Air gap
829   0       302 -501 675 -685  $ Air gap
c
830   5 -7.92     -301 610 -620  $ MPC baseplate
840   5 -7.92     -301 675 -680  $ MPC lid (both)
850   0           -301 680 -685  $ Air gap
c     OVERPACK \/ \/ \/ \/ \/
c
1001  8 -7.82 501 -502 630 -670 $ steel shell
1002  8 -7.82 502 -503 630 -670 $ steel shell
1003  8 -7.82 503 -504 630 -670 $ steel shell
1004  8 -7.82 504 -505 630 -670 $ steel shell
1005  8 -7.82 505 -506 630 -670 $ steel shell
1006  8 -7.82 506 -507 630 -670 $ steel shell
1007  8 -7.82 507 -508 630 -670 $ steel shell
1008  0       508 -509 630 -670  fill=20
1009  0       509 -510 630 -670  fill=20
1010  0       510 -511 630 -670  fill=20
1011  0       511 -512 630 -670  fill=20
1012  8 -7.82 512 -513 630 -670 $ outer steel shell
c     1012  8 -7.82  512 -513 640 -670             $ outer steel shell
c     1013  0        512 -513 630 -640  1103 -1102 $ air in pocket trun.
c     1014  0        512 -513 630 -640  2103 -2102 $ air in pocket trun.
c     1015  8 -7.82  512 -513 630 -640  1102  2102 $ outer steel shell
c     1016  8 -7.82  512 -513 630 -640  1102 -2103 $ outer steel shell
c     1017  8 -7.82  512 -513 630 -640 -1103 -2103 $ outer steel shell
c     1018  8 -7.82  512 -513 630 -640 -1103  2102 $ outer steel shell
c
c      steel spines and holtite
10101   8 -7.82   2000 -2002  645 -660   1000  u=20 $ steel spine
10102   7 -1.61   2002 -2011  645 -660   2000  u=20 $ holtite
```

```
10103   8 -7.82   2011 -2012  645 -660   2000  u=20 $ steel spine
10104   7 -1.61   2012 -2021  645 -660   2000  u=20 $ holtite
10105   8 -7.82   2021 -2022  645 -660   2000  u=20 $ steel spine
10106   7 -1.61   2022 -2031  645 -660   2000  u=20 $ holtite
10107   8 -7.82   2031 -2032  645 -660   2000  u=20 $ steel spine
10108   7 -1.61   2032 -2041  645 -660   2000  u=20 $ holtite
10109   8 -7.82   2041 -2042  645 -660   2000  u=20 $ steel spine
10110   7 -1.61   2042 -2051  645 -660   2000  u=20 $ holtite
10111   8 -7.82   2051 -2052  645 -660   2000  u=20 $ steel spine
10112   7 -1.61   2052 -2061  645 -660   2000  u=20 $ holtite
10113   8 -7.82   2061 -2062  645 -660   2000  u=20 $ steel spine
10114   7 -1.61   2062 -2071  645 -660   2000  u=20 $ holtite
10115   8 -7.82   2071 -2072  645 -660   2000  u=20 $ steel spine
10116   7 -1.61   2072 -2081  645 -660   2000  u=20 $ holtite
10117   8 -7.82   2081 -2082  645 -660   2000  u=20 $ steel spine
10118   7 -1.61   2082 -2091  645 -660   2000  u=20 $ holtite
10119   8 -7.82   2091 -2092  645 -660   2000  u=20 $ steel spine
10120   7 -1.61   2092  1002  645 -660   2000  u=20 $ holtite
10121   8 -7.82   1000 -1002  645 -660   2000  u=20 $ steel spine
c
10122   8 -7.82   1001 -1000  645 -660   2000  u=20 $ steel spine
10123   7 -1.61   1012 -1001  645 -660   2000  u=20 $ holtite
10124   8 -7.82   1011 -1012  645 -660   2000  u=20 $ steel spine
10125   7 -1.61   1022 -1011  645 -660   2000  u=20 $ holtite
10126   8 -7.82   1021 -1022  645 -660   2000  u=20 $ steel spine
10127   7 -1.61   1032 -1021  645 -660   2000  u=20 $ holtite
10128   8 -7.82   1031 -1032  645 -660   2000  u=20 $ steel spine
10129   7 -1.61   1042 -1031  645 -660   2000  u=20 $ holtite
10130   8 -7.82   1041 -1042  645 -660   2000  u=20 $ steel spine
10131   7 -1.61   1052 -1041  645 -660   2000  u=20 $ holtite
10132   8 -7.82   1051 -1052  645 -660   2000  u=20 $ steel spine
10133   7 -1.61   1062 -1051  645 -660   2000  u=20 $ holtite
10134   8 -7.82   1061 -1062  645 -660   2000  u=20 $ steel spine
10135   7 -1.61   1072 -1061  645 -660   2000  u=20 $ holtite
10136   8 -7.82   1071 -1072  645 -660   2000  u=20 $ steel spine
10137   7 -1.61   1082 -1071  645 -660   2000  u=20 $ holtite
10138   8 -7.82   1081 -1082  645 -660   2000  u=20 $ steel spine
10139   7 -1.61   1092 -1081  645 -660   2000  u=20 $ holtite
10140   8 -7.82   1091 -1092  645 -660   2000  u=20 $ steel spine
10141   7 -1.61   2002 -1091  645 -660   2000  u=20 $ holtite
10142   8 -7.82   2000 -2002  645 -660  -1000  u=20 $ steel spine
c
10143   8 -7.82   2001 -2000  645 -660  -1000  u=20 $ steel spine
10144   7 -1.61   2012 -2001  645 -660  -2000  u=20 $ holtite
10145   8 -7.82   2011 -2012  645 -660  -2000  u=20 $ steel spine
10146   7 -1.61   2022 -2011  645 -660  -2000  u=20 $ holtite
10147   8 -7.82   2021 -2022  645 -660  -2000  u=20 $ steel spine
10148   7 -1.61   2032 -2021  645 -660  -2000  u=20 $ holtite
10149   8 -7.82   2031 -2032  645 -660  -2000  u=20 $ steel spine
10150   7 -1.61   2042 -2031  645 -660  -2000  u=20 $ holtite
10151   8 -7.82   2041 -2042  645 -660  -2000  u=20 $ steel spine
10152   7 -1.61   2052 -2041  645 -660  -2000  u=20 $ holtite
10153   8 -7.82   2051 -2052  645 -660  -2000  u=20 $ steel spine
10154   7 -1.61   2062 -2051  645 -660  -2000  u=20 $ holtite
10155   8 -7.82   2061 -2062  645 -660  -2000  u=20 $ steel spine
10156   7 -1.61   2072 -2061  645 -660  -2000  u=20 $ holtite
10157   8 -7.82   2071 -2072  645 -660  -2000  u=20 $ steel spine
10158   7 -1.61   2082 -2071  645 -660  -2000  u=20 $ holtite
10159   8 -7.82   2081 -2082  645 -660  -2000  u=20 $ steel spine
10160   7 -1.61   2092 -2081  645 -660  -2000  u=20 $ holtite
10161   8 -7.82   2091 -2092  645 -660  -2000  u=20 $ steel spine
10162   7 -1.61  -1001 -2091  645 -660  -2000  u=20 $ holtite
10163   8 -7.82   1001 -1000  645 -660  -2000  u=20 $ steel spine
c
10164   8 -7.82   1000 -1002  645 -660  -2000  u=20 $ steel spine
10165   7 -1.61   1002 -1011  645 -660  -2000  u=20 $ holtite
10166   8 -7.82   1011 -1012  645 -660  -2000  u=20 $ steel spine
10167   7 -1.61   1012 -1021  645 -660  -2000  u=20 $ holtite
10168   8 -7.82   1021 -1022  645 -660  -2000  u=20 $ steel spine
```

```
10169   7 -1.61   1022 -1031  645 -660  -2000  u=20 $ holtite
10170   8 -7.82   1031 -1032  645 -660  -2000  u=20 $ steel spine
10171   7 -1.61   1032 -1041  645 -660  -2000  u=20 $ holtite
10172   8 -7.82   1041 -1042  645 -660  -2000  u=20 $ steel spine
10173   7 -1.61   1042 -1051  645 -660  -2000  u=20 $ holtite
10174   8 -7.82   1051 -1052  645 -660  -2000  u=20 $ steel spine
10175   7 -1.61   1052 -1061  645 -660  -2000  u=20 $ holtite
10176   8 -7.82   1061 -1062  645 -660  -2000  u=20 $ steel spine
10177   7 -1.61   1062 -1071  645 -660  -2000  u=20 $ holtite
10178   8 -7.82   1071 -1072  645 -660  -2000  u=20 $ steel spine
10179   7 -1.61   1072 -1081  645 -660  -2000  u=20 $ holtite
10180   8 -7.82   1081 -1082  645 -660  -2000  u=20 $ steel spine
10181   7 -1.61   1082 -1091  645 -660  -2000  u=20 $ holtite
10182   8 -7.82   1091 -1092  645 -660  -2000  u=20 $ steel spine
10183   7 -1.61   1092 -2001  645 -660  -2000  u=20 $ holtite
10184   8 -7.82   2001 -2000  645 -660   1000  u=20 $ steel spine
c
c    10201   8 -7.82   2000 -2002  635 -645   1000  u=20 $ steel spine
c    10202   7 -1.61   2002 -2011  635 -645   2000  u=20 $ holtite
10202   7 -1.61   2101 -2011  635 -645   2000  u=20 $ holtite
10203   8 -7.82   2011 -2012  635 -645   2000  u=20 $ steel spine
10204   7 -1.61   2012 -2021  635 -645   2000  u=20 $ holtite
10205   8 -7.82   2021 -2022  635 -645   2000  u=20 $ steel spine
10206   7 -1.61   2022 -2031  635 -645   2000  u=20 $ holtite
10207   8 -7.82   2031 -2032  635 -645   2000  u=20 $ steel spine
10208   7 -1.61   2032 -2041  635 -645   2000  u=20 $ holtite
10209   8 -7.82   2041 -2042  635 -645   2000  u=20 $ steel spine
10210   7 -1.61   2042 -2051  635 -645   2000  u=20 $ holtite
10211   8 -7.82   2051 -2052  635 -645   2000  u=20 $ steel spine
10212   7 -1.61   2052 -2061  635 -645   2000  u=20 $ holtite
10213   8 -7.82   2061 -2062  635 -645   2000  u=20 $ steel spine
10214   7 -1.61   2062 -2071  635 -645   2000  u=20 $ holtite
10215   8 -7.82   2071 -2072  635 -645   2000  u=20 $ steel spine
10216   7 -1.61   2072 -2081  635 -645   2000  u=20 $ holtite
10217   8 -7.82   2081 -2082  635 -645   2000  u=20 $ steel spine
10218   7 -1.61   2082 -2091  635 -645   2000  u=20 $ holtite
10219   8 -7.82   2091 -2092  635 -645   2000  u=20 $ steel spine
c    10220   7 -1.61   2092  1101  635 -645   2000  u=20 $ holtite
10220   7 -1.61   2092  1002  635 -645   2000  u=20 $ holtite
10221   8 -7.82   1000 -1002  635 -645   2000  u=20 $ steel spine
c
10222   8 -7.82   1001 -1000  635 -645   2000  u=20 $ steel spine
10223   7 -1.61   1012 -1001  635 -645   2000  u=20 $ holtite
c    10223   7 -1.61   1012 -1104  635 -645   2000  u=20 $ holtite
10224   8 -7.82   1011 -1012  635 -645   2000  u=20 $ steel spine
10225   7 -1.61   1022 -1011  635 -645   2000  u=20 $ holtite
10226   8 -7.82   1021 -1022  635 -645   2000  u=20 $ steel spine
10227   7 -1.61   1032 -1021  635 -645   2000  u=20 $ holtite
10228   8 -7.82   1031 -1032  635 -645   2000  u=20 $ steel spine
10229   7 -1.61   1042 -1031  635 -645   2000  u=20 $ holtite
10230   8 -7.82   1041 -1042  635 -645   2000  u=20 $ steel spine
10231   7 -1.61   1052 -1041  635 -645   2000  u=20 $ holtite
10232   8 -7.82   1051 -1052  635 -645   2000  u=20 $ steel spine
10233   7 -1.61   1062 -1051  635 -645   2000  u=20 $ holtite
10234   8 -7.82   1061 -1062  635 -645   2000  u=20 $ steel spine
10235   7 -1.61   1072 -1061  635 -645   2000  u=20 $ holtite
10236   8 -7.82   1071 -1072  635 -645   2000  u=20 $ steel spine
10237   7 -1.61   1082 -1071  635 -645   2000  u=20 $ holtite
10238   8 -7.82   1081 -1082  635 -645   2000  u=20 $ steel spine
10239   7 -1.61   1092 -1081  635 -645   2000  u=20 $ holtite
10240   8 -7.82   1091 -1092  635 -645   2000  u=20 $ steel spine
10241   7 -1.61   2101 -1091  635 -645   2000  u=20 $ holtite
c    10241   7 -1.61   2002 -1091  635 -645   2000  u=20 $ holtite
c    10242   8 -7.82   2000 -2002  635 -645  -1000  u=20 $ steel spine
c
c    10243   8 -7.82   2001 -2000  635 -645  -1000  u=20 $ steel spine
c    10244   7 -1.61   2012 -2001  635 -645  -2000  u=20 $ holtite
10244   7 -1.61   2012 -2104  635 -645  -2000  u=20 $ holtite
10245   8 -7.82   2011 -2012  635 -645  -2000  u=20 $ steel spine
```

```
10246   7 -1.61   2022 -2011  635 -645  -2000  u=20 $ holtite
10247   8 -7.82   2021 -2022  635 -645  -2000  u=20 $ steel spine
10248   7 -1.61   2032 -2021  635 -645  -2000  u=20 $ holtite
10249   8 -7.82   2031 -2032  635 -645  -2000  u=20 $ steel spine
10250   7 -1.61   2042 -2031  635 -645  -2000  u=20 $ holtite
10251   8 -7.82   2041 -2042  635 -645  -2000  u=20 $ steel spine
10252   7 -1.61   2052 -2041  635 -645  -2000  u=20 $ holtite
10253   8 -7.82   2051 -2052  635 -645  -2000  u=20 $ steel spine
10254   7 -1.61   2062 -2051  635 -645  -2000  u=20 $ holtite
10255   8 -7.82   2061 -2062  635 -645  -2000  u=20 $ steel spine
10256   7 -1.61   2072 -2061  635 -645  -2000  u=20 $ holtite
10257   8 -7.82   2071 -2072  635 -645  -2000  u=20 $ steel spine
10258   7 -1.61   2082 -2071  635 -645  -2000  u=20 $ holtite
10259   8 -7.82   2081 -2082  635 -645  -2000  u=20 $ steel spine
10260   7 -1.61   2092 -2081  635 -645  -2000  u=20 $ holtite
10261   8 -7.82   2091 -2092  635 -645  -2000  u=20 $ steel spine
c    10262   7 -1.61  -1104 -2091  635 -645  -2000  u=20 $ holtite
10262   7 -1.61  -1001 -2091  635 -645  -2000  u=20 $ holtite
10263   8 -7.82   1001 -1000  635 -645  -2000  u=20 $ steel spine
c
10264   8 -7.82   1000 -1002  635 -645  -2000  u=20 $ steel spine
10265   7 -1.61   1002 -1011  635 -645  -2000  u=20 $ holtite
c    10265   7 -1.61   1101 -1011  635 -645  -2000  u=20 $ holtite
10266   8 -7.82   1011 -1012  635 -645  -2000  u=20 $ steel spine
10267   7 -1.61   1012 -1021  635 -645  -2000  u=20 $ holtite
10268   8 -7.82   1021 -1022  635 -645  -2000  u=20 $ steel spine
10269   7 -1.61   1022 -1031  635 -645  -2000  u=20 $ holtite
10270   8 -7.82   1031 -1032  635 -645  -2000  u=20 $ steel spine
10271   7 -1.61   1032 -1041  635 -645  -2000  u=20 $ holtite
10272   8 -7.82   1041 -1042  635 -645  -2000  u=20 $ steel spine
10273   7 -1.61   1042 -1051  635 -645  -2000  u=20 $ holtite
10274   8 -7.82   1051 -1052  635 -645  -2000  u=20 $ steel spine
10275   7 -1.61   1052 -1061  635 -645  -2000  u=20 $ holtite
10276   8 -7.82   1061 -1062  635 -645  -2000  u=20 $ steel spine
10277   7 -1.61   1062 -1071  635 -645  -2000  u=20 $ holtite
10278   8 -7.82   1071 -1072  635 -645  -2000  u=20 $ steel spine
10279   7 -1.61   1072 -1081  635 -645  -2000  u=20 $ holtite
10280   8 -7.82   1081 -1082  635 -645  -2000  u=20 $ steel spine
10281   7 -1.61   1082 -1091  635 -645  -2000  u=20 $ holtite
10282   8 -7.82   1091 -1092  635 -645  -2000  u=20 $ steel spine
10283   7 -1.61   1092 -2104  635 -645  -2000  u=20 $ holtite
c    10283   7 -1.61   1092 -2001  635 -645  -2000  u=20 $ holtite
c    10284   8 -7.82   2001 -2000  635 -645   1000  u=20 $ steel spine
c
11000   0         660 -665   u=20 $ foam
11001   8 -7.82   665        u=20 $ item 17 top
c    11002   8 -7.82   1101  2101  -635  u=20 $ item 17 bot
c    11003   8 -7.82  -2104  1101  -635  u=20 $ item 17 bot
c    11004   8 -7.82  -1104 -2104  -635  u=20 $ item 17 bot
c    11005   8 -7.82   2101 -1104  -635  u=20 $ item 17 bot
11002   8 -7.82         2101  -635  u=20 $ item 17 bot
11003   8 -7.82  -2104        -635  u=20 $ item 17 bot
c
c    pocket trunion
c
c    11101   8 -7.82  -514  1104 -1101 -640  u=20 $ pocket trunion before hole
c    11102   8 -7.82   514  1104 -1103 -640  u=20 $ steel on side of hole
c    11103   8 -7.82   514  1103 -1102 -640  u=20 $ hole
c    11104   8 -7.82   514  1102 -1101 -640  u=20 $ steel on side of hole
c    11105   8 -7.82        1104 -1101  640 -645  u=20 $ steel above hole
c
11111   8 -7.82  -514  2104 -2101 -640  u=20 $ pocket trunion before hole
11112   8 -7.82   514  2104 -2103 -640  u=20 $ steel on side of hole
11113   8 -7.82   514  2103 -2102 -640  u=20 $ hole
11114   8 -7.82   514  2102 -2101 -640  u=20 $ steel on side of hole
11115   8 -7.82        2104 -2101  640 -645  u=20 $ steel above hole
c
c     overpack base plate
c
```

```
2000  8 -7.82      -301 600 -610
2001  8 -7.82 301 -501 600 -610
2002  8 -7.82 501 -502 600 -630
2003  8 -7.82 502 -503 600 -630
2004  8 -7.82 503 -504 600 -630
2005  8 -7.82 504 -505 600 -630
2006  8 -7.82 505 -506 600 -630
2007  8 -7.82 506 -515 600 -630
2017  9 -1.17e-3   515 -507 600 -630 fill=27
2008  9 -1.17e-3   507 -508 600 -630 fill=27
2009  9 -1.17e-3   508 -509 600 -630
2010  9 -1.17e-3   509 -510 600 -630
2011  9 -1.17e-3   510 -511 600 -630
2012  9 -1.17e-3   511 -512 600 -630
2013  9 -1.17e-3   512 -513 600 -630
c
c     overpack lid
c
3000  8 -7.82      -301 685 -695
3001  8 -7.82 301 -501 685 -695
3002  8 -7.82 501 -502 685 -695
3003  8 -7.82 502 -503 685 -695
3004  8 -7.82 503 -504 685 -695
3005  8 -7.82 504 -505 685 -695
3006  8 -7.82 505 -518 685 -695
3007  9 -1.17e-3   518 -507 685 -695 fill=28
3008  9 -1.17e-3   507 -508 685 -695 fill=28
3009  9 -1.17e-3   508 -509 685 -695
3010  9 -1.17e-3   509 -510 685 -695
3011  9 -1.17e-3   510 -511 685 -695
3012  9 -1.17e-3   511 -512 685 -695
3013  9 -1.17e-3   512 -513 685 -695
c
3022  8 -7.82      501 -502 675 -685
3023  8 -7.82      502 -503 675 -685
3024  8 -7.82      503 -504 675 -685
3025  8 -7.82      504 -505 675 -685
3026  8 -7.82      505 -506 675 -677
3126  8 -7.82      505 -518 677 -685
3027  8 -7.82      506 -507 675 -676
3127  8 -7.82      506 -516 676 -677
3227  9 -1.17e-3   516 -507 676 -677
3327  9 -1.17e-3   518 -507 677 -685 fill=28
3028  8 -7.82      507 -508 675 -676
3128  9 -1.17e-3   507 -508 676 -677
3228  9 -1.17e-3   507 -508 677 -685 fill=28
3029  8 -7.82      508 -517 675 -676
3129  9 -1.17e-3   517 -509 675 -676
3229  9 -1.17e-3   508 -509 676 -685
3030  9 -1.17e-3   509 -510 675 -685
3031  9 -1.17e-3   510 -511 675 -685
3032  9 -1.17e-3   511 -512 675 -685
3033  9 -1.17e-3   512 -513 675 -685
c
3042  8 -7.82      501 -502 670 -675
3043  8 -7.82      502 -503 670 -675
3044  8 -7.82      503 -504 670 -675
3045  8 -7.82      504 -505 670 -675
3046  8 -7.82      505 -506 670 -675
3047  8 -7.82      506 -507 670 -675
3048  8 -7.82      507 -508 670 -675
3049  8 -7.82      508 -517 670 -675
3149  9 -1.17e-3   517 -509 670 -675
3050  9 -1.17e-3   509 -510 670 -675
3051  9 -1.17e-3   510 -511 670 -675
3052  9 -1.17e-3   511 -512 670 -675
3053  9 -1.17e-3   512 -513 670 -675
c
c     surrounding air regions
```

```
9000  9 -1.17e-3        -301 695 -723  fill=26
9001  9 -1.17e-3   301 -501 695 -723  fill=26
9002  9 -1.17e-3   501 -502 695 -723  fill=26
9003  9 -1.17e-3   502 -503 695 -723  fill=26
9004  9 -1.17e-3   503 -504 695 -723  fill=26
9005  9 -1.17e-3   504 -505 695 -723  fill=26
9006  9 -1.17e-3   505 -506 695 -723  fill=26
9007  9 -1.17e-3   506 -507 695 -723  fill=28
9008  9 -1.17e-3   507 -508 695 -723  fill=28
9009  9 -1.17e-3   508 -509 695 -723
9010  9 -1.17e-3   509 -510 695 -723
9011  9 -1.17e-3   510 -511 695 -723
9012  9 -1.17e-3   511 -512 695 -723
9013  9 -1.17e-3   512 -513 695 -723
c
9100  9 -1.17e-3        -301 701 -600  fill=25
9101  9 -1.17e-3   301 -501 701 -600  fill=25
9102  9 -1.17e-3   501 -502 701 -600  fill=25
9103  9 -1.17e-3   502 -503 701 -600  fill=25
9104  9 -1.17e-3   503 -504 701 -600  fill=25
9105  9 -1.17e-3   504 -505 701 -600  fill=25
9106  9 -1.17e-3   505 -506 701 -600  fill=25
9107  9 -1.17e-3   506 -507 701 -600  fill=27
9108  9 -1.17e-3   507 -508 701 -600  fill=27
9109  9 -1.17e-3   508 -509 701 -600
9110  9 -1.17e-3   509 -510 701 -600
9111  9 -1.17e-3   510 -511 701 -600
9112  9 -1.17e-3   511 -512 701 -600
9113  9 -1.17e-3   512 -513 701 -600
c
9200  9 -1.17e-3   513 -521 701 -630
9201  9 -1.17e-3   521 -522 701 -630
9202  9 -1.17e-3   522 -523 701 -630
9203  9 -1.17e-3   523 -524 701 -630
9204  9 -1.17e-3   524 -525 701 -630
9205  9 -1.17e-3   525 -526 701 -630
9206  9 -1.17e-3   526 -527 701 -630
c
9210  9 -1.17e-3   513 -521 630 -670
9211  9 -1.17e-3   521 -522 630 -670
9212  9 -1.17e-3   522 -523 630 -670
9213  9 -1.17e-3   523 -524 630 -670
9214  9 -1.17e-3   524 -525 630 -670
9215  9 -1.17e-3   525 -526 630 -670
9216  9 -1.17e-3   526 -527 630 -670
c
9220  9 -1.17e-3   513 -521 670 -675
9221  9 -1.17e-3   521 -522 670 -675
9222  9 -1.17e-3   522 -523 670 -675
9223  9 -1.17e-3   523 -524 670 -675
9224  9 -1.17e-3   524 -525 670 -675
9225  9 -1.17e-3   525 -526 670 -675
9226  9 -1.17e-3   526 -527 670 -675
c
9230  9 -1.17e-3   513 -521 675 -685
9231  9 -1.17e-3   521 -522 675 -685
9232  9 -1.17e-3   522 -523 675 -685
9233  9 -1.17e-3   523 -524 675 -685
9234  9 -1.17e-3   524 -525 675 -685
9235  9 -1.17e-3   525 -526 675 -685
9236  9 -1.17e-3   526 -527 675 -685
c
9240  9 -1.17e-3   513 -521 685 -723
9241  9 -1.17e-3   521 -522 685 -723
9242  9 -1.17e-3   522 -523 685 -723
9243  9 -1.17e-3   523 -524 685 -723
9244  9 -1.17e-3   524 -525 685 -723
9245  9 -1.17e-3   525 -526 685 -723
9246  9 -1.17e-3   526 -527 685 -723
```

```
c
c
c     impact limiters both top and bottom
c
9508  7 -1.61          -870 803 -801 u=25 $ holtite
9509  8 -7.82     870  -871  803 -801 u=25 $ steel support item 2
9510  8 -7.82     871   852 -851  803 -801 u=25
9511  8 -7.82     871   854 -853  803 -801 u=25
9512  8 -7.82     871   856 -855   803 -801 u=25
9513  8 -7.82     871   858 -857   803 -801 u=25
9514  8 -7.82     871   860 -859   803 -801 u=25
9515  8 -7.82     871   862 -861   803 -801 u=25
9516  8 -7.82     871   864 -863   803 -801 u=25
9517  8 -7.82     871   866 -865   803 -801 u=25
9518  7 -1.61     871   851 -854 2000  803 -801 u=25
9519  7 -1.61     871   853 -856 2000  803 -801 u=25
9520  7 -1.61     871   855 -858 2000  803 -801 u=25
9521  7 -1.61     871   857  859 2000  803 -801 u=25
9522  7 -1.61     871   861 -860 2000  803 -801 u=25
9523  7 -1.61     871   863 -862 2000  803 -801 u=25
9524  7 -1.61     871   865 -864 2000  803 -801 u=25
9525  7 -1.61     871   851 -866 2000  803 -801 u=25
9526  7 -1.61     871   853 -852 -2000  803 -801 u=25
9527  7 -1.61     871   855 -854 -2000  803 -801 u=25
9528  7 -1.61     871   857 -856 -2000  803 -801 u=25
9529  7 -1.61     871   -858 -860 -2000  803 -801 u=25
9530  7 -1.61     871   859 -862 -2000  803 -801 u=25
9531  7 -1.61     871   861 -864 -2000  803 -801 u=25
9532  7 -1.61     871   863 -866 -2000  803 -801 u=25
9533  7 -1.61     871   865 -852 -2000  803 -801 u=25
c
9534  8 -7.82                  801 u=25 $ steel plate
9535  9 -1.17e-3              -803  u=25 $ air below
c
9536  8 -7.82     -519  803 u=27
9537  9 -1.17e-3  519   803 u=27
9538  9 -1.17e-3       -803 u=27
c
9608  7 -1.61          -870 821 -823 u=26 $ holtite
9609  8 -7.82     870  -871  821 -823 u=26 $ steel support item 2
9610  8 -7.82     871   852 -851  821 -823 u=26
9611  8 -7.82     871   854 -853  821 -823 u=26
9612  8 -7.82     871   856 -855   821 -823 u=26
9613  8 -7.82     871   858 -857   821 -823 u=26
9614  8 -7.82     871   860 -859   821 -823 u=26
9615  8 -7.82     871   862 -861   821 -823 u=26
9616  8 -7.82     871   864 -863   821 -823 u=26
9617  8 -7.82     871   866 -865   821 -823 u=26
9618  7 -1.61     871   851 -854 2000  821 -823 u=26
9619  7 -1.61     871   853 -856 2000  821 -823 u=26
9620  7 -1.61     871   855 -858 2000  821 -823 u=26
9621  7 -1.61     871   857  859 2000  821 -823 u=26
9622  7 -1.61     871   861 -860 2000  821 -823 u=26
9623  7 -1.61     871   863 -862 2000  821 -823 u=26
9624  7 -1.61     871   865 -864 2000  821 -823 u=26
9625  7 -1.61     871   851 -866 2000  821 -823 u=26
9626  7 -1.61     871   853 -852 -2000  821 -823 u=26
9627  7 -1.61     871   855 -854 -2000  821 -823 u=26
9628  7 -1.61     871   857 -856 -2000  821 -823 u=26
9629  7 -1.61     871   -858 -860 -2000  821 -823 u=26
9630  7 -1.61     871   859 -862 -2000  821 -823 u=26
9631  7 -1.61     871   861 -864 -2000  821 -823 u=26
9632  7 -1.61     871   863 -866 -2000  821 -823 u=26
9633  7 -1.61     871   865 -852 -2000  821 -823 u=26
c
9634  8 -7.82                 -821 u=26 $ steel plate
9635  9 -1.17e-3              823  u=26 $ air above
9637  8 -7.82     -519       -823 u=28
9638  9 -1.17e-3              823 u=28
```

```
9639  9 -1.17e-3   519       -823 u=28
c
9999  0  527:-701:723
c
c     BLANK LINE

c     BLANK LINE
c
c     MPC surfaces\/ \/ \/ \/ \/
c
1     cz         0.52832
2     cz         0.53213
3     cz         0.61341
4     cz         0.67437
5     cz         0.75057
6     px         0.8128
7     px        -0.8128
8     py         0.8128
9     py        -0.8128
10    px        -4.445
11    px         4.445
12    py        -4.445
13    py         4.445
c     14    px         -8.2423
14    px        -8.242301
15    px        -7.9248
16    px        -7.66826
17    px        -7.47776
18    px        -6.0325
19    px         6.0325
20    px         7.9248
c     21    px         8.2423
c     22    py        -8.2423
21    px         8.242301
22    py        -8.242301
23    py        -7.9248
24    py        -6.0325
25    py         6.0325
26    py         7.47776
27    py         7.66826
28    py         7.9248
c     29    py         8.2423
29    py         8.242301
c
30    px   -6.56082
31    px    6.56082
32    py   -6.56082
33    py    6.56082
c
101   px  -98.9076
102   px  -82.423
103   px  -65.9384
104   px  -49.4538
105   px  -32.9692
106   px  -16.4846
107   px   0.0
108   px   16.4846
109   px   32.9692
110   px   49.4538
111   px   65.9384
112   px   82.423
113   px   98.9076
c
201   py  -98.9076
202   py  -82.423
203   py  -65.9384
204   py  -49.4538
205   py  -32.9692
206   py  -16.4846
```

```
207   py   0.0
208   py   16.4846
209   py   32.9692
210   py   49.4538
211   py   65.9384
212   py   82.423
213   py   98.9076
c
301   cz   85.4075
302   cz   86.6775
c
c     620   pz    21.59     $ MPC baseplate        - 2.5 inches
c     400   pz   24.765  $ start of egg crate
400   pz   23.876  $ start of egg crate
410   pz   33.9725  $ start of boral
420   pz   40.3479 $ beginning of fuel
425   pz   406.1079 $ end of fuel
430   pz   421.3479 $ space
435   pz   430.2125  $ end of boral
440   pz   445.4271 $ plenum
445   pz   448.8561 $ expansion springs
450   pz   457.3397 $ top end fitting
455   pz   468.63   $ top of element
460   pz   466.344  $ top of egg crate
c
c     MPC surfaces/\ /\ /\ /\ /\
c
c
c     OVERPACK survaces \/ \/ \/ \/ \/
c
501   cz    87.3125  $ IR for overpack
502   cz    90.4875  $ item 2  1.25 inch
503   cz    93.6625  $ item 2  1.25 inch
504   cz    96.8375    $ item 12  1.25 inch
505   cz    100.0125   $ item 13  1.25 inch
506   cz    103.1875   $ item 14  1.25 inch
507   cz    106.3625   $ item 15  1.25 inch
508   cz    108.9025   $ item 16  1 inch
509   cz    111.521875  $ holtite
510   cz    114.14125   $ holtite
511   cz    116.760625  $ holtite
512   cz    119.53875      $ holtite - total 4.1875 inches
513   cz    120.80875      $ outer steel shell - 0.5 inches
c     512   cz    119.38      $ holtite - total 4.125 inches
c     513   cz    120.65      $ outer steel shell - 0.5 inches
514   cz    111.54      $ hole in pocket trunion
515   cz    105.7275    $ flange bottom of overpack
516   cz    105.7275    $ flange top    of overpack
517   cz    109.5375    $ shear ring
518   cz    103.1875    $ item 14  1.25 inch
519   cz    108.2675    $ impact limiter - 2 inch steel
c
521   cz    162.56      $ surface of impact limiters
522   cz    203.1875    $ 1 meter from 506 - upper and lower part overpack
523   cz    220.80875   $ 1 meter from 513 - outer steel
524   cz    303.1875    $ 2 meter from 506 - upper and lower part overpack
525   cz    320.80875   $ 2 meter from 513 - outer steel
526   cz    362.56      $ 2 meter from 521 - edge of impact limiters
527   cz    400.00
c
600   pz    0.0       $ bottom of overpack
610   pz    15.24     $ overpack baseplate   - 6 inches
620   pz    21.59     $ MPC baseplate        - 2.5 inches
630   pz    22.225    $ beginning of item 17 - 0.25 inches
635   pz    23.495    $ item 17              - 0.5 inches
640   pz    41.75125  $ hole in pocket trun  - 7.6875 inches from 630
645   pz    54.61     $ top of pocket trun   - 12.75 inches from 630
660   pz    455.6125  $ top of holtite       - 170.125 inches from 635
665   pz    460.6925  $ top of foam          - 2 inches
```

```
670   pz    461.9625  $ top of item 17 on top- 0.5 inches
675   pz    474.98    $ bottom of MPC in lid - 178.5 inches from 620
676   pz    476.5675  $ top of shear ring
677   pz    494.03    $ top of add steel
680   pz    499.11    $ top of MPC outer lid - 7.5 inches from 675
685   pz    500.6975  $ bot of overpack lid  - 5/8 inch
695   pz    515.9375  $ top of overpack lid  - 6 inches
c
c     tally segment surfaces
c
701   pz    -121.92
702   pz    -91.44
703   pz    -60.96
704   pz    -30.48
c     600   pz    0.0       $ bottom of overpack
c     630   pz    22.225    $ beginning of item 17 - 0.25 inches
705   pz    51.5408
706   pz    80.8567
707   pz    110.1725
708   pz    139.4883
709   pz    168.8042
710   pz    198.1200
711   pz    227.4358
712   pz    256.7517
713   pz    286.0675
714   pz    315.3833
715   pz    344.6992
716   pz    374.0150
717   pz    403.3308
718   pz    432.6467
c     670   pz    461.9625  $ top of item 17 on top- 0.5 inches
719   pz    488.3150
c     695   pz    514.6675  $ top of overpack lid  - 6 inches
720   pz    545.1475
721   pz    575.6275
722   pz    606.1075
723   pz    636.5875
c
801   pz    -2.54    $ steel disk
802   pz    -5.715   $ holtite
803   pz    -8.89    $ holtite
804   pz    -9.2075  $ cover over holtite
805   pz    -53.34   $ item 2 on impact limiters
810   pz    -100.0   $ 1 meter from surface overpack
811   pz    -105.7275 $ edge of impact limiter
812   pz    -200.0    $ 2 meter from surface overpack
813   pz    -305.7275 $ 2 meter from surface impact limiter
814   pz    -427.6475 $ 2 meter + 4 feet
815   pz    -488.6075 $ 2 meter + 6 feet
816   pz    -671.4875 $ 2 meter + 12 feet
817   pz    -700.00
c
821   pz    517.2075    $ steel disk
822   pz    520.3825    $ holtite
823   pz    523.5575    $ holtite
824   pz    523.875     $ cover over holtite
825   pz    568.0075    $ item 2 on impact limiters
830   pz    614.6675    $ 1 meter from surface overpack
831   pz    620.3950    $ edge of impact limiter
832   pz    714.6675    $ 2 meter from surface overpack
833   pz    820.395     $ 2 meter from surface impact limiter
834   pz    942.3150    $ 2 meter + 4 feet
835   pz    1003.275    $ 2 meter + 6 feet
836   pz    1186.155    $ 2 meter + 12 feet
837   pz    1200.00
c
851       py    1.5875
852       py   -1.5875
853   11  py    1.5875
```

```
854  11  py   -1.5875
855  12  py    1.5875
856  12  py   -1.5875
857  13  py    1.5875
858  13  py   -1.5875
859      px    1.5875
860      px   -1.5875
861  11  px    1.5875
862  11  px   -1.5875
863  12  px    1.5875
864  12  px   -1.5875
865  13  px    1.5875
866  13  px   -1.5875
c
870      cz    38.1
871      cz    41.91
c         steel spine and holtite cells
c
1000      px    0.0
1001      px  -0.635
1002      px   0.635
1011   1  px  -0.635
1012   1  px   0.635
1021   2  px  -0.635
1022   2  px   0.635
1031   3  px  -0.635
1032   3  px   0.635
1041   4  px  -0.635
1042   4  px   0.635
1051   5  px  -0.635
1052   5  px   0.635
1061   6  px  -0.635
1062   6  px   0.635
1071   7  px  -0.635
1072   7  px   0.635
1081   8  px  -0.635
1082   8  px   0.635
1091   9  px  -0.635
1092   9  px   0.635
c
1101   px   15.71625  $ pocket trunion
1102   px   8.09625   $ pocket trunion opening
1103   px  -8.09625   $ pocket trunion opening 6 3/8 inches thick
1104   px  -15.71625  $ pocket trunion - 9 3/8 inches thick
c
2000      py   0.0
2001      py  -0.635
2002      py   0.635
2011   1  py  -0.635
2012   1  py   0.635
2021   2  py  -0.635
2022   2  py   0.635
2031   3  py  -0.635
2032   3  py   0.635
2041   4  py  -0.635
2042   4  py   0.635
2051   5  py  -0.635
2052   5  py   0.635
2061   6  py  -0.635
2062   6  py   0.635
2071   7  py  -0.635
2072   7  py   0.635
2081   8  py  -0.635
2082   8  py   0.635
2091   9  py  -0.635
2092   9  py   0.635
c
2101   py   15.71625  $ pocket trunion
2102   py   8.09625   $ pocket trunion opening
```

```
2103   py  -8.09625   $ pocket trunion opening 6 3/8 inches thick
2104   py  -15.71625  $ pocket trunion - 9 3/8 inches thick
c
c     OVERPACK surfaces /\ /\ /\ /\ /\
c
c     BLANK LINE

c     BLANK LINE
c
*tr1    0 0 0  9 279 90  99  9 90 90 90 0
*tr2    0 0 0 18 288 90 108 18 90 90 90 0
*tr3    0 0 0 27 297 90 117 27 90 90 90 0
*tr4    0 0 0 36 306 90 126 36 90 90 90 0
*tr5    0 0 0 45 315 90 135 45 90 90 90 0
*tr6    0 0 0 54 324 90 144 54 90 90 90 0
*tr7    0 0 0 63 333 90 153 63 90 90 90 0
*tr8    0 0 0 72 342 90 162 72 90 90 90 0
*tr9    0 0 0 81 351 90 171 81 90 90 90 0
*tr11   0 0 0 22.5 292.5 90 112.5 22.5 90 90 90 0
*tr12   0 0 0 45.0 315.0 90 135.0 45.0 90 90 90 0
*tr13   0 0 0 67.5 337.5 90 157.5 67.5 90 90 90 0
c
c         PHOTON MATERIALS
c
c     fuel 3.4 w/o U235  10.412 gm/cc
m1            92235.01p   -0.029971
              92238.01p   -0.851529
              8016.01p    -0.1185
c     homogenized fuel  density 4.29251 gm/cc
m2            92235.01p   -0.024966
              92238.01p   -0.709315
               8016.01p   -0.098709
              40000.01p   -0.16701
c     zirconium 6.55 gm/cc
m3            40000.01p   1.           $ Zr Clad
c     stainless steel 7.92 gm/cc
m5            24000.01p   -0.19
              25055.01p   -0.02
              26000.01p   -0.695
              28000.01p   -0.095
c     boral  2.644 gm/cc
m6            5010.01p    -0.044226
              5011.01p    -0.201474
              13027.01p   -0.6861
              6000.01p    -0.0682
c     holtite 1.61 gm/cc
m7            6000.01p  -0.2766039
             13027.01p  -0.21285
              1001.01p  -0.0592
              8016.01p  -0.42372
              7014.01p  -0.0198
              5010.01p  -0.0014087
              5011.01p  -0.0064174
c     carbon steel 7.82 gm/cc
m8      6000.01p -0.005 26000.01p -0.995
c     air density 1.17e-3 gm/cc
m9      7014.01p 0.78 8016.01p 0.22
c     c
c     c         NEUTRON MATERIALS
c
c     fuel 3.4 w/o U235  10.412 gm/cc
c     m1           92235.50c   -0.029971
c                  92238.50c   -0.851529
c                  8016.50c    -0.1185
c     c     homogenized fuel  density 4.29251 gm/cc
c     m2           92235.50c   -0.024966
c                  92238.50c   -0.709315
c                   8016.50c   -0.098709
c                  40000.35c   -0.16701
```

```
c     c     zirconium 6.55 gm/cc
c     m3          40000.35c   1.          $ Zr Clad
c     c     stainless steel 7.92 gm/cc
c     m5          24000.50c   -0.19
c                 25055.50c   -0.02
c                 26000.55c   -0.695
c                 28000.50c   -0.095
c     c     boral  2.644 gm/cc
c     m6          5010.50c    -0.044226
c                 5011.56c    -0.201474
c                 13027.50c   -0.6861
c                 6000.50c    -0.0682
c     c     holtite 1.61 gm/cc
c     m7          6000.50c  -0.2766039
c                13027.50c  -0.21285
c                 1001.50c  -0.0592
c                 8016.50c  -0.42372
c                 7014.50c  -0.0198
c                 5010.50c  -0.0014087
c                 5011.56c  -0.0064174
c     mt7    lwtr.01t
c     c     carbon steel 7.82 gm/cc
c     m8      6000.50c -0.005 26000.55c -0.995
c     c     air density 1.17e-3 gm/cc
c     m9      7014.50c 0.78 8016.50c 0.22
c
phys:n   20 0.0
phys:p   100 0
c     imp:n   1 228r 0
c     imp:p   1 228r 0
nps     2000000
prdmp    j   -30   1   2
c     print   10 110 160 161 20 170
print
mode  p
c
sdef  par=2  erg=d1 axs=0 0 1 x=d4 y=fx d5 z=d3
c
c    energy dist for gammas in the fuel
c
c    si1  h  0.7 1.0 1.5 2.0 2.5 3.0
c    sp1     0  0.31 0.31 0.15 0.15 0.08
c
c    energy dist for neutrons in the fuel
c
c    si1  h  0.1 0.4 0.9 1.4 1.85 3.0 6.43 20.0
c    sp1     0   0.03787 0.1935 0.1773 0.1310 0.2320 0.2098 0.01853
c
c    energy dist for Co60 gammas
c
si1  l 1.3325 1.1732
sp1    0.5    0.5
c
c    axial dist for neut and phot in fuel
c
c    si3  h 40.3479 55.5879 70.8279 101.3079 162.2679 223.2279
c           284.1879 345.1479 375.6279 390.8679 406.1079
c    sp3    0 0.009167 0.031667 0.086250 0.194583 0.199167
c           0.193750 0.178750 0.072083 0.025833 0.009167
c
c    axial dist for Co60 - a zero prob is in the fuel
c
si3  h 21.59 40.3479 421.3479 445.4271 448.8561 457.3397 468.63
sp3    0     0.547   0.0      0.125    0.045    0.227    0.056
c
si4  s               15 16
              13 14 15 16 17 18
           12 13 14 15 16 17 18 19
           12 13 14 15 16 17 18 19
```

```
         11 12 13 14 15 16 17 18 19 20
         11 12 13 14 15 16 17 18 19 20
            12 13 14 15 16 17 18 19
            12 13 14 15 16 17 18 19
               13 14 15 16 17 18
                     15 16
sp4  1 67r
c
ds5  s               30 30
               29 29 29 29 29 29
            28 28 28 28 28 28 28 28
            27 27 27 27 27 27 27 27
         26 26 26 26 26 26 26 26 26 26
         25 25 25 25 25 25 25 25 25 25
            24 24 24 24 24 24 24 24
            23 23 23 23 23 23 23 23
               22 22 22 22 22 22
                     21 21
c
si11  -80.74152 -67.61988
si12  -64.25692 -51.13528
si13  -47.77232 -34.65068
si14  -31.28772 -18.16608
si15  -14.80312 -1.68148
si16   1.68148   14.80312
si17   18.16608  31.28772
si18   34.65068  47.77232
si19   51.13528  64.25692
si20   67.61988  80.74152
c
si21  -80.74152 -67.61988
si22  -64.25692 -51.13528
si23  -47.77232 -34.65068
si24  -31.28772 -18.16608
si25  -14.80312 -1.68148
si26   1.68148   14.80312
si27   18.16608  31.28772
si28   34.65068  47.77232
si29   51.13528  64.25692
si30   67.61988  80.74152
sp11  0 1
sp12  0 1
sp13  0 1
sp14  0 1
sp15  0 1
sp16  0 1
sp17  0 1
sp18  0 1
sp19  0 1
sp20  0 1
sp21  0 1
sp22  0 1
sp23  0 1
sp24  0 1
sp25  0 1
sp26  0 1
sp27  0 1
sp28  0 1
sp29  0 1
sp30  0 1
c
#           imp:p
   301        1
   302        1
   303        1
   304        1
   305        1
   306        1
   307        1
```

308	1
309	3
310	3
311	3
312	3
314	1
315	1
316	1
317	1
318	1
319	1
320	1
321	1
322	1
323	1
324	1
325	1
326	1
327	1
328	1
329	1
330	1
331	1
332	1
333	1
338	1
339	1
340	1
341	1
342	1
343	1
344	1
345	3
346	3
347	1
348	1
349	1
350	1
401	1
402	1
403	1
404	1
405	1
406	1
407	1
408	1
409	3
410	3
411	3
412	3
414	1
415	1
416	1
417	1
438	1
439	1
440	1
441	1
442	1
443	1
444	1
445	3
446	3
447	1
448	1
449	1
450	1
501	1
502	1

503	1
504	1
505	1
506	1
507	1
508	1
509	3
510	3
511	3
512	3
514	1
515	1
516	1
517	1
518	1
519	1
522	1
523	1
526	1
527	1
528	1
529	1
530	1
531	1
532	1
533	1
538	1
539	1
540	1
541	1
542	1
543	1
544	1
545	3
546	3
547	1
548	1
549	1
550	1
601	1
602	1
603	1
604	1
605	1
606	1
607	1
608	1
609	3
610	3
611	3
612	3
614	1
615	1
616	1
617	1
620	1
621	1
624	1
625	1
626	1
627	1
628	1
629	1
630	1
631	1
632	1
633	1
638	1
639	1

640	1
641	1
642	1
643	1
644	1
645	3
646	3
647	1
648	1
649	1
650	1
701	1
702	1
704	3
705	3
706	3
710	1
711	1
713	3
714	3
715	3
720	1
721	1
722	1
724	3
725	3
726	3
727	3
730	1
731	1
739	1
740	3
741	3
745	1
753	1
754	1
755	1
756	3
757	3
758	3
760	1
772	1
773	1
774	1
775	3
776	3
777	3
780	1
788	1
789	1
790	3
791	3
795	1
803	1
804	1
805	1
806	3
807	3
808	3
201	1
202	1
203	1
204	1
205	1
206	1
207	1
101	1
102	1
208	1

209	1
210	1
211	1
212	1
103	1
104	1
105	1
106	1
107	1
108	1
213	1
214	1
215	1
109	1
110	1
111	1
112	1
113	1
114	1
115	1
116	1
216	1
217	1
218	1
117	1
118	1
119	1
120	1
121	1
122	1
123	1
124	1
219	1
220	1
221	1
125	1
126	1
127	1
128	1
129	1
130	1
131	1
132	1
133	1
134	1
222	1
223	1
135	1
136	1
137	1
138	1
139	1
140	1
141	1
142	1
143	1
144	1
224	1
225	1
226	1
145	1
146	1
147	1
148	1
149	1
150	1
151	1
152	1
227	1

228	1
229	1
153	1
154	1
155	1
156	1
157	1
158	1
159	1
160	1
230	1
231	1
232	1
161	1
162	1
163	1
164	1
165	1
166	1
233	1
234	1
235	1
236	1
237	1
167	1
168	1
238	1
239	1
240	1
241	1
242	1
243	1
244	1
821	9
822	9
823	3
824	3
825	9
826	9
827	27
828	27
829	27
830	3
840	9
850	9
1001	9
1002	27
1003	81
1004	243
1005	729
1006	2187
1007	6561
1008	13122
1009	13122
1010	26244
1011	26244
1012	52488
10101	1
10102	1
10103	1
10104	1
10105	1
10106	1
10107	1
10108	1
10109	1
10110	1
10111	1
10112	1

10113	1
10114	1
10115	1
10116	1
10117	1
10118	1
10119	1
10120	1
10121	1
10122	1
10123	1
10124	1
10125	1
10126	1
10127	1
10128	1
10129	1
10130	1
10131	1
10132	1
10133	1
10134	1
10135	1
10136	1
10137	1
10138	1
10139	1
10140	1
10141	1
10142	1
10143	1
10144	1
10145	1
10146	1
10147	1
10148	1
10149	1
10150	1
10151	1
10152	1
10153	1
10154	1
10155	1
10156	1
10157	1
10158	1
10159	1
10160	1
10161	1
10162	1
10163	1
10164	1
10165	1
10166	1
10167	1
10168	1
10169	1
10170	1
10171	1
10172	1
10173	1
10174	1
10175	1
10176	1
10177	1
10178	1
10179	1
10180	1
10181	1

10182	1
10183	1
10184	1
10202	1
10203	1
10204	1
10205	1
10206	1
10207	1
10208	1
10209	1
10210	1
10211	1
10212	1
10213	1
10214	1
10215	1
10216	1
10217	1
10218	1
10219	1
10220	1
10221	1
10222	1
10223	1
10224	1
10225	1
10226	1
10227	1
10228	1
10229	1
10230	1
10231	1
10232	1
10233	1
10234	1
10235	1
10236	1
10237	1
10238	1
10239	1
10240	1
10241	1
10244	1
10245	1
10246	1
10247	1
10248	1
10249	1
10250	1
10251	1
10252	1
10253	1
10254	1
10255	1
10256	1
10257	1
10258	1
10259	1
10260	1
10261	1
10262	1
10263	1
10264	1
10265	1
10266	1
10267	1
10268	1
10269	1

10270	1
10271	1
10272	1
10273	1
10274	1
10275	1
10276	1
10277	1
10278	1
10279	1
10280	1
10281	1
10282	1
10283	1
11000	1
11001	1
11002	1
11003	1
11111	1
11112	1
11113	1
11114	1
11115	1
2000	3
2001	9
2002	27
2003	81
2004	243
2005	729
2006	2187
2007	6561
2017	6561
2008	19683
2009	39366
2010	39366
2011	78732
2012	78732
2013	157464
3000	27
3001	81
3002	243
3003	729
3004	2187
3005	6561
3006	19683
3007	59049
3008	177147
3009	354294
3010	354294
3011	708588
3012	708588
3013	1417176
3022	81
3023	243
3024	729
3025	2181
3026	6561
3126	6561
3027	19683
3127	19683
3227	19683
3327	19683
3028	59049
3128	59049
3228	59049
3029	118098
3129	118098
3229	118098
3030	118098

3031	236196
3032	236196
3033	472392
3042	27
3043	81
3044	243
3045	729
3046	2187
3047	6561
3048	19683
3049	39366
3149	39366
3050	39366
3051	78732
3052	78732
3053	157464
9000	27
9001	81
9002	243
9003	729
9004	2187
9005	6561
9006	19683
9007	59049
9008	177147
9009	354294
9010	354294
9011	708588
9012	708588
9013	1417176
9100	3
9101	9
9102	27
9103	81
9104	243
9105	729
9106	2187
9107	6561
9108	19683
9109	39366
9110	39366
9111	78732
9112	78732
9113	157464
9200	157464
9201	157464
9202	157464
9203	157464
9204	157464
9205	157464
9206	157464
9210	52488
9211	52488
9212	52488
9213	52488
9214	52488
9215	52488
9216	52488
9220	157464
9221	157464
9222	157464
9223	157464
9224	157464
9225	157464
9226	157464
9230	472392
9231	472392
9232	472392
9233	472392

9234	472392
9235	472392
9236	472392
9240	1417176
9241	1417176
9242	1417176
9243	1417176
9244	1417176
9245	1417176
9246	1417176
9508	1
9509	1
9510	1
9511	1
9512	1
9513	1
9514	1
9515	1
9516	1
9517	1
9518	1
9519	1
9520	1
9521	1
9522	1
9523	1
9524	1
9525	1
9526	1
9527	1
9528	1
9529	1
9530	1
9531	1
9532	1
9533	1
9534	1
9535	1
9536	1
9537	1
9538	1
9608	1
9609	1
9610	1
9611	1
9612	1
9613	1
9614	1
9615	1
9616	1
9617	1
9618	1
9619	1
9620	1
9621	1
9622	1
9623	1
9624	1
9625	1
9626	1
9627	1
9628	1
9629	1
9630	1
9631	1
9632	1
9633	1
9634	1
9635	1

```
  9637        1
  9638        1
  9639        1
  9999        0
c
c       neutron dose factors
c
c    2.5e-8   1.0e-7   1.0e-6   1.0e-5   1.0e-4   1.0e-3   1.0e-2     0.1
c        0.5      1.0      2.5      5.0      7.0      10.0      14.0     20.0
c    3.67e-6  3.67e-6  4.46e-6  4.54e-6  4.18e-6  3.76e-6  3.56e-6 2.17e-5
c        9.26e-5  1.32e-4  1.25e-4  1.56e-4  1.47e-4  1.47e-4  2.08e-4 2.27e-4
c
c       photon dose factors
c
c    0.01  0.03  0.05  0.07  0.1  0.15  0.2  0.25  0.3  0.35  0.4  0.45
c         0.5  0.55  0.6  0.65  0.7  0.8  1.0  1.4  1.8  2.2  2.6  2.8  3.25
c         3.75  4.25  4.75  5.0  5.25  5.75  6.25  6.75  7.5  9.0  11.0
c         13.0  15.0
c   3.96e-06  5.82e-07  2.90e-07  2.58e-07  2.83e-07  3.79e-07  5.01e-07
c        6.31e-07  7.59e-07  8.78e-07  9.85e-07  1.08e-06  1.17e-06  1.27e-06
c        1.36e-06  1.44e-06  1.52e-06  1.68e-06  1.98e-06  2.51e-06  2.99e-06
c        3.42e-06  3.82e-06  4.01e-06  4.41e-06  4.83e-06  5.23e-06  5.60e-06
c        5.80e-06  6.01e-06  6.37e-06  6.74e-06  7.11e-06  7.66e-06  8.77e-06
c        1.03e-05  1.18e-05  1.33e-05
c
c      PHOTON TALLIES
c
f102:p   515 517 516 518
fc102    bot  shear top very-top
ft102    scx 3
de102    0.01  0.03  0.05  0.07  0.1  0.15  0.2  0.25  0.3  0.35  0.4  0.45
         0.5  0.55  0.6  0.65  0.7  0.8  1.0  1.4  1.8  2.2  2.6  2.8  3.25
         3.75  4.25  4.75  5.0  5.25  5.75  6.25  6.75  7.5  9.0  11.0
         13.0  15.0
df102   3.96e-06  5.82e-07  2.90e-07  2.58e-07  2.83e-07  3.79e-07  5.01e-07
        6.31e-07  7.59e-07  8.78e-07  9.85e-07  1.08e-06  1.17e-06  1.27e-06
        1.36e-06  1.44e-06  1.52e-06  1.68e-06  1.98e-06  2.51e-06  2.99e-06
        3.42e-06  3.82e-06  4.01e-06  4.41e-06  4.83e-06  5.23e-06  5.60e-06
        5.80e-06  6.01e-06  6.37e-06  6.74e-06  7.11e-06  7.66e-06  8.77e-06
        1.03e-05  1.18e-05  1.33e-05
fq102   u s
c
f112:p   513 521 522 523 524 525 526
fs112    -702 -703 -704 -600 -630 -705 -706 -707 -708 -709 -710
        -711 -712 -713 -714 -715 -716 -717 -718 -670 -719 -695
        -720 -721 -722 t
fc112    1ft     1ft     1ft     1ft     8.75in   11.54in  11.54in 11.54in
        11.54in 11.54in 11.54in 11.54in 11.54in  11.54in  11.54in 11.54in
        11.54in 11.54in 11.54in 11.54in 10.375in 10.375in 1ft     1ft
        1ft     1ft
ft112    scx 3
de112    0.01  0.03  0.05  0.07  0.1  0.15  0.2  0.25  0.3  0.35  0.4  0.45
         0.5  0.55  0.6  0.65  0.7  0.8  1.0  1.4  1.8  2.2  2.6  2.8  3.25
         3.75  4.25  4.75  5.0  5.25  5.75  6.25  6.75  7.5  9.0  11.0
         13.0  15.0
df112   3.96e-06  5.82e-07  2.90e-07  2.58e-07  2.83e-07  3.79e-07  5.01e-07
        6.31e-07  7.59e-07  8.78e-07  9.85e-07  1.08e-06  1.17e-06  1.27e-06
        1.36e-06  1.44e-06  1.52e-06  1.68e-06  1.98e-06  2.51e-06  2.99e-06
        3.42e-06  3.82e-06  4.01e-06  4.41e-06  4.83e-06  5.23e-06  5.60e-06
        5.80e-06  6.01e-06  6.37e-06  6.74e-06  7.11e-06  7.66e-06  8.77e-06
        1.03e-05  1.18e-05  1.33e-05
fq112   u s
c
```

SUPPLEMENT 5.I

SHIELDING EVALUATION OF THE MPC-HB

5.I.0 INTRODUCTION

This supplement is focused on providing a shielding evaluation of the HI-STAR 100 System with the MPC-HB. The evaluation presented herein supplements those evaluations of the HI-STAR System contained in the main body of Chapter 5 of this SAR and information in the main body of Chapter 5 that remains applicable to the HI-STAR 100 System with the MPC-HB is not repeated in this supplement. To aid the reader, the sections in this supplement are numbered in the same fashion as the corresponding sections in the main body of this chapter, i.e., Sections 5.I.1 through 5.I.5 correspond to Sections 5.1 through 5.5. Tables and figures in this supplement are labeled sequentially.

5.I.1 DISCUSSION AND RESULTS

The MPC-HB is designed to accommodate 80 Humboldt Bay fuel assemblies. The maximum burnup of these assemblies is 23,000 MWD/MTU with a minimum cooling time of 29 years. The minimum enrichment is 2.09 wt% ^{235}U. Since the burnup of these assemblies is very low and the cooling time is long, an explicit evaluation of the dose rate outside a HI-STAR 100 overpack is not performed. Rather, the neutron and gamma source and assembly hardware activation inside an MPC-HB is compared to the corresponding values from an MPC-68 with design basis fuel to demonstrate that the MPC-HB is bounded by the analysis of the MPC-68. This comparison is performed in Section 5.I.4.

5.I.2 SOURCE SPECIFICATION

The neutron and gamma source term for the Humboldt Bay fuel assemblies were calculated using the same techniques described in Section 5.2. Table 5.I.1 provides the fuel characteristics for the Humboldt Bay fuel assemblies as analyzed in this supplement. These fuel characteristics are the same as those used in reference [5.I.1], except for an additional amount of 1.5 kg of stainless steel cladding that has been added for the DFCs. This is to allow for loading of stainless steel clad fuel rod fragments, should this be necessary. The value of 1.5 kg is a conservative upper bound value of the expected amount, based on the expected total amount of fuel fragments to be loaded, and the assumption that all those fragments have stainless steel clad.

Table 5.I.2 and 5.I.3 provide the neutron and gamma source term for Humboldt Bay fuel. Table 5.I.4 shows the fuel hardware activation. The activity of the stainless steel cladding fragments is directly derived from the activity of the lower tie plate by adjustment for the difference in steel weight (5.73 vs 1.5) and the flux factor (0.2 vs 1). Note that the source for the stainless steel clad is for the entire amount of steel, while all other values are per assembly. Note that the stainless steel clad source is smaller than the total source from steel from a single assembly, and therefore negligible compared to the total source from steel activation in an entire MPC with 80 assemblies.

5.I.3 MODEL SPECIFICATIONS

Generally, the same as in Section 5.3. However, the Holtite thickness in the HI-STAR HB is only 4.0 inches, compared to 4.3 Inches in the HI-STAR 100. A study shows that this could result in an increase in neutron dose rates of up to 30%. This increase is considered in the source term comparison in Section 5.I.4 below. Additionally, the Holtite composition for the HI-STAR HB is slightly different from the composition described in Section 5.3, with a Hydrogen content of 5.6 wt% instead of 5.92 wt%. A study shows that the effect on dose rates of this difference is less than 5%. This is more than compensated by the margins in the source terms discussed in Section 5.I.4 below. The Holtite composition with 5.6 wt% Hydrogen is therefore acceptable for the HI-STAR HB.

The MPC-HB is manufactured with Metamic neutron absorbing materials, while the MPCs discussed in the main part of this chapter are manufactured with Boral neutron absorber material. Both materials are made of aluminum and B_4C powder. The Boral contains an aluminum and B_4C powder mixture sandwiched between two aluminum plates while the Metamic is a single plate of aluminum and B_4C. The materials are therefore essentially equivalent and there is no distinction between the two materials from a shielding perspective.

5.I.4 SHIELDING EVALUATION

5.I.4.1 Normal Condition

The acceptability of transporting the MPC-HB was determined by comparing the source terms for the MPC-HB to the source terms for an MPC-68 containing BWR fuel with a burnup and cooling time of 24,500 MWD/MTU and 8 years. The neutron and gamma source terms for this burnup and cooling time can be found in Tables 5.2.5 and 5.2.13 in the main portion of this chapter, respectively. The source term in each energy group was multiplied by the number of assemblies and then divided by the active fuel length (144 inches for the MPC-68 and 77.5 inches for the MPC-HB) to determine the source strength per unit length. For neutrons, the total number of assemblies in the basket (68 or 80) is used for the comparison. For gammas, where the dose rates are dominated by the contributions of the assemblies on the periphery of the basket, the number of assemblies in the outer rows of the basket is used. These are 36 for the MPC-68, and 48 for the MPC-HB. Additionally, for neutrons in the HI-STAR HB, an increase of 30% (factor of 1.3) is applied as discussed in 5.I.3. In all cases, the design basis source term for the MPC-68 bounds the source term for the MPC-HB, and in most cases by a substantial margin. Therefore, the dose rates from a HI-STAR containing the MPC-HB will be bounded by the dose rates from a HI-STAR containing the MPC-68 under normal conditions.

5.I.4.2 Accident Condition

The accident condition was evaluated in the same manner as the normal condition. However, similar to the analysis in Section 5.4.2, it was assumed that fuel assemblies that are not intact are

compacted. The effect of this compaction is discussed below for damaged and undamaged assemblies.

- For damaged fuel in DFCs, it is assumed that 50% of the volume in the DFC cross-section is filled with fuel rods and cladding. Given the amount of fuel and cladding in a HB assembly, this corresponds to an active fuel height of 55 inches inside the DFC, i.e. an increase in the source per unit of active length by a factor of 77.5/55 = 1.41.
- For the undamaged assemblies, fuel relocation would be limited by the intact peripheral rods, so the compaction, if any, would also be limited. For a 6x6 assembly it is reasonable to assume that the 4x4 rods inside of the periphery could at most be replaced by a 5x5 rod array, resulting in a maximum number of rods in a cross section of 6x6-4x4+5x5 = 45 rods. This represents an increase by factor 1.25 compared to the intact assembly. Correspondingly, for a 7x7 assembly the maximum number would be 7x7-5x5+6x6 = 60, or an increase by factor 1.22.

As a bounding approach, an increase in source term per unit of active length of 1.41, corresponding to an active length reduced to 55 inch, was assumed for all assemblies in the basket, i.e. for both damaged and undamaged assemblies. The source term for the MPC-68, assuming an active height of 144 inches, was then compared, on a per inch basis, to the source term from the MPC-HB for an active height of 55 inches. In all neutron and gamma energy groups, the design basis source term for the MPC-68 bounds the source term for the MPC-HB, in most cases by a substantial margin. Therefore, the dose rates from a HI-STAR containing the MPC-HB will be bounded by the dose rates from a HI-STAR containing the MPC-68 during the design basis accident for all assembly conditions.

5.I.5 REGULATORY COMPLIANCE

In summary it can be concluded that dose rates from the HI-STAR 100 System with the MPC-HB are bounded by the dose rates for the MPCs analyzed in the main body of the report. The shielding system of the HI-STAR 100 System is therefore in compliance with 10CFR71.

5.I.6 REFERENCES

[5.I.1] "Humboldt Bay Independent Spent Fuel Storage Installation Safety Analysis Report", Pacific Gas and Electric Company, Docket No. 72-27.

Table 5.I.1

DESCRIPTION OF HUMBOLDT BAY FUEL

Description	Value
Fuel type	6x6
Active fuel length (in.)	77.5
No. of fuel rods	36
Rod pitch (in.)	0.740
Cladding material	Zircaloy-2
Rod diameter (in.)	0.563
Cladding thickness (in.)	0.032
Pellet diameter (in.)	0.488
Pellet material	UO_2
Pellet density (gm/cc)	10.412 (945% of theoretical)
Enrichment (w/o ^{235}U)	2.09
Burnup (MWD/MTU)	23,000
Cooling Time (years)	29
Specific power (MW/MTU)	17.836
Lower tie plate mass (kg)	5.73 Steel
Grid spacer mass (kg)	0.16 Inconel 0.84 Steel
Plenum springs mass (kg)	0.027 Inconel
Compression / expansion springs mass (kg)	0.11 Inconel
Upper tie plate mass (kg)	1.55 Steel
Stainless Steel Cladding on Fuel Fragments in DFC (kg)	1.5

Table 5.I.2

CALCULATED NEUTRON SOURCE PER ASSEMBLY
FOR HUMBOLDT BAY FUEL

Lower Energy (MeV)	**Upper Energy (MeV)**	**23,000 MWD/MTU 29-Year Cooling (Neutrons/sec)**
1.0E-01	4.0E-01	1.27E+05
4.0E-01	9.0E-01	6.48E+05
9.0E-01	1.4	6.06E+05
1.4	1.85	4.66E+05
1.85	3.0	8.85E+05
3.0	6.43	7.41E+05
6.43	20.0	6.17E+04
Total		3.53E+06

Table 5.I.3

CALCULATED FUEL GAMMA SOURCE PER ASSEMBLY
FOR HUMBOLDT BAY FUEL

Lower Energy	**Upper Energy**	**23,000 MWD/MTU 29-Year Cooling**	
(MeV)	(MeV)	(MeV/s)	(Photons/s)
0.45	0.7	6.31E+13	1.10E+14
0.7	1.0	7.96E+11	9.37E+11
1.0	1.5	7.47E+11	5.98E+11
1.5	2.0	5.26E+10	3.01E+10
2.0	2.5	5.67E+08	2.52E+08
2.5	3.0	1.94E+07	7.04E+06
Totals		6.47E+13	1.12E+14

Table 5.I.4
Non Fuel Hardware Sources
(23,000 MWD/MTU Burnup)

Location	**29-Year Cooling (curies)**
Lower Tie Plate	2.218
Active Fuel Zone (grid spacers)	4.107
Plenum Springs	0.065
Compression / Expansion Springs	0.133
Upper Tie Plate	0.400
Stainless Steel Cladding Fragments	2.9

CHAPTER 6: CRITICALITY EVALUATION

This chapter documents the criticality evaluation of the HI-STAR 100 System for the packaging and transportation of radioactive materials (spent nuclear fuel) in accordance with 10CFR71. The results of this evaluation demonstrate that, for the designated fuel assembly classes and basket configurations, an infinite number of HI-STAR 100 Systems with variations in internal and external moderation remain subcritical with a margin of subcriticality greater than 0.05Δk. This corresponds to a Criticality Safety Index (CSI) of zero (0) and demonstrates compliance with 10CFR71 criticality requirements for normal and hypothetical accident conditions of transport.

The criticality design is based on favorable geometry, fixed neutron poisons , an administrative limit on the maximum allowable enrichment, and an administrative limit on the minimum average assembly burnup for the MPC-32. Criticality safety of the HI-STAR 100 System does *not* rely on credit for: (1) fuel burnup except for the MPC-32; (2) fuel-related burnable absorbers; or (3) more than 75% of the manufacturer's minimum B-10 content for the fixed neutron absorber when subject to standard acceptance tests[†].

In addition to demonstrating that the criticality safety acceptance criteria are satisfied, this chapter describes the HI-STAR 100 System design structures and components important to criticality safety and limiting fuel characteristics in sufficient detail to identify the package accurately and provide a sufficient basis for the evaluation of the package.

[†] For greater credit allowance, fabrication tests capable of verifying the presence and uniformity of the neutron absorber are needed.

6.1 DISCUSSION AND RESULTS

In conformance with the principles established in 10CFR71 [6.1.1], NUREG-1617 [6.1.2], and NUREG-0800 Section 9.1.2 [6.1.3], the results in this chapter demonstrate that the effective multiplication factor (k_{eff}) of the HI-STAR 100 System, including all biases and uncertainties evaluated with a 95% probability at the 95% confidence level, does not exceed 0.95 under all credible normal and hypothetical accident conditions of transport. This criterion provides a large subcritical margin, sufficient to assure the criticality safety of the HI-STAR 100 System when fully loaded with fuel of the highest permissible reactivity. In addition, the results of this evaluation demonstrate that the HI-STAR 100 System is in full compliance with the requirements outlined in the Standard Review Plan for Dry Cask Storage Systems, NUREG-1536.

Criticality safety of the HI-STAR 100 System depends on the following four principal design parameters:

1. The inherent geometry of the fuel basket designs within the MPC (and the flux-trap water gaps in the MPC-24),

2. The incorporation of permanent fixed neutron-absorbing panels in the fuel basket structure, and

3. An administrative limit on the maximum average enrichment for PWR fuel and maximum planar-average enrichment for BWR fuel, and

4. An administrative limit on the minimum average assembly burnup for PWR fuel in the MPC-32.

The HI-STAR 100 System is designed such that the fixed neutron absorber will remain effective for a period greater than 20 years, and there are no credible means to lose it. Therefore, there is no need to provide a surveillance or monitoring program to verify the continued efficacy of the neutron absorber.

Criticality safety of the HI-STAR 100 System does not rely on the use of any of the following credits:

- burnup of fuel, except for the MPC-32

- fuel-related burnable neutron absorbers

- more than 75 percent of the B-10 content for the Boral fixed neutron absorber.

- more than 90 percent of the B-10 content for the Metamic fixed neutron absorber, with comprehensive fabrication tests as described in Chapter 8.

The following basket designs are available for use in the HI-STAR 100 System:

- a 24-cell basket (MPC-24), designed for intact PWR fuel assemblies with a specified maximum enrichment.

- a 24-cell basket (MPC-24E/EF), designed for intact and damaged PWR fuel assemblies, and fuel debris. This is a variation of the MPC-24, with increased ^{10}B content in the fixed neutron absorber and with four cells capable of accommodating either intact fuel or a damaged fuel container (DFC). The MPC-24E and MPC-24EF is designed for fuel assemblies with a specified maximum enrichment. Although the MPC-24E/EF is designed and analyzed for damaged fuel and fuel debris, it is only certified for intact fuel assemblies.

- a 24-cell basket (MPC-24E/EF Trojan), design for intact and damaged PWR fuel assemblies, and fuel debris from the Trojan Nuclear Plant (TNP). This is a variation of the MPC-24E/EF, with a slightly reduced height, and increased cell sizes for the cells designated for damaged fuel and fuel debris. This increased cell size is required to accommodate the Trojan specific Failed Fuel Cans and DFCs.

- a 32-cell basket (MPC-32), designed for intact PWR fuel assemblies of a specified minimum burnup, and

- a 68-cell basket (MPC-68), designed for both intact and damaged BWR fuel assemblies with a specified maximum planar-average enrichment. Additionally, a variation in the MPC-68, designated MPC-68F, is designed for damaged BWR fuel assemblies and BWR fuel debris with a specified maximum planar-average enrichment.

- a 80-cell basket (MPC-HB), designed for Humboldt Bay fuel. See Supplement 6.I for details and evaluations for this basket version.

Two interchangeable neutron absorber materials are used in these baskets, Boral and Metamic. For Boral, 75 percent of the minimum B-10 content is credited in the criticality analysis, while for Metamic, 90 percent of the minimum B-10 content is credited, based on the neutron absorber tests specified in Chapter 8. However, the B-10 content in Metamic is chosen to be lower than the B-10 content in Boral, and is chosen so that the absolute B-10 content credited in the criticality analysis is the same for the two materials. This makes the two materials identical from a criticality perspective. This is confirmed by comparing results for a selected number of cases

that were performed with both materials (see Section 6.4.12). Calculations in this chapter are therefore only performed for the Boral neutron absorber, with results directly applicable to Metamic.

During the normal conditions of transport, the HI-STAR 100 System is dry (no moderator), and thus, the reactivity is very low ($k_{eff} < 0.50$). However, the HI-STAR 100 System for loading and unloading operations, as well as for the hypothetical accident conditions, is flooded, and thus, represents the limiting case in terms of reactivity. The calculational models for these conditions conservatively include: full flooding with ordinary water, corresponding to the highest reactivity, and the worst case (most conservative) combination of manufacturing and fabrication tolerances.

The MPC-24EF contains the same basket as the MPC-24E. More specifically, all dimensions relevant to the criticality analyses are identical between the MPC-24E and MPC-24EF. Therefore, all criticality results obtained for the MPC-24E are valid for the MPC-24EF and no separate analyses for the MPC-24EF are necessary.

Confirmation of the criticality safety of the HI-STAR 100 Systems under flooded conditions, when filled with fuel of the maximum permissible reactivity for which they are designed, was accomplished with the three-dimensional Monte Carlo code MCNP4a [6.1.4]. Independent confirmatory calculations were made with NITAWL-KENO5a from the SCALE-4.3 package. KENO5a [6.1.5] calculations used the 238-group SCALE cross-section library in association with the NITAWL-II program [6.1.6], which adjusts the uranium-238 cross sections to compensate for resonance self-shielding effects. The Dancoff factors required by NITAWL-II were calculated with the CELLDAN code [6.1.13], which includes the SUPERDAN code [6.1.7] as a subroutine. K-factors for one-sided statistical tolerance limits with 95% probability at the 95% confidence level were obtained from the National Bureau of Standards (now NIST) Handbook 91 [6.1.8].

For the burnup credit calculations, CASMO-4, a two-dimensional transport theory code [6.1.10-6.1.12] for fuel assemblies, was used to calculate the isotopic composition of the spent fuel. The criticality evaluations for burnup credit were performed with MCNP4a [6.1.4].

To assess the incremental reactivity effects due to manufacturing tolerances, CASMO and MCNP4a [6.1.4] were used. The CASMO and MCNP4a calculations identify those tolerances that cause a positive reactivity effect, enabling the Monte Carlo code input to define the worst case (most conservative) conditions. CASMO was not used for quantitative criticality evaluations, but only to qualitatively indicate the direction and approximate magnitude of the reactivity effects of the manufacturing tolerances.

Benchmark calculations were made to compare the primary code packages (MCNP4a, CASMO and KENO5a) with experimental data, using experiments selected to encompass, insofar as

practical, the design parameters of the HI-STAR 100 System. The most important parameters are (1) the enrichment, (2) the water-gap size (MPC-24) or cell spacing (MPC-32 and MPC-68), (3) the ^{10}B loading of the neutron absorber panels, and (4) the assembly burnup (MPC-32 only). Benchmark calculations are presented in Appendix 6.A and Appendix 6.E.

Applicable codes, standards, and regulations, or pertinent sections thereof, include the following:

- U.S. Code of Federal Regulations, "Packaging and Transportation of Radioactive Materials," Title 10, Part 71.
- NUREG-1617, "Standard Review Plan for Transportation Packages for Spent Nuclear Fuel" USNRC, Washington D.C., March 2000.
- U.S. Code of Federal Regulations, "Prevention of Criticality in Fuel Storage and Handling," Title 10, Part 50, Appendix A, General Design Criterion 62.
- USNRC Standard Review Plan, NUREG-0800, Section 9.1.2, Spent Fuel Storage, Rev. 3, July 1981.
- USNRC Interim Staff Guidance 8 (ISG-8), Revision 2, "Burnup Credit in the Criticality Safety Analyses of PWR Spent Fuel in Transport and Storage Casks".

To assure the true reactivity will always be less than the calculated reactivity, the following conservative assumptions were made:

- The MPCs are assumed to contain the most reactive fuel authorized to be loaded into a specific basket design.
- No credit for fuel burnup is assumed, either in depleting the quantity of fissile nuclides or in producing fission product poisons, except for fuel in the MPC-32.
- The criticality analyses assume 75% of the manufacturer's minimum Boron-10 content for the Boral neutron absorber and 90% of the manufacturer's minimum Boron-10 content for the Metamic neutron absorber.
- The fuel stack density is assumed to be 96% of theoretical (10.522 g/cm^3) for all criticality analyses. The fuel stack density is approximately equal to 98% of the pellet density. Therefore, while the pellet density of some fuels might be slightly greater than 96% of theoretical, the actual stack density will still be less.
- For fresh fuel, no credit is taken for the ^{234}U and ^{236}U in the fuel.

- When flooded, the moderator is assumed to be water at a temperature corresponding to the highest reactivity within the expected operating range (i.e., water density of 1.000 g/cc).

- Neutron absorption in minor structural members and optional heat conduction elements is neglected, i.e., spacer grids, basket supports, and optional aluminum heat conduction elements are replaced by water.

- The worst hypothetical combination of tolerances (most conservative values within the range of acceptable values), as identified in Section 6.3, is assumed.

- When flooded, the fuel rod pellet-to-clad gap regions are assumed to be flooded.

- Planar-averaged enrichments are assumed for BWR fuel. (Analyses are presented in Appendix 6.B to demonstrate that the use of planar-average enrichments produces conservative results.)

- Fuel-related burnable neutron absorbers, such as the Gadolinia normally used in BWR fuel and IFBA normally used in PWR fuel, are neglected.

- For evaluation of the reactivity bias, all benchmark calculations that result in a k_{eff} greater than 1.0 are conservatively truncated to 1.0000.

- For fuel assemblies that contain low-enriched axial blankets, the governing enrichment is that of the highest planar average, and the blankets are not included in determining the average enrichment.

- Regarding the position of assemblies in the basket, configurations with centered and eccentric positioning of assemblies in the fuel storage locations are considered. For further discussions see Section 6.3.3.

- For intact fuel assemblies, as defined in Chapter 1, missing fuel rods must be replaced with dummy rods that displace a volume of water that is equal to, or larger than, that displaced by the original rods.

- The burnup credit methodology for the MPC-32 contains significant additional conservative assumptions specific to burnup credit, as discussed in Appendix 6.E.

The principal calculational results, which address the following conditions:

- A single package, under the conditions of 10 CFR 71.55(b), (d), and (e);

- An array of undamaged packages, under the conditions of 10 CFR 71.59(a)(1); and
- An array of damaged packages, under the conditions of 10 CFR 71.59(a)(2)

are summarized in Table 6.1.4 for all MPCs and for the most reactive configuration and fuel condition in each MPC. These results demonstrate that the HI-STAR 100 System is in full compliance with 10CFR71 (71.55(b), (d), and (e) and 71.59(a)(1) and (a)(2)). The calculations for package arrays are performed for infinite arrays of HI-STAR 100 Systems under flooded conditions. Therefore, the Criticality Safety Index (CSI) is zero (0). It is noted that the results for the internally flooded single package and package arrays are statistically equivalent for each basket. This shows that the physical separation between overpacks and the steel radiation shielding are each adequate to preclude any significant neutronic coupling between casks in an array configuration. In addition, the table shows the result for an unreflected, internally flooded cask for each MPC. This configuration is used in many calculations and studies throughout this chapter, and is shown to yield results that are statistically equivalent to the results for the corresponding reflected package. Further analyses for the various conditions of flooding that support the conclusion that the fully flooded condition corresponds to the highest reactivity, and thus is most limiting, are presented in Section 6.4. These analyses also include cases with various internal and external moderator densities and various cask-to-cask spacings.

Additional results of the design basis criticality safety calculations for single unreflected, internally flooded casks (limiting cases) are listed in Tables 6.1.1 through 6.1.3 and 6.1.5 through 6.1.7, conservatively evaluated for the worst combination of manufacturing tolerances (as identified in Section 6.3), and including the calculational bias, uncertainties, and calculational statistics. For each of the MPC designs and fuel assembly classes†, Tables 6.1.1 through 6.1.3 and 6.1.5 through 6.1.7 list the bounding maximum k_{eff} value, the associated maximum allowable enrichment, and the minimum required assembly average burnup (if applicable), as required by 10CFR71.33(b)(2). The maximum enrichment and minimum burnup acceptance criteria are defined in Chapter 1. Additional results for each of the candidate fuel assemblies, that are bounded by those listed in Tables 6.1.1 through 6.1.3, are given in Section 6.2 for the MPC-24, MPC-68 and MPC-68F. The tables in Section 6.2 list the maximum k_{eff} (including bias, uncertainties, and calculational statistics), calculated k_{eff}, standard deviation, and energy of the average lethargy causing fission (EALF) for each of the candidate fuel assemblies and basket configurations analyzed. The capability of the MPC-68F to safely accommodate Dresden-1 and Humboldt Bay damaged fuel (fuel assembly classes 6x6A, 6x6B, 6x6C, 7x7A, and 8x8A) is demonstrated in Subsection 6.4.4.

---

† For each array size (e.g., 6x6, 7x7, 14x14, etc.), the fuel assemblies have been subdivided into a number of assembly classes, where an assembly class is defined in terms of the (1) number of fuel rods; (2) pitch; (3) number and location of guide tubes (PWR) or water rods (BWR); and (4) cladding material. The assembly classes for BWR and PWR fuel are defined in Section 6.2.

In Summary, these results confirm that the maximum k_{eff} values for the HI-STAR 100 System are below the limiting design criteria ($k_{eff} < 0.95$) when fully flooded and loaded with any of the candidate fuel assemblies and basket configurations. The Criticality Safety Index is zero (0).

Table 6.1.1

BOUNDING MAXIMUM k_{eff} VALUES FOR EACH ASSEMBLY CLASS IN THE MPC-24

Fuel Assembly Class	Maximum Allowable Enrichment (wt% ^{235}U)	Maximum† k_{eff}
14x14A	4.6	0.9296
14x14B	4.6	0.9228
14x14C	4.6	0.9307
14x14D	4.0	0.8507
14x14E	5.0	0.7627
15x15A	4.1	0.9227
15x15B	4.1	0.9388
15x15C	4.1	0.9361
15x15D	4.1	0.9367
15x15E	4.1	0.9392
15x15F	4.1	0.9410
15x15G	4.0	0.8907
15x15H	3.8	0.9337
16x16A	4.6	0.9287
17x17A	4.0	0.9368
17x17B	4.0	0.9355
17x17C	4.0	0.9349

Note: These calculations are for single unreflected, fully flooded casks. However, comparable reactivities were obtained for fully reflected casks and for arrays of casks.

† The term "maximum k_{eff}" as used here, and elsewhere in this document, means the highest possible k-effective, including bias, uncertainties, and calculational statistics, evaluated for the worst case combination of manufacturing tolerances.

Table 6.1.2

BOUNDING MAXIMUM k_{eff} VALUES FOR EACH ASSEMBLY CLASS IN THE MPC-68

Fuel Assembly Class	Maximum Allowable Planar-Average Enrichment (wt% ^{235}U)	Maximum† k_{eff}
6x6A	2.7††	0.7888†††
6x6B‡	2.7††	0.7824†††
6x6C	2.7††	0.8021†††
7x7A	2.7††	0.7974†††
7x7B	4.2	0.9386
8x8A	2.7††	0.7697†††
8x8B	4.2	0.9416
8x8C	4.2	0.9425
8x8D	4.2	0.9403
8x8E	4.2	0.9312
8x8F	4.0	0.9459

Note: These calculations are for single unreflected, fully flooded casks. However, comparable reactivities were obtained for fully reflected casks and for arrays of casks.

---

† The term "maximum k_{eff}" as used here, and elsewhere in this document, means the highest possible k-effective, including bias, uncertainties, and calculational statistics, evaluated for the worst case combination of manufacturing tolerances.

†† This calculation was performed for 3.0% planar-average enrichment, however, the authorized contents are limited to maximum planar-average enrichment of 2.7%. Therefore, the listed maximum k_{eff} value is conservative.

††† This calculation was performed for a ^{10}B loading of 0.0067 g/cm^2, which is 75% of a minimum ^{10}B loading of 0.0089 g/cm^2. The minimum ^{10}B loading in the MPC-68 is at least 0.0310 g/cm^2. Therefore, the listed maximum k_{eff} value is conservative.

‡ Assemblies in this class contain both MOX and UO_2 pins. The composition of the MOX fuel pins is given in Table 6.3.4. The maximum allowable planar-average enrichment for the MOX pins is given in the specification of authorized contents, Chapter 1.

Table 6.1.2 (continued)

BOUNDING MAXIMUM k_{eff} VALUES FOR EACH ASSEMBLY CLASS IN THE MPC-68

Fuel Assembly Class	Maximum Allowable Planar-Average Enrichment (wt% ^{235}U)	Maximum† k_{eff}
9x9A	4.2	0.9417
9x9B	4.2	0.9436
9x9C	4.2	0.9395
9x9D	4.2	0.9394
9x9E	4.0	0.9486
9x9F	4.0	0.9486
9x9G	4.2	0.9383
10x10A	4.2	0.9457††
10x10B	4.2	0.9436
10x10C	4.2	0.9433
10x10D	4.0	0.9376
10x10E	4.0	0.9185

Note: These calculations are for single unreflected, fully flooded casks. However, comparable reactivities were obtained for fully reflected casks and for arrays of casks.

† The term "maximum k_{eff}" as used here, and elsewhere in this document, means the highest possible k-effective, including bias, uncertainties, and calculational statistics, evaluated for the worst case combination of manufacturing tolerances.

†† KENO5a verification calculation resulted in a maximum k_{eff} of 0.9453.

Table 6.1.3

BOUNDING MAXIMUM k_{eff} VALUES FOR EACH ASSEMBLY CLASS IN THE MPC-68F

Fuel Assembly Class	Maximum Allowable Planar-Average Enrichment (wt% ^{235}U)	Maximum† k_{eff}
6x6A	2.7††	0.7888
6x6B†††	2.7	0.7824
6x6C	2.7	0.8021
7x7A	2.7	0.7974
8x8A	2.7	0.7697

Note:

1. These calculations are for single unreflected, fully flooded casks. However, comparable reactivities were obtained for fully reflected casks and for arrays of casks.

2. These calculations were performed for a ^{10}B loading of 0.0067 g/cm^2, which is 75% of a minimum ^{10}B loading of 0.0089 g/cm^2. The minimum ^{10}B loading in the MPC-68F is 0.010 g/cm^2. Therefore, the listed maximum k_{eff} values are conservative.

---

† The term "maximum k_{eff}" as used here, and elsewhere in this document, means the highest possible k-effective, including bias, uncertainties, and calculational statistics, evaluated for the worst case combination of manufacturing tolerances.

†† These calculations were performed for 3.0% planar-average enrichment, however, the authorized contents are limited to a maximum planar-average enrichment of 2.7%. Therefore, the listed maximum k_{eff} values are conservative.

††† Assemblies in this class contain both MOX and UO_2 pins. The composition of the MOX fuel pins is given in Table 6.3.4. The maximum allowable planar-average enrichment for the MOX pins is given in the specification of authorized contents, Chapter 1.

Table 6.1.4
SUMMARY OF THE CRITICALITY RESULTS FOR THE MOST REACTIVE ASSEMBLY FROM THE ASSEMBLY CLASSES IN EACH MPC†
TO DEMONSTRATE COMPLIANCE WITH 10CFR71.55 AND 10CFR71.59

MPC-24, Assembly Class 15x15F, 4.1 wt% ^{235}U				
Configuration	% Internal Moderation	% External Moderation	Applicable Requirement	Maximum‡ k_{eff}
Single Package, unreflected	100%	0%	n/a	0.9410
Single Package, fully reflected	100%	100%	10CFR71.55 (b), (d), and (e)	0.9397
Containment, fully reflected	100%	100%		0.9397
Infinite Array of Damaged Packages	100%	100%	10CFR71.59 (a)(2)	0.9436
Infinite Array of Undamaged Packages	0%	0%	10CFR71.59 (a)(1)	0.3950
MPC-68, Assembly Class 9x9E/F, 4.0 wt% ^{235}U				
Configuration	% Internal Moderation	% External Moderation	Applicable Requirement	Maximum k_{eff}
Single Package, unreflected	100%	0%	n/a	0.9486
Single Package, fully reflected	100%	100%	10CFR71.55 (b), (d), and (e)	0.9470
Containment, fully reflected	100%	100%		0.9461
Infinite Array of Damaged Packages	100%	100%	10CFR71.59 (a)(2)	0.9468
Infinite Array of Undamaged Packages	0%	0%	10CFR71.59 (a)(1)	0.3808
MPC-68F, Assembly Class 6x6C, 2.7 wt% ^{235}U				
Configuration	% Internal Moderation	% External Moderation	Applicable Requirement	Maximum k_{eff}
Single Package, unreflected	100%	0%	n/a	0.8021
Single Package, fully reflected	100%	100%	10CFR71.55 (b), (d), and (e)	0.8033
Containment, fully reflected	100%	100%		0.8033
Infinite Array of Damaged Packages	100%	100%	10CFR71.59 (a)(2)	0.8026
Infinite Array of Undamaged Packages	0%	0%	10CFR71.59 (a)(1)	0.3034

† See Supplement 6.I, Table 6.I.1 for results for the MPC-HB.

‡ The maximum k_{eff} is equal to the sum of the calculated k_{eff}, two standard deviations, the code bias, and the uncertainty in the code bias. For cases with 100% internal moderation, the standard deviation is between 0.0007 and 0.0009, for cases with 0% internal moderation, the standard deviation is between 0.0002 and 0.0004.

Table 6.1.4 (continued)
SUMMARY OF THE CRITICALITY RESULTS FOR THE MOST REACTIVE ASSEMBLY FROM THE ASSEMBLY CLASSES IN EACH MPC†
TO DEMONSTRATE COMPLIANCE WITH 10CFR71.55 AND 10CFR71.59

MPC-24E/EF, Assembly Class 15x15F, 4.5 wt% ^{235}U				
Configuration	% Internal Moderation	% External Moderation	Applicable Requirement	Maximum‡ k_{eff}
Single Package, unreflected	100%	0%	n/a	0.9495
Single Package, fully reflected	100%	100%	10CFR71.55 (b), (d), and (e)	0.9485
Containment, fully reflected	100%	100%		0.9486
Infinite Array of Damaged Packages	100%	100%	10CFR71.59 (a)(2)	0.9495
Infinite Array of Undamaged Packages	0%	0%	10CFR71.59 (a)(1)	0.4026
MPC-24E/EF TROJAN, Trojan Intact and Damaged Fuel, 3.7 wt% ^{235}U				
Configuration	% Internal Moderation	% External Moderation	Applicable Requirement	Maximum k_{eff}
Single Package, unreflected	100%	0%	n/a	0.9377
Single Package, fully reflected	100%	100%	10CFR71.55 (b), (d), and (e)	0.9366
Containment, fully reflected	100%	100%		0.9377
Infinite Array of Damaged Packages	100%	100%	10CFR71.59 (a)(2)	0.9383
Infinite Array of Undamaged Packages	0%	0%	10CFR71.59 (a)(1)	0.3518
MPC-32, Assembly Class 15x15F and 17x17C				
Configuration	% Internal Moderation	% External Moderation	Applicable Requirement	Maximum k_{eff}
Single Package, unreflected	100%	0%	n/a	0.9481
Single Package, fully reflected	100%	100%	10CFR71.55 (b), (d), and (e)	0.9476
Containment, fully reflected	100%	100%		0.9467
Infinite Array of Damaged Packages	100%	100%	10CFR71.59 (a)(2)	0.9476
Infinite Array of Undamaged Packages	0%	0%	10CFR71.59 (a)(1)	0.4205

† See Supplement 6.I, Table 6.I.1 for results for the MPC-HB.

‡ The maximum k_{eff} is equal to the sum of the calculated k_{eff}, two standard deviations, the code bias, and the uncertainty in the code bias. For cases with 100% internal moderation, the standard deviation is between 0.0004 and 0.0009, for cases with 0% internal moderation, the standard deviation is between 0.0002 and 0.0004.

Table 6.1.5

BOUNDING MAXIMUM k_{eff} VALUES FOR EACH ASSEMBLY CLASS IN THE MPC-24E/EF

Fuel Assembly Class	Maximum Allowable Enrichment (wt% ^{235}U)	Maximum† k_{eff}
14x14A	5.0	0.9380
14x14B	5.0	0.9312
14x14C	5.0	0.9365
14x14D	5.0	0.8875
14x14E	5.0	0.7651
15x15A	4.5	0.9336
15x15B	4.5	0.9487
15x15C	4.5	0.9462
15x15D	4.5	0.9445
15x15E	4.5	0.9471
15x15F	4.5	0.9495
15x15G	4.5	0.9062
15x15H	4.2	0.9455
16x16A	5.0	0.9358
17x17A	4.4	0.9447
17x17B	4.4	0.9438
17x17C	4.4	0.9433

† The term "maximum k_{eff}" as used here, and elsewhere in this document, means the highest possible k-effective, including bias, uncertainties, and calculational statistics, evaluated for the worst case combination of manufacturing tolerances.

Table 6.1.6

BOUNDING MAXIMUM k_{eff} VALUES IN THE MPC-24E/EF TROJAN

Fuel Assembly Class	Maximum Allowable Enrichment (wt% ^{235}U)	Content	Maximum† k_{eff}
17x17B	3.7	Intact Fuel	0.9187
17x17B	3.7	Intact Fuel, Damaged Fuel and Fuel Debris	0.9377

† The term "maximum k_{eff}" as used here, and elsewhere in this document, means the highest possible k-effective, including bias, uncertainties, and calculational statistics, evaluated for the worst case combination of manufacturing tolerances.

Table 6.1.7

BOUNDING MAXIMUM k_{eff} VALUES IN THE MPC-32
FOR ASSEMBLIES NOT EXPOSED TO CONTROL RODS DURING DEPLETION‡

Fuel Assembly Class	Maximum Allowable Enrichment†† (wt% ^{235}U)	Minimum Required Assembly Average Burnup†† (GWd/MTU)	Maximum† k_{eff}
15x15D, E, F, H	1.8	0	0.9281
	2.0	11.4	0.9466
	3.0	30.19	0.9444
	4.0	41.66	0.9471
	5.0	55.85	0.9476
17x17A, B, C	1.8	0	0.9226
	2.0	9.04	0.9466
	3.0	28.44	0.9445
	4.0	42.78	0.9442
	5.0	58.54	0.9462

‡ See Appendix 6.E for results for other conditions.

†† Other combinations of maximum enrichment and minimum burnup have been evaluated which result in the same maximum k_{eff}. See Appendix 6.E for a bounding polynomial function.

† The term "maximum k_{eff}" as used here, and elsewhere in this document, means the highest possible k-effective, including bias, uncertainties, and calculational statistics, evaluated for the worst case combination of manufacturing tolerances.

6.2 SPENT FUEL LOADING

Specifications for the BWR and PWR fuel assemblies that were analyzed in this criticality evaluation are given in Tables 6.2.1 and 6.2.2, respectively. For the BWR fuel characteristics, the number and dimensions for the water rods are the actual number and dimensions. For the PWR fuel characteristics, the actual number and dimensions of the control rod guide tubes and thimbles are used. Table 6.2.1 lists 72 unique BWR assemblies while Table 6.2.2 lists 46 unique PWR assemblies, all of which were explicitly analyzed for this evaluation. Examination of Tables 6.2.1 and 6.2.2 reveals that there are a large number of minor variations in fuel assembly dimensions.

Due to the large number of minor variations in fuel assembly dimensions, the use of explicit dimensions in defining the authorized contents could limit the applicability of the HI-STAR 100 System. To resolve this limitation, bounding criticality analyses are presented in this section for a number of defined fuel assembly classes for both fuel types (PWR and BWR). The results of the bounding criticality analyses justify using bounding fuel dimensions for defining the authorized contents.

6.2.1 Definition of Assembly Classes

For each array size (e.g., 6x6, 7x7, 15x15, etc.), the fuel assemblies have been subdivided into a number of defined classes, where a class is defined in terms of the (1) number of fuel rods; (2) pitch; (3) number and locations of guide tubes (PWR) or water rods (BWR); and (4) cladding material. The assembly classes for BWR and PWR fuel are defined in Tables 6.2.1 and 6.2.2, respectively. It should be noted that these assembly classes are unique to this evaluation and are not known to be consistent with any class designations in the open literature.

For each assembly class, calculations have been performed for all of the dimensional variations for which data is available (i.e., all data in Tables 6.2.1 and 6.2.2). These calculations demonstrate that the maximum reactivity corresponds to:

- maximum active fuel length,
- maximum fuel pellet diameter,
- minimum cladding outside diameter (OD),
- maximum cladding inside diameter (ID),
- minimum guide tube/water rod thickness, and
- maximum channel thickness (for BWR assemblies only).

Therefore, for each assembly class, a bounding assembly was defined based on the above characteristics and a calculation for the bounding assembly was performed to demonstrate compliance with the regulatory requirement of $k_{eff} < 0.95$. In some assembly classes this bounding assembly corresponds directly to one of the actual (real) assemblies; while in most

assembly classes, the bounding assembly is artificial (i.e., based on bounding dimensions from more than one of the actual assemblies). In classes where the bounding assembly is artificial, the reactivity of the actual (real) assemblies is typically much less than that of the bounding assembly; thereby providing additional conservatism. As a result of these analyses, the authorized contents (Chapter 1) are defined in terms of the bounding assembly parameters for each class.

To demonstrate that the aforementioned characteristics are bounding, a parametric study was performed for a reference BWR assembly, designated herein as 8x8C04 (identified generally as a GE8x8R). The results of this study are shown in Table 6.2.3, and verify the positive reactivity effect associated with (1) increasing the pellet diameter, (2) maximizing the cladding ID (while maintaining a constant cladding OD), (3) minimizing the cladding OD (while maintaining a constant cladding ID), (4) decreasing the water rod thickness, (5) artificially replacing the Zircaloy water rod tubes with water, (6) maximizing the channel thickness, and (7) increasing the active length. These results, and the many that follow, justify the approach for using bounding dimensions for defining the authorized contents. Where margins permit, the Zircaloy water rod tubes (BWR assemblies) are artificially replaced by water in the bounding cases to remove the requirement for water rod thickness from the specification of authorized contents.

As mentioned, the bounding approach used in these analyses often results in a maximum k_{eff} value for a given class of assemblies that is much greater than the reactivity of any of the actual (real) assemblies within the class, and yet, is still below the 0.95 regulatory limit.

6.2.2 PWR Fuel Assemblies in the MPC-24

For PWR fuel assemblies (specifications listed in Table 6.2.2) the 15x15F01 fuel assembly at 4.1% enrichment has the highest reactivity (see Table 6.2.13). The 17x17A01 assembly (otherwise known as a Westinghouse 17x17 OFA) has a similar reactivity (see Table 6.2.17) and was used throughout this criticality evaluation as a reference PWR assembly. The 17x17A01 assembly is a representative PWR fuel assembly in terms of design and reactivity and is useful for the reactivity studies presented in Sections 6.3 and 6.4. Calculations for the various PWR fuel assemblies in the MPC-24 are summarized in Tables 6.2.4 through 6.2.19 and 6.2.43 for the fully flooded condition with the fuel centered in each fuel storage location.

Tables 6.2.4 through 6.2.19 and 6.2.43 show the maximum k_{eff} values for the assembly classes that are acceptable for storage in the MPC-24. All maximum k_{eff} values include the bias, uncertainties, and calculational statistics, evaluated for the worst combination of manufacturing tolerances. All calculations for the MPC-24 were performed for a ^{10}B loading of 0.020 g/cm^2, which is 75% of the minimum loading of 0.0267 g/cm^2 for Boral, or 90% of the minimum loading of 0.0223 g/cm^2 for Metamic, specified for the MPC-24 in Section 1.4. The maximum allowable enrichment in the MPC-24 varies from 3.8 to 5.0 wt% ^{235}U, depending on the assembly class, and is defined in Tables 6.2.4 through 6.2.19 and 6.2.43. It should be noted that

the maximum allowable enrichment does not vary within an assembly class. Table 6.1.1 summarizes the maximum allowable enrichments for each of the assembly classes that are acceptable for storage in the MPC-24.

Tables 6.2.4 through 6.2.19 and 6.2.43 are formatted with the assembly class information in the top row, the unique assembly designations, dimensions, and k_{eff} values in the following rows above the bold double lines, and the bounding dimensions selected to define the authorized contents and corresponding bounding k_{eff} values in the final rows. Where the bounding assembly corresponds directly to one of the actual assemblies, the fuel assembly designation is listed in the bottom row in parentheses (e.g., Table 6.2.4). Otherwise, the bounding assembly is given a unique designation. For an assembly class that contains only a single assembly (e.g., 14x14D, see Table 6.2.7), the authorized contents dimensions are based on the assembly dimensions from that single assembly. Generally, the maximum k_{eff} values corresponding to the selected bounding dimensions are greater than or equal to those for the actual assembly dimensions, and all maximum k_{eff} values are below the 0.95 regulatory limit.

The results of the analyses for the MPC-24, which were performed for all assemblies in each class, further confirm the validity of the bounding dimensions established in Subsection 6.2.1. Thus, for all following calculations, namely analyses of the MPC-24E, only the bounding assembly in a class is analyzed. For the MPC-32 with burnup credit, the validity of the bounding dimensions is verified in Appendix 6.E.

6.2.3 BWR Fuel Assemblies in the MPC-68

For BWR fuel assemblies (specifications listed in Table 6.2.1) the artificial bounding assembly for the 10x10A assembly class at 4.2% enrichment has the highest reactivity (see Table 6.2.32). Calculations for the various BWR fuel assemblies in the MPC-68 are summarized in Tables 6.2.20 through 6.2.36 and 6.2.44 for the fully flooded condition. In all cases, the gadolinia (Gd_2O_3) normally incorporated in BWR fuel was conservatively neglected and the fuel assembly was assumed to be centered in the fuel storage location.

For calculations involving BWR assemblies, the use of a uniform (planar-average) enrichment, as opposed to the distributed enrichments normally used in BWR fuel, produces conservative results. Calculations confirming this statement are presented in Appendix 6.B for several representative BWR fuel assembly designs. These calculations justify the specification of planar-average enrichments to define acceptability of BWR fuel for loading into the MPC-68.

Tables 6.2.20 through 6.2.36 and 6.2.44 show the maximum k_{eff} values for assembly classes that are acceptable for storage in the MPC-68. All maximum k_{eff} values include the bias, uncertainties, and calculational statistics, evaluated for the worst combination of manufacturing tolerances. With the exception of assembly classes 6x6A, 6x6B, 6x6C, 7x7A, and 8x8A, which will be discussed in Section 6.2.4, all calculations for the MPC-68 were performed with a ^{10}B loading of 0.0279 g/cm^2, which is 75% of the minimum loading of 0.0372 g/cm^2 for Boral, or

90% of the minimum loading of 0.031 g/cm^2 for Metamic, specified for the MPC-68 in Section 1.4. Calculations for assembly classes 6x6A, 6x6B, 6x6C, 7x7A, and 8x8A were conservatively performed with a ^{10}B loading of 0.0067 g/cm^2. The maximum allowable enrichment in the MPC-68 varies from 2.7 to 4.2 wt% ^{235}U, depending on the assembly class. It should be noted that the maximum allowable enrichment does not vary within an assembly class. Table 6.1.2 summarizes the maximum allowable enrichments for all assembly classes that are acceptable for storage in the MPC-68.

Tables 6.2.20 through 6.2.36 and 6.2.44 are formatted with the assembly class information in the top row, the unique assembly designations, dimensions, and k_{eff} values in the following rows above the bold double lines, and the bounding dimensions selected to define the authorized contents and corresponding bounding k_{eff} values in the final rows. Where an assembly class contains only a single assembly (e.g., 8x8E, see Table 6.2.24), the authorized contents dimensions are based on the assembly dimensions from that single assembly. For assembly classes that are suspected to contain assemblies with thicker channels (e.g., 120 mils), bounding calculations are also performed to qualify the thicker channels (e.g. 7x7B, see Table 6.2.20). All of the maximum k_{eff} values corresponding to the selected bounding dimensions are shown to be greater than or equal to those for the actual assembly dimensions and are below the 0.95 regulatory limit.

For assembly classes that contain partial length rods (i.e., 9x9A, 10x10A, and 10x10B), calculations were performed for the actual (real) assembly configuration and for the axial segments (assumed to be full length) with and without the partial length rods. In all cases, the axial segment with only the full length rods present (where the partial length rods are absent) is bounding. Therefore, the bounding maximum k_{eff} values reported for assembly classes that contain partial length rods bound the reactivity regardless of the active fuel length of the partial length rods. As a result, the specification of authorized contents has no minimum requirement for the active fuel length of the partial length rods.

For BWR fuel assembly classes where margins permit, the Zircaloy water rod tubes are artificially replaced by water in the bounding cases to remove the requirement for water rod thickness from the specification of authorized contents. For these cases, the bounding water rod thickness is listed as zero.

As mentioned, the highest observed maximum k_{eff} value[†] corresponds to the artificial bounding assembly in the 10x10A assembly class. This assembly has the following bounding characteristics: (1) the partial length rods are assumed to be zero length (most reactive configuration); (2) the channel is assumed to be 120 mils thick; and (3) the active fuel length of the full length rods is 155 inches.

[†] Assuming assemblies are centered in their basket position. For cases with eccentric positioning see Section 6.3.3.

6.2.4 Damaged BWR Fuel Assemblies and BWR Fuel Debris

In addition to storing intact PWR and BWR fuel assemblies, the HI-STAR 100 System is designed to store damaged BWR fuel assemblies and BWR fuel debris. Damaged fuel assemblies and fuel debris are defined in Chapter 1. Both damaged BWR fuel assemblies and BWR fuel debris are required to be loaded into Damaged Fuel Containers (DFCs). Two different DFC types with slightly different cross sections are considered. DFCs containing fuel debris are only analyzed in the MPC-68F. DFCs containing damaged fuel assemblies may be stored in either the MPC-68 or MPC-68F. The criticality evaluation of various possible damaged conditions of the fuel is presented in Subsection 6.4.4 for both DFC types.

Tables 6.2.37 through 6.2.41 show the maximum k_{eff} values for the six assembly classes that may be stored as damaged fuel or fuel debris. All maximum k_{eff} values include the bias, uncertainties, and calculational statistics, evaluated for the worst combination of manufacturing tolerances. All calculations were performed for a ^{10}B loading of 0.0067 g/cm^2, which is 75% of a minimum loading, 0.0089 g/cm^2. However, because the practical manufacturing lower limit for minimum ^{10}B loading is 0.01 g/cm^2, the minimum ^{10}B loading of 0.01 g/cm^2 is specified in Section 1.4, for the MPC-68F. As an additional level of conservatism in the analyses, the calculations were performed for an enrichment of 3.0 wt% ^{235}U, while the maximum allowable enrichment for these assembly classes is limited to 2.7 wt% ^{235}U in the specification of authorized contents. Therefore, the maximum k_{eff} values for damaged BWR fuel assemblies and fuel debris are conservative. Calculations for the various BWR fuel assemblies in the MPC-68F are summarized in Tables 6.2.37 through 6.2.41 for the fully flooded condition.

For the assemblies that may be stored as damaged fuel or fuel debris, the 6x6C01 assembly at 3.0 wt% ^{235}U enrichment has the highest reactivity (see Table 6.2.39). Considering all of the conservatism built into this analysis (e.g., higher than allowed enrichment and lower than actual ^{10}B loading), the actual reactivity will be lower.

Because the analysis for the damaged BWR fuel assemblies and fuel debris was performed for a minimum ^{10}B loading of 0.0089 g/cm^2, which conservatively bounds damaged BWR fuel assemblies in a standard MPC-68 with a minimum ^{10}B loading of at least 0.0310 g/cm^2, damaged BWR fuel assemblies may also be stored in the standard MPC-68. However, fuel debris is limited to the MPC-68F by the specification of authorized contents in Chapter 1.

Tables 6.2.37 through 6.2.41 are formatted with the assembly class information in the top row, the unique assembly designations, dimensions, and k_{eff} values in the following rows above the bold double lines, and the bounding dimensions selected to define the authorized contents and corresponding bounding k_{eff} values in the final rows. Where an assembly class contains only a single assembly (e.g., 6x6C, see Table 6.2.39), the authorized contents dimensions are based on the assembly dimensions from that single assembly. All of the maximum k_{eff} values corresponding to the selected bounding dimensions are greater than or equal to those for the actual assembly dimensions and are well below the 0.95 regulatory limit.

6.2.5 Thoria Rod Canister

Additionally, the HI-STAR 100 System is designed to store a Thoria Rod Canister in the MPC68 or MPC68F. The canister is similar to a DFC and contains 18 intact Thoria Rods placed in a separator assembly. The reactivity of the canister in the MPC68 or MPC68F is very low compared to the reactivity of the approved fuel assemblies (The ^{235}U content of these rods corresponds to UO_2 rods with an initial enrichment of approximately 1.7 wt% ^{235}U). It is therefore permissible to store the Thoria Rod Canister together with any other approved content in a MPC68 or MPC68F. Specifications of the canister and the Thoria Rods that are used in the criticality evaluation are given in Table 6.2.42. The criticality evaluation is presented in Subsection 6.4.6.

6.2.6 PWR Assemblies in the MPC-24E and MPC-24EF

The MPC-24E and MPC-24EF are variations of the MPC-24, which provide for transportation of higher enriched fuel than the MPC-24 through an increased ^{10}B loading in the neutron absorber. The maximum allowable fuel enrichment varies between 4.2 and 5.0 wt% ^{235}U, depending on the assembly class. The maximum allowable enrichment for each assembly class is listed in Table 6.1.5, together with the maximum k_{eff} for the bounding assembly in the assembly class. All maximum k_{eff} values are below the 0.95 regulatory limit. The 15x15F assembly class at 4.5% enrichment has the highest reactivity.

6.2.7 PWR Intact Fuel, Damaged Fuel and Fuel Debris in the Trojan MPC-24E/EF

The Trojan MPC-24E and MPC-24EF are variations of the MPC-24E/EF, designed to transport Trojan intact and damaged PWR fuel assemblies and fuel debris. Damaged PWR fuel assemblies and fuel debris are required to be loaded into PWR Damaged Fuel Containers (DFCs) or Failed Fuel Cans. Up to four DFCs may be loaded in the MPC-24E or MPC-24EF. The maximum enrichment for intact fuel, damaged fuel and fuel debris is 3.7 wt% ^{235}U. Only the assembly class 17x17B is certified for the Trojan MPC-24E/EF. The maximum k_{eff} is listed in Table 6.1.6. The criticality evaluation of the damaged fuel is presented in Subsection 6.4.9.

6.2.8 PWR Assemblies in the MPC-32

Burnup credit is necessary to store PWR assemblies in the MPC-32, i.e. a required minimum average assembly burnup is specified as a function of the assembly initial enrichment. Only the assembly classes 15x15D, E, F, H and 17x17A, B, C are certified for transportation in the MPC-32. The maximum initial enrichment in 5.0 wt% ^{235}U. The criticality evaluations for burnup credit are presented in Appendix 6.E.

Table 6.2.1 (page 1 of 6)
BWR FUEL CHARACTERISTICS AND ASSEMBLY CLASS DEFINITIONS
(all dimensions are in inches)

Fuel Assembly Designation	Clad Material	Pitch	Number of Fuel Rods	Cladding OD	Cladding Thickness	Pellet Diameter	Active Fuel Length	Number of Water Rods	Water Rod OD	Water Rod ID	Channel Thickness	Channel ID
6x6A Assembly Class												
6x6A01	Zr	0.694	36	0.5645	0.0350	0.4940	110.0	0	n/a	n/a	0.060	4.290
6x6A02	Zr	0.694	36	0.5645	0.0360	0.4820	110.0	0	n/a	n/a	0.060	4.290
6x6A03	Zr	0.694	36	0.5645	0.0350	0.4820	110.0	0	n/a	n/a	0.060	4.290
6x6A04	Zr	0.694	36	0.5550	0.0350	0.4820	110.0	0	n/a	n/a	0.060	4.290
6x6A05	Zr	0.696	36	0.5625	0.0350	0.4820	110.0	0	n/a	n/a	0.060	4.290
6x6A06	Zr	0.696	35	0.5625	0.0350	0.4820	110.0	1	0.0	0.0	0.060	4.290
6x6A07	Zr	0.700	36	0.5555	0.03525	0.4780	110.0	0	n/a	n/a	0.060	4.290
6x6A08	Zr	0.710	36	0.5625	0.0260	0.4980	110.0	0	n/a	n/a	0.060	4.290
6x6B (MOX) Assembly Class												
6x6B01	Zr	0.694	36	0.5645	0.0350	0.4820	110.0	0	n/a	n/a	0.060	4.290
6x6B02	Zr	0.694	36	0.5625	0.0350	0.4820	110.0	0	n/a	n/a	0.060	4.290
6x6B03	Zr	0.696	36	0.5625	0.0350	0.4820	110.0	0	n/a	n/a	0.060	4.290
6x6B04	Zr	0.696	35	0.5625	0.0350	0.4820	110.0	1	0.0	0.0	0.060	4.290
6x6B05	Zr	0.710	35	0.5625	0.0350	0.4820	110.0	1	0.0	0.0	0.060	4.290
6x6C Assembly Class												
6x6C01	Zr	0.740	36	0.5630	0.0320	0.4880	77.5	0	n/a	n/a	0.060	4.542
7x7A Assembly Class												
7x7A01	Zr	0.631	49	0.4860	0.0328	0.4110	80	0	n/a	n/a	0.060	4.542

Table 6.2.1 (page 2 of 6)
BWR FUEL CHARACTERISTICS AND ASSEMBLY CLASS DEFINITIONS
(all dimensions are in inches)

Fuel Assembly Designation	Clad Material	Pitch	Number of Fuel Rods	Cladding OD	Cladding Thickness	Pellet Diameter	Active Fuel Length	Number of Water Rods	Water Rod OD	Water Rod ID	Channel Thickness	Channel ID
7x7B Assembly Class												
7x7B01	Zr	0.738	49	0.5630	0.0320	0.4870	150	0	n/a	n/a	0.080	5.278
7x7B02	Zr	0.738	49	0.5630	0.0370	0.4770	150	0	n/a	n/a	0.102	5.291
7x7B03	Zr	0.738	49	0.5630	0.0370	0.4770	150	0	n/a	n/a	0.080	5.278
7x7B04	Zr	0.738	49	0.5700	0.0355	0.4880	150	0	n/a	n/a	0.080	5.278
7x7B05	Zr	0.738	49	0.5630	0.0340	0.4775	150	0	n/a	n/a	0.080	5.278
7x7B06	Zr	0.738	49	0.5700	0.0355	0.4910	150	0	n/a	n/a	0.080	5.278
8x8A Assembly Class												
8x8A01	Zr	0.523	64	0.4120	0.0250	0.3580	110	0	n/a	n/a	0.100	4.290
8x8A02	Zr	0.523	63	0.4120	0.0250	0.3580	120	0	n/a	n/a	0.100	4.290

Table 6.2.1 (page 3 of 6)
BWR FUEL CHARACTERISTICS AND ASSEMBLY CLASS DEFINITIONS
(all dimensions are in inches)

Fuel Assembly Designation	Clad Material	Pitch	Number of Fuel Rods	Cladding OD	Cladding Thickness	Pellet Diameter	Active Fuel Length	Number of Water Rods	Water Rod OD	Water Rod ID	Channel Thickness	Channel ID
8x8B Assembly Class												
8x8B01	Zr	0.641	63	0.4840	0.0350	0.4050	150	1	0.484	0.414	0.100	5.278
8x8B02	Zr	0.636	63	0.4840	0.0350	0.4050	150	1	0.484	0.414	0.100	5.278
8x8B03	Zr	0.640	63	0.4930	0.0340	0.4160	150	1	0.493	0.425	0.100	5.278
8x8B04	Zr	0.642	64	0.5015	0.0360	0.4195	150	0	n/a	n/a	0.100	5.278
8x8C Assembly Class												
8x8C01	Zr	0.641	62	0.4840	0.0350	0.4050	150	2	0.484	0.414	0.100	5.278
8x8C02	Zr	0.640	62	0.4830	0.0320	0.4100	150	2	0.591	0.531	0.000	no channel
8x8C03	Zr	0.640	62	0.4830	0.0320	0.4100	150	2	0.591	0.531	0.080	5.278
8x8C04	Zr	0.640	62	0.4830	0.0320	0.4100	150	2	0.591	0.531	0.100	5.278
8x8C05	Zr	0.640	62	0.4830	0.0320	0.4100	150	2	0.591	0.531	0.120	5.278
8x8C06	Zr	0.640	62	0.4830	0.0320	0.4110	150	2	0.591	0.531	0.100	5.278
8x8C07	Zr	0.640	62	0.4830	0.0340	0.4100	150	2	0.591	0.531	0.100	5.278
8x8C08	Zr	0.640	62	0.4830	0.0320	0.4100	150	2	0.493	0.425	0.100	5.278
8x8C09	Zr	0.640	62	0.4930	0.0340	0.4160	150	2	0.493	0.425	0.100	5.278
8x8C10	Zr	0.640	62	0.4830	0.0340	0.4100	150	2	0.591	0.531	0.120	5.278
8x8C11	Zr	0.640	62	0.4830	0.0340	0.4100	150	2	0.591	0.531	0.120	5.215
8x8C12	Zr	0.636	62	0.4830	0.0320	0.4110	150	2	0.591	0.531	0.120	5.215

Table 6.2.1 (page 4 of 6)
BWR FUEL CHARACTERISTICS AND ASSEMBLY CLASS DEFINITIONS
(all dimensions are in inches)

Fuel Assembly Designation	Clad Material	Pitch	Number of Fuel Rods	Cladding OD	Cladding Thickness	Pellet Diameter	Active Fuel Length	Number of Water Rods	Water Rod OD	Water Rod ID	Channel Thickness	Channel ID
8x8D Assembly Class												
8x8D01	Zr	0.640	60	0.4830	0.0320	0.4110	150	2 large/ 2 small	0.591/ 0.483	0.531/ 0.433	0.100	5.278
8x8D02	Zr	0.640	60	0.4830	0.0320	0.4110	150	4	0.591	0.531	0.100	5.278
8x8D03	Zr	0.640	60	0.4830	0.0320	0.4110	150	4	0.483	0.433	0.100	5.278
8x8D04	Zr	0.640	60	0.4830	0.0320	0.4110	150	1	1.34	1.26	0.100	5.278
8x8D05	Zr	0.640	60	0.4830	0.0320	0.4100	150	1	1.34	1.26	0.100	5.278
8x8D06	Zr	0.640	60	0.4830	0.0320	0.4110	150	1	1.34	1.26	0.120	5.278
8x8D07	Zr	0.640	60	0.4830	0.0320	0.4110	150	1	1.34	1.26	0.080	5.278
8x8D08	Zr	0.640	61	0.4830	0.0300	0.4140	150	3	0.591	0.531	0.080	5.278
8x8E Assembly Class												
8x8E01	Zr	0.640	59	0.4930	0.0340	0.4160	150	5	0.493	0.425	0.100	5.278
8x8F Assembly Class												
8x8F01	Zr	0.609	64	0.4576	0.0290	0.3913	150	4†	0.291†	0.228†	0.055	5.390
9x9A Assembly Class												
9x9A01	Zr	0.566	74	0.4400	0.0280	0.3760	150	2	0.98	0.92	0.100	5.278
9x9A02	Zr	0.566	66	0.4400	0.0280	0.3760	150	2	0.98	0.92	0.100	5.278
9x9A03	Zr	0.566	74/66	0.4400	0.0280	0.3760	150/90	2	0.98	0.92	0.100	5.278
9x9A04	Zr	0.566	66	0.4400	0.0280	0.3760	150	2	0.98	0.92	0.120	5.278

† Four rectangular water cross segments dividing the assembly into four quadrants

Table 6.2.1 (page 5 of 6)
BWR FUEL CHARACTERISTICS AND ASSEMBLY CLASS DEFINITIONS
(all dimensions are in inches)

Fuel Assembly Designation	Clad Material	Pitch	Number of Fuel Rods	Cladding OD	Cladding Thickness	Pellet Diameter	Active Fuel Length	Number of Water Rods	Water Rod OD	Water Rod ID	Channel Thickness	Channel ID
9x9B Assembly Class												
9x9B01	Zr	0.569	72	0.4330	0.0262	0.3737	150	1	1.516	1.459	0.100	5.278
9x9B02	Zr	0.569	72	0.4330	0.0260	0.3737	150	1	1.516	1.459	0.100	5.278
9x9B03	Zr	0.572	72	0.4330	0.0260	0.3737	150	1	1.516	1.459	0.100	5.278
9x9C Assembly Class												
9x9C01	Zr	0.572	80	0.4230	0.0295	0.3565	150	1	0.512	0.472	0.100	5.278
9x9D Assembly Class												
9x9D01	Zr	0.572	79	0.4240	0.0300	0.3565	150	2	0.424	0.364	0.100	5.278
9x9E Assembly Class†												
9x9E01	Zr	0.572	76	0.4170	0.0265	0.3530	150	5	0.546	0.522	0.120	5.215
9x9E02	Zr	0.572	48 28	0.4170 0.4430	0.0265 0.0285	0.3530 0.3745	150	5	0.546	0.522	0.120	5.215
9x9F Assembly Class†												
9x9F01	Zr	0.572	76	0.4430	0.0285	0.3745	150	5	0.546	0.522	0.120	5.215
9x9F02	Zr	0.572	48 28	0.4170 0.4430	0.0265 0.0285	0.3530 0.3745	150	5	0.546	0.522	0.120	5.215
9x9G Assembly Class												
9x9G01	Zr	0.572	72	0.4240	0.0300	0.3565	150	1	1.668	1.604	0.120	5.278

† The 9x9E and 9x9F fuel assembly classes represent a single fuel type containing fuel rods with different dimensions (SPC 9x9-5). In addition to the actual configuration (9x9E02 and 9x9F02), the 9x9E class contains a hypothetical assembly with only small fuel rods (9x9E01), and the 9x9F class contains a hypothetical assembly with only large rods (9x9F01). This was done in order to simplify the specification of this assembly for the authorized contents.

Table 6.2.1 (page 6 of 6)
BWR FUEL CHARACTERISTICS AND ASSEMBLY CLASS DEFINITIONS
(all dimensions are in inches)

Fuel Assembly Designation	Clad Material	Pitch	Number of Fuel Rods	Cladding OD	Cladding Thickness	Pellet Diameter	Active Fuel Length	Number of Water Rods	Water Rod OD	Water Rod ID	Channel Thickness	Channel ID
10x10A Assembly Class												
10x10A01	Zr	0.510	92	0.4040	0.0260	0.3450	155	2	0.980	0.920	0.100	5.278
10x10A02	Zr	0.510	78	0.4040	0.0260	0.3450	155	2	0.980	0.920	0.100	5.278
10x10A03	Zr	0.510	92/78	0.4040	0.0260	0.3450	155/90	2	0.980	0.920	0.100	5.278
10x10B Assembly Class												
10x10B01	Zr	0.510	91	0.3957	0.0239	0.3413	155	1	1.378	1.321	0.100	5.278
10x10B02	Zr	0.510	83	0.3957	0.0239	0.3413	155	1	1.378	1.321	0.100	5.278
10x10B03	Zr	0.510	91/83	0.3957	0.0239	0.3413	155/90	1	1.378	1.321	0.100	5.278
10x10C Assembly Class												
10x10C01	Zr	0.488	96	0.3780	0.0243	0.3224	150	5	1.227	1.165	0.055	5.457
10x10D Assembly Class												
10x10D01	SS	0.565	100	0.3960	0.0200	0.3500	83	0	n/a	n/a	0.08	5.663
10x10E Assembly Class												
10x10E01	SS	0.557	96	0.3940	0.0220	0.3430	83	4	0.3940	0.3500	0.08	5.663

Table 6.2.2 (page 1 of 4)
PWR FUEL CHARACTERISTICS AND ASSEMBLY CLASS DEFINITIONS
(all dimensions are in inches)

Fuel Assembly Designation	Clad Material	Pitch	Number of Fuel Rods	Cladding OD	Cladding Thickness	Pellet Diameter	Active Fuel Length	Number of Guide Tubes	Guide Tube OD	Guide Tube ID	Guide Tube Thickness
14x14A Assembly Class											
14x14A01	Zr	0.556	179	0.400	0.0243	0.3444	150	17	0.527	0.493	0.0170
14x14A02	Zr	0.556	179	0.400	0.0243	0.3444	150	17	0.528	0.490	0.0190
14x14A03	Zr	0.556	179	0.400	0.0243	0.3444	150	17	0.526	0.492	0.0170
14x14B Assembly Class											
14x14B01	Zr	0.556	179	0.422	0.0243	0.3659	150	17	0.539	0.505	0.0170
14x14B02	Zr	0.556	179	0.417	0.0295	0.3505	150	17	0.541	0.507	0.0170
14x14B03	Zr	0.556	179	0.424	0.0300	0.3565	150	17	0.541	0.507	0.0170
14x14B04	Zr	0.556	179	0.426	0.0310	0.3565	150	17	0.541	0.507	0.0170
14x14C Assembly Class											
14x14C01	Zr	0.580	176	0.440	0.0280	0.3765	150	5	1.115	1.035	0.0400
14x14C02	Zr	0.580	176	0.440	0.0280	0.3770	150	5	1.115	1.035	0.0400
14x14C03	Zr	0.580	176	0.440	0.0260	0.3805	150	5	1.111	1.035	0.0380
14x14D Assembly Class											
14x14D01	SS	0.556	180	0.422	0.0165	0.3835	144	16	0.543	0.514	0.0145

Table 6.2.2 (page 2 of 4)
PWR FUEL CHARACTERISTICS AND ASSEMBLY CLASS DEFINITIONS
(all dimensions are in inches)

Fuel Assembly Designation	Clad Material	Pitch	Number of Fuel Rods	Cladding OD	Cladding Thickness	Pellet Diameter	Active Fuel Length	Number of Guide Tubes	Guide Tube OD	Guide Tube ID	Guide Tube Thickness
14x14E Assembly Class											
14x14E01†	SS	0.453 and 0.441	162 3 8	0.3415 0.3415 0.3415	0.0120 0.0285 0.0200	0.313 0.280 0.297	102	0	n/a	n/a	n/a
14x14E02†	SS	0.453 and 0.441	173	0.3415	0.0120	0.313	102	0	n/a	n/a	n/a
14x14E03†	SS	0.453 and 0.441	173	0.3415	0.0285	0.280	102	0	n/a	n/a	n/a
15x15A Assembly Class											
15x15A01	Zr	0.550	204	0.418	0.0260	0.3580	150	21	0.533	0.500	0.0165

† This is the fuel assembly used at Indian Point 1 (IP-1). This assembly is a 14x14 assembly with 23 fuel rods omitted to allow passage of control rods between assemblies. It has a different pitch in different sections of the assembly, and different fuel rod dimensions in some rods.

Table 6.2.2 (page 3 of 4)
PWR FUEL CHARACTERISTICS AND ASSEMBLY CLASS DEFINITIONS
(all dimensions are in inches)

Fuel Assembly Designation	Clad Material	Pitch	Number of Fuel Rods	Cladding OD	Cladding Thickness	Pellet Diameter	Active Fuel Length	Number of Guide Tubes	Guide Tube OD	Guide Tube ID	Guide Tube Thickness
15x15B Assembly Class											
15x15B01	Zr	0.563	204	0.422	0.0245	0.3660	150	21	0.533	0.499	0.0170
15x15B02	Zr	0.563	204	0.422	0.0245	0.3660	150	21	0.546	0.512	0.0170
15x15B03	Zr	0.563	204	0.422	0.0243	0.3660	150	21	0.533	0.499	0.0170
15x15B04	Zr	0.563	204	0.422	0.0243	0.3659	150	21	0.545	0.515	0.0150
15x15B05	Zr	0.563	204	0.422	0.0242	0.3659	150	21	0.545	0.515	0.0150
15x15B06	Zr	0.563	204	0.420	0.0240	0.3671	150	21	0.544	0.514	0.0150
15x15C Assembly Class											
15x15C01	Zr	0.563	204	0.424	0.0300	0.3570	150	21	0.544	0.493	0.0255
15x15C02	Zr	0.563	204	0.424	0.0300	0.3570	150	21	0.544	0.511	0.0165
15x15C03	Zr	0.563	204	0.424	0.0300	0.3565	150	21	0.544	0.511	0.0165
15x15C04	Zr	0.563	204	0.417	0.0300	0.3565	150	21	0.544	0.511	0.0165
15x15D Assembly Class											
15x15D01	Zr	0.568	208	0.430	0.0265	0.3690	150	17	0.530	0.498	0.0160
15x15D02	Zr	0.568	208	0.430	0.0265	0.3686	150	17	0.530	0.498	0.0160
15x15D03	Zr	0.568	208	0.430	0.0265	0.3700	150	17	0.530	0.499	0.0155
15x15D04	Zr	0.568	208	0.430	0.0250	0.3735	150	17	0.530	0.500	0.0150
15x15E Assembly Class											
15x15E01	Zr	0.568	208	0.428	0.0245	0.3707	150	17	0.528	0.500	0.0140
15x15F Assembly Class											
15x15F01	Zr	0.568	208	0.428	0.0230	0.3742	150	17	0.528	0.500	0.0140

Table 6.2.2 (page 4 of 4)
PWR FUEL CHARACTERISTICS AND ASSEMBLY CLASS DEFINITIONS
(all dimensions are in inches)

Fuel Assembly Designation	Clad Material	Pitch	Number of Fuel Rods	Cladding OD	Cladding Thickness	Pellet Diameter	Active Fuel Length	Number of Guide Tubes	Guide Tube OD	Guide Tube ID	Guide Tube Thickness
15x15G Assembly Class											
15x15G01	SS	0.563	204	0.422	0.0165	0.3825	144	21	0.543	0.514	0.0145
15x15H Assembly Class											
15x15H01	Zr	0.568	208	0.414	0.0220	0.3622	150	17	0.528	0.500	0.0140
16x16A Assembly Class											
16x16A01	Zr	0.506	236	0.382	0.0250	0.3255	150	5	0.980	0.900	0.0400
16x16A02	Zr	0.506	236	0.382	0.0250	0.3250	150	5	0.980	0.900	0.0400
17x17A Assembly Class											
17x17A01	Zr	0.496	264	0.360	0.0225	0.3088	150	25	0.474	0.442	0.0160
17x17A02	Zr	0.496	264	0.360	0.0250	0.3030	150	25	0.480	0.448	0.0160
17x17B Assembly Class											
17x17B01	Zr	0.496	264	0.374	0.0225	0.3225	150	25	0.482	0.450	0.0160
17x17B02	Zr	0.496	264	0.374	0.0225	0.3225	150	25	0.474	0.442	0.0160
17x17B03	Zr	0.496	264	0.376	0.0240	0.3215	150	25	0.480	0.448	0.0160
17x17B04	Zr	0.496	264	0.372	0.0205	0.3232	150	25	0.427	0.399	0.0140
17x17B05	Zr	0.496	264	0.374	0.0240	0.3195	150	25	0.482	0.450	0.0160
17x17B06	Zr	0.496	264	0.372	0.0205	0.3232	150	25	0.480	0.452	0.0140
17x17C Assembly Class											
17x17C01	Zr	0.502	264	0.379	0.0240	0.3232	150	25	0.472	0.432	0.0200
17x17C02	Zr	0.502	264	0.377	0.0220	0.3252	150	25	0.472	0.432	0.0200

Table 6.2.3
REACTIVITY EFFECT OF ASSEMBLY PARAMETER VARIATIONS
(all dimensions are in inches)

Fuel Assembly/ Parameter Variation	reactivity effect	calculated k_{eff}	standard deviation	cladding OD	cladding ID	cladding thickness	pellet OD	water rod thickness	channel thickness
8x8C04 (GE8x8R)	reference	0.9307	0.0007	0.483	0.419	0.032	0.410	0.030	0.100
increase pellet OD (+0.001)	+0.0005	0.9312	0.0007	0.483	0.419	0.032	0.411	0.030	0.100
decrease pellet OD (-0.001)	-0.0008	0.9299	0.0009	0.483	0.419	0.032	0.409	0.030	0.100
increase clad ID (+0.004)	+0.0027	0.9334	0.0007	0.483	0.423	0.030	0.410	0.030	0.100
decrease clad ID (-0.004)	-0.0034	0.9273	0.0007	0.483	0.415	0.034	0.410	0.030	0.100
increase clad OD (+0.004)	-0.0041	0.9266	0.0008	0.487	0.419	0.034	0.410	0.030	0.100
decrease clad OD (-0.004)	+0.0023	0.9330	0.0007	0.479	0.419	0.030	0.410	0.030	0.100
increase water rod thickness (+0.015)	-0.0019	0.9288	0.0008	0.483	0.419	0.032	0.410	0.045	0.100
decrease water rod thickness (-0.015)	+0.0001	0.9308	0.0008	0.483	0.419	0.032	0.410	0.015	0.100
remove water rods (i.e., replace the water rod tubes with water)	+0.0021	0.9328	0.0008	0.483	0.419	0.032	0.410	0.000	0.100
remove channel	-0.0039	0.9268	0.0009	0.483	0.419	0.032	0.410	0.030	0.000
increase channel thickness (+0.020)	+0.0005	0.9312	0.0007	0.483	0.419	0.032	0.410	0.030	0.120
reduced active length (120 Inches)	-0.0007	0.9300	0.0007	0.483	0.419	0.032	0.410	0.030	0.100
reduced active length (90 Inches)	-0.0043	0.9264	0.0007	0.483	0.419	0.032	0.410	0.030	0.100

Table 6.2.4
MAXIMUM K_{EFF} VALUES FOR THE 14X14A ASSEMBLY CLASS IN THE MPC-24
(all dimensions are in inches)

14x14A (4.6% Enrichment, Fixed neutron absorber ^{10}B minimum loading of 0.02 g/cm^2) 179 fuel rods, 17 guide tubes, pitch=0.556, Zr clad										
Fuel Assembly Designation	maximum k_{eff}	calculated k_{eff}	standard deviation	EALF	cladding OD	cladding ID	cladding thickness	pellet OD	fuel length	guide tube thickness
14x14A01	0.9295	0.9252	0.0008	0.2084	0.400	0.3514	0.0243	0.3444	150	0.017
14x14A02	0.9286	0.9242	0.0008	0.2096	0.400	0.3514	0.0243	0.3444	150	0.019
14x14A03	0.9296	0.9253	0.0008	0.2093	0.400	0.3514	0.0243	0.3444	150	0.017
Dimensions Listed for Authorized Contents					0.400 (min.)	0.3514 (max.)		0.3444 (max.)	150 (max.)	0.017 (min.)
bounding dimensions (14x14A03)	0.9296	0.9253	0.0008	0.2093	0.400	0.3514	0.0243	0.3444	150	0.017

Table 6.2.5
MAXIMUM K_{EFF} VALUES FOR THE 14X14B ASSEMBLY CLASS IN THE MPC-24
(all dimensions are in inches)

14x14B (4.6% Enrichment, Fixed neutron absorber ^{10}B minimum loading of 0.02 g/cm^2) 179 fuel rods, 17 guide tubes, pitch=0.556, Zr clad										
Fuel Assembly Designation	maximum k_{eff}	calculated k_{eff}	standard deviation	EALF	cladding OD	cladding ID	cladding thickness	pellet OD	fuel length	guide tube thickness
14x14B01	0.9159	0.9117	0.0007	0.2727	0.422	0.3734	0.0243	0.3659	150	0.017
14x14B02	0.9169	0.9126	0.0008	0.2345	0.417	0.3580	0.0295	0.3505	150	0.017
14x14B03	0.9110	0.9065	0.0009	0.2545	0.424	0.3640	0.0300	0.3565	150	0.017
14x14B04	0.9084	0.9039	0.0009	0.2563	0.426	0.3640	0.0310	0.3565	150	0.017
Dimensions Listed for Authorized Contents					0.417 (min.)	0.3734 (max.)		0.3659 (max.)	150 (max.)	0.017 (min.)
bounding dimensions (B14x14B01)	0.9228	0.9185	0.0008	0.2675	0.417	0.3734	0.0218	0.3659	150	0.017

Table 6.2.6
MAXIMUM K_{EFF} VALUES FOR THE 14X14C ASSEMBLY CLASS IN THE MPC-24
(all dimensions are in inches)

14x14C (4.6% Enrichment, Fixed neutron absorber ^{10}B minimum loading of 0.02 g/cm^2) 176 fuel rods, 5 guide tubes, pitch=0.580, Zr clad										
Fuel Assembly Designation	maximum k_{eff}	calculated k_{eff}	standard deviation	EALF	cladding OD	cladding ID	cladding thickness	pellet OD	fuel length	guide tube thickness
14x14C01	0.9258	0.9215	0.0008	0.2729	0.440	0.3840	0.0280	0.3765	150	0.040
14x14C02	0.9265	0.9222	0.0008	0.2765	0.440	0.3840	0.0280	0.3770	150	0.040
14x14C03	0.9287	0.9242	0.0009	0.2825	0.440	0.3880	0.0260	0.3805	150	0.038
Dimensions Listed for Authorized Contents					0.440 (min.)	0.3880 (max.)		0.3805 (max.)	150 (max.)	0.038 (min.)
bounding dimensions (14x14C03)	0.9287	0.9242	0.0009	0.2825	0.440	0.3880	0.0260	0.3805	150	0.038

Table 6.2.7
MAXIMUM K_{EFF} VALUES FOR THE 14X14D ASSEMBLY CLASS IN THE MPC-24
(all dimensions are in inches)

14x14D (4.0% Enrichment, Fixed neutron absorber ^{10}B minimum loading of 0.02 g/cm^2) 180 fuel rods, 16 guide tubes, pitch=0.556, SS clad										
Fuel Assembly Designation	maximum k_{eff}	calculated k_{eff}	standard deviation	EALF	cladding OD	cladding ID	cladding thickness	pellet OD	fuel length	guide tube thickness
14x14D01	0.8507	0.8464	0.0008	0.3308	0.422	0.3890	0.0165	0.3835	144	0.0145
Dimensions Listed for Authorized Contents					0.422 (min.)	0.3890 (max.)		0.3835 (max.)	144 (max.)	0.0145 (min.)

Table 6.2.8
MAXIMUM K_{EFF} VALUES FOR THE 15X15A ASSEMBLY CLASS IN THE MPC-24
(all dimensions are in inches)

15x15A (4.1% Enrichment, Fixed neutron absorber ^{10}B minimum loading of 0.02 g/cm^2) 204 fuel rods, 21 guide tubes, pitch=0.550, Zr clad										
Fuel Assembly Designation	maximum k_{eff}	calculated k_{eff}	standard deviation	EALF	cladding OD	cladding ID	cladding thickness	pellet OD	fuel length	guide tube thickness
15x15A01	0.9204	0.9159	0.0009	0.2608	0.418	0.3660	0.0260	0.3580	150	0.0165
Dimensions Listed for Authorized Contents					0.418 (min.)	0.3660 (max.)		0.3580 (max.)	150 (max.)	0.0165 (min.)

Table 6.2.9
MAXIMUM K_{EFF} VALUES FOR THE 15X15B ASSEMBLY CLASS IN THE MPC-24
(all dimensions are in inches)

15x15B (4.1% Enrichment, Fixed neutron absorber ^{10}B minimum loading of 0.02 g/cm^2) 204 fuel rods, 21 guide tubes, pitch=0.563, Zr clad										
Fuel Assembly Designation	maximum k_{eff}	calculated k_{eff}	standard deviation	EALF	cladding OD	cladding ID	cladding thickness	pellet OD	fuel length	guide tube thickness
15x15B01	0.9369	0.9326	0.0008	0.2632	0.422	0.3730	0.0245	0.3660	150	0.017
15x15B02	0.9338	0.9295	0.0008	0.2640	0.422	0.3730	0.0245	0.3660	150	0.017
15x15B03	0.9362	0.9318	0.0008	0.2632	0.422	0.3734	0.0243	0.3660	150	0.017
15x15B04	0.9370	0.9327	0.0008	0.2612	0.422	0.3734	0.0243	0.3659	150	0.015
15x15B05	0.9356	0.9313	0.0008	0.2606	0.422	0.3736	0.0242	0.3659	150	0.015
15x15B06	0.9366	0.9324	0.0007	0.2638	0.420	0.3720	0.0240	0.3671	150	0.015
Dimensions Listed for Authorized Contents					0.420 (min.)	0.3736 (max.)		0.3671 (max.)	150 (max.)	0.015 (min.)
bounding dimensions (B15x15B01)	0.9388	0.9343	0.0009	0.2626	0.420	0.3736	0.0232	0.3671	150	0.015

Table 6.2.10
MAXIMUM K_{EFF} VALUES FOR THE 15X15C ASSEMBLY CLASS IN THE MPC-24
(all dimensions are in inches)

15x15C (4.1% Enrichment, Fixed neutron absorber ^{10}B minimum loading of 0.02 g/cm^2) 204 fuel rods, 21 guide tubes, pitch=0.563, Zr clad										
Fuel Assembly Designation	maximum k_{eff}	calculated k_{eff}	standard deviation	EALF	cladding OD	cladding ID	cladding thickness	pellet OD	fuel length	guide tube thickness
15x15C01	0.9255	0.9213	0.0007	0.2493	0.424	0.3640	0.0300	0.3570	150	0.0255
15x15C02	0.9297	0.9255	0.0007	0.2457	0.424	0.3640	0.0300	0.3570	150	0.0165
15x15C03	0.9297	0.9255	0.0007	0.2440	0.424	0.3640	0.0300	0.3565	150	0.0165
15x15C04	0.9311	0.9268	0.0008	0.2435	0.417	0.3570	0.0300	0.3565	150	0.0165
Dimensions Listed for Authorized Contents					0.417 (min.)	0.3640 (max.)		0.3570 (max.)	150 (max.)	0.0165 (min.)
bounding dimensions (B15x15C01)	0.9361	0.9316	0.0009	0.2385	0.417	0.3640	0.0265	0.3570	150	0.0165

Table 6.2.11
MAXIMUM K_{EFF} VALUES FOR THE 15X15D ASSEMBLY CLASS IN THE MPC-24
(all dimensions are in inches)

15x15D (4.1% Enrichment, Fixed neutron absorber ^{10}B minimum loading of 0.02 g/cm^2) 208 fuel rods, 17 guide tubes, pitch=0.568, Zr clad										
Fuel Assembly Designation	maximum k_{eff}	calculated k_{eff}	standard deviation	EALF	cladding OD	cladding ID	cladding thickness	pellet OD	fuel length	guide tube thickness
15x15D01	0.9341	0.9298	0.0008	0.2822	0.430	0.3770	0.0265	0.3690	150	0.0160
15x15D02	0.9367	0.9324	0.0008	0.2802	0.430	0.3770	0.0265	0.3686	150	0.0160
15x15D03	0.9354	0.9311	0.0008	0.2844	0.430	0.3770	0.0265	0.3700	150	0.0155
15x15D04	0.9339	0.9292	0.0010	0.2958	0.430	0.3800	0.0250	0.3735	150	0.0150
Dimensions Listed for Authorized Contents					0.430 (min.)	0.3800 (max.)		0.3735 (max.)	150 (max.)	0.0150 (min.)
bounding dimensions (15x15D04)	0.9339†	0.9292	0.0010	0.2958	0.430	0.3800	0.0250	0.3735	150	0.0150

† The k_{eff} value listed for the 15x15D02 case is slightly higher than that for the case with the bounding dimensions. However, calculations with significantly increased number of particles show that the two cases are statistically equivalent, with a maximum k_{eff} value of 0.9339. Nevertheless, the 15x15D02 case is used in Table 6.3.5 for the eccentric positioning analysis.

Table 6.2.12
MAXIMUM K_{EFF} VALUES FOR THE 15X15E ASSEMBLY CLASS IN THE MPC-24
(all dimensions are in inches)

15x15E (4.1% Enrichment, Fixed neutron absorber ^{10}B minimum loading of 0.02 g/cm^2) 208 fuel rods, 17 guide tubes, pitch=0.568, Zr clad										
Fuel Assembly Designation	maximum k_{eff}	calculated k_{eff}	standard deviation	EALF	cladding OD	cladding ID	cladding thickness	pellet OD	fuel length	guide tube thickness
15x15E01	0.9368	0.9325	0.0008	0.2826	0.428	0.3790	0.0245	0.3707	150	0.0140
Dimensions Listed for Authorized Contents					0.428 (min.)	0.3790 (max.)		0.3707 (max.)	150 (max.)	0.0140 (min.)

Table 6.2.13
MAXIMUM K_{EFF} VALUES FOR THE 15X15F ASSEMBLY CLASS IN THE MPC-24
(all dimensions are in inches)

15x15F (4.1% Enrichment, Fixed neutron absorber ^{10}B minimum loading of 0.02 g/cm^2) 208 fuel rods, 17 guide tubes, pitch=0.568, Zr clad										
Fuel Assembly Designation	maximum k_{eff}	calculated k_{eff}	standard deviation	EALF	cladding OD	cladding ID	cladding thickness	pellet OD	fuel length	guide tube thickness
15x15F01	0.9395†	0.9350	0.0009	0.2903	0.428	0.3820	0.0230	0.3742	150	0.0140
Dimensions Listed for Authorized Contents					0.428 (min.)	0.3820 (max.)		0.3742 (max.)	150 (max.)	0.0140 (min.)

† KENO5a verification calculation resulted in a maximum k_{eff} of 0.9378.

Table 6.2.14
MAXIMUM K_{EFF} VALUES FOR THE 15X15G ASSEMBLY CLASS IN THE MPC-24
(all dimensions are in inches)

15x15G (4.0% Enrichment, Fixed neutron absorber ^{10}B minimum loading of 0.02 g/cm^2) 204 fuel rods, 21 guide tubes, pitch=0.563, SS clad										
Fuel Assembly Designation	maximum k_{eff}	calculated k_{eff}	standard deviation	EALF	cladding OD	cladding ID	cladding thickness	pellet OD	fuel† length	guide tube thickness
15x15G01	0.8876	0.8833	0.0008	0.3357	0.422	0.3890	0.0165	0.3825	144	0.0145
Dimensions Listed for Authorized Contents					0.422 (min.)	0.3890 (max.)		0.3825 (max.)	144 (max.)	0.0145 (min.)

† Calculations were conservatively performed for a fuel length of 150 inches.

Table 6.2.15
MAXIMUM K_{EFF} VALUES FOR THE 15X15H ASSEMBLY CLASS IN THE MPC-24
(all dimensions are in inches)

15x15H (3.8% Enrichment, Fixed neutron absorber ^{10}B minimum loading of 0.02 g/cm^2) 208 fuel rods, 17 guide tubes, pitch=0.568, Zr clad										
Fuel Assembly Designation	maximum k_{eff}	calculated k_{eff}	standard deviation	EALF	cladding OD	cladding ID	cladding thickness	pellet OD	fuel length	guide tube thickness
15x15H01	0.9337	0.9292	0.0009	0.2349	0.414	0.3700	0.0220	0.3622	150	0.0140
Dimensions Listed for Authorized Contents					0.414 (min.)	0.3700 (max.)		0.3622 (max.)	150 (max.)	0.0140 (min.)

Table 6.2.16
MAXIMUM K_{EFF} VALUES FOR THE 16X16A ASSEMBLY CLASS IN THE MPC-24
(all dimensions are in inches)

16x16A (4.6% Enrichment, Fixed neutron absorber ^{10}B minimum loading of 0.02 g/cm^2) 236 fuel rods, 5 guide tubes, pitch=0.506, Zr clad										
Fuel Assembly Designation	maximum k_{eff}	calculated k_{eff}	standard deviation	EALF	cladding OD	cladding ID	cladding thickness	pellet OD	fuel length	guide tube thickness
16x16A01	0.9287	0.9244	0.0008	0.2704	0.382	0.3320	0.0250	0.3255	150	0.0400
16x16A02	0.9263	0.9221	0.0007	0.2702	0.382	0.3320	0.0250	0.3250	150	0.0400
Dimensions Listed for Authorized Contents					0.382 (min.)	0.3320 (max.)		0.3255 (max.)	150 (max.)	0.0400 (min.)
bounding dimensions (16x16A01)	0.9287	0.9244	0.0008	0.2704	0.382	0.3320	0.0250	0.3255	150	0.0400

Table 6.2.17
MAXIMUM K_{EFF} VALUES FOR THE 17X17A ASSEMBLY CLASS IN THE MPC-24
(all dimensions are in inches)

17x17A (4.0% Enrichment, Fixed neutron absorber ^{10}B minimum loading of 0.02 g/cm^2) 264 fuel rods, 25 guide tubes, pitch=0.496, Zr clad										
Fuel Assembly Designation	maximum k_{eff}	calculated k_{eff}	standard deviation	EALF	cladding OD	cladding ID	cladding thickness	pellet OD	fuel length	guide tube thickness
17x17A01	0.9368	0.9325	0.0008	0.2131	0.360	0.3150	0.0225	0.3088	150	0.016
17x17A02	0.9329	0.9286	0.0008	0.2018	0.360	0.3100	0.0250	0.3030	150	0.016
Dimensions Listed for Authorized Contents					0.360 (min.)	0.3150 (max.)		0.3088 (max.)	150 (max.)	0.016 (min.)
bounding dimensions (17x17A01)	0.9368	0.9325	0.0008	0.2131	0.360	0.3150	0.0225	0.3088	150	0.016

Table 6.2.18
MAXIMUM K_{EFF} VALUES FOR THE 17X17B ASSEMBLY CLASS IN THE MPC-24
(all dimensions are in inches)

17x17B (4.0% Enrichment, Fixed neutron absorber ^{10}B minimum loading of 0.02 g/cm^2) 264 fuel rods, 25 guide tubes, pitch=0.496, Zr clad										
Fuel Assembly Designation	maximum k_{eff}	calculated k_{eff}	standard deviation	EALF	cladding OD	cladding ID	cladding thickness	pellet OD	fuel length	guide tube thickness
17x17B01	0.9288	0.9243	0.0009	0.2607	0.374	0.3290	0.0225	0.3225	150	0.016
17x17B02	0.9290	0.9247	0.0008	0.2596	0.374	0.3290	0.0225	0.3225	150	0.016
17x17B03	0.9243	0.9199	0.0008	0.2625	0.376	0.3280	0.0240	0.3215	150	0.016
17x17B04	0.9324	0.9279	0.0009	0.2576	0.372	0.3310	0.0205	0.3232	150	0.014
17x17B05	0.9266	0.9222	0.0008	0.2539	0.374	0.3260	0.0240	0.3195	150	0.016
17x17B06	0.9311	0.9268	0.0008	0.2593	0.372	0.3310	0.0205	0.3232	150	0.014
Dimensions Listed for Authorized Contents					0.372 (min.)	0.3310 (max.)		0.3232 (max.)	150 (max.)	0.014 (min.)
bounding dimensions (17x17B06)	0.9311†	0.9268	0.0008	0.2593	0.372	0.3310	0.0205	0.3232	150	0.014

† The k_{eff} value listed for the 17x17B04 case is slightly higher than that for the case with the bounding dimensions. However, the difference (0.0013) is well within the statistical uncertainties, and thus, the two values are statistically equivalent (within 2σ). Nevertheless, the17x17B04 case is used in Table 6.3.5 for the eccentric analysis.

Table 6.2.19
MAXIMUM K_{EFF} VALUES FOR THE 17X17C ASSEMBLY CLASS IN THE MPC-24
(all dimensions are in inches)

17x17C (4.0% Enrichment, Fixed neutron absorber ^{10}B minimum loading of 0.02 g/cm^2) 264 fuel rods, 25 guide tubes, pitch=0.502, Zr clad										
Fuel Assembly Designation	maximum k_{eff}	calculated k_{eff}	standard deviation	EALF	cladding OD	cladding ID	cladding thickness	pellet OD	fuel length	guide tube thickness
17x17C01	0.9293	0.9250	0.0008	0.2595	0.379	0.3310	0.0240	0.3232	150	0.020
17x17C02	0.9336	0.9293	0.0008	0.2624	0.377	0.3330	0.0220	0.3252	150	0.020
Dimensions Listed for Authorized Contents					0.377 (min.)	0.3330 (max.)		0.3252 (max.)	150 (max.)	0.020 (min.)
bounding dimensions (17x17C02)	0.9336	0.9293	0.0008	0.2624	0.377	0.3330	0.0220	0.3252	150	0.020

Table 6.2.20
MAXIMUM K_{EFF} VALUES FOR THE 7X7B ASSEMBLY CLASS IN THE MPC-68
(all dimensions are in inches)

7x7B (4.2% Enrichment, Fixed neutron absorber ^{10}B minimum loading of 0.0279 g/cm^2) 49 fuel rods, 0 water rods, pitch=0.738, Zr clad											
Fuel Assembly Designation	maximum k_{eff}	calculated k_{eff}	standard deviation	EALF	cladding OD	cladding ID	cladding thickness	pellet OD	fuel length	water rod thickness	channel thickness
7x7B01	0.9372	0.9330	0.0007	0.3658	0.5630	0.4990	0.0320	0.4870	150	n/a	0.080
7x7B02	0.9301	0.9260	0.0007	0.3524	0.5630	0.4890	0.0370	0.4770	150	n/a	0.102
7x7B03	0.9313	0.9271	0.0008	0.3438	0.5630	0.4890	0.0370	0.4770	150	n/a	0.080
7x7B04	0.9311	0.9270	0.0007	0.3816	0.5700	0.4990	0.0355	0.4880	150	n/a	0.080
7x7B05	0.9350	0.9306	0.0008	0.3382	0.5630	0.4950	0.0340	0.4775	150	n/a	0.080
7x7B06	0.9298	0.9260	0.0006	0.3957	0.5700	0.4990	0.0355	0.4910	150	n/a	0.080
Dimensions Listed for Authorized Contents					0.5630 (min.)	0.4990 (max.)		0.4910 (max.)	150 (max.)	n/a	0.120 (max.)
bounding dimensions (B7x7B01)	0.9375	0.9332	0.0008	0.3887	0.5630	0.4990	0.0320	0.4910	150	n/a	0.102
bounding dimensions with 120 mil channel (B7x7B02)	0.9386	0.9344	0.0007	0.3983	0.5630	0.4990	0.0320	0.4910	150	n/a	0.120

Table 6.2.21
MAXIMUM K_{EFF} VALUES FOR THE 8X8B ASSEMBLY CLASS IN THE MPC-68
(all dimensions are in inches)

8x8B (4.2% Enrichment, Fixed neutron absorber ^{10}B minimum loading of 0.0279 g/cm^2) 63 or 64 fuel rods, 1 or 0 water rods, pitch† = 0.636-0.642, Zr clad													
Fuel Assembly Designation	maximum k_{eff}	calculated k_{eff}	standard deviation	EALF	Fuel rods	pitch	cladding OD	cladding ID	cladding thickness	pellet OD	fuel length	water rod thickness	channel thickness
8x8B01	0.9310	0.9265	0.0009	0.2935	63	0.641	0.4840	0.4140	0.0350	0.4050	150	0.035	0.100
8x8B02	0.9227	0.9185	0.0007	0.2993	63	0.636	0.4840	0.4140	0.0350	0.4050	150	0.035	0.100
8x8B03	0.9299	0.9257	0.0008	0.3319	63	0.640	0.4930	0.4250	0.0340	0.4160	150	0.034	0.100
8x8B04	0.9236	0.9194	0.0008	0.3700	64	0.642	0.5015	0.4295	0.0360	0.4195	150	n/a	0.100
Dimensions Listed for Authorized Contents					63 or 64	0.636-0.642	0.4840 (min.)	0.4295 (max.)		0.4195 (max.)	150 (max.)	0.034	0.120 (max.)
bounding (pitch=0.636) (B8x8B01)	0.9346	0.9301	0.0009	0.3389	63	0.636	0.4840	0.4295	0.02725	0.4195	150	0.034	0.120
bounding (pitch=0.640) (B8x8B02)	0.9385	0.9343	0.0008	0.3329	63	0.640	0.4840	0.4295	0.02725	0.4195	150	0.034	0.120
bounding (pitch=0.641) (B8x8B03)	0.9416	0.9375	0.0007	0.3293	63	0.642	0.4840	0.4295	0.02725	0.4195	150	0.034	0.120

† This assembly class was analyzed and qualified for a small variation in the pitch and a variation in the number of fuel and water rods.

Table 6.2.22
MAXIMUM K_{EFF} VALUES FOR THE 8X8C ASSEMBLY CLASS IN THE MPC-68
(all dimensions are in inches)

8x8C (4.2% Enrichment, Fixed neutron absorber ^{10}B minimum loading of 0.0279 g/cm^2) 62 fuel rods, 2 water rods, pitch† = 0.636-0.641, Zr clad												
Fuel Assembly Designation	maximum k_{eff}	calculated k_{eff}	standard deviation	EALF	pitch	cladding OD	cladding ID	cladding thickness	pellet OD	fuel length	water rod thickness	channel thickness
8x8C01	0.9315	0.9273	0.0007	0.2822	0.641	0.4840	0.4140	0.0350	0.4050	150	0.035	0.100
8x8C02	0.9313	0.9268	0.0009	0.2716	0.640	0.4830	0.4190	0.0320	0.4100	150	0.030	0.000
8x8C03	0.9329	0.9286	0.0008	0.2877	0.640	0.4830	0.4190	0.0320	0.4100	150	0.030	0.800
8x8C04	0.9348††	0.9307	0.0007	0.2915	0.640	0.4830	0.4190	0.0320	0.4100	150	0.030	0.100
8x8C05	0.9353	0.9312	0.0007	0.2971	0.640	0.4830	0.4190	0.0320	0.4100	150	0.030	0.120
8x8C06	0.9353	0.9312	0.0007	0.2944	0.640	0.4830	0.4190	0.0320	0.4110	150	0.030	0.100
8x8C07	0.9314	0.9273	0.0007	0.2972	0.640	0.4830	0.4150	0.0340	0.4100	150	0.030	0.100
8x8C08	0.9339	0.9298	0.0007	0.2915	0.640	0.4830	0.4190	0.0320	0.4100	150	0.034	0.100
8x8C09	0.9301	0.9260	0.0007	0.3183	0.640	0.4930	0.4250	0.0340	0.4160	150	0.034	0.100
8x8C10	0.9317	0.9275	0.0008	0.3018	0.640	0.4830	0.4150	0.0340	0.4100	150	0.030	0.120
8x8C11	0.9328	0.9287	0.0007	0.3001	0.640	0.4830	0.4150	0.0340	0.4100	150	0.030	0.120
8x8C12	0.9285	0.9242	0.0008	0.3062	0.636	0.4830	0.4190	0.0320	0.4110	150	0.030	0.120
Dimensions Listed for Authorized Contents					0.636-0.641	0.4830 (min.)	0.4250 (max.)		0.4160 (max.)	150 (max.)	0.000 (min.)	0.120 (max.)
bounding (pitch=0.636) (B8x8C01)	0.9357	0.9313	0.0009	0.3141	0.636	0.4830	0.4250	0.0290	0.4160	150	0.000	0.120
bounding (pitch=0.640) (B8x8C02)	0.9425	0.9384	0.0007	0.3081	0.640	0.4830	0.4250	0.0290	0.4160	150	0.000	0.120
bounding (pitch=0.641) (B8x8C03)	0.9418	0.9375	0.0008	0.3056	0.641	0.4830	0.4250	0.0290	0.4160	150	0.000	0.120

† This assembly class was analyzed and qualified for a small variation in the pitch.

†† KENO5a verification calculation resulted in a maximum k_{eff} of 0.9343.

Table 6.2.23
MAXIMUM K_{EFF} VALUES FOR THE 8X8D ASSEMBLY CLASS IN THE MPC-68
(all dimensions are in inches)

8x8D (4.2% Enrichment, Fixed neutron absorber ^{10}B minimum loading of 0.0279 g/cm^2) 60 or 61 fuel rods, 1-4 water rods†, pitch=0.640, Zr clad											
Fuel Assembly Designation	maximum k_{eff}	calculated k_{eff}	standard deviation	EALF	cladding OD	cladding ID	cladding thickness	pellet OD	fuel length	water rod thickness	channel thickness
8x8D01	0.9342	0.9302	0.0006	0.2733	0.4830	0.4190	0.0320	0.4110	150	0.03/0.025	0.100
8x8D02	0.9325	0.9284	0.0007	0.2750	0.4830	0.4190	0.0320	0.4110	150	0.030	0.100
8x8D03	0.9351	0.9309	0.0008	0.2731	0.4830	0.4190	0.0320	0.4110	150	0.025	0.100
8x8D04	0.9338	0.9296	0.0007	0.2727	0.4830	0.4190	0.0320	0.4110	150	0.040	0.100
8x8D05	0.9339	0.9294	0.0009	0.2700	0.4830	0.4190	0.0320	0.4100	150	0.040	0.100
8x8D06	0.9365	0.9324	0.0007	0.2777	0.4830	0.4190	0.0320	0.4110	150	0.040	0.120
8x8D07	0.9341	0.9297	0.0009	0.2694	0.4830	0.4190	0.0320	0.4110	150	0.040	0.080
8x8D08	0.9376	0.9332	0.0009	0.2841	0.4830	0.4230	0.0300	0.4140	150	0.030	0.080
Dimensions Listed for Authorized Contents					0.4830 (min.)	0.4230 (max.)		0.4140 (max.)	150 (max.)	0.000 (min.)	0.120 (max.)
bounding dimensions (B8x8D01)	0.9403	0.9363	0.0007	0.2778	0.4830	0.4230	0.0300	0.4140	150	0.000	0.120

† Fuel assemblies 8x8D01 through 8x8D03 have 4 water rods that are similar in size to the fuel rods, while assemblies 8x8D04 through 8x8D07 have 1 large water rod that takes the place of the 4 water rods. Fuel assembly 8x8D08 contains 3 water rods that are similar in size to the fuel rods.

Table 6.2.24
MAXIMUM K_{EFF} VALUES FOR THE 8X8E ASSEMBLY CLASS IN THE MPC-68
(all dimensions are in inches)

8x8E (4.2% Enrichment, Fixed neutron absorber ^{10}B minimum loading of 0.0279 g/cm^2) 59 fuel rods, 5 water rods, pitch=0.640, Zr clad											
Fuel Assembly Designation	maximum k_{eff}	calculated k_{eff}	standard deviation	EALF	cladding OD	cladding ID	cladding thickness	pellet OD	fuel length	water rod thickness	channel thickness
8x8E01	0.9312	0.9270	0.0008	0.2831	0.4930	0.4250	0.0340	0.4160	150	0.034	0.100
Dimensions Listed for Authorized Contents					0.4930 (min.)	0.4250 (max.)		0.4160 (max.)	150 (max.)	0.034 (min.)	0.100 (max.)

Table 6.2.25
MAXIMUM K_{EFF} VALUES FOR THE 8X8F ASSEMBLY CLASS IN THE MPC-68
(all dimensions are in inches)

8x8F (4.0% Enrichment, Fixed neutron absorber ^{10}B minimum loading of 0.0279 g/cm^2) 64 fuel rods, 4 rectangular water cross segments dividing the assembly into four quadrants, pitch=0.609, Zr clad											
Fuel Assembly Designation	maximum k_{eff}	calculated k_{eff}	standard deviation	EALF	cladding OD	cladding ID	cladding thickness	pellet OD	fuel length	water rod thickness	channel thickness
8x8F01	0.9411	0.9366	0.0009	0.2264	0.4576	0.3996	0.0290	0.3913	150	0.0315	0.055
Dimensions Listed for Authorized Contents					0.4576 (min.)	0.3996 (max.)		0.3913 (max.)	150 (max.)	0.0315 (min.)	0.055 (max.)

Table 6.2.26
MAXIMUM K_{EFF} VALUES FOR THE 9X9A ASSEMBLY CLASS IN THE MPC-68
(all dimensions are in inches)

9x9A (4.2% Enrichment, Fixed neutron absorber ^{10}B minimum loading of 0.0279 g/cm^2) 74/66 fuel rods†, 2 water rods, pitch=0.566, Zr clad											
Fuel Assembly Designation	maximum k_{eff}	calculated k_{eff}	standard deviation	EALF	cladding OD	cladding ID	cladding thickness	pellet OD	fuel length	water rod thickness	channel thickness
9x9A01 (axial segment with all rods)	0.9353	0.9310	0.0008	0.2875	0.4400	0.3840	0.0280	0.3760	150	0.030	0.100
9x9A02 (axial segment with only the full length rods)	0.9388	0.9345	0.0008	0.2228	0.4400	0.3840	0.0280	0.3760	150	0.030	0.100
9x9A03 (actual three-dimensional representation of all rods)	0.9351	0.9310	0.0007	0.2837	0.4400	0.3840	0.0280	0.3760	150/90	0.030	0.100
9x9A04 (axial segment with only the full length rods)	0.9396	0.9355	0.0007	0.2262	0.4400	0.3840	0.0280	0.3760	150	0.030	0.120
Dimensions Listed for Authorized Contents					0.4400 (min.)	0.3840 (max.)		0.3760 (max.)	150 (max.)	0.000 (min.)	0.120 (max.)
bounding dimensions (axial segment with only the full length rods) (B9x9A01)	0.9417	0.9374	0.0008	0.2236	0.4400	0.3840	0.0280	0.3760	150	0.000	0.120

† This assembly class contains 66 full length rods and 8 partial length rods. In order to eliminate a requirement on the length of the partial length rods, separate calculations were performed for the axial segments with and without the partial length rods.

Table 6.2.27
MAXIMUM K_{EFF} VALUES FOR THE 9X9B ASSEMBLY CLASS IN THE MPC-68
(all dimensions are in inches)

9x9B (4.2% Enrichment, Fixed neutron absorber ^{10}B minimum loading of 0.0279 g/cm^2) 72 fuel rods, 1 water rod (square, replacing 9 fuel rods), pitch=0.569 to 0.572†, Zr clad												
Fuel Assembly Designation	maximum k_{eff}	calculated k_{eff}	standard deviation	EALF	pitch	cladding OD	cladding ID	cladding thickness	pellet OD	fuel length	water rod thickness	channel thickness
9x9B01	0.9380	0.9336	0.0008	0.2576	0.569	0.4330	0.3807	0.0262	0.3737	150	0.0285	0.100
9x9B02	0.9373	0.9329	0.0009	0.2578	0.569	0.4330	0.3810	0.0260	0.3737	150	0.0285	0.100
9x9B03	0.9417	0.9374	0.0008	0.2545	0.572	0.4330	0.3810	0.0260	0.3737	150	0.0285	0.100
Dimensions Listed for Authorized Contents					0.572	0.4330 (min.)	0.3810 (max.)		0.3740 (max.)	150 (max.)	0.000 (min.)	0.120 (max.)
bounding dimensions (B9x9B01)	0.9436	0.9394	0.0008	0.2506	0.572	0.4330	0.3810	0.0260	0.3740††	150	0.000	0.120

† This assembly class was analyzed and qualified for a small variation in the pitch.

†† This value was conservatively defined to be larger than any of the actual pellet diameters.

Table 6.2.28
MAXIMUM K_{EFF} VALUES FOR THE 9X9C ASSEMBLY CLASS IN THE MPC-68
(all dimensions are in inches)

9x9C (4.2% Enrichment, Fixed neutron absorber ^{10}B minimum loading of 0.0279 g/cm^2) 80 fuel rods, 1 water rods, pitch=0.572, Zr clad											
Fuel Assembly Designation	maximum k_{eff}	calculated k_{eff}	standard deviation	EALF	cladding OD	cladding ID	cladding thickness	pellet OD	fuel length	water rod thickness	channel thickness
9x9C01	0.9395	0.9352	0.0008	0.2698	0.4230	0.3640	0.0295	0.3565	150	0.020	0.100
Dimensions Listed for Authorized Contents					0.4230 (min.)	0.3640 (max.)		0.3565 (max.)	150 (max.)	0.020 (min.)	0.100 (max.)

Table 6.2.29
MAXIMUM K_{EFF} VALUES FOR THE 9X9D ASSEMBLY CLASS IN THE MPC-68
(all dimensions are in inches)

9x9D (4.2% Enrichment, Fixed neutron absorber ^{10}B minimum loading of 0.0279 g/cm^2) 79 fuel rods, 2 water rods, pitch=0.572, Zr clad											
Fuel Assembly Designation	maximum k_{eff}	calculated k_{eff}	standard deviation	EALF	cladding OD	cladding ID	cladding thickness	pellet OD	fuel length	water rod thickness	channel thickness
9x9D01	0.9394	0.9350	0.0009	0.2625	0.4240	0.3640	0.0300	0.3565	150	0.0300	0.100
Dimensions Listed for Authorized Contents					0.4240 (min.)	0.3640 (max.)		0.3565 (max.)	150 (max.)	0.0300 (min.)	0.100 (max.)

Table 6.2.30
MAXIMUM K_{EFF} VALUES FOR THE 9X9E ASSEMBLY CLASS IN THE MPC-68
(all dimensions are in inches)

9x9E (4.0% Enrichment, Fixed neutron absorber ^{10}B minimum loading of 0.0279 g/cm^2) 76 fuel rods, 5 water rods, pitch=0.572, Zr clad											
Fuel Assembly Designation	maximum k_{eff}	calculated k_{eff}	standard deviation	EALF	cladding OD	cladding ID	cladding thickness	pellet OD	fuel length	water rod thickness	channel thickness
9x9E01	0.9334	0.9293	0.0007	0.2227	0.4170	0.3640	0.0265	0.3530	150	0.0120	0.120
9x9E02	0.9401	0.9359	0.0008	0.2065	0.4170 0.4430	0.3640 0.3860	0.0265 0.0285	0.3530 0.3745	150	0.0120	0.120
Dimensions Listed for Authorized Contents†					0.4170 (min.)	0.3640 (max.)		0.3530 (max.)	150 (max.)	0.0120 (min.)	0.120 (max.)
bounding dimensions (9x9E02)	0.9401	0.9359	0.0008	0.2065	0.4170 0.4430	0.3640 0.3860	0.0265 0.0285	0.3530 0.3745	150	0.0120	0.120

† This fuel assembly, also known as SPC 9x9-5, contains fuel rods with different cladding and pellet diameters which do not bound each other. To be consistent in the way fuel assemblies are listed for Authorized Contents, two assembly classes (9x9E and 9x9F) are required to specify this assembly. Each class contains the actual geometry (9x9E02 and 9x9F02), as well as a hypothetical geometry with either all small rods (9x9E01) or all large rods (9x9F01). The Authorized Content lists the small rod dimensions for class 9x9E and the large rod dimensions for class 9x9F, and a note that both classes are used to qualify the assembly. The analyses demonstrate that all configurations, including the actual geometry, are acceptable.

Table 6.2.31
MAXIMUM K_{EFF} VALUES FOR THE 9X9F ASSEMBLY CLASS IN THE MPC-68
(all dimensions are in inches)

9x9F (4.0% Enrichment, Fixed neutron absorber ^{10}B minimum loading of 0.0279 g/cm^2) 76 fuel rods, 5 water rods, pitch=0.572, Zr clad											
Fuel Assembly Designation	maximum k_{eff}	calculated k_{eff}	standard deviation	EALF	cladding OD	cladding ID	cladding thickness	pellet OD	fuel length	water rod thickness	channel thickness
9x9F01	0.9307	0.9265	0.0007	0.2899	0.4430	0.3860	0.0285	0.3745	150	0.0120	0.120
9x9F02	0.9401	0.9359	0.0008	0.2065	0.4170 0.4430	0.3640 0.3860	0.0265 0.0285	0.3530 0.3745	150	0.0120	0.120
Dimensions Listed for Authorized Contents†					0.4430 (min.)	0.3860 (max.)		0.3745 (max.)	150 (max.)	0.0120 (min.)	0.120 (max.)
bounding dimensions (9x9F02)	0.9401	0.9359	0.0008	0.2065	0.4170 0.4430	0.3640 0.3860	0.0265 0.0285	0.3530 0.3745	150	0.0120	0.120

† This fuel assembly, also known as SPC 9x9-5, contains fuel rods with different cladding and pellet diameters which do not bound each other. To be consistent in the way fuel assemblies are listed for Authorized Contents, two assembly classes (9x9E and 9x9F) are required to specify this assembly. Each class contains the actual geometry (9x9E02 and 9x9F02), as well as a hypothetical geometry with either all small rods (9x9E01) or all large rods (9x9F01). The Authorized Content lists the small rod dimensions for class 9x9E and the large rod dimensions for class 9x9F, and a note that both classes are used to qualify the assembly. The analyses demonstrate that all configurations, including the actual geometry, are acceptable.

Table 6.2.32
MAXIMUM K_{EFF} VALUES FOR THE 10X10A ASSEMBLY CLASS IN THE MPC-68
(all dimensions are in inches)

10x10A (4.2% Enrichment, Fixed neutron absorber ^{10}B minimum loading of 0.0279 g/cm^2) 92/78 fuel rods†, 2 water rods, pitch=0.510, Zr clad											
Fuel Assembly Designation	maximum k_{eff}	calculated k_{eff}	standard deviation	EALF	cladding OD	cladding ID	cladding thickness	pellet OD	fuel length	water rod thickness	channel thickness
10x10A01 (axial segment with all rods)	0.9377	0.9335	0.0008	0.3170	0.4040	0.3520	0.0260	0.3450	155	0.030	0.100
10x10A02 (axial segment with only the full length rods)	0.9426	0.9386	0.0007	0.2159	0.4040	0.3520	0.0260	0.3450	155	0.030	0.100
10x10A03 (actual three-dimensional representation of all rods)	0.9396	0.9356	0.0007	0.3169	0.4040	0.3520	0.0260	0.3450	155/90	0.030	0.100
Dimensions Listed for Authorized Contents					0.4040 (min.)	0.3520 (max.)		0.3455 (max.)	150†† (max.)	0.030 (min.)	0.120 (max.)
bounding dimensions (axial segment with only the full length rods) (B10x10A01)	0.9457†††	0.9414	0.0008	0.2212	0.4040	0.3520	0.0260	0.3455‡	155	0.030	0.120

† This assembly class contains 78 full-length rods and 14 partial-length rods. In order to eliminate the requirement on the length of the partial length rods, separate calculations were performed for axial segments with and without the partial length rods.

†† Although the analysis qualifies this assembly for a maximum active fuel length of 155 inches, the specification for authorized contents limits the active fuel length to 150 inches. This is due to the fact that the Fixed neutron absorber panels are 156 inches in length.

††† KENO5a verification calculation resulted in a maximum k_{eff} of 0.9453.

‡ This value was conservatively defined to be larger than any of the actual pellet diameters.

Table 6.2.33
MAXIMUM K_{EFF} VALUES FOR THE 10X10B ASSEMBLY CLASS IN THE MPC-68
(all dimensions are in inches)

10x10B (4.2% Enrichment, Fixed neutron absorber ^{10}B minimum loading of 0.0279 g/cm^2) 91/83 fuel rods†, 1 water rods (square, replacing 9 fuel rods), pitch=0.510, Zr clad											
Fuel Assembly Designation	maximum k_{eff}	calculated k_{eff}	standard deviation	EALF	cladding OD	cladding ID	cladding thickness	pellet OD	fuel length	water rod thickness	channel thickness
10x10B01 (axial segment with all rods)	0.9384	0.9341	0.0008	0.2881	0.3957	0.3480	0.0239	0.3413	155	0.0285	0.100
10x10B02 (axial segment with only the full length rods)	0.9416	0.9373	0.0008	0.2333	0.3957	0.3480	0.0239	0.3413	155	0.0285	0.100
10x10B03 (actual three-dimensional representation of all rods)	0.9375	0.9334	0.0007	0.2856	0.3957	0.3480	0.0239	0.3413	155/90	0.0285	0.100
Dimensions Listed for Authorized Contents					0.3957 (min.)	0.3480 (max.)		0.3420 (max.)	150†† (max.)	0.000 (min.)	0.120 (max.)
bounding dimensions (axial segment with only the full length rods) (B10x10B01)	0.9436	0.9395	0.0007	0.2366	0.3957	0.3480	0.0239	0.3420†††	155	0.000	0.120

† This assembly class contains 83 full length rods and 8 partial length rods. In order to eliminate a requirement on the length of the partial length rods, separate calculations were performed for the axial segments with and without the partial length rods.

†† Although the analysis qualifies this assembly for a maximum active fuel length of 155 inches, the specification for authorized contents limits the active fuel length to 150 inches. This is due to the fact that the Fixed neutron absorber panels are 156 inches in length.

††† This value was conservatively defined to be larger than any of the actual pellet diameters.

Table 6.2.34
MAXIMUM K_{EFF} VALUES FOR THE 10X10C ASSEMBLY CLASS IN THE MPC-68
(all dimensions are in inches)

10x10C (4.2% Enrichment, Fixed neutron absorber ^{10}B minimum loading of 0.0279 g/cm^2) 96 fuel rods, 5 water rods (1 center diamond and 4 rectangular), pitch=0.488, Zr clad											
Fuel Assembly Designation	maximum k_{eff}	calculated k_{eff}	standard deviation	EALF	cladding OD	cladding ID	cladding thickness	pellet OD	fuel length	water rod thickness	channel thickness
10x10C01	0.9433	0.9392	0.0007	0.2416	0.3780	0.3294	0.0243	0.3224	150	0.031	0.055
Dimensions Listed for Authorized Contents					0.3780 (min.)	0.3294 (max.)		0.3224 (max.)	150 (max.)	0.031 (min.)	0.055 (max.)

Table 6.2.35
MAXIMUM K_{EFF} VALUES FOR THE 10X10D ASSEMBLY CLASS IN THE MPC-68
(all dimensions are in inches)

10x10D (4.0% Enrichment, Fixed neutron absorber ^{10}B minimum loading of 0.0279 g/cm^2) 100 fuel rods, 0 water rods, pitch=0.565, SS clad											
Fuel Assembly Designation	maximum k_{eff}	calculated k_{eff}	standard deviation	EALF	cladding OD	cladding ID	cladding thickness	pellet OD	fuel length	water rod thickness	channel thickness
10x10D01	0.9376	0.9333	0.0008	0.3355	0.3960	0.3560	0.0200	0.350	83	n/a	0.080
Dimensions Listed for Authorized Contents					0.3960 (min.)	0.3560 (max.)		0.350 (max.)	83 (max.)	n/a	0.080 (max.)

Table 6.2.36
MAXIMUM K_{EFF} VALUES FOR THE 10X10E ASSEMBLY CLASS IN THE MPC-68
(all dimensions are in inches)

10x10E (4.0% Enrichment, Fixed neutron absorber ^{10}B minimum loading of 0.0279 g/cm^2) 96 fuel rods, 4 water rods, pitch=0.557, SS clad											
Fuel Assembly Designation	maximum k_{eff}	calculated k_{eff}	standard deviation	EALF	cladding OD	cladding ID	cladding thickness	pellet OD	fuel length	water rod thickness	channel thickness
10x10E01	0.9185	0.9144	0.0007	0.2936	0.3940	0.3500	0.0220	0.3430	83	0.022	0.080
Dimensions Listed for Authorized Contents					0.3940 (min.)	0.3500 (max.)		0.3430 (max.)	83 (max.)	0.022 (min.)	0.080 (max.)

Table 6.2.37
MAXIMUM K_{EFF} VALUES FOR THE 6X6A ASSEMBLY CLASS IN THE MPC-68F
(all dimensions are in inches)

6x6A (3.0% Enrichment†, Fixed neutron absorber ^{10}B minimum loading of 0.0067 g/cm^2) 35 or 36 fuel rods††, 1 or 0 water rods††, pitch=0.694 to 0.710††, Zr clad													
Fuel Assembly Designation	maximum k_{eff}	calculated k_{eff}	standard deviation	EALF	pitch	fuel rods	cladding OD	cladding ID	cladding thickness	pellet OD	fuel length	water rod thickness	channel thickness
6x6A01	0.7539	0.7498	0.0007	0.2754	0.694	36	0.5645	0.4945	0.0350	0.4940	110	n/a	0.060
6x6A02	0.7517	0.7476	0.0007	0.2510	0.694	36	0.5645	0.4925	0.0360	0.4820	110	n/a	0.060
6x6A03	0.7545	0.7501	0.0008	0.2494	0.694	36	0.5645	0.4945	0.0350	0.4820	110	n/a	0.060
6x6A04	0.7537	0.7494	0.0008	0.2494	0.694	36	0.5550	0.4850	0.0350	0.4820	110	n/a	0.060
6x6A05	0.7555	0.7512	0.0008	0.2470	0.696	36	0.5625	0.4925	0.0350	0.4820	110	n/a	0.060
6x6A06	0.7618	0.7576	0.0008	0.2298	0.696	35	0.5625	0.4925	0.0350	0.4820	110	0.0	0.060
6x6A07	0.7588	0.7550	0.0007	0.2360	0.700	36	0.5555	0.4850	0.03525	0.4780	110	n/a	0.060
6x6A08	0.7808	0.7766	0.0007	0.2527	0.710	36	0.5625	0.5105	0.0260	0.4980	110	n/a	0.060
Dimensions Listed for Authorized Contents					0.710 (max.)	35 or 36	0.5550 (min.)	0.5105 (max.)	0.02225	0.4980 (max.)	120 (max.)	0.0	0.060 (max.)
bounding dimensions (B6x6A01)	0.7727	0.7685	0.0007	0.2460	0.694	35	0.5550	0.5105	0.02225	0.4980	120	0.0	0.060
bounding dimensions (B6x6A02)	0.7782	0.7738	0.0008	0.2408	0.700	35	0.5550	0.5105	0.02225	0.4980	120	0.0	0.060
bounding dimensions (B6x6A03)	0.7888	0.7846	0.0007	0.2310	0.710	35	0.5550	0.5105	0.02225	0.4980	120	0.0	0.060

† Although the calculations were performed for 3.0%, the enrichment is limited in the specification for authorized contents to 2.7%.

†† This assembly class was analyzed and qualified for a small variation in the pitch and a variation in the number of fuel and water rods.

Table 6.2.38
MAXIMUM K_{EFF} VALUES FOR THE 6X6B ASSEMBLY CLASS IN THE MPC-68F
(all dimensions are in inches)

6x6B (3.0% Enrichment†, Fixed neutron absorber ^{10}B minimum loading of 0.0067 g/cm^2) 35 or 36 fuel rods†† (up to 9 MOX rods), 1 or 0 water rods††, pitch=0.694 to 0.710††, Zr clad													
Fuel Assembly Designation	maximum k_{eff}	calculated k_{eff}	standard deviation	EALF	pitch	fuel rods	cladding OD	cladding ID	cladding thickness	pellet OD	fuel length	water rod thickness	channel thickness
6x6B01	0.7604	0.7563	0.0007	0.2461	0.694	36	0.5645	0.4945	0.0350	0.4820	110	n/a	0.060
6x6B02	0.7618	0.7577	0.0007	0.2450	0.694	36	0.5625	0.4925	0.0350	0.4820	110	n/a	0.060
6x6B03	0.7619	0.7578	0.0007	0.2439	0.696	36	0.5625	0.4925	0.0350	0.4820	110	n/a	0.060
6x6B04	0.7686	0.7644	0.0008	0.2286	0.696	35	0.5625	0.4925	0.0350	0.4820	110	0.0	0.060
6x6B05	0.7824	0.7785	0.0006	0.2184	0.710	35	0.5625	0.4925	0.0350	0.4820	110	0.0	0.060
Dimensions Listed for Authorized Contents					0.710 (max.)	35 or 36	0.5625 (min.)	0.4945 (max.)		0.4820 (max.)	120 (max.)	0.0	0.060 (max.)
bounding dimensions (B6x6B01)	0.7822†††	0.7783	0.0007	0.2190	0.710	35	0.5625	0.4945	0.0340	0.4820	120	0.0	0.060

Note:

1. These assemblies contain up to 9 MOX pins. The composition of the MOX fuel pins is given in Table 6.3.4.

† The ^{235}U enrichment of the MOX and UO_2 pins is assumed to be 0.711% and 3.0%, respectively.

†† This assembly class was analyzed and qualified for a small variation in the pitch and a variation in the number of fuel and water rods.

††† The k_{eff} value listed for the 6x6B05 case is slightly higher than that for the case with the bounding dimensions. However, the difference (0.0002) is well within the statistical uncertainties, and thus, the two values are statistically equivalent (within 1σ). Therefore, the 0.7824 value is listed in Tables 6.1.2 and 6.1.3 as the maximum.

Table 6.2.39
MAXIMUM K_{EFF} VALUES FOR THE 6X6C ASSEMBLY CLASS IN THE MPC-68F
(all dimensions are in inches)

6x6C (3.0% Enrichment†, Fixed neutron absorber ^{10}B minimum loading of 0.0067 g/cm^2) 36 fuel rods, 0 water rods, pitch=0.740, Zr clad											
Fuel Assembly Designation	maximum k_{eff}	calculated k_{eff}	standard deviation	EALF	cladding OD	cladding ID	cladding thickness	pellet OD	fuel length	water rod thickness	channel thickness
6x6C01	0.8021	0.7980	0.0007	0.2139	0.5630	0.4990	0.0320	0.4880	77.5	n/a	0.060
Dimensions Listed for Authorized Contents					0.5630 (min.)	0.4990 (max.)		0.4880 (max.)	77.5 (max.)	n/a	0.060 (max.)

† Although the calculations were performed for 3.0%, the enrichment is limited in the specification for authorized contents to 2.7%.

Table 6.2.40
MAXIMUM K_{EFF} VALUES FOR THE 7X7A ASSEMBLY CLASS IN THE MPC-68F
(all dimensions are in inches)

7x7A (3.0% Enrichment†, Fixed neutron absorber ^{10}B minimum loading of 0.0067 g/cm^2) 49 fuel rods, 0 water rods, pitch=0.631, Zr clad											
Fuel Assembly Designation	maximum k_{eff}	calculated k_{eff}	standard deviation	EALF	cladding OD	cladding ID	cladding thickness	pellet OD	fuel length	water rod thickness	channel thickness
7x7A01	0.7974	0.7932	0.0008	0.2015	0.4860	0.4204	0.0328	0.4110	80	n/a	0.060
Dimensions Listed for Authorized Contents					0.4860 (min.)	0.4204 (max.)		0.4110 (max.)	80 (max.)	n/a	0.060 (max.)

† Although the calculations were performed for 3.0%, the enrichment is limited in the specification for authorized contents to 2.7%.

Table 6.2.41
MAXIMUM K_{EFF} VALUES FOR THE 8X8A ASSEMBLY CLASS IN THE MPC-68F
(all dimensions are in inches)

8x8A (3.0% Enrichment†, Fixed neutron absorber ^{10}B minimum loading of 0.0067 g/cm^2) 63 or 64 fuel rods††, 0 water rods, pitch=0.523, Zr clad												
Fuel Assembly Designation	maximum k_{eff}	calculated k_{eff}	standard deviation	EALF	fuel rods	cladding OD	cladding ID	cladding thickness	pellet OD	fuel length	water rod thickness	channel thickness
8x8A01	0.7685	0.7644	0.0007	0.2227	64	0.4120	0.3620	0.0250	0.3580	110	n/a	0.100
8x8A02	0.7697	0.7656	0.0007	0.2158	63	0.4120	0.3620	0.0250	0.3580	120	n/a	0.100
Dimensions Listed for Authorized Contents					63	0.4120 (min.)	0.3620 (max.)		0.3580 (max.)	110 (max.)	n/a	0.100 (max.)
bounding dimensions (8x8A02)	0.7697	0.7656	0.0007	0.2158	63	0.4120	0.3620	0.0250	0.3580	120	n/a	0.100

† Although the calculations were performed for 3.0%, the enrichment is limited in the specification for authorized contents to 2.7%.

†† This assembly class was analyzed and qualified for a variation in the number of fuel rods.

Table 6.2.42

SPECIFICATION OF THE THORIA ROD CANISTER AND THE THORIA RODS

Canister ID	4.81"
Canister Wall Thickness	0.11"
Separator Assembly Plates Thickness	0.11"
Cladding OD	0.412"
Cladding ID	0.362"
Pellet OD	0.358"
Active Length	110.5"
Fuel Composition	1.8% UO_2 and 98.2% ThO_2
Initial Enrichment	93.5 wt% ^{235}U for 1.8% of the fuel
Maximum k_{eff}	0.1813
Calculated k_{eff}	0.1779
Standard Deviation	0.0004

Table 6.2.43
MAXIMUM K_{EFF} VALUES FOR THE 14X14E ASSEMBLY CLASS IN THE MPC-24
(all dimensions are in inches)

14x14E (5.0% Enrichment, Fixed neutron absorber ^{10}B minimum loading of 0.02 g/cm^2) 173 fuel rods, 0 guide tubes, pitch=0.453 and 0.441, SS clad†										
Fuel Assembly Designation	maximum k_{eff}	calculated k_{eff}	standard deviation	EALF	cladding OD	cladding ID	cladding thickness	pellet OD	fuel length††	guide tube thickness
14x14E01	0.7598	0.7555	0.0008	0.3890	0.3415	0.3175 0.2845 0.3015	0.0120 0.0285 0.0200	0.3130 0.2800 0.2970	102	0.0000
14x14E02	0.7627	0.7586	0.0007	0.3607	0.3415	0.3175	0.0120	0.3130	102	0.0000
14x14E03	0.6952	0.6909	0.0008	0.2905	0.3415	0.2845	0.0285	0.2800	102	0.0000
Dimensions Listed for Authorized Contents					0.3415 (min.)	0.3175 (max.)		0.3130 (max.)	102 (max.)	0.0000 (min.)
Bounding dimensions (14x14E02)	0.7627	0.7586	0.0007	0.3607	0.3415	0.3175	0.0120	0.3130	102	0.0000

† This is the IP-1 fuel assembly at Indian Point. This assembly is a 14x14 assembly with 23 fuel rods omitted to allow passage of control rods between assemblies. Fuel rod dimensions are bounding for each of the three types of rods found in the IP-1 fuel assembly.

†† Calculations were conservatively performed for a fuel length of 150 inches.

Table 6.2.44
MAXIMUM K_{EFF} VALUES FOR THE 9X9G ASSEMBLY CLASS IN THE MPC-68 and MPC-68FF
(all dimensions are in inches)

9x9G (4.2% Enrichment, Fixed neutron absorber ^{10}B minimum loading of 0.0279 g/cm^2) 72 fuel rods, 1 water rod (square, replacing 9 fuel rods), pitch=0.572, Zr clad											
Fuel Assembly Designation	maximum k_{eff}	calculated k_{eff}	standard deviation	EALF	cladding OD	cladding ID	cladding thickness	pellet OD	fuel length	water rod thickness	channel thickness
9x9G01	0.9309	0.9265	0.0008	0.2191	0.4240	0.3640	0.0300	0.3565	150	0.0320	0.120
Dimensions Listed for Authorized Contents					0.4240 (min.)	0.3640 (max.)		0.3565 (max.)	150 (max.)	0.0320 (min.)	0.120 (max.)

6.3 MODEL SPECIFICATION

In compliance with the requirements of 10CFR71.31(a)(1), 10CFR71.33(a)(5), and 10CFR71.33(b), this section provides a description of the HI-STAR 100 System in sufficient detail to identify the package accurately and provide a sufficient basis for the evaluation of the package.

6.3.1 Description of Calculational Model

Figures 6.3.1 through 6.3.3 show representative horizontal cross sections of the four types of cells used in the calculations, and Figures 6.3.4 through 6.3.6 illustrate the basket configurations used. Four different MPC fuel basket designs were evaluated as follows:

- a 24 PWR assembly basket,
- an optimized 24 PWR assembly basket (MPC-24E/EF and Trojan MPC-24E/EF),
- a 32 PWR assembly basket, and
- a 68 BWR assembly basket.

For all basket designs, the same techniques and the same level of detail are used in the calculational models.

Full three-dimensional calculations were used, assuming the axial configuration shown in Figure 6.3.7, and conservatively neglecting the absorption in the overpack neutron shielding material (Holtite-A). Although the fixed neutron absorber panels are 156 inches in length, which is much longer than the active fuel length (maximum of 150 inches), they are assumed equal to the active fuel length in the calculations, except for the Trojan MPC-24E/EF. Due to the reduced height of the Trojan MPCs, there is the potential of a misalignment of about 1 inch between the active length and the fixed neutron absorber at the bottom of the active region. Conservatively, a misalignment of 3 inches is assumed in the calculational model for the Trojan MPCs. As shown on the drawings in Section 1.4, 16 of the 24 periphery fixed neutron absorber panels on the MPC-24 have reduced width (i.e., 6.25 inches wide as opposed to 7.5 inches). However, the calculational models for the MPC-24 conservatively assume all of the periphery fixed neutron absorber panels are 6.25 inches in width. Note that Figures 6.3.1 through 6.3.3 show Boral as the fixed neutron absorber. The effect of using Metamic as fixed neutron absorber is discussed in Subsection 6.4.12.

The calculational model explicitly defines the fuel rods and cladding, the guide tubes (or water rods for BWR assemblies), the water-gaps and fixed neutron absorber panels on the stainless

steel walls of the basket cells. Under normal conditions of transport, when the MPC is dry, the resultant reactivity with the design basis fuel is very low ($k_{eff} < 0.5$). For the flooded condition (loading, unloading, and hypothetical accident condition), water was assumed to be present in the fuel rod pellet-to-clad gap regions (see Subsection 6.4.2.3 for justification). Appendix 6.D provides sample input files for the MPC-24 and MPC-68 basket designs in the HI-STAR 100 System.

The water thickness above and below the fuel is intentionally maintained less than or equal to the actual water thickness. This assures that any positive reactivity effect of the steel in the MPC is conservatively included.

As indicated in Figures 6.3.1 through 6.3.3 and in Tables 6.3.1 and 6.3.2, calculations were made with dimensions assumed to be at their most conservative value with respect to criticality. CASMO and MCNP4a were used to determine the direction of the manufacturing tolerances which produced the most adverse effect on criticality. After the directional effect (positive effect with an increase in reactivity; or negative effect with a decrease in reactivity) of the manufacturing tolerances was determined, the criticality analyses were performed using the worst case tolerances in the direction which would increase reactivity.

CASMO-3 and -4 were used for one of each of the two principal basket designs, i.e. for the fluxtrap design MPC-24 and for the non-fluxtrap design MPC-68. The effects are shown in Table 6.3.1 which also identifies the approximate magnitude of the tolerances on reactivity. The conclusions in Table 6.3.1 are directly applicable to the MPC-24E/EF and the MPC-32, due to the similarity in the basket designs.

Additionaly, MCNP4a calculations are performed to evaluate the tolerances of the various basket dimensions of the MPC-68, MPC-24 and MPC-32 in further detail. The various basket dimensions are inter-dependent, and therefore cannot be individually varied (i.e., reduction in one parameter requires a corresponding reduction or increase in another parameter). Thus, it is not possible to determine the reactivity effect of each individual dimensional tolerance separately. However, it is possible to determine the reactivity effect of the dimensional tolerances by evaluating the various possible dimensional combinations. To this end, an evaluation of the various possible dimensional combinations was performed using MCNP4a, with fuel assemblies centered in the fuel storage locations. Calculated k_{eff} results (which do not include the bias, uncertainties, or calculational statistics), along with the actual dimensions, for a number of dimensional combinations are shown in Table 6.3.2 for the reference PWR and BWR fuel assemblies. Each of the basket dimensions are evaluated for their minimum, nominal and maximum values. Due to the close similarity between the MPC-24 and MPC-24E, the basket dimensions are only evaluated for the MPC-24, and the same dimensional assumptions are applied to both MPC designs. For the MPC-32, the highest results are shown for the minimum and nominal pitch, and both results are statistically equivalent (the difference is less than 1

standard deviation). Consistent with the approach for MPC-68, the case with the minimum pitch is used in the design basis analyses.

Based on the MCNP4a and CASMO calculations, the conservative dimensional assumptions listed in Table 6.3.3 were determined for the MPC basket designs. Because the reactivity effect (positive or negative) of the manufacturing tolerances are not assembly dependent, these dimensional assumptions were employed for the criticality analyses.

The design parameters important to criticality safety are: fuel enrichment, the inherent geometry of the fuel basket structure, and the fixed neutron absorbing panels. None of these parameters are affected by the hypothetical accident conditions of transport.

During the hypothetical accident conditions of transport, the HI-STAR 100 System is assumed to be flooded to such an extent as to cause the maximum reactivity and to have full water reflection to such an extent as to cause the maximum reactivity. Further, arrays of packages under the hypothetical accident conditions must be evaluated to determine the maximum number of packages that may be transported in a single shipment. Thus, the only differences between the normal and hypothetical accident condition calculational models are the internal/external moderator densities and the boundary conditions (to simulate an infinite array of HI-STAR 100 Systems).

6.3.2 Cask Regional Densities

Composition of the various components of the principal designs of the HI-STAR 100 Systems are listed in Table 6.3.4. In this table, only the composition of fresh fuel is listed. For a discussion on the composition of spent fuel for burnup credit in the MPC-32 see Appendix 6.E.

The HI-STAR 100 System is designed such that the fixed neutron absorber will remain effective for a period greater than 20 years, and there are no credible means to lose it. A detailed physical description, historical applications, unique characteristics, service experience, and manufacturing quality assurance of fixed neutron absorbers are provided in Subsection 1.2.1.4.1.

The continued efficacy of the fixed neutron absorber is assured by acceptance testing, documented in Chapter 8, to validate the ^{10}B (poison) concentration in the fixed neutron absorber. To demonstrate that the neutron flux from the irradiated fuel results in a negligible depletion of the poison material, an MCNP4a calculation of the number of neutrons absorbed in the ^{10}B was performed. The calculation conservatively assumed a constant neutron source for 50 years equal to the initial source for the design basis fuel, as determined in Section 5.2, and shows that the fraction of ^{10}B atoms destroyed is only 2.6E-09 in 50 years. Thus, the reduction in ^{10}B concentration in the fixed neutron absorber by neutron absorption is negligible. In addition, the structural analysis demonstrates that the sheathing, which affixes the fixed neutron absorber

panel, remains in place during all hypothetical accident conditions, and thus, the fixed neutron absorber panel remains permanently fixed. Therefore, there is no need to provide a surveillance or monitoring program to verify the continued efficacy of the neutron absorber.

6.3.3 Eccentric Positioning of Assemblies in Fuel Storage Cells

Up to and including Revision 9 of this SAR, all criticality calculations were performed with fuel assemblies centered in the fuel storage locations since the effect of credible eccentric fuel positioning was judged to be not significant. Starting in Revision 10 of this SAR, the potential reactivity effect of eccentric positioning of assemblies in the fuel storage locations is accounted for in a conservatively bounding fashion, as described further in this subsection, for all new or changed MPC designs or assembly classes. The calculations in this subsection serve to determine the highest maximum k_{eff} value for each of these assembly class and basket combinations, that is then reported in the summary tables in Section 6.1 and the results tables in Section 6.4. Further, the calculations in this subsection are used to determine the assembly class in each basket with the highest maximum k_{eff} that is then used to demonstrate compliance with the requirements of 10CFR71.55 and 10CFR71.59. All other calculations throughout this chapter, such as studies to determine bounding fuel dimension, bounding basket dimensions, or bounding moderation conditions, are performed with assemblies centered in the fuel storage locations.

To conservatively account for eccentric fuel positioning in the fuel storage cells, three different configurations are analyzed, and the results are compared to determine the bounding configuration:

- Cell Center Configuration: All assemblies centered in their fuel storage cell; same configuration that is used in Section 6.2 and Section 6.3.1;
- Basket Center Configuration: All assemblies in the basket are moved as closely to the center of the basket as permitted by the basket geometry; and
- Basket Periphery Configuration: All assemblies in the basket are moved furthest away from the basket center, and as closely to the periphery of the basket as possible.

It needs to be noted that the two eccentric configurations are hypothetical, since there is no known physical effect that could move all assemblies within a basket consistently to the center or periphery. Instead, the most likely configuration would be that all assemblies are moved in the same direction when the cask is in a horizontal position, and that assemblies are positioned randomly when the cask is in a vertical position. Further, it is not credible to assume that any such configuration could exist by chance. Even if the probability for a single assembly placed in the corner towards the basket center would be 1/5 (i.e. assuming only the center and four corner positions in each cell, all with equal probability), then the probability that all assemblies would be located towards the center would be $(1/5)^{24}$ or approximately 10^{-17} for the MPC-24, $(1/5)^{32}$ or approximately 10^{-23} for the MPC-32, and $(1/5)^{68}$ or approximately 10^{-48} for the MPC-68.

However, since the configurations listed above bound all credible configurations, they are conservatively used in the analyses.

The results are presented in Table 6.3.5 for the MPC-24, Table 6.3.6 for the MPC-24E/EF, Table 6.3.7 for the Trojan MPC-24E/EF, and Table 6.3.8 for the MPC-68. For evaluations of eccentric fuel positions in the MPC-32 with burnup credit see Appendix 6.E. Each table shows the maximum k_{eff} value for centered and the two eccentric configurations for each of the assembly classes, and indicates the bounding configuration. The results are summarized as follows:

- In all cases, moving the assemblies to the periphery of the basket results in a reduction in reactivity, compared to the cell centered position.
- Most cases show the maximum reactivity for the basket center configuration, however, in some cases the reactivity is higher for the cell center configuration.

For each of the assembly class and basket combinations listed in Tables 6.3.5 through Table 6.3.8, the configuration showing the highest reactivity is used as the bounding configuration, and listed in the respective tables in Section 6.1. and 6.4. For evaluations of eccentric fuel positions in the MPC-32 with burnup credit see Appendix 6.E.

Table 6.3.1

CASMO-4 CALCULATIONS FOR EFFECT OF TOLERANCES AND TEMPERATURE

Change in Nominal Parameter†	Δk for Maximum Tolerance		Action/Modeling Assumption
	MPC-24	MPC-68‡	
Reduce fixed neutron absorber Width to Minimum	N/A††† min. = nom. = 7.5" and 6.25"	N/A††† min. = nom. = 4.75"	Assume minimum fixed neutron absorber width
Increase UO_2 Density to Maximum	+0.0017 max. = 10.522 g/cc nom. = 10.412 g/cc	+0.0014 max. = 10.522 g/cc nom. = 10.412 g/cc	Assume maximum UO_2 density
Reduce Box Inside Dimension (I.D.) to Minimum	-0.0005 min.= 8.86" nom. = 8.92"	See Table 6.3.2	Assume maximum box I.D. for the MPC-24
Increase Box Inside Dimension (I.D.) to Maximum	+0.0007 max. = 8.98" nom. = 8.92"	-0.0030 max. = 6.113" nom. = 6.053"	Assume minimum box I.D. for the MPC-68
Decrease Water Gap to Minimum	+0.0069 min. = 1.09" nom. = 1.15"	N/A	Assume minimum water gap in the MPC-24

† Reduction (or increase) in a parameter indicates that the parameter is changed to its minimum (or maximum) value.

‡ Calculations for the MPC-68 were performed with CASMO-3 [6.3.1 – 6.3.4].

††† The fixed neutron absorber width for the MPC-68 is 4.75" +0.125", -0" , the fixed neutron absorber widths for the MPC-24 are 7.5" +0.125", -0" and 6.25" +0.125" –0" (i.e., the nominal and minimum values are the same).

Table 6.3.1 (continued)

CASMO-4 CALCULATIONS FOR EFFECT OF TOLERANCES AND TEMPERATURE

Change in Nominal Parameter	Δk Maximum Tolerance		Action/Modeling Assumption
	MPC-24	MPC-68‡	
Increase in Temperature			Assume 20°C
20°C	Ref.	Ref.	
40°C	-0.0030	-0.0039	
70°C	-0.0089	-0.0136	
100°C	-0.0162	-0.0193	
10% Void in Moderator			Assume no void
20°C with no void	Ref.	Ref.	
20°C	-0.0251	-0.0241	
100°C	-0.0412	-0.0432	
Removal of Flow Channel (BWR)	N/A	-0.0073	Assume flow channel present for MPC-68

‡ Calculations for the MPC-68 were performed with CASMO-3 [6.3.1 – 6.3.4].

Table 6.3.2

MCNP4a EVALUATION OF BASKET MANUFACTURING TOLERANCES†

Pitch	Box I.D.	Box Wall Thickness	MCNP4a Calculated k_{eff}
MPC-24†† (17x17A01 @ 4.0% Enrichment)			
nominal (10.906")	maximum (8.98")	nominal (5/16")	0.9325±0.0008†††
minimum (10.846")	nominal (8.92")	nominal (5/16")	0.9300±0.0008
nominal (10.906")	nom. –0.04" (8.88")	nom. + 0.05" (0.3625")	0.9305±0.0007
MPC-68 (8x8C04 @ 4.2% Enrichment)			
minimum (6.43")	minimum (5.993")	nominal (1/4")	0.9307±0.0007
nominal (6.49")	nominal (6.053")	nominal (1/4")	0.9274±0.0007
maximum (6.55")	maximum (6.113")	nominal (1/4")	0.9272±0.0008
nom. + 0.05" (6.54")	nominal (6.053")	nom. + 0.05" (0.30")	0.9267±0.0007

Note: Values in parentheses are the actual value used.

† Tolerance for pitch and box I.D. are ± 0.06".
Tolerance for box wall thickness is +0.05", -0.00".

†† All calculations for the MPC-24 assume minimum water gap thickness (1.09").

††† Numbers are 1σ statistical uncertainties.

Table 6.3.2 (cont.)

MCNP4a EVALUATION OF BASKET MANUFACTURING TOLERANCES†

Pitch	Box I.D.	Box Wall Thickness	MCNP4a Calculated k_{eff}
MPC-32 (17x17A @ 4.0% Enrichment)			
minimum (9.158")	minimum (8.73")	nominal (9/32")	0.9171±0.0005†††
nominal (9.218")	nominal (8.79")	nominal (9/32")	0.9173±0.0005
maximum (9.278")	maximum (8.85")	nominal (9/32")	0.9157±0.0005
nominal+0.05" (9.268")	nominal (8.79")	nominal+0.05" (0.331")	0.9167±0.0005
minimum+0.05"(9.208")	minimum (8.73")	nominal+0.05" (0.331")	0.9168±0.0005
maximum (9.278")	Maximum-0.05" (8.80")	nominal+0.05" (0.331")	0.9142±0.0005

Notes:

1. Values in parentheses are the actual value used.

† Tolerance for pitch and box I.D. are ± 0.06".
Tolerance for box wall thickness is +0.05", -0.00".

††† Numbers are 1σ statistical uncertainties.

Table 6.3.3

BASKET DIMENSIONAL ASSUMPTIONS

Basket Type	Pitch	Box I.D.	Box Wall Thickness	Water-Gap Flux Trap
MPC-24	nominal (10.906")	maximum (8.98")	nominal (5/16")	minimum (1.09")
MPC-24E	nominal (10.847")	maximum (8.81", 9.11" for DFC Positions, 9.36" for DFC Positions in Trojan MPC)	nominal (5/16")	minimum (1.076", 0.776" for DFC Positions, 0.526" for DFC Positions in Trojan MPC)
MPC-32	minimum (9.158")	minimum (8.73")	nominal (9/32")	N/A
MPC-68	minimum (6.43")	minimum (5.993")	nominal (1/4")	N/A

Table 6.3.4

COMPOSITION OF THE MAJOR COMPONENTS OF THE HI-STAR 100 SYSTEM

MPC-24		
UO_2 4.0% ENRICHMENT, DENSITY (g/cc) = 10.522		
Nuclide	**Atom-Density**	**Wgt. Fraction**
8016	4.693E-02	1.185E-01
92235	9.505E-04	3.526E-02
92238	2.252E-02	8.462E-01
BORAL (0.02 g ^{10}B/cm sq), DENSITY (g/cc) = 2.660		
Nuclide	**Atom-Density**	**Wgt. Fraction**
5010	8.707E-03	5.443E-02
5011	3.512E-02	2.414E-01
6012	1.095E-02	8.210E-02
13027	3.694E-02	6.222E-01
MPC-32		
BORAL (0.0279 g ^{10}B/cm sq), DENSITY (g/cc) = 2.660		
Nuclide	**Atom-Density**	**Wgt. Fraction**
5010	8.071E-03	5.089E-02
5011	3.255E-02	2.257E-01
6012	1.015E-02	7.675E-02
13027	3.805E-02	6.467E-01

Table 6.3.4 (continued)

COMPOSITION OF THE MAJOR COMPONENTS OF THE HI-STAR 100 SYSTEM

MPC-68		
UO_2 4.2% ENRICHMENT, DENSITY (g/cc) = 10.522		
Nuclide	**Atom-Density**	**Wgt. Fraction**
8016	4.697E-02	1.185E-01
92235	9.983E-04	3.702E-02
92238	2.248E-02	8.445E-01
UO_2 3.0% ENRICHMENT, DENSITY (g/cc) = 10.522		
Nuclide	**Atom-Density**	**Wgt. Fraction**
8016	4.695E-02	1.185E-01
92235	7.127E-04	2.644E-02
92238	2.276E-02	8.550E-01
MOX FUEL†, DENSITY (g/cc) = 10.522		
Nuclide	**Atom-Density**	**Wgt. Fraction**
8016	4.714E-02	1.190E-01
92235	1.719E-04	6.380E-03
92238	2.285E-02	8.584E-01
94239	3.876E-04	1.461E-02
94240	9.177E-06	3.400E-04
94241	3.247E-05	1.240E-03
94242	2.118E-06	7.000E-05

† The Pu-238, which is an absorber, was conservatively neglected in the MOX description for analysis purposes.

Table 6.3.4 (continued)

COMPOSITION OF THE MAJOR COMPONENTS OF THE HI-STAR 100 SYSTEM

BORAL (0.0279 g ^{10}B/cm sq), DENSITY (g/cc) = 2.660		
Nuclide	**Atom-Density**	**Wgt. Fraction**
5010	8.071E-03	5.089E-02
5011	3.255E-02	2.257E-01
6012	1.015E-02	7.675E-02
13027	3.805E-02	6.467E-01
FUEL IN THORIA RODS, DENSITY (g/cc) = 10.522		
Nuclide	**Atom-Density**	**Wgt. Fraction**
8016	4.798E-02	1.212E-01
92235	4.001E-04	1.484E-02
92238	2.742E-05	1.030E-03
90232	2.357E-02	8.630E-01

Table 6.3.4 (continued)

COMPOSITION OF THE MAJOR COMPONENTS OF THE HI-STAR 100 SYSTEM

COMMON MATERIALS		
ZR CLAD, DENSITY (g/cc) = 6.550		
Nuclide	**Atom-Density**	**Wgt. Fraction**
40000	4.323E-02	1.000E+00
MODERATOR (H_2O), DENSITY (g/cc) = 1.000		
Nuclide	**Atom-Density**	**Wgt. Fraction**
1001	6.688E-02	1.119E-01
8016	3.344E-02	8.881E-01
STAINLESS STEEL, DENSITY (g/cc) = 7.840		
Nuclide	**Atom-Density**	**Wgt. Fraction**
24000	1.761E-02	1.894E-01
25055	1.761E-03	2.001E-02
26000	5.977E-02	6.905E-01
28000	8.239E-03	1.000E-01
ALUMINUM, DENSITY (g/cc) = 2.700		
Nuclide	**Atom-Density**	**Wgt. Fraction**
13027	6.026E-02	1.000E+00

Table 6.3.5

EFFECT OF ECCENTRIC FUEL POSITIONING IN THE MPC-24

Fuel Assembly Class	Maximum k_{eff}			Bounding Configuration	Bounding Maximum k_{eff}
	Cell Center Configuration	Basket Center Configuration	Basket Periphery Configuration		
14x14A	0.9296	0.9271	0.8951	Cell Center	0.9296
14x14B	0.9228	0.9207	0.8904	Cell Center	0.9228
14x14C	0.9287	0.9307	0.9068	Basket Center	0.9307
14x14D	0.8507	0.8498	0.8225	Cell Center	0.8507
14x14E	0.7627	0.7608	0.7003	Cell Center	0.7627
15x15A	0.9204	0.9227	0.9037	Basket Center	0.9227
15x15B	0.9388	0.9388	0.9240	Basket Center	0.9388
15x15C	0.9361	0.9351	0.9218	Cell Center	0.9361
15x15D	0.9367	0.9364	0.9248	Cell Center	0.9367
15x15E	0.9368	0.9392	0.9264	Basket Center	0.9392
15x15F	0.9395	0.9410	0.9271	Basket Center	0.9410
15x15G	0.8876	0.8907	0.8761	Basket Center	0.8907
15x15H	0.9337	0.9335	0.9214	Cell Center	0.9337
16x16A	0.9287	0.9284	0.9051	Cell Center	0.9287
17x17A	0.9368	0.9362	0.9221	Cell Center	0.9368
17x17B	0.9324	0.9355	0.9204	Basket Center	0.9355
17x17C	0.9336	0.9349	0.9225	Basket Center	0.9349

Table 6.3.6

EFFECT OF ECCENTRIC FUEL POSITIONING IN THE MPC-24E/EF

Fuel Assembly Class	Maximum k_{eff}			Bounding Configuration	Bounding Maximum k_{eff}
	Cell Center Configuration	Basket Center Configuration	Basket Periphery Configuration		
14x14A	0.9380	0.9327	0.9080	Cell Center	0.9380
14x14B	0.9312	0.9288	0.9029	Cell Center	0.9312
14x14C	0.9356	0.9365	0.9189	Basket Center	0.9365
14x14D	0.8875	0.8857	0.8621	Cell Center	0.8875
14x14E	0.7651	0.7536	0.7001	Cell Center	0.7651
15x15A	0.9336	0.9304	0.9188	Cell Center	0.9336
15x15B	0.9465	0.9487	0.9367	Basket Center	0.9487
15x15C	0.9462	0.9452	0.9348	Cell Center	0.9462
15x15D	0.9440	0.9445	0.9343	Basket Center	0.9445
15x15E	0.9455	0.9471	0.9372	Basket Center	0.9471
15x15F	0.9468	0.9495	0.9406	Basket Center	0.9495
15x15G	0.9054	0.9062	0.8970	Basket Center	0.9062
15x15H	0.9423	0.9455	0.9365	Basket Center	0.9455
16x16A	0.9341	0.9358	0.9183	Basket Center	0.9358
17x17A	0.9447	0.9443	0.9355	Cell Center	0.9447
17x17B	0.9421	0.9438	0.9303	Basket Center	0.9438
17x17C	0.9433	0.9431	0.9347	Cell Center	0.9433

Table 6.3.7

EFFECT OF ECCENTRIC FUEL POSITIONING IN THE TROJAN MPC-24E/EF

Fuel Assembly Class	Maximum k_{eff}			Bounding Configuration	Bounding Maximum k_{eff}
	Cell Center Configuration	Basket Center Configuration	Basket Periphery Configuration		
17x17B (Intact Fuel)	0.9161	0.9187	0.9059	Basket Center	0.9187
17x17B (Intact Fuel and Damaged Fuel/Fuel Debris)	0.9377	0.9353	0.9338	Cell Center	0.9377

Table 6.3.8

EFFECT OF ECCENTRIC FUEL POSITIONING IN THE MPC-68

Fuel Assembly Class	Maximum k_{eff}			Bounding Configuration	Bounding Maximum k_{eff}
	Cell Center Configuration	Basket Center Configuration	Basket Periphery Configuration		
8x8F	0.9411	0.9459	0.9193	Basket Center	0.9459
9x9E/F	0.9401	0.9486	0.9166	Basket Center	0.9486
9x9G	0.9309	0.9383	0.9124	Basket Center	0.9383

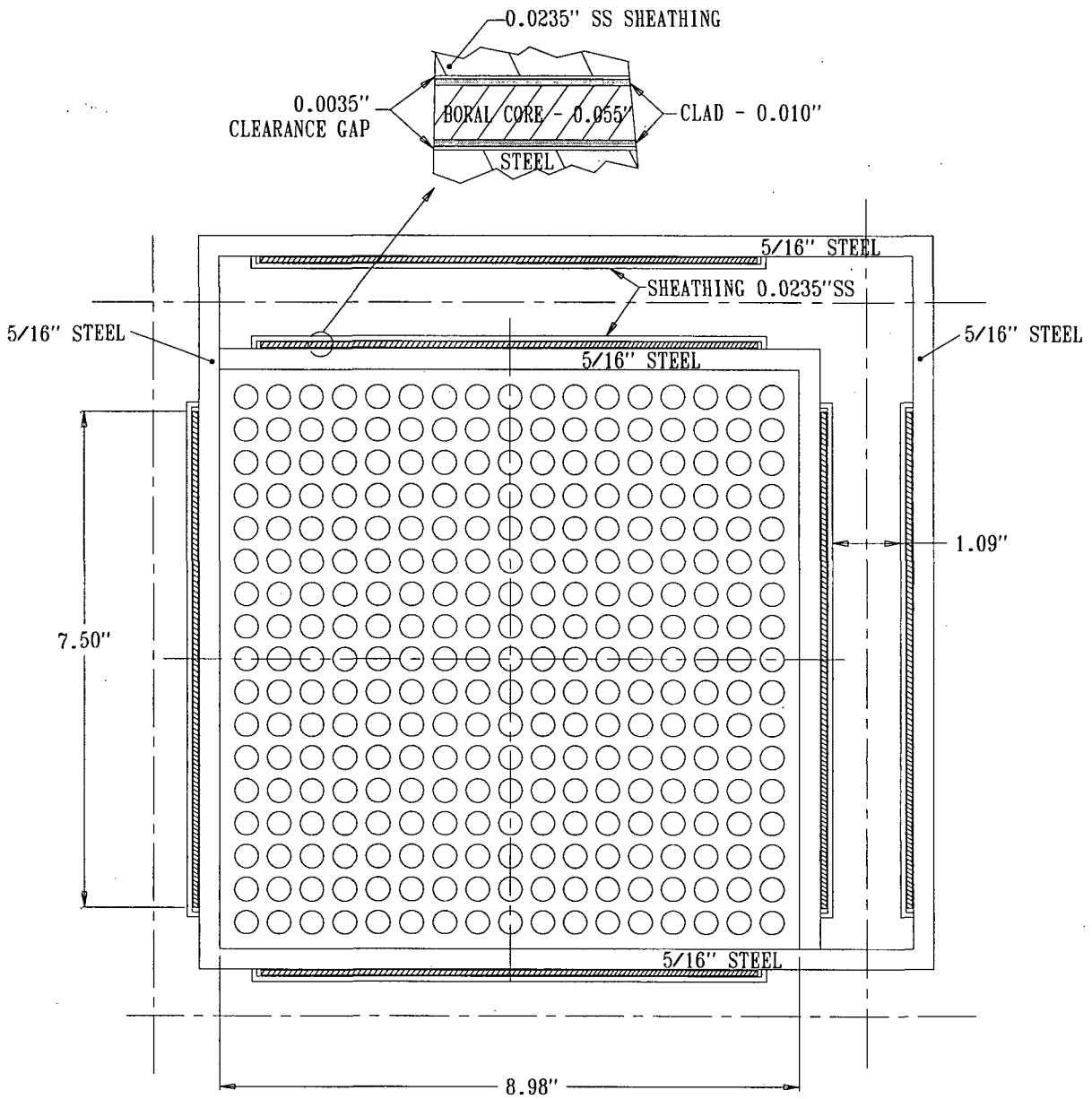

FIGURE 6.3.1; TYPICAL CELL IN THE CALCULATION MODEL (PLANAR CROSS-SECTION) WITH REPRESENTATIVE FUEL IN THE MPC-24 BASKET
(SEE CHAPTER 1 FOR TRUE BASKET DIMENSIONS)

NOTE: THESE DIMENSIONS WERE CONSERVATIVELY USED FOR CRITICALITY ANALYSES.

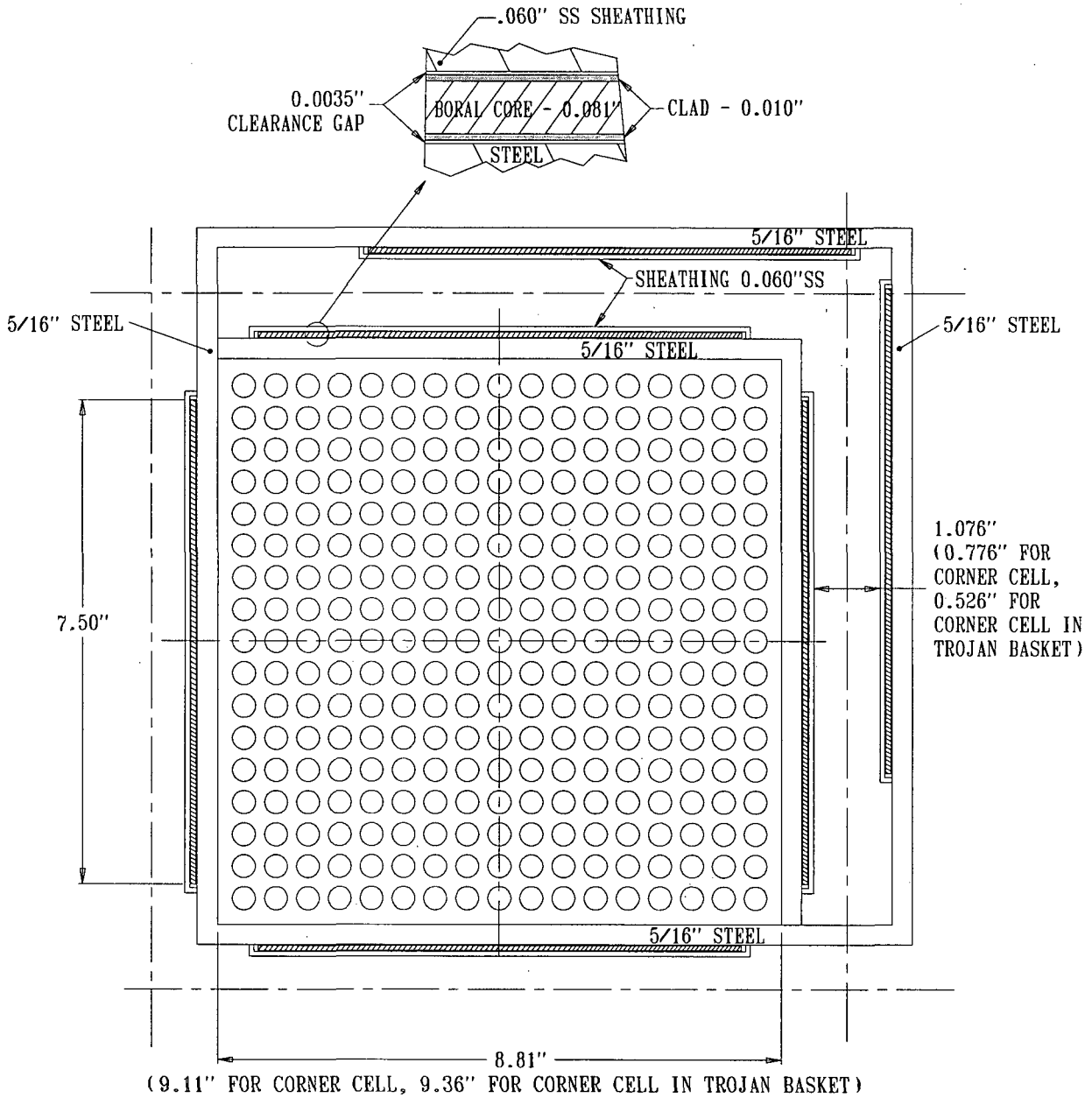

FIGURE 6.3.1A; TYPICAL CELL IN THE CALCULATION MODEL (PLANAR CROSS-SECTION) WITH REPRESENTATIVE FUEL IN THE MPC-24E & MPC-24E/EF TROJAN BASKET
(SEE CHAPTER 1 FOR TRUE BASKET DIMENSIONS)

NOTE: THESE DIMENSIONS WERE CONSERVATIVELY USED FOR CRITICALITY ANALYSES.

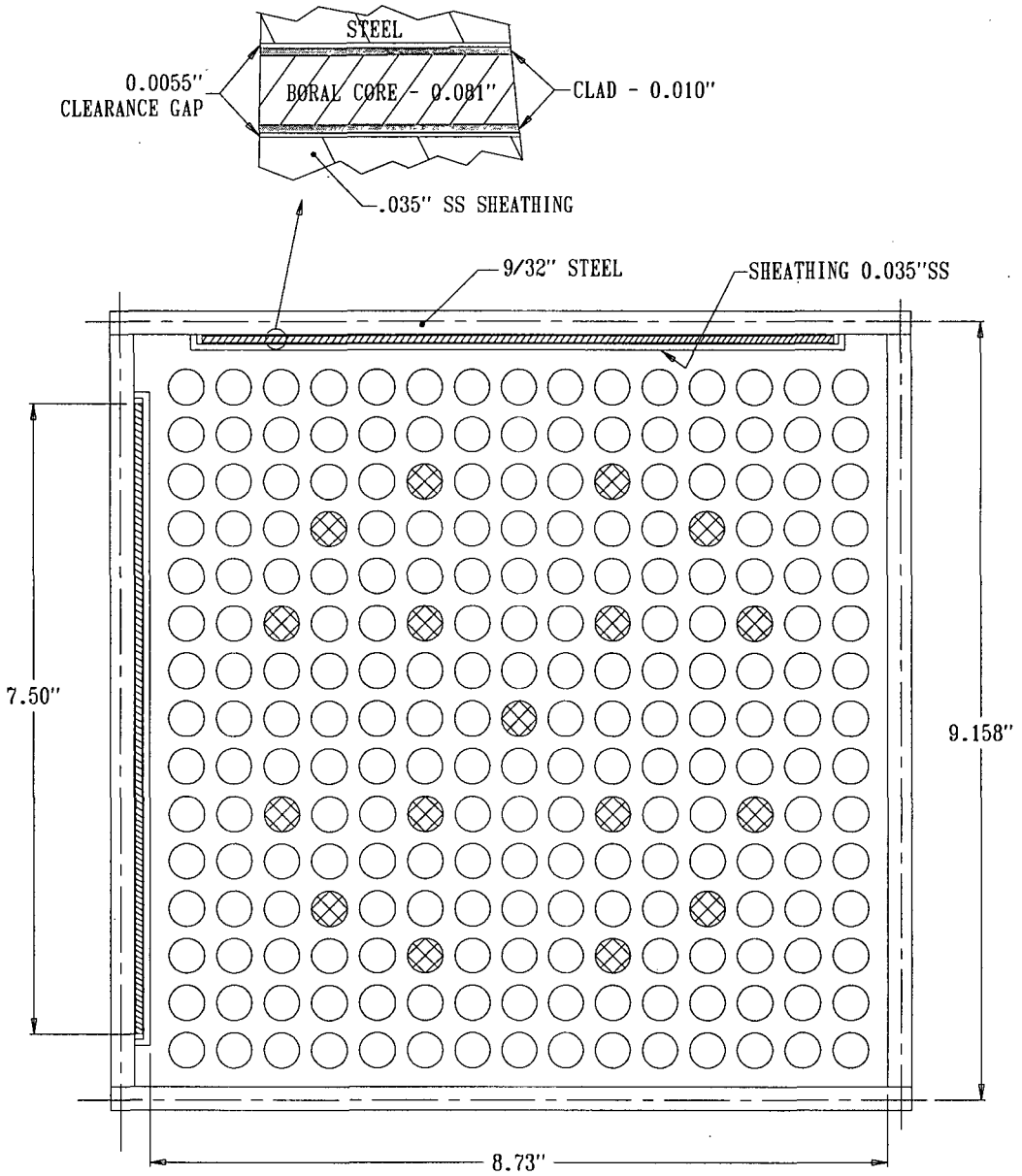

FIGURE 6.3.2; TYPICAL CELL IN THE CALCULATION MODEL (PLANAR CROSS-SECTION) WITH REPRESENTATIVE FUEL IN THE MPC-32 BASKET (SEE CHAPTER 1 FOR TRUE BASKET DIMENSIONS)

NOTE: THESE DIMENSIONS WERE CONSERVATIVELY USED FOR CRITICALITY ANALYSES.

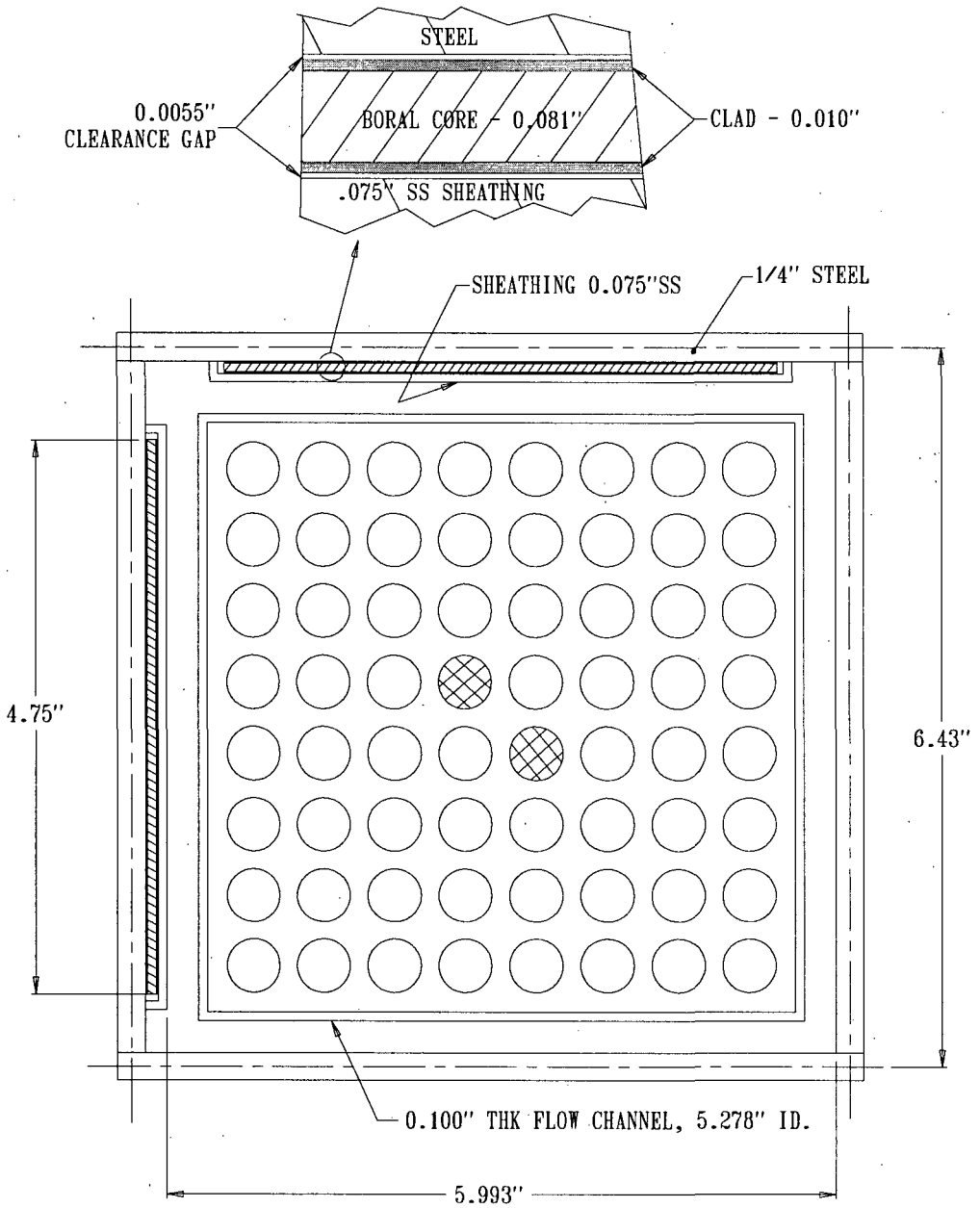

FIGURE 6.3.3; TYPICAL CELL IN THE CALCULATION MODEL (PLANAR CROSS-SECTION) WITH REPRESENTATIVE FUEL IN THE MPC-68 BASKET (SEE CHAPTER 1 FOR TRUE BASKET DIMENSIONS)

NOTE: THESE DIMENSIONS WERE CONSERVATIVELY USED FOR CRITICALITY ANALYSES.

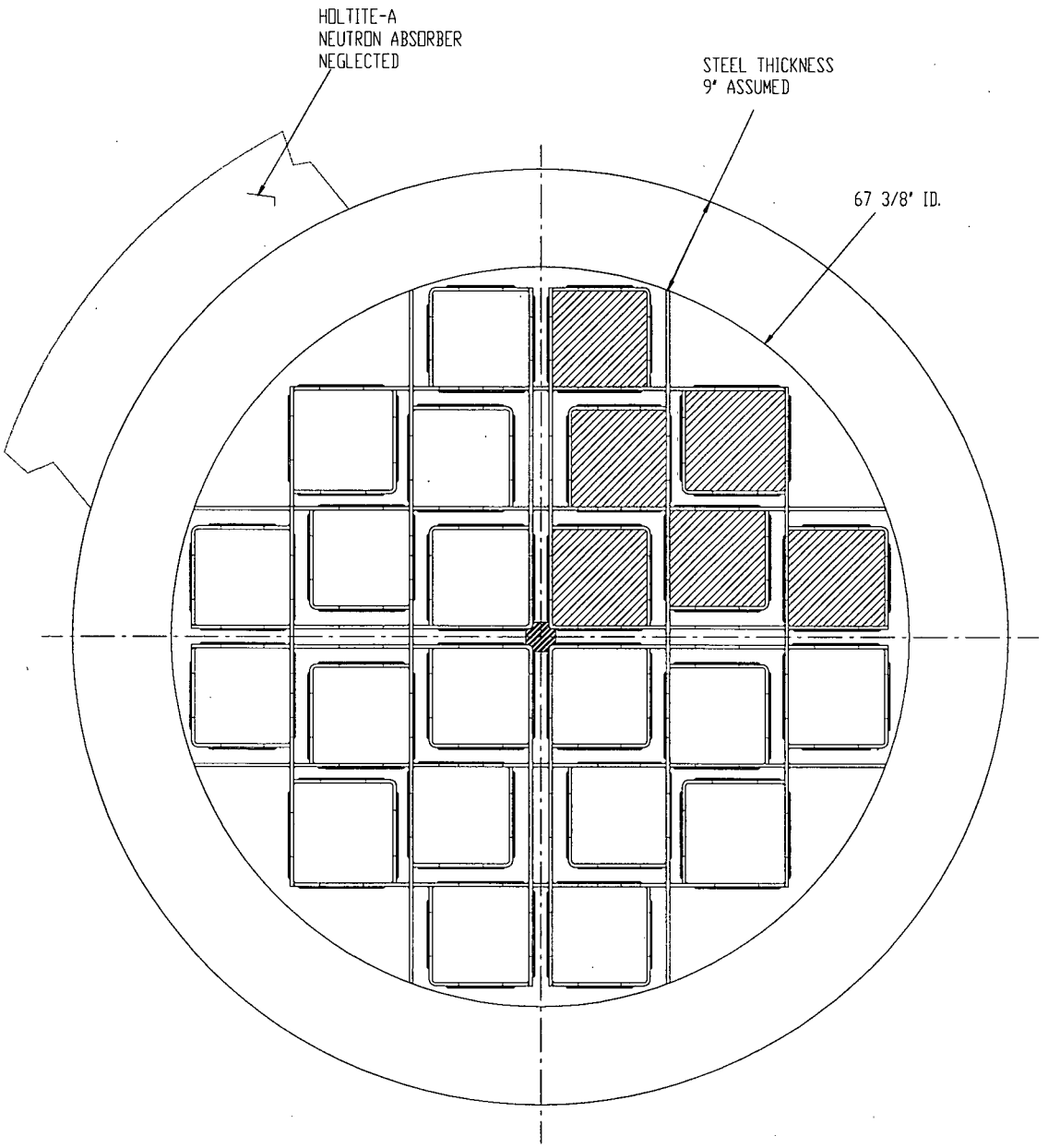

FIGURE 6.3.4; CALCULATION MODEL (PLANAR CROSS-SECTION) WITH FUEL ILLUSTRATED IN ONE QUADRANT OF THE MPC-24, MPC-24E AND MPC-24E/EF TROJAN.

(SEE CHAPTER 1 FOR TRUE BASKET DIMENSIONS)

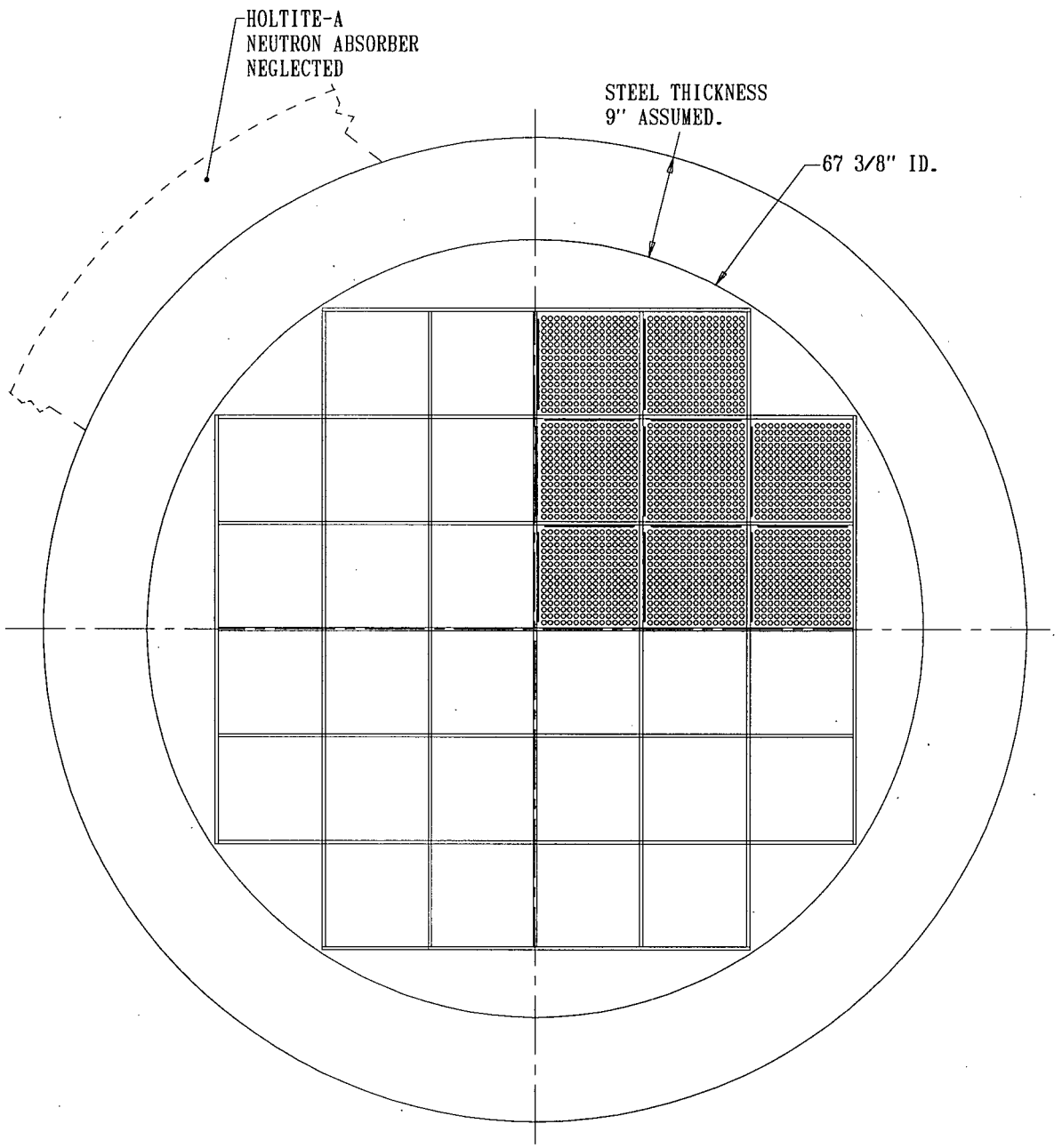

FIGURE 6.3.5; CALCULATION MODEL (PLANAR CROSS-SECTION) WITH FUEL ILLUSTRATED IN ONE QUADRANT OF THE MPC-32.
(SEE CHAPTER 1 FOR TRUE BASKET DIMENSIONS)

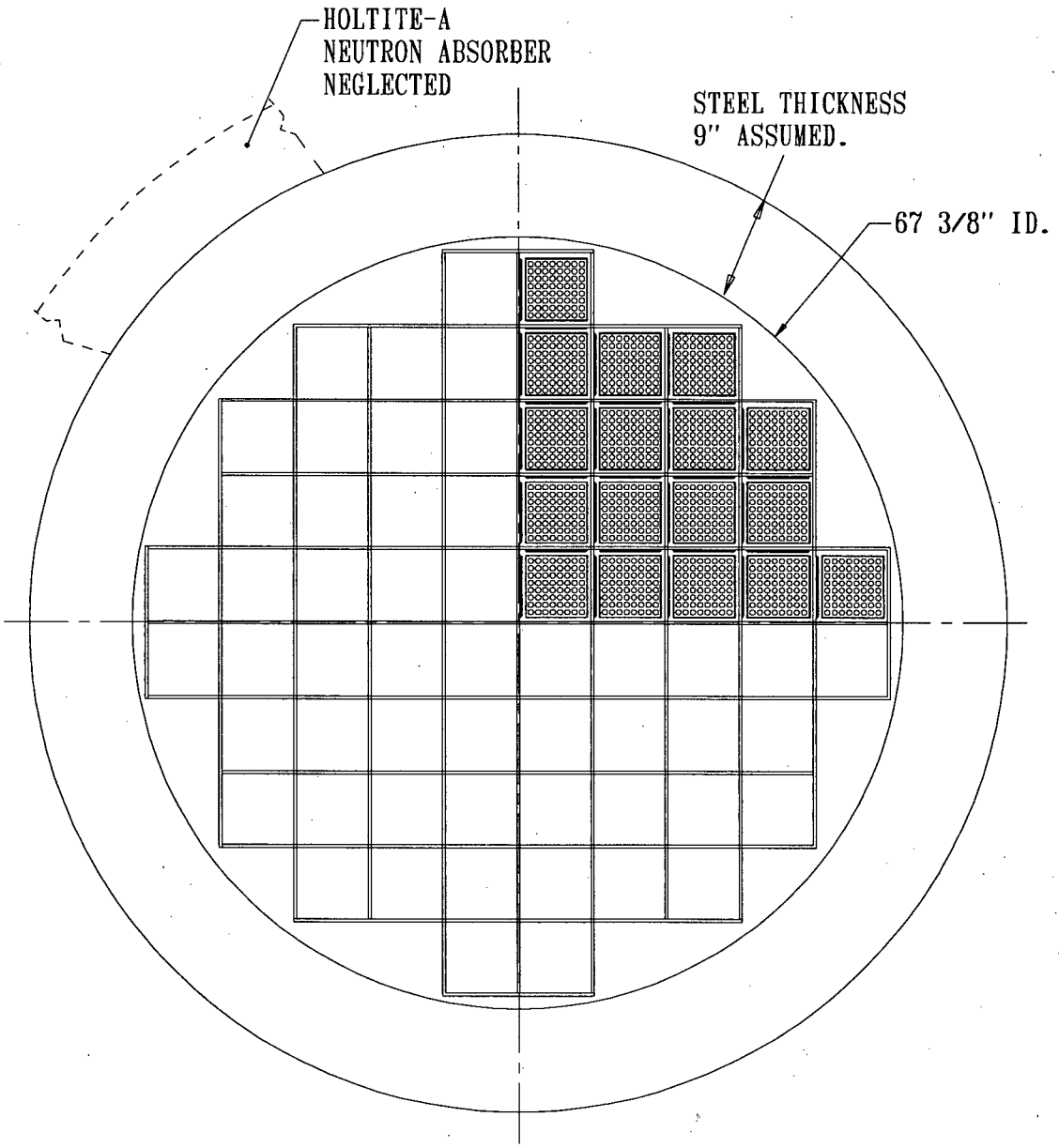

FIGURE 6.3.6; CALCULATION MODEL (PLANAR CROSS-SECTION) WITH FUEL ILLUSTRATED IN ONE QUADRANT OF THE MPC-68
(SEE CHAPTER 1 FOR TRUE BASKET DIMENSIONS)

	ACTIVE FUEL LENGTH	LOWER WATER THICKNESS	UPPER WATER THICKNESS
MPC-68	SEE TABLE 6.2.1	7.30 IN.	8.46 IN.
MPC-24-24E/ EF & -32	SEE TABLE 6.2.2	4.0 IN.	6.0 IN.

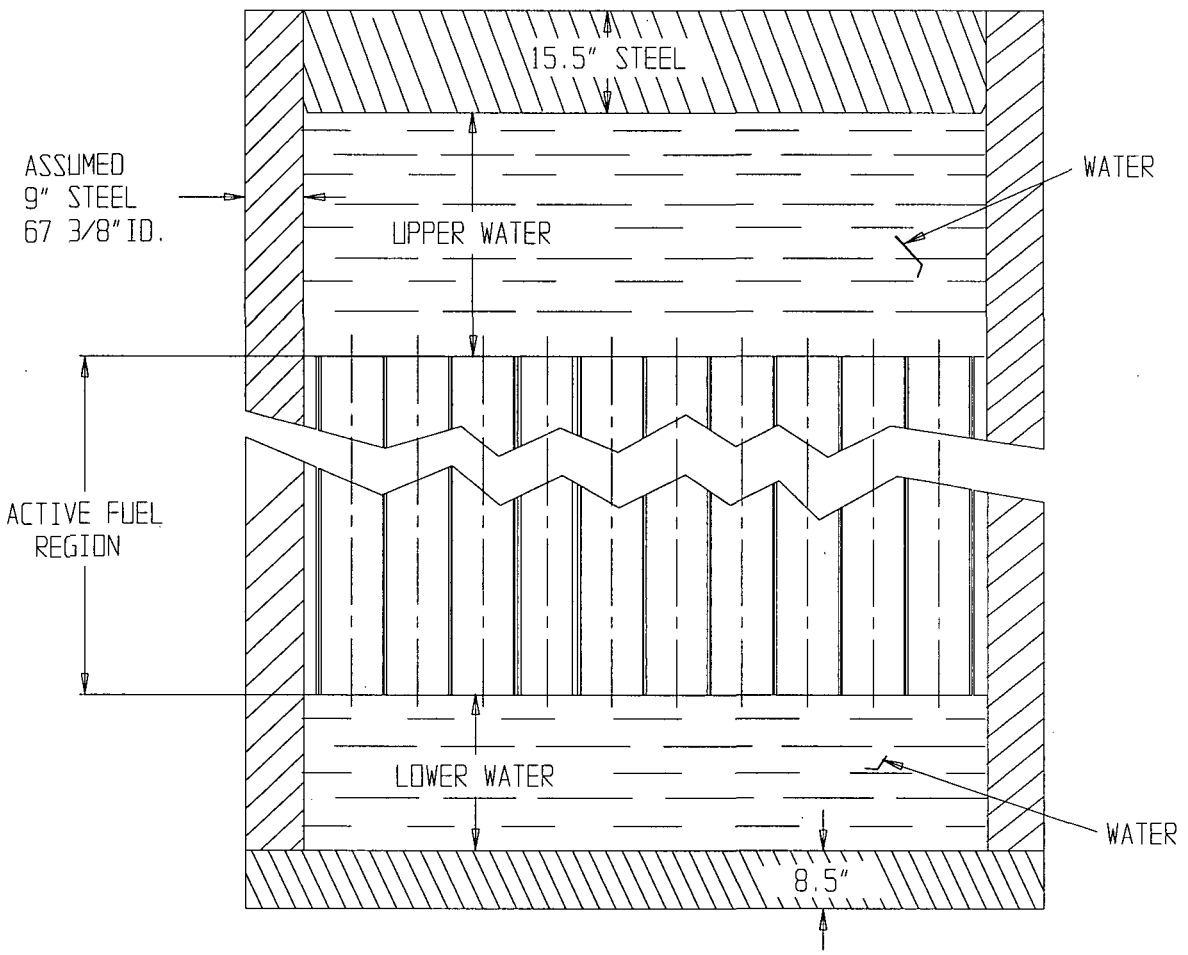

FIGURE 6.3.7; SKETCH OF THE CALCULATIONAL MODEL IN THE AXIAL DIRECTION

6.4 CRITICALITY CALCULATIONS

6.4.1 Calculational or Experimental Method

The principal method for the criticality analysis is the general three-dimensional continuous energy Monte Carlo N-Particle code MCNP4a [6.1.4] developed at the Los Alamos National Laboratory. MCNP4a was selected because it has been extensively used and verified and has all of the necessary features for this analysis. MCNP4a calculations used continuous energy cross-section data based on ENDF/B-V[†], as distributed with the code [6.1.4]. Independent verification calculations were performed with NITAWL-KENO5a [6.1.5], which is a three-dimensional multigroup Monte Carlo code developed at the Oak Ridge National Laboratory. The KENO5a calculations used the 238-group cross-section library, which is based on ENDF/B-V data and is distributed as part of the SCALE-4.3 package [6.4.1], in association with the NITAWL-II program [6.1.6], which adjusts the uranium-238 cross sections to compensate for resonance self-shielding effects. The Dancoff factors required by NITAWL-II were calculated with the CELLDAN code [6.1.13], which includes the SUPERDAN code [6.1.7] as a subroutine.

The convergence of a Monte Carlo criticality problem is sensitive to the following parameters: (1) number of histories per cycle, (2) the number of cycles skipped before averaging, (3) the total number of cycles and (4) the initial source distribution. The MCNP4a criticality output contains a great deal of useful information that may be used to determine the acceptability of the problem convergence. This information was used in parametric studies to develop appropriate values for the aforementioned criticality parameters to be used in the criticality calculations for this submittal. Based on these studies, calculations assuming fresh fuel used a minimum of 5,000 simulated histories per cycle, a minimum of 20 cycles were skipped before averaging, a minimum of 100 cycles were accumulated, and the initial source was specified as uniform over the fueled regions (assemblies). For parameters used in the burnup credit calculations see Appendix 6.E. Further, the output was examined to ensure that each calculation achieved acceptable convergence. These parameters represent an acceptable compromise between calculational precision and computational time. Appendix 6.D provides sample input files for the MPC-24 and MPC-68 basket in the HI-STAR 100 System.

CASMO-4 [6.1.10-6.1.12] was used for determining the small incremental reactivity effects of manufacturing tolerances. Although CASMO has been extensively benchmarked, these calculations are used only to establish direction of reactivity uncertainties due to manufacturing tolerances (and their magnitude). This allows the MCNP4a calculational model to use the worst combination of manufacturing tolerances. Table 6.3.1 shows results of the CASMO calculations. Additionally, CASMO-4 was used to determine the isotopic composition of spent fuel for burnup credit in the MPC-32 (see Appendix 6.E).

[†] For burnup credit calculations in the MPC-32, ENDF/B-VI cross sections are used for nuclides where ENDF/B-V cross sections are not available.

6.4.2 Fuel Loading or Other Contents Loading Optimization

The basket designs are intended to safely accommodate the candidate fuel assemblies with enrichments indicated in Tables 6.1.1 through 6.1.3 and 6.1.5 through 6.1.7. The calculations were based on the assumption that the HI-STAR 100 System was fully flooded with water. In all cases, the calculations include bias and calculational uncertainties, as well as the reactivity effects of manufacturing tolerances, determined by assuming the worst case geometry.

6.4.2.1 Internal and External Moderation

The regulations in 10CFR71.55 include the requirement that the system remains subcritical when assuming moderation to the most reactive credible extent. The regulations in 10CFR71.59 require subcriticality for package arrays under different moderation conditions. The calculations in this section demonstrate that the HI-STAR 100 System remains subcritical for all credible conditions of moderation, and that the system fulfills all requirements of 10CFR71.55 and 10CFR71.59. The following subsections 6.4.2.1.1 through 6.4.2.4 present various studies to confirm or identify the most reactive configuration or moderation condition. Specifically, the following conditions are analyzed:

- Reduced internal and external water density for single packages (6.4.2.1.1) and package arrays (6.4.2.1.2);
- Variation in package to package distance in package arrays (6.4.2.1.2);
- Partial internal flooding of package (6.4.2.2);
- Flooding of pellet to cladding gap of the fuel rods (6.4.2.3); and
- Preferential flooding, i.e. uneven flooding inside the package (6.4.2.4).

The calculations that specifically demonstrate compliance with the individual requirements of 10CFR71.55 and 10CFR71.59 are presented in Section 6.4.3. These calculations are performed for all MPCs.

The studies in subsections 6.4.2.1.1 through 6.4.2.4 have been performed for both principal basket designs (flux-trap and non-flux-trap) and for both fuel designs (BWR and PWR). Specifically, the studies are performed with the MPC-24 (flux-trap design / PWR fuel) and the MPC-68 (non-flux-trap design / BWR fuel). The results of the studies show a consistent behavior of the different basket designs and fuel types for different moderation conditions. Consequently, the conclusions drawn from these studies are directly applicable to the remaining baskets, namely the MPC-24E/EF (flux-trap design, PWR), MPC-32 (non-flux-trap design, PWR) and MPC-68F (non-flux-trap design, BWR), and no further studies are required for these baskets.

The studies in subsection 6.4.2.1.1 through 6.4.2.4 have been performed with the fuel assemblies centered in each storage location in the basket, which is not necessarily the most reactive position. However, this assumption is acceptable since the objective of these studies is to determine the most reactive moderation condition, not the highest reactivity. The calculations in Section 6.4.3 that demonstrate compliance with 10CFR71.55 and 19CFR71.59 are performed with the most reactive assembly position as discussed in Section 6.3.3.

Regarding the effect of low moderator density it is noted that with a neutron absorber present (i.e., the fixed neutron absorber sheets on the steel walls of the storage compartments), the phenomenon of a peak in reactivity at a hypothetical low moderator density (sometimes called "optimum" moderation) does not occur to any significant extent. In a definitive study, Cano, et al. [6.4.2] has demonstrated that the phenomenon of a peak in reactivity at low moderator densities does not occur when strong neutron absorbing material is present or in the absence of large water spaces between fuel assemblies in storage. Nevertheless, calculations for a single reflected cask and for infinite arrays of casks were made to confirm that the phenomenon does not occur with low density water inside or outside the HI-STAR 100 Systems.

6.4.2.1.1 Single Package Evaluation

Calculations for a single package are performed for the MPC-24 and MPC-68. The Calculational model consists of the HI-STAR System surrounded by a rectangular box filled with water. The neutron absorber on the outside of the HI-STAR is neglected, since it might be damaged under accident conditions, and since it is conservative to replace the neutron absorber (Holtite-A) with a neutron reflector (water). The minimum water thickness on each side of the cask is 30 cm, which effectively represents full water reflection. The outer surfaces of the surrounding box are conservatively set to be fully reflective, which effectively models a three dimensional array of cask systems with a minimum surface to surface distance of 60 cm. The calculations with internal and external moderators of various densities are shown in Table 6.4.1. For comparison purposes, a calculation for a single unreflected cask (Case 1) is also included in Table 6.4.1. At 100% external moderator density, Case 2 corresponds to a single fully-flooded cask, fully reflected by water. Figure 6.4.9 plots calculated k_{eff} values ($\pm 2\sigma$) as a function of internal moderator density for both MPC designs with 100% external moderator density (i.e., full water reflection).

Results listed in Table 6.4.1 and plotted in Figure 6.4.9 support the following conclusions:

- The calculated k_{eff} for a fully-flooded cask is independent of the external moderator (the small variations in the listed values are due to statistical uncertainties which are inherent to the calculational method (Monte Carlo)), and

- Reducing the internal moderation results in a monotonic reduction in reactivity, with no evidence of any optimum moderation. Thus, the fully flooded condition corresponds to the highest reactivity, and the phenomenon of optimum low-density moderation does not occur and is not applicable to the HI-STAR 100 System.

6.4.2.1.2 Evaluation of Package Arrays

In terms of reactivity, the normal conditions of transport (i.e., no internal or external moderation) are bounded by the hypothetical accident conditions of transport. Therefore, the calculations in this section evaluate arrays of HI-STAR 100 Systems under hypothetical accident conditions (i.e, internal and external moderation by water to the most reactive credible extent and no neutron shield present).

In accordance with 10CFR71.59 requirements, calculations were performed to simulate an infinite three-dimensional square array of internally fully-flooded (highest reactivity) casks with varying cask spacing and external moderation density. The MPC-24 was used for this analysis. The maximum k_{eff} results of these calculations are listed in Table 6.4.2 and confirm that the individual casks in a square-pitched array are independent of external moderation and cask spacing. The maximum value listed in Table 6.4.2 is statistically equivalent (within three standard deviations) to the reference value (Case 1 shown in Table 6.4.1) for a single unreflected fully flooded cask.

To further investigate the reactivity effects of array configurations, calculations were also performed to simulate an infinite three-dimensional hexagonal (triangular-pitched) array of internally fully-flooded (highest reactivity) MPC-24 casks with varying cask spacing and external moderation density. The maximum k_{eff} results of these calculations are listed in Table 6.4.3 and confirm that the individual casks in a hexagonal (triangular pitched) array are effectively independent of external moderation and cask spacing. The maximum value listed in Table 6.4.3 is statistically equivalent (within two standard deviations) to the reference value (Case 1 shown in Table 6.4.1) for a single unreflected fully flooded cask.

To assure that internal moderation does not result in increased reactivity, hexagonal array calculations were also performed for 10% internal moderator with 10% and 100% external moderation for varying cask spacing. Maximum k_{eff} results are summarized in Table 6.4.4 and confirm the very low values of k_{eff} for low values of internal moderation.

The results presented thus far indicate that neutronic interaction between casks is not enhanced by the neighboring casks or the water between the neighboring casks, and thus, the most reactive arrangement of casks corresponds to a tightly packed array with the cask surfaces touching. Therefore, calculations were performed for an infinite hexagonal (triangular pitched) array of touching casks (neglecting the Holtite-A neutron shield). These calculations were performed for

the MPC-24 and the MPC-68 designs, in the internally flooded (highest reactivity) and internally dry conditions, with and without external flooding. The results of these calculations are listed in Table 6.4.5. For both the MPC-24 and MPC-68, the maximum k_{eff} values are shown to be statistically equivalent (within one standard deviation) to that of a single internally flooded unreflected cask and are below the regulatory limit of 0.95.

The calculations demonstrate that the thick steel wall of the overpack is more than sufficient to preclude neutron coupling between casks, consistent with the findings of Cano, et al. Neglecting the Holtite-A neutron shielding in the calculational model provides further assurance of conservatism in the calculations.

6.4.2.2 Partial Flooding

To demonstrate that the HI-STAR 100 System would remain subcritical if water were to leak into the containment system, as required by 10CFR71.55, calculations in this section address partial flooding in the HI-STAR 100 System and demonstrate that the fully flooded condition is the most reactive.

The reactivity changes during the flooding process were evaluated in both the vertical and horizontal positions for the MPC-24 and MPC-68 designs. For these calculations, the cask is partially filled (at various levels) with full density (1.0 g/cc) water and the remainder of the cask is filled with steam consisting of ordinary water at partial density (0.002 g/cc). Results of these calculations are shown in Table 6.4.6. In all cases, the reactivity increases monotonically as the water level rises, confirming that the most reactive condition is fully flooded. This conclusion is also true for the other baskets that were not analyzed under partial flooding conditions, since increasing the water level always improves the moderation condition of the fuel and therefore results in an increase in reactivity[†]. The fully flooded case therefore represents the bounding condition for all MPC basket types.

6.4.2.3 Clad Gap Flooding

The reactivity effect of flooding the fuel rod pellet-to-clad gap regions, in the fully flooded condition, has been investigated. Table 6.4.7 presents maximum k_{eff} values that demonstrate the positive reactivity effect associated with flooding the pellet-to-clad gap regions. These results confirm that it is conservative to assume that the pellet-to-clad gap regions are flooded. For all cases that involve flooding, the pellet-to-clad gap regions are assumed to be flooded.

[†] The rate of increase in reactivity along the fuel length, though, could be different between different MPC designs. An example would be the MPC-32 with burnup credit where the reactivity is strongly affected by the lower burned ends of the fuel.

6.4.2.4 Preferential Flooding

Two different potential conditions of preferential flooding are considered: preferential flooding of the MPC basket itself (i.e. different water levels in different basket cells), and preferential flooding involving Damaged Fuel Containers.

Preferential flooding of the MPC basket itself for any of the MPC fuel basket designs is not possible because flow holes are present on all four walls of each basket cell and on the two flux trap walls at both the top and bottom of the MPC basket. The flow holes are sized to ensure that they cannot be blocked by crud deposits. Because the fuel cladding temperatures remain below their design limits (as demonstrated in Chapter 3) and the inertial loading remains below 63g's (Section 2.9), the cladding remains intact. For damaged BWR fuel assemblies and BWR fuel debris, the assemblies or debris are pre-loaded into stainless steel Damaged Fuel Containers fitted with 250x250 fine mesh screens (20x20 for Trojan FFC) which prevent damaged fuel assemblies or fuel debris from blocking the basket flow holes. Therefore, the flow holes cannot be blocked and the MPC fuel baskets cannot be preferentially flooded.

However, when DFCs are present in the MPC, a condition could exist during the draining of the MPC, where the DFCs are still partly filled with water while the remainder of the MPC is dry. This condition would be the result of the water tension across the mesh screens. The maximum water level inside the DFCs for this condition is calculated from the dimensions of the mesh screen and the surface tension of water. The wetted perimeter of the screen openings is up to 50 ft per square inch of screen. With a surface tension of water of 0.005 lbf/ft, this results in a maximum pressure across the screen of 0.25 psi, corresponding to a maximum water height in the DFC of 7 inches. For added conservatism, a value of 12 inches is used. Assuming this condition, calculations are performed for the two possible DFC configurations:

- MPC-68 or MPC-68F with 68 DFCs (Assembly Classes 6x6A/B/C, 7x7A and 8x8A, see Subsection 6.4.4)
- MPC-24E or MPC-24EF with 4 DFCs and 20 intact assemblies (Bounding all PWR assembly classes, see Subsection 6.4.9)

For each configuration, the case resulting in the highest maximum k_{eff} for the fully flooded condition (see Subsections 6.4.4 and 6.4.9) is re-analyzed assuming the preferential flooding condition. For these analyses, the lower 12 inches of the active fuel in the DFCs and the water region below the active fuel (see Figure 6.3.7) are filled with full density water (1.0 g/cc). The remainder of the cask is filled with steam consisting of ordinary water at partial density (0.002 g/cc). All calculations are performed for a single unreflected cask. Table 6.4.10 lists the maximum k_{eff} for the configurations in comparison with the maximum k_{eff} for the fully flooded condition. For all configurations, the preferential flooding condition results in a lower maximum k_{eff} than the fully flooded condition. Thus, the preferential flooding condition is bounded by the

fully flooded condition.

In summary, it is concluded that the MPC fuel baskets cannot be preferentially flooded, and that the potential preferential flooding conditions involving DFCs are bounded by the result for the fully flooded condition listed in Subsections 6.4.4 and 6.4.9.

6.4.2.5 Hypothetical Accidents Conditions of Transport

The analyses presented in Section 2.7 of Chapter 2 and Section 3.5 of Chapter 3 demonstrate that the damage resulting from the hypothetical accident conditions of transport are limited to a loss of the neutron shield material as a result of the hypothetical fire accident. Because the criticality analyses do not take credit for the neutron shield material (Holtite-A), this condition has no effect on the criticality analyses.

As reported in Table 2.7.1, the minimum factor of safety for all MPCs as a result of the hypothetical accident conditions of transport is larger than 1.0 against the Level D allowables for Subsection NG, Section III of the ASME Code. Therefore, because the maximum box wall stresses are well within the ASME Level D allowables, the flux-trap gap change in the MPC-24 and MPC-24E/EF will be insignificant compared to the characteristic dimension of the flux trap.

Regarding the fuel assembly integrity, SAR Section 2.9 contains an evaluation of the fuel under accident conditions that concludes that the fuel rod cladding remains intact under the design basis deceleration levels set for the HI-STAR 100.

In summary, the hypothetical transport accidents have no adverse effect on the geometric form of the package contents important to criticality safety, and thus, are limited to the effects on internal and external moderation evaluated in Subsection 6.4.2.1.

6.4.3 Criticality Results

In calculating the maximum reactivity, the analysis used the following equation:

$$k_{eff}^{max} = k_c + K_c\sigma_c + Bias + \sigma_B$$

where:

- ⇒ k_c is the calculated k_{eff} under the worst combination of tolerances;
- ⇒ K_c is the K multiplier for a one-sided statistical tolerance limit with 95% probability at the 95% confidence level [6.1.8]. Each final k_{eff} value calculated by MCNP4a (or KENO5a) is the result of averaging 100 (or more) cycle k_{eff} values, and thus, is based on

a sample size of 100. The K multiplier corresponding to a sample size of 100 is 1.93. However, for this analysis a value of 2.00 was assumed for the K multiplier, which is larger (more conservative) than the value corresponding to a sample size of 100;

⇒ σ_c is the standard deviation of the calculated k_{eff}, as determined by the computer code (MCNP4a or KENO5a);

⇒ ***Bias*** is the systematic error in the calculations (code dependent) determined by comparison with critical experiments; and

⇒ σ_B is the standard error of the bias (which includes the K multiplier for 95% probability at the 95% confidence level).

Appendix 6.A presents the critical experiment benchmarking for fresh UO2 and MOX fuel and the derivation of the corresponding bias and standard error of the bias (95% probability at the 95% confidence level).

See Appendix 6.E, Section 6.E.3, for the critical experiment benchmarking for spent fuel

The studies in sections 6.4.2.1 through 6.4.2.4 demonstrate that the moderation by water to the most reactive credible extent corresponds to the internally fully flooded condition of the MPC, with the pellet-to-clad gap in the fuel rods also flooded with water. The external moderation and/or the presence of other surrounding packages, however, has a statistically negligible effect. To demonstrate compliance with 10CFR71.55 and 10CFR71.59, the following set of four calculations is performed for each of the MPC designs:

- Single containment with full internal and external water moderation. The full external water moderation is modeled through an infinite array of containments with a 60cm surface to surface distance. The containment system corresponds to the 2.5 inch inner shell of the overpack. This case addresses the requirement of 10CFR71.55 (b).
- Single cask with full internal and external water moderation. As for the single containment, the full external water moderation is modeled through an infinite array. The external neutron moderator is conservatively neglected in the model. This case also addresses the requirement of 10CFR71.55 (b).
- Hexagonal array of touching casks with full internal and external water reflection. This addresses the requirement of 10CFR71.59 (a)(2) and the determination of the transport index based on criticality control according to 10CFR71.59 (b).
- Hexagonal array of touching casks, internally and externally dry. This addresses the requirement of 10CFR71.59 (a) (1) and the determination of the transport index based on criticality control according to 10CFR71.59 (b). This also addresses the requirement of 10CFR71.55 (d)(1).

To satisfy the requirements of 10CFR71.55 (b)(1), the calculations are performed

- with the assembly type that results in the highest reactivity in the MPC. This is the assembly class 15x15F for the MPC-24, MPC-24E/EF and MPC-32, the assembly class 17x17B with intact and damaged assemblies in the Trojan MPC-24E/EF, the assembly class 9x9E/F in the MPC-68, and the assembly class 6x6C for the MPC-68F; and
- with the bounding basket dimensions as determined in Section 6.3.1 for each basket; and
- with eccentric fuel positioning as necessary, as discussed in Section 6.3.3.

The maximum k_{eff} values for all these cases, calculated with 95% probability at the 95% confidence level, are listed in Table 6.4.12. Results of the criticality safety calculations for other assembly classes under the condition of full internal flooding with water are summarized in Section 6.1. Corresponding detailed results including the maximum k_{eff}, standard deviation and energy of the average lethargy causing fission (EALF) are listed for all MPCs except the MPC-32 in Tables 6.4.13 through 6.4.17. Results for the MPC-32 are presented in Appendix 6.E. Overall, these results confirm that for each of the candidate fuel assemblies and basket configurations the effective multiplication factor (k_{eff}), including all biases and uncertainties at a 95-percent confidence level, do not exceed 0.95 under all credible normal and hypothetical accident conditions of transport. Therefore, compliance with 10CFR71.55 for single packages and 10CFR71.59 for package arrays in both normal and hypothetical accident conditions of transport is demonstrated for all of the fuel assembly classes and basket configurations listed in Tables 6.1.1 through 6.1.3 and 6.1.5 through 6.1.7. It further demonstrates that the transportation index for criticality control is zero because an infinite number of HI-STAR 100 casks will remain subcritical (k_{eff}<0.95) under both normal and hypothetical accident conditions of transport.

Additional calculations (CASMO-4) at elevated temperatures confirm that the temperature coefficients of reactivity are negative as shown in Table 6.3.1. This confirms that the calculations for the storage baskets are conservative.

Tables listing the maximum k_{eff}, calculated k_{eff}, standard deviation, and energy of the average lethargy causing fission (EALF) for each of the candidate fuel assemblies in each assembly class for the MPC-24, MPC-68 and MPC-68F basket configurations, and with assemblies centered in the fuel storage locations, are provided in Section 6.2.

6.4.4 Damaged Fuel Container for BWR Fuel

Both damaged BWR fuel assemblies and BWR fuel debris are required to be loaded into Damaged Fuel Containers (DFCs). Two different DFC types with slightly different cross sections are analyzed. DFCs containing fuel debris are only analyzed in the MPC-68F. DFCs containing damaged fuel assemblies may be stored in either the MPC-68 or MPC-68F. Evaluation of the capability of storing damaged fuel and fuel debris (loaded in DFCs) is limited to very low reactivity fuel in the MPC-68F. Because the MPC-68 has a higher specified ^{10}B

loading, the evaluation of the MPC-68F conservatively bounds the storage of damaged BWR fuel assemblies in a standard MPC-68 Although the maximum planar-average enrichment of the damaged fuel is limited to 2.7% ^{235}U as specified in Chapter 1, analyses have been made for three possible scenarios, conservatively assuming fuel[††] of 3.0% enrichment. The scenarios considered included the following:

1. Lost or missing fuel rods, calculated for various numbers of missing rods in order to determine the maximum reactivity. The configurations assumed for analysis are illustrated in Figures 6.4.1 through 6.4.7.
2. Broken fuel assembly with the upper segments falling into the lower segment creating a close-packed array (described as a 8x8 array). For conservatism, the array analytically retained the same length as the original fuel assemblies in this analysis. This configuration is illustrated in Figure 6.4.8.
3. Fuel pellets lost from the assembly and forming powdered fuel dispersed through a volume equivalent to the height of the original fuel. (Flow channel and clad material assumed to disappear).

Results of the analyses, shown in Table 6.4.8, confirm that, in all cases, the maximum reactivity is well below the regulatory limit. There is no significant difference in reactivity between the two DFC types. Collapsed fuel reactivity (simulating fuel debris) is low because of the reduced moderation. Dispersed powdered fuel results in low reactivity because of the increase in ^{238}U neutron capture (higher effective resonance integral for ^{238}U absorption).

The loss of fuel rods results in a small increase in reactivity (i.e., rods assumed to collapse, leaving a smaller number of rods still intact). The peak reactivity occurs for 8 missing rods, and a smaller (or larger) number of intact rods will have a lower reactivity, as indicated in Table 6.4.8.

The analyses performed and summarized in Table 6.4.8 provides the relative magnitude of the effects on the reactivity. This information in combination with the maximum k_{eff} values listed in Table 6.1.3 and the conservatism in the analyses, demonstrate that the maximum k_{eff} of the damaged fuel in the most adverse post-accident condition will remain well below the regulatory requirement of $k_{eff} < 0.95$.

Appendix 6.D provides sample input files for the damaged fuel analysis.

[††] 6x6A01 and 7x7A01 fuel assemblies were used as representative assemblies.

6.4.5 Fuel Assemblies with Missing Rods

For fuel assemblies that are qualified for damaged fuel storage, missing and/or damaged fuel rods are acceptable. However, for fuel assemblies to meet the limitations of intact fuel assembly storage, missing fuel rods must be replaced with dummy rods that displace a volume of water that is equal to, or larger than, that displaced by the original rods.

6.4.6 Thoria Rod Canister

The Thoria Rod Canister is similar to a DFC with an internal separator assembly containing 18 intact fuel rods. The configuration is illustrated in Figure 6.4.10. The k_{eff} value for an MPC-68F filled with Thoria Rod Canisters is calculated to be 0.1813. This low reactivity is attributed to the relatively low content in ^{235}U (equivalent to UO_2 fuel with an enrichment of approximately 1.7 wt% ^{235}U), the large spacing between the rods (the pitch is approximately 1", the cladding OD is 0.412") and the absorption in the separator assembly. Together with the maximum k_{eff} values listed in Tables 6.1.2 and 6.1.3 this result demonstrates, that the k_{eff} for a Thoria Rod Canister loaded into the MPC68 or the MPC68F together with other approved fuel assemblies or DFCs will remain well below the regulatory requirement of $k_{eff} < 0.95$.

6.4.7 Sealed Rods Replacing BWR Water Rods

Some BWR fuel assemblies contain sealed rods filled with a non-fissile instead of water rods. Compared to the configuration with water rods, the configuration with sealed rods has a reduced amount of moderator, while the amount of fissile material is maintained. Thus, the reactivity of the configuration with sealed rods will be lower compared to the configuration with water rods. Any configuration containing sealed rods instead of water rods is therefore bounded by the analysis for the configuration with water rods and no further analysis is required to demonstrate the acceptability. Therefore, for all BWR fuel assemblies analyzed, it is permissible that water rods are replaced by sealed rods filled with a non-fissile material.

6.4.8 Neutron Sources in Fuel Assemblies

Fuel assemblies containing start-up neutron sources are permitted for storage in the HI-STAR 100 System. The reactivity of a fuel assembly is not affected by the presence of a neutron source (other than by the presence of the material of the source, which is discussed later). This is true because in a system with a keff less than 1.0, any given neutron population at any time, regardless of its origin or size, will decrease over time. Therefore, a neutron source of any strength will not increase reactivity, but only the neutron flux in a system, and no additional criticality analyses are required. Sources are inserted as rods into fuel assemblies, i.e. they replace either a fuel rod or water rod (moderator). Therefore, the insertion of the material of the source into a fuel assembly will not lead to an increase of reactivity either.

6.4.9 PWR Damaged Fuel and Fuel Debris

The MPC-24E, MPC-24EF, and Trojan MPC-24E and MPC-24EF are designed to contain damaged fuel and fuel debris, loaded into Damaged Fuel Containers (DFCs) or Failed Fuel Cans (FFCs). There is one generic DFC for the MPC-24E/EF, and two containers, a Holtec DFC and a Trojan FFC for the Trojan MPC-24E/EF. In this section, the term "DFC" is used to specify either of these components. In any case, the number of DFCs is limited to 4, and the permissible locations of the DFCs are shown in Figure 6.4.11.

Only the Trojan MPC-24E/EF is certified for damaged fuel and fuel debris. However, the generic MPC-24E/EF is also designed to accommodate damaged fuel and fuel debris, and the majority of criticality evaluations for damaged fuel and fuel debris are performed for the generic MPC-24E/EF, with only a smaller number of calculations performed for the Trojan MPCs. Therefore, criticality evaluations for both the generic MPC-24E/EF and the Trojan MPC-24E/EF are presented in this subsection, even though the Trojan MPC-24E/EF are the only MPCs authorized to transport damaged fuel and fuel debris.

Damaged fuel assemblies are assemblies with known or suspected cladding defects greater than pinholes or hairlines, or with missing rods, but excluding fuel assemblies with gross defects (for a full definition see Chapter 1). Therefore, apart from possible missing fuel rods, damaged fuel assemblies have the same geometric configuration as intact fuel assemblies and consequently the same reactivity. Missing fuel rods can result in a slight increase of reactivity. After a drop accident, however, it can not be assumed that the initial geometric integrity is still maintained. For a drop on either the top or bottom of the cask, the damaged fuel assemblies could collapse. This would result in a configuration with a reduced length, but increased amount of fuel per unit length. For a side drop, fuel rods could be compacted to one side of the DFC. In either case, a significant relocation of fuel within the DFC is possible, which creates a greater amount of fuel in some areas of the DFC, whereas the amount of fuel in other areas is reduced. Fuel debris can include a large variety of configurations ranging from whole fuel assemblies with severe damage down to individual fuel pellets.

In the cases of fuel debris or relocated damaged fuel, there is the potential that fuel could be present in axial sections of the DFCs that are outside the basket height covered with fixed neutron absorber. However, in these sections, the DFCs are not surrounded by any intact fuel, only by basket cell walls, non-fuel hardware and water. Studies have shown that this condition does not result in any significant effect on reactivity, compared to a condition where the damaged fuel and fuel debris is restricted to the axial section of the basket covered by fixed neutron absorber. All calculations for damaged fuel and fuel debris are therefore performed assuming that fuel is present only in the axial sections covered by the fixed neutron absorber,

and the results are directly applicable to any situation where damaged fuel and fuel debris is located outside these sections in the DFCs.

To address all the situations listed above and identify the configuration or configurations leading to the highest reactivity, it is impractical to analyze a large number of different geometrical configurations for each of the fuel classes. Instead, a bounding approach is taken which is based on the analysis of regular arrays of bare fuel rods without cladding. Details and results of the analyses are discussed in the following sections.

All calculations for generic damaged fuel and fuel debris are performed using a full cask model with the maximum permissible number of Damaged Fuel Containers. For the MPC-24E and MPC-24EF, the model consists of 20 intact assemblies, and 4 DFCs in the locations shown in Figure 6.4.11. The bounding assumptions regarding the intact assemblies and the modeling of the damaged fuel and fuel debris in the DFCs are discussed in the following sections.

6.4.9.1 Bounding Intact Assemblies

Intact PWR assemblies stored together with DFCs in the MPC-24E/EF are limited to a maximum enrichment of 4.0 wt% ^{235}U, regardless of the fuel class. Results presented in Table 6.1.5 for the MPC-24E/EF loaded with intact assemblies only are for different enrichments for each class, ranging between 4.2 and 5.0 wt% ^{235}U, making it difficult to directly identify the bounding assembly. However, the assembly class 15x15H is among the classes with the highest reactivity, but has the lowest initial enrichment. Therefore, the 15x15H assembly is used as the intact PWR assembly for all calculations with DFCs.

The Trojan MPC-24E/EF is only certified for the assembly class 17x17B, which bounds the fuel types used at the Trojan plant. Consequently, the assembly class 17x17B is used as the intact assembly in all calculations for the Trojan MPC-24E/EF.

6.4.9.2 Bare Fuel Rod Arrays

A conservative approach is used to model both damaged fuel and fuel debris in the DFCs, using arrays of bare fuel rods:

- Fuel in the DFCs is arranged in regular, rectangular arrays of bare fuel rods, i.e. all cladding and other structural material in the DFC is replaced by water.
- The active length of these rods is chosen to be the maximum active fuel length of all fuel assemblies listed in Section 6.2, which is 150 inch for PWR fuel.

- To ensure the configuration with optimum moderation and highest reactivity is analyzed, the amount of fuel per unit length of the DFC is varied over a large range. This is achieved by changing the number of rods in the array and the rod pitch. The number of rods are varied between 64 (8x8) and 729 (27x27) for PWR fuel.

- Analyses are performed for the minimum, maximum and typical pellet diameter of the fuel.

This is a very conservative approach to model damaged fuel, and to model fuel debris configurations such as severely damaged assemblies and bundles of individual fuel rods, as the absorption in the cladding and structural material is neglected.

This is also a conservative approach to model fuel debris configurations such as bare fuel pellets due to the assumption of an active length of 150 inch. For some of the analyzed cases, this assumption results in more uranium mass being modeled in the DFCs than is permitted by the uranium mass loading restrictions listed in Chapter 1.

To demonstrate the level of conservatism, additional analyses are performed with the DFC containing various realistic assembly configurations such as intact assemblies, assemblies with missing fuel rods and collapsed assemblies, i.e. assemblies with increased number of rods and decreased rod pitch.

As discussed in Subsection 6.4.9, all calculations are performed for full cask models, containing the maximum permissible number of DFCs together with intact assemblies.

Graphical presentations of the calculated maximum k_{eff} for each case as a function of the fuel mass per unit length of the DFC are shown in Figure 6.4.12. The results for the bare fuel rods show a distinct peak in the maximum k_{eff} at about 3.5 $kgUO_2$/inch.

The realistic assembly configurations are typically about 0.01 (delta-k) or more below the peak results for the bare fuel rods, demonstrating the conservatism of this approach to model damaged fuel and fuel debris configurations such as severely damaged assemblies and bundles of fuel rods.

For fuel debris configurations consisting of bare fuel pellets only, the fuel mass per unit length would be beyond the value corresponding to the peak reactivity. For example, for DFCs filled with a mixture of 60 vol% fuel and 40 vol% water the fuel mass per unit length is 7.92 $kgUO_2$/inch for the PWR DFC. The corresponding reactivities are significantly below the peak reactivies. The difference is about 0.01 (delta-k) or more for PWR fuel. Furthermore, the filling height of the DFC would be less than 70 inches in these examples due to the limitation of the fuel mass per basket position, whereas the calculation is conservatively performed for a height of

150 inch. These results demonstrate that even for the fuel debris configuration of bare fuel pellets, the model using bare fuel rods is a conservative approach.

To demonstrate that the bare fuel rod approach also bounds the potential presence of fuel fragments in the DFCs, additional calculations were performed with fuel fragments in the DFCs instead of bare fuel rods. The fuel fragments are modeled as regular 3-dimensional arrays of fuel cubes positioned inside water cubes. Both the dimension of the fuel cubes and the fuel-to-water-volume ratio are varied over a wide range. Calculations are performed for the MPC-24E/EF Trojan, and the results are presented in Table 6.4.18. The highest maximum k_{eff} is 0.9320 for a fragment outer dimension of 0.2 inches and a fuel to water volume ratio of 0.4. This maximum k_{eff} value is lower than the corresponding value for the bare fuel rod model, which is 0.9377 as shown in Table 6.4.17. The damaged fuel and fuel debris model based on bare fuel rods therefore bounds any condition involving fuel fragments in the DFCs.

6.4.9.3 Results for MPC-24E and MPC-24EF

The MPC-24E/EF is designed for the storage of up to four DFCs with damaged fuel or fuel debris in the four outer fuel baskets cells shaded in Figure 6.4.11. These locations are designed with a larger box ID to accommodate the DFCs. For an enrichment of 4.0 wt% ^{235}U for the intact fuel, damaged fuel and fuel debris, the results for the various configurations outlined in Subsection 6.4.9.2 are summarized in Figure 6.4.12 and in Table 6.4.11. Figure 6.4.12 shows the maximum k_{eff}, including bias and calculational uncertainties, for various actual and hypothetical damaged fuel and fuel debris configurations as a function of the fuel mass per unit length of the DFC. For the intact assemblies, the 15x15H assembly class was chosen (see Subsection 6.4.9.1). Table 6.4.11 lists the highest maximum k_{eff} for the various configurations. All maximum k_{eff} values are below the 0.95 regulatory limit.

6.4.9.4 Results for Trojan MPC-24E and MPC-24EF

For the Trojan MPC-24E/EF, bare fuel rod arrays with arrays sizes between 11x11 and 23x23 were analyzed as damaged fuel/fuel debris, with a pellet diameter corresponding to the 17x17B assembly class. The highest maximum k_{eff} value is shown in Table 6.1.6, and is below the 0.95 regulatory limit. The realistic damaged fuel assembly configurations in the DFC, such as assemblies with missing rods, were not analyzed in the Trojan MPC-24E/EF since the evaluations for the generic MPC-24E/EF demonstrate that these conditions are bounded by the fuel debris model using bare fuel pellets.

6.4.10 Non-fuel Hardware in PWR Fuel Assemblies

Non-fuel hardware such as Thimble Plugs (TPs), Burnable Poison Rod Assemblies (BPRAs), Rod Cluster Control Assemblies (RCCAs) and similar devices are permitted for storage with the

PWR fuel assemblies in the Trojan MC-24E/EF. Non-fuel hardware is inserted in the guide tubes of the assemblies. For pure water, the reactivity of any PWR assembly with inserts is bounded by (i.e. lower than) the reactivity of the same assembly without the insert. This is due to the fact that the insert reduces the amount of moderator in the assembly, while the amount of fissile material remains unchanged.

Therefore, from a criticality safety perspective, non-fuel hardware inserted into PWR assemblies are acceptable for all allowable PWR types, and, depending on the assembly class, can increase the safety margin.

6.4.11 Reactivity Effect of Potential Fixed Neutron Absorber Damage

During the manufacturing process of the fuel baskets, it is possible that minor damage to fixed neutron absorber panels occurs during welding operations. Criticality calculations have been performed for all basket types to determine whether this condition could have an effect on the reactivity of the system. Since the potential fixed neutron absorber damage is typically the result of welding operations, the damage would occur in a narrow area along the edge of the panel, and would only be present in a few panels within each basket. However, in order to maximize the potential reactivity effect of the damage in the calculations, it is assumed that the damage occurs in an area with a diameter of 1 inch at the center of the fixed neutron absorber panel, and that this condition exists in every panel in the basket. It is further assumed that the fixed neutron absorber in this area is completely replaced by water, while in reality only a relocation of the fixed neutron absorber would occur, since the fixed neutron absorber is completely covered by the sheathing. Calculations performed under these assumption demonstrate that the conservatively modeled fixed neutron absorber damage has a negligible effect on the reactivity, i.e. the difference to the condition without the damage is less than 2 standard deviations. For example, for the MPC-24 and MPC-24E, the change in reactivity is +0.0006 and -0.0004, respectively, for a standard deviation between 0.0004 and 0.0005. In the MPC-24E for Trojan, a specific potential damage was identified that is not bounded by the generic approach described above. To demonstrate that this condition is acceptable, a specific calculation was performed assuming a damage of 5 square-inches in a specific location in up to 8 fixed neutron absorber panels in the basket, and was found to have again a negligible effect on reactivity. In summary, these calculations demonstrate that fixed neutron absorber damage bounded by the configurations assumed in the analyses is acceptable and does not affect the reactivity of the HI-STAR System.

6.4.12 Fixed Neutron Absorber Material

The MPCs in the HI-STAR 100 System can be manufactured with one of two possible neutron absorber materials: Boral or Metamic. Both materials are made of aluminum and B_4C powder. Boral has an inner core consisting of B_4C and aluminum between two outer layers consisting of

aluminum only. This configuration is explicitly modeled in the criticality evaluation and shown in Figures 6.3.1 through 6.3.3 for each basket. Metamic is a single layer material with the same overall thickness and the same credited ^{10}B loading (in g/cm^2) for each basket. The majority of the criticality evaluations documented in this chapter are performed using Boral as the fixed neutron absorber. For a selected number of bounding cases, analyses are also performed using Metamic instead of Boral. The results for these cases are listed in Table 6.4.19, together with the corresponding result using Boral and the difference between the two materials for each case. Individual cases show small differences for the two materials. However, the differences are mostly below two times the standard deviation (the standard deviation is about 0.0008 for all cases in Table 6.4.19), indicating that the results are statistically equivalent. Furthermore, the average difference is well below two standard deviations, and all cases are below the regulatory limit of 0.95. The calculations therefore demonstrate that the two fixed neutron absorber materials are identical from a criticality perspective. All results obtained for Boral are therefore directly applicable to Metamic and no further evaluations using Metamic are required.

6.4.13 Reactivity Effect of Manufacturing Variations

For additional flexibility in manufacturing neutron absorber panels, the following condition for the poison panels is evaluated to demonstrate that this condition is acceptable and does not lead to an increase in reactivity. The condition is:

- A poison panel might show a reduced width in a small section along the length, while the average width is equal to or larger than the required minimum. To conservatively model this condition, it is assumed that all panels have a width reduction below the minimum by 1/32 inch over a length of 12 inches at the axial center of the active length. The width of the remainder of the panel is increased slightly to maintain the minimum width on average for a panel length of 156 inches.

The results for this case are listed in Table 6.4.20, together with the corresponding results for the design basis, i.e. with the minimum panels width, and the reactivity difference for each case is shown. The differences are either below two times the standard deviation (the standard deviation is between 0.0004 and 0.0008 for all cases in Table 6.4.20), or the conditions result in a reduction in reactivity. Furthermore, the average difference is well below two standard deviations, and all cases are below the regulatory limit of 0.95. The calculations therefore demonstrate that the condition stated above have a negligible effect on reactivity and is therefore acceptable.

Table 6.4.1

MAXIMUM REACTIVITIES WITH REDUCED WATER DENSITIES FOR CASK ARRAYS[†] WITH MPC-24 AND MPC-68

	Water Density		MCNP4a Results					
Case Number	Internal	External	MPC-24 (17x17A01 @ 4.0%)			MPC-68 (8x8C04 @ 4.2%)		
			Max. k_{eff}[††]	1 σ	EALF (eV)	Max. k_{eff}	1 σ	EALF (eV)
1	100%	single cask	0.9368	0.0008	0.2131	0.9348	0.0007	0.2915
2	100%	100%	0.9354	0.0009	0.2136	0.9339	0.0005	0.2922
3	100%	70%	0.9362	0.0008	0.2139	0.9339	0.0006	0.2921
4	100%	50%	0.9352	0.0008	0.2144	0.9347	0.0004	0.2924
5	100%	20%	0.9372	0.0008	0.2138	0.9338	0.0005	0.2921
6	100%	10%	0.9380	0.0009	0.2140	0.9336	0.0005	0.2920
7	100%	5%	0.9351	0.0008	0.2142	0.9333	0.0006	0.2936
8	100%	0%	0.9342	0.0008	0.2136	0.9338	0.0005	0.2922
9	70%	0%	0.8337	0.0007	0.4115	0.8488	0.0004	0.6064
10	50%	0%	0.7426	0.0008	0.8958	0.7631	0.0004	1.4515
11	20%	0%	0.5606	0.0007	15.444	0.5797	0.0006	26.5
12	10%	0%	0.4834	0.0005	160.28	0.5139	0.0003	241
13	5%	0%	0.4432	0.0004	1133.9	0.4763	0.0003	1770
14	10%	100%	0.4793	0.0005	171.79	0.4946	0.0003	342

† For an infinite square array of casks with 60 cm spacing between cask surfaces.

†† Maximum k_{eff} includes the bias, uncertainties, and calculational statistics, evaluated for the worst case combination of manufacturing tolerances.

Table 6.4.2

REACTIVITY EFFECTS OF SPACING AND WATER MODERATOR DENSITY FOR SQUARE ARRAYS OF MPC-24 CASKS
(17x17A01 @ 4.0% E)

Cask-to-Cask External Spacing (cm)					
External Moderator Density (%)	2	10	20	40	60
5	0.9352	0.9389	0.9356	0.9345	0.9351
10	0.9366	0.9353	0.9338	0.9357	0.9380
20	0.9368	0.9371	0.9359	0.9366	0.9372
50	0.9363	0.9363	0.9371	0.9352	0.9352
100	0.9355	0.9369	0.9354	0.9354	0.9354

Note:

1. All values are maximum k_{eff} which include the bias, uncertainties, and calculational statistics, evaluated for the worst case combination of manufacturing tolerances.
2. The standard deviation (σ) of the calculations ranges between 0.0007 and 0.0010.

Table 6.4.3

REACTIVITY EFFECTS OF SPACING AND WATER MODERATOR DENSITY FOR HEXAGONAL (TRIANGULAR-PITCHED) ARRAYS OF MPC-24 CASKS (17x17A01 @ 4.0% E)

Cask-to-Cask External Spacing (cm)					
External Moderator Density (%)	2	10	20	40	60
5	0.9358	0.9365	0.9369	0.9354	0.9354
10	0.9363	0.9372	0.9351	0.9368	0.9372
20	0.9354	0.9357	0.9345	0.9358	0.9381
50	0.9347	0.9361	0.9371	0.9365	0.9370
100	0.9373	0.9381	0.9354	0.9354	0.9354

Note:

1. All values are maximum k_{eff} which include the bias, uncertainties, and calculational statistics, evaluated for the worst case combination of manufacturing tolerances.
2. The standard deviation (σ) of the calculations ranges between 0.0007 and 0.0009.

Table 6.4.4

REACTIVITY EFFECTS OF SPACING AND EXTERNAL MODERATOR DENSITY FOR HEXAGONAL (TRIANGULAR-PITCHED) ARRAYS OF MPC-24 CASKS (17x17A01 @ 4.0% E) INTERNALLY FLOODED WITH WATER OF 10% FULL DENSITY

Cask-to-Cask External Spacing (cm)					
External Moderator Density (%)	2	10	20	40	60
10	0.4818	0.4808	0.4798	0.4795	0.4789
100	0.4798	0.4788	0.4781	0.4793	0.4793

Note:

1. All values are maximum k_{eff} which include the bias, uncertainties, and calculational statistics, evaluated for the worst case combination of manufacturing tolerances.
2. The standard deviation (σ) of the calculations ranges between 0.0004 and 0.0005.

Table 6.4.5

CALCULATIONS FOR HEXAGONAL (TRIANGULAR-PITCHED) ARRAYS OF TOUCHING CASKS WITH MPC-24 AND MPC-68

MPC-24 (17x17A01 @ 4.0% ENRICHMENT)		
Internal Moderation (%)	External Moderation (%)	Maximum k_{eff}
0	0	0.3910
0	100	0.3767
100	0	0.9366
100	100	0.9341
MPC-68 (8x8C04 @ 4.2% ENRICHMENT)		
Internal Moderation (%)	External Moderation (%)	Maximum k_{eff}
0	0	0.4036
0	100	0.3716
100	0	0.9351
100	100	0.9340

Note:

1. All values are maximum k_{eff} which include bias, uncertainties, and calculational statistics, evaluated for the worst case combination of manufacturing tolerances.
2. The standard deviation (σ) of the calculations ranges between 0.0007 and 0.0008 for 100% internal moderation, and between 0.0002 and 0.0003 for 0% internal moderation.

Table 6.4.6

REACTIVITY EFFECTS OF PARTIAL CASK FLOODING FOR MPC-24 AND MPC-68

MPC-24 (17x17A01 @ 4.0% ENRICHMENT)			
Flooded Condition (% Full)	Vertical Orientation	Flooded Condition (% Full)	Horizontal Orientation
25	0.9157	25	0.8766
50	0.9305	50	0.9240
75	0.9330	75	0.9329
100	0.9368	100	0.9368
MPC-68 (8x8C04 @ 4.2% ENRICHMENT)			
Flooded Condition (% Full)	Vertical Orientation	Flooded Condition (% Full)	Horizontal Orientation
25	0.9132	23.5	0.8586
50	0.9307	50	0.9088
75	0.9312	76.5	0.9275
100	0.9348	100	0.9348

Notes:

1. All values are maximum k_{eff} which include bias, uncertainties, and calculational statistics, evaluated for the worst case combination of manufacturing tolerances.
2. The standard deviation (σ) of the calculations ranges between 0.0007 and 0.0010.

Table 6.4.7

REACTIVITY EFFECT OF FLOODING THE PELLET-TO-CLAD GAP FOR MPC-24 AND MPC-68

Pellet-to-Clad Condition	**MPC-24 17x17A01 4.0% Enrichment**	**MPC-68 8x8C04 4.2% Enrichment**
dry	0.9295	0.9279
flooded	0.9368	0.9348

Notes:

1. All values are maximum k_{eff} which includes bias, uncertainties, and calculational statistics, evaluated for the worst case combination of manufacturing tolerances.
2. The standard deviation (σ) of the calculations ranges between 0.0007 and 0.0010.

Table 6.4.8

MAXIMUM k_{eff} VALUES† IN THE DAMAGED FUEL CONTAINER

Condition	MCNP4a Results					
	DFC Dimensions: ID 4.93" THK. 0.12"			DFC Dimensions: ID 4.81" THK. 0.11"		
	Max.†† k_{eff}	1 σ	EALF (eV)	Max.†† k_{eff}	1 σ	EALF (eV)
6x6 Fuel Assembly						
6x6 Intact Fuel	0.7086	0.0007	0.3474	0.7016	0.0006	0.3521
w/32 Rods Standing	0.7183	0.0008	0.2570	0.7117	0.0007	0.2593
w/28 Rods Standing	0.7315	0.0007	0.1887	0.7241	0.0006	0.1909
w/24 Rods Standing	0.7086	0.0007	0.1568	0.7010	0.0008	0.1601
w/18 Rods Standing	0.6524	0.0006	0.1277	0.6453	0.0007	0.1288
Collapsed to 8x8 array	0.7845	0.0007	1.1550	0.7857	0.0007	1.1162
Dispersed Powder	0.7628	0.0007	0.0926	0.7440	0.0007	0.0902
7x7 Fuel Assembly						
7x7 Intact Fuel	0.7463	0.0007	0.2492	0.7393	0.0006	0.2504
w/41 Rods Standing	0.7529	0.0007	0.1733	0.7481	0.0007	0.1735
w/36 Rods Standing	0.7487	0.0007	0.1389	0.7444	0.0006	0.1406
w/25 Rods Standing	0.6718	0.0007	0.1070	0.6644	0.0007	0.1082

† These calculations were performed with a planar-average enrichment of 3.0% and a ^{10}B loading of 0.0067 g/cm^2, which is 75% of a minimum ^{10}B loading of 0.0089 g/cm^2. The minimum ^{10}B loading in the MPC-68F is 0.010 g/cm^2. Therefore, the listed maximum k_{eff} values are conservative.

†† Maximum k_{eff} includes bias, uncertainties, and calculational statistics, evaluated for the worst case combination of manufacturing tolerances.

Table 6.4.9

DELETED

Table 6.4.10

REACTIVITY EFFECT OF PREFERENTIAL FLOODING OF THE DFCs

DFC Configuration	Preferential Flooding	Fully Flooded
MPC-68 or MPC-68F with 68 DFCs (Assembly Classes 6x6A/B/C, 7x7A and 8x8A)	0.6560	0.7857
MPC-24E or MPC-24EF with 4 DFCs (Bounding All PWR Assembly Classes)	0.7895	0.9480

Notes:

1. All values are maximum k_{eff} which includes bias, uncertainties, and calculational statistics, evaluated for the worst case combination of manufacturing tolerances.

Table 6.4.11

MAXIMUM k_{eff} VALUES IN THE GENERIC PWR DAMAGED FUEL CONTAINER FOR A MAXIMUM INITIAL ENRICHMENT OF 4.0 wt% ^{235}U.

Model Configuration inside the DFC	**Maximum k_{eff}**
Intact Assemblies (2 assemblies analyzed)	0.9340
Assemblies with missing rods (4 configurations analyzed)	0.9350
Collapsed Assemblies (6 configurations analyzed)	0.9360
Regular Arrays of Bare Fuel Rods (36 configurations analyzed)	0.9480

Notes:

1. All values are maximum k_{eff} which includes bias, uncertainties, and calculational statistics, evaluated for the worst case combination of manufacturing tolerances.
2. The standard deviation (σ) of the calculations ranges between 0.0007 and 0.0010.

Table 6.4.12
SUMMARY OF THE CRITICALITY RESULTS FOR THE MOST REACTIVE ASSEMBLY FROM THE MOST REACTIVE ASSEMBLY CLASS IN EACH MPC TO DEMONSTRATE COMPLIANCE WITH 10CFR71.55 AND 10CFR71.59

MPC-24, Assembly Class 15x15F, 4.1 wt% ^{235}U					
Configuration	% Internal Moderation	% External Moderation	Max.‡ k_{eff}	1 σ	EALF (eV)
Single Package, unreflected	100%	0%	0.9410	0.0007	0.2998
Single Package, fully reflected	100%	100%	0.9397	0.0008	0.3016
Containment, fully reflected	100%	100%	0.9397	0.0008	0.3006
Infinite Array of Damaged Packages	100%	100%	0.9436	0.0009	0.2998
Infinite Array of Undamaged Packages	0%	0%	0.3950	0.0004	82612.0
MPC-68, Assembly Class 9x9E/F, 4.0 wt% ^{235}U					
Configuration	% Internal Moderation	% External Moderation	Max. k_{eff}	1 σ	EALF (eV)
Single Package, unreflected	100%	0%	0.9486	0.0008	0.2095
Single Package, fully reflected	100%	100%	0.9470	0.0008	0.2079
Containment, fully reflected	100%	100%	0.9461	0.0007	0.2092
Infinite Array of Damaged Packages	100%	100%	0.9468	0.0008	0.2106
Infinite Array of Undamaged Packages	0%	0%	0.3808	0.0003	85218.0
MPC-68F, Assembly Class 6x6C, 2.7 wt% ^{235}U					
Configuration	% Internal Moderation	% External Moderation	Max. k_{eff}	1 σ	EALF (eV)
Single Package, unreflected	100%	0%	0.8021	0.0007	0.2139
Single Package, fully reflected	100%	100%	0.8033	0.0008	0.2142
Containment, fully reflected	100%	100%	0.8033	0.0008	0.2138
Infinite Array of Damaged Packages	100%	100%	0.8026	0.0008	0.2142
Infinite Array of Undamaged Packages	0%	0%	0.3034	0.0002	99463.0

‡ The maximum k_{eff} is equal to the sum of the calculated k_{eff}, two standard deviations, the code bias, and the uncertainty in the code bias.

Table 6.4.12 (continued)
SUMMARY OF THE CRITICALITY RESULTS FOR THE MOST REACTIVE ASSEMBLY FROM THE MOST REACTIVE ASSEMBLY CLASS IN EACH MPC TO DEMONSTRATE COMPLIANCE WITH 10CFR71.55 AND 10CFR71.59

MPC-24E/EF, Assembly Class 15x15F, 4.5 wt% ^{235}U					
Configuration	% Internal Moderation	% External Moderation	Max.‡ k_{eff}	1 σ	EALF (eV)
Single Package, unreflected	100%	0%	0.9495	0.0008	0.3351
Single Package, fully reflected	100%	100%	0.9485	0.0008	0.3313
Containment, fully reflected	100%	100%	0.9486	0.0008	0.3362
Infinite Array of Damaged Packages	100%	100%	0.9495	0.0008	0.3335
Infinite Array of Undamaged Packages	0%	0%	0.4026	0.0004	87546.0
MPC-24E/EF TROJAN, Trojan Intact and Damaged Fuel, 3.7 wt% ^{235}U					
Configuration	% Internal Moderation	% External Moderation	Max. k_{eff}	1 σ	EALF (eV)
Single Package, unreflected	100%	0%	0.9377	0.0008	n/c†
Single Package, fully reflected	100%	100%	0.9366	0.0008	n/c
Containment, fully reflected	100%	100%	0.9377	0.0008	n/c
Infinite Array of Damaged Packages	100%	100%	0.9383	0.0007	n/c
Infinite Array of Undamaged Packages	0%	0%	0.3518	0.0003	n/c
MPC-32, Assembly Class 15x15F and 17x17C					
Configuration	% Internal Moderation	% External Moderation	Max. k_{eff}	1 σ	EALF (eV)
Single Package, unreflected	100%	0%	0.9481	0.0005	0.3613
Single Package, fully reflected	100%	100%	0.9476	0.0005	0.4319
Containment, fully reflected	100%	100%	0.9467	0.0005	0.3629
Infinite Array of Damaged Packages	100%	100%	0.9476	0.0004	0.3600
Infinite Array of Undamaged Packages	0%	0%	0.4205	0.0002	39928

‡ The maximum k_{eff} is equal to the sum of the calculated k_{eff}, two standard deviations, the code bias, and the uncertainty in the code bias.
† n/c = not calculated

Table 6.4.13

RESULTS FOR EACH ASSEMBLY CLASS IN THE MPC-24

Fuel Assembly Class	Maximum Allowable Enrichment (wt% ^{235}U)	Max.† k_{eff}	1 σ	EALF (eV)
14x14A	4.6	0.9296	0.0008	0.2093
14x14B	4.6	0.9228	0.0008	0.2675
14x14C	4.6	0.9307	0.0008	0.3001
14x14D	4.0	0.8507	0.0008	0.3308
14x14E	5.0	0.7627	0.0007	0.3607
15x15A	4.1	0.9227	0.0007	0.2708
15x15B	4.1	0.9388	0.0009	0.2626
15x15C	4.1	0.9361	0.0009	0.2385
15x15D	4.1	0.9367	0.0008	0.2802
15x15E	4.1	0.9392	0.0008	0.2908
15x15F	4.1	0.9410	0.0007	0.2998
15x15G	4.0	0.8907	0.0008	0.3456
15x15H	3.8	0.9337	0.0009	0.2349
16x16A	4.6	0.9287	0.0008	0.2704
17x17A	4.0	0.9368	0.0008	0.2131
17x17B	4.0	0.9355	0.0008	0.2659
17x17C	4.0	0.9349	0.0009	0.2677

† The term "maximum k_{eff} " as used here, and elsewhere in this document, means the highest possible k-effective, including bias, uncertainties, and calculational statistics, evaluated for the worst case combination of manufacturing tolerances.

Table 6.4.14

RESULTS FOR EACH ASSEMBLY CLASS IN THE MPC-68

Fuel Assembly Class	Maximum Allowable Enrichment (wt% ^{235}U)	Max.† k_{eff}	1 σ	EALF (eV)
7x7B	4.2	0.9386	0.0007	0.3983
8x8B	4.2	0.9416	0.0007	0.3293
8x8C	4.2	0.9425	0.0007	0.3081
8x8D	4.2	0.9403	0.0006	0.2778
8x8E	4.2	0.9312	0.0008	0.2831
8x8F	4.0	0.9459	0.0007	0.2361
9x9A	4.2	0.9417	0.0008	0.2236
9x9B	4.2	0.9436	0.0008	0.2506
9x9C	4.2	0.9395	0.0008	0.2698
9x9D	4.2	0.9394	0.0009	0.2625
9x9E	4.0	0.9486	0.0008	0.2095
9x9F	4.0	0.9486	0.0008	0.2095
9x9G	4.2	0.9383	0.0008	0.2292
10x10A	4.2	0.9457	0.0008	0.2212
10x10B	4.2	0.9436	0.0007	0.2366
10x10C	4.2	0.9433	0.0007	0.2416
10x10D	4.0	0.9376	0.0008	0.3355
10x10E	4.0	0.9185	0.0007	0.2936

† The term "maximum k_{eff} " as used here, and elsewhere in this document, means the highest possible k-effective, including bias, uncertainties, and calculational statistics, evaluated for the worst case combination of manufacturing tolerances.

Table 6.4.15

RESULTS FOR EACH ASSEMBLY CLASS IN THE MPC-68F

Fuel Assembly Class	Maximum Allowable Enrichment (wt% ^{235}U)	Max.† k_{eff}	1 σ	EALF (eV)
6x6A	2.7††	0.7888	0.0007	0.2310
6x6B†††	2.7	0.7824	0.0006	0.2184
6x6C	2.7	0.8021	0.0007	0.2139
7x7A	2.7	0.7974	0.0008	0.2015
8x8A	2.7	0.7697	0.0007	0.2158

† The term "maximum k_{eff} " as used here, and elsewhere in this document, means the highest possible k-effective, including bias, uncertainties, and calculational statistics, evaluated for the worst case combination of manufacturing tolerances.

†† These calculations were performed for 3.0% planar-average enrichment; however, the authorized contents are limited to a maximum planar-average enrichment of 2.7%. Therefore, the listed maximum k_{eff} values are conservative.

††† Assemblies in this class contain both MOX and UO_2 pins. The composition of the MOX fuel pins is given in Table 6.3.4. The maximum allowable planar-average enrichment for the MOX pins is given in the specification of authorized contents, Chapter 1.

Table 6.4.16

RESULTS FOR EACH ASSEMBLY CLASS IN THE MPC-24E/EF

Fuel Assembly Class	Maximum Allowable Enrichment (wt% ^{235}U)	Max.† k_{eff}	1 σ	EALF (eV)
14x14A	5.0	0.9380	0.0008	0.2277
14x14B	5.0	0.9312	0.0008	0.2927
14x14C	5.0	0.9365	0.0008	0.3318
14x14D	5.0	0.8875	0.0009	0.4026
14x14E	5.0	0.7651	0.0007	0.3644
15x15A	4.5	0.9336	0.0008	0.2879
15x15B	4.5	0.9487	0.0009	0.3002
15x15C	4.5	0.9462	0.0008	0.2631
15x15D	4.5	0.9445	0.0008	0.3375
15x15E	4.5	0.9471	0.0008	0.3242
15x15F	4.5	0.9495	0.0008	0.3351
15x15G	4.5	0.9062	0.0008	0.3883
15x15H	4.2	0.9455	0.0009	0.2663
16x16A	5.0	0.9358	0.0008	0.3150
17x17A	4.4	0.9447	0.0007	0.2374
17x17B	4.4	0.9438	0.0008	0.2951
17x17C	4.4	0.9433	0.0008	0.2932

† The term "maximum k_{eff} " as used here, and elsewhere in this document, means the highest possible k-effective, including bias, uncertainties, and calculational statistics, evaluated for the worst case combination of manufacturing tolerances.

Table 6.4.17

RESULTS FOR THE MPC-24E/EF TROJAN

Fuel Assembly Class	Maximum Allowable Enrichment (wt% ^{235}U)	Content	Max.† k_{eff}	1 σ	EALF (eV)
17x17B	3.7	Intact Fuel	0.9187	0.0009	not calculated
17x17B	3.7	Intact Fuel, Damaged Fuel and Fuel Debris	0.9377	0.0008	not calculated

† The term "maximum k_{eff} " as used here, and elsewhere in this document, means the highest possible k-effective, including bias, uncertainties, and calculational statistics, evaluated for the worst case combination of manufacturing tolerances.

Table 6.4.18

RESULTS FOR THE MPC-24E/EF TROJAN USING A FUEL FRAGMENT MODEL FOR DAMAGED FUEL AND FUEL DEBRIS

Fuel Cube OD (Inches)	**Maximum k_{eff}**			
	Fuel Volume / Water Volume			
	0.2	**0.4**	**0.6**	**0.8**
1	0.9098	0.9223	0.9260	0.9204
0.5	0.9156	0.9310	0.9273	0.9168
0.2	0.9254	0.9320	0.9216	0.9137
0.1	0.9253	0.9274	0.9183	0.9135
0.05	0.9224	0.9228	0.9168	0.9126
0.02	0.9183	0.9213	0.9140	0.9122

Table 6.4.19

COMPARISON OF MAXIMUM k_{eff} VALUES FOR DIFFERENT FIXED NEUTRON ABSORBER MATERIALS

CASE	**Maximum k_{eff}**		Reactivity Difference
	BORAL	**METAMIC**	
MPC-68	0.9486	0.9470	-0.0016
MPC-68F with 68 DFCs	0.8021	0.8019	-0.0002
MPC-24	0.9410	0.9425	+0.0015
MPC-24E, Intact Assemblies	0.9495	0.9494	-0.0001
MPC-24E, with 4 DFCs	0.9480	0.9471	-0.0009
Average Difference			**-0.0003**

Table 6.4.20

COMPARISON OF MAXIMUM k_{eff} VALUES FOR DIFFERENT FIXED NEUTRON ABSORBER CONDITIONS

CASE	**Maximum k_{eff}**		Reactivity Difference
	DESIGN BASIS (SINGLE PART PANEL AND MINIMUM WIDTH)	**PANELS WITH WIDTH REDUCTION**	
MPC-68	0.9486	0.9464	-0.0022
MPC-68F with 68 DFCs	0.8021	0.8023	+0.0002
MPC-24	0.9410	0.9411	+0.0001
MPC-24E, Intact Assemblies	0.9495	0.9494	-0.0001
MPC-24E, with 4 DFCs	0.9480	0.9470	-0.0010
Average Difference			**-0.0006**

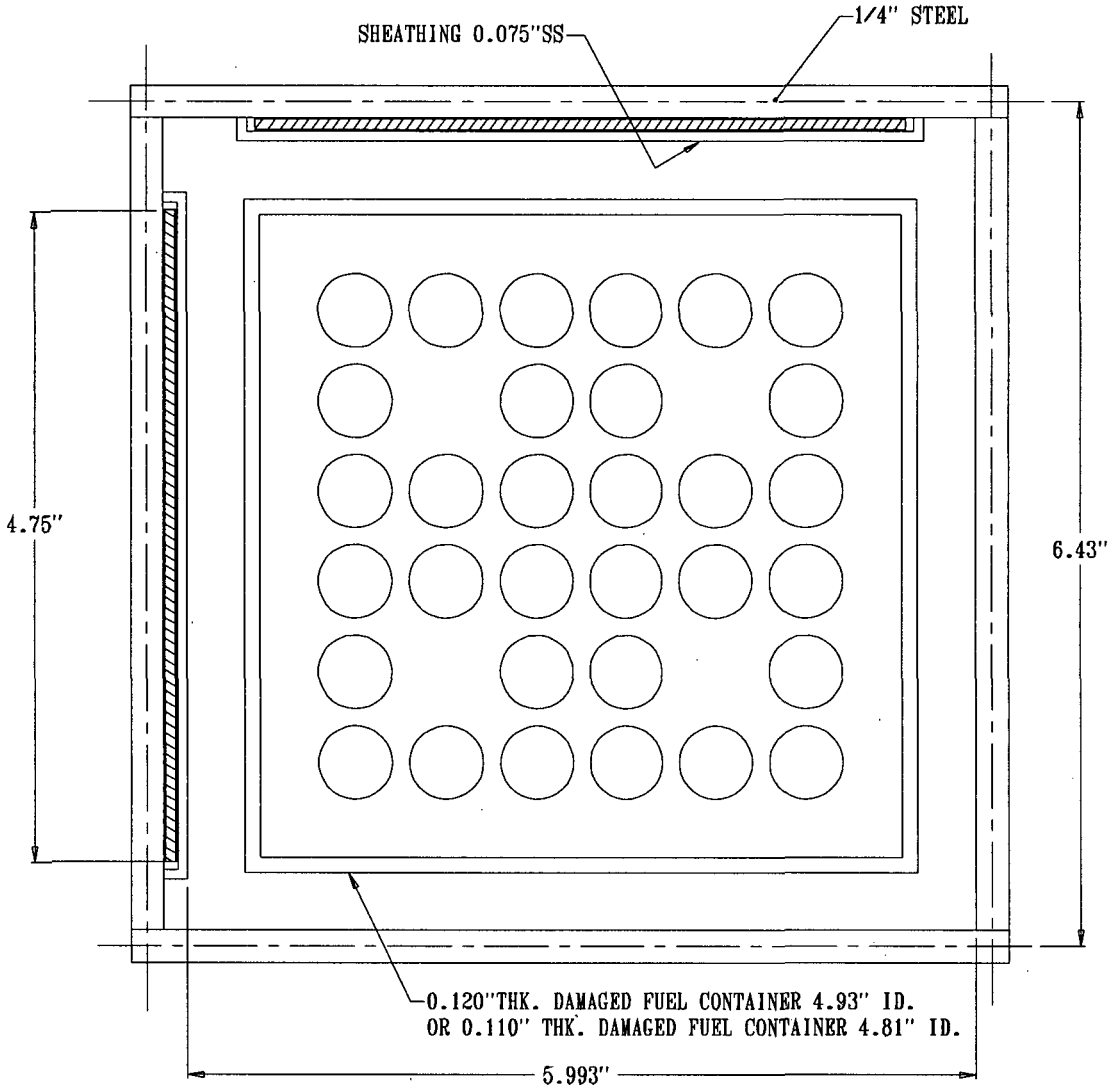

FIGURE 6.4.1; FAILED FUEL CALCULATION MODEL (PLANAR CROSS-SECTION) WITH 6X6 ARRAY WITH 4 MISSING RODS IN THE MPC-68 BASKET (SEE CHAPTER 1 FOR TRUE BASKET DIMENSIONS)

NOTE: THESE DIMENSIONS WERE CONSERVATIVELY USED FOR CRITICALITY ANALYSES.

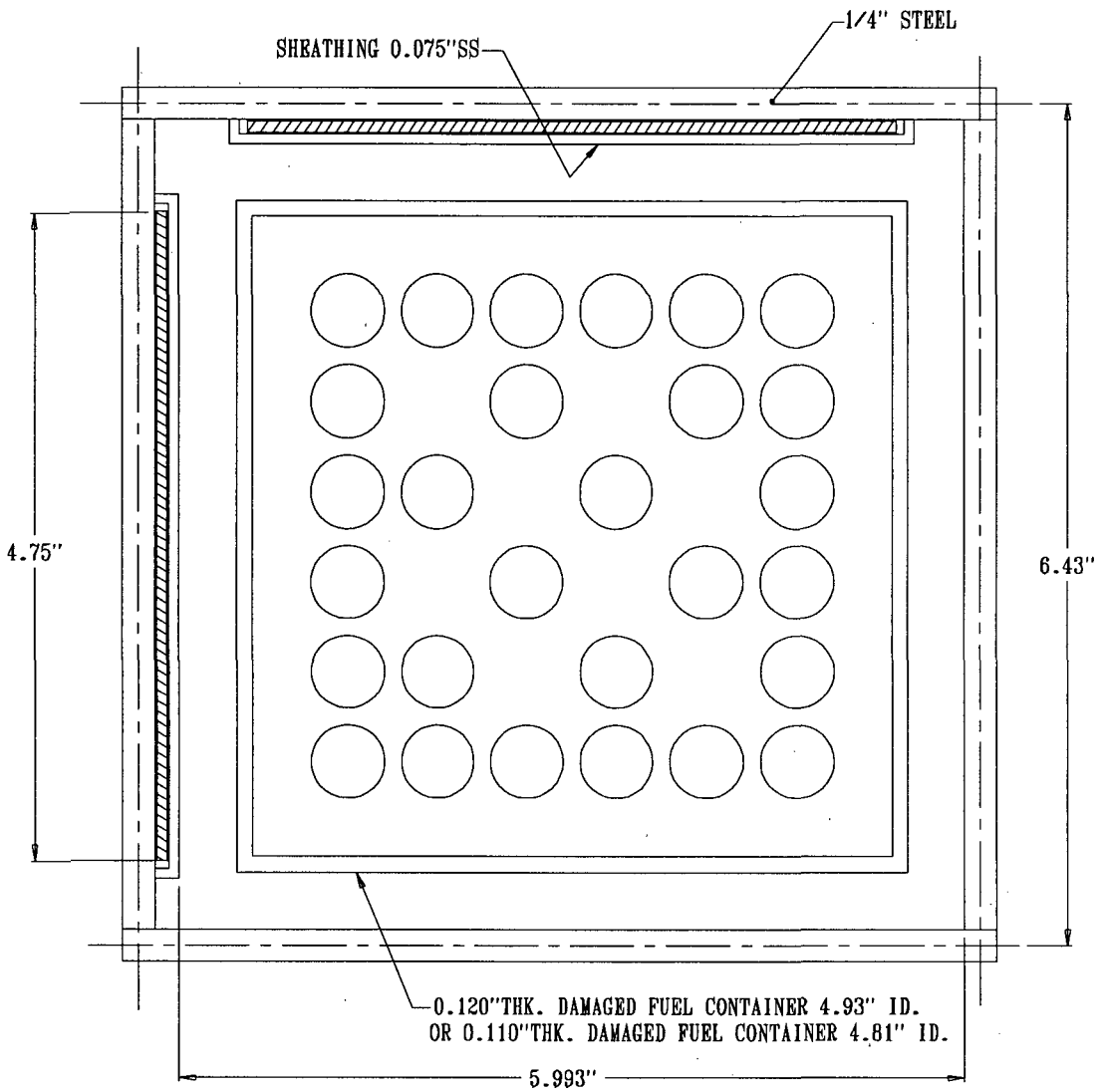

FIGURE 6.4.2; FAILED FUEL CALCULATION MODEL (PLANAR CROSS-SECTION) WITH 6X6 ARRAY WITH 8 MISSING RODS IN THE MPC-68 BASKET (SEE CHAPTER 1 FOR TRUE BASKET DIMENSIONS)

NOTE: THESE DIMENSIONS WERE CONSERVATIVELY USED FOR CRITICALITY ANALYSES.

REPORT HI-951251 | REVISION 9

e\PROJECTS\5014\HI951251\CH_6\6_4_2

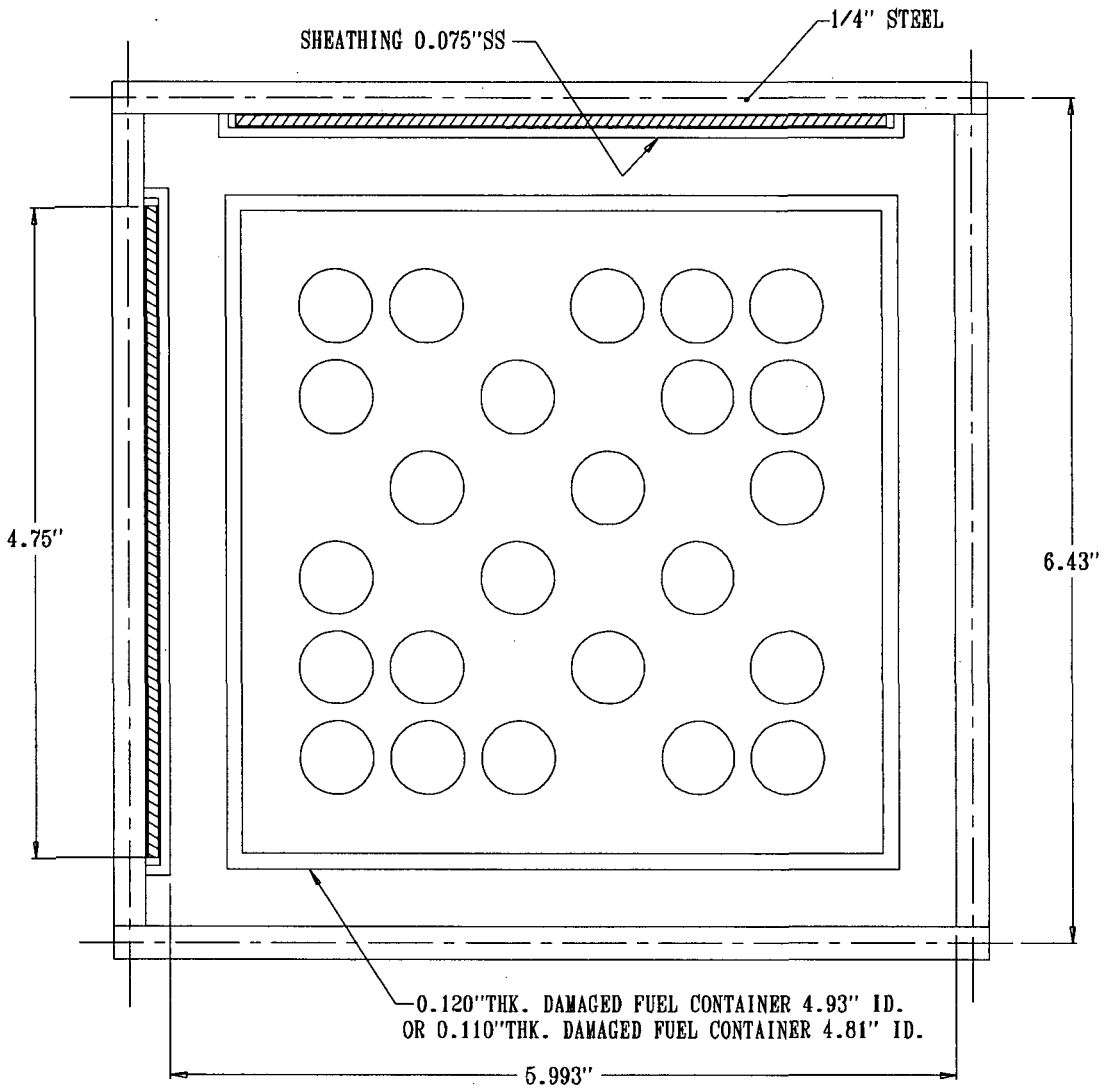

FIGURE 6.4.3; FAILED FUEL CALCULATION MODEL (PLANAR CROSS-SECTION) WITH 6X6 ARRAY WITH 12 MISSING RODS IN THE MPC-68 BASKET (SEE CHAPTER 1 FOR TRUE BASKET DIMENSIONS)

NOTE: THESE DIMENSIONS WERE CONSERVATIVELY USED FOR CRITICALITY ANALYSES.

REPORT HI-951251 | REVISION 9

e\PROJECTS\5014\HI951251\CH_6\6_4_3

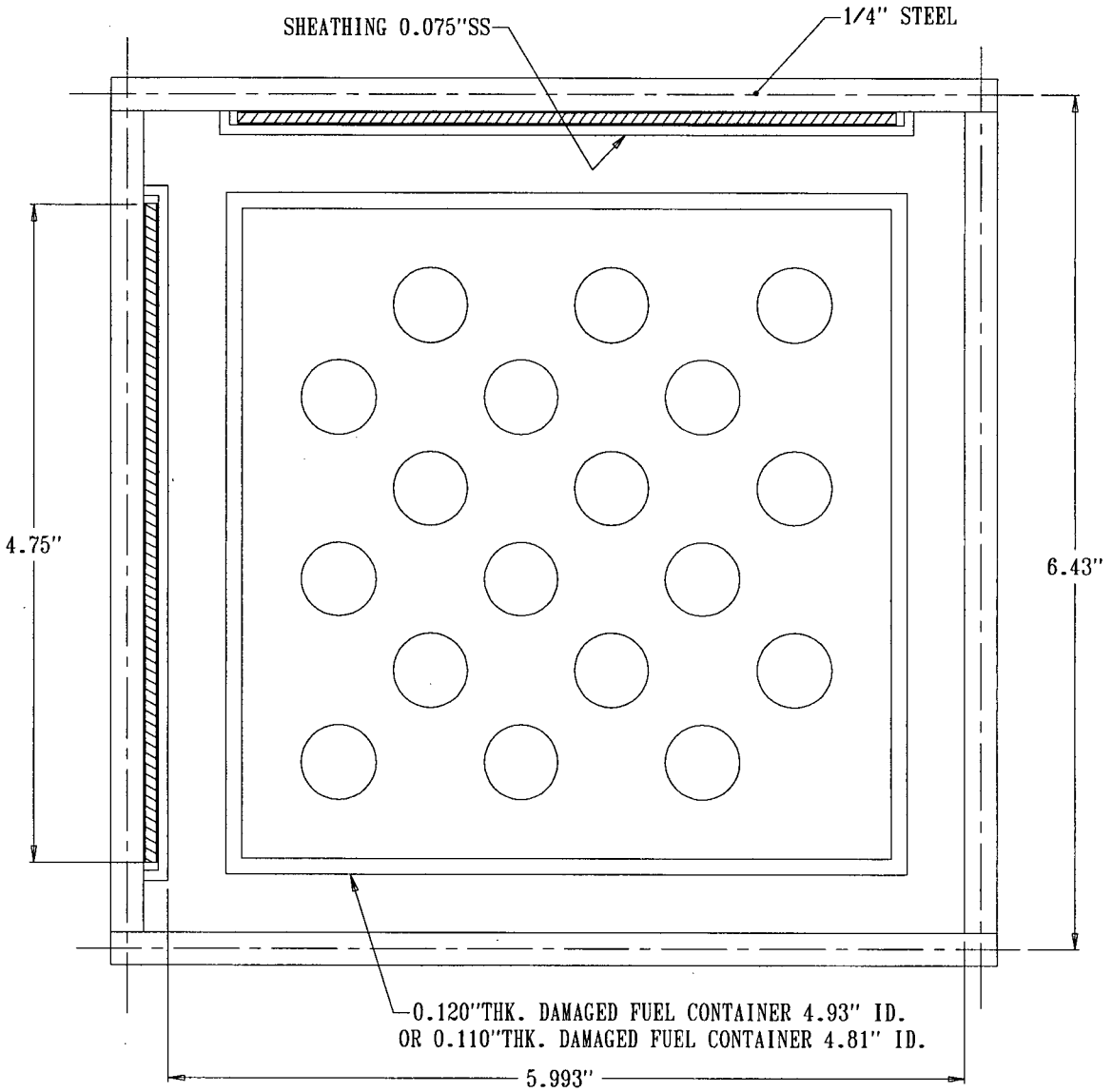

FIGURE 6.4.4; FAILED FUEL CALCULATION MODEL (PLANAR CROSS-SECTION) WITH 6X6 ARRAY WITH 18 MISSING RODS IN THE MPC-68 BASKET (SEE CHAPTER 1 FOR TRUE BASKET DIMENSIONS)

NOTE: THESE DIMENSIONS WERE CONSERVATIVELY USED FOR CRITICALITY ANALYSES.

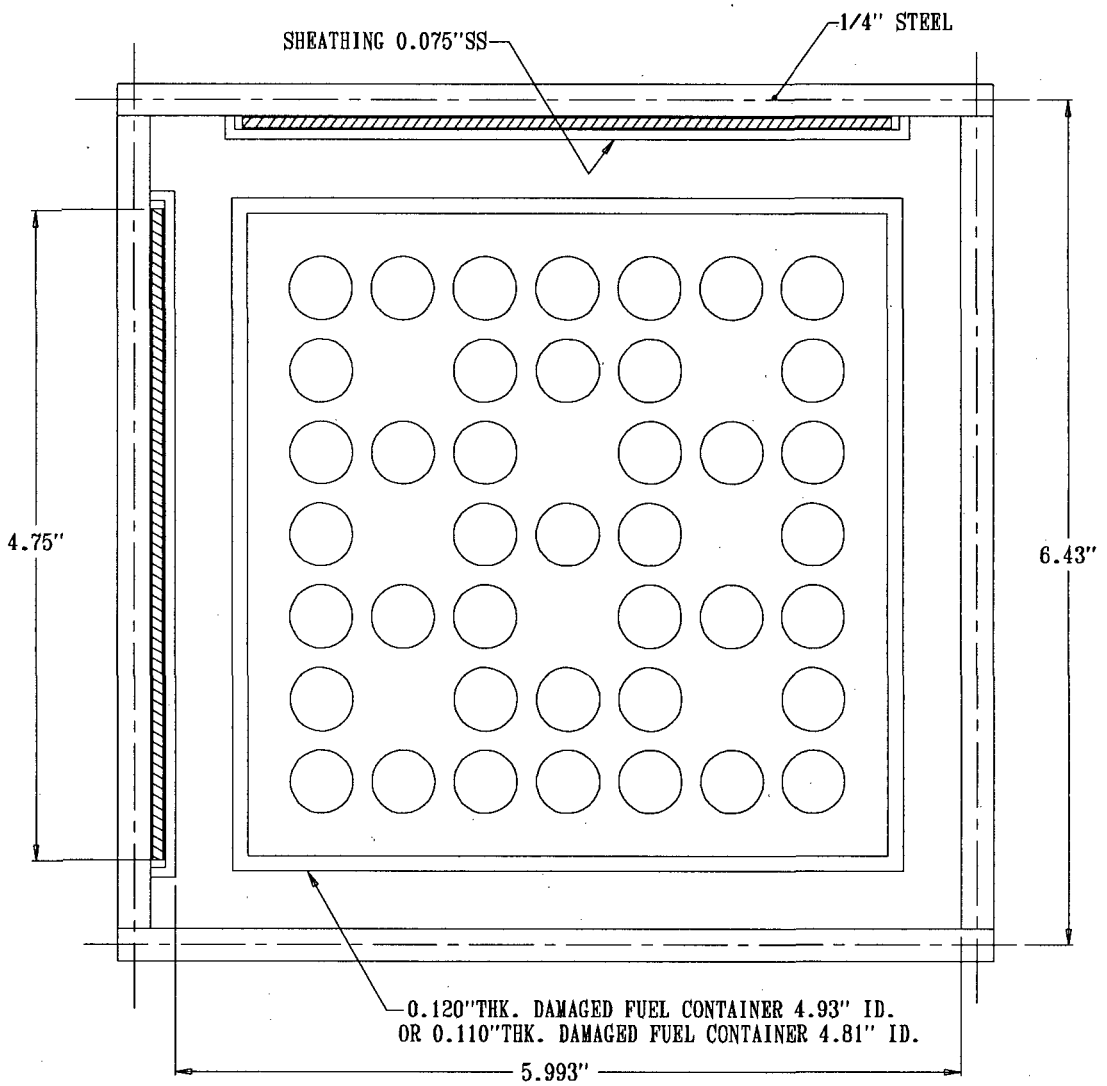

FIGURE 6.4.5; FAILED FUEL CALCULATION MODEL (PLANAR CROSS-SECTION) WITH 7X7 ARRAY WITH 8 MISSING RODS IN THE MPC-68 BASKET (SEE CHAPTER 1 FOR TRUE BASKET DIMENSIONS)

NOTE: THESE DIMENSIONS WERE CONSERVATIVELY USED FOR CRITICALITY ANALYSES.

REPORT HI-951251 | REVISION 9

@\PROJECTS\5014\HI951251\CH_6\6_4_5

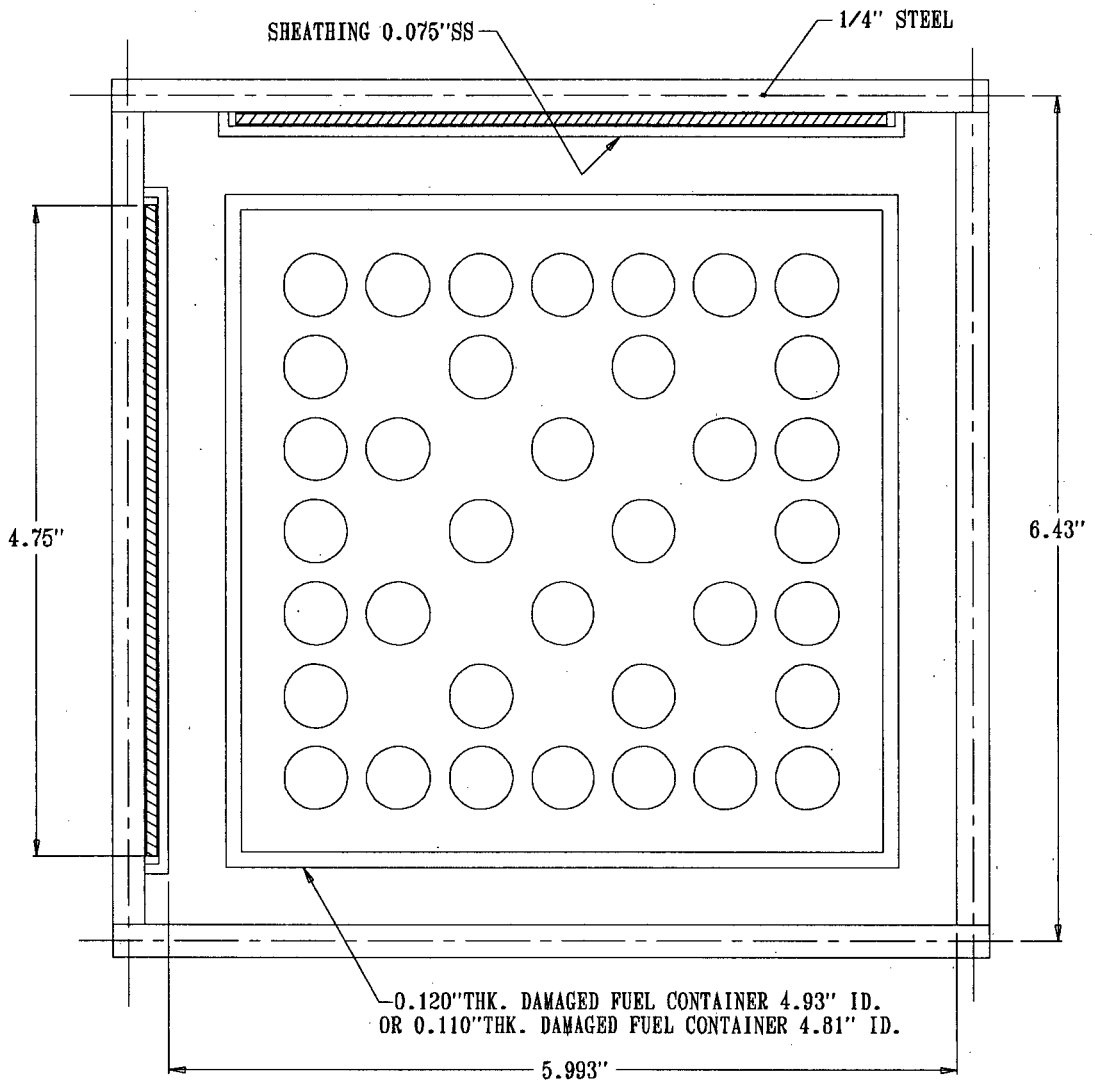

FIGURE 6.4.6; FAILED FUEL CALCULATION MODEL (PLANAR CROSS-SECTION) WITH 7X7 ARRAY WITH 13 MISSING RODS IN THE MPC-68 BASKET (SEE CHAPTER 1 FOR TRUE BASKET DIMENSIONS)

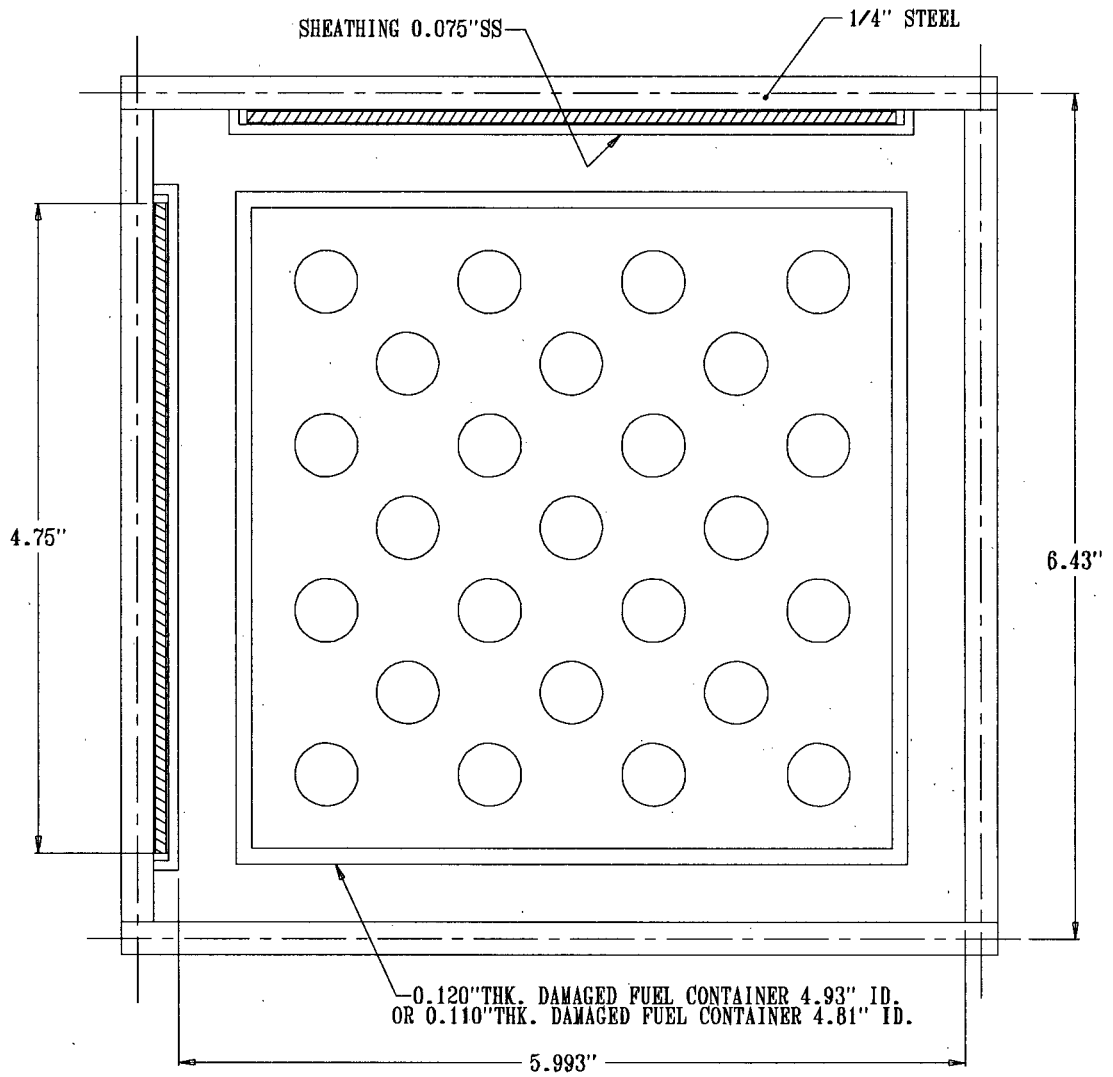

FIGURE 6.4.7; FAILED FUEL CALCULATION MODEL (PLANAR CROSS-SECTION) WITH 7X7 ARRAY WITH 24 MISSING RODS IN THE MPC-68 BASKET (SEE CHAPTER 1 FOR TRUE BASKET DIMENSIONS)

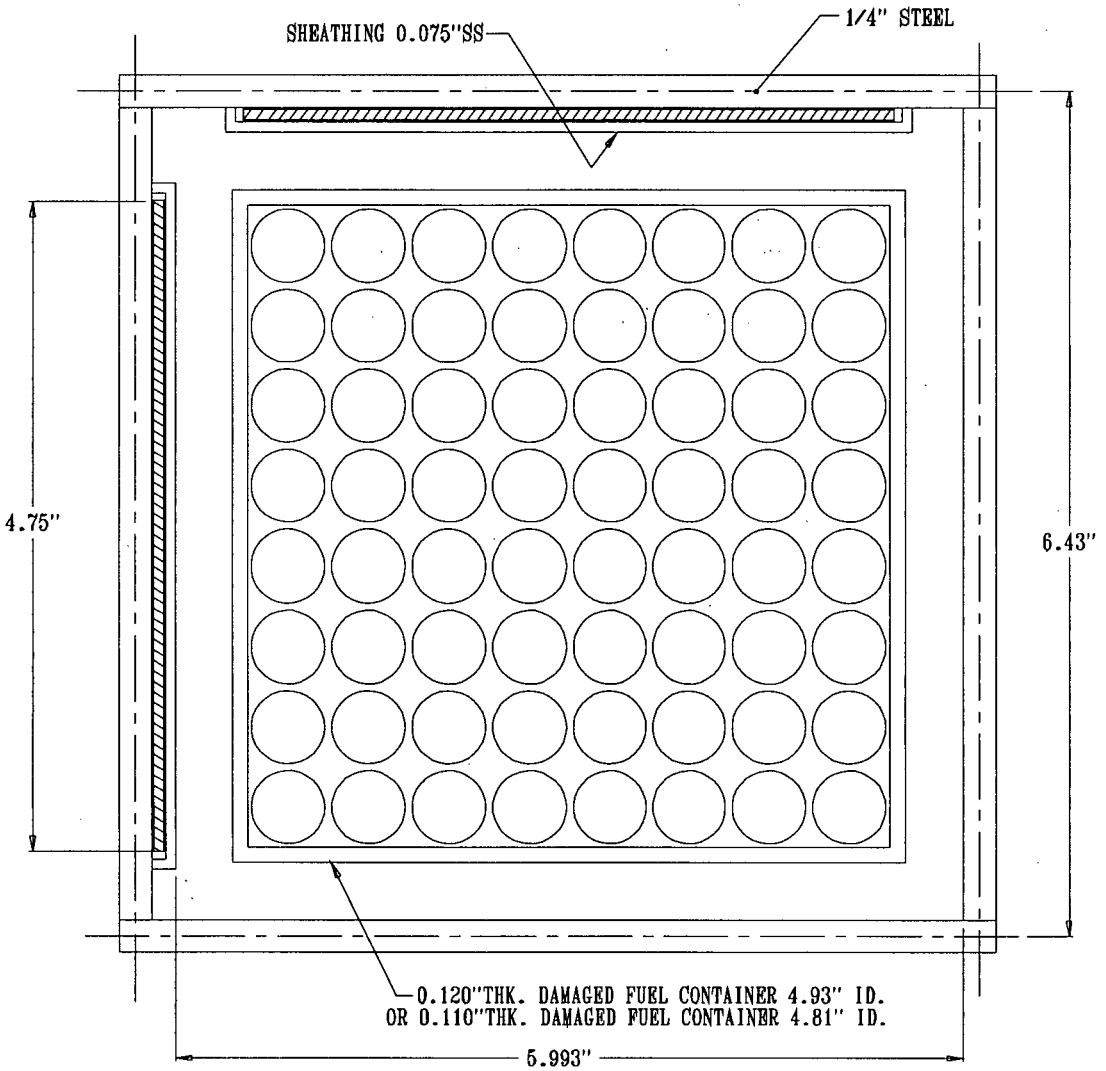

FIGURE 6.4.8; FAILED FUEL CALCULATION MODEL (PLANAR CROSS-SECTION) WITH DAMAGED FUEL COLLAPSED INTO 8X8 ARRAY IN THE MPC-68 BASKET (SEE CHAPTER 1 FOR TRUE BASKET DIMENSIONS)

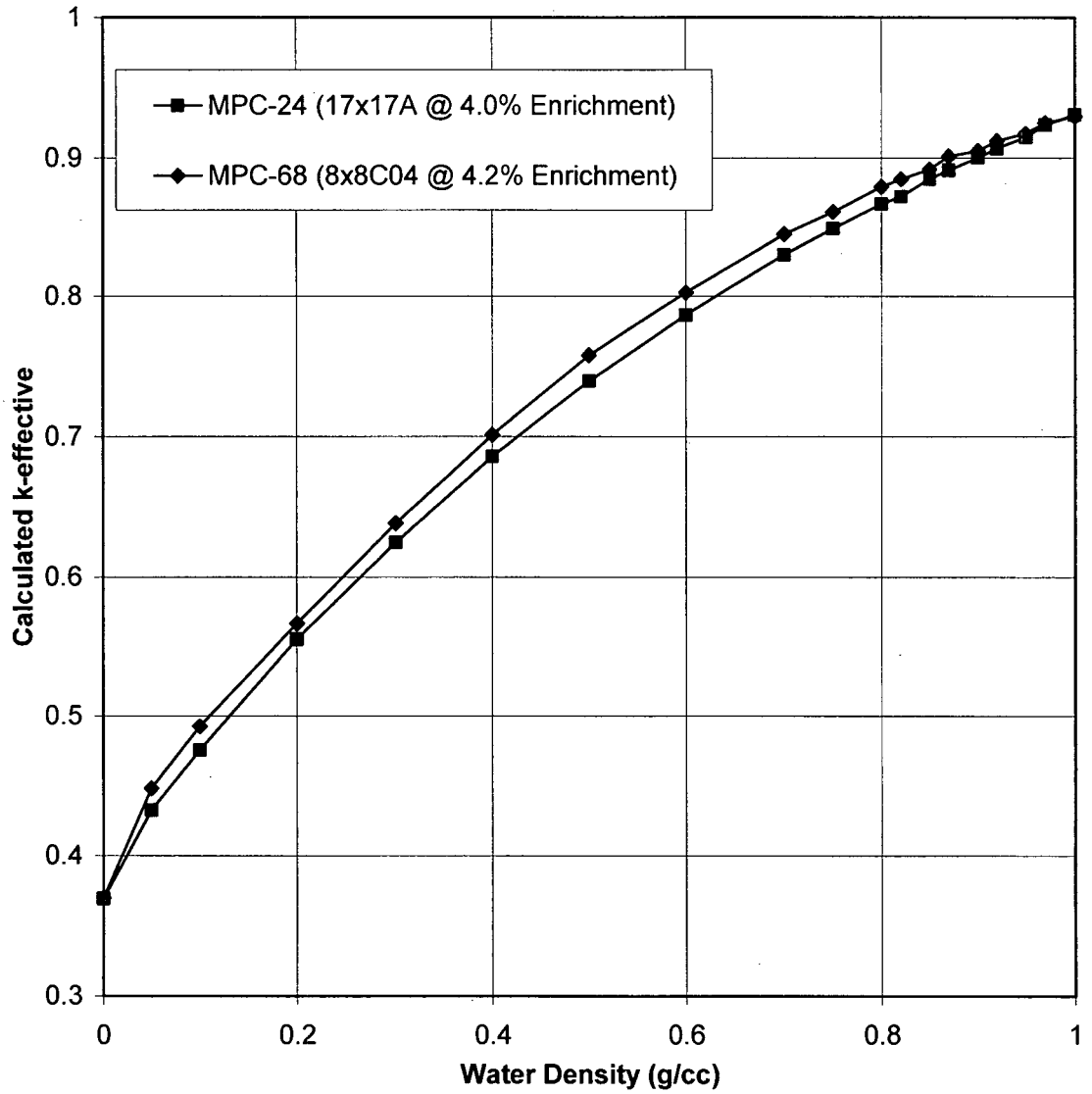

FIGURE 6.4.9; CALCULATED K-EFFECTIVE AS A FUNCTION OF INTERNAL MODERATOR DENSITY

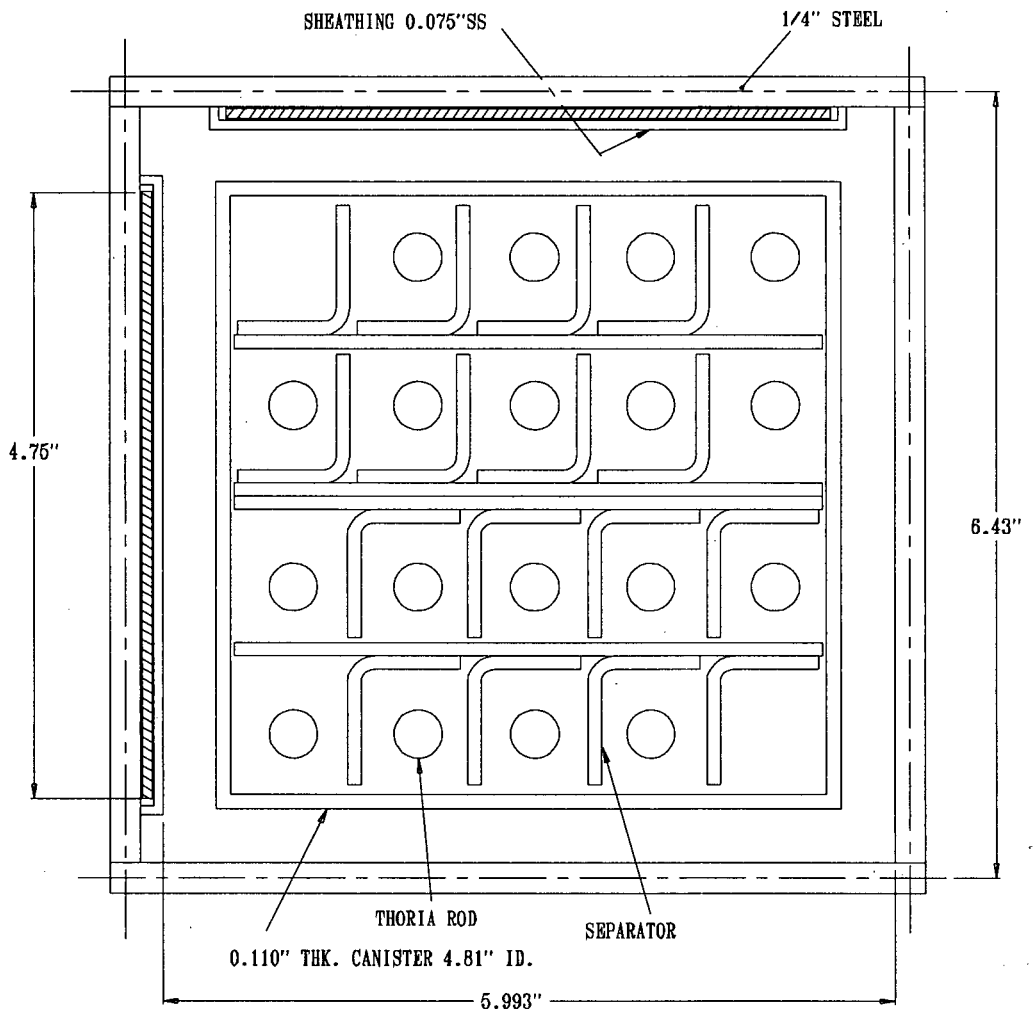

FIGURE 6.4.10; THORIA ROD CANISTER (PLANAR CROSS-SECTION) WITH 18 THORIA RODS IN THE MPC-68 BASKET (SEE CHAPTER 1 FOR TRUE BASKET DIMENSIONS)

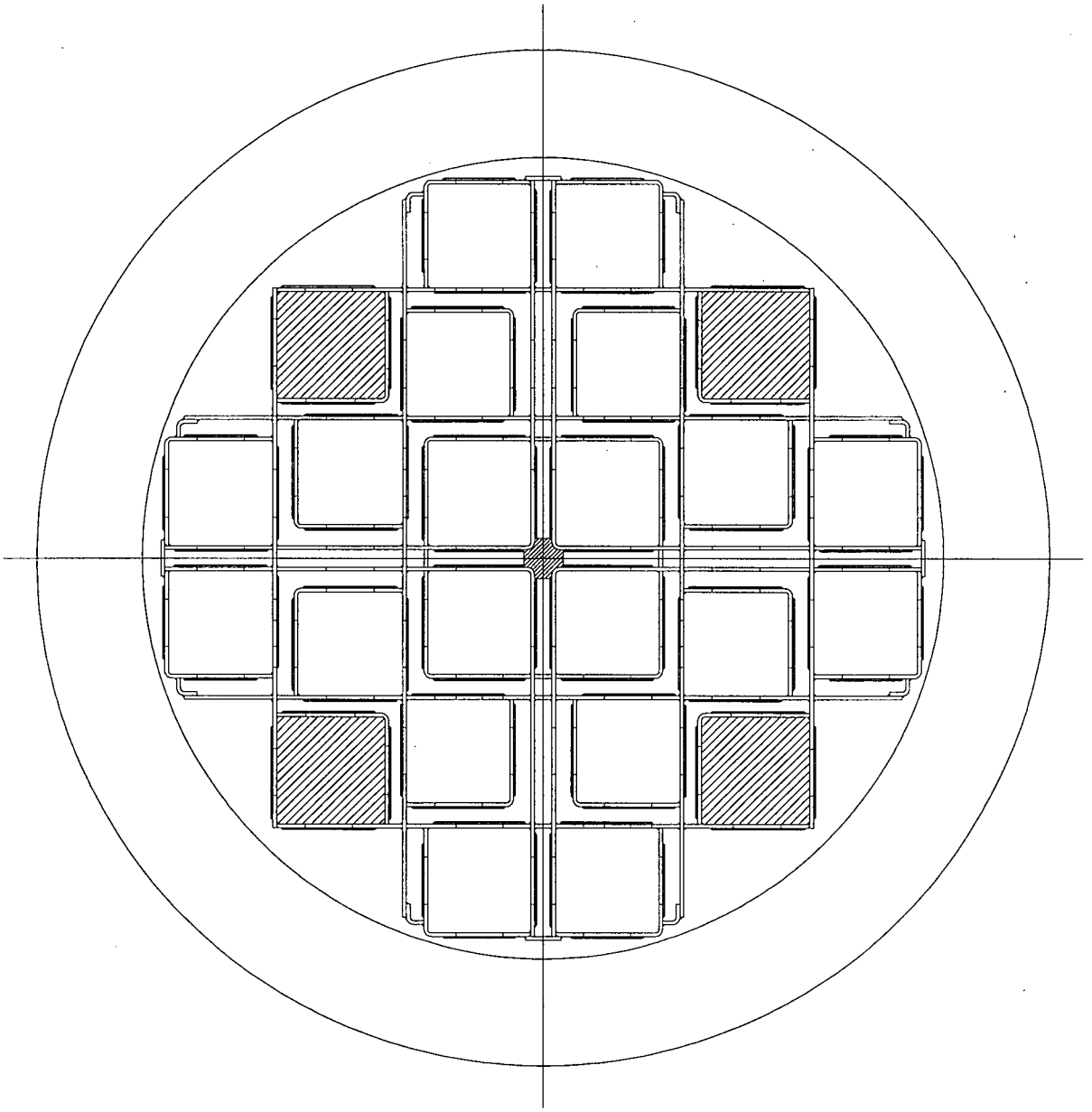

FIGURE 6.4.11: LOCATIONS OF THE DAMAGED FUEL CONTAINERS IN THE MPC-24E/EF

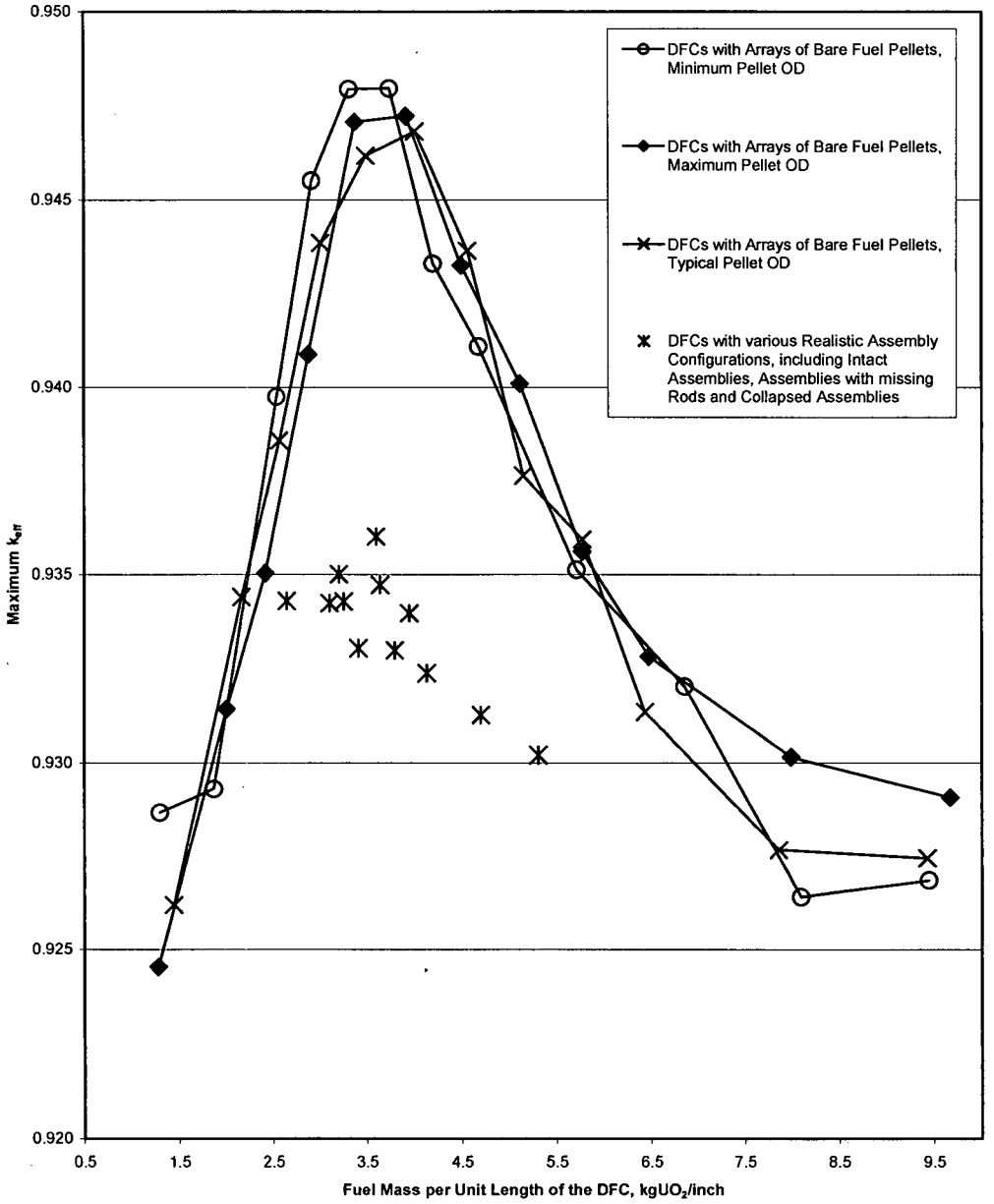

FIGURE 6.4.12: MAXIMUM K_{EFF} FOR THE MPC-24E/EF WITH GENERIC PWR DAMAGED FUEL CONTAINER, INITIAL ENRICHMENT OF 4.0 WT% FOR DAMAGED AND INTACT FUEL.

6.5 CRITICALITY BENCHMARK EXPERIMENTS

Benchmark calculations have been made on selected critical experiments, chosen, insofar as possible, to bound the range of variables in the cask designs. The most important parameters are (1) the enrichment, (2) the water-gap size (MPC-24) or cell spacing (MPC-68), and (3) the ^{10}B loading of the neutron absorber panels. Other parameters, within the normal range of cask and fuel designs, have a smaller effect, but are also included. No significant trends were evident in the benchmark calculations or the derived bias. Detailed benchmark calculations are presented in Appendix 6.A.

The benchmark calculations were performed with the same computer codes and cross-section data, described in Section 6.4, that were used to calculate the k_{eff} values for the cask. Further, all calculations were performed on the same computer hardware, specifically, personal computers using the pentium processor.

Additional benchmark calculations performed for the burnup methodology for the MPC-32 are presented in Appendix 6.E.

6.6 REGULATORY COMPLIANCE

This chapter documents the criticality evaluation of the HI-STAR 100 System for the packaging and transportation of radioactive materials (spent nuclear fuel). This evaluation demonstrates that the HI-STAR 100 System is in full compliance with the criticality safety requirements of 10CFR71.

The criticality design is based on favorable geometry, fixed neutron poisons (Boral), and an administrative limit on the maximum allowable enrichment and the minimum allowable burnup in the MPC-32. The HI-STAR 100 System design structures and components important to criticality safety are described in sufficient detail in this chapter to identify the package accurately and provide a sufficient basis for the evaluation of the package, including the maximum allowable enrichments and minimum allowable burnups.

The HI-STAR 100 System is designed to be subcritical under both normal and hypothetical accident conditions of transport. The evaluations presented in the chapter address the criticality safety requirements of 10CFR71 and demonstrate that a single HI-STAR 100 System remains subcritical under the most reactive normal and hypothetical accident conditions of transport and that the most reactive infinite array of HI-STAR 100 Systems is subcritical under both normal and hypothetical accident conditions of transport. This corresponds to a transport index of zero (0) and demonstrates compliance with 10CFR71 criticality requirements.

Therefore, it is concluded that the criticality design features for the HI-STAR 100 System are in compliance with 10CFR71 and that the applicable design and acceptance criteria have been satisfied. This criticality evaluation provides reasonable assurance that the HI-STAR 100 System will allow safe transport of spent fuel.

6.7 REFERENCES

[6.1.1] U.S. Code of Federal Regulations, "Packaging and Transportation of Radioactive Materials," Title 10, Part 71.

[6.1.2] NUREG-1617, Standard Review Plan for Transportation Packages for Spent Nuclear Fuel, USNRC, Washington, D.C., March 2000.

[6.1.3] USNRC Standard Review Plan, NUREG-0800, Section 9.1.2, Spent Fuel Storage, Rev. 2 - July 1981.

[6.1.4] J.F. Briesmeister, Ed., "MCNP - A General Monte Carlo N-Particle Transport Code, Version 4A," Los Alamos National Laboratory, LA-12625-M (1993).

[6.1.5] L.M. Petrie and N.F. Landers, "KENOVa - An Improved Monte Carlo Criticality Program with Supergrouping," Volume 2, Section F11 from "SCALE: A Modular System for Performing Standardized Computer Analysis for Licensing Evaluation," NUREG/CR-0200, Rev. 4, January 1990.

[6.1.6] N.M. Greene, L.M. Petrie and R.M. Westfall, "NITAWL-II: Scale System Module For Performing Resonance Shielding and Working Library Production," Volume 1, Section F1 from "SCALE: A Modular System for Performing Standardized Computer Analysis for Licensing Evaluation," NUREG/CR-0200, Rev. 4, January 1990.

[6.1.7] J.R. Knight, "SUPERDAN: Computer Programs for Calculating the Dancoff Factor of Spheres, Cylinders, and Slabs," Oak Ridge National Laboratory, ORNL/NUREG/CSD/TM-2, March 1978, with correction published in "Proceedings of Seminar on SCALE-4," Saclay, France, 1991.

[6.1.8] M.G. Natrella, Experimental Statistics, National Bureau of Standards, Handbook 91, August 1963.

[6.1.9] Deleted

[6.1.10] "CASMO-4 Methodology", Studsvik/SOA-95/2, Rev. 0, 1995.

[6.1.11] "CASMO-4 A Fuel Assembly Burnup Program, Users Manual," SSP-01/400, Rev. 1, Studsvik Scandpower, Inc., 2001.

[6.1.12] "CASMO-4 Benchmark Against Critical Experiments", Studsvik/SOA-94/13, Studsvik of America, 1995.

[6.1.13] "QA Validation Manual for Computer Code CELLDAN," Holtec International Report HI-90577.

[6.3.1] A. Ahlin, M. Edenius, and H. Haggblom, "CASMO - A Fuel Assembly Burnup Program," AE-RF-76-4158, Studsvik report.

[6.3.2] A. Ahlin and M. Edenius, "CASMO - A Fast Transport Theory Depletion Code for LWR Analysis," *Trans. Am. Nucl. Soc.*, **26**, 604 (1977).

[6.3.3] "CASMO-3 A Fuel Assembly Burnup Program, Users Manual," Studsvik/NFA-87/7, Studsvik Energitechnik AB, November 1986.

[6.3.4] M. Edenius and A. Ahlin, "CASMO-3: New Features, Benchmarking, and Advanced Applications," *Nucl. Sci. Eng.*, **100**, 342-351, (1988).

[6.4.1] "SCALE 4.3: A Modular System for Performing Standardized Computer Analysis for Licensing Evaluations," NUREG-CR-0200, Rev. 5, Oak Ridge National Laboratory (1995).

[6.4.2] J.M. Cano, R. Caro, and J.M Martinez-Val, "Supercriticality Through Optimum Moderation in Nuclear Fuel Storage," *Nucl. Technol.*, **48**, 251-260, (1980).

APPENDIX 6.A: BENCHMARK CALCULATIONS

6.A.1 INTRODUCTION AND SUMMARY

Benchmark calculations have been made on selected critical experiments, chosen, in so far as possible, to bound the range of variables in the cask designs. Two independent methods of analysis were used, differing in cross section libraries and in the treatment of the cross sections. MCNP4a [6.A.1] is a continuous energy Monte Carlo code and KENO5a [6.A.2] uses group-dependent cross sections. For the KENO5a analyses reported here, the 238-group library was chosen, processed through the NITAWL-II [6.A.2] program to create a working library and to account for resonance self-shielding in uranium-238 (Nordheim integral treatment). The 238 group library was chosen to avoid or minimize the errors[†] (trends) that have been reported (e.g., [6.A.3 through 6.A.5]) for calculations with collapsed cross section sets.

The results of the benchmark calculations presented herein are separated into two parts. The first part (Sections 6.A.1 through 6.A.5) presents the calculational bias for fresh fuel calculations and encompasses the benchmark critical experiments numbered 1 through 62 in Table 6.A.1. The second part (Section 6.A.6) presents the calculational bias for burnup credit and encompasses all of the benchmark critical experiments presented in Table 6.A.1.

In cask designs, the three most significant parameters affecting criticality are (1) the fuel enrichment, (2) the ^{10}B loading in the neutron absorber, and (3) the lattice spacing (or water-gap thickness if a flux-trap design is used). Other parameters, within the normal range of cask and fuel designs, have a smaller effect, but are also included in the analyses.

Table 6.A.1 summarizes results of the benchmark calculations for all cases selected and analyzed, as referenced in the table. The effect of the major variables are discussed in subsequent sections below. It is important to note that there is obviously considerable overlap in parameters since it is not possible to vary a single parameter and maintain criticality; some other parameter or parameters must be concurrently varied to maintain criticality.

One possible way of representing the data is through a spectrum index that incorporates all of the variations in parameters. KENO5a computes and prints the "energy of the average lethargy causing fission". In MCNP4a, by utilizing the tally option with the identical 238-group energy structure as in KENO5a, the number of fissions in each group may be collected and the energy of the average lethargy causing fission determined (post-processing).

Figures 6.A.1 and 6.A.2 show the calculated k_{eff} for the benchmark critical experiments as a function of the "energy of the average lethargy causing fission" for MCNP4a and KENO5a, respectively (UO_2 fuel only). The scatter in the data (even for comparatively minor variation in

[†] Small but observable trends (errors) have been reported for calculations with the 27-group and 44-group collapsed libraries. These errors are probably due to the use of a single collapsing spectrum when the spectrum should be different for the various cases analyzed, as evidenced by the spectrum indices.

critical parameters) represents experimental error[††] in performing the critical experiments within each laboratory, as well as between the various testing laboratories. The B&W critical experiments show a larger experimental error than the PNL criticals. This would be expected since the B&W criticals encompass a greater range of critical parameters than the PNL criticals.

Linear regression analysis of the data in Figures 6.A.1 and 6.A.2 show that there are no trends, as evidenced by very low values of the correlation coefficient (0.13 for MCNP4a and 0.21 for KENO5a). The total bias (systematic error, or mean of the deviation from a k_{eff} of exactly 1.000) for the two methods of analysis are shown in the table below.

Calculational Bias of MCNP4a and KENO5a		
	Total	Truncated
MCNP4a	0.0009 ± 0.0011	0.0021 ± 0.0007
KENO5a	0.0030 ± 0.0012	0.0036 ± 0.0009

The values of bias shown in this table include both the bias derived directly from the calculated k_{eff} values in Table 6.A.1, and a more conservative value derived by arbitrarily truncating to 1.000 any calculated value that exceeds 1.000. The bias and standard error of the bias were calculated by the following equations[†], with the standard error multiplied by the one-sided K-factor for 95% probability at the 95% confidence level from NBS Handbook 91 [6.A.18] (for the number of cases analyzed, the K-factor is ~2.05 or slightly more than 2).

$$\bar{k} = \frac{1}{n}\sum_{i=1}^{n} k_i \qquad (6.A.1)$$

$$\sigma_{\bar{k}}^2 = \frac{\sum_{i=1}^{n} k_i^2 - (\sum_{i=1}^{n} k_i)^2 / n}{n(n-1)} \qquad (6.A.2)$$

$$\text{Bias} = (1 - \bar{k}) \pm K\sigma_{\bar{k}} \qquad (6.A.3)$$

where k_i are the calculated reactivities for n critical experiments; $\sigma_{\bar{k}}$ is the unbiased estimator of the standard deviation of the mean (also called the standard error of the bias (mean)); and K is the one-sided multiplier for 95% probability at the 95% confidence level (NBS Handbook 91 [6.A.18]).

[††] A classical example of experimental error is the corrected enrichment in the PNL experiments, first as an addendum to the initial report and, secondly, by revised values in subsequent reports for the same fuel rods.

[†]These equations may be found in any standard text on statistics, for example, reference [6.A.6] (or the MCNP4a manual) and is the same methodology used in MCNP4a and in KENO5a.

Formula 6.A.3 is based on the methodology of the National Bureau of Standards (now NIST) and is used to calculate the values presented on page 6.A-2. The first portion of the equation, $(1-\bar{k})$, is the actual bias which is added to the MCNP4a and KENO5a results. The second term, $K\sigma_{\bar{k}}$, which corresponds to σ_B in Section 6.4.3, is the uncertainty or standard error associated with the bias. The K values used were obtained from the National Bureau of Standards Handbook 91 and are for one-sided statistical tolerance limits for 95% probability at the 95% confidence level. The actual K values for the 56 critical experiments evaluated with MCNP4a and the 53 critical experiments evaluated with KENO5a are 2.04 and 2.05, respectively.

The larger of the calculational biases (truncated bias) was used to evaluate the maximum k_{eff} values for the cask designs.

6.A.2 Effect of Enrichment

The benchmark critical experiments include those with enrichments ranging from 2.46% to 5.74% and therefore span the enrichment range for the MPC designs. Figures 6.A.3 and 6.A.4 show the calculated k_{eff} values (Table 6.A.1) as a function of the fuel enrichment reported for the critical experiments. Linear regression analyses for these data confirms that there are no trends, as indicated by low values of the correlation coefficients (0.08 for MCNP4a and 0.37 for KENO5a). Thus, there are no corrections to the bias for the various enrichments.

As further confirmation of the absence of any trends with enrichment, the MPC-68 configuration was calculated with both MCNP4a and KENO5a for various enrichments. The cross-comparison of calculations with codes of comparable sophistication is suggested in Reg. Guide 3.41. Results of this comparison, shown in Table 6.A.2 and Figure 6.A.5, confirm no significant difference in the calculated values of k_{eff} for the two independent codes as evidenced by the 45° slope of the curve. Since it is very unlikely that two independent methods of analysis would be subject to the same error, this comparison is considered confirmation of the absence of an enrichment effect (trend) in the bias.

6.A.3 Effect of ^{10}B Loading

Several laboratories have performed critical experiments with a variety of thin absorber panels similar to the Boral panels in the cask designs. Of these critical experiments, those performed by B&W are the most representative of the cask designs. PNL has also made some measurements with absorber plates, but, with one exception (a flux-trap experiment), the reactivity worth of the absorbers in the PNL tests is very low and any significant errors that might exist in the treatment of strong thin absorbers could not be revealed.

Table 6.A.3 lists the subset of experiments using thin neutron absorbers (from Table 6.A.1) and shows the reactivity worth (Δk) of the absorber.[†]

[†]The reactivity worth of the absorber panels was determined by repeating the calculation with the absorber analytically removed and calculating the incremental (Δk) change in reactivity due to the absorber.

No trends with reactivity worth of the absorber are evident, although based on the calculations shown in Table 6.A.3, some of the B&W critical experiments seem to have unusually large experimental errors. B&W made an effort to report some of their experimental errors. Other laboratories did not evaluate their experimental errors.

To further confirm the absence of a significant trend with ^{10}B concentration in the absorber, a cross-comparison was made with MCNP4a and KENO5a (as suggested in Reg. Guide 3.41). Results are shown in Figure 6.A.6 and Table 6.A.4 for the MPC-68 cask[††] geometry. These data substantiate the absence of any error (trend) in either of the two codes for the conditions analyzed (data points fall on a 45° line, within an expected 95% probability limit).

6.A.4 Miscellaneous and Minor Parameters

6.A.4.1 Reflector Material and Spacings

PNL has performed a number of critical experiments with thick steel and lead reflectors.[†] Analysis of these critical experiments are listed in Table 6.A.5 (subset of data in Table 6.A.1). There appears to be a small tendency toward overprediction of k_{eff} at the lower spacing, although there are an insufficient number of data points in each series to allow a quantitative determination of any trends. The tendency toward overprediction at close spacing means that the cask calculations may be slightly more conservative than otherwise.

6.A.4.2 Fuel Pellet Diameter and Lattice Pitch

The critical experiments selected for analysis cover a range of fuel pellet diameters from 0.311 to 0.444 inches, and lattice spacings from 0.476 to 1.00 inches. In the cask designs, the fuel pellet diameters range from 0.303 to 0.3835 inches O.D. (0.496 to 0.580 inch lattice spacing) for PWR fuel and from 0.3224 to 0.498 inches O.D. (0.488 to 0.740 inch lattice spacing) for BWR fuel. Thus, the critical experiments analyzed provide a reasonable representation of the fuel in the MPC designs. Based on the data in Table 6.A.1, there does not appear to be any observable trend with either fuel pellet diameter or lattice pitch, at least over the range of the critical experiments or the cask designs.

6.A.4.3 Soluble Boron Concentration Effects

Various soluble boron concentrations were used in the B&W series of critical experiments and in one PNL experiment, with boron concentrations ranging up to 2550 ppm. Results of MCNP4a (and one KENO5a) calculations are shown in Table 6.A.6. Analyses of the very high boron

[††]The MPC-68 geometry was chosen for this comparison since it contains the greater number of Boral panels and would therefore be expected to be the most sensitive to trends (errors) in calculations.

[†]Parallel experiments with a depleted uranium reflector were also performed but not included in the present analysis since they are not pertinent to the Holtec cask design. A lead reflector is also not directly pertinent, but might be used in future designs.

concentration experiments (>1300 ppm) show a tendency to slightly overpredict reactivity for the three experiments exceeding 1300 ppm.

6.A.5 MOX Fuel Critical Experiments

The number of critical experiments with PuO_2 bearing fuel (MOX) is more limited than for UO_2 fuel. However, a number of MOX critical experiments have been analyzed and the results are shown in Table 6.A.7. Results of these analyses are generally above a k_{eff} of 1.00, indicating that when Pu is present, MCNP4a and KENO5a overpredict the reactivity.

This may indicate that calculation of k_{eff} for MOX fuel will be expected to be conservative, especially with MCNP4a. It may be noted that for the larger lattice spacings, the KENO5a calculated reactivities are below 1.00, suggested that a small trend may exist with KENO5a. It is also possible that the overprediction in k_{eff} in both codes may be due to a small inadequacy in the determination of the Pu-241 decay and Am-241 growth. This possibility is supported by the consistency in calculated k_{eff} over a wide range of the spectral index (energy of the average lethargy causing fission).

6.A.6 Burnup Credit Benchmark Experiments

The use of burnup credit in a spent fuel transportation cask license requires benchmarking of the appropriate codes to spent fuel critical experiments. However, spent fuel critical experiments are not available, therefore benchmarking with an extended set of mixed oxide fuel critical experiments is performed. Fifty MOX fuel critical experiments (31 from reference [6.A.21], eight additional MOX critical experiments from Section 6.A.5 and eleven MOX critical experiments from [6.A.22]) have been selected for validating MCNP4a for burnup credit. The total bias (systematic error, or mean of the deviation from a k_{eff} of exactly 1.000) for MCNP4a for the entire set of 98 critical experiments identified in Table 6.A.1 is shown in the table below.

Calculational Bias of MCNP4a and KENO5a		
	Total	Truncated
MCNP4a	-0.0004 ± 0.0008	0.0015 ± 0.0004

The values of bias shown in this table include both the bias derived directly from the calculated k_{eff} values in Table 6.A.1, and a more conservative value derived by arbitrarily truncating to 1.000 any calculated value that exceeds 1.000. The bias and standard error of the bias were calculated with the equations in Section 6.A.1, with the standard error multiplied by the one-sided K-factor for 95% probability at the 95% confidence level from NBS Handbook 91 [6.A.18] (for the number of cases analyzed, the K-factor is ~1.95 or slightly less than 2).

6.A.6.1 Effect of EALF

Figure 6.A.7 shows the MOX fuel calculated k_{eff} values as a function of the calculated EALF from MCNP4a during post-processing as described in Section 6.A.1. Linear regression analysis for this data confirms that the MCNP4a results do not exhibit any trends with respect to the

EALF as evidenced by the low value of the correlation coefficient (-0.03). Thus there is no correction to the bias as a function of the EALF.

6.A.6.2 Effect of Cladding OD

The MOX critical experiments selected for analysis cover a range of cladding outside diameters from 0.230 to 0.565 inches. In the Holtec cask designs, the allowable cladding outside diameters range from 0.342 to 0.440 inches O.D. for PWR fuel and from 0.378 to 0.563 inches O.D. for BWR and PWR fuel. Thus, the critical experiments analyzed provide a reasonable representation of the fuel in the MPC designs. Linear regression analysis for this data confirms that the MCNP4a results do not exhibit any trends with respect to the Cladding O.D. as evidenced by the low value of the correlation coefficient (-0.17). Thus there is no correction to the bias as a function of the Cladding O.D.

6.A.7 References

[6.A.1] J.F. Briesmeister, Ed., "MCNP - A General Monte Carlo N-Particle Transport Code, Version 4A; Los Alamos National Laboratory, LA-12625-M (1993).

[6.A.2] SCALE 4.3, "A Modular Code System for Performing Standardized Computer Analyses for Licensing Evaluation", NUREG-0200 (ORNL-NUREG-CSD-2/U2/R5, Revision 5, Oak Ridge National Laboratory, September 1995.

[6.A.3] M.D. DeHart and S.M. Bowman, "Validation of the SCALE Broad Structure 44-G Group ENDF/B-Y Cross-Section Library for Use in Criticality Safety Analyses", NUREG/CR-6102 (ORNL/TM-12460) Oak Ridge National Laboratory, September 1994.

[6.A.4] W.C. Jordan et al., "Validation of KENOV.a", CSD/TM-238, Martin Marietta Energy Systems, Inc., Oak Ridge National Laboratory, December 1986.

[6.A.5] O.W. Hermann et al., "Validation of the Scale System for PWR Spent Fuel Isotopic Composition Analysis", ORNL-TM-12667, Oak Ridge National Laboratory, undated.

[6.A.6] R.J. Larsen and M.L. Marx, An Introduction to Mathematical Statistics and its Applications, Prentice-Hall, 1986.

[6.A.7] M.N. Baldwin et al., Critical Experiments Supporting Close Proximity Water Storage of Power Reactor Fuel, BAW-1484-7, Babcock and Wilcox Company, July 1979.

[6.A.8] G.S. Hoovier et al., Critical Experiments Supporting Underwater Storage of Tightly Packed Configurations of Spent Fuel Pins, BAW-1645-4, Babcock & Wilcox Company, November 1991.

[6.A.9] L.W. Newman et al., Urania Gadolinia: Nuclear Model Development and Critical Experiment Benchmark, BAW-1810, Babcock and Wilcox Company, April 1984.

[6.A.10] J.C. Manaranche et al., "Dissolution and Storage Experimental Program with 4.75% Enriched Uranium-Oxide Rods," Trans. Am. Nucl. Soc. 33: 362-364 (1979).

[6.A.11] S.R. Bierman and E.D. Clayton, Criticality Experiments with Subcritical Clusters of 2.35 wt % and 4.31 wt % ^{235}U Enriched UO_2 Rods in Water with Steel Reflecting Walls, PNL-3602, Battelle Pacific Northwest Laboratory, April 1981.

[6.A.12] S.R. Bierman et al., Criticality Experiments with Subcritical Clusters of 2.35 Wt% and 4.31 Wt% ^{235}U Enriched UO_2 Rods in Water with Uranium or Lead Reflecting Walls, PNL-3926, Battelle Pacific Northwest Laboratory, December, 1981.

[6.A.13] S.R. Bierman et al., Critical Separation Between Subcritical Clusters of 4.31 Wt % ^{235}U Enriched UO_2 Rods in Water with Fixed Neutron Poisons, PNL-2615, Battelle Pacific Northwest Laboratory, October 1977.

[6.A.14] S.R. Bierman, Criticality Experiments with Neutron Flux Traps Containing Voids, PNL-7167, Battelle Pacific Northwest Laboratory, April 1990.

[6.A.15] B.M. Durst et al., Critical Experiments with 4.31 wt % ^{235}U Enriched UO_2 Rods in Highly Borated Water Lattices, PNL-4267, Battelle Pacific Northwest Laboratory, August 1982.

[6.A.16] S.R. Bierman, Criticality Experiments with Fast Test Reactor Fuel Pins in Organic Moderator, PNL-5803, Battelle Pacific Northwest Laboratory, December 1986.

[6.A.17] E.G. Taylor et al., Saxton Plutonium Program Critical Experiments for the Saxton Partial Plutonium core, WCAP-3385-54, Westinghouse Electric Corp., Atomic Power Division, December 1965.

[6.A.18] M.G. Natrella, Experimental Statistics, National Bureau of Standards, Handbook 91, August 1963.

[6.A.19] R. I. Smith and G.J. Konzek, April 1976 and September 1978. *Clean Critical Experiment Benchmarks for Plutonium Recycle in LWRs,* Volumes I and II, EPRI NP-196, Electric Power Research Institute.

[6.A.20] V. O. Uotinen, et al., August 1972. "Lattices of Plutonium-Enriched Rods in Light Water – Part I: Experimental Results," *Nuclear Technology,* 15, 257.

[6.A.21] *Topical Report on Actinide-Only Burnup Credit for PWR Spent Nuclear Fuel Packages,* DOE/RW-0472, Rev. 1, U.S. Department of Energy, Office of Civilian Radioactive Waste Management, May 1997.

[6.A.22] "Critical Arrays of Mixed Plutonium-Uranium Fuel Rods with Water-to-Fuel Volume Ratios Ranging from 2.4 to 5.6", from "*International Handbook of Evaluated Criticality Safety Benchmark Experiments", NEA/NSC/DOC(95)03, Volume VI, MIX-COMP-THERM-004*

Table 6.A.1
Summary of Criticality Benchmark Calculations

	Reference	Identification	Enrich.	Calculated k_{eff} MCNP4a	Calculated k_{eff} KENO5a	EALF (eV) MCNP4a	EALF (eV) KENO5a
1	B&W-1484 (6.A.7)	Core I	2.46	0.9964 ± 0.0010	0.9898 ± 0.0006	0.1759	0.1753
2	B&W-1484 (6.A.7)	Core II	2.46	1.0008 ± 0.0011	1.0015 ± 0.0005	0.2553	0.2446
3	B&W-1484 (6.A.7)	Core III	2.46	1.0010 ± 0.0012	1.0005 ± 0.0005	0.1999	0.1939
4	B&W-1484 (6.A.7)	Core IX	2.46	0.9956 ± 0.0012	0.9901 ± 0.0006	0.1422	0.1426
5	B&W-1484 (6.A.7)	Core X	2.46	0.9980 ± 0.0014	0.9922 ± 0.0006	0.1513	0.1499
6	B&W-1484 (6.A.7)	Core XI	2.46	0.9978 ± 0.0012	1.0005 ± 0.0005	0.2031	0.1947
7	B&W-1484 (6.A.7)	Core XII	2.46	0.9988 ± 0.0011	0.9978 ± 0.0006	0.1718	0.1662
8	B&W-1484 (6.A.7)	Core XIII	2.46	1.0020 ± 0.0010	0.9952 ± 0.0006	0.1988	0.1965
9	B&W-1484 (6.A.7)	Core XIV	2.46	0.9953 ± 0.0011	0.9928 ± 0.0006	0.2022	0.1986
10	B&W-1484 (6.A.7)	Core XV††	2.46	0.9910 ± 0.0011	0.9909 ± 0.0006	0.2092	0.2014
11	B&W-1484 (6.A.7)	Core XVI††	2.46	0.9935 ± 0.0010	0.9889 ± 0.0006	0.1757	0.1713
12	B&W-1484 (6.A.7)	Core XVII	2.46	0.9962 ± 0.0012	0.9942 ± 0.0005	0.2083	0.2021

Table 6.A.1
Summary of Criticality Benchmark Calculations

	Reference	Identification	Enrich.	Calculated k_{eff} MCNP4a	Calculated k_{eff} KENO5a	EALF (eV) MCNP4a	EALF (eV) KENO5a
13	B&W-1484 (6.A.7)	Core XVIII	2.46	1.0036 ± 0.0012	0.9931 ± 0.0006	0.1705	0.1708
14	B&W-1484 (6.A.7)	Core XIX	2.46	0.9961 ± 0.0012	0.9971 ± 0.0005	0.2103	0.2011
15	B&W-1484 (6.A.7)	Core XX	2.46	1.0008 ± 0.0011	0.9932 ± 0.0006	0.1724	0.1701
16	B&W-1484 (6.A.7)	Core XXI	2.46	0.9994 ± 0.0010	0.9918 ± 0.0006	0.1544	0.1536
17	B&W-1645 (6.A.8)	S-type Fuel, w/886 ppm B	2.46	0.9970 ± 0.0010	0.9924 ± 0.0006	1.4475	1.4680
18	B&W-1645 (6.A.8)	S-type Fuel, w/746 ppm B	2.46	0.9990 ± 0.0010	0.9913 ± 0.0006	1.5463	1.5660
19	B&W-1645 (6.A.8)	SO-type Fuel, w/1156 ppm B	2.46	0.9972 ± 0.0009	0.9949 ± 0.0005	0.4241	0.4331
20	B&W-1810 (6.A.9)	Case 1 1337 ppm B	2.46	1.0023 ± 0.0010	NC	0.1531	NC
21	B&W-1810 (6.A.9)	Case 12 1899 ppm B	2.46/4.02	1.0060 ± 0.0009	NC	0.4493	NC
22	French (6.A.10)	Water Moderator 0 gap	4.75	0.9966 ± 0.0013	NC	0.2172	NC
23	French (6.A.10)	Water Moderator 2.5 cm gap	4.75	0.9952 ± 0.0012	NC	0.1778	NC
24	French (6.A.10)	Water Moderator 5 cm gap	4.75	0.9943 ± 0.0010	NC	0.1677	NC

Table 6.A.1
Summary of Criticality Benchmark Calculations

	Reference	Identification	Enrich.	Calculated k_{eff} MCNP4a	Calculated k_{eff} KENO5a	EALF (eV) MCNP4a	EALF (eV) KENO5a
25	French (6.A.10)	Water Moderator 10 cm gap	4.75	0.9979 ± 0.0010	NC	0.1736	NC
26	PNL-3602 (6.A.11)	Steel Reflector, 0 cm separation	2.35	NC	1.0004 ± 0.0006	NC	0.1018
27	PNL-3602 (6.A.11)	Steel Reflector, 1.321 cm separation	2.35	0.9980 ± 0.0009	0.9992 ± 0.0006	0.1000	0.0909
28	PNL-3602 (6.A.11)	Steel Reflector, 2.616 cm separation	2.35	0.9968 ± 0.0009	0.9964 ± 0.0006	0.0981	0.0975
29	PNL-3602 (6.A.11)	Steel Reflector, 3.912 cm separation	2.35	0.9974 ± 0.0010	0.9980 ± 0.0006	0.0976	0.0970
30	PNL-3602 (6.A.11)	Steel Reflector, Infinite separation	2.35	0.9962 ± 0.0008	0.9939 ± 0.0006	0.0973	0.0968
31	PNL-3602 (6.A.11)	Steel Reflector, 0 cm separation	4.306	NC	1.0003 ± 0.0007	NC	0.3282
32	PNL-3602 (6.A.11)	Steel Reflector, 1.321 cm separation	4.306	0.9997 ± 0.0010	1.0012 ± 0.0007	0.3016	0.3039
33	PNL-3602 (6.A.11)	Steel Reflector, 2.616 cm separation	4.306	0.9994 ± 0.0012	0.9974 ± 0.0007	0.2911	0.2927
34	PNL-3602 (6.A.11)	Steel Reflector, 5.405 cm separation	4.306	0.9969 ± 0.0011	0.9951 ± 0.0007	0.2828	0.2860
35	PNL-3602 (6.A.11)	Steel Reflector, Infinite separation	4.306	0.9910 ± 0.0020	0.9947 ± 0.0007	0.2851	0.2864
36	PNL-3602 (6.A.11)	Steel Reflector, with Boral Sheets	4.306	0.9941 ± 0.0011	0.9970 ± 0.0007	0.3135	0.3150

Table 6.A.1
Summary of Criticality Benchmark Calculations

	Reference	Identification	Enrich.	Calculated k_{eff} MCNP4a	Calculated k_{eff} KENO5a	EALF (eV) MCNP4a	EALF (eV) KENO5a
37	PNL-3626 (6.A.12)	Lead Reflector, 0 cm sepn.	4.306	NC	1.0003 ± 0.0007	NC	0.3159
38	PNL-3626 (6.A.12)	Lead Reflector, 0.55 cm sepn.	4.306	1.0025 ± 0.0011	0.9997 ± 0.0007	0.3030	0.3044
39	PNL-3626 (6.A.12)	Lead Reflector, 1.956 cm sepn.	4.306	1.0000 ± 0.0012	0.9985 ± 0.0007	0.2883	0.2930
40	PNL-3626 (6.A.12)	Lead Reflector, 5.405 cm sepn.	4.306	0.9971 ± 0.0012	0.9946 ± 0.0007	0.2831	0.2854
41	PNL-2615 (6.A.13)	Experiment 004/032 – no absorber	4.306	0.9925 ± 0.0012	0.9950 ± 0.0007	0.1155	0.1159
42	PNL-2615 (6.A.13)	Experiment 030 – Zr plates	4.306	NC	0.9971 ± 0.0007	NC	0.1154
43	PNL-2615 (6.A.13)	Experiment 013 – Steel plates	4.306	NC	0.9965 ± 0.0007	NC	0.1164
44	PNL-2615 (6.A.13)	Experiment 014 – Steel plates	4.306	NC	0.9972 ± 0.0007	NC	0.1164
45	PNL-2615 (6.A.13)	Exp. 009 1.05% Boron Steel plates	4.306	0.9982 ± 0.0010	0.9981 ± 0.0007	0.1172	0.1162
46	PNL-2615 (6.A.13)	Exp. 009 1.62% Boron Steel plates	4.306	0.9996 ± 0.0012	0.9982 ± 0.0007	0.1161	0.1173
47	PNL-2615 (6.A.13)	Exp. 031 – Boral plates	4.306	0.9994 ± 0.0012	0.9969 ± 0.0007	0.1165	0.1171
48	PNL-7167 (6.A.14)	Experiment 214R – with flux traps	4.306	0.9991 ± 0.0011	0.9956 ± 0.0007	0.3722	0.3812

Table 6.A.1
Summary of Criticality Benchmark Calculations

	Reference	Identification	Enrich.	Calculated k_{eff} MCNP4a	Calculated k_{eff} KENO5a	EALF (eV) MCNP4a	EALF (eV) KENO5a
49	PNL-7167 (6.A.14)	Experiment 214V3 –with flux trap	4.306	0.9969 ± 0.0011	0.9963 ± 0.0007	0.3742	0.3826
50	PNL-4267 (6.A.15)	Case 173 – 0 ppm B	4.306	0.9974 ± 0.0012	NC	0.2893	NC
51	PNL-4267 (6.A.15)	Case 177 – 2550 ppm B	4.306	1.0057 ± 0.0010	NC	0.5509	NC
52	PNL-5803 (6.A.16)	MOX Fuel – Type 3.2 Exp. 21	20% Pu	1.0041 ± 0.0011	1.0046 ± 0.0006	0.9171	0.8868
53	PNL-5803 (6.A.16)	MOX Fuel – Type 3.2 Exp. 43	20% Pu	1.0058 ± 0.0012	1.0036 ± 0.0006	0.2968	0.2944
54	PNL-5803 (6.A.16)	MOX Fuel – Type 3.2 Exp. 13	20% Pu	1.0083 ± 0.0011	0.9989 ± 0.0006	0.1665	0.1706
55	PNL-5803 (6.A.16)	MOX Fuel – Type 3.2 Exp. 32	20% Pu	1.0079 ± 0.0011	0.9966 ± 0.0006	0.1339	0.1165
56	WCAP-3385 (6.A.17)	Saxton Case 52 PuO_2 0.52" pitch	6.6% Pu	0.9996 ± 0.0011	1.0005 ± 0.0006	0.8665	0.8417
57	WCAP-3385 (6.A.17)	Saxton Case 52 U 0.52" pitch	5.74	1.0000 ± 0.0010	0.9956 ± 0.0007	0.4476	0.4580
58	WCAP-3385 (6.A.17)	Saxton Case 56 PuO_2 0.56" pitch	6.6% Pu	1.0036 ± 0.0011	1.0047 ± 0.0006	0.5289	0.5197
59	WCAP-3385 (6.A.17)	Saxton Case 56 borated PuO_2	6.6% Pu	1.0008 ± 0.0010	NC	0.6389	NC
60	WCAP-3385 (6.A.17)	Saxton Case 56 U 0.56" pitch	5.74	0.9994 ± 0.0011	0.9967 ± 0.0007	0.2923	0.2954

Table 6.A.1
Summary of Criticality Benchmark Calculations

	Reference	Identification	Enrich.	Calculated k_{eff} MCNP4a	Calculated k_{eff} KENO5a	EALF (eV) MCNP4a	EALF (eV) KENO5a
61	WCAP-3385 (6.A.17)	Saxton Case 79 PuO_2 0.79" pitch	6.6% Pu	1.0063 ± 0.0011	1.0133 ± 0.0006	0.1520	0.1555
62	WCAP-3385 (6.A.17)	Saxton Case 79 U 0.79" pitch	5.74	1.0039 ± 0.0011	1.0008 ± 0.0006	0.1036	0.1047
Additional MOX							
63	EPRI Exp22 (6.A.19)	0.700-in. pitch 0 ppm B	2% Pu	1.0065 ± 0.0011	NC	0.5458	NC
64	EPRI Exp23 (6.A.19)	0.700-in. pitch 688 ppm B	2% Pu	1.0069 ± 0.0010	NC	0.7256	NC
65	EPRI Exp24 (6.A.19)	0.870-in. pitch 0 ppm B	2% Pu	1.0037 ± 0.0011	NC	0.1963	NC
66	EPRI Exp25 (6.A.19)	0.870-in. pitch 1090 ppm B	2% Pu	1.0073 ± 0.0011	NC	0.2880	NC
67	EPRI Exp26 (6.A.19)	0.990-in. pitch 0 ppm B	2% Pu	1.0057 ± 0.0010	NC	0.1386	NC
68	EPRI Exp27 (6.A.19)	0.990-in. pitch 767 ppm B	2% Pu	1.0079 ± 0.0010	NC	0.1849	NC
69	WCAP-3385 (6.A.17)	Saxton Case PuO_2 0.735" pitch	6.6% Pu	1.0081 ± 0.0012	NC	0.1843	NC
70	WCAP-3385 (6.A.17)	Saxton Case PuO_2 1.04" pitch	6.6% Pu	1.0085 ± 0.0011	NC	0.0999	NC
71	PUP Exp35 (6.A.20)	8 wt% ^{240}Pu 0.80" pitch	2% Pu	0.9971 ± 0.0010	NC	0.3582	NC
72	PUP Exp36 (6.A.20)	8 wt% ^{240}Pu 0.93" pitch	2% Pu	1.0018 ± 0.0011	NC	0.1883	NC

Table 6.A.1
Summary of Criticality Benchmark Calculations

	Reference	Identification	Enrich.	Calculated k_{eff} MCNP4a	Calculated k_{eff} KENO5a	EALF (eV) MCNP4a	EALF (eV) KENO5a
73	PUP Exp37 (6.A.20)	8 wt% ^{240}Pu 1.05" pitch	2% Pu	0.9959 ± 0.0011	NC	0.1377	NC
74	PUP Exp38 (6.A.20)	8 wt% ^{240}Pu 1.143" pitch	2% Pu	1.0017 ± 0.0010	NC	0.1170	NC
75	PUP Exp39 (6.A.20)	8 wt% ^{240}Pu 1.32" pitch	2% Pu	1.0000 ± 0.0010	NC	0.0956	NC
76	PUP Exp40 (6.A.20)	8 wt% ^{240}Pu 1.386" pitch	2% Pu	0.9994 ± 0.0009	NC	0.0908	NC
77	PUP Exp41 (6.A.20)	16 wt% ^{240}Pu 0.93" pitch	2% Pu	1.0042 ± 0.0010	NC	0.1981	NC
78	PUP Exp42 (6.A.20)	16 wt% ^{240}Pu 1.05" pitch	2% Pu	1.0018 ± 0.0010	NC	0.1408	NC
79	PUP Exp43 (6.A.20)	16 wt% ^{240}Pu 1.143" pitch	2% Pu	1.0029 ± 0.0009	NC	0.1200	NC
80	PUP Exp44 (6.A.20)	16 wt% ^{240}Pu 1.32" pitch	2% Pu	1.0019 ± 0.0008	NC	0.0970	NC
81	PUP Exp45 (6.A.20)	24 wt% ^{240}Pu 0.80" pitch	2% Pu	0.9947 ± 0.0010	NC	0.3988	NC
82	PUP Exp46 (6.A.20)	24 wt% ^{240}Pu 0.93" pitch	2% Pu	0.9993 ± 0.0008	NC	0.2006	NC
83	PUP Exp47 (6.A.20)	24 wt% ^{240}Pu 1.05" pitch	2% Pu	1.0014 ± 0.0008	NC	0.1414	NC
84	PUP Exp48 (6.A.20)	24 wt% ^{240}Pu 1.143" pitch	2% Pu	1.0019 ± 0.0009	NC	0.1196	NC

Table 6.A.1
Summary of Criticality Benchmark Calculations

	Reference	Identification	Enrich.	Calculated k_{eff} MCNP4a	Calculated k_{eff} KENO5a	EALF (eV) MCNP4a	EALF (eV) KENO5a
85	PUP Exp49 (6.A.20)	24 wt% ^{240}Pu 1.32" pitch	2% Pu	1.0049 ± 0.0008	NC	0.0973	NC
86	PUP Exp50 (6.A.20)	24 wt% ^{240}Pu 1.386" pitch	2% Pu	1.0040 ± 0.0008	NC	0.0917	NC
87	PUP Exp51 (6.A.20)	18 wt% ^{240}Pu 0.85" pitch	4% Pu	0.9993 ± 0.0011	NC	0.3918	NC
88	PUP Exp52 (6.A.20)	18 wt% ^{240}Pu 0.93" pitch	4% Pu	0.9991 ± 0.0010	NC	0.2565	NC
89	PUP Exp53 (6.A.20)	18 wt% ^{240}Pu 1.05" pitch	4% Pu	1.0073 ± 0.0011	NC	0.1757	NC
90	PUP Exp54 (6.A.20)	18 wt% ^{240}Pu 1.143" pitch	4% Pu	1.0065 ± 0.0010	NC	0.1454	NC
91	PUP Exp55 (6.A.20)	18 wt% ^{240}Pu 1.386" pitch	4% Pu	1.0093 ± 0.0009	NC	0.1068	NC
92	PUP Exp56 (6.A.20)	18 wt% ^{240}Pu 1.60" pitch	4% Pu	1.0086 ± 0.0010	NC	0.0932	NC
93	PUP Exp57 (6.A.20)	18 wt% ^{240}Pu 1.70" pitch	4% Pu	1.0106 ± 0.0009	NC	0.0884	NC
94	MCT004 (6.A.22)	2.42Pu Lattics, 59.55 cm Water	3% Pu	0.9962 ± 0.0007	NC	0.1461	NC
95	MCT004 (6.A.22)	2.42Pu Lattics, 61.90 cm Water	3% Pu	0.9959 ± 0.0006	NC	0.1453	NC
96	MCT004 (6.A.22)	2.42Pu Lattics, 64.06 cm Water	3% Pu	0.9973 ± 0.0006	NC	0.1447	NC
97	MCT004 (6.A.22)	2.98Pu Lattics, 61.50 cm Water	3% Pu	0.9984 ± 0.0006	NC	0.1196	NC
98	MCT004 (6.A.22)	2.98Pu Lattics, 64.40 cm Water	3% Pu	0.9980 ± 0.0007	NC	0.1195	NC
99	MCT004 (6.A.22)	2.98Pu Lattics, 69.40 cm Water	3% Pu	0.9988 ± 0.0006	NC	0.1181	NC
100	MCT004 (6.A.22)	4.24Pu Lattics, 60.32 cm Water	3% Pu	0.9996 ± 0.0006	NC	0.0929	NC
101	MCT004 (6.A.22)	4.24Pu Lattics, 62.99 cm Water	3% Pu	0.9998 ± 0.0006	NC	0.0928	NC
102	MCT004 (6.A.22)	4.24Pu Lattics, 65.63 cm Water	3% Pu	1.0015 ± 0.0006	NC	0.0921	NC
103	MCT004 (6.A.22)	5.55Pu Lattics, 62.05 cm Water	3% Pu	1.0000 ± 0.0006	NC	0.0800	NC
104	MCT004 (6.A.22)	5.55Pu Lattics, 64.53 cm Water	3% Pu	1.0025 ± 0.0006	NC	0.0794	NC

Notes: NC stands for not calculated.

† EALF is the energy of the average lethargy causing fission

†† The experimental results appear to be statistical outliers (>3σ) suggesting the possibility of unusually large experimental error. Although they could be justifiably excluded, for conservatism, they were retained in determining the calculational basis.

Table 6.A.2

COMPARISON OF MCNP4a AND KENO5a CALCULATED REACTIVITIES†
FOR VARIOUS ENRICHMENTS (UO_2)

Enrichment	Calculated $k_{eff} \pm 1\sigma$	
	MCNP4a	**KENO5a**
3.0	0.8465 ± 0.0011	0.8478 ± 0.0004
3.5	0.8820 ± 0.0011	0.8841 ±0.0004
3.75	0.9019 ± 0.0011	0.8987 ± 0.0004
4.0	0.9132 ± 0.0010	0.9140 ± 0.0004
4.2	0.9276 ± 0.0011	0.9237 ± 0.0004
4.5	0.9400 ± 0.0011	0.9388 ± 0.0004

† Based on the MPC-68 with the GE 8x8R

Table 6.A.3

MCNP4a CALCULATED REACTIVITIES FOR
CRITICAL EXPERIMENTS WITH NEUTRON ABSORBERS (UO_2)

Ref.	Experiment		Δk Worth of Absorber	MCNP4a Calculated k_{eff}	EALF† (eV)
6.A.13	PNL-2615	Boral Sheet	0.0139	0.9994 ± 0.0012	0.1165
6.A.7	BAW-1484	Core XX	0.0165	1.0008 ± 0.0011	0.1724
6.A.13	PNL-2615	1.62% Boron-steel	0.0165	0.9996 ± 0.0012	0.1161
6.A.7	BAW-1484	Core XIX	0.0202	0.9961 ± 0.0012	0.2103
6.A.7	BAW-1484	Core XXI	0.0243	0.9994 ± 0.0010	0.1544
6.A.7	BAW-1484	Core XVII	0.0519	0.9962 ± 0.0012	0.2083
6.A.11	PNL-3602	Boral Sheet	0.0708	0.9941 ± 0.0011	0.3135
6.A.7	BAW-1484	Core XV	0.0786	0.9910 ± 0.0011	0.2092
6.A.7	BAW-1484	Core XVI	0.0845	0.9935 ± 0.0010	0.1757
6.A.7	BAW-1484	Core XIV	0.1575	0.9953 ± 0.0011	0.2022
6.A.7	BAW-1484	Core XIII	0.1738	1.0020 ± 0.0011	0.1988
6.A.14	PNL-7167	Expt 214R flux trap	0.1931	0.9991 ± 0.0011	0.3722

† EALF is the energy of the average lethargy causing fission

Table 6.A.4
COMPARISON OF MCNP4a AND KENO5a
CALCULATED REACTIVITIES† FOR VARIOUS BORON LOADINGS (UO_2)

^{10}B, g/cm^2	**Calcualted $k_{eff} \pm 1\sigma$**	
	MCNP4a	**KENO5a**
0.005	1.0381 ± 0.0012	1.0340 ± 0.0004
0.010	0.9960 ±0.0010	0.9941 ± 0.0004
0.015	0.9727 ± 0.0009	0.9713 ± 0.0004
0.020	0.9541 ± 0.0012	0.9560 ± 0.0004
0.025	0.9433 ± 0.0011	0.9428 ± 0.0004
0.030	0.9325 ± 0.0011	0.9338 ± 0.0004
0.035	0.9234 ± 0.0011	0.9251 ± 0.0004
0.040	0.9173 ± 0.0011	0.9179 ± 0.0004

† based on 4.5% enrichment GE 8x8R in the MPC-68 cask.

Table 6.A.5

CALCULATIONS FOR CRITICAL EXPERIMENTS WITH THICK LEAD AND STEEL REFLECTORS† (UO_2)

Ref.	Case	Enrichment, wt%	Separation, cm	MCNP4a k_{eff}	KENO5a k_{eff}
6.A.11	Steel Reflector	2.35	1.321	0.9980 ± 0.0009	0.9992 ± 0.0006
		2.35	2.616	0.9968 ± 0.0009	0.9964 ± 0.0006
		2.35	3.912	0.9974 ± 0.0010	0.9980 ± 0.0006
		2.35	∞	0.9962 ± 0.0008	0.9939 ± 0.0006
6.A.11	Steel Reflector	4.306	1.321	0.9997 ± 0.0010	1.0012 ± 0.0007
		4.306	2.616	0.9994 ± 0.0012	0.9974 ± 0.0007
		4.306	3.405	0.9969 ± 0.0011	0.9951 ± 0.0007
		4.306	∞	0.9910 ± 0.0020	0.9947 ± 0.0007
6.A.11	Lead Reflector	4.306	0.55	1.0025 ± 0.0011	0.9997 ± 0.0007
		4.306	1.956	1.0000 ± 0.0012	0.9985 ± 0.0007
		4.306	5.405	0.9971 ± 0.0012	0.9946 ± 0.0007

† Arranged in order of increasing reflector fuel spacing.

Table 6.A.6

CALCULATIONS FOR CRITICAL EXPERIMENTS WITH VARIOUS SOLUBLE BORON CONCENTRATIONS (UO_2)

Reference	Experiment	Boron Concentration ppm	Calculated k_{eff}	
			MCNP4a	KENO5a
6.A.15	PNL-4267	0	0.9974 ± 0.0012	-
6.A.8	BAW-1645-4	886	0.9970 ± 0.0010	0.9924 ± 0.0006
6.A.9	BAW-1810	1337	1.0023 ± 0.0010	-
6.A.9	BAW-1810	1899	1.0060 ± 0.0009	-
6.A.15	PNL-4267	2550	1.0057 ± 0.0010	-

Table 6.A.7

CALCULATIONS FOR CRITICAL EXPERIMENTS WITH MOX FUEL

Reference	Case†	MCNP4a		KENO 5a	
		k_{eff}	EALF†† (eV)	k_{eff}	EALF†† (eV)
PNL-5803 [6.A.16]	MOX Fuel – Exp No 21	1.0041±0.0011	0.9171	1.0046±0.0006	0.8868
	MOX Fuel – Exp No 43	1.0058±0.0012	0.2968	1.0036±0.0006	0.2944
	MOX Fuel – Exp No 13	1.0083±0.0011	0.1665	0.9989±0.0006	0.1706
	MOX Fuel – Exp No 32	1.0079±0.0011	0.1139	0.9966±0.0006	0.1165
WCAP- 3385-54 [6.A.17]	Saxton @ 0.52" pitch	0.9996±0.0011	0.8665	1.0005±0.0006	0.8417
	Saxton @ 0.56" pitch	1.0036±0.0011	0.5289	1.0047±0.0006	0.5197
	Saxton @ 0.56" pitch borated	1.0008±0.0010	0.6389	NC	NC
	Saxton @ 0.79" pitch	1.0063±0.0011	0.1520	1.0133±0.0006	0.1555

† Arranged in order of increasing lattice spacing.

†† EALF is the energy of the average lethargy causing fission.

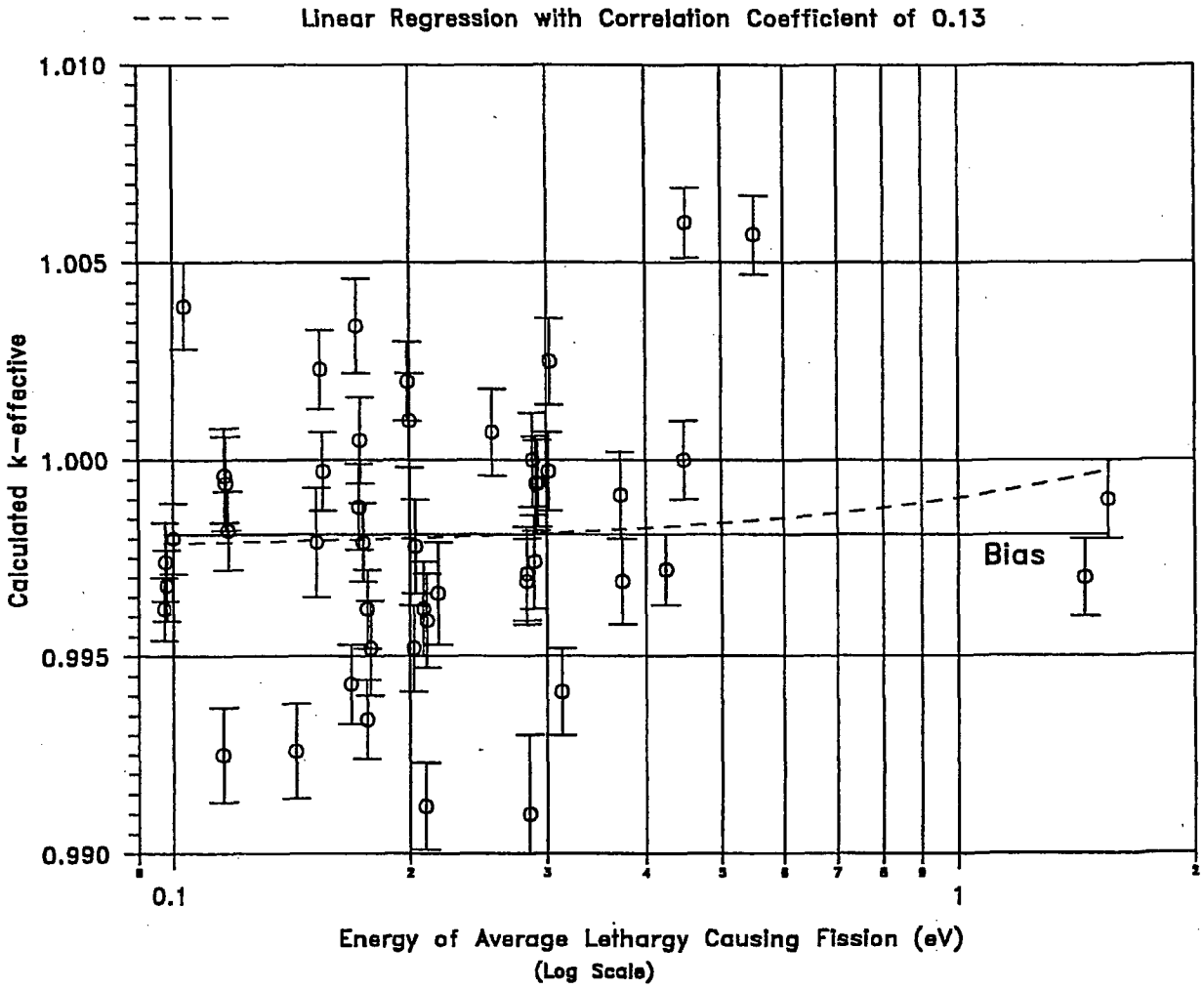

FIGURE 6.A.1 MCNP4a CALCULATED k-eff VALUES FOR VARIOUS VALUES OF THE SPECTRAL INDEX

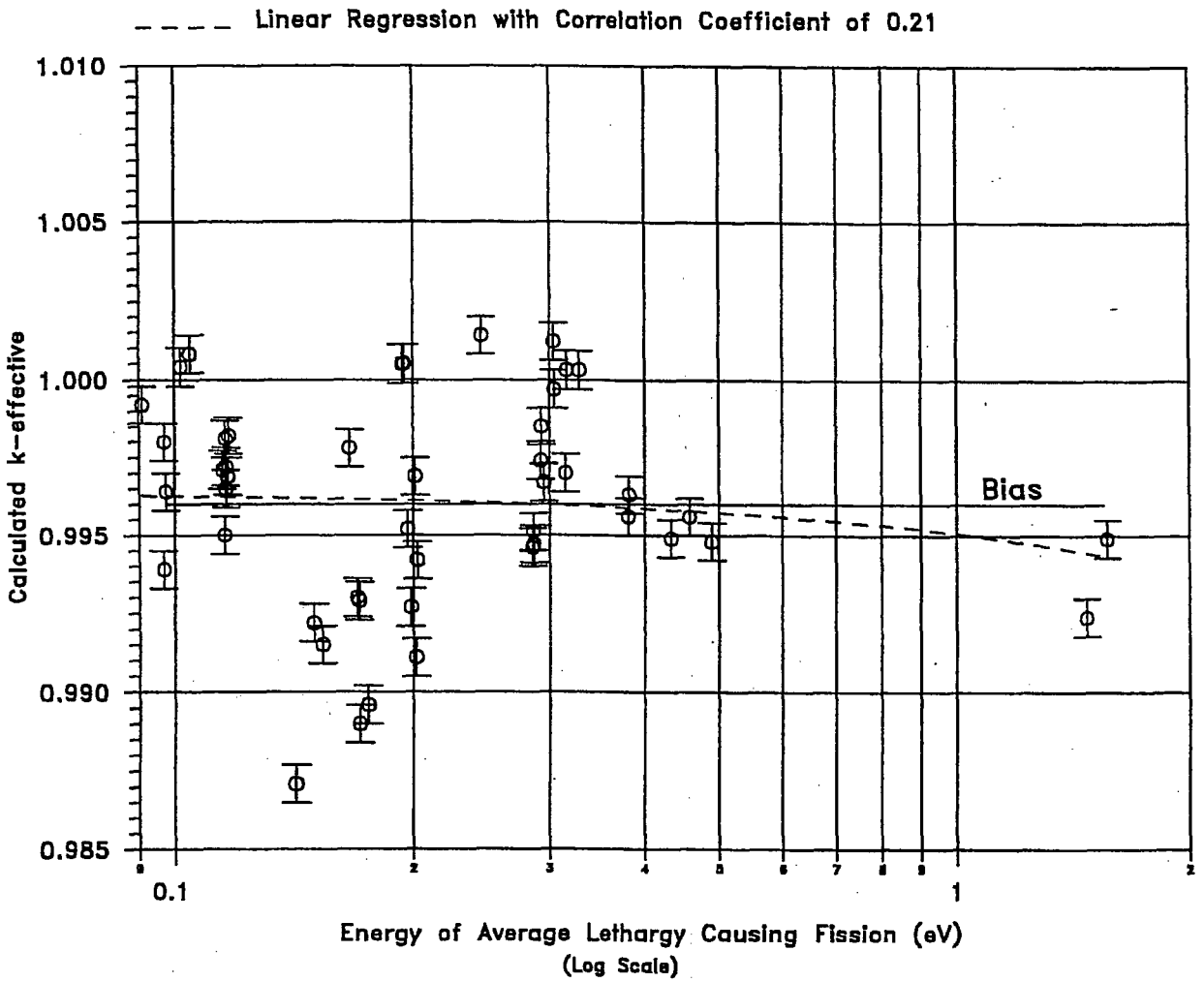

FIGURE 6.A.2 KENO5a CALCULATED k-eff VALUES FOR VARIOUS VALUES OF THE SPECTRAL INDEX

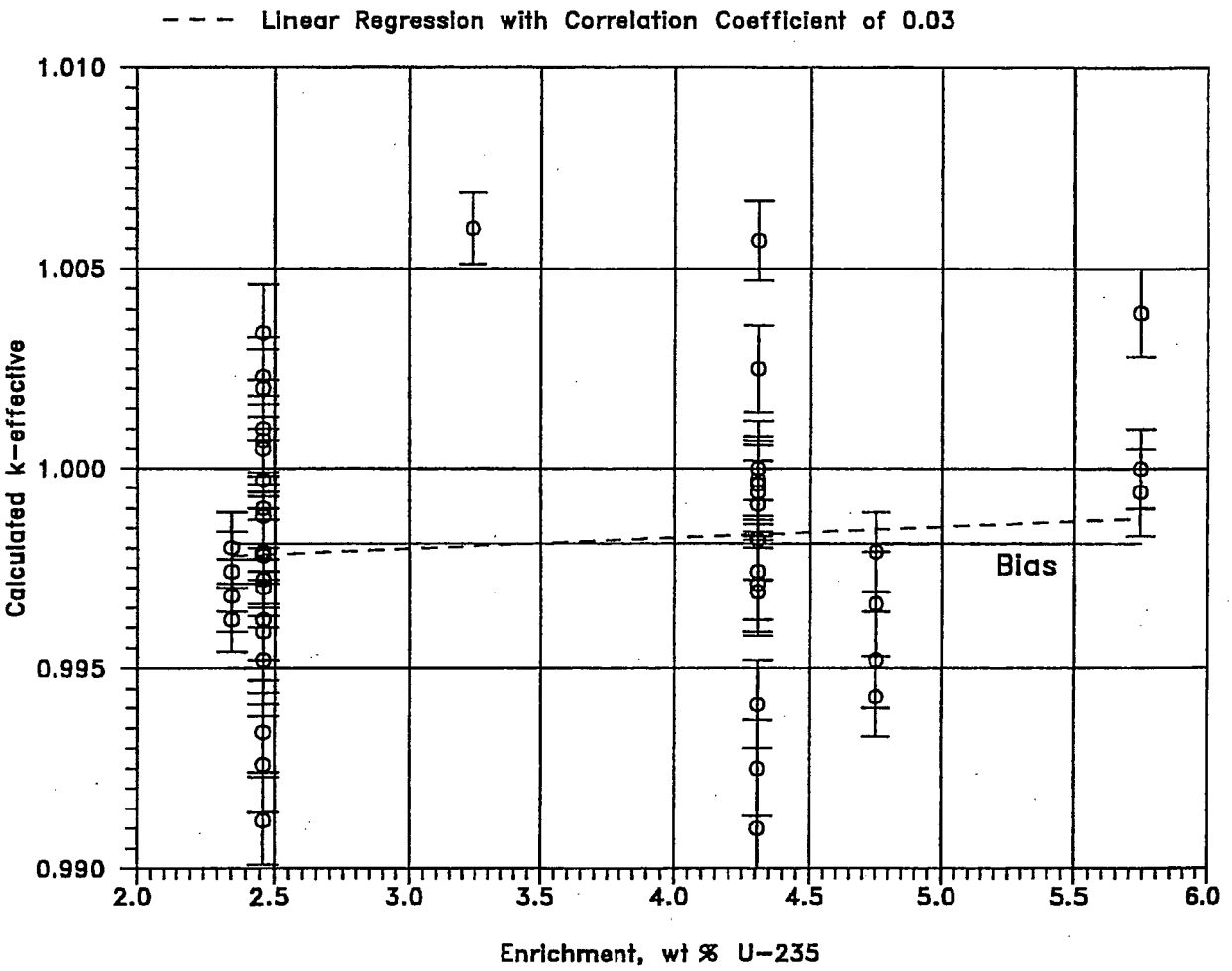

FIGURE 6.A.3 MCNP4a CALCULATED k-eff VALUES AT VARIOUS U-235 ENRICHMENTS

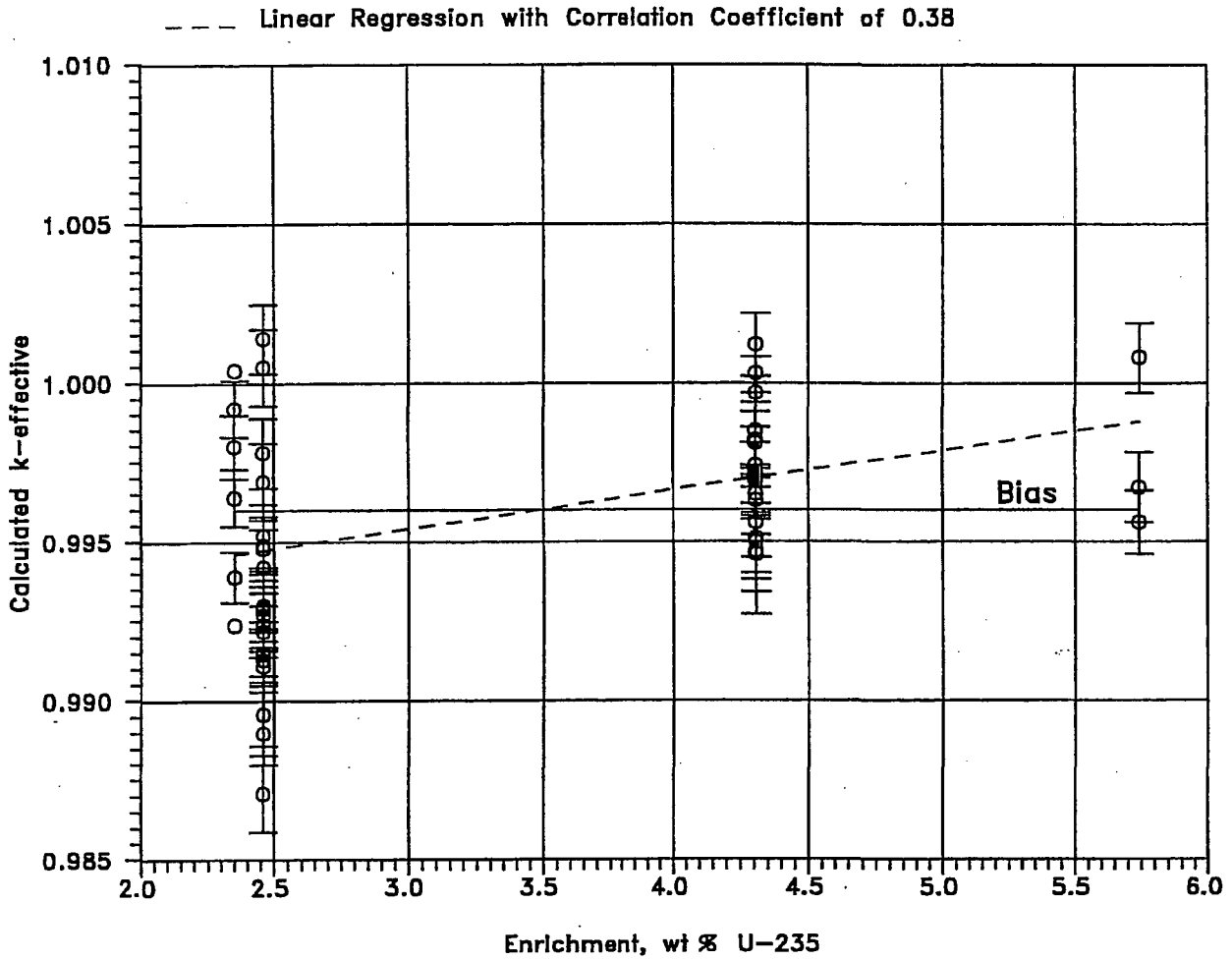

FIGURE 6.A.4 KENO5a CALCULATED k-eff VALUES AT VARIOUS U-235 ENRICHMENTS

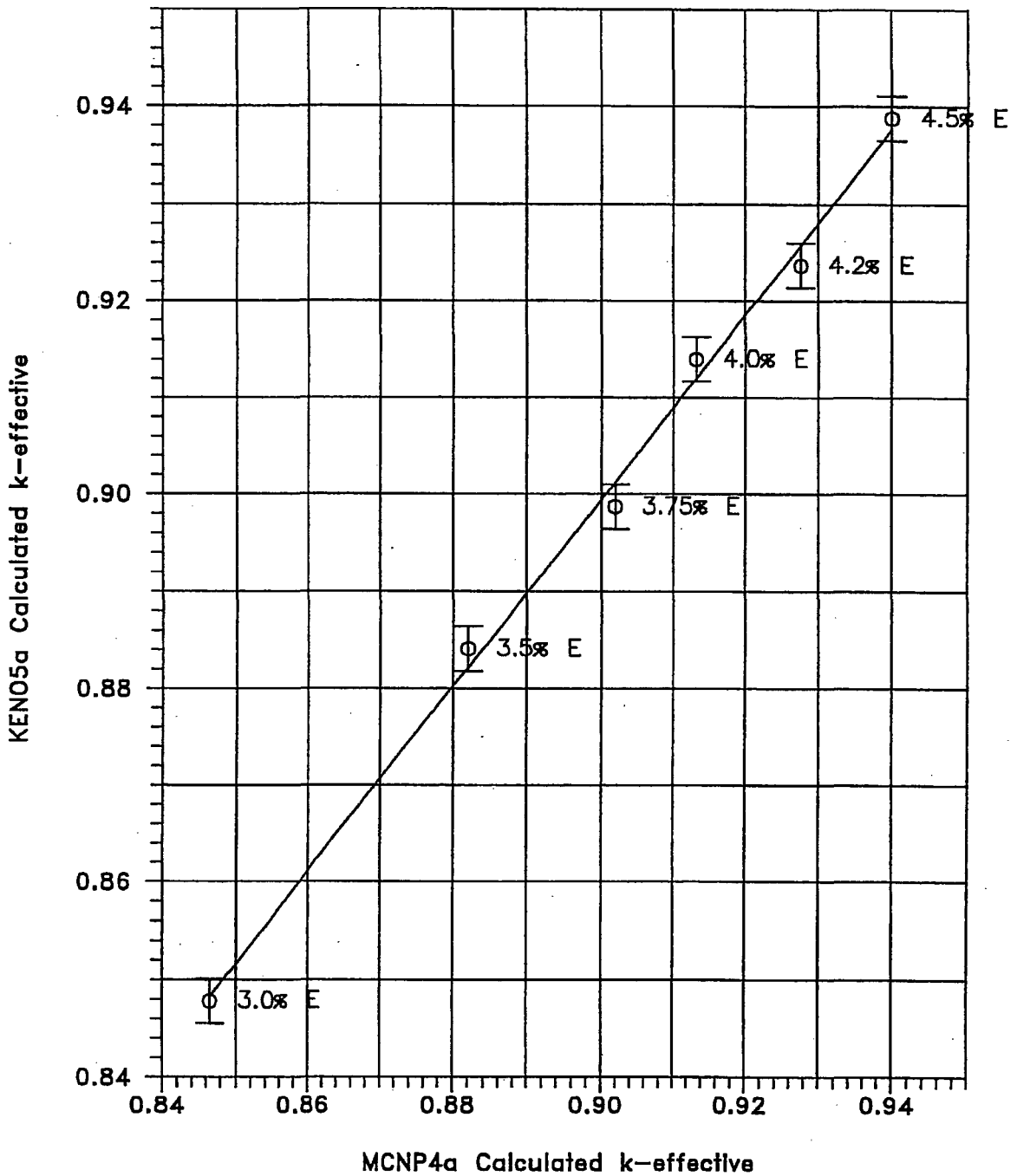

FIGURE 6.A.5 COMPARISON OF MCNP4a AND KENO5a CALCULATIONS FOR VARIOUS FUEL ENRICHMENTS

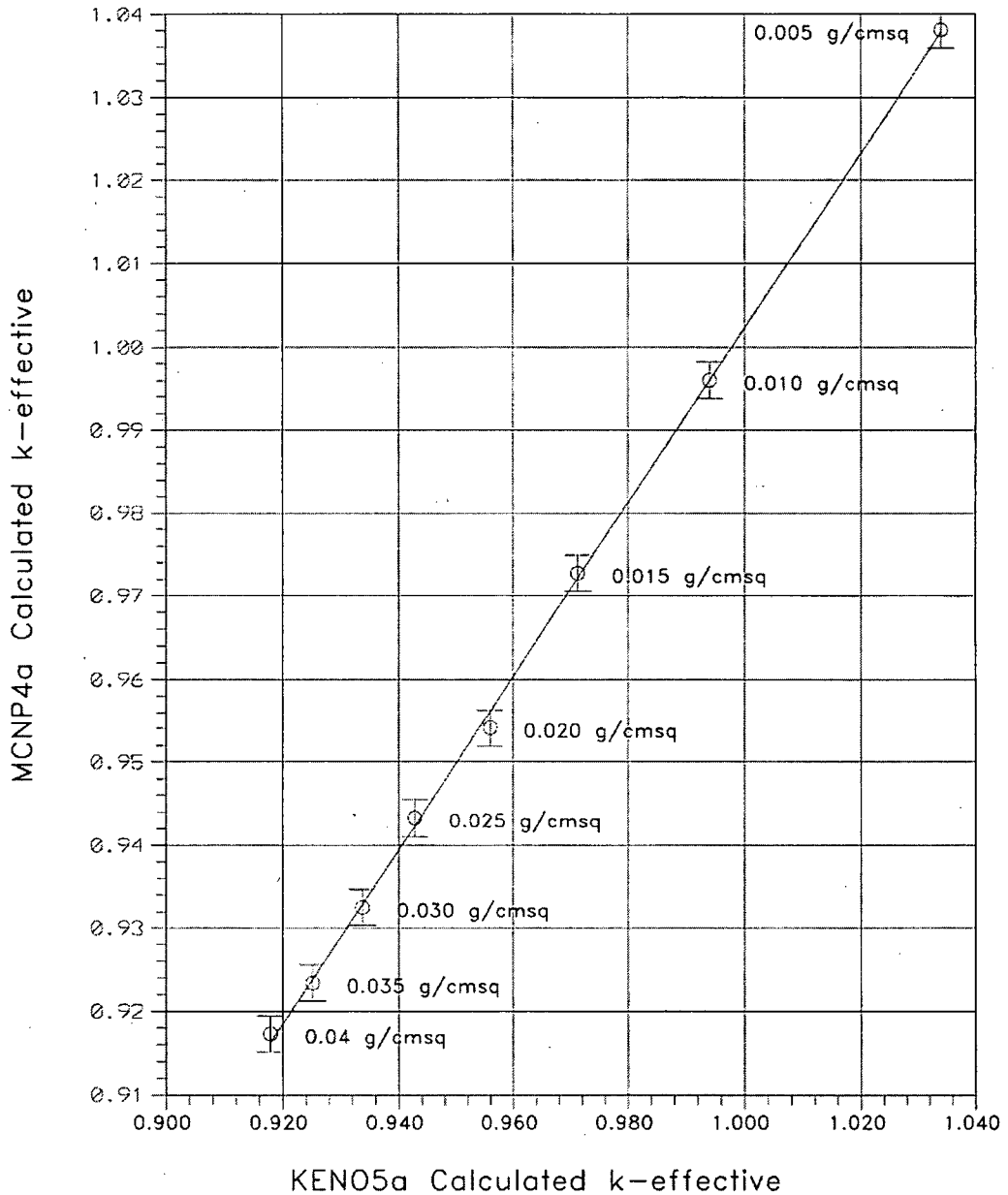

FIGURE 6.A.6 COMPARISON OF MCNP4a AND KENO5a CALCULATIONS FOR VARIOUS BORON-10 AREAL DENSITIES

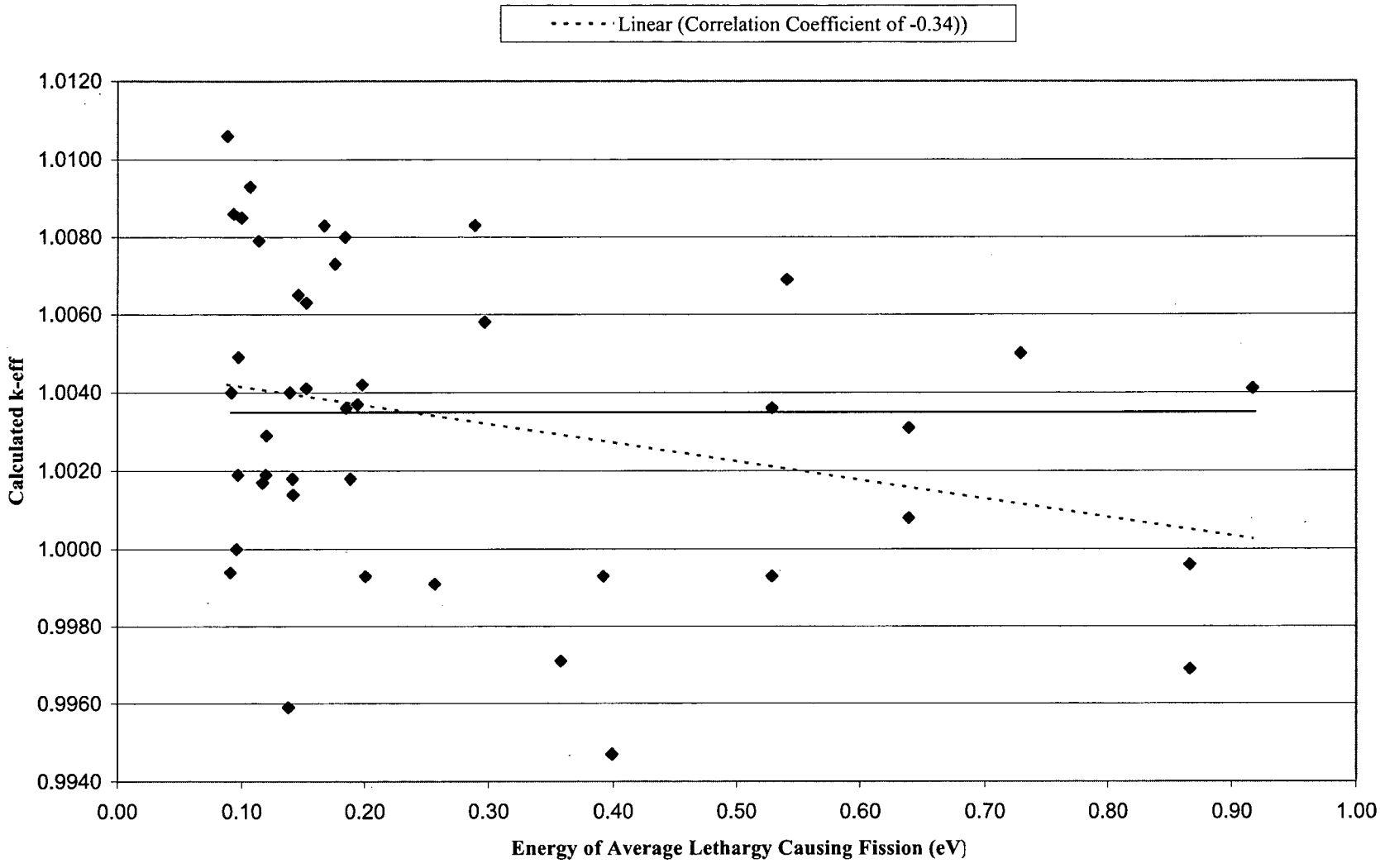

Figure 6.A.7: MCNP4a CALCULATED k-eff VALUES FOR VARIOUS VALUES OF THE SPECTRAL INDEX

APPENDIX 6.B: DISTRIBUTED ENRICHMENTS IN BWR FUEL

Fuel assemblies used in BWRs utilize fuel rods of varying enrichments as a means of controlling power peaking during in-core operation. For calculations involving BWR assemblies, the use of a uniform (planar-average) enrichment, as opposed to the distributed enrichments normally used in BWR fuel, produces conservative results. Calculations have been performed to confirm that this statement remains valid in the geometry of the MPC-68. These calculations are based on fuel assembly designs currently in use and two hypothetical distributions, all intended to illustrate that calculations with uniform average enrichments are conservative.

The average enrichment is calculated as the linear average of the various fuel rod enrichments, i.e.,

$$\overline{E} = \frac{1}{n} \sum_{i=1}^{n} E_i,$$

where E_i is the enrichment in each of the n rods, and $\overline{E}$ is the assembly average enrichment. This parameter conservatively characterizes the fuel assembly and is readily available for specific fuel assemblies in determining the acceptability of the assembly for placement in the MPC-68 cask.

The criticality calculations for average and distributed enrichment cases are compared in Table 6.B.1 to illustrate and confirm the conservatism inherent in using average enrichments. With two exceptions, the cases analyzed represent realistic designs currently in use and encompass fuel with different ratios of maximum pin enrichment to average assembly enrichment. The two exceptions are hypothetical cases intended to extend the models to higher enrichments and to demonstrate that using the average enrichment remains conservative.

Table 6.B.1 shows that, in all cases, the averaged enrichment yields conservative values of reactivity relative to distributed enrichments for both the actual fuel designs and the hypothetical higher enrichment cases. Thus, it is concluded that uniform average enrichments will always yield higher (more conservative) values for reactivity than the corresponding distributed enrichments.†

† This conclusion implicitly assumes the higher enrichment fuel rods are located internal to the assembly (as in BWR fuel), and the lower enriched rods are on the outside.

Table 6.B.1

COMPARISON CALCULATIONS FOR BWR FUEL WITH AVERAGE AND DISTRIBUTED ENRICHMENTS

Case	Average %E	Peak Rod E%	Calculated k_{eff}	
			Average E	Distributed E
8x8C04	3.01	3.80	0.8549	0.8429
8x8C04	3.934	4.9	0.9128	0.9029
8x8D05	3.42	3.95	0.8790	0.8708
8x8D05	3.78	4.40	0.9030	0.8974
8x8D05	3.90	4.90	0.9062	0.9042
9x9B01	4.34	4.71	0.9347	0.9285
9x9D01	3.35	4.34	0.8793	0.8583
Hypothetical #1 (48 outer rods of 3.967%E,14 inner rods of 5.0%)	4.20	5.00	0.9289	0.9151
Hypothetical #2 (48 outer rods of 4.354%E,14 inner rods of 5.0%)	4.50	5.00	0.9422	0.9384

APPENDIX 6.C: CALCULATIONAL SUMMARY

DELETED

APPENDIX 6.D: SAMPLE INPUT FILES

(Total number of pages in this appendix : 46)

File Description	Starting Page
MCNP4a input file for MPC-24	Appendix 6.D-2
MCNP4a input file for MPC-68	Appendix 6.D-13
MCNP4a input file for MPC-68F	Appendix 6.D-19
MCNP4a input file for MPC-68F with Dresden damaged fuel in the Damaged Fuel Container	Appendix 6.D-25
MCNP4a input file for MPC-68F with Humbolt Bay damaged fuel in the Damaged Fuel Container	Appendix 6.D-31
KENO5a input file for MPC-24	Appendix 6.D-37
KENO5a input file for MPC-68	Appendix 6.D-42

```
 message:   outp=4rf5f45o  srctp=4rf5f45s  runtpe=4rf5f45r

4rf5f45
c
c
c Bounding Assembly in Class 15x15F
c
c MPC-24/24E cell configuration
c
c HI-STAR with active length 150 inch
c
c Cask Input Preprocessor
c cskinp 15f 15f mpc24n mpc24n histar star150 4.1 4rf5f45 pure
c ------     10580 30-Jul-101 09:38 cpp\15f.bat
c   added 15f.co
c   added 15f.ce
c   added 15f.su
c   added 15f.sp
c ------     37966 21-Aug-101 10:10 cpp\mpc24n.bat
c   added mpc24n.co
c   added mpc24n.ce
c   added mpc24n.su
c   added mpc24n.sp
c ------      5620 22-Aug-101 14:05 cpp\histar.bat
c   added histar.co
c   added histar.ce
c   added histar.su
c   added histar.sp
c end of comments
c
c start of cells
c
c 15x15f
c
c number of cells: 6
c cell numbers:      1 to 7 and 201 to 299
c univers numbers:   1 to 3 and 201 to 299
c surface numbers:   1 to 9 and 201 to 299
c
c number of cells: 1
1     1 -10.522     -1  u=2       $ fuel
2     4 -1.0     1  -2  u=2       $ gap
3     3 -6.55    2  -3  u=2       $ Zr Clad
4     4 -1.0        3  u=2       $ water in fuel region
5     4 -1.0  -4:5     u=3       $ water in guide tubes
6     3 -6.55   4 -5    u=3       $ guide tubes
7     4 -1.0  -6   +7   -8  +9   u=1  lat=1
      fill= -8:8    -8:8   0:0
      1 1 1 1 1 1 1 1 1 1 1 1 1 1 1 1 1
      1 2 2 2 2 2 2 2 2 2 2 2 2 2 2 2 1
      1 2 2 2 2 2 2 2 2 2 2 2 2 2 2 2 1
      1 2 2 2 2 2 3 2 2 2 3 2 2 2 2 2 1
      1 2 2 2 3 2 2 2 2 2 2 2 3 2 2 2 1
      1 2 2 2 2 2 2 2 2 2 2 2 2 2 2 2 1
      1 2 2 3 2 2 3 2 2 2 3 2 2 3 2 2 1
      1 2 2 2 2 2 2 2 2 2 2 2 2 2 2 2 1
      1 2 2 2 2 2 2 2 3 2 2 2 2 2 2 2 1
      1 2 2 2 2 2 2 2 2 2 2 2 2 2 2 2 1
      1 2 2 3 2 2 3 2 2 2 3 2 2 3 2 2 1
      1 2 2 2 2 2 2 2 2 2 2 2 2 2 2 2 1
      1 2 2 2 3 2 2 2 2 2 2 2 3 2 2 2 1
```

```
      1 2 2 2 2 2 3 2 2 2 3 2 2 2 2 2 1
      1 2 2 2 2 2 2 2 2 2 2 2 2 2 2 2 1
      1 2 2 2 2 2 2 2 2 2 2 2 2 2 2 2 1
      1 1 1 1 1 1 1 1 1 1 1 1 1 1 1 1 1
c
c     MPC-24
c
c number of cells: 102
c cell numbers :       400   to  699
c universe numbers :     4   to    9
c surface numbers :    400   to  699
c
c     Right Side
c
408     0          -410   411  -412   413    u=4 fill=1 (1)
409     5  -7.84    410  -424   413  -426    u=4
410    4 -1.0      424  -428   448  -445    u=4
411    7  -2.7      428  -528  448  -445    u=4
412    6  -2.66    528  -532  448  -445    u=4
413    7  -2.7     532  -432   448  -445    u=4
414    4 -1.0      432  -436   448  -445    u=4
415    5  -7.84     436  -440   448  -445    u=4
416    4 -1.0      440         413         u=4
417    4 -1.0      424  -440   413  -447    u=4
418    4 -1.0      424  -440   446         u=4
419    5  -7.84     424  -440   447  -448    u=4
420    5  -7.84     424  -440   445  -446    u=4
c
c    Left Side
c
421    5  -7.84     425  -411   413         u=4
422    4 -1.0      429  -425   448  -445    u=4
423    7  -2.7     529  -429   448  -445    u=4
424    6  -2.66    533 -529   448  -445    u=4
425    7  -2.7      433 -533   448  -445    u=4
426    4 -1.0      437  -433   448  -445    u=4
427    5  -7.84     441  -437   448  -445    u=4
428    4 -1.0          -441   413         u=4
429    4 -1.0      441  -425   413  -447    u=4
430    4 -1.0      441  -425   446         u=4
431    5  -7.84     441  -425   447  -448    u=4
432    5  -7.84     441  -425   445  -446    u=4
c
c     Top
c
433    5  -7.84     411  -410   412  -426    u=4
434    4 -1.0      451  -452   426  -430    u=4
435    7  -2.7      451  -452   430 -530    u=4
436    6  -2.66     451  -452  530 -534    u=4
437    7  -2.7      451  -452  534  -434    u=4
438    4 -1.0      451  -452   434  -438    u=4
439    5  -7.84     451  -452   438  -442    u=4
440    4 -1.0      411  -424   442         u=4
441    4 -1.0      411  -450   426  -442    u=4
442    4 -1.0      453  -424   426  -442    u=4
443    5  -7.84     450  -451   426  -442    u=4
444    5  -7.84     452  -453   426  -442    u=4
c
c     Bottom
c
445    5  -7.84     427            -413    u=4
```

```
446    4 -1.0     451  -452   431  -427    u=4
447    7  -2.7     451  -452  531  -431    u=4
448    6  -2.66    451  -452  535 -531    u=4
449    7  -2.7     451  -452   435 -535    u=4
450    4 -1.0     451  -452   439  -435    u=4
451    5  -7.84    451  -452   443  -439    u=4
452    4 -1.0     411            -443    u=4
453    4 -1.0     411  -450   443  -427    u=4
454    4 -1.0     453        443  -427    u=4
455    5  -7.84    450  -451   443  -427    u=4
456    5  -7.84    452  -453   443  -427    u=4
457    5  -7.84    425  -411       -427    u=4
458    4 -1.0         -425       -427    u=4
c
c     TYPE B CELL  -  Short Boral on top and right
c
c     Right Side
c
459    0          -410   411  -412   413    u=5 fill=1 (1)
460    5  -7.84    410  -424   413  -426    u=5
470    4 -1.0     424  -428  548 -545    u=5
471    7  -2.7     428  -528 548 -545    u=5
472    6  -2.66   528  -532 548 -545    u=5
473    7  -2.7    532  -432  548 -545    u=5
474    4 -1.0     432  -436  548 -545    u=5
475    5  -7.84    436  -440  548 -545    u=5
476    4 -1.0     440        413         u=5
477    4 -1.0     424  -440   413 -547    u=5
478    4 -1.0     424  -440  546         u=5
479    5  -7.84    424  -440  547 -548    u=5
480    5  -7.84    424  -440  545 -546    u=5
c
c    Left Side
c
481    5  -7.84    425  -411  413         u=5
482    4 -1.0     429  -425   448  -445    u=5
483    7  -2.7    529  -429   448  -445    u=5
484    6  -2.66   533 -529   448  -445    u=5
485    7  -2.7     433 -533   448  -445    u=5
486    4 -1.0     437  -433   448  -445    u=5
487    5  -7.84    441  -437   448  -445    u=5
488    4 -1.0         -441   413         u=5
489    4 -1.0     441  -425   413  -447    u=5
490    4 -1.0     441  -425   446         u=5
491    5  -7.84    441  -425   447  -448    u=5
492    5  -7.84    441  -425   445  -446    u=5
c
c     Top
c
493    5  -7.84    411  -410   412  -426    u=5
494    4 -1.0    551 -552   426  -430    u=5
495    7  -2.7    551 -552   430 -530    u=5
496    6  -2.66   551 -552  530 -534    u=5
497    7  -2.7    551 -552  534  -434    u=5
498    4 -1.0    551 -552   434  -438    u=5
499    5  -7.84   551 -552   438  -442    u=5
500   4 -1.0     411  -424   442         u=5
501   4 -1.0     411 -550   426  -442    u=5
502   4 -1.0    553  -424   426  -442    u=5
503   5  -7.84   550 -551   426  -442    u=5
504   5  -7.84   552 -553   426  -442    u=5
```

```
c
c     Bottom
c
505   5  -7.84    427            -413    u=5
506   4 -1.0     451  -452   431  -427    u=5
507   7  -2.7     451  -452  531  -431    u=5
508   6  -2.66    451  -452  535 -531    u=5
509   7  -2.7     451  -452   435 -535    u=5
510   4 -1.0     451  -452   439  -435    u=5
511   5  -7.84    451  -452   443  -439    u=5
512   4 -1.0     411            -443    u=5
513   4 -1.0     411  -450   443  -427    u=5
514   4 -1.0     453        443  -427    u=5
515   5  -7.84    450  -451   443  -427    u=5
516   5  -7.84    452  -453   443  -427    u=5
517   5  -7.84    425  -411       -427    u=5
518   4 -1.0         -425       -427    u=5
c
c
c
c     TYPE D CELL  -  Short Boral on left and bottom, different cell ID
c
c number of cells: 51
c
c     Right Side
c
1570   0          -1410   1411  -1412   1413    u=17 fill=1 (1)
1571   5  -7.84    1410  -1424   1413  -1426    u=17
1572   4 -1.0     1424  -1428   1448  -1445    u=17
1573   7  -2.7     1428  -1528  1448  -1445    u=17
1574   6  -2.66   1528  -1532  1448  -1445    u=17
1575   7  -2.7    1532  -1432   1448  -1445    u=17
1576   4 -1.0     1432  -1436   1448  -1445    u=17
1577   5  -7.84    1436  -1440   1448  -1445    u=17
1578   4 -1.0     1440        1413         u=17
1579   4 -1.0     1424  -1440   1413  -1447    u=17
1580   4 -1.0     1424  -1440   1446         u=17
1581   5  -7.84    1424  -1440   1447  -1448    u=17
1582   5  -7.84    1424  -1440   1445  -1446    u=17
c
c    Left Side
c
1583   5  -7.84    1425  -1411   1413         u=17
1584   4 -1.0     1429  -1425  1548 -1545    u=17
1585   7  -2.7    1529  -1429  1548 -1545    u=17
1586   6  -2.66   1533 -1529  1548 -1545    u=17
1587   7  -2.7     1433 -1533  1548 -1545    u=17
1588   4 -1.0     1437  -1433  1548 -1545    u=17
1589   5  -7.84    1441  -1437  1548 -1545    u=17
1590   4 -1.0         -1441   1413         u=17
1591   4 -1.0     1441  -1425   1413 -1547    u=17
1592   4 -1.0     1441  -1425  1546         u=17
1593   5  -7.84    1441  -1425  1547 -1548    u=17
1594   5  -7.84    1441  -1425  1545 -1546    u=17
c
c     Top
c
1595   5  -7.84    1411  -1410   1412  -1426    u=17
1596   4 -1.0     1451  -1452   1426  -1430    u=17
1597   7  -2.7     1451  -1452   1430 -1530    u=17
1598   6  -2.66    1451  -1452  1530 -1534    u=17
```

```
1599   7  -2.7     1451  -1452  1534  -1434    u=17
1600   4 -1.0     1451  -1452   1434  -1438    u=17
1601   5  -7.84    1451  -1452   1438  -1442    u=17
1602   4 -1.0     1411  -1424   1442         u=17
1603   4 -1.0     1411  -1450   1426  -1442    u=17
1604   4 -1.0     1453  -1424   1426  -1442    u=17
1605   5  -7.84    1450  -1451   1426  -1442    u=17
1606   5  -7.84    1452  -1453   1426  -1442    u=17
c
c     Bottom
c
1607   5  -7.84    1427            -1413    u=17
1608   4 -1.0    1551 -1552   1431  -1427    u=17
1609   7  -2.7    1551 -1552  1531  -1431    u=17
1610   6  -2.66   1551 -1552  1535 -1531    u=17
1611   7  -2.7    1551 -1552   1435 -1535    u=17
1612   4 -1.0    1551 -1552   1439  -1435    u=17
1613   5  -7.84   1551 -1552   1443  -1439    u=17
1614   4 -1.0     1411            -1443    u=17
1615   4 -1.0     1411 -1550   1443  -1427    u=17
1616   4 -1.0    1553         1443  -1427    u=17
1617   5  -7.84   1550 -1551   1443  -1427    u=17
1618   5  -7.84   1552 -1553   1443  -1427    u=17
1619   5  -7.84    1425  -1411       -1427    u=17
1620   4 -1.0         -1425       -1427    u=17
c
c number of cells: 29
c
c empty cell no boral, no top
c
c
751     4 -1.0   -410   411  -412   413    u=14
752     5  -7.84    410  -424   413  -426    u=14
753    5  -7.84    425  -411   413         u=14
754    4 -1.0     411  -410   412  -426    u=14
755    5  -7.84    427            -413    u=14
756    5  -7.84    425  -411      -427    u=14
757    4 -1.0     411   426             u=14
758    4 -1.0     411  -427              u=14
759    4 -1.0    -425   413              u=14
760    4 -1.0     424   413   -426       u=14
761    4 -1.0    -425  -427              u=14
c
c
701   5   -7.84   701 -702 711 -713     u=9   $ steel post
702   5   -7.84   702 -703 711 -712     u=9   $ steel post
c
711   0           701 -705 711 -715 (702:713) (703:712)
                  fill=4 (13.8506 13.8506 0) u=9
712   0           704 (-706:-716) (705:715) -717 -710
                  fill=4 (17.9489 41.5518 0  0 1 0  -1 0 0   0 0 1) u=9
713   0           (705:715) -707 714 (-706:-716)  710
                  fill=4 (41.5518 17.9489 0  0 -1 0  1 0 0   0 0 1) u=9
714   0           701 -705 717 -719
                  fill=5 (13.8506 69.253 0) u=9
715   0           707 -709 711 -715
                  fill=5 (69.253 13.8506 0) u=9
716   0           706 -708 716 -718
                  fill=17 (45.6501 45.6501 0  -1 0 0  0 -1 0  0 0 1) u=9
717   0           705 -706 717 -719
                  fill=14 (41.5518 69.253 0) u=9
```

```
718    0            707 -709 715 -716
                    fill=14 (69.253 41.5518 0 0 1 0   1 0 0   0 0 1) u=9
719    0            701 -704 715 -717
                    fill=14 (-9.75233 41.5518 0  -1 0 0  0 1 0   0 0 1) u=9
720    0            705 -707 711 -714
                    fill=14 (41.5518 -9.75233 0   0 -1 0  1 0 0   0 0 1) u=9
721    4 -1.0      (706:719) (708:718) (709:716) u=9
c
c
c q-offset  0 inch
c
731    4 -1.0       720  721   fill=9 (0 0 0) u=19
732    4 -1.0      -720  721   fill=9 (0 0 0
                                -1 0 0  0  1 0  0 0 1) u=19
733    4 -1.0       720 -721   fill=9 (0 0 0
                                 1 0 0  0 -1 0  0 0 1) u=19
734    4 -1.0      -720 -721   fill=9 (0 0 0
                                -1 0 0  0 -1 0  0 0 1) u=19
c
673    0            -41                39  -40  fill=19
c
c number of cells: 6
102    4  -1.0     -41       40  -44            $ 6.0" Water above Fuel
103    5  -7.84    -41       44  -45            $ 15.5" Steel above Fuel
104    4  -1.0     -41      -39   43            $ 7.3" Water below Fuel
105    5  -7.84    -41      -43   46            $ 8.5" Steel below Fuel
106    5  -7.84    46  -45 41 -42               $ 6.0" Radial Steel Shield
107    0             -46:45:42                  $ Outside world
c end of cells
c --- empty line

c --- empty line
c start of surfaces
1      cz          0.4752    $ fuel
2      cz          0.4851    $ clad ID
3      cz          0.5436    $ clad OD
4      cz          0.6350    $ guide ID
5      cz          0.6706    $ guide OD
6      px          0.7214    $ pin pitch
7      px         -0.7214
8      py          0.7214
9      py         -0.7214
c
c
c cell-id       8.98
c cell-pitch    10.906
c wall-thkns    5/16
c angle-thkns   5/16
c boral-gap     0.0035
c boral-gap-o   0.0035
c boral-thkns   0.075
c boral-clad    0.01
c sheathing     0.0235
c boral-wide    7.5
c boral-narrow  6.25
c
c gap size      1.09
c basket-od     67.335
c
410    px          11.40460 $x 8.98/2
411    px         -11.40460 $x {410} *-1
```

```
412    py         11.40460 $x {410}
413    py        -11.40460 $x {411}
416    px         13.85062 $x (10.906 + 5/16 - 5/16) /2
417    px        -13.85062 $x -10.906 + {416}
418    py         13.85062 $x {416}
419    py        -13.85062 $x {417}
424    px         12.19835 $x {410} + 5/16     $ angle
425    px        -12.19835 $x {411} - 5/16     $ box wall
426    py         12.19835 $x {412} + 5/16
427    py        -12.19835 $x {413} - 5/16
428    px         12.20724 $x {424} + 0.0035   $ wall to boral gap
429    px        -12.20724 $x {425} - 0.0035
430    py         12.20724 $x {426} + 0.0035
431    py        -12.20724 $x {427} - 0.0035
432    px         12.39774 $x {428} + 0.075    $ boral
433    px        -12.39774 $x {429} - 0.075
434    py         12.39774 $x {430} + 0.075
435    py        -12.39774 $x {431} - 0.075
436    px         12.40663 $x {432} + 0.0035   $ boral to sheathing gap
437    px        -12.40663 $x {433} - 0.0035
438    py         12.40663 $x {434} + 0.0035
439    py        -12.40663 $x {435} - 0.0035
440    px         12.46632 $x {436} + 0.0235   $ sheathing
441    px        -12.46632 $x {437} - 0.0235
442    py         12.46632 $x {438} + 0.0235
443    py        -12.46632 $x {439} - 0.0235
445    py          9.52500 $x 7.5/2
446    py          9.58469 $x {445} + 0.0235   $ sheathing
447    py         -9.58469 $x {446} *-1
448    py         -9.52500 $x {445} *-1
450    px         -9.58469 $x {447}
451    px         -9.52500 $x {448}
452    px          9.52500 $x {445}
453    px          9.58469 $x {446}
528   px         12.23264 $x {428} + 0.01  $ Aluminum on the outside of boral
529   px        -12.23264 $x {429} - 0.01
530   py         12.23264 $x {430} + 0.01
531   py        -12.23264 $x {431} - 0.01
532   px         12.37234 $x {432} - 0.01
533   px        -12.37234 $x {433} + 0.01
534   py         12.37234 $x {434} - 0.01
535   py        -12.37234 $x {435} + 0.01
545   py         7.93750 $x 6.25/2
546   py         7.99719 $x {545} + 0.0235   $ sheathing
547   py        -7.99719 $x {546} *-1
548   py        -7.93750 $x {545} *-1
550   px        -7.99719 $x {547}
551   px        -7.93750 $x {548}
552   px         7.93750 $x {545}
553   px         7.99719 $x {546}
c
c cell-id-2 8.98
c gap-o     1.09
c
701   px        -5.0
702   px        1.90627 $x (10.906 - 8.98)/2 - 5/16 + 0.1
703   px        3.45694 $x 2.722/2
704   px        4.09829 $x 10.906 - 8.98 - 5/16
705   px        27.70124 $x 10.906
706   px        31.79953 $x 2 * 10.906 - (8.98+8.98)/2 - 5/16
707   px        55.40248 $x 2 * 10.906
```

```
708   px        59.50077 $x {707} + {704}
709   px        83.10372 $x 3 * 10.906
710   p     1  -1  0  0.1 $ diagonal x=y, offset by 0.1 to avoid intersecting corners
711   py        -4.99999 $x {701}
712   py        1.90627 $x {702}
713   py        3.45694 $x {703}
714   py        4.09829 $x {704}
715   py        27.70124 $x {705}
716   py        31.79953 $x {706}
717   py        55.40248 $x {707}
718   py        59.50077 $x {708}
719   py        83.10372 $x {709}
720   px        0.0
721   py        0.0
1410    px         11.40460 $x 8.98/2
1411    px        -11.40460 $x {1410} *-1
1412    py         11.40460 $x {1410}
1413    py        -11.40460 $x {1411}
1424    px         12.19835 $x {1410} + 5/16     $ angle
1425    px        -12.19835 $x {1411} - 5/16     $ box wall
1426    py         12.19835 $x {1412} + 5/16
1427    py        -12.19835 $x {1413} - 5/16
1428    px         12.20724 $x {1424} + 0.0035   $ wall to boral gap
1429    px        -12.20724 $x {1425} - 0.0035
1430    py         12.20724 $x {1426} + 0.0035
1431    py        -12.20724 $x {1427} - 0.0035
1432    px         12.39774 $x {1428} + 0.075    $ boral
1433    px        -12.39774 $x {1429} - 0.075
1434    py         12.39774 $x {1430} + 0.075
1435    py        -12.39774 $x {1431} - 0.075
1436    px         12.40663 $x {1432} + 0.0035   $ boral to sheathing gap
1437    px        -12.40663 $x {1433} - 0.0035
1438    py         12.40663 $x {1434} + 0.0035
1439    py        -12.40663 $x {1435} - 0.0035
1440    px         12.46632 $x {1436} + 0.0235   $ sheathing
1441    px        -12.46632 $x {1437} - 0.0235
1442    py         12.46632 $x {1438} + 0.0235
1443    py        -12.46632 $x {1439} - 0.0235
1445    py          9.52500 $x 7.5/2
1446    py          9.58469 $x {1445} + 0.0235   $ sheathing
1447    py         -9.58469 $x {1446} *-1
1448    py         -9.52500 $x {1445} *-1
1450    px         -9.58469 $x {1447}
1451    px         -9.52500 $x {1448}
1452    px          9.52500 $x {1445}
1453    px          9.58469 $x {1446}
1528   px         12.23264 $x {1428} + 0.01  $ Aluminum on the outside of boral
1529   px        -12.23264 $x {1429} - 0.01
1530   py         12.23264 $x {1430} + 0.01
1531   py        -12.23264 $x {1431} - 0.01
1532   px         12.37234 $x {1432} - 0.01
1533   px        -12.37234 $x {1433} + 0.01
1534   py         12.37234 $x {1434} - 0.01
1535   py        -12.37234 $x {1435} + 0.01
1545   py         7.93750 $x 6.25/2
1546   py         7.99719 $x {1545} + 0.0235   $ sheathing
1547   py        -7.99719 $x {1546} *-1
1548   py        -7.93750 $x {1545} *-1
1550   px        -7.99719 $x {1547}
1551   px        -7.93750 $x {1548}
1552   px         7.93750 $x {1545}
```

```
1553   px         7.99719 $x {1546}
46    pz         -31.75       $ 8.5"  lower steel thickness
43    pz         -10.16       $ lower water thickness
39    pz           0.0        $ bottom of active fuel assembly
40    pz         381.0        $ top of active fuel assembly
44    pz         396.24       $ upper water thickness
45    pz         435.61       $ 15.5" upper steel thickness
41    cz          85.57       $ mpc steel ID
42    cz         108.43       $ mpc water
c end of surfaces
c --- empty line

c --- empty line
tr1 0 0 0
kcode    10000  .94  20  120
sdef  par=1  erg=d1 axs=0 0 1 x=d4 y=fx d5 z=d3
c
sp1  -2 1.2895
c
sp3  0 1
c
si4  s         13 14
            12 13 14 15
         11 12 13 14 15 16
         11 12 13 14 15 16
            12 13 14 15
               13 14
sp4  1 23r
c
ds5  s                26 26
                   25 25 25 25
               24 24 24 24 24 24
               23 23 23 23 23 23
                   22 22 22 22
                      21 21
c
si11  -79.25435 -57.61355
si12  -51.88077 -30.23997
si13  -24.50719 -2.86639
si14   2.86639   24.50719
si15   30.23997  51.88077
si16   57.61355  79.25435
c
si21  -79.25435 -57.61355
si22  -51.88077 -30.23997
si23  -24.50719 -2.86639
si24   2.86639   24.50719
si25   30.23997  51.88077
si26   57.61355  79.25435
c
sp11  0 1
sp12  0 1
sp13  0 1
sp14  0 1
sp15  0 1
sp16  0 1
sp21  0 1
sp22  0 1
sp23  0 1
sp24  0 1
sp25  0 1
```

```
sp26  0 1
c
m3          40000.56c   1.           $ Zr Clad
m4          1001.50c    0.6667       $ Water
            8016.50c    0.3333
m5          24000.50c   0.01761      $ Steel
            25055.50c   0.001761
            26000.55c   0.05977
            28000.50c   0.008239
m6          5010.50c   -0.054427     $ Boral Central Section @ 0.02 g/cmsq
            5011.50c   -0.241373
            13027.50c  -0.6222
            6000.50c   -0.0821
m7          13027.50c   1.0
mt4        lwtr.01t
prdmp    j   -120   j   2
fm4      1000   1   -6
f4:n   1
sd4      1000
e4    1.000E-11   1.000E-10   5.000E-10   7.500E-10   1.000E-09   1.200E-09
      1.500E-09   2.000E-09   2.500E-09   3.000E-09
      4.700E-09   5.000E-09   7.500E-09   1.000E-08   2.530E-08
      3.000E-08   4.000E-08   5.000E-08   6.000E-08   7.000E-08
      8.000E-08   9.000E-08   1.000E-07   1.250E-07   1.500E-07
      1.750E-07   2.000E-07   2.250E-07   2.500E-07   2.750E-07
      3.000E-07   3.250E-07   3.500E-07   3.750E-07   4.000E-07
      4.500E-07   5.000E-07   5.500E-07   6.000E-07   6.250E-07
      6.500E-07   7.000E-07   7.500E-07   8.000E-07   8.500E-07
      9.000E-07   9.250E-07   9.500E-07   9.750E-07   1.000E-06
      1.010E-06   1.020E-06   1.030E-06   1.040E-06   1.050E-06
      1.060E-06   1.070E-06   1.080E-06   1.090E-06   1.100E-06
      1.110E-06   1.120E-06   1.130E-06   1.140E-06   1.150E-06
      1.175E-06   1.200E-06   1.225E-06   1.250E-06   1.300E-06
      1.350E-06   1.400E-06   1.450E-06   1.500E-06   1.590E-06
      1.680E-06   1.770E-06   1.860E-06   1.940E-06   2.000E-06
      2.120E-06   2.210E-06   2.300E-06   2.380E-06   2.470E-06
      2.570E-06   2.670E-06   2.770E-06   2.870E-06   2.970E-06
      3.000E-06   3.050E-06   3.150E-06   3.500E-06   3.730E-06
      4.000E-06   4.750E-06   5.000E-06   5.400E-06   6.000E-06
      6.250E-06   6.500E-06   6.750E-06   7.000E-06   7.150E-06
      8.100E-06   9.100E-06   1.000E-05   1.150E-05   1.190E-05
      1.290E-05   1.375E-05   1.440E-05   1.510E-05   1.600E-05
      1.700E-05   1.850E-05   1.900E-05   2.000E-05   2.100E-05
      2.250E-05   2.500E-05   2.750E-05   3.000E-05   3.125E-05
      3.175E-05   3.325E-05   3.375E-05   3.460E-05   3.550E-05
      3.700E-05   3.800E-05   3.910E-05   3.960E-05   4.100E-05
      4.240E-05   4.400E-05   4.520E-05   4.700E-05   4.830E-05
      4.920E-05   5.060E-05   5.200E-05   5.340E-05   5.900E-05
      6.100E-05   6.500E-05   6.750E-05   7.200E-05   7.600E-05
      8.000E-05   8.200E-05   9.000E-05   1.000E-04   1.080E-04
      1.150E-04   1.190E-04   1.220E-04   1.860E-04   1.925E-04
      2.075E-04   2.100E-04   2.400E-04   2.850E-04   3.050E-04
      5.500E-04   6.700E-04   6.830E-04   9.500E-04   1.150E-03
      1.500E-03   1.550E-03   1.800E-03   2.200E-03   2.290E-03
      2.580E-03   3.000E-03   3.740E-03   3.900E-03   6.000E-03
      8.030E-03   9.500E-03   1.300E-02   1.700E-02   2.500E-02
      3.000E-02   4.500E-02   5.000E-02   5.200E-02   6.000E-02
      7.300E-02   7.500E-02   8.200E-02   8.500E-02   1.000E-01
      1.283E-01   1.500E-01   2.000E-01   2.700E-01   3.300E-01
      4.000E-01   4.200E-01   4.400E-01   4.700E-01   4.995E-01
      5.500E-01   5.730E-01   6.000E-01   6.700E-01   6.790E-01
```

```
      7.500E-01   8.200E-01   8.611E-01   8.750E-01   9.000E-01
      9.200E-01   1.010E+00   1.100E+00   1.200E+00   1.250E+00
      1.317E+00   1.356E+00   1.400E+00   1.500E+00   1.850E+00
      2.354E+00   2.479E+00   3.000E+00   4.304E+00   4.800E+00
      6.434E+00   8.187E+00   1.000E+01   1.284E+01   1.384E+01
      1.455E+01   1.568E+01   1.733E+01   2.000E+01
si3  h 0 381.00
imp:n 1 193r 0
c fuel enrichment 4.1 %
m1      92235.50c     -0.03614
        92238.50c     -0.84536
         8016.50c     -0.11850
c end of file
c
```

```
HI-STAR containing MPC68, 08x08 @ 4.2 wt% Enrich.
c     4.20 % uniform enrichment,  unreflected cask, 0.0279 g/cmsq B-10 in Boral
c
c
1     1 -10.522      -1  u=2       $ fuel
2     4 -1.0      1  -2  u=2       $ gap
3     3 -6.55    2  -3  u=2       $ Zr Clad
4     4 -1.0          3  u=2       $ water in fuel region
5     4 -1.0   -4:5     u=3       $ water in guide tubes
6     3 -6.55   4 -5    u=3       $ guide tubes
7     4 -1.0   -6   +7   -8   +9   u=1  lat=1
      fill= -5:4    -5:4   0:0
      1  1 1 1 1 1 1 1 1  1
      1  2 2 2 2 2 2 2 2  1
      1  2 2 2 2 2 2 2 2  1
      1  2 2 2 2 2 2 2 2  1
      1  2 2 2 3 2 2 2 2  1
      1  2 2 2 2 3 2 2 2  1
      1  2 2 2 2 2 2 2 2  1
      1  2 2 2 2 2 2 2 2  1
      1  2 2 2 2 2 2 2 2  1
      1  1 1 1 1 1 1 1 1  1
c
C  BOX TYPE R
c
8     0  -10   11  -12   13          u=4 fill=1 (0.8128  0.8128  0)
9     3  -6.55    60   -61    62   -63  #8      u=4     $ Zr flow channel
10    4  -1.      64   -65    66   -67  #8 #9   u=4     $ water
11    5  -7.84    20   -23    67   -14          u=4     $ 0.075" STEEL
12    4  -1.      20   -23    14   -15          u=4     $ WATER POCKET
13    7  -2.7     20   -23    15   -16          u=4     $ Al CLAD
14    6  -2.66    20   -23    16   -17          u=4     $ BORAL Absorber
15    7  -2.7     20   -23    17   -18          u=4     $ Al Clad
16    4  -1.      20   -23    18  -118          u=4     $ Water
17    5  -7.84    118:-129:65:-66               u=4     $ Steel
18    4  -1.      64   -21    67   -118         u=4     $ Water
19    4  -1.      24   -65    67   -118         u=4     $ water
20    5  -7.84    21   -20    67   -118         u=4     $ Steel
21    5  -7.84    23   -24    67   -118         u=4     $ Steel
22    4  -1.     129   -64    33   -118         u=4     $ Water
c
23    5  -7.84    25   -64    30   -31          u=4     $ Steel
24    4  -1.      26   -25    30   -31          u=4     $ Water
25    7  -2.7     27   -26    30   -31          u=4     $ Al clad
26    6  -2.66    28   -27    30   -31          u=4     $ Boral
27    7  -2.7     29   -28    30   -31          u=4     $ Al clad
28    4  -1.     129   -29    30   -31          u=4     $ water
29    5  -7.84   129   -64    32   -30          u=4     $ Steel ends
30    5  -7.84   129   -64    31   -33          u=4     $ Steel ends
31    4  -1.     129   -64    66   -32          u=4     $ Water
c
c    Type A box - Boral only on left side
c
32    0  -10   11  -12   13          u=6 fill=1 (0.8128  0.8128  0)
33    3  -6.55    60   -61    62   -63  #8      u=6     $ Zr flow channel
34    4  -1.      64   -65    66  -118  #8 #9   u=6     $ water
35    5  -7.84    118:-129:65:-66               u=6     $ Steel
36    4  -1.     129   -64    67   -118         u=6     $ Water
c
37    5  -7.84    25   -64    30   -31          u=6     $ Steel
38    4  -1.      26   -25    30   -31          u=6     $ Water
```

```
39    7  -2.7     27   -26    30   -31          u=6     $ Al clad
40    6  -2.66    28   -27    30   -31          u=6     $ Boral
41    7  -2.7     29   -28    30   -31          u=6     $ Al clad
42    4  -1.     129   -29    30   -31          u=6     $ water
43    4  -1.     129   -64    33   -67          u=6     $ Water
44    5  -7.84   129   -64    32   -30          u=6     $ Steel ends
45    5  -7.84   129   -64    31   -33          u=6     $ Steel ends
46    4  -1.     129   -64    66   -32          u=6     $ Water
c
c    Type B box -  Boral on Top only
c
47    0  -10   11  -12   13         u=7 fill=1 (0.8128  0.8128  0)
48    3  -6.55    60   -61    62   -63  #8      u=7     $ Zr flow channel
49    4  -1.      64   -65    66   -67  #8 #9   u=7     $ water
50    5  -7.84    20   -23    67   -14          u=7     $ 0.075" STEEL
51    4  -1.      20   -23    14   -15          u=7     $ WATER POCKET
52    7  -2.7     20   -23    15   -16          u=7     $ Al CLAD
53    6  -2.66    20   -23    16   -17          u=7     $ BORAL Absorber
54    7  -2.7     20   -23    17   -18          u=7     $ water
55    4  -1.      20   -23    18  -118          u=7     $ Water
56    5  -7.84    118:-129:65:-66               u=7     $ Steel
57    4  -1.      64   -21    67   -118         u=7     $ Water
58    4  -1.      24   -65    67   -118         u=7     $ water
59    5  -7.84    21   -20    67   -118         u=7     $ Steel
60    5  -7.84    23   -24    67   -118         u=7     $ Steel
61    4  -1.     129   -64    66   -118         u=7     $ Water
c
c    Type E box  - No Boral Panels
c
62    0  -10   11  -12   13         u=8 fill=1 (0.8128  0.8128  0)
63    3  -6.55    60   -61    62   -63  #8      u=8     $ Zr flow channel
64    4  -1.     129   -65    66  -118  #8 #9   u=8     $ water
65    5  -7.84    118:-129:65:-66               u=8     $ Steel
c
c    Type F box  - No Boral Panels or fuel
c
66    4  -1.     129   -65    66  -118          u=9     $ water
67    5  -7.84    118:-129:65:-66               u=9     $ Steel
c
68    4  -1.0    -34  35  -36  37  u=5  lat=1  fill=-7:6  -7:6  0:0
               5 5 5 5 5 5 5 5 5 5 5 5 5 5
               5 9 9 9 9 9 9 9 9 9 9 9 9 5
               5 9 9 9 9 9 7 4 9 9 9 9 9 5
               5 9 9 9 7 4 4 4 4 4 9 9 9 5
               5 9 9 7 4 4 4 4 4 4 4 9 9 5
               5 9 9 7 4 4 4 4 4 4 4 9 9 5
               5 9 7 4 4 4 4 4 4 4 4 4 9 5
               5 9 8 4 4 4 4 4 4 4 4 6 9 5
               5 9 9 7 4 4 4 4 4 4 4 9 9 5
               5 9 9 8 4 4 4 4 4 4 6 9 9 5
               5 9 9 9 8 4 4 4 6 6 9 9 9 5
               5 9 9 9 9 9 8 6 9 9 9 9 9 5
               5 9 9 9 9 9 9 9 9 9 9 9 9 5
               5 5 5 5 5 5 5 5 5 5 5 5 5 5
69    0          -41                 50  -49  fill=5 (8.1661  8.1661  0)
70    4  -1.0    -41        43  -50             $ Water below Fuel
71    4  -1.0    -41        49  -44             $ Water above Fuel
72    5  -7.84   -42        68  -43             $ Steel below Fuel
73    5  -7.84   -42        44  -69             $ Steel above Fuel
74    5  -7.84    41  -42  43  -44              $ Radial Steel
75    0            42 :-68:  69                 $ outside world
```

```
1      cz        0.5207      $ Fuel OD
2      cz        0.5321      $ Clad ID
3      cz        0.6134      $ Clad OD
4      cz        0.6744      $ Thimble ID
5      cz        0.7506      $ Thimble OD
6      px        0.8128      $ Pin Pitch
7      px       -0.8128
8      py        0.8128
9      py       -0.8128
10     px        6.7031      $ Channel ID
11     px       -6.7031
12     py        6.7031
13     py       -6.7031
14     py        7.8016
15     py        7.8155
16     py        7.8410
17     py        8.0467
18     py        8.0721
118    py        8.0861
20     px       -6.0325
21     px       -6.2230
23     px        6.0325
24     px        6.2230
25     px       -7.8016
26     px       -7.8155
27     px       -7.8410
28     px       -8.0467
29     px       -8.0721
129    px       -8.0861
30     py       -6.0325
31     py        6.0325
32     py       -6.2230
33     py        6.2230
34     px        7.6111
35     px       -8.7211
36     py        8.7211
37     py       -7.6111
41     cz        85.57
42     cz        108.43
43     pz       -18.54
44     pz        402.5
49     pz        381.         $ Top of Active Fuel
50     pz          0          $ Start of Active Fuel
60     px       -6.9571      $ Channel OD
61     px        6.9571
62     py       -6.9571
63     py        6.9571
64     px       -7.6111      $ Cell Box ID
65     px        7.6111
66     py       -7.6111
67     py        7.6111
68     pz       -40.13
69     pz        441.9

imp:n     1 73r 0
kcode   10000  0.94   20  120
c
sdef  par=1  erg=d1 axs=0 0 1 x=d4 y=fx d5 z=d3
c
sp1 -2 1.2895
```

```
c
c
si3  h 0 365.76
sp3  0 1
c
c
si4  s                15 16
                 13 14 15 16 17 18
             12 13 14 15 16 17 18 19
             12 13 14 15 16 17 18 19
          11 12 13 14 15 16 17 18 19 20
          11 12 13 14 15 16 17 18 19 20
             12 13 14 15 16 17 18 19
             12 13 14 15 16 17 18 19
                 13 14 15 16 17 18
                       15 16
sp4  1 67r
c
ds5  s                30 30
                 29 29 29 29 29 29
             28 28 28 28 28 28 28 28
             27 27 27 27 27 27 27 27
          26 26 26 26 26 26 26 26 26 26
          25 25 25 25 25 25 25 25 25 25
             24 24 24 24 24 24 24 24
             23 23 23 23 23 23 23 23
                 22 22 22 22 22 22
                       21 21
c
si11  -80.6831 -67.6783
si12  -64.1985 -51.1937
si13  -47.7139 -34.7091
si14  -31.2293 -18.2245
si15  -14.7447 -1.7399
si16   1.7399   14.7447
si17   18.2245  31.2293
si18   34.7091  47.7139
si19   51.1937  64.1985
si20   67.6783  80.6831
c
si21  -80.6831 -67.6783
si22  -64.1985 -51.1937
si23  -47.7139 -34.7091
si24  -31.2293 -18.2245
si25  -14.7447 -1.7399
si26   1.7399   14.7447
si27   18.2245  31.2293
si28   34.7091  47.7139
si29   51.1937  64.1985
si30   67.6783  80.6831
sp11  0 1
sp12  0 1
sp13  0 1
sp14  0 1
sp15  0 1
sp16  0 1
sp17  0 1
sp18  0 1
sp19  0 1
sp20  0 1
sp21  0 1
```

```
sp22  0 1
sp23  0 1
sp24  0 1
sp25  0 1
sp26  0 1
sp27  0 1
sp28  0 1
sp29  0 1
sp30  0 1
c
m1          92235.50c   9.98343E-04  $ 4.20% E Fuel
            92238.50c   0.022484
            8016.50c    0.046965
m2          8016.50c    1.           $ Void
m3          40000.56c   1.           $ Zr Clad
m4          1001.50c    0.6667       $ Water
            8016.50c    0.3333
m5          24000.50c   0.01761      $ Steel
            25055.50c   0.001761
            26000.55c   0.05977
            28000.50c   0.008239
m6          5010.50c    8.0707E-03   $ Boral
            5011.50c    3.2553E-02
            6000.50c    1.0146E-02
            13027.50c   3.8054E-02
m7          13027.50c    1.           $ Al Clad
mt4        lwtr.01t
prdmp    j   -30   1   2
fm4      1000   1   -6
f4:n   1
sd4      1000
e4    1.000E-11   1.000E-10   5.000E-10   7.500E-10   1.000E-09   1.200E-09
      1.500E-09   2.000E-09   2.500E-09   3.000E-09
      4.700E-09   5.000E-09   7.500E-09   1.000E-08   2.530E-08
      3.000E-08   4.000E-08   5.000E-08   6.000E-08   7.000E-08
      8.000E-08   9.000E-08   1.000E-07   1.250E-07   1.500E-07
      1.750E-07   2.000E-07   2.250E-07   2.500E-07   2.750E-07
      3.000E-07   3.250E-07   3.500E-07   3.750E-07   4.000E-07
      4.500E-07   5.000E-07   5.500E-07   6.000E-07   6.250E-07
      6.500E-07   7.000E-07   7.500E-07   8.000E-07   8.500E-07
      9.000E-07   9.250E-07   9.500E-07   9.750E-07   1.000E-06
      1.010E-06   1.020E-06   1.030E-06   1.040E-06   1.050E-06
      1.060E-06   1.070E-06   1.080E-06   1.090E-06   1.100E-06
      1.110E-06   1.120E-06   1.130E-06   1.140E-06   1.150E-06
      1.175E-06   1.200E-06   1.225E-06   1.250E-06   1.300E-06
      1.350E-06   1.400E-06   1.450E-06   1.500E-06   1.590E-06
      1.680E-06   1.770E-06   1.860E-06   1.940E-06   2.000E-06
      2.120E-06   2.210E-06   2.300E-06   2.380E-06   2.470E-06
      2.570E-06   2.670E-06   2.770E-06   2.870E-06   2.970E-06
      3.000E-06   3.050E-06   3.150E-06   3.500E-06   3.730E-06
      4.000E-06   4.750E-06   5.000E-06   5.400E-06   6.000E-06
      6.250E-06   6.500E-06   6.750E-06   7.000E-06   7.150E-06
      8.100E-06   9.100E-06   1.000E-05   1.150E-05   1.190E-05
      1.290E-05   1.375E-05   1.440E-05   1.510E-05   1.600E-05
      1.700E-05   1.850E-05   1.900E-05   2.000E-05   2.100E-05
      2.250E-05   2.500E-05   2.750E-05   3.000E-05   3.125E-05
      3.175E-05   3.325E-05   3.375E-05   3.460E-05   3.550E-05
      3.700E-05   3.800E-05   3.910E-05   3.960E-05   4.100E-05
      4.240E-05   4.400E-05   4.520E-05   4.700E-05   4.830E-05
      4.920E-05   5.060E-05   5.200E-05   5.340E-05   5.900E-05
      6.100E-05   6.500E-05   6.750E-05   7.200E-05   7.600E-05
```

8.000E-05	8.200E-05	9.000E-05	1.000E-04	1.080E-04
1.150E-04	1.190E-04	1.220E-04	1.860E-04	1.925E-04
2.075E-04	2.100E-04	2.400E-04	2.850E-04	3.050E-04
5.500E-04	6.700E-04	6.830E-04	9.500E-04	1.150E-03
1.500E-03	1.550E-03	1.800E-03	2.200E-03	2.290E-03
2.580E-03	3.000E-03	3.740E-03	3.900E-03	6.000E-03
8.030E-03	9.500E-03	1.300E-02	1.700E-02	2.500E-02
3.000E-02	4.500E-02	5.000E-02	5.200E-02	6.000E-02
7.300E-02	7.500E-02	8.200E-02	8.500E-02	1.000E-01
1.283E-01	1.500E-01	2.000E-01	2.700E-01	3.300E-01
4.000E-01	4.200E-01	4.400E-01	4.700E-01	4.995E-01
5.500E-01	5.730E-01	6.000E-01	6.700E-01	6.790E-01
7.500E-01	8.200E-01	8.611E-01	8.750E-01	9.000E-01
9.200E-01	1.010E+00	1.100E+00	1.200E+00	1.250E+00
1.317E+00	1.356E+00	1.400E+00	1.500E+00	1.850E+00
2.354E+00	2.479E+00	3.000E+00	4.304E+00	4.800E+00
6.434E+00	8.187E+00	1.000E+01	1.284E+01	1.384E+01
1.455E+01	1.568E+01	1.733E+01	2.000E+01	

```
HI-STAR containing MPC68F, 06x06 @ 3.0 wt% Enrich.
c     3.00 % uniform enrichment, unreflected cask, 0.0067 g/cmsq B-10 in Boral
c     Dresden-1 6x6
c
c
1     1 -10.522     -1  u=2       $ fuel
2     4 -1.0     1  -2  u=2       $ gap
3     3 -6.55    2  -3  u=2       $ Zr Clad
4     4 -1.0         3  u=2       $ water in fuel region
5     4 -1.0   -4:5     u=3       $ water in guide tubes
6     3 -6.55   4 -5    u=3       $ guide tubes
7     4 -1.0   -6   +7   -8   +9   u=1  lat=1
      fill= -4:3    -4:3   0:0
      1  1 1 1 1 1 1  1
      1  2 2 2 2 2 2  1
      1  2 2 2 2 2 2  1
      1  2 2 2 2 2 2  1
      1  2 2 2 2 2 2  1
      1  2 2 2 2 2 2  1
      1  2 2 2 2 2 2  1
      1  1 1 1 1 1 1  1
c
C  BOX TYPE R
c
8     0  -10   11  -12   13         u=4 fill=1 (0.8814  0.8814  0)
9     3  -6.55    60   -61    62   -63  #8      u=4     $ Zr flow channel
10    4  -1.      64   -65    66   -67  #8 #9   u=4     $ water
11    5  -7.84    20   -23    67   -14          u=4     $ 0.075" STEEL
12    4  -1.      20   -23    14   -15          u=4     $ WATER POCKET
13    7  -2.7     20   -23    15   -16          u=4     $ Al CLAD
14    6  -2.66    20   -23    16   -17          u=4     $ BORAL Absorber
15    7  -2.7     20   -23    17   -18          u=4     $ Al Clad
16    4  -1.      20   -23    18  -118          u=4     $ Water
17    5  -7.84    118:-129:65:-66               u=4     $ Steel
18    4  -1.      64   -21    67   -118         u=4     $ Water
19    4  -1.      24   -65    67   -118         u=4     $ water
20    5  -7.84    21   -20    67   -118         u=4     $ Steel
21    5  -7.84    23   -24    67   -118         u=4     $ Steel
22    4  -1.     129   -64    33   -118         u=4     $ Water
c
23    5  -7.84    25   -64    30   -31          u=4     $ Steel
24    4  -1.      26   -25    30   -31          u=4     $ Water
25    7  -2.7     27   -26    30   -31          u=4     $ Al clad
26    6  -2.66    28   -27    30   -31          u=4     $ Boral
27    7  -2.7     29   -28    30   -31          u=4     $ Al clad
28    4  -1.     129   -29    30   -31          u=4     $ water
29    5  -7.84   129   -64    32   -30          u=4     $ Steel ends
30    5  -7.84   129   -64    31   -33          u=4     $ Steel ends
31    4  -1.     129   -64    66   -32          u=4     $ Water
c
c    Type A box - Boral only on left side
c
32    0  -10   11  -12   13         u=6 fill=1 (0.8814  0.8814  0)
33    3  -6.55    60   -61    62   -63  #8      u=6     $ Zr flow channel
34    4  -1.      64   -65    66  -118  #8 #9   u=6     $ water
35    5  -7.84    118:-129:65:-66               u=6     $ Steel
36    4  -1.     129   -64    67   -118         u=6     $ Water
c
37    5  -7.84    25   -64    30   -31          u=6     $ Steel
38    4  -1.      26   -25    30   -31          u=6     $ Water
39    7  -2.7     27   -26    30   -31          u=6     $ Al clad
```

```
40    6  -2.66    28   -27    30   -31          u=6     $ Boral
41    7  -2.7     29   -28    30   -31          u=6     $ Al clad
42    4  -1.     129   -29    30   -31          u=6     $ water
43    4  -1.     129   -64    33   -67          u=6     $ Water
44    5  -7.84   129   -64    32   -30          u=6     $ Steel ends
45    5  -7.84   129   -64    31   -33          u=6     $ Steel ends
46    4  -1.     129   -64    66   -32          u=6     $ Water
c
c    Type B box -  Boral on Top only
c
47    0  -10   11  -12   13         u=7 fill=1 (0.8814  0.8814  0)
48    3  -6.55    60   -61    62   -63  #8      u=7     $ Zr flow channel
49    4  -1.      64   -65    66   -67  #8 #9   u=7     $ water
50    5  -7.84    20   -23    67   -14          u=7     $ 0.075" STEEL
51    4  -1.      20   -23    14   -15          u=7     $ WATER POCKET
52    7  -2.7     20   -23    15   -16          u=7     $ Al CLAD
53    6  -2.66    20   -23    16   -17          u=7     $ BORAL Absorber
54    7  -2.7     20   -23    17   -18          u=7     $ water
55    4  -1.      20   -23    18  -118          u=7     $ Water
56    5  -7.84    118:-129:65:-66               u=7     $ Steel
57    4  -1.      64   -21    67   -118         u=7     $ Water
58    4  -1.      24   -65    67   -118         u=7     $ water
59    5  -7.84    21   -20    67   -118         u=7     $ Steel
60    5  -7.84    23   -24    67   -118         u=7     $ Steel
61    4  -1.     129   -64    66   -118         u=7     $ Water
c
c    Type E box  - No Boral Panels
c
62    0  -10   11  -12   13         u=8 fill=1 (0.8814  0.8814  0)
63    3  -6.55    60   -61    62   -63  #8      u=8     $ Zr flow channel
64    4  -1.     129   -65    66  -118  #8 #9   u=8     $ water
65    5  -7.84    118:-129:65:-66               u=8     $ Steel
c
c    Type F box  - No Boral Panels or fuel
c
66    4  -1.     129   -65    66  -118          u=9     $ water
67    5  -7.84    118:-129:65:-66               u=9     $ Steel
c
68    4  -1.0    -34  35  -36  37  u=5  lat=1  fill=-7:6  -7:6  0:0
               5 5 5 5 5 5 5 5 5 5 5 5 5 5
               5 9 9 9 9 9 9 9 9 9 9 9 9 5
               5 9 9 9 9 9 7 4 9 9 9 9 9 5
               5 9 9 9 7 4 4 4 4 4 9 9 9 5
               5 9 9 7 4 4 4 4 4 4 4 9 9 5
               5 9 9 7 4 4 4 4 4 4 4 9 9 5
               5 9 7 4 4 4 4 4 4 4 4 4 9 5
               5 9 8 4 4 4 4 4 4 4 4 6 9 5
               5 9 9 7 4 4 4 4 4 4 4 9 9 5
               5 9 9 8 4 4 4 4 4 4 6 9 9 5
               5 9 9 9 8 4 4 4 6 6 9 9 9 5
               5 9 9 9 9 9 8 6 9 9 9 9 9 5
               5 9 9 9 9 9 9 9 9 9 9 9 9 5
               5 5 5 5 5 5 5 5 5 5 5 5 5 5
69    0           -41                 50  -49  fill=5 (8.1661  8.1661  0)
70    4  -1.0    -41        43  -50             $ Water below Fuel
71    4  -1.0    -41        49  -44             $ Water above Fuel
72    5  -7.84   -42        68  -43             $ Steel below Fuel
73    5  -7.84   -42        44  -69             $ Steel above Fuel
74    5  -7.84    41  -42  43  -44              $ Radial Steel
75    0            42 :-68:  69                 $ outside world
```

```
1      cz        0.6274       $ Fuel OD
2      cz        0.6280       $ Clad ID
3      cz        0.7169       $ Clad OD
4      cz        0.6280       $ Thimble ID
5      cz        0.7169       $ Thimble OD
6      px        0.8814       $ Pin Pitch
7      px       -0.8814
8      py        0.8814
9      py       -0.8814
10     px        5.4483       $ Channel ID
11     px       -5.4483
12     py        5.4483
13     py       -5.4483
14     py        7.8016
15     py        7.8155
16     py        7.8410
17     py        8.0467
18     py        8.0721
118    py        8.0861
20     px       -6.0325
21     px       -6.2230
23     px        6.0325
24     px        6.2230
25     px       -7.8016
26     px       -7.8155
27     px       -7.8410
28     px       -8.0467
29     px       -8.0721
129    px       -8.0861
30     py       -6.0325
31     py        6.0325
32     py       -6.2230
33     py        6.2230
34     px        7.6111
35     px       -8.7211
36     py        8.7211
37     py       -7.6111
41     cz        85.57
42     cz        108.43
43     pz        11.46
44     pz        331.0
49     pz        309.4         $ Top of Active F
50     pz         30.          $ Start of Active
60     px       -5.6007        $ Channel OD
61     px        5.6007
62     py       -5.6007
63     py        5.6007
64     px       -7.6111        $ Cell Box ID
65     px        7.6111
66     py       -7.6111
67     py        7.6111
68     pz       -10.13
69     pz        370.36

imp:n     1 73r 0
kcode    10000  0.94   20  120
c
sdef  par=1  erg=d1 axs=0 0 1 x=d4 y=fx d5 z=d3
c
sp1 -2 1.2895
c
```

```
si3  h 30. 309.
sp3  0 1
c
c
si4  s                15 16
                 13 14 15 16 17 18
             12 13 14 15 16 17 18 19
             12 13 14 15 16 17 18 19
         11 12 13 14 15 16 17 18 19 20
         11 12 13 14 15 16 17 18 19 20
             12 13 14 15 16 17 18 19
             12 13 14 15 16 17 18 19
                 13 14 15 16 17 18
                       15 16
sp4  1 67r
c
ds5  s                30 30
                 29 29 29 29 29 29
             28 28 28 28 28 28 28 28
             27 27 27 27 27 27 27 27
         26 26 26 26 26 26 26 26 26 26
         25 25 25 25 25 25 25 25 25 25
             24 24 24 24 24 24 24 24
             23 23 23 23 23 23 23 23
                 22 22 22 22 22 22
                       21 21
c
si11  -80.6831 -67.6783
si12  -64.1985 -51.1937
si13  -47.7139 -34.7091
si14  -31.2293 -18.2245
si15  -14.7447 -1.7399
si16   1.7399   14.7447
si17   18.2245  31.2293
si18   34.7091  47.7139
si19   51.1937  64.1985
si20   67.6783  80.6831
c
si21  -80.6831 -67.6783
si22  -64.1985 -51.1937
si23  -47.7139 -34.7091
si24  -31.2293 -18.2245
si25  -14.7447 -1.7399
si26   1.7399   14.7447
si27   18.2245  31.2293
si28   34.7091  47.7139
si29   51.1937  64.1985
si30   67.6783  80.6831
sp11  0 1
sp12  0 1
sp13  0 1
sp14  0 1
sp15  0 1
sp16  0 1
sp17  0 1
sp18  0 1
sp19  0 1
sp20  0 1
sp21  0 1
sp22  0 1
sp23  0 1
```

```
sp24  0 1
sp25  0 1
sp26  0 1
sp27  0 1
sp28  0 1
sp29  0 1
sp30  0 1
c
m1          92235.50c   -0.02644      $ 3.00% E Fuel
            92238.50c   -0.85504
            8016.50c    -0.11852
m3          40000.56c   1.            $ Zr Clad
m4          1001.50c    0.6667        $ Water
            8016.50c    0.3333
m5          24000.50c   0.01761       $ Steel
            25055.50c   0.001761
            26000.55c   0.05977
            28000.50c   0.008239
m6          5010.50c  1.9592E-03       $ Boral 0.0067 gm/cm2
            5011.50c  8.1175E-03
            6000.50c  2.5176E-03
            13027.50c 5.4933E-02
m7          13027.50c    1.            $ Al Clad
mt4        lwtr.01t
prdmp    j   -120   j   2
fm4      1000   1   -6
f4:n   1
sd4      1000
e4    1.000E-11   1.000E-10   5.000E-10   7.500E-10   1.000E-09   1.200E-09
      1.500E-09   2.000E-09   2.500E-09   3.000E-09
      4.700E-09   5.000E-09   7.500E-09   1.000E-08   2.530E-08
      3.000E-08   4.000E-08   5.000E-08   6.000E-08   7.000E-08
      8.000E-08   9.000E-08   1.000E-07   1.250E-07   1.500E-07
      1.750E-07   2.000E-07   2.250E-07   2.500E-07   2.750E-07
      3.000E-07   3.250E-07   3.500E-07   3.750E-07   4.000E-07
      4.500E-07   5.000E-07   5.500E-07   6.000E-07   6.250E-07
      6.500E-07   7.000E-07   7.500E-07   8.000E-07   8.500E-07
      9.000E-07   9.250E-07   9.500E-07   9.750E-07   1.000E-06
      1.010E-06   1.020E-06   1.030E-06   1.040E-06   1.050E-06
      1.060E-06   1.070E-06   1.080E-06   1.090E-06   1.100E-06
      1.110E-06   1.120E-06   1.130E-06   1.140E-06   1.150E-06
      1.175E-06   1.200E-06   1.225E-06   1.250E-06   1.300E-06
      1.350E-06   1.400E-06   1.450E-06   1.500E-06   1.590E-06
      1.680E-06   1.770E-06   1.860E-06   1.940E-06   2.000E-06
      2.120E-06   2.210E-06   2.300E-06   2.380E-06   2.470E-06
      2.570E-06   2.670E-06   2.770E-06   2.870E-06   2.970E-06
      3.000E-06   3.050E-06   3.150E-06   3.500E-06   3.730E-06
      4.000E-06   4.750E-06   5.000E-06   5.400E-06   6.000E-06
      6.250E-06   6.500E-06   6.750E-06   7.000E-06   7.150E-06
      8.100E-06   9.100E-06   1.000E-05   1.150E-05   1.190E-05
      1.290E-05   1.375E-05   1.440E-05   1.510E-05   1.600E-05
      1.700E-05   1.850E-05   1.900E-05   2.000E-05   2.100E-05
      2.250E-05   2.500E-05   2.750E-05   3.000E-05   3.125E-05
      3.175E-05   3.325E-05   3.375E-05   3.460E-05   3.550E-05
      3.700E-05   3.800E-05   3.910E-05   3.960E-05   4.100E-05
      4.240E-05   4.400E-05   4.520E-05   4.700E-05   4.830E-05
      4.920E-05   5.060E-05   5.200E-05   5.340E-05   5.900E-05
      6.100E-05   6.500E-05   6.750E-05   7.200E-05   7.600E-05
      8.000E-05   8.200E-05   9.000E-05   1.000E-04   1.080E-04
      1.150E-04   1.190E-04   1.220E-04   1.860E-04   1.925E-04
      2.075E-04   2.100E-04   2.400E-04   2.850E-04   3.050E-04
```

5.500E-04	6.700E-04	6.830E-04	9.500E-04	1.150E-03
1.500E-03	1.550E-03	1.800E-03	2.200E-03	2.290E-03
2.580E-03	3.000E-03	3.740E-03	3.900E-03	6.000E-03
8.030E-03	9.500E-03	1.300E-02	1.700E-02	2.500E-02
3.000E-02	4.500E-02	5.000E-02	5.200E-02	6.000E-02
7.300E-02	7.500E-02	8.200E-02	8.500E-02	1.000E-01
1.283E-01	1.500E-01	2.000E-01	2.700E-01	3.300E-01
4.000E-01	4.200E-01	4.400E-01	4.700E-01	4.995E-01
5.500E-01	5.730E-01	6.000E-01	6.700E-01	6.790E-01
7.500E-01	8.200E-01	8.611E-01	8.750E-01	9.000E-01
9.200E-01	1.010E+00	1.100E+00	1.200E+00	1.250E+00
1.317E+00	1.356E+00	1.400E+00	1.500E+00	1.850E+00
2.354E+00	2.479E+00	3.000E+00	4.304E+00	4.800E+00
6.434E+00	8.187E+00	1.000E+01	1.284E+01	1.384E+01
1.455E+01	1.568E+01	1.733E+01	2.000E+01	

```
HI-STAR containing MPC68F, 06x06 in DFC with 08 missing rods
c     3.00 % uniform enrichment, unreflected cask, 0.0067 g/cmsq B-10 in Boral
c
c
1     1 -10.522     -1  u=2       $ fuel
2     4 -1.0     1  -2  u=2       $ gap
3     3 -6.55    2  -3  u=2       $ Zr Clad
4     4 -1.0         3  u=2       $ water in fuel region
5     4 -1.0   -4:5     u=3       $ water in guide tubes
6     3 -6.55   4 -5    u=3       $ guide tubes
7     4 -1.0   -6   +7   -8   +9   u=1  lat=1
      fill= -4:3    -4:3   0:0
      1  1 1 1 1 1 1  1
      1  2 2 2 2 2 2  1
      1  2 1 2 1 2 2  1
      1  2 2 1 2 1 2  1
      1  2 1 2 1 2 2  1
      1  2 2 1 2 1 2  1
      1  2 2 2 2 2 2  1
      1  1 1 1 1 1 1  1
c
C  BOX TYPE R
c
8     0  -10   11  -12   13         u=4 fill=1 (0.8814  0.8814  0)
9     3  -6.55    60   -61    62   -63  #8      u=4     $ Zr flow channel
100   5  -7.84   74 -75 76 -77 (-70:71:-72:73)  u=4     $ DFC
10    4  -1.      64   -65    66   -67  #8 #9 #100  u=4 $ water
11    5  -7.84    20   -23    67   -14          u=4     $ 0.075" STEEL
12    4  -1.      20   -23    14   -15          u=4     $ WATER POCKET
13    7  -2.7     20   -23    15   -16          u=4     $ Al CLAD
14    6  -2.66    20   -23    16   -17          u=4     $ BORAL Absorber
15    7  -2.7     20   -23    17   -18          u=4     $ Al Clad
16    4  -1.      20   -23    18  -118          u=4     $ Water
17    5  -7.84    118:-129:65:-66               u=4     $ Steel
18    4  -1.      64   -21    67   -118         u=4     $ Water
19    4  -1.      24   -65    67   -118         u=4     $ water
20    5  -7.84    21   -20    67   -118         u=4     $ Steel
21    5  -7.84    23   -24    67   -118         u=4     $ Steel
22    4  -1.     129   -64    33   -118         u=4     $ Water
c
23    5  -7.84    25   -64    30   -31          u=4     $ Steel
24    4  -1.      26   -25    30   -31          u=4     $ Water
25    7  -2.7     27   -26    30   -31          u=4     $ Al clad
26    6  -2.66    28   -27    30   -31          u=4     $ Boral
27    7  -2.7     29   -28    30   -31          u=4     $ Al clad
28    4  -1.     129   -29    30   -31          u=4     $ water
29    5  -7.84   129   -64    32   -30          u=4     $ Steel ends
30    5  -7.84   129   -64    31   -33          u=4     $ Steel ends
31    4  -1.     129   -64    66   -32          u=4     $ Water
c
c    Type A box - Boral only on left side
c
32    0  -10   11  -12   13         u=6 fill=1 (0.8814  0.8814  0)
33    3  -6.55    60   -61    62   -63  #8      u=6     $ Zr flow channel
101   5  -7.84   74 -75 76 -77 (-70:71:-72:73)  u=6     $ DFC
34    4  -1.      64   -65    66  -118  #8 #9 #101 u=6  $ water
35    5  -7.84    118:-129:65:-66               u=6     $ Steel
36    4  -1.     129   -64    67   -118         u=6     $ Water
c
37    5  -7.84    25   -64    30   -31          u=6     $ Steel
38    4  -1.      26   -25    30   -31          u=6     $ Water
```

```
39    7  -2.7     27   -26    30   -31          u=6     $ Al clad
40    6  -2.66    28   -27    30   -31          u=6     $ Boral
41    7  -2.7     29   -28    30   -31          u=6     $ Al clad
42    4  -1.     129   -29    30   -31          u=6     $ water
43    4  -1.     129   -64    33   -67          u=6     $ Water
44    5  -7.84   129   -64    32   -30          u=6     $ Steel ends
45    5  -7.84   129   -64    31   -33          u=6     $ Steel ends
46    4  -1.     129   -64    66   -32          u=6     $ Water
c
c    Type B box -  Boral on Top only
c
47    0  -10   11  -12   13         u=7 fill=1 (0.8814  0.8814  0)
48    3  -6.55    60   -61    62   -63  #8      u=7     $ Zr flow channel
102   5  -7.84   74 -75 76 -77 (-70:71:-72:73)  u=7     $ DFC
49    4  -1.      64   -65    66   -67  #8 #9 #102 u=7  $ water
50    5  -7.84    20   -23    67   -14          u=7     $ 0.075" STEEL
51    4  -1.      20   -23    14   -15          u=7     $ WATER POCKET
52    7  -2.7     20   -23    15   -16          u=7     $ Al CLAD
53    6  -2.66    20   -23    16   -17          u=7     $ BORAL Absorber
54    7  -2.7     20   -23    17   -18          u=7     $ water
55    4  -1.      20   -23    18  -118          u=7     $ Water
56    5  -7.84    118:-129:65:-66               u=7     $ Steel
57    4  -1.      64   -21    67   -118         u=7     $ Water
58    4  -1.      24   -65    67   -118         u=7     $ water
59    5  -7.84    21   -20    67   -118         u=7     $ Steel
60    5  -7.84    23   -24    67   -118         u=7     $ Steel
61    4  -1.     129   -64    66   -118         u=7     $ Water
c
c    Type E box  - No Boral Panels
c
62    0  -10   11  -12   13         u=8 fill=1 (0.8814  0.8814  0)
63    3  -6.55    60   -61    62   -63  #8      u=8     $ Zr flow channel
103   5  -7.84   74 -75 76 -77 (-70:71:-72:73)  u=8     $ DFC
64    4  -1.     129   -65    66  -118  #8 #9 #103 u=8  $ water
65    5  -7.84    118:-129:65:-66               u=8     $ Steel
c
c    Type F box  - No Boral Panels or fuel
c
66    4  -1.     129   -65    66  -118          u=9     $ water
67    5  -7.84    118:-129:65:-66               u=9     $ Steel
c
68    4  -1.0    -34  35  -36  37  u=5  lat=1  fill=-7:6  -7:6  0:0
                5 5 5 5 5 5 5 5 5 5 5 5 5 5
                5 9 9 9 9 9 9 9 9 9 9 9 9 5
                5 9 9 9 9 9 7 4 9 9 9 9 9 5
                5 9 9 9 7 4 4 4 4 4 9 9 9 5
                5 9 9 7 4 4 4 4 4 4 4 9 9 5
                5 9 9 7 4 4 4 4 4 4 4 9 9 5
                5 9 7 4 4 4 4 4 4 4 4 4 9 5
                5 9 8 4 4 4 4 4 4 4 4 6 9 5
                5 9 9 7 4 4 4 4 4 4 4 9 9 5
                5 9 9 8 4 4 4 4 4 4 6 9 9 5
                5 9 9 9 8 4 4 4 6 6 9 9 9 5
                5 9 9 9 9 9 8 6 9 9 9 9 9 5
                5 9 9 9 9 9 9 9 9 9 9 9 9 5
                5 5 5 5 5 5 5 5 5 5 5 5 5 5
69    0          -41                 50  -49  fill=5 (8.1661  8.1661  0)
70    4  -1.0    -41        43  -50             $ Water below Fuel
71    4  -1.0    -41        49  -44             $ Water above Fuel
72    5  -7.84   -42        68  -43             $ Steel below Fuel
73    5  -7.84   -42        44  -69             $ Steel above Fuel
```

```
74     5  -7.84     41  -42  43  -44              $ Radial Steel
75     0             42 :-68:  69                 $ outside world

1      cz          0.6274       $ Fuel OD
2      cz          0.6280       $ Clad ID
3      cz          0.7169       $ Clad OD
4      cz          0.6280       $ Thimble ID
5      cz          0.7169       $ Thimble OD
6      px          0.8814       $ Pin Pitch
7      px         -0.8814
8      py          0.8814
9      py         -0.8814
10     px          5.4483       $ Channel ID
11     px         -5.4483
12     py          5.4483
13     py         -5.4483
14     py          7.8016
15     py          7.8155
16     py          7.8410
17     py          8.0467
18     py          8.0721
118    py          8.0861
20     px         -6.0325
21     px         -6.2230
23     px          6.0325
24     px          6.2230
25     px         -7.8016
26     px         -7.8155
27     px         -7.8410
28     px         -8.0467
29     px         -8.0721
129    px         -8.0861
30     py         -6.0325
31     py          6.0325
32     py         -6.2230
33     py          6.2230
34     px          7.6111
35     px         -8.7211
36     py          8.7211
37     py         -7.6111
41     cz          85.57
42     cz          108.43
43     pz          11.46
44     pz          331.0
49     pz          309.4         $ Top of Active F
50     pz           30.          $ Start of Active
60     px         -5.6007        $ Channel OD
61     px          5.6007
62     py         -5.6007
63     py          5.6007
64     px         -7.6111        $ Cell Box ID
65     px          7.6111
66     py         -7.6111
67     py          7.6111
68     pz         -10.13
69     pz          370.36
70     px         -6.2611        $ DFC ID
71     px          6.2611
72     py         -6.2611
73     py          6.2611
74     px         -6.5659        $ DFC OD
```

```
75    px          6.5659
76    py         -6.5659
77    py          6.5659

imp:n     1 77r 0
kcode    10000  0.94   20  120
c
sdef  par=1  erg=d1 axs=0 0 1 x=d4 y=fx d5 z=d3
c
sp1 -2 1.2895
c
si3  h 30. 309.
sp3  0 1
c
c
si4  s                15 16
                 13 14 15 16 17 18
             12 13 14 15 16 17 18 19
             12 13 14 15 16 17 18 19
          11 12 13 14 15 16 17 18 19 20
          11 12 13 14 15 16 17 18 19 20
             12 13 14 15 16 17 18 19
             12 13 14 15 16 17 18 19
                 13 14 15 16 17 18
                       15 16
sp4  1 67r
c
ds5  s                30 30
                 29 29 29 29 29 29
             28 28 28 28 28 28 28 28
             27 27 27 27 27 27 27 27
          26 26 26 26 26 26 26 26 26 26
          25 25 25 25 25 25 25 25 25 25
             24 24 24 24 24 24 24 24
             23 23 23 23 23 23 23 23
                 22 22 22 22 22 22
                       21 21
c
si11  -80.6831 -67.6783
si12  -64.1985 -51.1937
si13  -47.7139 -34.7091
si14  -31.2293 -18.2245
si15  -14.7447 -1.7399
si16   1.7399   14.7447
si17   18.2245  31.2293
si18   34.7091  47.7139
si19   51.1937  64.1985
si20   67.6783  80.6831
c
si21  -80.6831 -67.6783
si22  -64.1985 -51.1937
si23  -47.7139 -34.7091
si24  -31.2293 -18.2245
si25  -14.7447 -1.7399
si26   1.7399   14.7447
si27   18.2245  31.2293
si28   34.7091  47.7139
si29   51.1937  64.1985
si30   67.6783  80.6831
sp11  0 1
sp12  0 1
```

```
sp13  0 1
sp14  0 1
sp15  0 1
sp16  0 1
sp17  0 1
sp18  0 1
sp19  0 1
sp20  0 1
sp21  0 1
sp22  0 1
sp23  0 1
sp24  0 1
sp25  0 1
sp26  0 1
sp27  0 1
sp28  0 1
sp29  0 1
sp30  0 1
c
m1          92235.50c   -0.02644      $ 3.00% E Fuel
            92238.50c   -0.85504
            8016.50c    -0.11852
m3          40000.56c   1.           $ Zr Clad
m4          1001.50c    0.6667       $ Water
            8016.50c    0.3333
m5          24000.50c   0.01761      $ Steel
            25055.50c   0.001761
            26000.55c   0.05977
            28000.50c   0.008239
m6          5010.50c  1.9592E-03      $ Boral 0.0067 gm/cm2
            5011.50c  8.1175E-03
            6000.50c  2.5176E-03
            13027.50c 5.4933E-02
m7          13027.50c    1.           $ Al Clad
mt4        lwtr.01t
prdmp    j   -120   j   2
fm4      1000   1   -6
f4:n   1
sd4      1000
e4    1.000E-11   1.000E-10   5.000E-10   7.500E-10   1.000E-09   1.200E-09
      1.500E-09   2.000E-09   2.500E-09   3.000E-09
      4.700E-09   5.000E-09   7.500E-09   1.000E-08   2.530E-08
      3.000E-08   4.000E-08   5.000E-08   6.000E-08   7.000E-08
      8.000E-08   9.000E-08   1.000E-07   1.250E-07   1.500E-07
      1.750E-07   2.000E-07   2.250E-07   2.500E-07   2.750E-07
      3.000E-07   3.250E-07   3.500E-07   3.750E-07   4.000E-07
      4.500E-07   5.000E-07   5.500E-07   6.000E-07   6.250E-07
      6.500E-07   7.000E-07   7.500E-07   8.000E-07   8.500E-07
      9.000E-07   9.250E-07   9.500E-07   9.750E-07   1.000E-06
      1.010E-06   1.020E-06   1.030E-06   1.040E-06   1.050E-06
      1.060E-06   1.070E-06   1.080E-06   1.090E-06   1.100E-06
      1.110E-06   1.120E-06   1.130E-06   1.140E-06   1.150E-06
      1.175E-06   1.200E-06   1.225E-06   1.250E-06   1.300E-06
      1.350E-06   1.400E-06   1.450E-06   1.500E-06   1.590E-06
      1.680E-06   1.770E-06   1.860E-06   1.940E-06   2.000E-06
      2.120E-06   2.210E-06   2.300E-06   2.380E-06   2.470E-06
      2.570E-06   2.670E-06   2.770E-06   2.870E-06   2.970E-06
      3.000E-06   3.050E-06   3.150E-06   3.500E-06   3.730E-06
      4.000E-06   4.750E-06   5.000E-06   5.400E-06   6.000E-06
      6.250E-06   6.500E-06   6.750E-06   7.000E-06   7.150E-06
      8.100E-06   9.100E-06   1.000E-05   1.150E-05   1.190E-05
```

1.290E-05	1.375E-05	1.440E-05	1.510E-05	1.600E-05
1.700E-05	1.850E-05	1.900E-05	2.000E-05	2.100E-05
2.250E-05	2.500E-05	2.750E-05	3.000E-05	3.125E-05
3.175E-05	3.325E-05	3.375E-05	3.460E-05	3.550E-05
3.700E-05	3.800E-05	3.910E-05	3.960E-05	4.100E-05
4.240E-05	4.400E-05	4.520E-05	4.700E-05	4.830E-05
4.920E-05	5.060E-05	5.200E-05	5.340E-05	5.900E-05
6.100E-05	6.500E-05	6.750E-05	7.200E-05	7.600E-05
8.000E-05	8.200E-05	9.000E-05	1.000E-04	1.080E-04
1.150E-04	1.190E-04	1.220E-04	1.860E-04	1.925E-04
2.075E-04	2.100E-04	2.400E-04	2.850E-04	3.050E-04
5.500E-04	6.700E-04	6.830E-04	9.500E-04	1.150E-03
1.500E-03	1.550E-03	1.800E-03	2.200E-03	2.290E-03
2.580E-03	3.000E-03	3.740E-03	3.900E-03	6.000E-03
8.030E-03	9.500E-03	1.300E-02	1.700E-02	2.500E-02
3.000E-02	4.500E-02	5.000E-02	5.200E-02	6.000E-02
7.300E-02	7.500E-02	8.200E-02	8.500E-02	1.000E-01
1.283E-01	1.500E-01	2.000E-01	2.700E-01	3.300E-01
4.000E-01	4.200E-01	4.400E-01	4.700E-01	4.995E-01
5.500E-01	5.730E-01	6.000E-01	6.700E-01	6.790E-01
7.500E-01	8.200E-01	8.611E-01	8.750E-01	9.000E-01
9.200E-01	1.010E+00	1.100E+00	1.200E+00	1.250E+00
1.317E+00	1.356E+00	1.400E+00	1.500E+00	1.850E+00
2.354E+00	2.479E+00	3.000E+00	4.304E+00	4.800E+00
6.434E+00	8.187E+00	1.000E+01	1.284E+01	1.384E+01
1.455E+01	1.568E+01	1.733E+01	2.000E+01	

```
HI-STAR containing MPC68F, 07x07 in DFC with 13 missing rods
c     3.00 % uniform enrichment, unreflected cask, 0.0067 g/cmsq B-10 in Boral
c
c
1     1 -10.522      -1  u=2        $ fuel
2     4 -1.0      1  -2  u=2        $ gap
3     3 -6.55     2  -3  u=2        $ Zr Clad
4     4 -1.0          3  u=2        $ water in fuel region
5     4 -1.0   -4:5      u=3        $ water in guide tubes
6     3 -6.55   4 -5     u=3        $ guide tubes
7     4 -1.0   -6   +7   -8   +9   u=1  lat=1
      fill= -4:4    -4:4   0:0
      1  1 1 1 1 1 1 1  1
      1  2 2 2 2 2 2 2  1
      1  2 1 2 1 2 1 2  1
      1  2 2 1 2 1 2 2  1
      1  2 1 2 1 2 1 2  1
      1  2 2 1 2 1 2 2  1
      1  2 1 2 1 2 1 2  1
      1  2 2 2 2 2 2 2  1
      1  1 1 1 1 1 1 1  1
c
C  BOX TYPE R
c
8     0  -10   11  -12   13          u=4 fill=1
9     3  -6.55    60   -61    62   -63  #8      u=4      $ Zr flow channel
100   5  -7.84   74 -75 76 -77 (-70:71:-72:73)  u=4      $ DFC
10    4  -1.      64   -65    66   -67  #8 #9 #100 u=4   $ water
11    5  -7.84    20   -23    67   -14          u=4      $ 0.075" STEEL
12    4  -1.      20   -23    14   -15          u=4      $ WATER POCKET
13    7  -2.7     20   -23    15   -16          u=4      $ Al CLAD
14    6  -2.66    20   -23    16   -17          u=4      $ BORAL Absorber
15    7  -2.7     20   -23    17   -18          u=4      $ Al Clad
16    4  -1.      20   -23    18  -118          u=4      $ Water
17    5  -7.84    118:-129:65:-66               u=4      $ Steel
18    4  -1.      64   -21    67   -118         u=4      $ Water
19    4  -1.      24   -65    67   -118         u=4      $ water
20    5  -7.84    21   -20    67   -118         u=4      $ Steel
21    5  -7.84    23   -24    67   -118         u=4      $ Steel
22    4  -1.     129   -64    33   -118         u=4      $ Water
c
23    5  -7.84    25   -64    30   -31          u=4      $ Steel
24    4  -1.      26   -25    30   -31          u=4      $ Water
25    7  -2.7     27   -26    30   -31          u=4      $ Al clad
26    6  -2.66    28   -27    30   -31          u=4      $ Boral
27    7  -2.7     29   -28    30   -31          u=4      $ Al clad
28    4  -1.     129   -29    30   -31          u=4      $ water
29    5  -7.84   129   -64    32   -30          u=4      $ Steel ends
30    5  -7.84   129   -64    31   -33          u=4      $ Steel ends
31    4  -1.     129   -64    66   -32          u=4      $ Water
c
c    Type A box - Boral only on left side
c
32    0  -10   11  -12   13          u=6 fill=1
33    3  -6.55    60   -61    62   -63  #8      u=6      $ Zr flow channel
101   5  -7.84   74 -75 76 -77 (-70:71:-72:73)  u=6      $ DFC
34    4  -1.      64   -65    66   -118 #8 #9 #101 u=6   $ water
35    5  -7.84    118:-129:65:-66               u=6      $ Steel
36    4  -1.     129   -64    67   -118         u=6      $ Water
c
37    5  -7.84    25   -64    30   -31          u=6      $ Steel
```

```
38    4  -1.      26   -25    30   -31          u=6     $ Water
39    7  -2.7     27   -26    30   -31          u=6     $ Al clad
40    6  -2.66    28   -27    30   -31          u=6     $ Boral
41    7  -2.7     29   -28    30   -31          u=6     $ Al clad
42    4  -1.     129   -29    30   -31          u=6     $ water
43    4  -1.     129   -64    33   -67          u=6     $ Water
44    5  -7.84   129   -64    32   -30          u=6     $ Steel ends
45    5  -7.84   129   -64    31   -33          u=6     $ Steel ends
46    4  -1.     129   -64    66   -32          u=6     $ Water
c
c    Type B box -  Boral on Top only
c
47    0  -10   11  -12   13         u=7 fill=1
48    3  -6.55    60   -61    62   -63  #8      u=7     $ Zr flow channel
102   5  -7.84   74 -75 76 -77 (-70:71:-72:73)  u=7     $ DFC
49    4  -1.      64   -65    66   -67  #8 #9 #102 u=7  $ water
50    5  -7.84    20   -23    67   -14          u=7     $ 0.075" STEEL
51    4  -1.      20   -23    14   -15          u=7     $ WATER POCKET
52    7  -2.7     20   -23    15   -16          u=7     $ Al CLAD
53    6  -2.66    20   -23    16   -17          u=7     $ BORAL Absorber
54    7  -2.7     20   -23    17   -18          u=7     $ water
55    4  -1.      20   -23    18  -118          u=7     $ Water
56    5  -7.84    118:-129:65:-66               u=7     $ Steel
57    4  -1.      64   -21    67   -118         u=7     $ Water
58    4  -1.      24   -65    67   -118         u=7     $ water
59    5  -7.84    21   -20    67   -118         u=7     $ Steel
60    5  -7.84    23   -24    67   -118         u=7     $ Steel
61    4  -1.     129   -64    66   -118         u=7     $ Water
c
c    Type E box  - No Boral Panels
c
62    0  -10   11  -12   13         u=8 fill=1
63    3  -6.55    60   -61    62   -63  #8      u=8     $ Zr flow channel
103   5  -7.84   74 -75 76 -77 (-70:71:-72:73)  u=8     $ DFC
64    4  -1.     129   -65    66  -118  #8 #9 #103 u=8  $ water
65    5  -7.84    118:-129:65:-66               u=8     $ Steel
c
c    Type F box  - No Boral Panels or fuel
c
66    4  -1.     129   -65    66  -118          u=9     $ water
67    5  -7.84    118:-129:65:-66               u=9     $ Steel
c
68    4  -1.0    -34  35  -36  37  u=5  lat=1  fill=-7:6  -7:6  0:0
             5 5 5 5 5 5 5 5 5 5 5 5 5 5
             5 9 9 9 9 9 9 9 9 9 9 9 9 5
             5 9 9 9 9 9 7 4 9 9 9 9 9 5
             5 9 9 9 7 4 4 4 4 4 9 9 9 5
             5 9 9 7 4 4 4 4 4 4 4 9 9 5
             5 9 9 7 4 4 4 4 4 4 4 9 9 5
             5 9 7 4 4 4 4 4 4 4 4 4 9 5
             5 9 8 4 4 4 4 4 4 4 4 6 9 5
             5 9 9 7 4 4 4 4 4 4 4 9 9 5
             5 9 9 8 4 4 4 4 4 4 6 9 9 5
             5 9 9 9 8 4 4 4 6 6 9 9 9 5
             5 9 9 9 9 9 8 6 9 9 9 9 9 5
             5 9 9 9 9 9 9 9 9 9 9 9 9 5
             5 5 5 5 5 5 5 5 5 5 5 5 5 5
69    0          -41                 50  -49  fill=5 (8.1661  8.1661  0)
70    4  -1.0    -41        43  -50             $ Water below Fuel
71    4  -1.0    -41        49  -44             $ Water above Fuel
72    5  -7.84   -42        68  -43             $ Steel below Fuel
```

```
73    5  -7.84   -42        44  -69            $ Steel above Fuel
74    5  -7.84    41  -42  43  -44             $ Radial Steel
75    0            42 :-68:  69                $ outside world

1     cz         0.5220     $ Fuel OD
2     cz         0.5334     $ Clad ID
3     cz         0.6172     $ Clad OD
4     cz         0.5398     $ Thimble ID
5     cz         0.6261     $ Thimble OD
6     px         0.8014     $ Pin Pitch
7     px        -0.8014
8     py         0.8014
9     py        -0.8014
10    px         5.7684     $ Channel ID
11    px        -5.7684
12    py         5.7684
13    py        -5.7684
14    py         7.8016
15    py         7.8155
16    py         7.8410
17    py         8.0467
18    py         8.0721
118   py         8.0861
20    px        -6.0325
21    px        -6.2230
23    px         6.0325
24    px         6.2230
25    px        -7.8016
26    px        -7.8155
27    px        -7.8410
28    px        -8.0467
29    px        -8.0721
129   px        -8.0861
30    py        -6.0325
31    py         6.0325
32    py        -6.2230
33    py         6.2230
34    px         7.6111
35    px        -8.7211
36    py         8.7211
37    py        -7.6111
41    cz         85.57
42    cz         108.43
43    pz         11.46
44    pz         252.15
49    pz         230.66      $ Top of Active Fuel
50    pz         30.         $ Start of Active Fuel
60    px        -5.9207      $ Channel OD
61    px         5.9207
62    py        -5.9207
63    py         5.9207
64    px        -7.6111      $ Cell Box ID
65    px         7.6111
66    py        -7.6111
67    py         7.6111
68    pz        -10.13
69    pz         291.52
70    px        -6.2611        $ DFC ID
71    px         6.2611
72    py        -6.2611
73    py         6.2611
```

```
74    px         -6.5659       $ DFC OD
75    px          6.5659
76    py         -6.5659
77    py          6.5659

imp:n     1 77r 0
kcode   10000  0.94   20  120
c
sdef  par=1  erg=d1 axs=0 0 1 x=d4 y=fx d5 z=d3
c
sp1 -2 1.2895
c
si3  h 30. 230.66
sp3  0 1
c
c
si4  s                15 16
                 13 14 15 16 17 18
             12 13 14 15 16 17 18 19
             12 13 14 15 16 17 18 19
          11 12 13 14 15 16 17 18 19 20
          11 12 13 14 15 16 17 18 19 20
             12 13 14 15 16 17 18 19
             12 13 14 15 16 17 18 19
                 13 14 15 16 17 18
                       15 16
sp4  1 67r
c
ds5  s                30 30
                 29 29 29 29 29 29
             28 28 28 28 28 28 28 28
             27 27 27 27 27 27 27 27
          26 26 26 26 26 26 26 26 26 26
          25 25 25 25 25 25 25 25 25 25
             24 24 24 24 24 24 24 24
             23 23 23 23 23 23 23 23
                 22 22 22 22 22 22
                       21 21
c
si11  -80.6831 -67.6783
si12  -64.1985 -51.1937
si13  -47.7139 -34.7091
si14  -31.2293 -18.2245
si15  -14.7447 -1.7399
si16   1.7399   14.7447
si17   18.2245  31.2293
si18   34.7091  47.7139
si19   51.1937  64.1985
si20   67.6783  80.6831
c
si21  -80.6831 -67.6783
si22  -64.1985 -51.1937
si23  -47.7139 -34.7091
si24  -31.2293 -18.2245
si25  -14.7447 -1.7399
si26   1.7399   14.7447
si27   18.2245  31.2293
si28   34.7091  47.7139
si29   51.1937  64.1985
si30   67.6783  80.6831
sp11  0 1
```

```
sp12  0 1
sp13  0 1
sp14  0 1
sp15  0 1
sp16  0 1
sp17  0 1
sp18  0 1
sp19  0 1
sp20  0 1
sp21  0 1
sp22  0 1
sp23  0 1
sp24  0 1
sp25  0 1
sp26  0 1
sp27  0 1
sp28  0 1
sp29  0 1
sp30  0 1
c
m1          92235.50c   -0.02644      $ 3.00% E Fuel
            92238.50c   -0.85504
            8016.50c    -0.11852
m3          40000.56c   1.           $ Zr Clad
m4          1001.50c    0.6667       $ Water
            8016.50c    0.3333
m5          24000.50c   0.01761      $ Steel
            25055.50c   0.001761
            26000.55c   0.05977
            28000.50c   0.008239
m6          5010.50c  1.9592E-03      $ Boral 0.0067 gm/cm2
            5011.50c  8.1175E-03
            6000.50c  2.5176E-03
            13027.50c 5.4933E-02
m7          13027.50c    1.           $ Al Clad
mt4        lwtr.01t
prdmp    j   -120   j   2
fm4      1000   1   -6
f4:n   1
sd4      1000
e4    1.000E-11   1.000E-10   5.000E-10   7.500E-10   1.000E-09   1.200E-09
      1.500E-09   2.000E-09   2.500E-09   3.000E-09
      4.700E-09   5.000E-09   7.500E-09   1.000E-08   2.530E-08
      3.000E-08   4.000E-08   5.000E-08   6.000E-08   7.000E-08
      8.000E-08   9.000E-08   1.000E-07   1.250E-07   1.500E-07
      1.750E-07   2.000E-07   2.250E-07   2.500E-07   2.750E-07
      3.000E-07   3.250E-07   3.500E-07   3.750E-07   4.000E-07
      4.500E-07   5.000E-07   5.500E-07   6.000E-07   6.250E-07
      6.500E-07   7.000E-07   7.500E-07   8.000E-07   8.500E-07
      9.000E-07   9.250E-07   9.500E-07   9.750E-07   1.000E-06
      1.010E-06   1.020E-06   1.030E-06   1.040E-06   1.050E-06
      1.060E-06   1.070E-06   1.080E-06   1.090E-06   1.100E-06
      1.110E-06   1.120E-06   1.130E-06   1.140E-06   1.150E-06
      1.175E-06   1.200E-06   1.225E-06   1.250E-06   1.300E-06
      1.350E-06   1.400E-06   1.450E-06   1.500E-06   1.590E-06
      1.680E-06   1.770E-06   1.860E-06   1.940E-06   2.000E-06
      2.120E-06   2.210E-06   2.300E-06   2.380E-06   2.470E-06
      2.570E-06   2.670E-06   2.770E-06   2.870E-06   2.970E-06
      3.000E-06   3.050E-06   3.150E-06   3.500E-06   3.730E-06
      4.000E-06   4.750E-06   5.000E-06   5.400E-06   6.000E-06
      6.250E-06   6.500E-06   6.750E-06   7.000E-06   7.150E-06
```

8.100E-06	9.100E-06	1.000E-05	1.150E-05	1.190E-05
1.290E-05	1.375E-05	1.440E-05	1.510E-05	1.600E-05
1.700E-05	1.850E-05	1.900E-05	2.000E-05	2.100E-05
2.250E-05	2.500E-05	2.750E-05	3.000E-05	3.125E-05
3.175E-05	3.325E-05	3.375E-05	3.460E-05	3.550E-05
3.700E-05	3.800E-05	3.910E-05	3.960E-05	4.100E-05
4.240E-05	4.400E-05	4.520E-05	4.700E-05	4.830E-05
4.920E-05	5.060E-05	5.200E-05	5.340E-05	5.900E-05
6.100E-05	6.500E-05	6.750E-05	7.200E-05	7.600E-05
8.000E-05	8.200E-05	9.000E-05	1.000E-04	1.080E-04
1.150E-04	1.190E-04	1.220E-04	1.860E-04	1.925E-04
2.075E-04	2.100E-04	2.400E-04	2.850E-04	3.050E-04
5.500E-04	6.700E-04	6.830E-04	9.500E-04	1.150E-03
1.500E-03	1.550E-03	1.800E-03	2.200E-03	2.290E-03
2.580E-03	3.000E-03	3.740E-03	3.900E-03	6.000E-03
8.030E-03	9.500E-03	1.300E-02	1.700E-02	2.500E-02
3.000E-02	4.500E-02	5.000E-02	5.200E-02	6.000E-02
7.300E-02	7.500E-02	8.200E-02	8.500E-02	1.000E-01
1.283E-01	1.500E-01	2.000E-01	2.700E-01	3.300E-01
4.000E-01	4.200E-01	4.400E-01	4.700E-01	4.995E-01
5.500E-01	5.730E-01	6.000E-01	6.700E-01	6.790E-01
7.500E-01	8.200E-01	8.611E-01	8.750E-01	9.000E-01
9.200E-01	1.010E+00	1.100E+00	1.200E+00	1.250E+00
1.317E+00	1.356E+00	1.400E+00	1.500E+00	1.850E+00
2.354E+00	2.479E+00	3.000E+00	4.304E+00	4.800E+00
6.434E+00	8.187E+00	1.000E+01	1.284E+01	1.384E+01
1.455E+01	1.568E+01	1.733E+01	2.000E+01	

```
=NITAWL
' k4rf5f45, HI-STAR containing MPC24, 15x15 assembly a17 @ 4.1% E
0$$ 84 E
1$$ 0 13  0  4R0  1  E T
2$$ 92235    92238
    40000    1001     8016     5010      5011      6012
    13027    24000    25055     26000     28000
3** 92238 294.6    2   .4752    .1928     0.      0.02251     1
   16.0   7.8209   1   235.04  0.5154    1      1.0           T
END
=KENO5A
k4rf5f45, HI-STAR containing MPC24, 15x15 assembly a17 @ 4.1% E
READ PARAM TME=10000 GEN=300 NPG=10000 NSK=50 LIB=4 TBA=5
END PARAM
READ MIXT SCT=2  EPS=1.0
MIX=1   92235  9.7463E-04
        92238  0.02251
        8016   0.04694
MIX=2   40000  0.04323
MIX=3   1001   0.06688
        8016   0.03344
MIX=4   24000  0.01761
        25055  0.001761
        26000  0.05977
        28000  0.008239
MIX=5   5010   8.7066E-03
        5011   3.5116E-02
        6012   1.0948E-02
        13027  3.6936E-02
MIX=6   1001   0.06688
        8016   0.03344
MIX=7   13027  0.06026
END MIXT
'
' cell-id      8.98
' cell-pitch   10.906
' wall-thkns   5/16
' angle-thkns  5/16
' boral-gap    0.0035
' boral-pocket 0.082
' boral-thkns  0.075
' boral-clad   0.01
' boral-core   0.055
' sheathing    0.0235
' boral-wide   7.500
' boral-narrow 6.250
'
' gap size     1.09
'
READ GEOM
UNIT           1
COM="FUEL ROD"
CYLINDER        1  1  0.4752                                   381.0   0.
CYLINDER        3  1  0.4851                                   381.0   0.
CYLINDER        2  1  0.5436                                   381.0   0.
CUBOID          3  1  0.7214   -0.7214    0.7214    -0.7214    381.0   0.
UNIT           2
COM="GUIDE  TUBE CELL"
CYLINDER        3  1  0.6350                                   381.0   0.
CYLINDER        2  1  0.6706                                   381.0   0.
CUBOID          3  1  0.7214   -0.7214    0.7214    -0.7214    381.0   0.
```

```
UNIT            4
COM="LONG HORIZONTAL BORAL PANEL - NORTH"
CUBOID          5  1  9.525  -9.525   0.06985    -0.06985     381.0   0.
CUBOID          7  1  9.525  -9.525   0.09525    -0.09525     381.0   0.
CUBOID          3  1  9.525  -9.525   0.10414    -0.10414     381.0   0.
CUBOID          4  1  9.58469  -9.58469   0.16383      -0.10414     381.0   0.
UNIT            5
COM="LONG VERTICAL BORAL PANEL - EAST"
CUBOID          5  1  0.06985    -0.06985    9.525  -9.525    381.0   0.
CUBOID          7  1  0.09525    -0.09525    9.525  -9.525    381.0   0.
CUBOID          3  1  0.10414    -0.10414    9.525  -9.525    381.0   0.
CUBOID          4  1  0.16383      -0.10414    9.58469  -9.58469    381.0   0.
UNIT            6
COM="LONG HORIZONTAL BORAL PANEL - SOUTH"
CUBOID          5  1  9.525  -9.525    0.06985   -0.06985     381.0   0.
CUBOID          7  1  9.525  -9.525    0.09525   -0.09525     381.0   0.
CUBOID          3  1  9.525  -9.525    0.10414   -0.10414     381.0   0.
CUBOID          4  1  9.58469  -9.58469    0.10414   -0.16383       381.0   0.
UNIT            7
COM="LONG VERTICAL BORAL PANEL - WEST"
CUBOID          5  1  0.06985    -0.06985    9.525  -9.525    381.0   0.
CUBOID          7  1  0.09525    -0.09525    9.525  -9.525    381.0   0.
CUBOID          3  1  0.10414    -0.10414    9.525  -9.525    381.0   0.
CUBOID          4  1  0.10414    -0.16383      9.58469  -9.58469    381.0   0.
UNIT            8  ARRAY 1  -10.8204    -10.8204       0.
COM="CENTRAL FUEL ASSEMBLIES - 4 BORAL PANELS"
CUBOID          3  1  11.4046  -11.4046   11.4046  -11.4046     381.0   0.
CUBOID          4  1  12.1984  -12.1984   12.1984  -12.1984     381.0   0.
CUBOID          3  1  12.4673  -12.4673   12.4673  -12.4673     381.0   0.
HOLE            4    0.         12.3026     0.
HOLE            5   12.3026       0.        0.
HOLE            6  0.          -12.3026    0.
HOLE            7  -12.3026      0.        0.
' HOLE           17   -11.9802    11.9805    0.
' HOLE           17   -11.9802   -13.59      0.
' HOLE           18   -13.59     -11.90      0.
UNIT           21  ARRAY 1  -10.8204    -10.8204       0.
COM="CENTRAL FUEL ASSEMBLIES - 4 BORAL PANELS, W/O EAST WALL"
CUBOID          3  1  11.4046  -11.4046   11.4046  -11.4046     381.0   0.
CUBOID          4  1  11.4046  -12.1984   12.1984  -12.1984     381.0   0.
CUBOID          3  1  11.4046  -12.4673   12.4673  -12.4673     381.0   0.
HOLE            4    0.         12.3026     0.
HOLE            6  0.          -12.3026    0.
HOLE            7  -12.3026      0.        0.
UNIT           22  ARRAY 1  -10.8204    -10.8204       0.
COM="CENTRAL FUEL ASSEMBLIES - 4 BORAL PANELS, W/O WEST WALL"
CUBOID          3  1  11.4046  -11.4046   11.4046  -11.4046     381.0   0.
CUBOID          4  1  12.1984  -11.4046   12.1984  -12.1984     381.0   0.
CUBOID          3  1  12.4673  -11.4046   12.4673  -12.4673     381.0   0.
HOLE            4    0.         12.3026     0.
HOLE            5   12.3026       0.        0.
HOLE            6  0.          -12.3026    0.
UNIT           23
COM="CELL WALL BETWEEN UNITS 21 AND 22"
CUBOID          4  1  0.396775  -0.396775   23.9998  -23.9998     381.0   0.
UNIT            9
COM="SHORT HORIZONTAL BORAL PANEL - NORTH"
CUBOID          5  1  7.9375  -7.9375   0.06985    -0.06985     381.0   0.
CUBOID          7  1  7.9375  -7.9375   0.09525    -0.09525     381.0   0.
CUBOID          3  1  7.9375  -7.9375   0.10414    -0.10414     381.0   0.
CUBOID          4  1  7.99719  -7.99719   0.16383      -0.10414     381.0   0.
```

```
UNIT          10
COM="SHORT VERTICAL BORAL PANEL - EAST"
CUBOID          5  1  0.06985    -0.06985    7.9375  -7.9375    381.0   0.
CUBOID          7  1  0.09525    -0.09525    7.9375  -7.9375    381.0   0.
CUBOID          3  1  0.10414    -0.10414    7.9375  -7.9375    381.0   0.
CUBOID          4  1  0.16383      -0.10414    7.99719  -7.99719    381.0   0.
UNIT          11
COM="SHORT HORIZONTAL BORAL PANEL - SOUTH"
CUBOID          5  1  7.9375  -7.9375    0.06985   -0.06985     381.0   0.
CUBOID          7  1  7.9375  -7.9375    0.09525   -0.09525     381.0   0.
CUBOID          3  1  7.9375  -7.9375    0.10414   -0.10414     381.0   0.
CUBOID          4  1  7.99719  -7.99719    0.10414   -0.16383       381.0   0.
UNIT          12
COM="SHORT VERTICAL BORAL PANEL - WEST"
CUBOID          5  1  0.06985    -0.06985    7.9375  -7.9375    381.0   0.
CUBOID          7  1  0.09525    -0.09525    7.9375  -7.9375    381.0   0.
CUBOID          3  1  0.10414    -0.10414    7.9375  -7.9375    381.0   0.
CUBOID          4  1  0.10414    -0.16383      7.99719  -7.99719    381.0   0.
UNIT          13  ARRAY 1  -10.8204    -10.8204       0.
COM="Array B short Boral N & E "
CUBOID          3  1  11.4046  -11.4046   11.4046  -11.4046     381.0   0.
CUBOID          4  1  12.1984  -12.1984   12.1984  -12.1984     381.0   0.
CUBOID          3  1  12.4673  -12.4673   12.4673  -12.4673     381.0   0.
HOLE            9    0.         12.3026     0.
HOLE           10   12.3026       0.        0.
HOLE            6  0.          -12.3026    0.
HOLE            7  -12.3026      0.        0.
' HOLE           17   -11.9802    11.9805    0.
' HOLE           17   -11.9802   -13.59      0.
' HOLE           18   -13.59     -11.90      0.
UNIT          14  ARRAY 1  -10.8204    -10.8204       0.
COM="Array C short Boral E & S "
CUBOID          3  1  11.4046  -11.4046   11.4046  -11.4046     381.0   0.
CUBOID          4  1  12.1984  -12.1984   12.1984  -12.1984     381.0   0.
CUBOID          3  1  12.4673  -12.4673   12.4673  -12.4673     381.0   0.
HOLE            4    0.         12.3026     0.
HOLE           10   12.3026       0.        0.
HOLE           11  0.          -12.3026    0.
HOLE            7  -12.3026      0.        0.
' HOLE           17   -11.9802    11.9805    0.
' HOLE           17   -11.9802   -13.59      0.
' HOLE           18   -13.59     -11.90      0.
UNIT          15  ARRAY 1  -10.8204    -10.8204       0.
COM="Array D short Boral S & W "
CUBOID          3  1  11.4046  -11.4046   11.4046  -11.4046     381.0   0.
CUBOID          4  1  12.1984  -12.1984   12.1984  -12.1984     381.0   0.
CUBOID          3  1  12.4673  -12.4673   12.4673  -12.4673     381.0   0.
HOLE            4    0.         12.3026     0.
HOLE            5   12.3026       0.        0.
HOLE           11  0.          -12.3026    0.
HOLE           12  -12.3026      0.        0.
' HOLE           17   -11.9802    11.9805    0.
' HOLE           17   -11.9802   -13.59      0.
' HOLE           18   -13.59     -11.90      0.
UNIT          16  ARRAY 1  -10.8204    -10.8204       0.
COM="Array E short Boral N & W "
CUBOID          3  1  11.4046  -11.4046   11.4046  -11.4046     381.0   0.
CUBOID          4  1  12.1984  -12.1984   12.1984  -12.1984     381.0   0.
CUBOID          3  1  12.4673  -12.4673   12.4673  -12.4673     381.0   0.
HOLE            9    0.         12.3026     0.
HOLE            5   12.3026       0.        0.
```

```
HOLE            6  0.          -12.3026    0.
HOLE           12  -12.3026      0.        0.
' HOLE           17   -11.9802    11.9805    0.
' HOLE           17   -11.9802   -13.59      0.
' HOLE           18   -13.59     -11.90      0.
UNIT           17
CUBOID          4  1  0.7938   -0.        1.60      -0.         381.0   0.
UNIT           18
CUBOID          4  1  1.60     -0.        0.7938    -0.         381.0   0.
UNIT           30
CUBOID          4  1  1.37332  -1.37332   3.4925  -3.4925     381.0   0.
UNIT           31
CUBOID          4  1  1.05959  -1.05959   1.37332  -1.37332     381.0   0.
UNIT           41
CUBOID          3  1  14.6768  -14.6768   1.65227  -1.65227     381.0   0.
CUBOID          4  1  14.6768  -14.6768   2.44602  -2.44602     381.0   0.
UNIT           42
CUBOID          3  1  1.65227  -1.65227   14.6768  -14.6768     381.0   0.
CUBOID          4  1  2.44602  -2.44602   14.6768  -14.6768     381.0   0.
GLOBAL
UNIT           19
COM="ASSEMBLY ARRAY + X DIRECTION"
CYLINDER        3  1  86.57                                   396.24  -10.16
HOLE            8   13.8506    13.8506    0.
HOLE            8   13.8506   -13.8506    0.
HOLE           21   17.949    41.5519    0.
HOLE           21   17.949   -41.5519    0.
HOLE           13   13.8506    69.2531    0.
HOLE           14   13.8506   -69.2531    0.
HOLE           22   41.5519    17.949    0.
HOLE           22   41.5519   -17.949    0.
HOLE           13   45.6502    45.6502    0.
HOLE           14   45.6502   -45.6502    0.
HOLE           13   69.2531    13.8506    0.
HOLE           14   69.2531   -13.8506    0.
HOLE            8  -13.8506    13.8506    0.
HOLE            8  -13.8506   -13.8506    0.
HOLE           22  -17.949    41.5519    0.
HOLE           22  -17.949   -41.5519    0.
HOLE           16  -13.8506    69.2531    0.
HOLE           15  -13.8506   -69.2531    0.
HOLE           21  -41.5519    17.949    0.
HOLE           21  -41.5519   -17.949    0.
HOLE           16  -45.6502    45.6502    0.
HOLE           15  -45.6502   -45.6502    0.
HOLE           16  -69.2531    13.8506    0.
HOLE           15  -69.2531   -13.8506    0.
HOLE           23   29.7505    29.7505    0.
HOLE           23  -29.7505    29.7505    0.
HOLE           23   29.7505   -29.7505    0.
HOLE           23  -29.7505   -29.7505    0.
HOLE            5   30.2516    41.5519    0.
HOLE            5   30.2516   -41.5519    0.
HOLE            7  -30.2516    41.5519    0.
HOLE            7  -30.2516   -41.5519    0.
HOLE            7   29.2494    17.949    0.
HOLE            7   29.2494   -17.949    0.
HOLE            5  -29.2494    17.949    0.
HOLE            5  -29.2494   -17.949    0.
HOLE           30      0.       0.    0.
HOLE           31   2.43291       0.    0.
```

```
HOLE            31  -2.43291       0.    0.
HOLE            41   41.5519       0.    0.
HOLE            41  -41.5519       0.    0.
HOLE            42      0.    41.5519    0.
HOLE            42      0.   -41.5519    0.
CYLINDER         4  1  108.43                                435.61  -31.75
CUBOID           3  1  139   -139    139   -139    435.61   -31.75
END GEOM
READ ARRAY
ARA=1  NUX=15  NUY=15  NUZ=1
COM="15 X 15 FUEL ASSEMBLY"
FILL
      1 1 1 1 1 1 1 1 1 1 1 1 1 1 1
      1 1 1 1 1 1 1 1 1 1 1 1 1 1 1
      1 1 1 1 1 2 1 1 1 2 1 1 1 1 1
      1 1 1 2 1 1 1 1 1 1 1 2 1 1 1
      1 1 1 1 1 1 1 1 1 1 1 1 1 1 1
      1 1 2 1 1 2 1 1 1 2 1 1 2 1 1
      1 1 1 1 1 1 1 1 1 1 1 1 1 1 1
      1 1 1 1 1 1 1 2 1 1 1 1 1 1 1
      1 1 1 1 1 1 1 1 1 1 1 1 1 1 1
      1 1 2 1 1 2 1 1 1 2 1 1 2 1 1
      1 1 1 1 1 1 1 1 1 1 1 1 1 1 1
      1 1 1 2 1 1 1 1 1 1 1 2 1 1 1
      1 1 1 1 1 2 1 1 1 2 1 1 1 1 1
      1 1 1 1 1 1 1 1 1 1 1 1 1 1 1
      1 1 1 1 1 1 1 1 1 1 1 1 1 1 1
END FILL
END ARRAY
END DATA
END
```

```
=NITAWL
' HI-STAR containing MPC68, 08x08 @ 4.2% E
0$$ 84 E
1$$ 0 13  0  4R0  1  E T
2$$ 92235    92238
    40000    1001     8016     5010      5011      6012
    13027    24000    25055     26000     28000
3** 92238 294.6    2   .5207    .1623     0.      0.02248     1
   16.0   7.8330   1   235.04  0.5662    1      1.0           T
END
=KENO5A
HI-STAR containing MPC68, 08x08 @ 4.2% E
'  GE 8X8R FUEL 2 WATER HOLES
READ PARAM TME=10000 GEN=1100 NPG=5000 NSK=100
     LIB=4 TBA=5  LNG=400000   NB8=900
END PARAM
READ MIXT SCT=2  EPS=1.
MIX=1   92235  9.983E-04
        92238  0.02248
        8016   0.04697
MIX=2   40000  0.04323
MIX=3   1001   0.06688
        8016   0.03344
MIX=4   24000  0.01761
        25055  0.001761
        26000  0.05977
        28000  0.008239
MIX=5   5010   8.071E-03
        5011   3.255E-02
        6012   1.015E-02
        13027  3.805E-02
MIX=6   13027  0.06026
END MIXT
READ GEOM
UNIT           1
COM=           "FUEL ROD"
CYLINDER        1  1  0.5207                                    381.0   0.
CYLINDER        3  1  0.5321                                    381.0   0.
CYLINDER        2  1  0.6134                                    381.0   0.
CUBOID          3  1  0.8128   -0.8128    0.8128    -0.8128     381.0   0.
UNIT           2
COM=           "GUIDE  TUBE CELL"
CYLINDER        3  1  0.6744                                    381.0   0.
CYLINDER        2  1  0.7506                                    381.0   0.
CUBOID          3  1  0.8128   -0.8128    0.8128    -0.8128     381.0   0.
UNIT           4
COM=           "HORIZONTAL BORAL PANEL"
CUBOID          5  1  6.0325   -6.0325    0.1027    -0.1027     381.0   0.
CUBOID          6  1  6.0325   -6.0325    0.1283    -0.1283     381.0   0.
CUBOID          3  1  6.0325   -6.0325    0.1422    -0.1422     381.0   0.
CUBOID          4  1  6.4611   -6.4611    0.1422    -0.3327     381.0   0.
UNIT           5
COM=           "VERTICAL BORAL PANEL"
CUBOID          5  1  0.1027   -0.1027     6.0325   -6.0325    381.0   0.
CUBOID          6  1  0.1283   -0.1283     6.0325   -6.0325    381.0   0.
CUBOID          3  1  0.1422   -0.1422     6.0325   -6.0325    381.0   0.
CUBOID          4  1  0.3327   -0.1422     6.4611   -6.4611    381.0   0.
UNIT           8  ARRAY 1  -6.5024     -6.5024        0.
COM=           "FUEL ASSEMBLIES - 2 BORAL PANELS"
CUBOID          3  1  6.7031   -6.7031    6.7031   -6.7031          381.0   0.
CUBOID          2  1  6.9571   -6.9571    6.9571   -6.9571          381.0   0.
```

```
CUBOID          3  1  7.6111   -8.0861    8.0861   -7.6111          381.0   0.
HOLE            4    0.         7.9438     0.
HOLE            5  -7.9438       0.         0.
CUBOID          4  1  7.6111   -8.7211    8.7211   -7.6111          381.0   0.
UNIT            9  ARRAY 1  -6.5024     -6.5024        0.
COM=            "FUEL ASSEMBLIES - Type A"
CUBOID          3  1  6.7031   -6.7031    6.7031   -6.7031          381.0   0.
CUBOID          2  1  6.9571   -6.9571    6.9571   -6.9571          381.0   0.
CUBOID          3  1  7.6111   -8.0861    8.0861   -7.6111          381.0   0.
HOLE            5  -7.9438       0.         0.
CUBOID          4  1  8.2461   -8.7211    8.7211   -7.6111          381.0   0.
UNIT           10  ARRAY 1  -6.5024     -6.5024        0.
COM=            "FUEL ASSEMBLIES - Type B"
CUBOID          3  1  6.7031   -6.7031    6.7031   -6.7031          381.0   0.
CUBOID          2  1  6.9571   -6.9571    6.9571   -6.9571          381.0   0.
CUBOID          3  1  7.6111   -8.0861    8.0861   -7.6111          381.0   0.
HOLE            5  -7.9438       0.         0.
CUBOID          4  1  7.6111   -8.7211    8.7211   -7.6111          381.0   0.
UNIT           11  ARRAY 1  -6.5024     -6.5024        0.
COM=            "FUEL ASSEMBLIES - Type C"
CUBOID          3  1  6.7031   -6.7031    6.7031   -6.7031          381.0   0.
CUBOID          2  1  6.9571   -6.9571    6.9571   -6.9571          381.0   0.
CUBOID          3  1  7.6111   -8.0861    8.0861   -7.6111          381.0   0.
HOLE            4    0.         7.9438     0.
HOLE            5  -7.9438       0.         0.
CUBOID          4  1  8.2461   -8.7211    8.7211   -7.6111          381.0   0.
UNIT           12  ARRAY 1  -6.5024     -6.5024        0.
COM=            "FUEL ASSEMBLIES - Type D"
CUBOID          3  1  6.7031   -6.7031    6.7031   -6.7031          381.0   0.
CUBOID          2  1  6.9571   -6.9571    6.9571   -6.9571          381.0   0.
CUBOID          3  1  7.6111   -8.0861    8.0861   -7.6111          381.0   0.
HOLE            4    0.         7.9438     0.
HOLE            5  -7.9438       0.         0.
CUBOID          4  1  8.2461   -8.7211    8.7211   -8.2461          381.0   0.
UNIT           13  ARRAY 1  -6.5024     -6.5024        0.
COM=            "FUEL ASSEMBLIES - Type E"
CUBOID          3  1  6.7031   -6.7031    6.7031   -6.7031          381.0   0.
CUBOID          2  1  6.9571   -6.9571    6.9571   -6.9571          381.0   0.
CUBOID          3  1  7.6111   -8.0861    8.0861   -7.6111          381.0   0.
HOLE            4    0.         7.9438     0.
HOLE            5  -7.9438       0.         0.
CUBOID          4  1  7.6111   -8.7211    8.7211   -8.2461          381.0   0.
UNIT           14  ARRAY 1  -6.5024     -6.5024        0.
COM=            "FUEL ASSEMBLIES - Type F"
CUBOID          3  1  6.7031   -6.7031    6.7031   -6.7031          381.0   0.
CUBOID          2  1  6.9571   -6.9571    6.9571   -6.9571          381.0   0.
CUBOID          3  1  7.6111   -8.0861    8.0861   -7.6111          381.0   0.
HOLE            4    0.         7.9438     0.
CUBOID          4  1  7.6111   -8.7211    8.7211   -8.2461          381.0   0.
UNIT           15  ARRAY 1  -6.5024     -6.5024        0.
COM=            "FUEL ASSEMBLIES - TYPE G"
CUBOID          3  1  6.7031   -6.7031    6.7031   -6.7031          381.0   0.
CUBOID          2  1  6.9571   -6.9571    6.9571   -6.9571          381.0   0.
CUBOID          3  1  7.6111   -8.0861    8.0861   -7.6111          381.0   0.
HOLE            4    0.         7.9438     0.
CUBOID          4  1  7.6111   -8.7211    8.7211   -7.6111          381.0   0.
UNIT           16  ARRAY 1  -6.5024     -6.5024        0.
COM=            "FUEL ASSEMBLIES - TYPE H"
CUBOID          3  1  6.7031   -6.7031    6.7031   -6.7031          381.0   0.
CUBOID          2  1  6.9571   -6.9571    6.9571   -6.9571          381.0   0.
CUBOID          3  1  7.6111   -8.0861    8.0861   -7.6111          381.0   0.
```

```
CUBOID          4  1  7.6111   -8.7211    8.7211   -7.6111          381.0   0.
UNIT           17  ARRAY 2     -48.9966  -48.9966          0
UNIT           18  ARRAY 3     -16.3322  -7.6111           0.
UNIT           19  ARRAY 4     -48.9966  -7.6111           0.
UNIT           20  ARRAY 5     -8.7211   -16.3322          0.
UNIT           21  ARRAY 6     -8.7211   -50.1068          0.
UNIT           22  ARRAY 7     -8.7211   -16.3322          0.
UNIT           23  ARRAY 8     -8.7211   -16.3322          0.
UNIT           24  ARRAY 9     -8.7211   -16.3322          0.
UNIT           25  ARRAY 10    -8.7211   -16.3322          0.
UNIT           26  ARRAY 11    -16.3322  -8.7213           0.
UNIT           27  ARRAY 12    -16.3322  -7.6111           0.
UNIT           28  ARRAY 13    -16.3322  -8.7213           0.
UNIT           29  ARRAY 14    -16.3322  -8.7213           0.
GLOBAL
UNIT           30
CYLINDER        3  1   85.57                                        402.5   -18.54.
HOLE           17      0.0        0.0        0.
HOLE           18      0.0       73.4949     0.
HOLE           19      0.0       57.1627     0.
HOLE           20     -73.4949    0.0        0.
HOLE           21     -56.6077    0.0        0.
HOLE           22      57.7177   32.6644     0.
HOLE           23      57.7177    0.0        0.
HOLE           24      74.052     0.0        0.
HOLE           25      57.7177  -32.6644     0.
HOLE           26      32.6644  -57.7177     0.
HOLE           27       0.0     -57.7177     0.
HOLE           28     -32.6644  -57.7177     0.
HOLE           29       0.0     -74.052      0.
CYLINDER        4   1   108.43                                  441.85  -40.13
CUBOID          3   1   109.     -109.      109.     -109.    442     -40.2
END GEOM
READ ARRAY
ARA=1  NUX=8   NUY=8   NUZ=1
COM=   "8 X 8 FUEL ASSEMBLY"
FILL
 1 1 1 1 1 1 1 1
 1 1 1 1 1 1 1 1
 1 1 1 1 1 1 1 1
 1 1 1 2 1 1 1 1
 1 1 1 1 2 1 1 1
 1 1 1 1 1 1 1 1
 1 1 1 1 1 1 1 1
 1 1 1 1 1 1 1 1
END FILL
ARA=2  NUX=6   NUY=6   NUZ=1
COM=   "6 X 6 CENTRAL ARRAY OF FUEL ASSEMBLIES"
FILL
  8 8 8 8 8 8
  8 8 8 8 8 8
  8 8 8 8 8 8
  8 8 8 8 8 8
  8 8 8 8 8 8
  8 8 8 8 8 8
END FILL
ARA=3  NUX=2   NUY=1   NUZ=1
COM=   "2 X 1  ARRAY OF FUEL ASSEMBLIES - TOP ROW"
FILL
 16  9
END FILL
```

```
ARA=4  NUX=6   NUY=1   NUZ=1
COM=   "6 X 1  ARRAY OF FUEL ASSEMBLIES - 2ND ROW"
FILL
  16  10  8  8  10  9
END FILL
ARA=5  NUX=1   NUY=2   NUZ=1
COM=   "2 X 1  ARRAY OF FUEL ASSEMBLIES - OUTER LEFT"
FILL
  14
  16
END FILL
ARA=6  NUX=1   NUY=6   NUZ=1
COM=   "1 X 6  ARRAY OF FUEL ASSEMBLIES - 2ND ROW LEFT"
FILL
  14  15  8  8  15  16
END FILL
ARA=7  NUX=1   NUY=2   NUZ=1
COM=   "1 X 2  ARRAY OF FUEL ASSEMBLIES - UPPER RIGHT"
FILL
  11
   9
END FILL
ARA=8  NUX=1   NUY=2   NUZ=1
COM=   "1 X 2  ARRAY OF FUEL ASSEMBLIES - MIDDLE RIGHT"
FILL
   8
   8
END FILL
ARA=9  NUX=1   NUY=2   NUZ=1
COM=   "1 X 2  ARRAY OF FUEL ASSEMBLIES - MIDDLE RIGHT"
FILL
   11
    9
END FILL
ARA=10  NUX=1   NUY=2   NUZ=1
COM=   "1 X 2  ARRAY OF FUEL ASSEMBLIES - LOWER RIGHT"
FILL
  11
  11
END FILL
ARA=11  NUX=2   NUY=1   NUZ=1
COM=   "2 X 1  ARRAY OF FUEL ASSEMBLIES - 2ND BOTTOM ROW"
FILL
  13  13
END FILL
ARA=12  NUX=2   NUY=1   NUZ=1
COM=   "2 X 1  ARRAY OF FUEL ASSEMBLIES - BOTTOM ROW"
FILL
  8  8
END FILL
ARA=13  NUX=2   NUY=1   NUZ=1
COM=   "2 X 1  ARRAY OF FUEL ASSEMBLIES - BOTTOM ROW"
FILL
  14  13
END FILL
ARA=14  NUX=2   NUY=1   NUZ=1
COM=   "2 X 1  ARRAY OF FUEL ASSEMBLIES - BOTTOM ROW"
FILL
  14 13
END FILL
END ARRAY
```

```
END DATA
END
```